Akademiya Nauk SSSR

COSMIC RAYS AND PROBLEMS OF SPACE PHYSICS

Edited by Yu. G. Shafer

N67-38201 N67-38234
(ACCESSION NUMBER) (THRU)
353 1
(PAGES) (CODE)
29
(NASA CR OR TMX OR AD NUMBER) (CATEGORY)
FACILITY FORM 602

TRANSLATED FROM RUSSIAN

Published for the National Aeronautics and Space Administration
and the National Science Foundation, Washington, D.C.
by the Israel Program for Scientific Translations

AKADEMIYA NAUK SSSR·SIBIRSKOE OTDELENIE
USSR Academy of Sciences · Siberian Division

COSMIC RAYS AND PROBLEMS OF SPACE PHYSICS

(Kosmicheskie luchi i problemy kosmofiziki)

Edited by Yu. G. Shafer

Proceedings of the All-Union Conference on the
Space Physics Aspects of Cosmic-Ray Research,
Yakutsk, August-September 1962

Redaktsionno-izdatel'skii otdel
Sibirskogo otdeleniya AN SSSR
Novosibirsk 1965

Translated from Russian

Israel Program for Scientific Translations
Jerusalem 1967

NASA TT F-428
TT 67-51365

Published Pursuant to an Agreement with
NATIONAL AERONAUTICS AND SPACE ADMINISTRATION, U.S.A.
and
THE NATIONAL SCIENCE FOUNDATION, WASHINGTON, D.C.

Copyright © 1967
Israel Program for Scientific Translations Ltd.
IPST Cat. No. 1814

Translated and Edited by R. Hardin

Printed in Jerusalem by S. Monson
Binding: Wiener Bindery, Ltd., Jerusalem

Available from the
U.S. DEPARTMENT OF COMMERCE
Clearinghouse for Federal Scientific and Technical Information
Springfield, Va. 22151

V/13/5

CONTENTS

PREFACE vii

V. L. GINZBURG. The Emphasis on Space Physics in Cosmic-Ray Research 1

V. L. GINZBURG and S. I. SYROVATSKII. The Present State of Ideas on the Origin of Cosmic Rays (Synopsis) 3

V. L. GINZBURG, L. V. KURNOSOVA, V. I. LOGACHEV, L. A. RAZORENOV, and M. I. FRADKIN. The Primary Component of Cosmic Radiation (Review of some experimental data) 4

BRUNO PONTECORVO. The Neutrino and its Importance in Astrophysics 20

G. F. KRYMSKII. Application of a Unidimensional-Diffusion Model to the Propagation of Solar Cosmic Rays . . . 41

A. E. CHUDAKOV, V. L. DADYKIN, V. I. ZATSEPIN, and N. M. NESTEROVA. A Search for High-Energy Photons from Discrete Sources of Cosmic Radio Emission. 45

Yu. G. SHAFER. Studies of Variations in the Primary Cosmic Radiation 48

V. V. VITKEVICH. The Predominantly Radial Magnetic Field in the Space about the Sun (Synopsis) 57

V. I. SHISHOV. The Influence of the Radial Magnetic Field on the Diffusion of Cosmic Rays (Synopsis) 60

A. A. POMANSKII and O. I. DOVZHENKO. The Radiation Length . 63

S. I. NIKOL'SKII. Extensive Air Showers of Cosmic Radiation . 86

S. N. VERNOV, V. I. SOLOV'EVA, B. A. KHRENOV, and G. B. KHRISTIANSEN. Primary Cosmic Radiation in the Ultra-high-Energy Range and Extensive Air Showers 103

D. D. KRASIL'NIKOV, M. M. ATAKOVA, N. N. EFIMOV, M. A. NIFONTOV, and F. K. SHAMSUTDINOVA. Atmospheric-Density Effects in the EAS Frequency During Cyclones and Seasonal Fluctuations in Atmospheric Temperature . 112

D. D. KRASIL'NIKOV. The μ-Meson Spectrum for Energies from 10^{11} TO 10^{13} eV at Sea Level 118

A. I. KUZ'MIN and G. F. KRYMSKII. Cosmic-Ray Bursts . . . 133

A. I. KUZ'MIN and G. F. KRYMSKII. The Effect on Cosmic Rays of a Variation in the Geomagnetic Thresholds 140

L. I. DORMAN, E. V. KOLOMEETS, L. V. KOZAK, V. T. PIVNEVA, and G. A. SERGEEVA. The Variation in Cosmic-Ray Intensity at the Time of a Forbush Decrease 144

A. I. KUZ'MIN, G. F. KRYMSKII, G. V. SKRIPIN, N. P. CHIRKOV, Yu. G. SHAFER, and G. V. SHAFER. Cosmic Rays in July 1961 156

A. I. KUZ'MIN, G. V. SKRIPIN, S. N. DRUZHININ, G. F. KRYMSKII, and P. A. KRIVOSHAPKIN. Some Results of Azimuthal Measurements of Cosmic-Ray Variations at Yakutsk . . . 164

L. I. DORMAN and O. I. INOZEMTSEVA. A Local Source of the Diurnal Cosmic-Ray Variation During Magnetic Storms (Synopsis) 173

G. V. SKRIPIN, G. F. KRYMSKII, and L. P. BOLTRUSHKO. The Contribution of Solar Particles to the Diurnal Variation of the Neutron Intensity. 174

N. N. EFIMOV, M. M. ATAKOVA, T. A. EGOROV, D. D. KRASIL'NIKOV, S. V. MAKSIMOV, M. A. NIFONTOV, and F. K. SHAMSUTDINOVA. The EAS Frequency During Periods of Various Effects in the Intensity of Intermediate-Energy Cosmic Rays 180

G. V. SKRIPIN. Diurnal Variations in Cosmic-Ray Intensity . . . 184

N. P. CHIRKOV, A. I. KUZ'MIN, G. F. KRYMSKII, G. V. SHAFER, and V. A. FILIPPOV. The Unusual Phenomena Related to the Cosmic-Ray Variations in December 1957 197

N. P. CHIRKOV. Ionization-Burst Variations 206

N. P. CHIRKOV. Rhythmic Trends in the Secular Variations of Cosmic-Ray Intensity 211

D. D. KRASIL'NIKOV. Correlation of the Frequency of Large Ionization Bursts with the 11-Year Solar-Activity Cycle. . 216

E. F. VERSHININ and E. A. PONOMAREV. Observations of the Ultralow-Frequency (ULF) Radiation of Polar Aurorae . . 221

N. P. BEN'KOVA and A. N. SUKHODOL'SKAYA. The Variability of Ionospheric Parameters 232

E. G. BOSS, L. I. DORMAN, E. V. KOLOMEETS, and Zh. S. TAKIBAEV. Coupling Coefficients for Particle Passage Through the Atmosphere, Taking into Account Nuclear Interactions 237

A. I. KUZ'MIN, P. A. KRIVOSHAPKIN, G. F. KRYMSKII, and G. V. SKRIPIN. A Study of Temperature Fluctuations of the Upper Atmosphere, According to Data of Underground Cosmic-Ray Measurements 246

V. V. SMIRNOV and K. K. FEDCHENKO. The Barometric Effect for the ASK-3 Ionization Chamber at Murmansk (Synopsis) . 254

A. A. DANILOV. A Comparison between the Diurnal Variations of the Geomagnetic Field and the Corresponding Variations of Cosmic-Ray Intensity 255

A. T. ABROSIMOV and Ya. L. BLOKH. The Study of Short-Period Variations and Microvariations in Cosmic-Ray Intensity by Means of Single Scintillation Counters 266

M. M. DAION and G. A. LEKSIN. Spark Detectors for Charged Particles (Synopsis) 277

N. N. NURGOZHIN and R. A. NAM. An Air-Filled Spark Chamber . 278

M. I. PAK and Yu. T. LUKIN. A Spark Counter for Recording Cosmic-Radiation Particles 281

I. Ya. CHASNIKOV. The Use of δ Electrons to Determine the Nature and Energy of Charged Particles 286

E. T. FRANTSUZ. The Organization of Stratospheric Cosmic-Ray Observations at Apatity. 290

R. Z. DENIKAEV, E. V. KOLOMEETS, L. V. KOZAK, L. A. MIRKIN, B. A. PRILEPSKII, and V. G. ROSHCHUPKIN. Operation of a Neutron Monitor and μ-Meson Telescope 291

I. N. KAPUSTIN and A. V. KAPUSTINA. A Possible Cause of Instrumental Errors for a Neutron Monitor 294

I. N. KAPUSTIN. Visible Recording of the Cosmic-Ray Intensity by Means of a Multiple-Point Automatic Potentiometer . . 297

L. V. GRANITSKII, A. F. NEERMOLOV, Yu. K. VOROB'EV, and G. V. KONONOVA. An Automatic Programed Scaler . . . 300

LIST OF ABBREVIATIONS 304

INDEX 305

PRECEDING PAGE BLANK NOT FILMED.

PREFACE

Cosmic-ray physics is now entering a new stage of development, a characteristic feature of which is a definite emphasis on space physics in cosmic-ray research. In addition, the nuclear aspect of cosmic-ray physics is receiving special study in the range of ultrahigh energies as yet unattainable in the laboratory.

The enormous advances made so far in the conquest of space have stimulated interest in space physics even more. The use of artificial satellites and rockets makes it possible to solve certain important theoretical problems in astrophysics and also some purely practical problems, especially with regard to the prediction of solar radiation bursts and their space-time distribution, in order to guarantee the safety of manned space flights.

The First All-Union Conference on the Space Physics Aspect of Cosmic-Ray Research, held in Yakutsk from 23 August to 2 September 1962, is a further indication of the radical changes currently taking place in cosmic-ray physics. This conference stirred up a lively interest among Soviet scientists, and as a result a large number of problems were posed and discussed.

One hundred and ten scientists participated in the conference, which was convened under the joint auspices of the Cosmic-Ray Council of the USSR Academy of Sciences, the Siberian Division of the Academy, and the Yakutsk Branch of the Siberian Division of the Academy. The scientists taking part represented twenty-six scientific institutions and universities in the Soviet Union.

At the conference, seventy-five reports were read and discussed. These dealt with the following subjects in space physics and related fields: geophysics, solar physics and astronomy, neutrino physics, the neutrino and cosmogony, the origin of cosmic rays, cosmic-ray variations, electromagnetic conditions in interplanetary space, solar cosmic rays, primary galactic and extragalactic radiation, extensive air showers of cosmic rays, nuclear interactions and spectra of μ mesons at high and ultrahigh energies, meteorological effects in cosmic rays, the ionosphere, the upper atmosphere, research methods, experimental techniques.

Forty two of the reports submitted at the conference are given in this collection. Several others, which were still in preparation when this collection went to press, will be published in scientific journals.

V. L. Ginzburg

THE EMPHASIS ON SPACE PHYSICS IN COSMIC-RAY RESEARCH

The first article on cosmic rays was published at the beginning of this century, in 1900. By chance, quantum physics also came into being at that time, and the basic law of blackbody radiation was formulated. However, whereas quantum theory rapidly became one of the most discussed fields of physics, for many years cosmic rays did not attract any special attention. In fact, it took a quarter of a century just to prove that highly penetrating radiation continually reaches the earth from outer space.

During this period, cosmic rays could be recorded only by means of the ionization which they produced in ionization chambers. At the same time, some ionization always resulted from the presence of radioactive elements in the chamber walls, in surrounding objects, and in the soil. Consequently, the proof of the existence of cosmic rays had to await the ascent of equipment in balloons. In a balloon the effects of terrestrial radioactivity are reduced, while, conversely, the intensity of cosmic radiation is higher. Such experiments, which at present are quite simple, were very complicated undertakings early in this century. That is why it took until 1926 to complete the first stage in the study of cosmic rays, namely to demonstrate that such rays actually exist.

It is natural to assume that the next step would have been to determine the origin of cosmic rays. However, in the second stage of cosmic-ray research the main attention was focused on the study of various elementary particles by means of cosmic rays.

Such a trend of the investigations was not fortuitous. First of all, at that time there was no means of studying cosmic rays beyond the earth's atmosphere or even at altitudes higher than 20 km. Moreover, primary cosmic rays approaching the earth produce various secondary particles in the atmosphere, and to determine the origin of cosmic rays it is of course necessary to have information on the primary particles. Second, it was found that even in the secondary cosmic rays in the atmosphere particles of very high energy, which have extremely interesting properties, are present. These particles and their behavior in cosmic rays constituted the main object of study until 1955–1957. Consequently, some discoveries were made which were of great significance for physics as a whole. Almost all the so-called elementary particles, apart from the previously known electron, proton, and photon, were discovered in cosmic rays.

These discoveries and the physics research related to them were so important that huge amounts were spent on producing artificial cosmic-ray beams of fast particles in accelerators (cyclotrons, phasotrons, synchrotons, etc.). The flux of fast particles in an accelerator is much

greater than the particle fluxes in cosmic rays. Therefore, if particles of a given energy can be obtained in an accelerator, it is quite impractical to study them in cosmic rays. Accelerators are now available which can provide particles with energies up to 30 BeV. The energies of most cosmic rays are less than 30 BeV, and cosmic-ray particles with energies higher than this are comparatively few. For example, in an hour 1 m^2 of the earth's surface receives only one particle with an energy of 10^6 BeV or more. On the other hand, particles with energies higher than 30 BeV cannot now be produced artificially, whereas their study is extremely interesting. Consequently, the continued use of cosmic rays as a means of studying elementary particles is both desirable and in fact inevitable.

In such studies it is also possible to utilize artificial earth satellites and high-altitude space stations (in the USSR there are three such stations). Nevertheless, the research on elementary particles in cosmic rays began to take a different direction some years ago, becoming oriented more toward studies of the primary cosmic rays, the cosmic rays emitted by the sun, etc.

In general, it may be stated that the emphasis of studies in cosmic-ray physics changed radically after 1955–1957, and that a third stage of development, which is still in progress, has begun.

At present the objects of research in this new field related to space physics are: primary cosmic rays near the earth, studied using balloons, rockets, and artificial satellites; cosmic rays in the universe in general, studied mainly by radio-astronomical methods (the major source of radio emission in space is cosmic rays); solar cosmic rays; cosmic-ray variations and their application in the study of interplanetary space; the radiation belts of the earth and of other planets; the origin of cosmic rays, and their motions and accelerations in outer space.

A large, ever-increasing number of institutes, laboratories, and scientific groups, both in the Soviet Union and elsewhere, are studying problems of this type, often in connection with related problems in physics, geophysics, astronomy, and engineering.

The great advances made in the conquest of space, beginning with the launching of Sputnik I on 4 October 1957, have increased even more the importance and interest of the space-physics aspect of cosmic-ray research. Artificial satellites and space (interplanetary) rockets open up whole new vistas in the study of various astrophysical problems, in particular with regard to primary cosmic rays and radiation belts.

All these facts are evidence of the radical changes in cosmic-ray physics mentioned above, and they signal the beginning of a new development phase in which research is predominantly oriented toward space physics.

V. L. Ginzburg and S. I. Syrovatskii

THE PRESENT STATE OF IDEAS ON THE ORIGIN OF COSMIC RAYS (Synopsis)

This report attempts to do two things: to review the present state of ideas on the origin of cosmic rays (apart from questions related to the sun and the solar system); and to present some new results on this subject obtained by the authors. In the review portion of the report the following topics were discussed.

1. Recent data on primary cosmic rays (nuclei, γ rays, and electrons). Data on γ rays and electrons are discussed in particular detail (includes a study in which an electron component of solar cosmic rays is detected).
2. Some radio-astronomical results. The nature and the spectrum of the electron component of cosmic rays in the galaxy.
3. The nature of the motion of cosmic rays in interstellar space (diffusion approximation, Compton losses, etc.).
4. An overall look at the theory of cosmic-ray origins. The results of some calculations described in more detail in the second part of the report.

The second part of the report discusses three main subjects: the concentration of cosmic rays in the metagalaxy; the chemical composition of galactic cosmic rays; and the spectrum of the total galactic radio emission associated with the secondary electron component of cosmic rays in the galaxy.

All the material touched upon in the report is discussed in detail in the authors' monograph "The Origin of Cosmic Rays".*

P. N. Lebedev Institute of Physics of the USSR Academy of Sciences

* [Proiskhozhdenie kosmicheskikh luchei — Moskva, Izdatel'stvo AN SSSR, 1963.]

NC: 38202

V.L. Ginzburg, L.V. Kurnosova, V.I. Logachev, L.A. Razorenov, and M.I. Fradkin

THE PRIMARY COMPONENT OF COSMIC RADIATION

*(Review of some experimental data)**

Many experimenters have studied the primary component of cosmic rays using various types of apparatus, and these studies have made it possible to determine the general composition of primary cosmic radiation. However, there are still not enough data on the fluxes of the nuclei of different elements, apart from protons and α particles, and in most investigations only fluxes of groups of nuclei are considered.

Nuclei with charges $Z \geqslant 3$ are usually divided into the following groups:

1) light nuclei with $3 \leqslant Z \leqslant 5$ (L group);
2) nuclei of the middle group, with $6 \leqslant Z \leqslant 9$ (M group);
3) heavy nuclei with $Z \geqslant 10$ (H group).

The designation S is also used for the group of nuclei with charges $Z \geqslant 6$ ($S = M + H$).

The flux magnitude for each group of nuclei depends on the rigidity $R = \frac{Apc}{Ze}$ of the nuclei being recorded, where A is the atomic weight, Z is the atomic number, and p is the momentum of each nucleon.

Measurements show that the rigidity spectra of different nuclei are close to one another, if not identical. For multiply charged nuclei $\frac{A}{Z} \approx 2$, and the rigidity of the nucleus is determined by the momentum p of each of the nucleons (and thus by the energy E per nucleon). Consequently, identity of the rigidity spectra indicates identity of the energy spectra for the different groups of nuclei. For energies from about 1.8 to 7.5 BeV/nucleon, the spectra of nuclei with $Z \geqslant 2$, $Z \geqslant 5$, and $Z \geqslant 12$ to 14 have been found to be the same; this was shown, in particular, by measurements /1, 2/ of the latitude effect during flights of Soviet satellite vehicles. Figure 1 shows the latitude dependences for different nucleus groups, on the basis of measurements made with Sputnik VI. Figures 2 and 3 give the integral energy spectra of nuclei with various charges. Certain data from measurements using photoemulsions (see review article /3/) indicate that for groups M and H the spectra remain identical up to energies of the order of 100 BeV/nucleon.

* **Note.** A more detailed review of this subject, making use of a greater amount of data, was published in the journal, "Uspekhi fizicheskikh nauk" (**82**, 585. 1964). New data published after the close of the Conference on the Space Physics Aspects of Cosmic-Ray Research were also presented in a report at the Cosmic-Ray Conference in Apatity (August 1964); the results of this conference will be published in the journal, "Izvestiya Akademii Nauk SSSR, seriya fizicheskaya."

The situation is somewhat different for protons, since in this case $\frac{A}{Z} = 1$, so that for the same energy per nucleon the rigidities of protons and nuclei

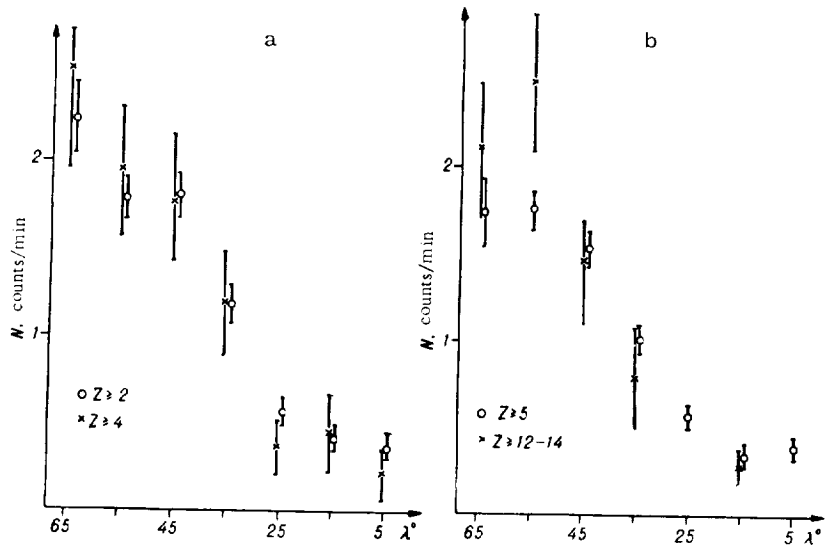

FIGURE 1. Latitude dependence of counting rate, according to data obtained with Sputnik VI: a-nuclei with $z \geqslant 2$ and $z \geqslant 4$; b-nuclei with $Z \geqslant 5$ and $Z \geqslant 12$ to 14.

are different at low energies. Identity of the rigidity spectra of protons and multiply charged nuclei indicates a difference in their energy spectra. Consequently, the flux ratio for protons and multiply charged nuclei depends on the energy, and only for $E \gg mc^2$ will this ratio be constant. For example, the ratio of proton flux to α-particle flux for a given rigidity is $\frac{I_p(R)}{I_\alpha(R)} = 7.2 \pm 0.2$ for rigidities $R > 10^9$ volts, and this ratio remains constant up to $R \approx 5 \cdot 10^{12}$ volts. However, this flux ratio for a given energy per nucleon increases with a rise in energy, approaching the value $\frac{I_p(E)}{I_\alpha(E)} = 19.8 \pm 1.2$ for $E \gg mc^2$.

Therefore, if the fluxes of different nuclei (including protons) are to be compared, this should be done for a specified value of their rigidity.

With respect to the chemical composition of cosmic rays, one characteristic feature is particularly important: heavier nuclei are present in cosmic rays in a comparatively greater proportion than in nature. Thus, the ratio of the flux of nuclei of charge Z in cosmic rays to their abundance in nature increases with Z. This relation is roughly proportional, so that in cosmic rays nuclei of an element with an atomic number Z are Z times more abundant than in nature /4/.

In several cases (for instance, for light nuclei of the L group) this rule is not obeyed, and it should therefore be considered as an indication of the general tendency, rather than any kind of strict law. Figure 4 shows the

dependence on Z of the ratio k between the percentage of various nuclei in cosmic rays (for a given rigidity) and the mean abundance of these nuclei in nature. The data on the mean abundances in nature were collected by Suess and Urey /5/. The data on the percent contents of various nuclei in cosmic rays were taken from /3/ and /6/, and also from the results of measurements made during flights of Soviet space rockets and satellites /1, 2, 7, 8/. The ratio k for protons was taken as unity. When data from

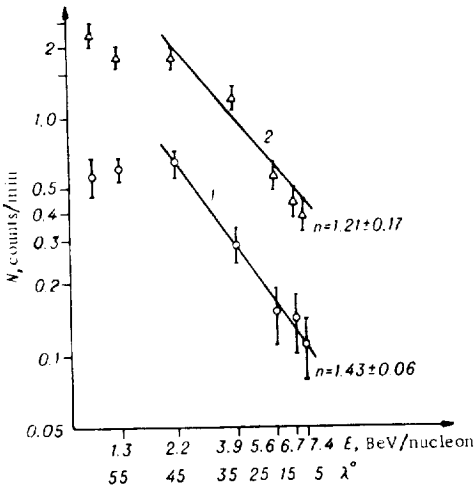

FIGURE 2. Integral energy spectra of nuclei with $Z \geqslant 2$, according to data from two Čerenkov counters aboard Sputnik VI.

1-data of first counter; 2-data of second counter. The difference in counting rate for the two counters was due to a difference in sensitivity (see /1/).

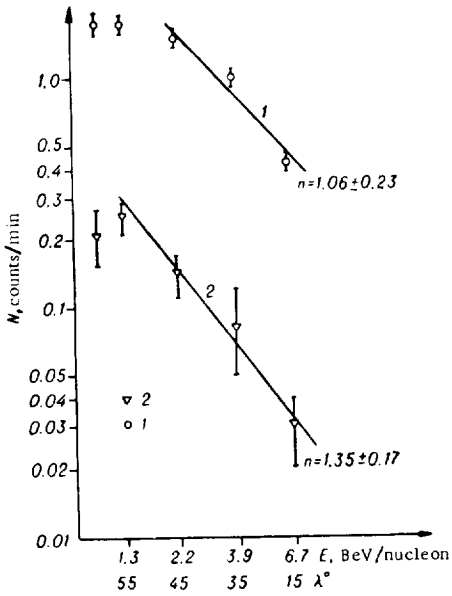

FIGURE 3. Integral energy spectra of nuclei with $Z \geqslant 5$(1) and $Z \geqslant 12$ to 14 (2), according to data from an integral Čerenkov counter aboard Sputnik VI.

space rockets and satellites were used, the value of k for α particles was normalized to 2. Although Figure 4 shows that the increase in k is roughly proportional to the increase in Z, it should be stipulated once again that this rule is quite arbitrary. For example, for nuclei with $Z \geqslant 15$ the experimental point obtained in /7/ agrees more or less with the rule, whereas the flux usually observed for these nuclei is about twice as great, so that the corresponding point lies considerably higher. Some uncertainty is also introduced due to insufficient knowledge of the abundances of the elements in nature. For instance, for the abundance ratio of helium and hydrogen, Cameron /9/ gave a value which was about twice the one used. Such a relation between the helium and hydrogen abundances agrees with their percent content in cosmic rays, and, if it is accepted, the value of k turns out to be the same for $Z = 1$ and $Z = 2$.

Since in the calculation of k the flux values for the nucleus groups must be used, there is some uncertainty in the value of Z corresponding to a given k. This uncertainty is negligible for nuclei in the M group (the value of k corresponding to $Z=7$). For the group with $Z \geqslant 12$ to 14, the value of k is calculated for $Z=13$; for nuclei with $Z \geqslant 15$, it is calculated for $Z=20$; and for nuclei with $Z > 30$ to 40, it is calculated for $Z=35$. The value of k obtained for nuclei with $Z > 30$ to 40, according to data obtained with Sputnik III /8/, represents only an upper limit for the k values of this nucleus group.

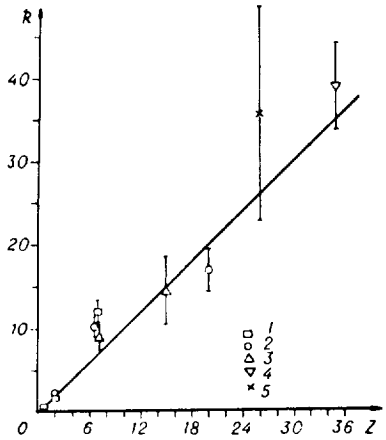

FIGURE 4. Ratio k between percent content of various nuclei in cosmic rays and their mean abundance in nature, as a function of Z:

1-data of /3/; 2-, 3-, 4-data of second lunar probe, Sputnik VI, and Sputnik III, respectively; 5-data of /6/.

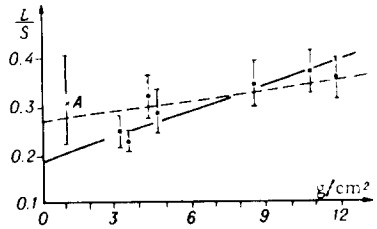

FIGURE 5. Flux ratio for nuclei of groups L and S, for various atmospheric depths, from data of /3/ (point A indicates the value of L/S according to data from Sputnik VI).

The overall regularity of the increase of k with Z apparently indicates the nature of the acceleration of heavy nuclei in the cosmic-ray sources. A possible mechanism for the predominant acceleration of the nuclei has been suggested by Korchak and Syrovatskii /10, 11/.

With regard to the origin of cosmic rays, it is essential to specify very accurately the cosmic-ray chemical compositions. It was especially important to ascertain the relative contents in cosmic rays of the nuclei of certain elements which are not very abundant in nature, for example, light nuclei of the L group. For a long time, the fluxes of these nuclei in cosmic rays were not known with any certainty, and conflicting data were obtained. Now, however, it has been established that considerable quantities of these nuclei are present in cosmic rays. Figure 5, which was taken from Waddington /3/, gives the flux ratio L/S for nuclei of groups L and S (the latter group includes the groups M and H). The abscissa indicates the depth of the atmospheric layers at which the various measurements were made. The dashed line shows an extrapolation to the limit of atmosphere of the measurements carried out by Waddington /12/ at a depth of 12 g/cm^2. As is evident from the figure, the points obtained by other experimenters

fit this line quite well, except for the data of O'Dell, Shapiro, and Stiller /13/, obtained in 1961 at a depth of about 3 g/cm^2. The solid line was drawn (method of least squares) through all the points used by Waddington except the point from the Sputnik-VI measurements.

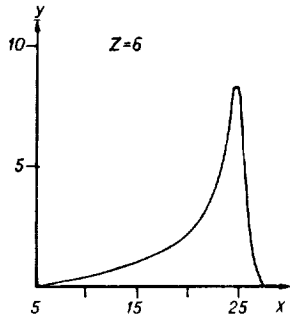

FIGURE 6. Amplitude distribution of pulses at photomultiplier output for carbon nuclei, taking into account the velocity spectrum of the nuclei.

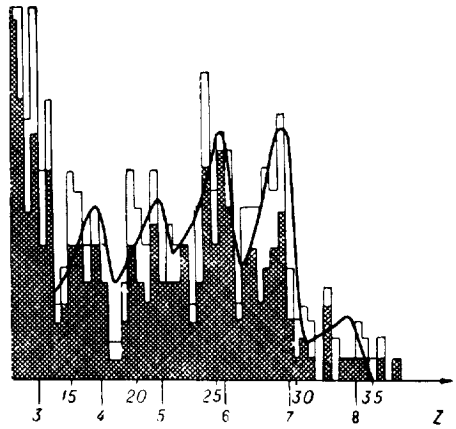

FIGURE 7. Charge distribution of nuclei, according to measurements carried out with Sputnik VI. The curve shows the distribution obtained, matched to the experimental data, taking into account the velocity spectrum of the nuclei.

During the flights of Sputnik V and Sputnik VI, the fluxes of various groups of nuclei, including light and intermediate nuclei, were measured. The data were obtained using Čerenkov counters of the so-called differential type. The amplitude of each counter pulse caused by the passage of a charged particle within a certain solid angle was measured, the solid angle being determined by a telescope of gas-discharge counters. The counters were calibrated at the earth's surface using singly charged particles, so that the amplitude of a pulse obtained during flight was an indication of the charge of each nucleus passing through the detector.

The determination of the fluxes of different nucleus groups proved to be difficult, mainly due to the fact that for the energies of the particles counted in this case the amplitude of a pulse in a Čerenkov counter depends not only on the nuclear charge but also on the velocity. Because of this velocity dependence, heavier nuclei with low velocities exceeding the threshold value ($v \approx 0.67\,c$) required to excite Čerenkov radiation may contribute to the flux recorded for light nuclei. It would be easy to get around this difficulty by using only the data of equatorial regions, for which the energies of recorded nuclei are quite high and the pulse amplitude is practically independent of velocity. However, the use of equatorial data only was not possible, due to the insufficiency of statistical information available for the region of the equator. Therefore, during the data processing the results obtained at all latitudes were added together, and the velocity dependence of the pulse amplitude had to be taken into account by means of a correction. When nuclei with fairly high energies are recorded, in which case the

velocity does not affect the pulse amplitude, nuclei with the same charge will have a Gaussian amplitude distribution at the equipment output, the halfwidth of the Gaussian depending on the efficiency of the photocathode and the multiplier. For low-velocity nuclei the shape of the distribution curve is different, the left "wing" of the curve becoming spread out as shown in Figure 6. The abscissa is a quantity X proportional to $\sqrt{A}$ (where A is the pulse amplitude), and thus proportional to the recorded charge Z; the ordinate is the number of pulses of amplitude A, calculated taking into account the efficiency of the photomultiplier photocathode and the dependence of A on the velocity of the nucleus.

The curve in Figure 6 was obtained theoretically, using the integral energy spectrum of particles with an index γ of 1.5 and for a 5% efficiency of the multiplier photocathode. This curve can be evaluated according to ground-level measurements of the amplitude distribution for singly charged particles. However, with regard to the energy spectrum, this calculated curve does not depend greatly on the index of the spectrum. The curve in Figure 6 is for carbon nuclei; similar curves were obtained for other nuclei by means of numerical integration using a computer. These curves, whose areas were initially normalized to unity, were next fitted to the experimentally obtained charge spectrum by multiplying the ordinates by appropriate coefficients (beginning with oxygen, heavier nuclei not being considered here). The curve thus obtained is shown in Figure 7. The coefficients used to fit the curves were an indication of the relative fluxes of the different elements. In the region corresponding to nitrogen and oxygen, saturation of the photomultiplier is apparently important, as a result of which the peak for nitrogen nuclei appears to be higher. The peak for lithium nuclei is "wiped out" by the α-particle peak. The situation would probably have been similar if, having constructed the amplitude-distribution curve for α particles, an attempt had been made to consider lithium nuclei separately. However, at present this is not done, and the relative flux of lithium nuclei is taken as 1/3 of the flux of boron nuclei, according to data in the references (for example, /3/ and /13/).

The shaded area in Figure 7 refers to "single-shot" recordings of nuclei. The unshaded part corresponds to cases when the passage of a nucleus through the detector was followed by the triggering of more than one counter in a lower tray of the counter telescope.

Without analyzing the chemical composition according to different elements, since this composition may be distorted by saturation for nuclear charges of 7 or 8, it is possible to estimate the flux ratio between nuclei of the L group and heavier nuclei [S group]. This ratio was found to be $31.0 \pm 9.6\%$, a value differing from the value of 50% predicted earlier /1/ because the velocity dependence of the amplitude distribution was taken into account. A ratio of $\frac{L}{S} = 0.31 \pm 0.10$ is consistent with the recent measurements of O'Dell, Shapiro, and Stiller /13/, who obtained $\frac{L}{S} = 0.18 \pm 0.04$ for extrapolation to the limit of atmosphere. This extrapolated value may vary somewhat depending on the fragmentation parameters used for the extrapolation. For example, for the same experimental data (that is, $\frac{L}{S} = 0.24$), Waddington obtained an extrapolated value of $\frac{L}{S} = 0.19 \pm 0.02$. Our ratio of $\frac{L}{S} = 0.31 \pm 0.10$ agrees somewhat better with Waddington's extrapolation

(which gives $\frac{L}{S}=0.27$, see Figure 5), and also with Webber's data /14/ obtained with Čerenkov counters at an atmospheric depth of 6 g/cm^2. Webber's measurements were carried out for the same threshold energy as our measurements ($E_{\text{kin thr}} \approx 0.5$ BeV/nucleon), and they gave a ratio of $\frac{L}{S}=0.31\pm0.09$ (for the 1958 flight). Our data were cited in Figure 2. This value was not corrected for the presence of an overlying aluminum layer (1 g/cm^2), or for fragmentation in the detector itself. It should be noted, however, that such corrections are small, since the aluminum layer was thin, while in addition the products of decay in this layer did not succeed in dispersing when they entered the detector, so that they produced pulses which did not correspond to any determined charge value, and they just increased the background radiation. Some of these events are excluded by the triggering of more than one counter in each bank of the telescope.

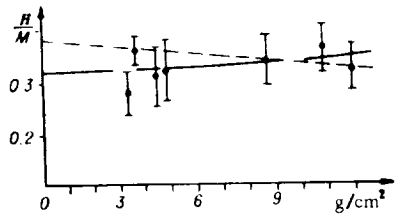

FIGURE 8. Flux ratio for nuclei of groups H and M at different atmospheric depths, according to data of /3/.

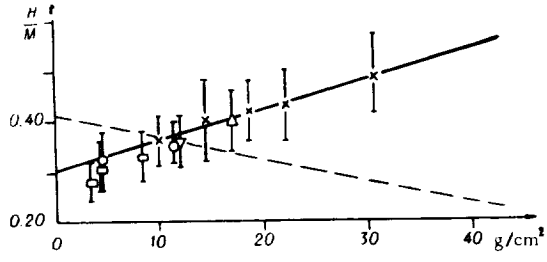

FIGURE 9. Dependence of H/M ratio on quantity of overlying matter, according to data of /6/. Dashed line shows Waddington's extrapolation /12/.

Experiments at high altitudes indicate definitely that nuclei of lithium, beryllium, and boron are present in the primary cosmic radiation; the number of these nuclei is from 20 to 30% of the heavier nuclei. Such a quantity corresponds to the penetration of cosmic rays in interstellar space through 5 to 10 g/cm^2 of matter /11, 15/, if we assume that in the primary cosmic radiation at the source there are practically no nuclei of these elements, just as is the case, on the average, in nature. However, some uncertainty enters into the estimate of the amount of matter penetrated by cosmic rays in space, since the values of the fragmentation parameters for heavy nuclei in the interstellar medium are not precisely known.

Different investigators have found similar values for the flux ratio of nuclei in groups H and M. O'Dell, Shapiro, and Stiller /13/ obtained $\frac{H}{M}=0.38\pm0.04$ (photoemulsion method), while Webber /14/ obtained $\frac{H}{M}=0.25\pm0.07$ using a Čerenkov counter (1958 flight at a depth of 6 g/cm^2; the nuclei had energies $E_{\text{kin}}>0.55$ BeV/nucleon). Figure 8 shows the H/M ratios measured at different atmospheric depths by different investigators. The dashed line gives the extrapolation to the limit of atmosphere for Waddington's data /12/, obtained at a depth of 12 g/cm^2. The solid line was drawn through all the points in the figure by means of the method of least squares. Waddington /3/ took $\frac{H}{M}=0.34\pm0.04$ as the best value; this ratio

agrees with the value $\frac{H}{M} = 0.30 \pm 0.02$ obtained by Daniel and Durgaprasad /6/. It should be noted that according to the data of /6/ the ratio *H/M* does not drop, but rather increases somewhat, with the depth of the residual layer of matter above the measuring equipment (Figure 9).

TABLE 1. Percent contents of nuclei of various elements in cosmic radiation (% of total flux of nuclei with $Z \geqslant 3$)

Element	Data of /3/ (photoemulsion method)*		Data of /14/ (Čerenkov counter, $E_{kin} \gtrsim 0.5$ BeV/nucleon)		Data of /13/ (photoemulsion method)		Data of measurements made with Sputnik VI
Li	3.9		–		5.3		4.00**
Be	1.7		6.7		2.3		8.0
B	11.6		10.1		7.4		12.0
C	26.0		28.6		30.1		25.0
N	12.4	56.8	13.3	47.8	9.7	54.9	52.5
O	17.9		17.9		19.4		
F	2.6		–		2.4		
$Z \geqslant 10$	23.9		16.6		23.4		

* Errors in values cited are ± 20–30%.

** A value equal to 1/3 of that for boron nuclei was taken.

As mentioned above, reliable data on the percent contents of the nuclei of different elements in cosmic rays are not yet available. Nevertheless, some data which have been obtained so far are listed in Table 1. The table shows that, although the flux data for the various elements disagree, still certain overall features are evident. For example, the number of carbon nuclei exceeds the number of oxygen nuclei (the fluxes of carbon and oxygen nuclei stand in a ratio of about 3 to 2 to one another), and the content of nitrogen nuclei is lower than the contents of carbon and oxygen.

The isotopic content of the nuclei of different elements in cosmic radiation is a very interesting subject. For example, in nature deuterium is about 0.01% as abundant as hydrogen. In cosmic rays, on the other hand, it could be expected that from 1 to 5% deuterium would be present, due to the interaction of cosmic rays with interstellar matter (according to calculations of Singer /16/ and Hayakawa /17/). Therefore, isotope studies can, in the same way as charge-spectrum studies, give important information on the conditions of generation and propagation of cosmic rays in the universe. At present the only data on the isotopic composition of the nuclear component of cosmic rays are those given in /18/ and /19/ for helium isotopes. According to /18/, $\frac{He^3}{He^3+He^4} = 0.41 \pm 0.09$, whereas more recent measurements by the same author /19/ give 0.31 ± 0.08.

However, the isotopic composition of the helium in cosmic rays cannot yet be considered as finally determined (for instance, according to the data of /20/, the He^3 content is considerably lower).

Some data will now be cited on the electron-positron component of cosmic rays. The flux of electrons and positrons in the galactic radiation is small. So far, a comparatively small number of measurements of the electron component have been made, and no information at all is available on electrons and positrons separately.

In 1948–1950 Ney and Oleksa /21/ measured the electron flux by means of a Wilson cloud chamber with lead plates, under an atmospheric layer of 13 to 18 g/cm^2. The electrons were recorded from showers produced in the plates. According to these data, the flux of electrons with energies $E \geqslant 1.1$ BeV (corrected for the formation of secondary electrons in the overlying atmosphere) was about 0.6% of the proton flux.

For a long time after these measurements, no new data appeared on the electrons in cosmic rays. Then, not so long ago (1961), Earl's measurements /22/ at depths from 4 to 6.5 g/cm^2 were published. The method of electron recording was the same as in /21/. Cascade showers produced by a single primary electron were studied. The number of secondary electrons produced in the matter above the measuring equipment obviously will increase with the drop in their energies down to the minimum energy, which is determined by the sensitivity of the equipment. This minimum energy was 0.25 BeV in Earl's measurements. However, the increase in the number of recorded electrons stopped at $E \approx 0.7$ BeV, in accordance with the geomagnetic threshold at the observation point, which indicates that the electrons were primary. The number of electrons recorded was $3 \pm 1\%$ of the number of protons.

However, it should be noted that the minimum recorded electron energy of $E \approx 0.7$ BeV is lower than the high-latitude cutoff energy. This makes it necessary to treat Earl's results with a certain amount of reserve. It may be that in part he recorded secondary electrons or electrons of solar origin.

Meyer and Vogt /23/ made electron recordings using scintillation counters, interbedded with lead plates, under an atmospheric layer of 3 to 5 g/cm^2; at the latitude of the measurements, the geomagnetic threshold energy was 0.1 BeV. Cases were chosen in which showers were produced in the equipment. The flux of electrons with $E > 1.3$ BeV was about 4% of the proton flux. Meyer and Vogt /24/ also used a Wilson cloud chamber with lead plates to record what was apparently a flux of solar electrons with energies from 0.1 to 1.3 BeV; this flux was about three times the flux of galactic electrons measured by these authors.

Further measurements are necessary before the problem of galactic electrons can really be solved. Separate measurements of the electron and positron fluxes must also be made. Finally, the electron flux in solar cosmic rays is also a subject of great interest (for a more detailed account, see /2/).

It should be noted, too, that recently the first measurements of the flux of cosmic γ rays were made /34/. Although these measurements were only preliminary, they nevertheless demonstrated the great potentialities inherent in γ-ray astronomy.

Let us now go on to consider the chemical composition of solar cosmic rays. At the cosmic-ray conference in Yerevan (1961), certain short-term variations of the nuclear component of cosmic rays were reported which could be correlated with solar chromospheric flares and bursts of solar radio emission /32/. These variations were characterized by a short-term rise in the nuclear intensity, the intensity for heavy nuclei increasing more than that for lighter nuclei. Such brief intensity variations are caused by the acceleration of nuclei during solar flares, when apparently there is a preferential acceleration of heavier nuclei. Figure 10 shows a typical short-term increase in the intensity of nuclei recorded on 12 September 1959,

during the flight of the second [Soviet] space probe /2, 25/. Since as yet there are not enough data available on the acceleration of nuclei at the sun, definite conclusions concerning their generation mechanism cannot be drawn. It appears, however, that at any rate solar cosmic rays are generated by two different mechanisms. One of these, the more common

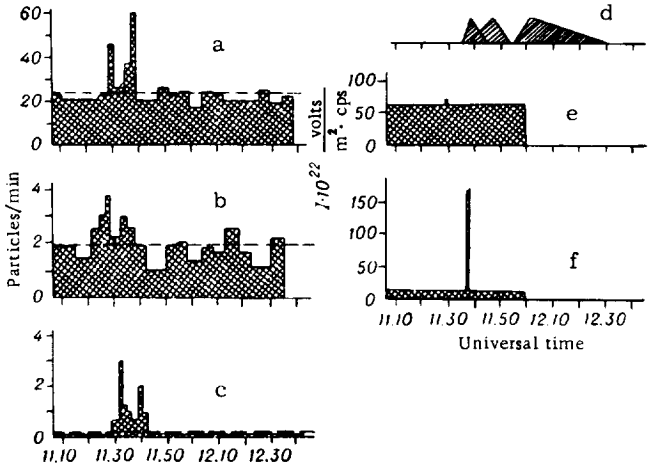

FIGURE 10. A short-term increase in the intensity of nuclei, recorded on 12 September 1959 during the flight of the second lunar probe.

a–, b–, c–counting rates for nuclei with $z \geq 2$, $z \geq 5$, and $z \geq 15$, respectively; dashed line shows average counting rate; d–schematic representation of chromospheric flares; e–, f–schematic representation of radio-emission bursts at 810 and 208 Mc, respectively.

one, leads to the acceleration of protons, and perhaps to an equally efficient acceleration of other nuclei as well (indicating that the percent of accelerated nuclei corresponds approximately to the relative number of the nuclei in the solar atmosphere). The second mechanism, on the other hand, leads to a preferential acceleration not of protons but of nuclei, mainly just heavier nuclei (the acceleration of α particles in this case may be related mainly to the greater abundance of He^4, which compensates for the low acceleration efficiency). This type of generation mechanism is discussed in /10/ and /11/. The introduction of two or even more mechanisms of particle acceleration at the sun, by the way, should not be surprising; for example, in a similar way, sporadic solar radio emission is explained in terms of several mechanisms of radio-wave generation. Let us note, too, that in some cases (after weak flares) the cosmic-ray pressure in the solar atmosphere may not be high enough to change the solar and near-solar magnetic fields significantly. As a result, the escape of particles beyond the corona will be difficult, so that only relatively fast nuclei with energies of the order of hundreds of MeV/nucleon will be observed in the solar system (and in particular near the earth). Consequently, short-term increases in the intensity of nuclei recorded by a Čerenkov counter may not be accompanied by a subsequent increase in the intensity of nuclei with lower energies.

It is possible that the greater increase in intensity observed for heavy nuclei is related to the conditions of escape from the solar atmosphere rather than to their higher velocities. Heavy nuclei which are not fully ionized can escape from the sun more easily than fully ionized light nuclei with the same energy per nucleon, and this is probably the reason for the observed greater intensity rise for heavier nuclei.*

Recently, some new studies have reported observations of nuclei of solar origin. Let us now consider in some detail the findings of Fichtel et al /26/. These authors recorded protons and nuclei by means of thick-layered photoemulsions, taken up by rocket following the onset of intense chromospheric flares. The measurements were made at a geomagnetic latitude of 60.7°N, so that it was possible to record low-energy particles. At altitudes up to 130 km, the emulsions were irradiated for a few minutes under an atmospheric layer less than 0.01 g/cm^2 in depth. A 0.19 g/cm^2 layer of material heavier than aluminum was placed above the emulsions.

TABLE 2

Beginning of flare (universal time)	3 September 1960 00 h 40 min	12 November 1960 13 h 22 min	15 November 1960 02 h 00 min
Time of flight (universal time)	3 September 1960 14 h 08 min	12 November 1960 18 h 40 min	16 November 1960 19 h 41 min
Flux of group-M nuclei with $E_{kin} > 42.7$ MeV/nucleon (particles/m^2·sec·sterad)	19±4	1530±210	258±40

In the three cases described by Fichtel /26, 27/, there was an intensity increase for protons, α particles, group-M nuclei, and heavier nuclei. Table 2 /27/ shows the fluxes of group-M nuclei with kinetic energies $E_{kin} > 42.7$ MeV/nucleon, obtained during three rocket flights following intense chromospheric flares. During control flights made during periods of quiet sun, on the other hand, only particles of galactic cosmic rays were recorded.

The results pertaining to the intensity rise for protons and nuclei during the Class-3 flare which began at 13 h 22 min on 12 November 1960 are described in /26/. This flare was accompanied by a strong increase in the cosmic-ray intensity, the neutron monitors having begun to indicate an intensity rise 18 minutes after the onset of the flare. A monitor at the Deep-River Station recorded an intensity increase which reached 200% of the normal cosmic-ray intensity and continued for many hours. It should be noted, though, that the flare occurred shortly after the two intense flares of 10 and 11 November 1960. Consequently, it may be that the particles generated during the flare on 12 November had been trapped magnetically by the corpuscular stream emitted during the flare on 11 November /26/.

During the flare which began on 12 November, two rockets carrying emulsions were sent up, one at 18 h 40 min on the 12th and one at 16 h 03 min on the 13th. On both flights high intensities for protons, α particles, M-group nuclei, and heavier nuclei were recorded.

* This was noted by Syrovatskii during discussion of the report at the Yakutsk conference.

The differential energy spectra and rigidity spectra were determined for protons and nuclei (Figures 11 and 12). The figures show that the rigidity spectra for protons and nuclei agree, within the limits of observational accuracy, whereas the energy spectra do not. The relative abundances of protons and nuclei in a specific energy range turned out to be close on the two flights (on the 12th and the 13th), and also on other flights (after other flares). The fluxes recorded on the 12 November flight for α particles, nuclei of group L, nuclei of group M, and nuclei with $Z \geqslant 10$ were 680 ± 10; < 0.1; 10; and 1.0 ± 0.3, respectively (the group-M flux was taken as 10). These ratios are close to those obtained from spectroscopic data (for the elements for which such data are available).

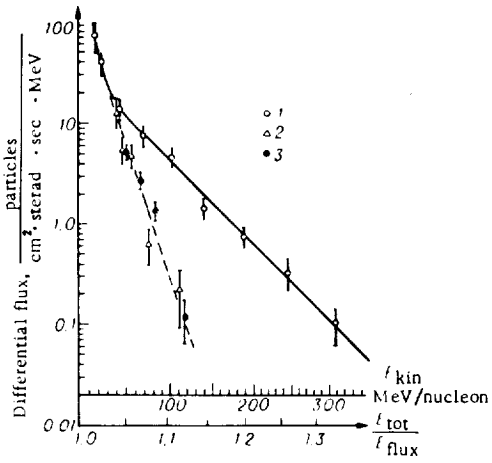

FIGURE 11. Differential energy spectra of solar protons and nuclei, according to data of /26/.

1-proton flux; 2-α-particle flux, multiplied by 10; 3-flux of nuclei of group μ, multiplied by 700.

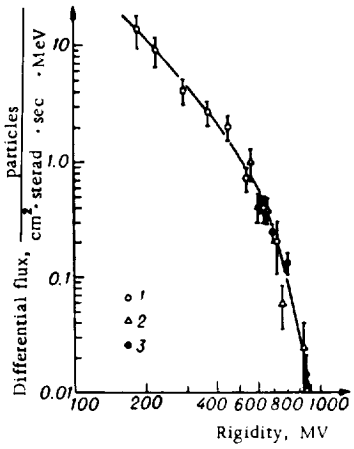

FIGURE 12. Differential rigidity spectra for protons and nuclei, according to data of /26/.

1-proton flux; 2-α-particle flux, multiplied by 5; 3-flux of nuclei of group μ, multiplied by 350.

The authors concluded that their ratios between the fluxes of the various multiply charged nuclei indicate the relative abundances of the corresponding elements at the sun. This interpretation is confirmed by the identity of the flux ratios for He, C, O, Ne, and heavier nuclei for three different chromospheric flares, two of which even occurred in different parts of the sun. On the flights of 12 and 13 November 1960, the same flux ratios were recorded. The authors' conclusion is also verified by the agreement of the flux ratios obtained from spectroscopic data. In particular, the flux ratio obtained for carbon and oxygen nuclei was 3/5, which is in good agreement with solar spectroscopic data (in galactic cosmic rays this ratio is about 3/2). Therefore, at least for the three large flares studied in /26/ and /27/, there was apparently no preferential acceleration of heavy nuclei, and the composition of the nuclear flux generated at the sun was an indication of the abundances of the elements in the outer layers of the sun. In Table 3 /27/, the fluxes of nuclei of various elements recorded in these cases are compared with the abundances of the elements on the sun and with the fluxes

of the nuclei in galactic cosmic rays. All the data are referred to carbon, for which the fluxes and the relative abundance are taken as 10.

TABLE 3

Element	P	Be, B	C	N	O
Number of nuclei generated at sun (in a specified rigidity range)	$2.6 \cdot 10^3 - 50 \cdot 10^3$	≤ 0.5	10	≤ 6	19
Relative abundance on sun	$2 \cdot 10^{-3}$	10^{-5}	10	2	18
Number of nuclei in galactic cosmic rays (in a specified rigidity range)	$2.8 \cdot 10^3$	5	10	≤ 5	6

Yagoda et al /28/ also used thick-layered photoemulsions, the emulsion stacks being irradiated during balloon ascents or mounted on artificial satellites. The mean intensities for nuclei with $Z \geqslant 6$, obtained from the data for emulsions on balloons and on the Discoverer XVIII satellite, turned out to be close. The mean intensities obtained from the processing of emulsions recovered from Discoverer XVII, on the other hand, were about 100 times higher, since during this flight an intense flare (Class 3^+) occurred.

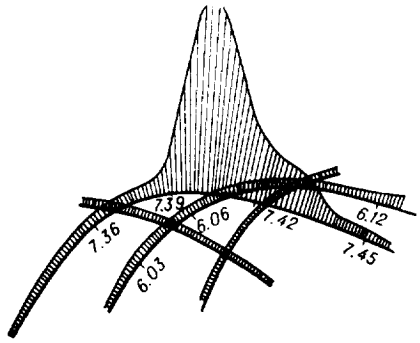

FIGURE 13. Variation of telescope counting rate along part of trajectory of Sputnik V.

In these measurements /27, 28/ a preferential increase in the intensities of heavier nuclei was not recorded. In connection with this, the recordings which were made during the flight of Sputnik V /29/ may be interpreted as indicating a short-term intensity rise for protons and for nuclei with $Z > 5$. Nuclei with $Z > 5$ and $Z \geqslant 15$ were recorded by an integral Čerenkov counter. Moreover, the counting rate of a telescope of gas-discharge counters was also measured. In the case mentioned, a sharp rise in the telescope counting rate was observed, accompanied by an intensity increase for the nuclei with $Z > 5$ recorded on the integral Čerenkov counter. At the same time, no noticeable intensity rise for nuclei with $Z \geqslant 15$ was observed. Figure 13 shows the variation of the telescope counting rate along

the trajectory of the satellite. It was found that a sharp rise occurred at 07 h 40 min (universal time) on 20 August 1960. On the adjacent trajectory turns over the same geographical region, the intensity was considerably less, confirming the short-term nature of the intensity rise.

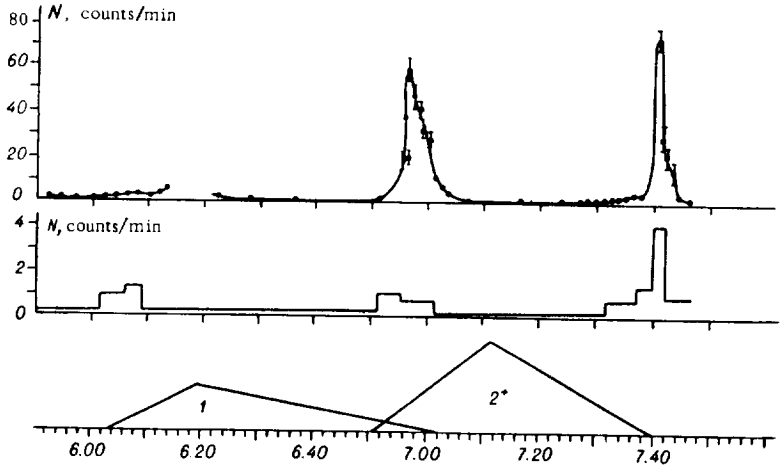

FIGURE 14. Counting rates of telescope and of integral Čerenkov counter recording nuclei with $Z \geqslant 5$, as functions of time.

Figure 14 shows the counting rates of the telescope and of the integral Čerenkov counter recording nuclei with $Z > 5$, as functions of time. A Class-2^+ flare preceding the intensity rise is shown schematically. It can also be seen from the figure that at the previous passage of the satellite over the north-polar region (where an intensity burst was recorded) the counting rates of the telescope and the Čerenkov counter were appreciably lower. The large intensity peak recorded by the telescope at about 6 h 46 min corresponds to flight of the satellite through the region of the southern radiation anomaly /2, 30, 31/.

It would seem that the generation mechanism in this case, just as in the cases described in references /27, 28, 29/, differs from the generation mechanism for nuclei with $E_{kin} \gtrsim 10^9$ eV/nucleon, for which there is a preferential acceleration of heavy nuclei /2, 25, 32, 33/.

At present, thanks to a number of experimental studies, it is possible to discuss the acceleration at the sun not only of protons but also of multiply charged nuclei. However, the mechanism by which particles are accelerated at the sun is still not clear. Also, as noted in this report, it is quite possible that different acceleration mechanisms exist, one of which accelerates all nuclei with the same efficiency, and the other of which causes a preferential acceleration of heavier nuclei.

P. N. Lebedev Institute of Physics of
the USSR Academy of Sciences

REFERENCES

1. KURNOSOVA, L.V., L.A.RAZORENOV, and M.I.FRADKIN. — Sbornik: "Iskusstvennye sputniki Zemli," No.12, p.16, Moskva, Izd. AN SSSR. 1962.

2. GINZBURG, V.L., L.V.KURNOSOVA, L.A.RAZORENOV, and M.I.FRADKIN. — Geomagnetizm i aeronomiya, **2**, 193. 1962.

3. WADDINGTON, C.J. Contribution to 1961 Kyoto Conference, NASA, Goddard Space Flight Center.

4. NEY, E.P. — Astrophys. J., Suppl. Series, **4**, 371. 1960.

5. SUESS, H. and H.C.UREY. — UFN, **62**, 101. 1957.

6. DANIEL, R.R. and N.DURGAPRASAD. — Nuovo Cimento Suppl., **23**, 82. 1962.

7. KURNOSOVA, L.V., V.I.LOGACHEV, L.A.RAZORENOV, and M.I.FRADKIN. — Sbornik: "Iskusstvennye sputniki Zemli," No.5, p.30, Moskva, Izd. AN SSSR. 1960.

8. KURNOSOVA, L.V., L.A.RAZORENOV, and M.I.FRADKIN. — Sbornik: "Iskusstvennye sputniki Zemli," No.2, p.70, Moskva, Izd. AN SSSR. 1958.

9. CAMERON, A.G. — Astrophys. J., Suppl. Series 3, **129**, 676. 1959.

10. KORCHAK, A.A. and S.I.SYROVATSKII. — DAN SSSR, **122**, 792. 1958.

11. GINZBURG, V.L. and S.I.SYROVATSKII. — UFN, **71**, 411. 1960.

12. WADDINGTON, C.J. — Phil.Mag., **2**, 1059, 1957; **5**, 1105. 1960.

13. O'DELL, F.W., M.M.SHAPIRO, and B. STILLER. — J. Phys. Soc. Japan, **17**, Suppl. A-111, 23. 1962.

14. McDONALD, F.B. and W.R.WEBBER. Contribution to 1960 Kyoto Conference, NASA, Goddard Space Flight Center.

15. GINZBURG, V.L. — UFN, **74**, 521. 1961.

16. SINGER, S.F. — Nuovo Cimento Suppl., **8**, 549. 1958.

17. HAYAKAWA, S., K.ITO, and Y.TERASHIMA. — Progr. Theor. Phys., Suppl. No.6, 1. 1958.

18. APPA RAO, M.V.K. — Phys. Rev., **123**, 295. 1961.

19. APPA RAO, M.V.K. — J. Geoph. Res., **67**, 1289. 1962.

20. AIZU, H., Y.FUJIMOTO, S.HASEGAWA, M.KOSHIBA, I.MITO, J.NISHIMURA, K.YOKOI, and M.SCHEIN. — Phys. Rev., **121**, 1206. 1961.

21. CRITCHFIELD, C.L., E.P.NEY, and S.OLEKSA. — Phys. Rev., **85**, 461. 1952.

22. EARL, J.A. — Phys. Rev. Letters, **6**, 125. 1961.

23. MEYER, P. and R.VOGT. — Phys. Rev. Letters, **6**, 193. 1961.

24. MEYER, P. and R. VOGT. — Phys. Rev. Letters, **6**, 3950. 1962.

25. KURNOSOVA, L.V., L.A.RAZORENOV, and M.I.FRADKIN. — Sbornik: "Iskusstvennye sputniki Zemli," No.6, p.131, Moskva, Izd. AN SSSR. 1961.

26. BISWAS, S., C.E.FICHTEL, and D.E. GUSS. Contribution to 1961 Kyoto Conference, NASA, Goddard Space Flight Center (preprint).

27. FICHTEL, C.E. and D.E.GUSS. Contribution to 1961 Kyoto Conference, NASA, Goddard Space Flight Center.

28. YAGODA, H., R.FILZ, and K.FUKUI. — Phys. Rev. Letters, **6**, 629. 1961.

29. KURNOSOVA, L.V., L.A.RAZORENOV, and M.I.FRADKIN. — Sbornik: "Iskusstvennye sputniki Zemli," No.15, Moskva, Izd. AN SSSR. (in press).

30. KURNOSOVA, L.V., T.N.KOLOBYANINA, V.I.LOGACHEV, L.A.RAZORENOV, I.A.SIROTKIN, and M.I.FRADKIN. — Sbornik: "Iskusstvennye sputniki Zemli," No.8, p.87, Moskva, Izd. AN SSSR. 1961.

31. GINZBURG, V. L., L. V. KURNOSOVA, V. I. LOGACHEV, L. A. RAZORENOV, I. A. SIROTKIN, and M. I. FRADKIN. — Sbornik: "Iskusstvennye sputniki Zemli," No. 10, p. 22, Moskva, Izd. AN SSSR. 1961.

32. GINZBURG, V. L., L. V. KURNOSOVA, V. I. LOGACHEV, L. A. RAZORENOV, and M. I. FRADKIN. — Izv. AN SSSR, seriya fizicheskaya, **26**, 782. 1961.

33. KURNOSOVA, L. V., L. A. RAZORENOV, and M. I. FRADKIN. — Sbornik: "Iskusstvennye sputniki Zemli," No. 12, p. 31, Moskva, Izd. AN SSSR. 1962.

34. KRAUSHAAR, W. L. and G. W. CLARK. — Phys. Rev. Letters, **8**, 106. 1962.

N67 38203

Bruno Pontecorvo

THE NEUTRINO AND ITS IMPORTANCE IN ASTROPHYSICS

I wish to demonstrate in this report that neutrinos play an essential role in macroscopic phenomena. The reader should be warned at the outset, however, that in neutrino physics there are still several questions of qualitative nature to which simple answers of "yes" or "no" cannot be given. I intend to discuss how such problems have arisen and how physicists are going to solve them experimentally. First, though, let us review briefly the principal known properties of the neutrino.

1. THE KNOWN PROPERTIES OF THE NEUTRINO

During various processes of elementary-particle decay, it often turns out that the total energy and momentum of the particles in the initial state do not equal the total energy and momentum in the final state. In such cases, as we now know, the apparent violation of the conservation laws is due to neutrino emission.

Most of the properties of the neutrino became known immediately after Pauli, about 30 years ago, "invented" the neutrino in order to explain the apparent violation of the conservation laws. At that time, only the β decays of certain radioactive elements had been studied, although it was known that the spectrum of electrons is continuous. This "invention" of the neutrino to account for the apparent energy disappearance during β decay required considerable imagination. We now know that the continuity of the β-decay spectrum is related to the fact that the following three particles are present in the final state: an electron (e), a neutrino (ν), and the final nucleus. After the discovery of several new elementary particles, two-particle decays were noted in which the "disappearing" energy is always the same (for example, during $\pi-\mu$ decay, 28 MeV always disappears). During the muon capture $\mu^- + He^3 \rightarrow H^3 + \nu$, which was discovered at OIYaI in 1960, 100 MeV are lost. Figure 1 shows an example of this reaction in a diffusion chamber filled with He^3: the tritium produced always has a definite mean free path. If two-particle processes in which the neutrino participates had only been known earlier, Pauli's genius might not have been necessary to "invent" this particle.

The main decay processes involving the neutrino are: $n \rightarrow p + e^- + \tilde{\nu}$ (β decay); $\mu + p \rightarrow n + \nu$ (μ capture); $\mu \rightarrow e + \nu + \tilde{\nu}$ (μ decay); $\pi \rightarrow \mu + \nu$ ($\pi-\mu$ decay); $\pi \rightarrow \pi^0 + e + \nu$; $K \rightarrow \mu + \nu$, $K \rightarrow \mu + \nu + \pi$, $K \rightarrow e + \nu + \pi$, $\Lambda^0 \rightarrow p + e^- + \tilde{\nu}$.

The basic properties of the neutrino are given more or less by definition: zero charge; a mass much less than the electronic mass; a spin of one half; and colossal penetrating power. Let us try to see what such a particle will be like. Neutrino collisions due to the interactions causing β decay of nuclei must take place in matter. In other words, processes such as

$$\tilde{\nu} + p \rightarrow e^{+} + n, \tag{1}$$

must occur, this being the reverse of the ordinary β decay of a neutron:

$$n \rightarrow p + e^{-} + \tilde{\nu}.$$

The maximum cross section for process (1) is found from dimensional considerations to be

$$\sigma \leqslant \frac{1}{\tau} \frac{\lambda}{c} \lambda^{2}.$$

Here, τ is the time characteristic of β decay (some tens of seconds for electron energies of ~ 1 MeV), and λ is the neutrino wavelength (the highest wavelength involved in the given process). For a neutrino with an energy of ~ 1 MeV, it has been calculated that $\sigma \leqslant 10^{-43}\,\mathrm{cm}^2$, which means that the neutrino mean free path through dense matter is around 10^{16} km!

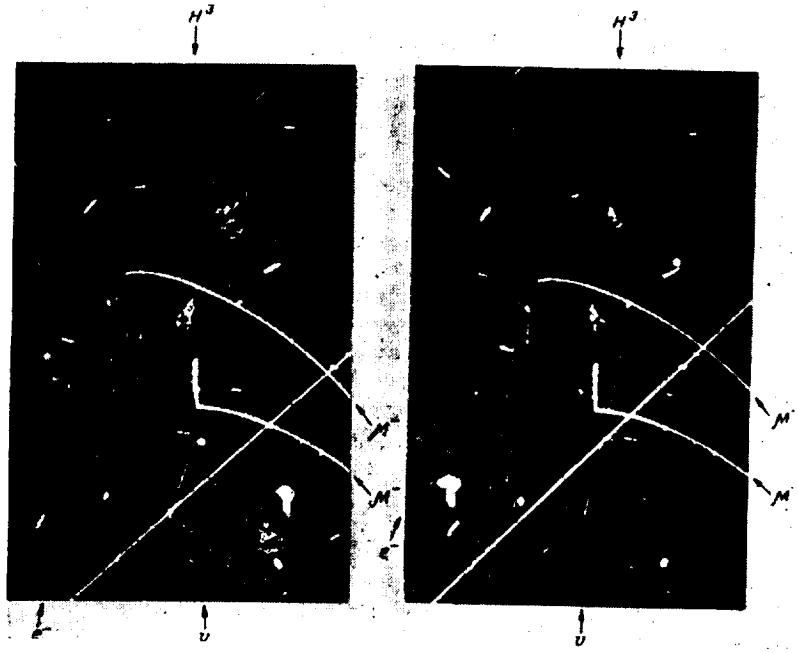

FIGURE 1. Typical photograph of $\mu^{-} + He^{3} \rightarrow H_{3} + \nu$ reaction.

Processes in which neutrinos participate are called slow processes, since they have low probability; they are due to so-called weak interactions. Although all other particles undergo weak interactions as well (such interactions being the most common type of all), neutrinos can be considered the main participants in these interactions. This is because neutrinos take part only in weak interactions, while all other particles enter into electromagnetic or strong interactions, or both of these, in addition to weak interactions. Since the intensities of strong, electromagnetic, and weak interactions stand roughly in a ratio of 1, 10^{-2}, 10^{-12} to one another (the intensity being proportional to the square of the coupling constant), it is clear why the penetrating power of the neutrino is unique among elementary particles.

Recently, "free" neutrinos, that is, neutrinos far away from their source, were observed by Reines and Cowan. The interactions between these particles and matter correspond roughly to the mean free paths predicted by the dimensional considerations referred to above. Experiments with free neutrinos promise to play an important part in the solution of the problems which will be discussed below. Since so far only a few experiments have been carried out using free neutrinos, it will be advisable here to discuss some of these briefly.

Beams of antineutrinos ($\tilde{\nu}$) with energies of a few MeV were obtained from a reactor. An antineutrino flux of about $10^{13}\,cm^{-2}\,sec^{-1}$ can be obtained from a very powerful reactor (with a power, say, of several hundred thousand kw), this being the flux beyond the reactor shield under conditions ensuring an antineutrino beam which is quite free of neutrons and γ rays.

Reines and Cowan used a liquid scintillation counter $\sim 1\,m^3$ in volume as an antineutrino detector. While recording reaction (1), the energy of the positron was measured, the two quanta from the positron annihilation were isolated, and, after moderation of the neutron, the γ rays characteristic of its nuclear capture were recorded. Thus, the striking succession of events characteristic of reaction (1) were all used to reduce the background. Several events were recorded per hour. This experiment was significant in that for the first time neutrino effects which were independent of the neutrino-creation processes were observed, which divested the neutrino of its somewhat mystical quality. These measurements were accurate enough to verify that the cross section for reaction (1), in agreement with the theory of the longitudinal neutrino (see below), is twice the cross section to be expected if parity is conserved. The nonconservation of parity will be discussed later in this report.

Now I would like to say a few words about the nonidentity of the neutrino and antineutrino. That these two are different particles was demonstrated recently by means of a quite difficult experiment. It will be worthwhile to describe this experiment briefly at this point, first because it shows the nonidentity of ν and $\tilde{\nu}$, and second because of its usefulness in determining the flux of cosmic neutrinos, especially those from the sun (incidentally, neutrinos from the sun have not yet been recorded).

The antineutrino was defined as a particle emitted during the β^- decay of a neutron, and the neutrino as a particle emitted during the β^+ decay of a proton. Such a definition does not specify whether the two particles are identical or not. It is known that reaction (1) has the expected cross section. Now, the reaction

$$\nu + n \rightarrow p + e^-$$

is caused by the same interaction as (1), so that it can be used to detect neutrinos. However, since a target of free neutrons does not exist, complex nuclei can be used, for example, deuterium or heavier nuclei. The reaction

$$\nu + Cl^{37} \rightarrow A^{37} + e^- \qquad (2)$$

is very convenient for technical reasons (CCl_4 is cheap, for one thing, and also trace amounts of radioactive A^{37} can be separated from large amounts of CCl_4). On the other hand, it is impossible to tell a priori if the reaction

$$\tilde{\nu} + Cl^{37} \rightarrow A^{37} + e^- \qquad (3)$$

is observable or not. This will depend on whether ν and $\tilde{\nu}$ are identical. Since experiment has shown that the cross section for reaction (3) is 5% less than that predicted for reaction (2), it is safe to assume that $\nu \neq \tilde{\nu}$. But in what way do ν and $\tilde{\nu}$ differ? It is now known that neutrinos are longitudinally polarized, the neutrino being left-handed and the antineutrino being right-handed. Consequently, it would appear that ν differs from $\tilde{\nu}$ in the sense of its "helicity." However, it is still not certain that the difference in helicity sense is the only feature which differentiates the neutrino from the

TABLE 1. Some properties of the neutrino

	According to theory of longitudinal neutrino	Experiment
Electric charge	0	0
Mass	0	<250 eV
Spin	$1/2\ \hbar$	$1/2\ \hbar$
"Neutrality"	$\nu \neq \tilde{\nu}$	$\nu \neq \tilde{\nu}$
Helicity	Fully longitudinally polarized	Degree of polarization $>97\%$ ν – left-handed, $\tilde{\nu}$ – right-handed
Magnetic moment	0	$<10^{-9}\ \mu_B$*

* μ_B = Bohr magneton.

antineutrino. It should be noted that the behavior of the neutrino described by the theory of the longitudinal neutrino, according to which it is fully polarized in the direction of the momentum, serves as a sort of prototype for the behavior of all other particles (with respect, of course, only to their weak interactions). Table 1 lists some properties of the neutrino.

The longitudinally polarized neutrino is a clear case of nonconservation of parity and noninvariance of charge conjugation (transformation of a particle into its antiparticle). I will say a few words about this subject here just so that astrophysicists will get the impression (be it correct or not, I don't know) that the nonconservation of parity may well have macroscopic consequences. This is a subject which should be considered further.

The law of invariance under a spatial inversion P (all coordinates are reversed in sign) may be formulated as follows: every mirror image of a physical process is itself an actually existing process. Consequently, every correlation of the spin-momentum σp is incompatible with parity conservation, since for the mirror image σ does not change sign but p does. In particular, the longitudinal polarization of elementary particles, such as

the longitudinal polarization of neutrinos and electrons in β decay, is incompatible with parity conservation.

Similarly, the conception of a left-handed neutrino and a right-handed antineutrino is incompatible with invariance under the charge-conjugation operation C. However, if invariance exists under the "combined inversion" operation PC of Landau (an operation in which each particle is transformed into its antiparticle with simultaneous sign reversal of all the coordinates), then the longitudinal neutrino is a completely law-abiding particle. Let us now consider what macroscopic effects may result from the longitudinal polarization of the neutrino, on the basis of a simple example.

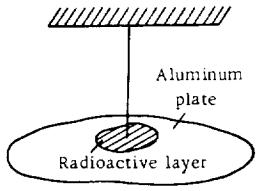

FIGURE 2. An ideal experiment for detecting the macroscopic consequences of parity nonconservation.

A β-active thin plate glued onto an aluminum plate is suspended freely on a thin wire (Figure 2). Electrons escape only upward, since in the downward direction they are absorbed by the aluminum. The electrons are longitudinally polarized, so that the system will rotate. This experiment is very difficult to carry out in practice; however, in nature and on a universal scale, phenomena which seem insignificant under laboratory conditions may be very important. The most striking example of this is gravitation. I am not completely convinced that there are macroscopic effects of parity nonconservation, but I do think that this question should be gone into further.

2. PHYSICS OF HIGH-ENERGY NEUTRINOS

Now I wish to discuss some unsolved problems in neutrino physics which are of great importance in elementary-particle theory. In recent years a new branch of the physics of elementary particles, the physics of high-energy neutrinos, has come into being. An accurate definition of this field would include all neutrino processes except β decay. However, by convention, the physics of high-energy neutrinos now includes mainly interactions between high-energy neutrinos and other particles. Various experiments have been suggested and several theoretical predictions made in this new branch of physics. It is quite likely that the experimental results forthcoming in this branch will be decisive factors in the establishment of a future theory of elementary particles.

I will now list some of these problems, laying particular stress on aspects related to experiments with free neutrinos.

3. IS A FOUR-FERMION INTERACTION PRIMARY?

It is a well-known fact that all weak processes can be explained, at least phenomenologically, in terms of an interaction between four fermions. However, the question immediately arises as to whether a four-fermion interaction is primary. In his first studies of nuclear forces, Yukawa

attempted to explain β decay as the virtual emission of a meson by a nucleon, followed by a decay of this meson.

We denote by B the intermediate meson, which is considered to be the carrier of the weak interaction. (Of course, this B meson must have a spin of unity.) We define g_B as the constant for coupling of a B meson with a nucleon, or with fermions in general. Here, the four-fermion weak interaction is not primary, and it is characterized by a phenomenological Fermi constant

$$G=\frac{10^{-5}}{M^2}(\hbar=c=1),$$

where M is the mass of the nucleon. This describes a second-order interaction with respect to the constant of the B-meson primary interaction, which has an "intermediate" intensity. Since g_B, like e and g_π, is a dimensionless constant, dimensional considerations indicate that $G\sim\frac{g_B^2}{M_B^2}$, where M_B is the mass of the intermediate boson. Therefore, if $M_B\sim M$, we have $g_B^2\sim 10^{-5}$, a value which must be compared with $e^2=\frac{1}{137}$ and $g_\pi^2\sim 10$. This B particle will decay with a characteristic time

$$\frac{1}{\tau}\sim g_B^2 M_B\sim 10^{18}\ \text{sec}^{-1}$$

along the decay channels

$$\begin{aligned} B&\to\pi+\pi;\\ &\to K+\pi;\\ &\to e+\nu;\\ &\to\mu+\nu,\ \text{etc.}\end{aligned}$$

When the energy of the weak interactions is insufficient for the actual creation of B, the nonlocalization effects related to the existence of the B meson are small and difficult to detect. However, if B can actually be produced, the effects will be perceptible. This is related to the fact that once B has been produced it must decay, in particular along one of the lepton decay channels. It follows from this that if $M_B\sim M$, leptons should be ejected from the "stars" during nuclear interactions at high energies. Their number will be $\sim 10^{-5}$ per star, a relatively large amount of leptons. The difficulty in observing the leptons from the "stars" is not because of the small number of events but rather is related to the evaluation of the large number of events involved. In any case, it would be extremely interesting to establish the emission of leptons (or their absence) in "stars."

Another very interesting possibility for detecting B mesons is the bombardment of nuclei of A with high-energy neutrinos:

$$\left.\begin{aligned} \nu+A&\to B+\left\{\begin{matrix}\mu\\ e\end{matrix}\right\}+A;\\ &\left|\begin{aligned}&\to\mu+\nu;\\ &\to e+\nu.\end{aligned}\right.\end{aligned}\right\} \qquad (4)$$

For this process dimensional considerations give a cross section

$$\sigma\sim Z^2e^4\frac{g_B^2}{M_B^2}$$

(see Figure 3).

For neutrinos with energies of several BeV and $M_B=M$, we have $\sigma\sim$ $\sim 10^{-37}$ cm^2/nucleon (for Fe). This is larger than the cross section obtained

for a local weak interaction, taking into account, of course, the formation of the nucleon. The section for reaction (4) increases rapidly with the neutrino energy and decreases with an increase in M_B. In this respect, it should be noted that:

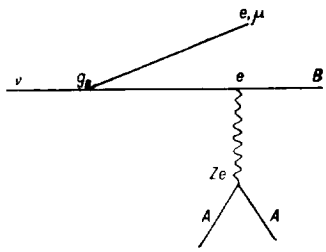

FIGURE 3. Process (4).

1) the mass of the B meson must obey the relation $M_B \geqslant M_K$, so that the process $K \rightarrow B + \pi$ does not occur;

2) in reaction (4) the "unnatural" pair μe may be observed. The appearance of such an "unnatural" pair is very typical of reactions where B is produced by means of high-energy neutrinos.

Energetic neutrinos are obtained from the decay of π mesons in flight. Since the neutrinos from pion decay have energies from zero to a maximum of $0.42\,E_\pi$, the energy of the forming neutrinos will be quite low, and synchrophasotrons of very high energy will be required in the search for the B mesons.

Neutrino-beam intensities of 10^3 to 10^4 per cm^2 per pulse can be obtained from 30-BeV accelerators like the ones at CERN or Brookhaven, at distances of ~ 100 m from an internal target; the neutrino energies in this case will be more than 1 BeV. A comparison between experiments with high-energy neutrinos from accelerators and experiments with neutrinos from reactors makes it clear that the absolute number of events in the second case is several orders of magnitude higher than in the first case. However, the background conditions are much more favorable in the experiments with high-energy neutrinos, especially since the neutrinos from the accelerator arrive in pulses. The present state of research experiments with high-energy neutrinos will be discussed below.

4. ARE ν_e AND ν_μ IDENTICAL PARTICLES?

It is completely unknown whether the neutrino emitted during β decay and the neutrino emitted during $\pi - \mu$ decay are identical. The electron neutrino ν_e and the muon neutrino ν_μ are defined as follows:

$$e^- + p \rightarrow n + \nu_e;$$
$$\mu^- + p \rightarrow n + \nu_\mu,$$

without going into the question of their identity, since this can only be decided experimentally. The idea that ν_e and ν_μ may not be identical arose because certain decay processes, such as $\mu \rightarrow e + \gamma$ and $\mu \rightarrow e + e + e$, are not observed (at least they have not been detected so far). This implies that $\mu \rightarrow e$ transitions may be forbidden because certain quantum numbers (or "charges") exist whose conservation is required by the laws of nature. If this is so, then ν_μ has a muon "charge" while ν_e does not.

The idea of an experiment to decide the identity of ν_e and ν_μ is reminiscent of the experiment using Cl^{37} suggested to decide whether the neutrino and antineutrino are identical. The cross section of the reaction

$$\tilde{\nu}_\mu + p \rightarrow n + e^+$$

will be zero if $\nu_e \neq \nu_\mu$ and it will be calculable if $\nu_e \equiv \nu_\mu$. For a neutrino with

an energy of 2 BeV, the cross section will be $(0.4 \text{ to } 0.8) \cdot 10^{-38}$ cm^2, which corresponds approximately to the section of the reaction

$$\tilde{\nu}_\mu + p \to n + \mu^+.$$

Experiments are now being carried out at the Brookhaven Laboratory in an attempt to solve this problem, and a definite answer should be obtained in the near future (see proofreading note at end of report).

A large spark chamber with aluminum plates about 2.5 cm thick is used to detect charged leptons in neutrino-caused reactions. The total weight of the aluminum used is around 10 tons. Several events per day per ton of matter can be expected. In order to reduce the background interference, which may be caused by cosmic radiation, the length of the pulses from the synchrophasotron are increased to 35 microseconds. In addition, the beam has a fine structure: once every 200 millimicroseconds a 10-millimicrosecond "break" is inserted. Thus, the difference in the travel times of the neutron and neutrino under these conditions makes possible considerable reduction of the neutron background.

5. DOES AN ANOMALOUS $\nu_\mu - N$ INTERACTION EXIST?

The theoretical aspect of this question was discussed by Kobzarev and Okun'. Let us assume that two types of neutrino exist. The various experiments performed, such as the experiment determining $g-2$ for a muon or the experiment checking for large-angle muon scattering at nuclei, do not rule out a relatively strong anomalous (that is, nonelectromagnetic) muon interaction.

If the anomalous interaction is represented in terms of some four-fermion interaction with a constant F, then the maximum value F_{max} compatible with the experiment determining $g-2$ will be $F_{max} < \frac{10^{-1}}{M^2}$. Obviously, F_{max} will be four orders of magnitude greater than G, the weak-interaction constant.

If both muon neutrinos and nucleons experience anomalous interaction, Okun' and Kobzarev recommend that neutrino scattering at the nucleon ($\nu_\mu - N$ scattering) be sought. The maximum possible cross section for energies of 2 BeV is 10^{-31} cm^2. Naturally, the experimental information available leaves a wide scope for the possibility of an anomalous interaction.

In experiments made with the synchrophasotron at OIYaI, the anomalous scattering of muon neutrinos by protons was checked for. Since the maximum possible cross section for this process is several orders of magnitude higher than the section expected for the weak interaction, it was possible to use a high-energy-neutrino beam of relatively low intensity, and to make use of a neutrino "detector" with a relatively small mass. The experiments showed that the section for $\nu_\mu - N$ scattering is less than 10^{-32} cm^2. Studies of the cosmic-ray intensity deep in the earth give even more accurate values, namely $\sigma_{\nu_\mu N} < 10^{-34}$ cm^2. This reduces considerably the probability that an anomalous interaction exists.

From a purely phenomenological point of view, experiments other than those suggested by Okun' and Kobzarev would also be of interest.

Actually, no data are available on $\nu - N$ scattering. Finally, since this process is in no way related to the known weak interaction, independent studies will be required.

6. DOES A $\nu - e$ INTERACTION EXIST?

Theory answers this question in the affirmative, but experimental studies are obviously necessary. Of course, here $\nu - e$ scattering which is first-order with respect to the weak-interaction constant is referred to. The experiments can in principle be carried out with low-energy neutrinos (for example, reactor neutrinos of about 1 MeV), and such an experiment is now being set up by Reines. On the other hand, it should also be possible to use high-energy neutrinos.

The main problem in setting up experiments with low-energy neutrinos is the radiation background. Reines intends to use several hundred NaI "anticoincidence" scintillation counters with a total weight of about two tons. The cross section for the process $\nu + e \rightarrow \nu + e$ has been calculated as $8 \cdot 10^{-42} E\,\mathrm{cm}^2$, where E is the neutrino energy in BeV.

Instead of using a reactor, monoenergetic neutrinos from reactions caused by stopped mesons, such as

$$\pi^+ \rightarrow \mu^+ + \nu;$$
$$\mu^- + A \rightarrow A' + \nu,$$

can be used. In the first reaction the neutrino has an energy of 28 MeV, and in the second about 100 MeV. The accelerator in this case can be a cyclotron with a spatial variation of the magnetic field, since this provides a current of accelerated protons which is close to a milliampere. The use of monoenergetic neutrinos makes it possible to utilize the kinematic properties of the reactions in question to reduce the background.*

7. DO NEUTRAL CURRENTS EXIST IN WEAK INTERACTIONS?

The most popular theory describing weak interactions, that proposed by Feynman and Gell-Mann, assumes that only "charged" currents exist: the Lagrangian is such that an interaction of a charged pair of fermions with one another or with some other charged pair is necessary in order for a four-fermion weak interaction to take place. Now, it cannot be assumed a priori that "neutral" currents such as (ee), $(\mu\mu)$, $(\nu\nu)$, (pp), (nn), $(\Lambda\Lambda)$, (μe), and (Λn) do not exist. To be sure, a (μe) current cannot exist, since this would imply a relatively high probability for the process $\mu \rightarrow e + \nu$, to which experimental data assign a low probability. Therefore, Feynman and Gell-Mann assumed that in general there are no neutral currents. However, the absence of (μe) currents does not mean that all the possible neutral currents are absent, and it has not yet been decided whether the symmetric neutral

* After it was found that two kinds of neutrinos exist, the above type of experiment became impossible: the scattering of muon neutrinos at electrons will not be first-order with respect to the weak-interaction constant.

currents $(ee),(\mu\mu),(\nu\nu),(pp),(nn)$, and $(\Lambda\Lambda)$ exist or not. Actually, not a single experimental result has been obtained which is at variance with the hypothesis of symmetric neutral currents. Moreover, the low probability of the process $\mu \rightarrow e + \gamma$ may even be related to the existence of such currents. The presence of neutral currents would have the following consequences.

1. Certain weak interactions, such as the scattering of electrons by protons and by other electrons without parity conservation, would have to take place. No experimental data are available on this, and such data will be extremely difficult to obtain.

2. Excited nuclei must emit $\nu\bar{\nu}$ pairs. This effect is practically not observable at all under laboratory conditions, because of its low probability compared to those of ordinary electromagnetic processes. However, the presence of neutral symmetric currents would have important astrophysical consequences, and that is why I have discussed them here.

3. In experiments with beams of high-energy neutrinos, neutrino-nucleon scattering must be observed (and in complex nuclei, stars), unaccompanied by charged leptons. Searches for such processes with cross sections of the order of 10^{-38} to 10^{-40} cm^2/nucleon may indicate whether neutral currents are present during weak interactions.

8. SOME REMARKS ON MACROSCOPIC EFFECTS RELATED TO NEUTRINOS

I will now mention briefly some data which indicate that neutrinos definitely affect macroscopic phenomena. First, within stars a large number of neutrinos are formed during nuclear transformations (see following section), especially during the β decay of various unstable nuclei. As mentioned previously, the penetrating power of neutrinos is stupendous. In order to get an idea of how great it is, let us imagine a cast-iron plate a billion times thicker than the distance from the earth to the sun. This is the mean free path of a neutrino with an energy of about 1 MeV! Naturally, neutrinos can escape from the sun without any difficulty, and the energy transfer associated with the solar-neutrino flux at the earth's surface constitutes several percent of the solar constant.

There is still another example of a macroscopic effect. A uranium reactor with an output of hundreds of thousands of kilowatts "wastes" tens of thousands of kilowatts as neutrinos.

These examples should indicate the importance of neutrinos in the macrocosm. However, quite often situations arise in which the quantitative effects of neutrinos in some phenomenon cannot be evaluated, due to the lack of information on certain neutrino properties. The answers to the very subtle questions raised by elementary-particle physics (for example, the existence of $e\nu$ interactions or of neutral currents in weak interactions) have far-reaching astrophysical consequences. On the other hand, there are also cases in which neutrinos would have an enormous effect on stellar processes under certain density and temperature conditions, but it is not known whether these conditions actually exist.

9. NEUTRINOS AND THE SUN

Although many problems related to neutrino production in stars are still unsolved, nevertheless a few definite statements on this subject can be made. The flux of solar neutrinos, for instance, is known to be of the order of 10^{11} neutrinos/cm^2 sec at the earth's surface. In addition, it is known that the sun ejects neutrinos but not antineutrinos. This happens because of the types of nuclear reactions which can take place in stars (as opposed to antistars, if the latter exist).

The sun and the other stars liberate energy via hydrogen and carbon cycles, in which hydrogen is converted into helium. In these processes, about 5% of the energy of the sun and the main-sequence stars is emitted as neutrinos (Table 2).

TABLE 2. Processes responsible for energy release on the sun

	Type of neutrino spectrum	Neutrino energy, MeV
Hydrogen cycles		
a) $^1H + {}^1H \to {}^2H + e^+ + \nu$; $^2H + {}^1H \to {}^3He + \gamma$; $^3He + {}^3He \to {}^4He + {}^1H + {}^1H$	Continuous	$E_{max} \sim 0.4$
b) $^3He + {}^4He \to Be^7 + \gamma$; $^7Be + e \to$ $^7Li + \nu$ / $^7Li^* + \nu$; $Li^{7*} \to Li^7 + \gamma$; $Li^7 + {}^1H \to {}^4He + {}^4He$	Monochromatic Monochromatic	$E \sim 0.9$ $E \sim 0.4$
c) $^7Be + {}^1H \to {}^8B + \gamma$; $^8B \to {}^8Be^* + e^+ + \nu$; $^8Be^* \to {}^4He + {}^4He$	Continuous	$E_{max} \sim 14$
Carbon cycle		
$^{12}C + {}^1H \to {}^{13}N + \gamma$; $^{13}N \to {}^{13}C + e^+ + \nu$; $^{13}C + {}^1H \to {}^{14}N + \beta$	Continuous	$E_{max} \sim 1.2$
$^{14}N + {}^1H \to {}^{15}O + \gamma$; $^{15}O \to {}^{15}N + e^+ + \nu$; $^{15}N + {}^1H \to {}^{12}C + {}^4He$	Continuous	$E_{max} \sim 1.7$

However, the relative importance of each cycle is unknown. It has been established only that the sun and the "cold" stars operate mainly on the hydrogen cycle, while in the hotter stars the carbon cycle prevails. The carbon cycle apparently occurs in the central parts of the sun as well. So far, practically nothing is known about the different reaction channels of the hydrogen cycle.

As Table 2 shows, the neutrinos emitted by the sun and by other main-sequence stars have various spectra. In particular, intensive monochromatic neutrinos resulting from electron capture exist. The possibility of recording solar neutrinos and the value of the pertinent investigations will be discussed below. Let us only remark here that the different mechanisms for the ejection of neutrino-antineutrino pairs accompanying the electron-neutrino interaction (see below) are not important on the sun or on stars with low temperatures and densities.

10. THE EMISSION OF NEUTRINO-ANTINEUTRINO PAIRS ACCOMPANYING THE ELECTRON-NEUTRINO INTERACTION

As we saw in Section 6, the most popular theory describing weak interactions assumes a probability for the $\nu + e \rightarrow \nu + e$ reaction which is comparable with the probabilities for all other weak interactions. Let me stress that no experimental proof of this has been found. If we make the foregoing assumption, however, then there will be some very interesting astrophysical consequences.

The electron-neutrino interaction may be accompanied by electron-positron annihilation and the emission of a neutrino-antineutrino pair ($\nu + e \rightarrow \nu + e$, and therefore $e^+ + e^- \rightarrow \tilde{\nu} + \nu$). Consequently, in electromagnetic processes, there will be a possibility of $\nu\tilde{\nu}$-pair emission (via the virtual pair $e^+ e^-$) instead of photon emission. This general fundamental relation between electromagnetic phenomena and lepton processes is a direct consequence of the electron-neutrino interaction (when only charged currents are present). Granted that $\nu\tilde{\nu}$-pair emission during the elementary interaction has extremely low probability compared to photon emission, still the enormous penetrating power of the neutrino forces us to consider the possibility of effects of neutrino-electron interactions in large bodies at high temperatures. Apparently, at some stage of stellar evolution, the energy emitted into space as neutrino-antineutrino pairs becomes comparable to the energy emitted as photons. Then, during the subsequent evolution of the star, its neutrino luminosity considerably exceeds its photon luminosity. I will discuss here only some results of studies of the stellar neutrino luminosity associated with the electron-neutrino interaction.

1. The neutrino-emitting mechanisms related to the electron-neutrino interaction here refer to the emission of neutrino-antineutrino pairs rather than the emission of neutrinos separately which takes place as a result of solar nuclear transformations (see Table 2).

2. The effects of the electron-neutrino interaction are important only on stars with high density and temperature, when the light elements have practically burned up ($Z \geqslant 10$). Consequently, these effects do not influence the energy balance of the sun much. The predominance of the neutrino luminosity over the photon luminosity for large Z is also related to the fact that, as Z increases, the mean free paths of gamma quanta decrease while the cross section for $\nu\tilde{\nu}$-pair production increases.

3. The electron-neutrino interaction causes certain processes whose importance depends on the stellar temperature and density. The main ones are:

$e^- + Z \rightarrow e^- + Z + \nu + \tilde{\nu}$, neutrino bremsstrahlung;
$\gamma + e^- \rightarrow e^- + \nu + \tilde{\nu}$, electron photoneutrino effect;
$\gamma + Z \rightarrow Z + \nu + \tilde{\nu}$, nuclear photoneutrino effect;
$e^+ + e^- \rightarrow \nu + \tilde{\nu}$, neutrino annihilation of an electron-positron pair.

4. The neutrino luminosity becomes comparable to the photon luminosity at $T \sim 10$ keV, $\rho = 2$ to $3 \cdot 10^3$ g/cm^3, and $Z = 12$. For denser, hotter stars the photon luminosity is quite negligible compared to the neutrino luminosity. For stars with densities $\rho \sim 10^4$ g/cm^3, the energy $q\nu\tilde{\nu}$ released by 1 cm^3 of stellar matter per second, as a result of the $e\nu$ interaction, is from 10^4 to 10^{14} erg/cm^3 sec, for temperatures from 10 to 100 keV. The relative contribution of the neutrino processes listed above depends on T.

For fixed values of $Z = 12$ and $\rho = 10^4\,\mathrm{g/cm^3}$, neutrino-bremsstrahlung emission will predominate at low temperatures ($T < 10\,\mathrm{keV}$), photoneutrino effects will predominate up to $T = 50$ keV, and neutrino annihilation of electron-positron pairs will predominate at $T \geqslant 50$ keV.

5. Neutrino processes associated with the electron-neutrino interaction should be very important factors in the evolution of white dwarfs. Also, they should have a considerable effect on the dynamics of supernovae.

In conclusion, let us note that at very high densities and temperatures the "transfer" of energy to the neutrino-antineutrino component of the radiation is a quite general property of matter.

11. THE URCA PROCESS

There is still another process which can, under favorable conditions, contribute to the neutrino luminosity. For reasons which are not very clear, it is referred to in the literature as the urca process.

In this process, a $\nu\tilde{\nu}$ pair is not emitted due to an $e\nu$ interaction; rather, $\tilde{\nu}$ and ν are produced separately by the catalytic action of electrons:

$$\begin{cases} e^- + Z \to (Z-1) + \nu; \\ (Z-1) \to Z + e^- + \tilde{\nu}. \end{cases}$$

At high temperatures, electrons may induce reverse β processes in which ν and a radioactive nucleus are formed, after which the nucleus decays emitting a $\nu\tilde{\nu}$ pair.

The urca process differs fundamentally from the mechanisms of $\nu\tilde{\nu}$-pair emission based on the $e\nu$ interaction. The latter is a nonthreshold process, whereas the urca process has a definite threshold. For this reason, the importance of the urca process depends greatly on the chemical composition of the stars and is difficult to assess.

12. NEUTRAL CURRENTS AND ASTROPHYSICS

We have seen that the absence of symmetric neutral currents such as (ee), $(\nu\nu)$, $(\mu\mu)$, (pp), and (nn) in weak interactions has not been proven. If such currents do exist, the emission of $\nu\tilde{\nu}$ pairs from excited nuclei will be possible. These emissions are analogous to the β radioactivity of nuclei, except that instead of an electron and a neutrino a $\nu\tilde{\nu}$ pair is emitted. This neutrino radioactivity is unrelated to electromagnetic processes, and it differs from the $\nu\tilde{\nu}$-pair emission caused by the electron-neutrino interaction in that it is a process of the order of G^2 and not G^2e^4. Therefore, neutrino radioactivity may be of great importance for astrophysics, provided only that neutral currents actually exist in nature.

13. NEUTRINOS AND COSMOGONY

Recently, several discussions of the possible role played by neutrinos in cosmogony have appeared. Since a proper treatment of this

subject would be very time-consuming, I will just list some of the more interesting questions. The literature on this subject, however, will be represented quite fully.

The red shift of astronomical objects is usually explained as being due to the expansion of the universe. According to the general theory of relativity, the "homogeneous" model of Friedman leads to various cosmogonical possibilities, depending on the (mean) density ρ of the matter in the universe. If ρ is less than some critical value ρ_{cr}, estimated as being about $2 \cdot 10^{-29}$ g/cm^3, then the universe will expand indefinitely (open model). However, if $\rho > \rho_{cr}$ (closed model), the universe will stop expanding at some period and will begin to contract, after which there will be another expansion, etc. (pulsating universe).

The mean nucleon density ρ_N in the universe is of the order of 10^{-29} g/cm$^3 \sim 10^{-2}$ MeV/cm^3. Since this value is not known with much accuracy, however, it is impossible to tell whether it is larger or smaller than ρ_{cr}.

The following question may be asked: is it not possible that the energy density of neutrinos and antineutrinos in the universe is comparable with (or even greater than) the hydrogen energy density ρ_N? The question of a higher density of neutrinos and antineutrinos arises, naturally, during discussions of the *PC* asymmetry of the world, in connection with the hypothesis of the existence of antiworlds. The possibility that antiworlds may be created due to fluctuation of the charge-symmetric universe has been discussed repeatedly in the literature. So far no experimental verification of the existence of antiworlds has been obtained. However, the fluctuation hypothesis requires that there exist in the universe (now or at some time in the past) a large charge-symmetric "background." Such a background would in principle have to consist, to a considerable degree, of ν and $\bar{\nu}$ (with equal densities of each).

What is known about the neutrino energy density? For neutrinos with energies $\geqslant 1$ BeV, measurements of the underground cosmic-ray intensity have indicated an energy density lower than ρ_N by at least three orders of magnitude. For neutrinos of several MeV, on the other hand, the experimental data (obtained from an analysis of the experiments of Reines and Cowan and Davis, assuming that the "background" in their apparatus was due to cosmic neutrinos) do not rule out an energy density of neutrinos and antineutrinos which is considerably greater than ρ_N.

However, a study of the gravitational consequences for neutrinos of any energy compatible with an expanding universe indicates that the maximum neutrino energy density $\rho_{\tilde{\nu}}$ cannot exceed ρ_N by much ($\rho \approx \rho_N + \rho_{\tilde{\nu}} < 10\rho_N$). In this case ($E_\nu \leqslant 1$ MeV), nuclear experiments give less information than an estimate based on the gravitational effects of neutrinos. Be that as it may, it would seem that the energy density of ν and $\bar{\nu}$ at present is small in comparison with that of hydrogen. At first glance, this is inconsistent with the fluctuation hypothesis, since apparently a "background" is not available out of which fluctuations can arise. This inconsistency, however, has a natural explanation.

According to the general theory of relativity, the mean energy of relativistic particles (in this case, neutrinos) drops in proportion to the curvature of space (that is, it drops as a^{-1}, while the energy density of the particles drops as a^{-4}). In other words, in the past the mean energy of neutrinos must have been as many times greater than the present value as

the curvature of space was greater. Thus, in the past, when the density of matter was colossal, the energy density of neutrinos (as well as of protons, and in general the density of the "symmetric" energy not related to the rest mass) may have exceeded by many orders of magnitude the density of the total energy of nucleons. These may well have been the conditions under which the fluctuations originated. Naturally, the fluctuation mechanism is not being discussed here, and the question of the priority of neutrino-antineutrino pairs must remain open. It can be stated, however, that the above-mentioned mechanism of energy "transfer" to the neutrino-antineutrino component, which is related to neutrino scattering by electrons, should ensure that the "symmetric form" of energy as $\nu\tilde{\nu}$ pairs will predominate over other symmetric forms of energy (thermal energy, energy of photons, etc.).

Consequently, irrespective of the fluctuation hypothesis, it seems quite probable that for a universe which really pulsates, the dynamics of the universe will be determined by the energy density of ν and $\tilde{\nu}$, at any rate during the compression phase. During this phase neutrinos have very high energies.

14. EXPERIMENTAL NEUTRINO ASTRONOMY

Introduction. Neutrino astrophysics and neutrino astronomy are the sciences describing the numerous phenomena in which neutrinos are of paramount importance. There are two separate aspects of neutrino astrophysics.

First, neutrinos participate in processes occurring inside of stars and in space in general. Thus, astrophysics and cosmology as theoretical sciences must take into account the role which these particles play in such processes. This aspect of neutrino science has been discussed in the foregoing.

Second, the neutrinos emitted by stars and by outer space as a whole can be recorded on the earth itself or on spacecraft, which provides us with valuable information concerning the universe. This view of neutrino astronomy, as an experimental science, is a very tempting one, and I wish to discuss it briefly. Up to the present, essentially only one type of radiation incident on the earth from outer space could be studied, and that was electromagnetic waves. Here, I said "essentially only one" type of radiation, since recently cosmic rays have begun to be studied from the point of view of astrophysics. However, there is no need to go into this further.

The possibility of recording the intensities, energies, and directions of neutrinos and antineutrinos arriving from stars and from outer space provides us with a powerful tool for solving astrophysical problems. When astronomers record electromagnetic waves, they do not "look deeply" into a star, since such waves come only from the surface layer of the celestial body. However, because of the enormous penetrating power of neutrinos, their recording makes possible a very "deep look" into the stars. This extremely interesting possibility is really practicable only for the study of nuclear reactions within the sun and will be discussed later.

Now, if you will let me be a bit imaginative, that is, to speak of some things which are less practicable, I would like to point out some of the main potentialities of experimental neutrino astronomy. The practical realization of these potentialities, however, is quite far-off and perhaps may never be achieved.

After the neutrino fluxes from the sun have been recorded, a further step will be necessary, namely to measure the neutrino fluxes from outer space (we have already seen how important this is) and from other galaxies. To do this, the sensitivity of contemporary recording methods must be increased by a factor of more than one million. Consequently, I will not discuss these problems in detail here, but will just illustrate one of the main possibilities inherent in neutrino astronomy. This has to do with antiworlds, which are worlds completely made up of antiparticles.

Can observations made on the earth tell us whether antiworlds exist? Let us assume that we wish to know whether some celestial body is made up of matter or antimatter. It is clear from the outset that observations of light, or of electromagnetic waves in general, cannot tell us what we want to know. The light emitted, let us say, by a hydrogen atom is identical to the light emitted by an atom of antihydrogen (photons are intrinsically neutral; they have no charge and are indistinguishable from their antiparticles).

But what is the situation for neutrino emission? We have seen that the sun emits neutrinos but not antineutrinos. This will be the case for all stars whose main energy sources are thermonuclear reactions converting hydrogen into helium. Now, let us imagine an antisun with internal processes similar to those of the sun. On it, the energy will be provided by the conversion of antihydrogen to antihelium. Although the light from such antisuns will not differ from sunlight, they will emit antineutrinos rather than neutrinos. This indicates the potentialities inherent in neutrino astronomy. Of course, an overly optimistic view of the possibility of solving this problem should be warned against. The difficulty is not just the extremely low intensity of neutrinos and antineutrinos; the greatest problem is that it is not known how to construct an effective neutrino telescope. In order to verify that a neutrino emission comes from a definite celestial body, the angular distribution of the neutrino-caused fission products must be measured. However, it appears that the angular distribution with respect to the direction of the incident beam is completely insensitive (for neutrinos with energies of a few MeV or less). This difficulty is so great that the previously cited problem may well be insolvable. Nevertheless, the possibility in principle is in itself very interesting.

The construction of a neutrino telescope is considerably simpler for high-energy neutrinos ($E_\nu \gtrsim 1$ BeV), and this will be discussed below.

The neutrino intensity of cosmic rays underground. The determination of the intensity and direction of high-energy cosmic neutrinos is of great interest. A complicated assembly of scintillation counters, placed at a great depth and recording the neutrino-produced muons from reactions of the type

$$\nu + N \rightarrow \mu + N'$$

may be used as a neutrino detector.

According to Markov, underground equipment records muons produced by neutrinos coming from the inner hemisphere, that is, by neutrinos passing through the whole earth. This is possible, of course, since the mean free path of a neutrino is incomparably greater than the earth's diameter. Moreover, the background of cosmic muons not produced by neutrinos will not interfere, since charged particles cannot pass through the earth. In principle it is possible to record, first, "atmospheric" neutrinos, that is, neutrinos from the decay of the pions produced during atmospheric collisions of the proton component of cosmic rays. Such studies are more interesting from the point of view of elementary-particle physics than from the point of view of astronomy. Second, it may be possible to study the direction in space of localized sources of cosmic neutrinos; if such sources exist, new possibilities for astronomy may be created. Experimental neutrino astrophysics is a very young science, and it may even seem that it has not yet come into being, since I always refer to the future when discussing it. However, some experiments giving information on cosmic fluxes of neutrinos have already been carried out. It is true that the neutrinos themselves have not been detected as yet, and that the results are negative. But it has been found that the energy density of high-energy neutrinos ($E_\nu \gtrsim 1$ BeV) is less than 10^{-5} MeV/cm^3, which is at least three orders of magnitude less than the energy density of hydrogen in the universe. It is significant that this result was obtained from an analysis of high-quality measurements of the underground intensity of cosmic rays, measurements not intended to give information on neutrinos.

Solar experimental neutrino astrophysics. We have seen (Table 2) that the various reactions responsible for the solar energy are accompanied by the emission of neutrinos with different intensities and different spectra. Of great interest from the theoretical point of view is the question: what nuclear reactions take place deep in the interior of the sun? Since the probability that a neutrino interaction will occur (and thus will be measurable) depends greatly on the neutrino energy, such interactions are unique means of obtaining valuable information about the sun. The primary task of neutrino astronomy will obviously be to record solar neutrinos. But how can this be done? The following interaction between a neutrino and the ^{37}Cl nucleus was referred to above: $\nu + {}^{37}\mathrm{Cl} \rightarrow {}^{37}\mathrm{A} + e^-$. The threshold for this reaction (that is, the threshold of the neutrino detector) is about 0.8 MeV, and so the recording of solar neutrinos will be impossible if the only neutrino source is the reaction $p + p \rightarrow d + e^+ + \nu$ (see Table 2). On the other hand, the decay processes

$$^{13}\mathrm{N} \rightarrow {}^{13}\mathrm{C} + e^+ + \nu;$$
$$^{15}\mathrm{O} \rightarrow {}^{15}\mathrm{N} + e^+ + \nu;$$

and especially

$$^{8}\mathrm{B} \rightarrow {}^{8}\mathrm{Be} + e^+ + \nu$$

produce neutrinos with energies higher than the detector threshold.

At present only one method for recording neutrinos with energies of a few MeV is known, and that is by means of the reaction $\nu + \mathrm{Cl}^{37} \rightarrow \mathrm{A}^{37} + e^-$. The sensitivity of this method is such that recordings of solar neutrinos, though extremely difficult, are nevertheless practicable. It may be that in the future a new efficient means of recording megavolt neutrinos will be devised.

To complete the picture, let us recall that a good method for recording megavolt antineutrinos is one based on the Reines-Cowan reaction $\tilde{\nu} + p \rightarrow \rightarrow n + e^+$. However, for $\tilde{\nu}$ and ν with energies $\ll 1$ MeV, there is unfortunately no recording method available.

CONCLUSION

Table 1 lists the known properties of the neutrino. Some of its properties are still unknown; in particular, it is not known whether neutrino-electron scattering, which is very important for astrophysics, exists. Neutrinos have tremendous penetrating power, and the role played by the neutrino in the cosmos as a whole is closely related to this property. The sun and the main-sequence stars emit neutrinos but not antineutrinos. The energy given off as neutrinos by these stars constitutes a few percent of the total energy release.

For heavy stars ($\bar{Z} \sim 12$) with high temperatures ($T > 10$ keV) and densities ($\rho > 3 \cdot 10^3$ g/cm^3) the neutrino luminosity exceeds the photon luminosity. These bodies emit neutrino-antineutrino pairs by various mechanisms (neutrino bremsstrahlung, photoneutrino effects, neutrino annihilation of a positron and an electron) which have the following property in common: they are all associated with neutrino-electron interactions which are first-order with respect to the weak-interaction constant.

Neutrinos and antineutrinos are apparently very important factors in the evolution of white dwarfs and in the explosion dynamics of supernovae. It is also quite possible that neutrinos play a large part in cosmogony.

Experimental neutrino astrophysics is a very promising science, but one which is just coming into being. Its primary task is to record neutrinos coming from the sun, so as to enable us to "look into" the solar depths.

Proofreading note. An American experiment (Brookhaven Laboratory) designed to test whether muon neutrinos are identical to electron neutrinos indicated that the two types of neutrinos are in fact different particles.

Joint Institute for
Nuclear Research, Dubna

REFERENCES

1. General articles on elementary-particle physics

GELL-MANN, M. and E. ROZENBAUM.—UFN, **64**, 391. 1958.

SALAM, A.—UFN, **84**, 141. 1961.

2. Theoretical works on weak interactions

FERMI, E.—Zs. Phys., **88**, 161. 1934 (first version of β-decay theory).

LEE, T. D. and C. N. YANG.—Phys. Rev., **104**, 254. 1956 (is parity conserved in weak interactions?).

FEYNMAN, R. P. and M. GELL-MANN.—Phys. Rev., **109**, 193. 1958 (universal theory of weak interactions).

OKUN', L. Lektsii po teorii slabykh vzaimodeistvii elementarnykh chastits (Lectures on the Theory of Weak Interactions of Elementary Particles). Preprint P-318, Dubna. 1961.

3. Theoretical studies of the two-component neutrino

SALAM, A.—Nuovo Cimento, **5**, 299. 1957.

LANDAU, L. D.—ZhETF, **32**, 405. 1957.

LEE, T. D. and C. N. YANG.—Phys. Rev., **105**, 1671. 1957.

4. General articles on invariance principles in nuclear physics

CHEN, NING-YANG.—UFN, **66**, 79. 1958.

CHIANG, TAO-LI.—UFN, **66**, 89. 1958.

LANDAU, L. D.—ZhETF, **32**, 405. 1957.

VIK, G.—UFN, **68**, 201. 1959.

5. Experimental studies of neutrinos

REINES, F. and C. L. COWAN.—Phys. Rev., **92**, 830. 1953.

REINES, F., C. L. COWAN et al.—Phys. Rev., **117**, 159. 1960 (the first experiments in which an interaction of free reactor-produced antineutrinos with protons was detected).

DAVIS, R.—Phys. Rev., **97**, 666. 1955; Bull. Amer. Phys. Soc., **4**, 217. 1959.

PONTECORVO, B.—Nat. Res. Council, Canada, Rept. P. D., 205. 1946 ($\nu + Cl^{37} \rightarrow A^{37} + e^-$ reaction).

COWAN, C. and F. REINES.—Phys. Rev., **107**, 528. 1957 (determination of the upper limit for the magnetic moment of ν).

WU, C. S. et al.—Phys. Rev., **105**, 1413. 1957 (discovery of parity nonconservation in β decay).

GARWIN, R. L., L. M. LEDERMAN, and M. WEINRICH.—Phys. Rev., **105**, 1415. 1957 (discovery of parity nonconservation in $\pi \rightarrow \mu \rightarrow e$ decay; the longitudinal polarization of neutrinos).

GOLDHABER, M. et al.—Phys. Rev., **109**, 1015. 1958 (determination of the neutrino helicity).

REINES, F.—Ann. Rev. Nucl. Sci., **10(1)**, 1960 (review of neutrino interactions).

6. The physics of high-energy neutrinos

MARKOV, M. A., Editor. K fizike neitrino vysokikh energii (Contributions to the Physics of High-Energy Neutrinos). Preprint, Dubna. 1960 (review of Soviet studies in the physics of high-energy neutrinos).

PONTECORVO, B. and R. M. RYNDIN.—IX International Conference on High-Energy Physics, Kiev. 1959.

LEE, T. D. and C. N. YANG.—Phys. Rev., **119**, 1410. 1960 (experiments using neutrino beams are suggested to solve the problem of the intermediate boson).

PONTECORVO, B.—ZhETF, **37**, 1751. 1959.

MARKOV, M. A. Hyperonen und K-mesonen.—Verlag der Wissenschaften, Berlin. 1960 (experiments are suggested to solve the problem of the identity of ν_e and ν_μ).

DANDY, G., I. GALLARD, K. GOULIANOS, L. M. LEDERMAN, N. MISTRY, M. SCHWARTZ, and I. STEINBERGER.—Phys. Rev. Letts., **9**, 36. 1962 (experimental verification of the nonidentity of ν_e and ν_μ).

KOBZAREV, P. Yu. and L. B. OKUN'.—ZhETF, **41**, 1205. 1961 (theoretical study of the possibility of an anomalous ν_μ interaction).

VASILEVSKY, N.M., V.I.VEKSLER, V.V.VISHNYKOV, B.PONTECORVO, and A.A.TYAPKIN.— Phys. Letts., **1**, 345. 1962 (checks for an anomalous ν_μ interaction).

BLUDMAN, S.S.—Nuovo Cimento, **2**, 433. 1958.

PONTECORVO, B.—Phys. Letts., **1**, 287. 1962 (do neutral currents exist in weak interactions?).

7. Neutrinos in cosmic rays

MARKOV, M.A.—In the collection: Proc. 1960. Ann. Int. Conf. on High Energy Physics at Rochester.

GREISEN, K.—Ann. Rev.Nucl. Sci., 1960.

ZATSEPIN, G.T. and V.A.KUZ'MIN.—ZhETF, **41**, 1818. 1961 (possible experiments on recording neutrino fluxes in cosmic rays are discussed).

MIYAKE, S., V.S.NARASIMHAN, and P.V.RAMANA MURTYH.—Proc. Int. Conf. on Cosmic Rays and the Earthstorm, Part III. 1961 (measurements of the cosmic-ray intensity at great depths).

PONTECORVO, B. and A.E.CHUDAKOV.—Proc.1962 Ann. Int. Conf. on High Energy Physics at Geneva (measurements of the cosmic-ray intensity at great depths lead to conclusions concerning the energy density of high-energy neutrinos and concerning the absence of an anomalous ν_N interaction).

8. Neutrino astronomy (the sun)

FRANK-KAMENETSKII, D.A. Fizicheskie protsessy vnutri zvezd (Physical Processes in Stellar Interiors).— Fizmatgiz, Moskva. 1959* (nuclear reactions in the interior of stars).

MARX, G. and N.MENYHÁRD.—Science, **131**, 299. 1960.

PONTECORVO, B.— Znanie-sila, No. 2, Feb. 1961.

REEVES, H. Istochniki zvezdnoi energii (Sources of Stellar Energy). Preprint. 1962.

MORRISON, P. Neutrino Astronomy.— Sci. Amer., **207**(2), 90. 1962 (the prospects of experimental neutrino astronomy).

9. $\nu\bar{\nu}$ -pair emission

GAMOW, G. and M.SCHOENBERG.—Phys. Rev., **59**, 539. 1941 (urca process).

PONTECORVO, B.— ZhETF, **36**, 1615. 1959 (the e—ν interaction and its significance in astrophysics).

GANDEL'MAN, G.M. and V.S.PINAEV.— ZhETF, **37**, 1072. 1959 (neutrino bremsstrahlung in stars).

RITUS, V.I.— ZhETF, **41**, 1285. 1961 (photoneutrino effect at an electron, in stars).

MATINYAN, S.G. and N.N.TSPLOSANI.— ZhETF, **41**, 1681. 1961 (photoneutrino effect at a nucleus, in stars).

CHIU, H.Y. and Ph.MORRISON.—Phys. Rev. Letts., **5**, 573. 1960 (neutrino annihilation of electron-positron pair, in stars).

MATINYAN, S.G. Lektsiya, prochitannaya v vesennei shkole teoreticheskoi i eksperimental'noi fiziki Nor-Amberd, Aprel' 1962 (A Lecture Read at the Spring School of Theoretical and Experimental Physics at Nor-Amberd, April 1962).—Izdatel'stvo Akademii Nauk ArmSSR.

PINAEV, V.S. Lektsiya, prochitannaya v shkole astrofiziki v Tartu (A Lecture Read at the School of Astrophysics in Tartu).—Voprosy kosmogonii (in press) (reviews of $\widetilde{\nu\nu}$-pair emission in stars).

10. Neutrinos and cosmogony

PONTECORVO, B. and Ya.A.SMORODINSKII.— ZhETF, **41**, 239. 1961 (neutrinos and the density of matter in the universe).

[English translation: IPST Cat. No.815, TT 67-51366.]

ZEL'DOVICH, Ya.B. and Ya. A. SMORODINSKII. — ZhETF, **41**, 907. 1961 (the upper limit for the neutrino density in the universe).

KHARITONOV, V.M. Lektsiya, prochitannaya v vesennei shkole teoreticheskoi i eksperimental'noi fiziki Nor-Amberd, Aprel' 1961 (A Lecture Read at the Spring School of Theoretical and Experimental Physics at Nor-Amberd, April 1961). — Izdatel'stvo Akademii Nauk ArmSSR (cosmogonic aspects of neutrino physics).

WEINBERG, S. Preprint. 1962 (universal neutrino degeneration).

N67 38204

G. F. Krymskii

APPLICATION OF A UNIDIMENSIONAL-DIFFUSION MODEL TO THE PROPAGATION OF SOLAR COSMIC RAYS

Magnetic fields exist within the solar system which are strong enough to scatter protons with energies above 1 BeV. Therefore, the propagation of particles accelerated at the sun can be described as a diffusion of these particles at inhomogeneities in a magnetic field. If the field is random or is represented in terms of a system of magnetic "clouds," the diffusion can be taken as isotropic.

Many authors (for instance, /1–4/) have tried to describe the time dependence of the solar-cosmic-ray intensity by means of isotropic diffusion. In each case, however, the agreement with experiment for the period of intensity decay was not good enough. The drop in cosmic-ray intensity takes place more rapidly than according to the $t^{-3/2}$ law describing isotropic diffusion in an unbounded space.

If unidimensional diffusion takes place within a bounded layer of thickness l with an absorbing boundary, then we can solve the diffusion equation

$$\Delta n = D \frac{\partial n}{\partial t} \tag{1}$$

for the following boundary and initial conditions:

$$n|_{x=l} = 0; \quad \operatorname{grad} n|_{x=0} = 0; \quad n|_{t=0} = Q\delta(x), \tag{2}$$

where n is the density of cosmic-ray particles, D is the diffusion coefficient, and Q is the total number of emitted particles. A particle density of zero at $x = l$ is justified for a diffusion approximation assuming particle velocities which approach infinity and a scattering mean free path λ which approaches zero. Actually, of course, this density is not zero.

The solution of equation (1) for boundary conditions (2) is

$$n(x, t) = \frac{2Q}{(4\pi Dt)^{3/2}} \left\{ \sum_{j=-\infty}^{\infty} e^{-\frac{[x+4jl]^2}{4Dt}} - \sum_{j=-\infty}^{\infty} e^{-\frac{[x+l(4j+2)]^2}{4Dt}} \right\}. \tag{3}$$

The number of particles reaching the absorbing boundary (or leaving the diffusion region) per unit time is

$$q(t) = -D \operatorname{grad} n|_{x=l}. \tag{4}$$

By substituting the gradient of (3) into (4), we obtain

$$q(t) = \frac{8QD}{\sqrt{\pi} l^3} \tau^{-\frac{3}{2}} \sum_{j=-\infty}^{\infty} (4j+1) e^{-\frac{(4j+1)^2}{\tau}}, \tag{5}$$

where $\tau = \frac{4D}{l^2} t$.

Equation (5) can also be obtained by taking into account that the number of particles leaving the diffusion region equals the decrease in the number of particles participating in the diffusion:

$$q(t) = -\frac{\partial}{\partial t}\left[\int_0^l n(x, t)\, dx\right].$$

In equation (5) the term with $j = 0$ is the most important one for $\tau \leq 1$; the other terms become significant when $\tau \geqslant 1$, that is, during the decay period.

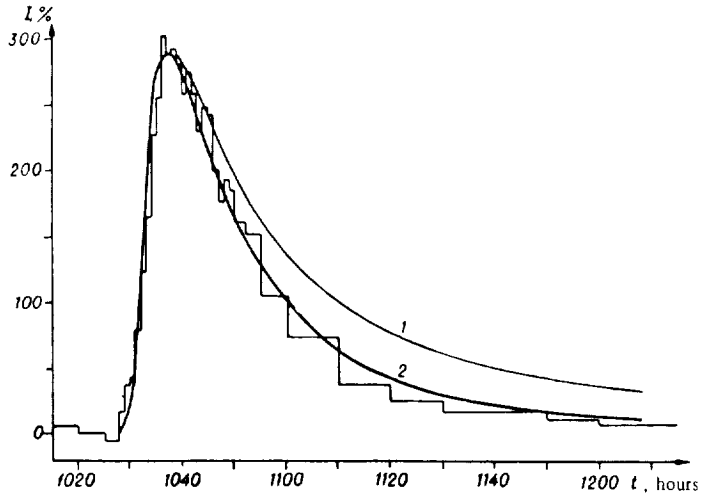

FIGURE 1. The rise in the cosmic-ray neutron component on 4 May 1960 (Churchill Station).

Predicted time dependence of the rise: 1–according to the model of isotropic diffusion in an unbounded space; 2–according to the model of unidimensional diffusion in a bounded region.

If it is assumed that solar cosmic rays undergo unidimensional diffusion within a bounded layer located inside the earth's orbit, then law (5) gives the variation in the number of particles leaving the layer and also the change in particle intensity at the earth.

Figures 1 and 2 show the intensity (I) as a function of time (t) for the flares of 23 February 1956 and 4 May 1960. The curves show this function: (1) calculated assuming isotropic diffusion in unbounded space; and (2) calculated assuming diffusion "luminescence" of a two-dimensional layer. The best fit of curves 1 and 2 with experiment is obtained when the onsets of the intensity rise are taken as 10 h 28 min for the flare on 4 May 1960 and 3 h 45 min for the flare on 23 February 1956. These times agree with the directly determined flare onsets: 10 h 28 min /5/ and 3 h 42 min /6/.

The satisfactory fit between the experimental data and the curve according to (5) enables us to assume that on 23 February 1956 and 4 May 1960 the region of solar-cosmic-ray diffusion was bounded and that the diffusion was sharply anisotropic:

$$D_{\parallel} \gg D_{\perp}, \qquad (6)$$

where $D_{\parallel}$ and $D_{\perp}$ are respectively the coefficients of diffusion along the main direction of particle propagation and along the direction transverse to this.

The anisotropy of the diffusion coefficient indicates that during these periods there is a cosmic-ray "channel" between the earth and the region of the corresponding chromospheric flares observed near the western limb of the sun. Such a channel can exist if the magnetic field between the earth and the sun has an ordered structure, with approximately radial orientation.

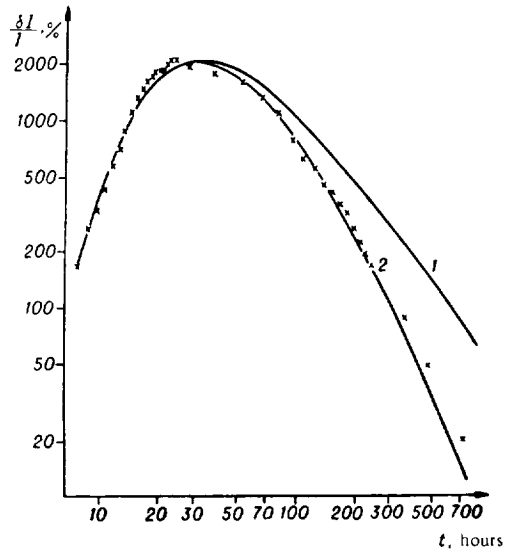

FIGURE 2. Time dependence of cosmic-ray intensity on 23 February 1956, according to data of neutron monitor at Churchill (points). The meaning of curves 1 and 2 is the same as in Figure 1.

The boundedness of the diffusion region obviously agrees with the fact that further from the sun the path becomes freer. Consequently, l is an effective dimension of the diffusion region, which however has a very diffuse boundary.

Since the parameter

$$\varkappa = \frac{D}{l^2} \tag{7}$$

entering into (5) is known experimentally, and since

$$D \sim \lambda c/_3, \tag{8}$$

the upper limit for l can be estimated roughly. For the diffusion approximation to be valid, the scattering mean free path must be much less than the dimension l of the diffusion region. If $\lambda \leqslant 0.3\ l$ is a reasonable value, then from (7) and (8) we have

$$l \leqslant 0.1 \frac{c}{\varkappa}. \tag{9}$$

The dimensions of the diffusion region given by formula (9) are $\leqslant 0.7$ A.U. for the flare of 4 May 1960 and $\leqslant 3$ A.U. for the flare of 23 February 1956.

An analysis of the distribution over the earth's surface of the effect of the 23-February flare /6/ indicates that during the decay period the intensity of solar cosmic rays is approximately isotropic. Therefore, it can be assumed that during this period the diffusion region extended to beyond the earth's orbit.

The pronounced anisotropy of the solar-cosmic-ray flux on 4 May 1960 /7/ indicates that then the diffusion region lay mainly inside of the earth's orbit.

The results obtained agree with the picture of a radial interplanetary magnetic field, twisted by the solar rotation; such a field is suggested by an analysis of the distribution over the solar disk of chromospheric flares causing the emission of high-energy particles /8, 9, 10/.

Institute of Space-Physics Research and
Aeronomy, Yakutsk Branch of Siberian
Division of USSR Academy of Sciences

REFERENCES

1. DORMAN, L.I. Voprosy magnitnoi gidrodinamiki i dinamiki plazmy (Problems in Magnetohydrodynamics and Plasma Dynamics), p.13. Riga. 1959.
2. KAMINER, N.S., Ya.L. BLOKH, and L.I. DORMAN. - Trudy MGG, Section VII, **4**, 146. 1961.
3. CHARAKHCH'YAN, A.N., V.F. TULINOV, and T.N. CHARAKHCH'YAN. - ZhETF, **41**, 735. 1961.
4. STEPANYAN, A.N. Polnoe chislo chastits vysokoi energii, ispushchennoe vo vremya vspyshki 4 Maya 1960 g. (The Total Number of High-Energy Particles Emitted During the Flare on 4 May 1960). In Press.
5. KUZ'MIN, A.I., G.V. KUKLIN, A.V. SERGEEV, G.V. SKRIPIN, N.P. CHIRKOV, and G.V. SHAFER. - Trudy Yakutskogo filiala Sibirskogo otdeleniya Akademii nauk SSSR, seriya fizicheskaya, **4**, 132. 1962.
6. DORMAN, L.I. and G.I. FREIDMAN. - Trudy Yakutskogo filiala Sibirskogo otdeleniya Akademii nauk SSSR, seriya fizicheskaya, **2**, 129. 1958.
7. Mc CRACKEN, K.G. - J. Geoph. Res., **67**, 435. 1962.
8. REID, G.C. and H. LEINBACH. - J. Geoph. Res., **64**, 1801. 1959.
9. DVORYASHIN, A.S., L.S. LEVITSKII, and A.K. PANKRATOV. - Izv. KAO, **26**, 90. 1961.
10. Mc CRACKEN, K.G. - J. Geoph. Res., **67**, 447. 1962.

N67 38205

A.E. Chudakov, V.L. Dadykin, V.I. Zatsepin, and N.M. Nesterova

A SEARCH FOR HIGH-ENERGY PHOTONS FROM DISCRETE SOURCES OF COSMIC RADIO EMISSION

It is now known that many sources of radio emission have a comparatively large concentration of high-energy electrons. It has been suggested that these electrons are products of the interaction of protons and high-energy nuclei with matter.

This hypothesis would be verified experimentally if high-energy photons could be detected in these sources. Such photons should be produced during the interaction of cosmic rays with the nuclei of interstellar-gas atoms, as a result of the formation of π^0 mesons and the subsequent decay of these. The photons will arrive from the direction of the source, since, in contrast to the trajectories of charged particles, their trajectories are not bent by magnetic fields in the interstellar medium.

In 1958 Cocconi /1/ suggested that, if the directions of cores of extensive air showers of cosmic rays could be determined with an accuracy of $\sim 1°$, it would be possible to distinguish which showers are produced by primary photons coming from discrete sources on the celestial sphere.

Cocconi's estimates of the intensity of high-energy photons from certain celestial objects, however, were very exaggerated, and subsequent theoretical calculations /2/ gave a lower photon flux.

In spite of this, in 1960–1961, we attempted to detect experimentally photons arriving from discrete sources of cosmic radio emission. To do this, the extensive air showers were recorded by means of the Čerenkov radiation which they produce in the earth's atmosphere.*

The observations were made in the Crimea, at sea level and on cloudless, moonless nights.

"Photon" showers were separated from the general mass of showers produced by primary protons and nuclei solely on the basis of the angular anisotropy expected for the primary photons.

Bursts of Čerenkov radiation were recorded by photomultipliers located at the foci of parabolic mirrors 150 cm in diameter. In 1960 4 such telescopes were used, and in 1961 the number was increased to 12, in order to raise the aperture ratio of the equipment. Figure 1 shows an overall view of the telescope assembly.

The optical axes of all the telescopes were parallel and directed toward the point on the celestial sphere through which the object studied must pass after ~ 30 minutes. Then, for an hour a continuous record of the shower

* This method was used by us in 1953–1958 for a series of studies of extensive air showers.

counting rate was made. The same object could be observed several times during the night by reorienting the telescopes and "catching up with" a source. All the results pertaining to a given source were then combined.

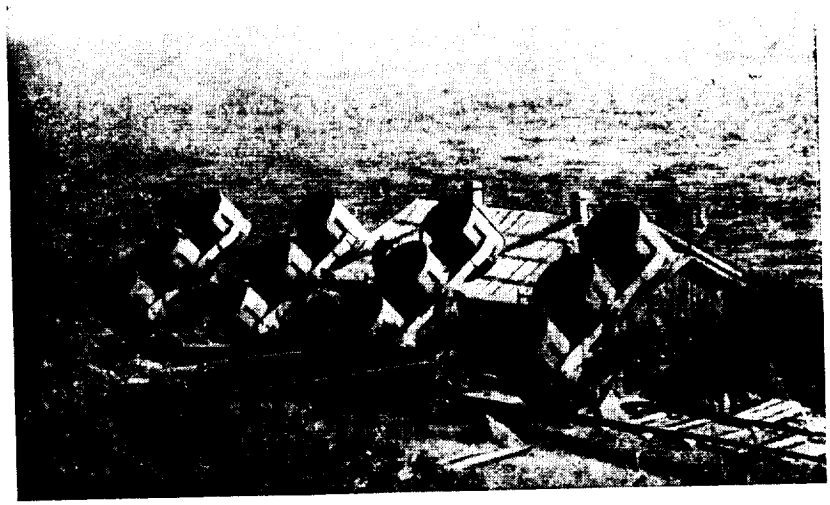

FIGURE 1.

A rise in counting rate was to be expected during the passage of the object through the viewing angle of the telescopes. The viewing angle of the optical system in this case was ± 2°. There was an additional angular distance of about 1° in which showers could probably be recorded, due to the angular dispersion of the luminous flux. Consequently, a rise in counting rate was to be expected during a time interval of 20 to 30 minutes for the observation of object Cygnus A and during an interval of 16 to 24 minutes for the observation of object Taurus A.

The energy threshold of the equipment for recording showers from primary photons was $5 \cdot 10^{12}$ eV in 1960 and $3 \cdot 10^{12}$ eV in 1961. The counting rate for showers from the charged cosmic-ray component within a solid angle of 1/300 steradian was correspondingly 80 and 200 counts per minute.

The results. For all the objects examined: Cassiopeia A, Taurus A (Crab Nebula), Cygnus A, Virgo A, and several other less powerful sources of radio emission, a sharp rise in counting rate was not observed. If such a rise does exist, it does not exceed 1 or 2%. Figures 2 and 3 show the results of the 1960 and 1961 measurements of Cygnus A and Taurus A, respectively. The abscissa is the time relative to the moment when the source passed through the optical axis of the telescopes; α is the right ascension of the source. The upper histograms show the total number of showers N counted in the given time interval.

The curves below the histograms show the variation in photomultiplier current due to the passage of more or less bright stars through the viewing angle of the telescopes.

The effective shower-recording area, determined by the maximum impact parameter for which a shower is still recorded, was $\sim 10^9$ cm^2 for showers with energies of 10^{13} eV. Taking into account the statistical

accuracy of the experiment (± 0.02 pulse/sec), it is possible to obtain an upper limit for the photon intensity. According to our data, the photon flux for the objects studied did not exceed 10^{11} photons/cm^2 sec. This result is not at variance with estimates of the probable flux made on the basis of data for the magnetic-field strength and gas density in the objects /2/.

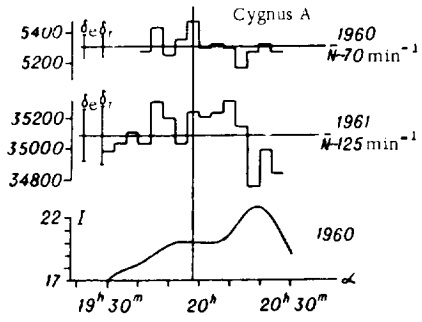

FIGURE 2.

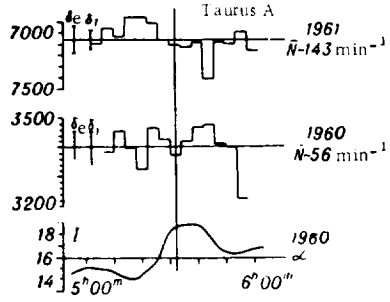

FIGURE 3.

However, this result does contradict the hypothesis that the electrons producing the synchrotronic radiation of the Crab Nebula are generated and continually replenished as a result of nuclear collisions. On the collision hypothesis, a photon flux about 100 times greater than the upper limit obtained in the experiment would be expected. Consequently, the high-energy electrons in the Crab Nebula either were produced during the first stage of a supernova outburst or else are now being accelerated by some very efficient mechanism. Both of these explanations involve considerable difficulty.

In the 1960 measurements a slight, but nevertheless noticeable, increase in counting rate was observed for object Cygnus A. Consequently, in the 1961 measurements most of the attention was focused on this object. 70 passages of the object were recorded and more than 500,000 showers counted.

The 1960 data showed a very striking effect within a narrow angular interval (1°), an effect which decreased abruptly when the interval was widened. This result, which contradicted the expected wide angular characteristic (± 2 to 3°), was not confirmed by the measurements repeated in 1961. After averaging over a wide angular interval, the effect noted in 1960 amounted to 1.6 ± 0.8 % for the Cygnus-A source. The 1961 measurements gave an effect of 0.68 ± 0.28%. The probability that in this case the positive effect is just statistical chance is quite high (2%).

Therefore, the existence of a photon flux from object Cygnus A, which was detected a second time by our equipment but again at the limit of statistical accuracy, can only be decided definitely by further experiments.

P. N. Lebedev Institute of Physics of the USSR Academy of Sciences

REFERENCES

1. COCCONI, G. - Trudy MKKL, **2**, 327. Izd. AN SSSR, 1960.

2. ZATSEPIN, G. T. and A. E. CHUDAKOV. - ZhETF, **41**, 655. 1961.

N67 38206

Yu. G. Shafer

STUDIES OF VARIATIONS IN THE PRIMARY COSMIC RADIATION

During the last few years, spatial and temporal variations in the intensity, energy spectrum, and chemical composition of primary cosmic rays have begun to be studied particularly widely. These studies have been made from the point of view of space physics.

This progress in the study of cosmic-ray variations was caused, first of all, by the accumulation and thorough analysis of the unusually extensive and detailed material collected at ground-level stations during the International Geophysical Year and the International Year of the Quiet Sun.

However, for a real understanding of the phenomena associated with variations in the low-energy primary particles, which are mostly of solar origin, cosmic-ray measurements at high altitudes, using sounding balloons, were necessary. The first such measurements were designed and carried out by Vernov in 1934.

At present, even more progressive methods of cosmic-ray research, using rockets and artificial satellites, are beginning to be applied successfully.

From the point of view of space physics, cosmic-ray research has as its goal the determination of: (1) the nature and the sources of cosmic rays of various energies; (2) the mechanisms of acceleration of the primaries in the galaxy; (3) the laws describing the spatial and temporal distributions of electromagnetic conditions in different parts of space.

The basic technique of such studies is the use of cosmic rays as a means for finding out about the physical state of the upper atmosphere and magnetosphere of the earth, the interplanetary space, the vicinity of the sun, and the galaxy as a whole.

From the experimental point of view, this means obtaining accurate data from continuous recordings over long periods of time (several decades, if possible). These recordings will be of the various parameters describing the flux of primaries over a very wide interval of the energy spectrum.

Experiments show that cosmic rays of galactic origin enter the solar system with intensities which are constant in time and with complete spatial isotropy. As a result, in spite of the great interest of variations in ultrahigh-energy particles (10^{13}–10^{20} eV), in this part of the spectrum it is unlikely that variations will occur with periods comparable to the time scales of terrestrial and solar phenomena.

Particles of lower energy, from a few BeV up to 10^{12} eV, undergo considerable spatial and temporal variations in intensity and in energy

spectrum. These variations take place according to terrestrial or even solar-system time scales. They are related to particle acceleration at the sun or else are produced by the modulation of galactic cosmic rays by electromagnetic fields in the interplanetary medium.

The temporal parameters of these variations are more accessible to a terrestrial observer than galactic times are, since primary particles of intermediate and high energy have low Larmor radii in comparison with ultrahigh-energy particles.

Studies of variations in cosmic rays of intermediate and high energy indicate a regular correlation between these cosmic rays and geophysical and solar phenomena. On the basis of such data, important dynamical and structural characteristics have been specified for the electromagnetic conditions in the vicinity of the earth, in interplanetary space at a distance of 1 A. U., and at the sun, during various stages of solar activity. One very significant outcome of these studies was the detection of large increases in cosmic-ray intensity accompanying solar chromospheric flares; in addition, the mechanism of solar modulation of galactic cosmic rays was discovered.

The flux variations for particles of intermediate and high energy give information concerning large-scale processes in the solar system and concerning the general structure of outer space. Analogously, studies of low-energy primaries should tell us about the fine structure of the magnetosphere and upper atmosphere of the earth and also about phenomena and inhomogeneities in the space around the sun (at a distance of 1 A.U.). The low-energy primaries can be used as a probing tool for a more thorough study of the following subjects: the space-time distribution and geometry of magnetic and electric fields; solar corpuscular streams; the nature and mechanism of terrestrial radiation belts; the characteristics of the interplanetary magnetic field; and the low-energy part of the galactic-cosmic-ray spectrum. This means of study should be quite effective, since it is now commonly assumed that low-energy particles are the main participants in cosmic-ray variations and that thus their variations should be particularly great.

There are two kinds of low-energy particles. The cosmic rays generated at the sun during flares generally include particles with momenta of 0.2 to 2.0 Bev/c (kinetic energy of protons from 20 MeV to 1 BeV). The lower energy limit for these particles is determined by their acceleration mechanism, by the escape from the sun's vicinity, and by the propagation earthward.

During a period of undisturbed solar activity, the plasma temperature in the solar supercorona (which is $\sim 10^5$°K) is sometimes assumed to determine the lower energy limit. This leads to the assumption that there is a continuous transition over the energy range from 10^5°K to 2 BeV.

The upper limit for solar cosmic particles is determined mainly by the dimensions and size of the region in which the acceleration originates.

When low-energy galactic cosmic rays are modulated, particles with momenta of 0.5 BeV/c and above undergo the greatest variations in intensity. The lower limit has not been established accurately, but the intensity of primaries with momenta of 0.5 BeV/c is known to be low. The upper limit is also quite arbitrary, but it can be assumed that the effect of solar modulation drops sharply for particles with energies above several BeV. Cases have been known in which galactic particles with momenta up to 800 BeV/c were subject to modulation. Studies of such variations are a

part of the physics of cosmic rays with intermediate and high energies, and special techniques, experiments, and theories are necessary.

Until 1950, only ionization chambers located near sea level were used to study cosmic-ray variations. Such detectors could not, of course, be used to record low-energy primary cosmic rays.

The situation did not change much when neutron monitors, which are about 50 times more sensitive to low-energy particles than ionization chambers are, were introduced in ground-level measurements of the variations. However, beginning in 1955, neutron monitors were used to record some cosmic-ray bursts which were genetically related to solar-activity displays; three of these recordings were made simultaneously with ionization chambers as well.

These first experimental data led to the general opinion that cosmic rays can be generated during solar flares only under very special, unusual circumstances.

This opinion was not refuted by the investigations of Pomerantz (1956) and Neher (1957). Their experiments did not indicate whether the results of the cosmic-ray measurements made by them with balloon-borne equipment differed from the results of ground-level measurements.

Beginning in 1957, especially after the detailed observations of solar cosmic rays at high latitudes made by Winckler and Anderson (USA) and by Charakhch'yan (USSR), it became clear that changes in the intensity of the low-energy component of the primary radiation were often unaccompanied by variations in the cosmic rays of intermediate and high energy. Also, it was found that studies of the primary flux in the energy range from 0 to 1 BeV imposed special requirements on the measuring equipment and on the observation site.

It turned out that particles with these energies can be found only at the limits of the atmosphere, over the polar caps of the planet (at the knee of the latitude cutoff), or outside of the earth's magnetosphere. At these places the lower energy limits for recorded particles are due only to the shielding effect of the instrument cases.

The penetration of these particles into the ionosphere produces secondary electrons there. In addition, ionospheric ionization, recombination, and capture take place, which in turn lead to polar blackouts and to the absorption of cosmic radio noise in definite parts of the radio-frequency range at altitudes of 50 to 100 km.

By means of riometers and ionospheric stations located in the polar latitudes, we can get an idea of the spatial and temporal morphology of these phenomena, in relation to fluctuations in the influx of solar protons with energies of 10 to 100 MeV, these being the cause of the electron maximum at the indicated level.

The latitude distribution of the absorption makes possible a rough estimate of the intensity and the energy characteristics of low-energy cosmic radiation.

Due to the residual atmosphere above high-latitude equipment, the sounding-balloon method now widely used to study low-energy cosmic rays makes it possible to measure particles of solar origin with energies of 100 MeV or more. At altitudes of 200 to 400 km over the geomagnetic poles, of course, the absolute intensity and the energy spectrum of primary cosmic rays can be determined for energies ranging from tens of electron volts to 10^8 electron volts; at these altitudes the temporal and spatial variations of this radiation can also be studied.

A basic stage in the study of cosmic-ray variations and their relations to various geophysical and solar phenomena is the statistical analysis of series of data on the intensity of the different cosmic-ray components, collected over many years.

This experimental material is being gathered by means of systematic, long-term, uninterrupted observations of cosmic rays of various energies. Only in this way is it possible to record the flux variations in cosmic rays of different intensity and direction which accompany solar flares, disturbances of the geomagnetic field, and other phenomena, since such flux variations are difficult to predict, are sudden, and have unexpected amplitudes.

Just as in ground-level experiments, the particle flux must also be recorded continuously during studies of variations in the low-energy primaries. However, in this case the measuring equipment must remain for an extended period in the upper strata of the atmosphere over the polar regions of our planet or else at some point in interplanetary space beyond the magnetosphere (from which the transmission of information to an earthbound observer by radio is reliable). This is an extremely difficult technical problem.

Considerable effort has been made recently to develop recorders which will operate in the stratosphere for long periods. Recorders borne aloft in rigid polyethylene jackets filled with hydrogen can "float" for many hours at altitudes of 25 to 30 km or even higher.

With the advent of artificial earth satellites, it became much easier, from the experimental point of view, to study the variations of low-energy cosmic rays. Studies of this kind were first attempted by the Soviet scientists working with Vernov, at the time of the launching of the first artificial satellite (1957). Later, such investigations were also initiated in America, by Rothwell and McIlwain (1959), and by Simpson, van Allen, Hoffman, and Winckler (1960).

These first experiments using artificial satellites, and also the many others which have been made up to the present, were mainly exploratory in nature.

Most such cosmic-ray research turned out to be devoted to the unexpectedly discovered radiation belts, and to the structure, composition, energy characteristics, nature, and formation mechanism of these belts. As a corollary of the uninterrupted studies of the radiation belts, scientists have recently begun to be interested in the structure of the interplanetary magnetic field, the solar wind, and the physics of solar phenomena. Studies of primary-radiation variations by means of continuous, long-term observations with artificial satellites, however, are still practically not made at all, in spite of the lack of the very important data on the variations of low-energy cosmic rays and on their spectra.

With the development of extra-atmospheric research, and after processing the enormous amount of data collected during the International Geophysical Year, it became clear that systematic launchings of artificial satellites with "polar" orbits were necessary for the study of low-energy cosmic rays. Here, a "polar" orbit is one which is inclined to the equatorial plane of the earth by not less than 80°. These satellites should have at least one Geiger counter on board. In addition to satellite flights, geophysical rockets should be launched sporadically, from points with geomagnetic latitudes of at least 70–75°, at the times of solar flares, geomagnetic storms, and other phenomena.

Cosmic-ray variations can probably be studied most effectively by means of simple, uniform, calibrated equipment making simultaneous measurements from two artificial satellites. These satellites will serve as cosmic-ray patrol stations revolving about the earth in different orbits.

One of these satellites will be "low," following a circular "polar" orbit at altitudes of 300 to 500 km. It should operate for at least a year. The other, "high," satellite, also moving along a circular "polar" orbit, will revolve about the earth beyond the limits of the magnetosphere. The "high" space station serving as this satellite can exist for as long as is thought necessary. Its service period will be limited only by the reserves of solar batteries, radio elements, and cosmic-ray detectors. With this in mind, all the equipment on board the satellite must be operated as economically as possible. This means that an efficient program for communications with a terrestrial observation point must be employed, implemented according to signals from automatic programming equipment on board the satellite. When additional information is required, it should be obtained via a control radio channel. Such a patrol-station system will probably be able to operate adequately for a few years. To ensure continuity of the measurements, similar satellites must be kept in readiness on the earth during operation of the space stations. It will be possible to launch these quite accurately into specified orbits at any time, in place of stations going out of operation or after the period of dependable service of the satellite has elapsed.

To study cosmic-ray variations by means of space stations, the equipment used must be simple, reliable, stable with respect to vibrational and line overloads, and compact. In addition, it should have low power consumption and minimum requirements with respect to telemetering channels for communication with points on the earth's surface.

Such studies using a patrol satellite can be made satisfactorily with a transducer assembly recording the number of particles and the ionization of the cosmic rays; provision should also be made for separate measurements of energies from 10^5 to 10^8 eV.

The following units are recommended as parts of the standard assembly: (a) an ionization chamber controlled by a single master Geiger counter; (b) a circular counter arrangement of coincidence telescopes, with a central shielded counter; (c) a rugged scintillation detector, mounted 2 or 3 meters away from the satellite on a special bar; (d) a single Geiger counter which records the intensity over a wide range (at least three orders of magnitude); and (e) a three-component magnetometer.

The ionization chamber measures the global cosmic-ray intensity according to the ionization current, which is produced mainly by penetrating particles. Due to the low gamma sensitivity of the chamber, when the satellite passes the outer radiation belt the γ-ray current will be less than 10% of the current set up by the primary radiation.

The circular arrangement measures the cosmic-ray intensity (number of particles) according to three energy cutoffs specified by the inner and outer shielding of the arrangement. The counter telescopes are also almost insensitive to γ rays and to x rays.

The scintillation detector measures the intensity and energy release of the flux of low-energy particles (electrons with energies of a few or some tens of keV).

To develop this detector assembly, experiments must first be made to determine the recording efficiency of each detector for γ rays, electrons, and protons at energies corresponding to the primaries studied. In addition, it is very important, as a preparation, to calibrate the satellite-borne equipment for the natural cosmic-radiation background and to compare the response of each unit with data from one of them chosen as a standard.

The use of such relatively simple, and thus reliable, equipment installed in patrol stations or other types of satellites will make available a large amount of important experimental data pertaining to cosmic-ray variations.

With proper pinpointing of the satellite in orbit (± 25 km in altitude and 1° in longitude and latitude), the "low" satellite can make use of the geomagnetic field as a spectrum analyzer for the magnetic rigidity. Data on the latitude distribution of the primary flux obtained in this way can then be used to evaluate the cosmic-ray energy spectrum. This spectrum will begin with the minimum energy of protons arriving to the limit of atmosphere at the geomagnetic equator and will end with the minimum energies of particles recorded by means of satellites over the polar regions of our planet.

It will also be possible to distinguish quite accurately periodic and irregular variations of the primary cosmic rays in discrete intervals of magnetic rigidity and to take the energy spectrum of these variations. Such measurements will be especially important during solar flares, magnetic storms, and Forbush decreases. A comparison of the data thus obtained with measurements of the undisturbed spectrum will indicate the spectral sensitivity of the mechanisms modulating these effects.

During intense magnetic storms, the patrol satellites will also be able to record changes in the geomagnetic cutoffs of cosmic rays, since any distortion of the geomagnetic field during a storm will affect the low-energy particles.

The position of the maximum in the differential spectrum of the primary flux gives us important information on the diffusion of cosmic rays through magnetic inhomogeneities in the solar system. This maximum can be specified only using satellites, geophysical rockets, or balloon-borne equipment. If it is found that the spectral maximum is not shifted into the low-energy range during years of solar minimum, this will tell us a great deal about the transformation of galactic cosmic rays in the solar system. The existence of such a shift, on the other hand, will indicate an energy dependence of the diffusion coefficient, within the framework of models of interplanetary space. Consequently, we will know something definite about the structure and dimensions of magnetic inhomogeneities and about the solar wind. Data of this kind will be especially valuable for checking different models of interplanetary space during periods of solar activity.

It will also be very important to verify the intensity rise in the low-energy part of the spectrum against the background of a Forbush decrease. Many authors have explained this increase as a change in the conditions for energy cutoff of the particle flux, as a result of distortion of the magnetic field during a storm. Usually, only the decrease in the field within the current ring responsible for the main phase of the storm is considered. Outside of this ring, the same current enhances the field. Therefore, the effective geomagnetic moment must then increase, while at the same time the energy limit for cutoff must be shifted to a high value, causing a drop in the cosmic-ray intensity.

Measurements of the Forbush effect in interplanetary space should help to explain the long recovery time after a Forbush decrease, and also to describe the leading edge of the flux. In addition, it is important to clarify the function of the earth and the moon as absorbers during the development of a Forbush decrease. If the Forbush effect is due to the diffusion of galactic cosmic rays in a turbulent cloud of magnetic plasma, then an appreciable gradient of the cosmic-ray density must exist in the vicinity of the earth and the moon, which are absorbing bodies. For the scattering of cosmic rays by the regular magnetic fields of the solar plasma, this phenomenon does not exist.

Measurements of the cosmic-ray density gradient far from the earth, either toward the sun or away from it or else perpendicular to the ecliptic plane, will be very useful. The results of such measurements, to their respective accuracies, may give information about the propagation of cosmic rays in the solar system, about the interplanetary heliocentric or other field, and about the presence or absence of a magnetic barrier shutting the solar system off from galactic cosmic rays. All this information is essential for checking different models of the interplanetary field and for evaluating solar-wind hypotheses. Finally, these data are necessary for the theory of the origin of cosmic rays and for studies of the 11-year variations.

The primary radiation in the low-energy part of the spectrum during periods of minimum solar activity is of particular interest. Since 1964 and 1965 constitute one of these periods, beginning on 1 January 1964 scientists of many lands will carry out extensive complex studies according to an internationally agreed-upon plan. Some of these will be studies of cosmic-ray variations.

Contrary to the period of solar maximum, during years of minimum activity inhomogeneities of various kinds and solar-activity effects in interplanetary space are relatively few. Therefore, it is natural to expect that at this time the spectrum of the primary flux in the vicinity of the earth will be moderated.

The considerable modification of the electromagnetic conditions in interplanetary space during this period can be judged according to the intensity variations of primaries with energies from 10^5 to 10^{12} eV. Thus, an analysis of the variations in low-energy particles gives us information on the fine structure of the circumsolar space out to 10^{10} or 10^{12} cm, while the variations in high-energy particles inform us about the general contours of space within a radius of 1 to 10 A.U.

At the minimum of the 11-year cycle, conditions are more favorable for studying the various types of irregular, periodic, and solar cosmic rays. This is because at other times, particularly in the years of maximum, much of the space in the solar system is full of inhomogeneities. These inhomogeneities may be turbulent or ordered, they may be local or may encompass considerable space, and they may be different in nature and character. Also, during the period of maximum, solar physical phenomena are superimposed on one another, and it is impossible to tell where one disturbance begins and another ends. Consequently, a strict classification of the different types of solar activity is impossible, and it is difficult to establish reliably the quantitative relations between solar activity and the phenomena studied in space physics and aeronomy.

During years of minimum activity, solar effects on cosmic rays and especially solar flares will be rare phenomena, and in the absence of disturbing factors they will show up particularly clearly against the background of low activity.

Measurements of all the characteristics of the relativistic particles produced by high acceleration in active regions of the sun are exceptionally important.

Solar cosmic rays mainly arrive at the earth when a chromospheric flare has occurred on the western side of the solar disk. The delay time for particle arrival at the earth increases with the distance of the flare from the western limb of the sun, and the time required to reach maximum intensity also increases.

It is important to find out whether all chromospheric flares produce cosmic rays. It may be that cosmic rays are always produced, but that conditions for particle escape from the solar atmosphere or particle propagation to the earth are not always favorable.

Cosmic-ray bursts can be studied effectively by means of satellite-borne equipment. This is because the rapid pass of the satellite through the space around the earth will make it possible to trace, with an as yet unattained accuracy, the so-called "entry zones" for solar cosmic rays, located at the limit of the terrestrial atmosphere. In this same experiment, it will be possible to find the latitude dependence of the burst effect, which will give information on the spectrum of the particles responsible for the cosmic-ray burst. The study of bursts of solar cosmic rays is very important for developing methods of predicting radiation danger.

Cosmic-ray studies at the time of the solar-activity minimum may make it possible to ascertain the cutoff limit of the spectrum in the low-energy range, in relation to the residual modulation of galactic cosmic rays by the interplanetary magnetic field. As a result, we may find out to what degree the primary radiation in the solar system indicates the composition and the energy spectrum of the galactic cosmic rays.

Data on the intensity, composition, energy spectra, and variations of α particles and other heavy primary nuclei are of great interest with respect to the origin of cosmic rays. Such data are obtainable only by means of rockets and artificial satellites. The first measurements of the nuclear component were made by Ginzburg during the flight of Sputnik III, made in 1959. From this, important information was gained on the latitude distribution of intensity for nuclei with $Z \geqslant 2$ and $Z \geqslant 5$. From 1959 to 1961, Winckler's group (USA) made some important studies of the nuclear composition of the primaries.

These and subsequent measurements were sporadic, and they were not designed to study intensity variations of the multiply charged component. However, it was still possible to record short-lived bursts of the fluxes of nuclei. So far, no more detailed data on variations of the nuclear component, and on the relation between changes in the primary-proton intensity and variations in the flux of the multiply charged component, have been obtained. Direct measurements of variations in the heavy primary nuclei during changes in the intensity of the general cosmic-ray flux, especially at the time of chromospheric flares, should provide valuable data on the solar accelerating and modulating mechanisms and on the nature of galactic cosmic rays.

Data on the maximum of the proton and α-particle spectra are also important. If these maxima will be observed for different rigidities, this may imply that cosmic rays originating in the galaxy undergo fragmentation on the way to the earth, as a result of which the secondary protons observed by us in cosmic rays are produced. If, however, the positions of these maxima will coincide, then there is no fragmentation. This effect should be studied for various levels of solar activity.

The proposed experiments using patrol satellites to investigate the variations of heavy nuclei can include simultaneous measurements of the primary radiation using ionization chambers and counter assemblies. The mean ionizing capacity of the primary flux is more than twice that of the relativistic particles. This is due to the presence of heavy nuclei in cosmic rays. The proposed experiment will make it possible to find the relation between the number of particles and their ionizing capacity, and from this the percent content of multiply charged particles in the primary flux as well.

Two questions arise in connection with the prospective implementation of an extensive study of the surroundings of the earth, the sun, and outer space using rockets and artificial satellites.

1. Will rocket and satellite studies of cosmic-ray variations in the near future eliminate analogous measurements at the earth's surface as being less effective?

2. Will the indirect method of space research by means of cosmic rays be replaced at some time by the direct measurement, with rocket-borne and satellite-borne equipment, of the state of the interplanetary plasma, the parameters of the electromagnetic fields, and the composition, geometry, and structure of the various inhomogeneities?

We assume that these two questions must be answered in the negative. For example, ground-level studies of cosmic rays cover a range of the energy spectrum (up to tens of BeV and above) which is unattainable using any airborne [or spaceborne] equipment. True, flux recordings for some primary particles, which are impossible at the earth's surface because of the shielding action of the atmosphere, must be obtained using stratospheric and extra-atmospheric methods. However, cosmic rays of higher energies can be studied only by means of super monitors located under the earth and at sea level. Such measurements should be made at different points throughout the world, using the geomagnetic field in the given case as a gigantic spectrum analyzer for the magnetic rigidity.

Now let us consider the possible elimination of variation studies as an indirect means of investigating the interplanetary plasma and earth-sun problems, and the replacement of this method by direct measurements of various space phenomena. With respect to this, a basic feature of cosmic-ray variations should be noted, namely that their study is apparently a unique and absolute means of obtaining high-accuracy, reliable, continuous measurements, on a patrol and global basis, of the electromagnetic conditions in the space surrounding our planet. It is impossible to fill the solar system with large numbers of rockets and satellites just in order to provide direct measurements of this type.

Institute of Space-Physics Research and Aeronomy, Yakutsk Branch of Siberian Division of USSR Academy of Sciences

V. V. Vitkevich

THE PREDOMINANTLY RADIAL MAGNETIC FIELD IN THE SPACE ABOUT THE SUN (Synopsis)

I. RESEARCH METHOD

1. It was noted by the author /1/ that one of the discrete radio-emission sources, the Crab Nebula, is covered each year by the solar corona. This unusual eclipse is observed in the middle of June. The distance of closest approach between the center of the sun and the source on 15 June is 4.5 $R_\odot$.

2. The selection of radio waves from the source, which approach against the background of the more intense solar radio emission, is based on a radio-interference method. A radio interferometer with a resolving power (angular distance between lobes) of 15' to 45' (200λ to 60λ) will respond only to the source, and it will usually not pick up the solar radio emission. This method was used by the author, and subsequently by several non-Soviet researchers, to study the space about the sun "by transillumination."

II. MAIN RESULTS

3. The first results obtained indicated an attenuation of the intensity of radio reception from the source (1951 data, and then subsequent data which were more reliable from the numerical point of view). More recent investigations by the author in the USSR /3/ (and similar results obtained in England by Hewish) have developed and refined these data. The influence of the "supercorona" was observed at distances of $10R_\odot$, then at $20R_\odot$ and $30R_\odot$, and now it has been detected up to 40 or 50 $R_\odot$. For an active sun the influence of the supercorona may even extend out to 100 $R_\odot$ on certain days (data of Slee, Australia).

4. Observations using two or three radio-interferometer bases of different lengths /4/ indicate that scattering of the radio waves takes place in the solar supercorona rather than damping. Consequently, the space about the sun is nonuniform, due to the electron production there (plasma production).

III. RADIAL INHOMOGENEITIES. THE MAGNETIC FIELD

5. Vitkevich and Panovkin /5, 6/ were the first to demonstrate the "elongation" of the inhomogeneities, which are roughly radial in orientation.

This result was obtained from measurements of the effect of scattering in different directions; for these measurements, an interferometer oriented in various ways to the meridian was used.

6. Electron inhomogeneities in the form of "jets" could not exist long if their corresponding magnetic field did not prevent them from diffusing. The magnetic field in the space about the sun is predominantly radial, with a structure generally the same as the inhomogeneities. The magnetic field keeps the radial electron inhomogeneities from dispersing.

In the vicinity of the photosphere, the field cannot be more than 0.1 oersted. Thus, for a square-law decrease, at $30\,R_\odot$ the field strength will be about 10^{-4} oersted.

IV. THE NATURE OF THE MAGNETIC FIELD

7. Two factors are apparently responsible for the radial magnetic fields. On one hand, as observed by Piddington, solar flares (in which the kinetic energy of the matter may be higher than the magnetic energy) produce enormous radial magnetic "loops." Apparently, this effect really takes place. On the other hand, such an explanation does not apply to the circumpolar regions of the sun, where the structure of the plasma is also nonuniform.

8. In the polar regions, the formation of extended inhomogeneities apparently is inherently different. According to the author's analysis, the solar magnetic field is basically a dipole field. The motion of plasma in the corona at velocities of 2 or 3 km/sec (such velocities are usually observed in the corona during eclipses, by means of the Doppler effect) ensures a kinetic energy of $\frac{SV^2}{2} \approx \frac{H^2}{8\pi}$. Because of this motion, the plasmas deform the magnetic field, transforming it from a "dipole" field to a nearly dipole field, and then to a radial field. Such is the probable nature of the second component of the magnetic field in the solar supercorona.

V. DEVIATIONS FROM THE PICTURE OF A "QUIET" SUPERCORONA

Sometimes sudden irregular phenomena are observed during studies using the "transillumination" method:

9. Refraction of radio waves, which in some cases may be as much as 30' for a 5-meter wave. The refraction is caused by coronal rays which penetrate into the supercorona and have an electron concentration an order of magnitude higher than the "background." The magnetic field confining the coronal rays is apparently higher than the "average" field in the supercorona.

10. Rapid changes in signal amplitude, caused by plasma motions with velocities up to 2000 km/sec and above.

11. Scattering at distances up to $100\,R_\odot$ (observed by Slee in Australia), apparently due to corpuscular streams.

All these electron-production phenomena are related to the corresponding structure of the magnetic fields. However, these problems are still far from being worked out and require more study.

The radial nature of the magnetic field detected by radio-astronomical research is an important key to understanding a number of physical processes in the space about the sun. In particular, the radial magnetic field affects the dynamics of both solar and galactic cosmic rays. This problem is posed and in part solved in the following report by Shishov.

P. N. Lebedev Institute of Physics of
the USSR Academy of Sciences.

REFERENCES

1. VITKEVICH, V. V. – DAN SSSR, **77**, No. 4, 1951.
2. VITKEVICH, V. V. – DAN SSSR, **101**, No. 3, 1955.
3. VITKEVICH, V. V. – AZh, **35**, No. 1, 1958.
4. VITKEVICH, V. V. – AZh, **38**, No. 1, 1960.
5. VITKEVICH, V. V. and B. N. PANOVKIN. – AZh, **36**, No. 3, 1959.
6. VITKEVICH, V. V. and N. A. LOTOVA. – Izvestiya vysshikh uchebnykh zavedenii, Radiofizika, No. 5, 1961.

V.I. Shishov

THE INFLUENCE OF THE RADIAL MAGNETIC FIELD ON THE DIFFUSION OF COSMIC RAYS (Synopsis)

1. Recently many works have appeared giving data which indicate that approximately radial, somewhat twisted, magnetic fields exist in interplanetary space, in addition to random fields. These data are listed briefly below:

a) electron inhomogeneities observed during eclipse of the Crab Nebula by the solar supercorona are extended in a predominantly radial direction /1, 2/;

b) solar flares accompanied by cosmic-ray bursts are grouped together more toward the western limb of the solar disk. Cosmic rays produced on the western side of the disk arrive at the earth much more rapidly than rays produced on the eastern side (see, for example, /3, 4/), the impact zones being clearly pronounced only for the former /5/.

2. Let us consider that a radial magnetic field with a strength $H(r)$, where r is the distance from the sun, exists in interplanetary space. In addition, magnetic inhomogeneities are present at which cosmic particles are scattered isotropically. The influence of the radial field will be effective only for $\omega > \frac{1}{\tau}$ (where $\omega = \frac{eH}{mc}$ and τ is the constant time for transit of the mean free path). Since ω decreases with the distance from the sun, the domain of this influence is limited by some surface at $r = R$.

With reference to a flare, let us assume that at a moment $t = 0$ N relativistic particles are ejected from a point on the surface of the sun; the particles are ejected radially, and each has the same velocity v.

3. We denote as $n(r, \theta, t)$ the particle density at a point with coordinates r and θ (where θ is the angular coordinate reckoned from the direction of initial escape of the particle). For $r > R$ the function $n(r, \theta, t)$ must satisfy the ordinary diffusion equation. For $r < R$, however, $n(r, \theta, t)$ obeys the equation:

$$\frac{\partial (r^2 n)}{\partial t} = D_r \frac{\partial^2 (r^2 n)}{\partial r^2} + D_\theta \frac{1}{\sin\theta} \frac{\partial}{\partial \theta} \sin\theta \frac{\partial (r^2 n)}{\partial \theta}; \qquad (1)$$

where

$$D_r = \frac{v \cdot l}{3}; \quad D_\theta = \frac{\rho^2}{3r^2\tau}, \text{ and } \rho = \frac{v}{\omega}.$$

The following conditions apply to this equation:

$$SndV = N; \qquad (2)$$

$$n_{t=0} = \frac{1}{4\pi l}\,\delta\left(\frac{(r-R_\odot)}{l}\right)\delta\left(1-\cos\theta\right)\frac{1}{r^2}, \tag{3}$$

where $l = v \cdot \tau$.

If we take D_θ=constant, that is, if we choose some effective value $\bar{D}_\theta$, then we can separate the variables r and θ:

$$n = \Psi(\theta, t)\cdot T(r, t). \tag{4}$$

For $r > R$, the function $T(r, t)$ is a spherical-symmetric solution of the diffusion equation. For $\frac{1}{4\bar{D}_\theta} > t$ and $\theta < 1$, the function $\Psi(\theta, t)$ is

$$\Psi = \frac{1}{4\bar{D}_\theta t}\exp\left(-\frac{\theta^2}{4\bar{D}_\theta t}\right). \tag{5}$$

For large t, the function Ψ can be expanded in terms of Legendre polynomials:

$$\Psi = \sum_{k=1}^{\infty}(2k+1)\,P_k(\cos\theta)\,e^{-k(k+1)\bar{D}_\theta t}. \tag{6}$$

Within certain limits the formula

$$t_{\max} = \frac{1}{10}\left[\frac{(r-R_\odot)^2}{D_r} + \frac{\theta^2}{\bar{D}_\theta}\right] \tag{7}$$

is valid, where $t_{\max}$ is the time at which the particle-density maximum occurs at the point with coordinates r and θ.

4. If the twisting of the magnetic field is roughly taken into account, θ must be replaced by $|\theta \pm \theta_0|$ (where plus corresponds to the eastern side and minus to the western side). Here, θ_0 is the angle between the direction of the force line of the regular field at the point of particle ejection and the direction toward the intersection point of this line and the surface $r = R$.

5. Comparison with experimental data on the time of maximum particle density as a function of the heliographic longitude of a flare /3/ gives $\theta_0 = 75°$; $\frac{1}{D_\theta}$=300 minutes; and $\bar{D}_\theta \approx \frac{D_\theta}{2}\Big|_{r=R}$ for $H \sim \frac{1}{r^2}$. Since $\frac{A^2}{D_r} \approx$ $\approx$200 minutes, therefore

$$R = 0.8\cdot A;\quad H|_{r=A} = H_0 = 7\cdot 10^{-6}\ \text{gauss}\ \ (A = 1\,\text{A.U.}).$$

According to theory, for a flare on the western side of the sun, the drop after the maximum should be sharper than in the spherical-symmetric case. This was actually observed for the flare of 4 May 1960 in the energy range from 1 to 2 BeV /6/. Matching of the theoretical curve with the observations gave $l = 5\cdot 10^{12}$ cm and $H_0 = 4\cdot 10^{-7}$ gauss.

Flares on the eastern side of the sun, on the other hand, should have a wide, diffuse maximum. This was observed for the flare on 3 September 1960 (for protons with energies around 100 MeV) /7/. The values $l = 1.3\cdot 10^{12}$ cm and $H_0 = 8\cdot 10^{-7}$ gauss gave a satisfactory fit with the observations.

The difference between the value of the field (according to the 1960 flares) and the average field strength obtained from the dependence of the delay time on the heliographic longitude of the flare may be attributed to the fact that the conditions in the interplanetary medium in 1960 were not average.

Therefore, on the average, $H = 5 \cdot 10^{-6}$ gauss near the earth's orbit and $H = 0,1$ gauss at the surface of the sun.

P. N. Lebedev Institute of Physics of
the USSR Academy of Sciences

REFERENCES

1. VITKEVICH, V. V. and B. N. PANOVKIN. – AZh, **36**, 544. 1959.
2. ERICKSON, W. C. – Astron. J., **67**, No. 2. 1962.
3. ELLISON, M. A., S. M. P. McKENNA, and J. H. REID. – Dunsink Observatory Publications, **1**, No. 3. 1962.
4. DVORYASHIN, A. S., L. S. LEVITSKII, and A. K. PANKRATOV. – Izv. KAO, **26**, 90. 1961.
5. McCRACKEN, K. G. – J. Geophys. Res., **67**, 447. 1962.
6. STEPANYAN, A. A. – Izv. KAO, 178. 1962.
7. CHARAKHCH'YAN, A. N., V. F. TULINOV, and T. N. CHARAKHCH'YAN. – ZhETF, **41**, 735. 1961.

N67 38207

A.A. Pomanskii and O.I. Dovzhenko

THE RADIATION LENGTH

I. INTRODUCTION

In processes related to the passage of high-energy electrons and photons through matter, the energy losses are mainly caused by bremsstrahlung and pair production, respectively. In this case, the mean free paths of the particles can be expressed conveniently in so-called radiation, or cascade, units of length.* The introduction of such a unit makes it possible to solve the cascade equations in a form which is independent of the substance in which the electron-photon shower develops /1/.

The advisability of adopting the cascade unit becomes evident from a consideration of the cross sections for bremsstrahlung and electron-positron pair production. Actually, at high energies ($E \gg mc^2$), when these two processes will occur mainly at large distances from a nucleus, the screening of the field of the nucleus by the field of atomic electrons may be considered to be total (this case is the most important for studies of cascade processes). Then, the effective cross sections for bremsstrahlung and pair production, according to the Born approximation, are given by Bethe and Heitler /2, 3/ as:

$$d\sigma_{rad} = 4\frac{N}{A}\alpha r_0^2 Z^2 \frac{d\nu}{\nu E_0^2}\left[\left(E_0^2 + E^2 - \frac{2}{3}E_0E\right)L^{rad} + \frac{1}{9}E_0E\right]; \qquad (1)$$

$$d\sigma_{pair} = 4\frac{N}{A}\alpha r_0^2 Z^2 \frac{dE_+}{\nu^3}\left[\left(E_+^2 + E_-^2 + \frac{2}{3}E_+E_-\right)L^{rad} - \frac{1}{9}E_+E_-\right], \qquad (2)$$

where ν is the energy of a γ quantum; E_0 and E in (1) are the electron energies in the initial and final states of the bremsstrahlung; E_+ and E_- in (2) are the energies of the positron and the electron, respectively; $\alpha = \frac{e^2}{\hbar c} = \frac{1}{137}$; $r_0 = \frac{e^2}{mc^2}$ is the "classical radius" of the electron; N is Avogadro's number; A is the atomic weight; and L^{rad} is the so-called radiation logarithm, which determines the effect of total screening of the field of the nucleus by the field of atomic electrons.

Following Carlson and Oppenheimer /1/, we define the cascade unit t_0 as

$$\frac{1}{t_0} = 4\frac{N}{A}\alpha r_0^2 Z^2 L^{rad}. \qquad (3)$$

The effective cross sections, $d\sigma^t_{rad}$ of bremsstrahlung (1) and $d\sigma^t_{pair}$ of pair production (2), in cascade units are then

$$d\sigma^t_{rad} = \frac{d\nu}{E_0^2\nu}\left[E_0^2 + E^2 - E_0E\left(\frac{2}{3} - 2b\right)\right]; \qquad (4)$$

* [The radiation length, or cascade unit, is alternatively known as the shower unit.]

$$d\sigma'_{pair} = \frac{dE_+}{\nu^3}\left[E_+^2 + E_-^2 + E_+E_-\left(\frac{2}{3} - 2b\right)\right], \qquad (5)$$

where

$$b = \frac{1}{18L^{rad}} \sim 10^{-2}.$$

It can be shown /4/ that when an electron penetrates one cascade unit of matter its energy falls, on the average, to $1/e$ of its original value, due to bremsstrahlung. Similarly, the intensity of a photon beam is reduced to approximately 1/2.2 of its original value over one cascade unit, due to pair production.

Expression (3) for t_0 was written assuming that the Born approximation is valid and that bremsstrahlung and pair production take place only in the field of the nucleus. However, as will be shown below, the Born approximation gives values of the cascade units for heavy elements which are $\sim 10\%$ too low. The following expressions for $d\sigma_{rad}$ and $d\sigma_{pair}$, incorporating corrections to the Born approximation for the case of total screening, are more accurate /5/:

$$d\sigma_{rad} = 4\frac{N}{A}\alpha r_0^2 Z^2 \frac{d\nu}{\nu E_0^2}\left[\left(E_0^2 + E^2 - \frac{2}{3}E_0E\right)\{L^{rad} - f(z)\} + \frac{1}{9}E_0E\right]; \qquad (6)$$

$$d\sigma_{pair} = 4\frac{N}{A}\alpha r_0^2 Z^2 \frac{dE_+}{\nu^3}\left[\left(E_+^2 + E_-^2 + \frac{2}{3}E_+E_-\right)\{L^{rad} - f(z)\} - \frac{1}{9}E_+E_-\right], \qquad (7)$$

where $f(z)$ is the correction for the inaccuracy of the Born approximation and all the other quantities are the same as in (1) and (2).

For bremsstrahlung and pair production in a field of atomic electrons, the following expressions give the corresponding cross sections /6/:

$$d\sigma^e_{rad} = 4\frac{N}{A}Z\alpha r_0^2 \frac{d\nu}{\nu E_0^2}\left[\left(E_0^2 + E^2 - \frac{2}{3}E_0E\right)l^{rad} + \frac{1}{9}E_0E\right]; \qquad (8)$$

$$d\sigma^e_{pair} = 4\frac{N}{A}Z\alpha r_0^2 \frac{dE_+}{\nu^3}\left[\left(E_+^2 + E_-^2 + \frac{2}{3}E_+E_-\right)l^{rad} - \frac{1}{9}E_+E_-\right], \qquad (9)$$

where l^{rad} is a quantity taking into account the screening (it is analogous to L^{rad}).

By combining equations (6) through (9), we obtain the total cross sections:

$$d\sigma^{tot}_{rad} = 4\frac{N}{A}\alpha r_0^2 Z(Z+\zeta)\left[\left(E_0^2 + E^2 - \frac{2}{3}E_0E\right)\{L^{rad} - f(z)\} + \frac{1}{9}E_0E\frac{Z+1}{Z+\zeta}\right]\frac{d\nu}{\nu E_0^2}; \qquad (10)$$

$$d\sigma^{tot}_{pair} = 4\frac{N}{A}\alpha r_0^2 Z(Z+\zeta)\left[E_+^2 + E_-^2 + \frac{2}{3}E_+E_-\right)\{L^{rad} - f(z)\} - \frac{1}{9}E_+E_-\frac{Z+1}{Z+\zeta}\Big]\frac{dE_+}{\nu^3}, \qquad (11)$$

where

$$\zeta = \frac{l^{rad}}{L^{rad} - f(z)}.$$

Taking into account the corrections for inaccuracy of the Born approximation and for the effects of a field of atomic electrons, we can define the cascade unit by the expression

$$\frac{1}{t_0} = 4\frac{N}{A}\alpha r_0^2 Z(Z+\zeta)[L^{rad} - f(z)]. \qquad (12)$$

Consequently, cross sections (10) and (11), in terms of the cascade unit (12), may be described by equations (4) and (5) provided b is replaced by

$$b' = \frac{Z+1}{Z+\zeta} \cdot \frac{1}{18\,|L^{rad} - f(z)|} . \qquad (13)$$

In the calculations of cascade units made by different authors, the influence of total screening of processes in a field of atomic electrons and the inaccuracy of the Born approximation were allowed for differently. This led to discrepancies of ~ 10 to 20% in the values of the cascade units. Such a large discrepancy can distort considerably the interpretation of experimental results on the interactions of high-energy particles ($E \gg mc^2$) with matter.

In this report, the reasons for these discrepancies will be analyzed in detail. In addition, the values of the cascade units which are most accurate in the light of recent theoretical and experimental results will be given.

II. THE RADIATION LOGARITHM

As we have seen, the quantity $L^{rad} = \int_0^{mc/\hbar} [1 - F(q)]^2 \frac{dq}{q} + 1$, the radiation logarithm, enters into the expression for the cascade unit and allows for the effect of total screening. The radiation logarithm depends on $F(q)$, the atomic form factor (a function of the atomic scattering), which provides a measure of the amplitude of the scattered wave produced when radiation of a given amplitude encounters an atom. The amplitude of the scattering at a free classical electron is usually taken as the amplitude unit for the scattered radiation. Although electrons in an atom cannot be considered completely free, they are so weakly bound to the atom that they scatter radiation like free electrons. In addition, the amplitude of the radiation scattered by a given atom can be assumed to be Z times the amplitude of the scattering by a single classical electron under the same conditions. For radiation with a frequency higher than any of the atomic-absorption frequencies and for small scattering angles, the value of $f(q)$* is close to the number of electrons in the atom (Z). With an increase in the scattering angle, however, the form factor drops rapidly, the nature of the drop being a function of the distribution of electrons in the atom.

For scattering in the direction of the incident radiation, there will be no path difference for waves scattered by electrons in different parts of the atom. If we assume that the electrons in an atom are weakly bound, then the phase variation during scattering will be the same for each electron, and the amplitude of the wave scattered by an atom will be Z times the amplitude of the wave scattered by an individual electron.

If the direction of the scattered radiation lies at some angle to the direction of the incident radiation, there will be a difference in path for waves scattered by electrons in different parts of the atom. Thus, interference of these waves will make the resultant scattering amplitude less than Z times the amplitude of the scattering at a single electron.

* Here and in the following, $F(q) = \frac{f(q)}{Z}$.

If $D(r)$ is a function characterizing the spatial distribution of electrons in the atom, and dv is a volume element of the atom, then the scattering power of this volume element will be proportional to $D(r)dv$. Let us assume that a wave $e^{i(\vec{K}_0\vec{r})}$ impinges upon an atom, where $\vec{K}_0$ is the wave vector, with a modulus $|K_0| = \frac{2\pi}{\lambda}$. The wave vector of the scattered wave is $\vec{K}$. Since the incident wave $e^{i(\vec{K}_0\vec{r})}$ arrives at points r_1 and r_2 with different phases (Figure 1), the scattered waves $e^{i(\vec{K}\vec{r}_i)}$ leaving these points and observed at a distant point with $R \gg r$ will have different phases. The phase difference is $r(K-K_0)$. For elastic scattering $q = |K - K_0| = 4\pi\frac{\sin\theta}{\lambda}$ (see Figure 2), where θ is the scattering half-angle.

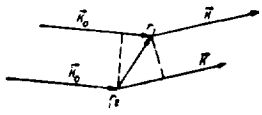

FIGURE 1.

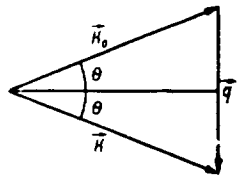

FIGURE 2.

In order to obtain the amplitude of the scattering from the entire volume, the scattered elementary waves $e^{i(\vec{K}-\vec{K}_0)\vec{r}}$ with amplitudes proportional to $D(r)$ must be integrated over all the volume elements (actually, over all the electrons in the atom).

Therefore, the amplitude of atomic scattering is given by the Fourier integral $f = \int D(r)e^{i(\vec{K}-\vec{K}_0)\vec{r}}dv$, where the integral is over the entire volume of a single atom. Let us make the trivial assumption that $D(r)$ depends only on $|\vec{r}|$, and not on the direction of $\vec{r}$. In this case the atom may be considered on the average to be spherically symmetric. After some elementary operations, we find that $f(q) = \int_0^\infty D(r)\frac{\mathrm{Sin}\, qr}{qr}dr$, where $q = 4\pi\frac{\mathrm{Sin}\,\theta}{\lambda}$.

Consequently, if $D(r) = 4\pi r^2\rho(r)$ is known (where $\rho(r)$ is the number of electrons per unit volume at a distance r from the nucleus), the function $f(q)$ can be calculated for any q. Also, by using the reversibility property of the Fourier integral, it is possible to calculate the distribution of electrons in the atom when experimental data on the scattering of X rays are available:

$$D(r) = \frac{2r}{\pi}\int_0^\infty qf(q)\sin qr\,dq.$$

A comparison of the distribution thus obtained with the distribution calculated theoretically provides a check of the reliability of the theoretical premises.

L^{rad} was first evaluated by Bethe /2/. He calculated $F(q)$ using the statistical model of Thomas and Fermi /8, 7/, which gives the following expression for the electron density in an atom:

$$\rho = \frac{Z}{4\pi\mu^3}\left(\frac{\Phi}{\varkappa}\right)^3 = \frac{Z}{4\pi\mu^3}\cdot\frac{\Phi^3}{\varkappa},$$

where the function Φ satisfies the equation $\Phi'' = \frac{\Phi^{3/2}}{x^{1/2}}$ with boundary conditions $\Phi(0) = 1$ and $\Phi(\infty) = \Phi'(\infty) = 0$. Here $x = \frac{r}{\mu}$, $\mu = \mu_0 Z^{-1/3}$, $\mu_0 = \frac{(3\pi)^{2/3}}{2^{7/3}} a_0$, and a_0 is the radius of the hydrogen atom.

Bethe introduced the variable $\xi = \frac{\sin\theta}{\lambda} Z^{-1/3} \cdot 10^{-8}$, so that $F(q)$ was a function only of $q\mu = 5.887\xi$ and not of Z and $\frac{\sin\theta}{\lambda}$ separately. Then, he calculated /9/ the atomic form factor $F_{T\text{-}F}$ on the basis of the Thomas-Fermi model up to values of $\xi = 0.5$. The value of L^{rad} obtained by Bethe /2/ was $\ln(183 Z^{-1/3})$. Subsequent calculations /10, 11/ of L^{rad} according to the Thomas-Fermi model gave a value of $L^{rad}_{T\text{-}F}$ closer to $\ln(190 Z^{-1/3})$. Our calculations of $L^{rad}_{T\text{-}F}$ using accurate values of Φ and Φ' obtained recently /12/ gave $L^{rad}_{T\text{-}F} = \ln(191 Z^{-1/3})$, the same value as obtained by Kirpichev and Pomeranchuk /10/. The Fourier integral $F(q) = \frac{1}{Z}\int_0^\infty D(r)\frac{\sin qr}{qr} dr$ was calculated by us graphically. The values of $F_{T\text{-}F}$ for certain ξ were compared with the values computed using Filon's method /13/.

Rossi and Greisen /14/ used the value $L^{rad}_{T\text{-}F} = \ln(183 Z^{-1/3})$ to calculate the cascade unit. Then, Kirpichev and Pomeranchuk /10/ demonstrated that the Thomas-Fermi method is inapplicable to light elements. They suggested computing L^{rad} using experimental values of the atomic form factor, obtained from studies of X-ray scattering. For calculating the radiation logarithm, these authors used data on the atomic form factor cited in a 1931 handbook /15/. The radiation logarithms calculated on the basis of the Thomas-Fermi model and according to the form-factor data used by Kirpichev and Pomeranchuk differed by about 10%. Consequently, Belen'kii raised the theoretical (Thomas-Fermi) value of the radiation logarithm by 10% for all elements, and on the basis of this constructed a table of the cascade units /4/. Therefore, Belen'kii's cascade units were about 10% less than the values given by Rossi and Greisen.

This difference was assumed by Belen'kii to be the same for both light and heavy elements, irrespective of the fact that, the more electrons there are in an atom, the better will the Thomas-Fermi model serve as an approximation. However, the data used by Kirpichev and Pomeranchuk did not agree with theory either, at any rate not for higher Z.

Let us consider the data on the atomic form factor used by Kirpichev and Pomeranchuk more closely. The table of values of $f(q)$ in handbook /15/ was taken from Bragg and West /16/. When these data are used, it must be kept in mind that in crystal-structure analysis estimates of the scattering by the various atoms in the crystal lattice are necessary. Such estimates are useful for comparing experimental values of $f(q)$ with values calculated for the structure in question. The f curves (expressing the atomic form factor as a function of $\frac{\sin\theta}{\lambda} \cdot 10^{-8}$) which are valid for atoms or ions must be modified for the direct observation of scattering by crystals. This modification is related to the thermal oscillations of atoms in a crystal lattice, to the zero-point energy of the lattice, and also to the overlapping of the lattice atoms.* These factors reduce the observed values

* Here, the term "overlapping" refers to cases when the very same electrons are present in the shells of different atoms in the crystal lattice.

of $f(q)$ in comparison to the true values; the greater $\frac{\sin\theta}{\lambda}$ is, the more this reduction will be. Moreover, in nonisotropic crystals the reduction of $f(q)$ will also be affected by extinction phenomena.* Overlapping of the atoms in crystals has a very small effect on the value of the radiation logarithm, since the difference between f curves for a given element and its ions becomes appreciable only for very low values of $\frac{\sin\theta}{\lambda}$ (see Table 1). This

TABLE 1. Values of $f(q)$ for Ag, Ag^-, Ag^{--}, and Ag^{---}

$\frac{\sin\theta}{\lambda}\cdot 10^{-8}$	0.00	0.1	0.2	0.3	0.4	0.5	0.6	0.7
Ag	47.00	43.63	37.57	32.44	28.16	24.71	21.85	19.50
Ag^-	46.00	43.37	37.71	32.38	28.18	24.70	21.85	19.50
Ag^{--}	46.00	42.85	37.79	32.44	28.13	24.72	21.86	19.49
Ag^{---}	44.00	42.19	37.72	32.56	28.13	24.68	21.88	19.50

is related to the weakening of the effect of the outer electrons upon the f curve as $\frac{\sin\theta}{\lambda}$ increases (see Figure 3). The figure shows: (a) a schematic curve of the electron distribution in the argon atom, as a function of r; and (b) the corresponding atomic form factor as a function of $4\pi\frac{\sin\theta}{\lambda}$.

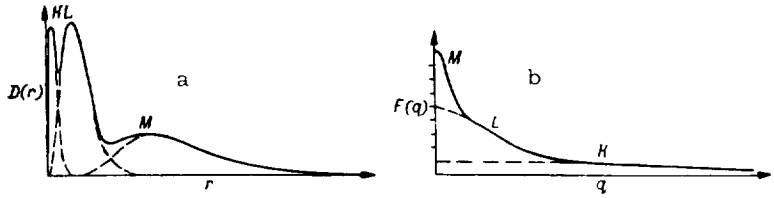

FIGURE 3. Curve a: schematic representation of radial distribution of electrons in an atom with $2K$ electrons, $8L$ electrons, and $8M$ electrons; curve b: the corresponding atomic form factor.

Calculations indicate that this difference in $f(q)$ has practically no effect on the value of the radiation logarithm. Therefore, the shape of the f curve (and thus the value of L^{rad}) is affected only by the inner electrons, which are not influenced by the chemical bonds of the atom.

As a result of thermal motion of atoms in the lattice, the f curves for scattering by crystals will drop more steeply with a rise in $\frac{\sin\theta}{\lambda}$ than the curves for free atoms. This is because the thermal vibration of the atoms in a crystal affects the mean distribution of the charge density. Moreover, for large scattering angles the radiation intensity will be very low, so that the measurement errors will grow with an increase in $\frac{\sin\theta}{\lambda}$. Thus, in studies of crystal structure two alternatives are possible. First, the calculated f curves can be used and a more rapid drop in f can be expected, as $\frac{\sin\theta}{\lambda}\cdot 10^{-8}$ increases, than is indicated by theory. Second, it is possible

* In crystallography, extinction usually refers to attenuation of the incident and reflected radiation, due to reflections from nonparallel crystal planes.

to modify the f curves beforehand in such a way that the properties of scattering by crystals will be taken into account and the curves can be used subsequently to analyze an experiment. Bragg and West chose this second alternative, when they constructed f curves on the basis of their empirical estimates of the scattering. They did not introduce corrections for the above-mentioned factors distorting the shape of the f curves, in particular for the thermal motion of the atoms in the crystal lattice. Therefore, the data used by Kirpichev and Pomeranchuk are actually not the results of experimental measurements of the atomic form factor. Rather, they are a set of $f(q)$ values which are practically useful for analyzing experiments in crystal-structure research.

It had been shown even earlier than this /17/ that the f curves calculated using Hartree's method fit the experimental curves very accurately, provided the latter were corrected for extinction, the zero-point energy of the lattice, and thermal motion. Since experimental techniques at that time were not very accurate, in their article Bragg and West stressed that the good agreement between the experimental and theoretical results proved the reliability of the methods used for the quantitative measurements, and also that the f curves calculated using Hartree's model portray the atomic scattering accurately. It should also be noted that the values of $f(q)$ used by Kirpichev and Pomeranchuk applied only to values of $\frac{\sin\theta}{\lambda} \cdot 10^{-8}$ up to 1.3, whereas $f(q)$ for considerably higher values of $\frac{\sin\theta}{\lambda} \cdot 10^{-8}$ should be known in order to integrate with an accuracy up to a percent (as was done by Kirpichev and Pomeranchuk).

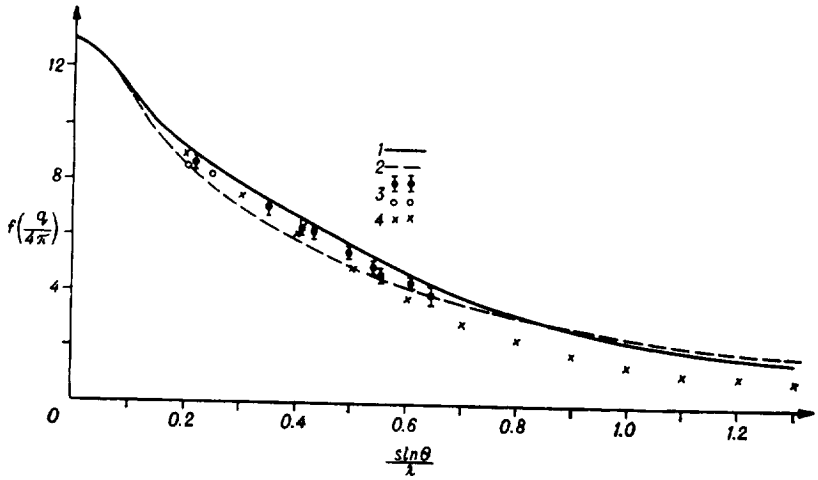

FIGURE 4. A comparison of experimental and theoretical data for the atomic form factor of aluminum $f = f\left(\frac{\sin\theta}{\lambda}\right)$: 1–Hartree-Fok model; 2–Thomas-Fermi model; 3–experiment /21–24, 26/; 4–Bragg and West /16/.

Using the experimental techniques of those years, perfectly accurate values of the atomic-scattering amplitude were not sought. Only an overall, mainly qualitative, study of the function $f = f(q)$ was necessary. Nevertheless, most of the experiments made at that time still verified the

applicability of the method of the self-consistent field to calculations of the atomic-scattering amplitude /18/.

In the experimental determination of $f(q)$, sometimes the same authors have obtained different results using different techniques /19, 20, 22, 26/. After due consideration, we have decided that the data (obtained using a powder rather than crystals) which agree with the calculations of the atomic form factor using the Hartree-Fok method are valid.

During the last decade several experiments were made to determine the amplitude of atomic scattering /22–26/ in various substances. In most cases the scattering materials were in powder form; special consideration was given to preparing the powder, which was cold-pressed into disks and then carefully buffed. In addition, very accurate measurements were made of the intensity of the radiation source, which was chosen to be as monochromatic as possible. The results of these experiments /21–24, 26/, for scattering from aluminum and iron samples, are shown in Figures 4 and 5. The figures give the f curves calculated using the Hartree-Fok model ($f_{H\text{-}F}$), taking into account exchange, and using the Thomas-Fermi model ($f_{T\text{-}F}$). The data of Bragg and West used by Kirpichev and Pomeranchuk ($f_{K\text{-}P}$) are also plotted in each figure. It is clear that:

1) the discrepancy between $f_{T\text{-}F}$ and $f_{H\text{-}F}$ is considerably less than that between $f_{H\text{-}F}$ and $f_{K\text{-}P}$;

2) as $\frac{\sin\theta}{\lambda} \cdot 10^{-8}$ increases, f_{exp}, $f_{T\text{-}F}$ and $f_{H\text{-}F}$ approach one another, while $f_{K\text{-}P}$ deviates from these;

3) f_{exp} in general agrees with $f_{H\text{-}F}$;

4) as Z increases, f_{exp}, $f_{T\text{-}F}$ and $f_{H\text{-}F}$ approach one another.

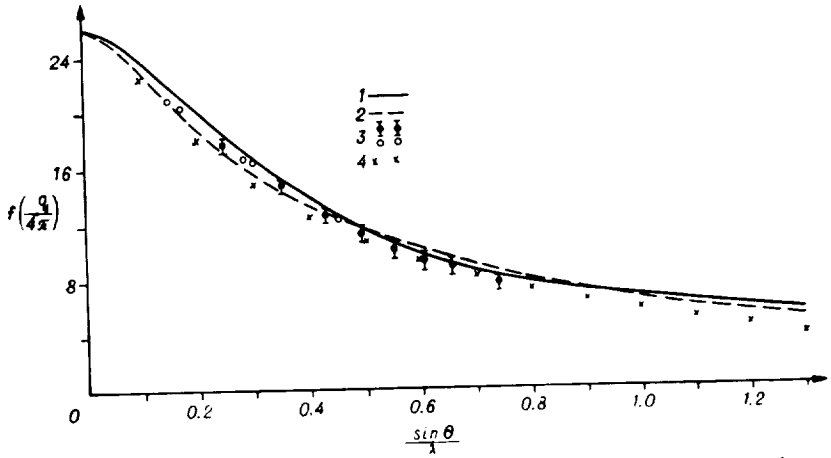

FIGURE 5. A comparison of experimental and theoretical data for the atomic form factor of iron $f = f\left(\frac{\sin\theta}{\lambda}\right)$: 1–Hartree-Fok model; 2–Thomas-Fermi model; 3–experiment /21–24, 26/; 4–Bragg and West /16/.

To complete our survey of the available experimental data on the determination of the atomic form factors, let us turn to a study /27/ in which $f(q)$ was found from experimental data on the diffraction of electrons. As early

as 1930, Compton showed /28/ that the technical difficulties related to the study of X-ray scattering by crystals can be avoided if $f(q)$ is determined from the scattering of X rays by the atoms of a rarefied gas. However, this method also involves certain difficulties: the accuracy of measurements of the intensity as a function of the scattering angle must be higher, and the radiation wavelength must be as small as possible. Since a short-wave monochromatic electron beam can be obtained quite easily, it is apparently more advisable to use electron-diffraction data to obtain the electron distribution in the atoms, and from this to find $f(q)$. The authors of the article in question /27/ chose argon for their experiment, since this element is sufficiently light and the Born scattering theory applies to it; at the same time, argon is sufficiently structural (three electronic shells) to provide a critical control of the method used.

Figure 6 shows the atomic form factor as a function of $4\pi\frac{\sin\theta}{\lambda}\cdot 10^{-8}$, calculated according to the method of Hartree and Fok and also obtained experimentally. The results of this carefully devised and executed experiment /27/ agreed beautifully with theory. This verifies the general conclusion, drawn from the experiments considered previously, that the radiation logarithm should be calculated using the theoretical values of $f(q)$ obtained by means of the method of the self-consistent field, since these values agree very well with experiment.

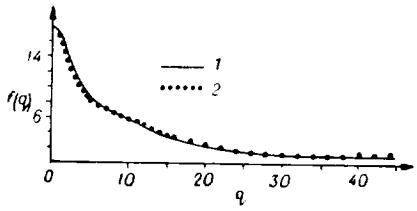

FIGURE 6.

1–Hartree-Fok model; 2–experiment /27/.

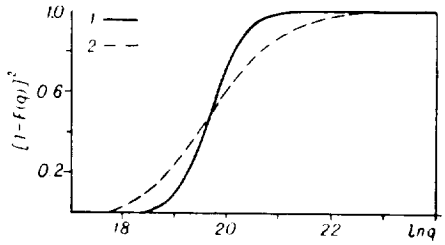

FIGURE 7. $[1-F(q)]^2$ as a function of $\ln q$, for hydrogen. The scale of the coordinate axes is such that the area under the curve equals $L^{rad}-1$.

1–exact wave function; 2–Thomas-Fermi model.

The method of the self-consistent field was suggested by Hartree /29/, and then developed by Fok, who took electron transfer into account /30/. The difference between the electron distributions in the atom according to Hartree and Fok is slight. In the interior of the atom, the electron density given by Fok is on the average larger than that of Hartree, while in the outer parts of the atom it is smaller than Hartree's. In the immediate vicinity of the nucleus the density variations according to the two authors are the same. Therefore, the difference in density distribution mainly affects the atomic properties, which are caused mostly by the outer parts of the atoms.

Since the method of the self-consistent field is very laborious, until recently it was applied to calculate the form factors of only a few atoms. In the last decade, however, with the increasing development of computers, this method was used to calculate $f(q)$ for most of the atoms in the

periodic system /31/. For elements with $Z > 25$, $f(q)$ was calculated statistically taking into account transfer /32/.

To calculate L^{rad}, we used theoretically obtained values of $f(q)$ listed in the third volume of a recent edition of International Tables /31/, and also in some other works which have appeared recently /33, 34/.

We calculated L^{rad} for all elements of practical interest. For hydrogen, values of $f(q)$ obtained by means of exact quantum-mechanical wave functions were used. For the other elements, L^{rad} was calculated using the most recent version of the method of the self-consistent field, taking into account electron transfer. Moreover, for atoms with $Z > 20$, the distribution of electron density according to the Thomas-Fermi-Dirac model was introduced /35/. However, the calculated values of $f(q)$ in the tables in several cases could not give an accurate value of L^{rad}, since $f(q)$ was listed for values of $\frac{\sin\theta}{\lambda} \cdot 10^{-8}$ usually not exceeding 2; for an accurate evaluation of L^{rad}, on the other hand, $f(q)$ must be known for somewhat higher values of $\frac{q}{4\pi}$ (Figures 7 and 8). Therefore, in such cases we calculated $f(q)$ for higher values of q. To do this, we assumed that the scattering at very large angles is governed only by the K electrons, which can be described in terms of hydrogenlike wave functions in the $1S$ state /27/. Figure 3 confirms the feasibility of this assumption. This extrapolation was applied to the $f(q)$ values calculated by means of the method of the self-consistent field.

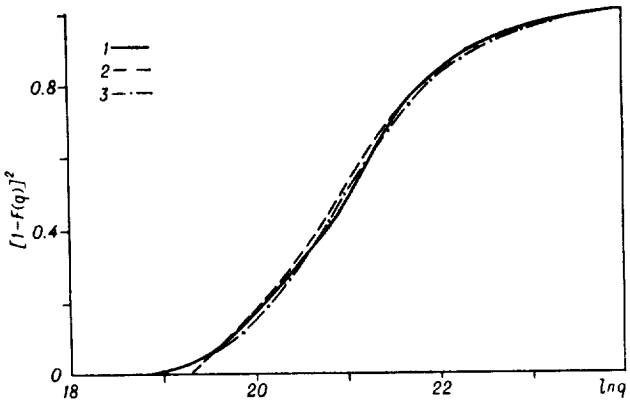

FIGURE 8. $[1-F(q)]^2$ as a function of ln q, for silver. The scale of the coordinate axes is such that the area under the curve equals $L^{rad}-1$.

1–Hartree-Fok model; 2–Thomas-Fermi model; 3–Thomas-Fermi-Dirac model.

If the calculation was made according to the electron-density distribution given by the Thomas-Fermi-Dirac method, then for large angles (that is, close to the nucleus) we extrapolated $f(q)$ according to the Thomas-Fermi model, without taking into account electron transfer. The error in L^{rad} introduced by this extrapolation is negligible /32/ (see Figure 8). In Figure 9 the radiation logarithms for different elements, calculated according to the various assumptions, are plotted as a function of log Z. We will not

attempt here to discover any regularities in the behavior of the L^{rad} values calculated using the method of the self-consistent field and the statistical method taking into account transfer. Let us remark only that these values

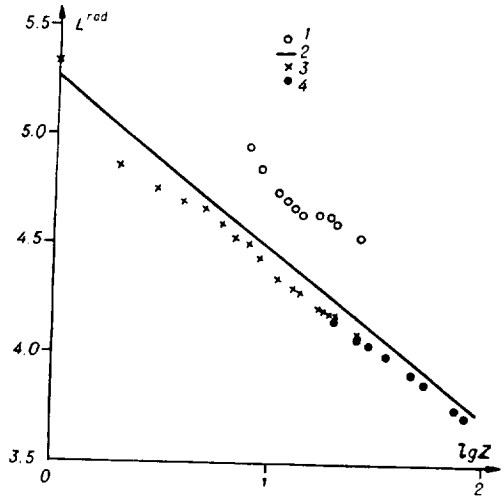

FIGURE 9.

1–according to Kirpichev and Pomeranchuk; 2–Thomas-Fermi model; 3–Hartree-Fok model; 4–Thomas-Fermi-Dirac model.

are very close to the L^{rad} obtained with the Thomas-Fermi model, and that they are quite different from the values of Kirpichev and Pomeranchuk. The radiation logarithms obtained in our study were calculated using $f(q)$ values which agreed very well with the experimental data. Consequently, these are the values of L^{rad} which must be used to calculate the cascade unit.

III. BREMSSTRAHLUNG AND PAIR PRODUCTION IN A FIELD OF ATOMIC ELECTRONS

Everything discussed in the previous section referred to elastic-scattering processes. Actually, since processes in the field of a nucleus are being considered, we can neglect the momentum imparted to the nucleus, and thus we can assume that the wavelengths of the scattered and incident radiation are the same. However, as early as 1934, Perrin /36/ demonstrated that pair production and bremsstrahlung in the field of an electron are an inevitable consequence of quantum electrodynamics. He showed that in the laboratory system the minimum energy required for pair production in a field of electrons is twice that required in the field of a nucleus and is equal to $4mc^2$. Perrin estimated that the cross section for this process approximately equals that for pair production in the field of a nucleus with unit charge. When the electrons in whose field pairs and bremsstrahlung photons are created are parts of an atom, it is important to distinguish between the cross sections for coherent and incoherent pair

production and bremsstrahlung; this can be done on the basis of the energy imparted to the atom. In a coherent process, the collisions are such that an atomic electron is in the same energy state at the beginning and the end of the process. In such a case, of course, the electron can be considered as bound to the atom. The recoil momentum is here imparted to the atom as a whole, which has remained practically unexcited. However, collisions will also occur in which the recoil momentum will be imparted to an individual atomic electron. In such a case the atom will become excited and will pass from the ground state to an excited state (incoherent process).

For high energies of the incident electron (photon) the determining factor will be the large interaction parameters associated with low momentum transfers due to excitation energies which are low in comparison with mc^2. In this case the atomic electrons can be considered bound, and their intratomic motion can be neglected. The explanation of this is as follows: the time required for the incident particle to cross the atom must be short compared to the period of motion of the atomic electrons. Therefore, the validity of the result depends on whether the energy of the incident particle is large enough, and the recoil momentum small enough, to allow us to neglect the motion of the atomic electrons during the passage of the particle through the atom. This condition will be satisfied sufficiently well if the energy of the incident particle is large in comparison with mc^2.

However, if the energy imparted to an atomic electron exceeds the ionization energy, the binding forces can be neglected and, to a first approximation, the electron can be considered free. Since collisions are possible in which the atom becomes excited, a fast electron passing through the nucleus will emit at a higher velocity than that which would be expected if the atom appeared to the electron as just a static force field. Similarly, γ quanta will produce pairs at a higher energy.

Landau and Rumer, in their discussion of cascade showers /37/, first pointed out the necessity to take into account emission and pair production in a field of atomic electrons. These authors assumed that the cross section for radiation processes in the field of an electron equals the cross section for these processes at a proton. Also, they assumed correspondingly that the contribution of these electrons is determined by the formulas of Bethe and Heitler (formulas (1) and (2)), with Z^2 replaced by Z,* where Z is the number of electrons in the atom. On the basis of these assumptions, Landau and Rumer concluded that the total cross section is proportional to $Z(Z+\zeta)$, where ζ was taken as unity.

However, the replacement of Z^2 by $Z(Z+1)$ is justified only for heavy nuclei. For low Z, the effect of radiation processes in the field of atomic electrons must be taken into account more accurately. For example, one of the main electromagnetic processes contributing to the absorption of high-energy photons in light elements is the production of electron-positron pairs by photons in the Coulomb field of an electron (usually known as triplet production).

Wheeler and Lamb /6, 38/ worked out a theory describing the radiation processes occurring in a field of atomic electrons. They calculated the cross sections using the Born approximation, taking into account screening. It was assumed in these calculations that:

1) an atomic electron picks up a momentum $\leqslant mc$; for low recoil momenta the cross sections in the field of an electron do not differ from

* [Apparently this should read: "with Z^2 replaced by $Z(Z+1)$."]

those in the field of a proton, and for recoil momenta close to mc the electrons can be considered free;

2) the exchange effect related to the indistinguishability of two electrons at the end of the process is not taken into account;

3) the contribution of the γ—e interaction is not taken into account; in this interaction an atomic electron first absorbs an incident photon and then emits it, after which the emitted photon produces a pair.

The importance of the latter two processes drops sharply with an increase in energy, since they are always associated with transfers of large momenta. As the energy increases, the transfer of large momenta becomes less likely, and thus the interaction parameter increases. Wheeler and Lamb obtained the following general expression giving the cross section for the emission of a γ quantum with an energy between ν and $(\nu + d\nu)$ during an incoherent emission process:

$$d\nu \int \left(\frac{4\pi e}{q}\right)^2 ZS(q)\, G(q, \nu, E_1)\, dq. \qquad (14)$$

Here $G(q, \nu, E_1)$ is a function combining all the effects involving γ quanta and electrons (just as in coherent emission processes), and $S(q)$ is a function taking into account the incoherent scattering of X rays at the atom (the value of $S(q)$ varies from 0 to 1). Heisenberg /39/ demonstrated how

TABLE 2

Element	Z	ζ		
		Bethe, Ashkin /41/	Joseph, Rohrlich /42/	Our results
Hydrogen	1	1.39	1.20	1.16
Lithium	3	1.35	1.14	1.18
Nitrogen	7	1.31	1.09	1.20
Aluminum	13	1.28	1.04	1.22
Iron	26	1.24	0.99	1.24
Silver	47	1.20	0.94	1.24
Lead	82	1.16	0.89	1.27

to calculate $S(q)$ using the Thomas-Fermi model. Earlier, calculations of $S(q)$ had been made by Wheeler and Lamb /40/ down to very low values of q. As a result, the cross sections given in formulas (8) and (9) were obtained, where $l^{rad} = \ln 1440\, Z^{-2/3}$. In order to verify the applicability of the Thomas-Fermi model to the calculation of cross sections (1), (2), (9), and (10), the authors of /6/ integrated (14) using the atomic wave functions for two elements: for nitrogen in the case of total screening and for hydrogen at all energies.* The results of Wheeler and Lamb were taken into account when Bethe and Ashkin calculated the cascade unit /41/. For all elements including hydrogen they took the values for ζ given by the Thomas-Fermi model. Moreover, in the expression for ζ they did not allow for the correction to the Born approximation. This gave values of ζ which dropped with an increase of Z (see Table 2), from 1.39 for hydrogen to 1.16 for lead. As noted above, for hydrogen and nitrogen Wheeler and Lamb computed cross sections for both coherent and incoherent processes, using exact wave functions rather than the Thomas-Fermi model. In this case $\zeta^H = 1.16$ was used instead of 1.39 and $\zeta^N = 1.2$ instead of 1.31. We used

* For the coherent case, the results of Wheeler and Lamb agreed with ours.

these values of ζ^H and ζ^N as starting points in the interpolation of ζ for the intermediate elements. We determined ζ for the heavy elements using the Thomas-Fermi model, but taking into account the Coulomb correction to the Born approximation:

$$\zeta = \frac{\ln 1440\, Z^{-2/3}}{\ln 191\, Z^{-1/3} - f(Z)}.$$

For the intermediate elements a smooth interpolation was made from the value of ζ^{Pb} obtained with the Thomas-Fermi model to ζ^N. This gave values of ζ which increased slightly with increasing Z (Table 2). In their review article /42/, Joseph and Rohrlich attempted to take into account the exchange character of the interactions, and also the γ—e interaction. The values which they obtained for the cross sections differed from those of Wheeler and Lamb by a constant which was independent of the screening and the energy. These values are also listed in Table 2.

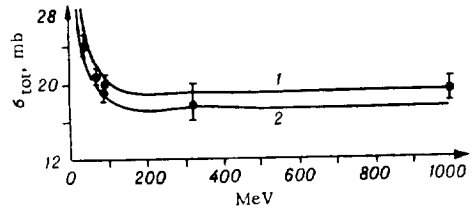

FIGURE 10. Total cross section for absorption of γ quanta in hydrogen, as a function of energy:

1—curve obtained from calculations of Wheeler and Lamb /6/; 2—curve obtained from calculations of Joseph and Rohrlich /42/.

In a more recent theoretical study of this subject /43/, it was demonstrated that the distribution of recoil momenta in the corresponding variables is independent of the mass of the recoiling particle, which verifies the correctness of the assumptions of Wheeler and Lamb.

Several recent experiments on the absorption of beams of photons and electrons in different substances agree well with the theoretical calculations of Wheeler and Lamb. For instance, a study of pair production in the field of an electron and the field of a proton /44/, by photons with energies from 10 to 1000 MeV, gave results agreeing with the calculations of Wheeler and Lamb.

Measurements of the absorption of 1-BeV photons in 12 different materials were made using the Cornell synchrotron /45/. These experiments gave data which agreed much better with the cross sections of Wheeler and Lamb than with those calculated by Joseph and Rohrlich. The results of experiments /45–53/ on the absorption of photons with energies over 40 MeV in different substances were collected in /45/, and they are shown in Figures 10, 11, 12, and 13. For hydrogen, at photon energies below 100 MeV the experimental cross sections are between the values calculated by Wheeler and Lamb /6/ and by Joseph and Rohrlich /42/. For Li, the experimental values agree with the calculations of Wheeler and Lamb, provided the values of ζ obtained by us (see Table 2) are used instead of those calculated according to the Thomas-Fermi model (see Figure 11).

For all the other elements the fit between the theoretical predictions of Wheeler and Lamb and the experimental data is very good. One of the most recent studies of electron-triplet production in hydrogen by high-energy

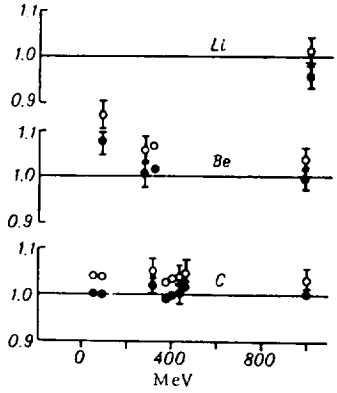

FIGURE 11. Ratios of experimental total cross sections for pair production to theoretical values of Wheeler and Lamb and of Joseph and Rohrlich, as functions of energy, for Li, Be, and C:

$$\bullet - \frac{\sigma_{exp}}{\sigma_{W\text{-}L}}; \quad \circ - \frac{\sigma_{exp}}{\sigma_{J\text{-}R}}.$$

photons /54/ gives a positron energy distribution agreeing with the predictions of Wheeler and Lamb. The distribution obtained for the recoil

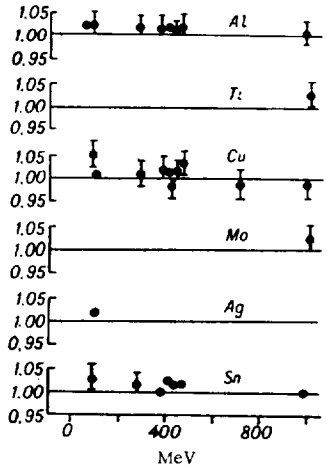

FIGURE 12. Ratios of experimental total cross sections for pair production to theoretical values, as functions of energy, for Al, Ti, Mo, Cu, Ag, and Sn.

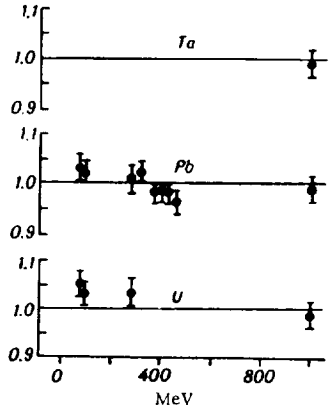

FIGURE 13. Same as Figure 12, but for the heavy elements Ta, Pb, and U.

momenta agrees with the calculations of Such and Bethe /43/, which also confirm the basic assumptions of Wheeler and Lamb. On the basis of this, the authors conclude that the correction for the γ—e interaction, and also the exchange correction, are negligible.

Experimental data are also available which check the theory of bremsstrahlung at high energies. For example, Bernstein and Panofsky /55/ give a ratio of 0.976 ± 0.028 between the experimental cross section for bremsstrahlung in hydrogen and the theoretical value of Wheeler and Lamb; thus, the agreement between experiment and theory is very good.

Everything discussed in this section indicates that bremsstrahlung and pair production in the field of atomic electrons must be taken into account in calculations of the radiation length. For these calculations, the theoretical results of Wheeler and Lamb should be used, that is, the values of ζ given in Table 2. Of course, the replacement of $Z(Z+1)$ by $Z(Z+\zeta)$ is important only for very light elements.

IV. CORRECTIONS FOR INACCURACY OF THE BORN APPROXIMATION

The Born approximation in collision theory considers the Coulomb interaction as a small perturbation. It stipulates that the kinetic energy of the incident particle at the beginning and end of the collision be high enough that

$$\frac{2\pi Z}{137\beta_0} \ll 1 \text{ and } \frac{2\pi Z}{137\beta} \ll 1,$$

where Z is the atomic number of the scattering center of force, and β_0 and β are the velocities of the incident particle at the beginning and end of the collision, respectively. These inequalities indicate that the lighter the substance is, the better will be the approximation according to the Born theory. Bethe and Heitler used the Born approximation to obtain the cross sections for processes at high energies /3/. They represented the wave functions of the electrons in the initial and final states as plane waves, thereby neglecting the Coulomb field of the nucleus.

Because of the inaccuracy of the Born cross sections for bremsstrahlung and pair production in the nuclear field of a heavy element, several authors have calculated these cross sections without using the Born approximation. They assumed the energy of the incident particle to be quite large in comparison with mc^2 at the beginning and the end of the collision process. In the first calculations of accurate integral and differential cross sections for bremsstrahlung and pair production, the wave functions of the incident particle at the beginning and end of the process were represented by a plane wave with a diverging spherical wave added to it /56, 57/. Calculations of the differential cross sections at extremely high energies (total screening) indicated /56/ that for bremsstrahlung the correction to the Born approximation because of Coulomb interaction is negligible, whereas for pair production it differs appreciably from zero. In the subsequent article /57/ the differential cross sections were integrated over the angles. As also shown by several experimental studies, the correction to the Born approximation was nearly proportional to Z^2 and

was independent of the amount of screening. The integral cross section for bremsstrahlung decreased to the same extent as the cross section for pair production, in comparison with the cross section calculated using the Born approximation.

However, subsequently /58/ it was shown that the representation of the wave functions of the electron by a plane wave plus a diverging spherical wave is valid only for the initial period of a collision. At the end of a collision the electron wave functions must be represented in the form of a plane wave with a converging spherical wave added to it. While calculating the bremsstrahlung cross section, these authors found that the correction to the Born approximation was practically zero. This result led to two subsequent accurate calculations /59, 60/ of the cross sections for bremsstrahlung and pair production; here, in the matrix element for pair production, the wave functions of the electron and positron were described, in accordance with the foregoing, by converging waves. In this case, contrary to the Born approximation, there was considerable difference between the processes. The authors explained the resulting difference between the accurate values of the cross sections as follows: the waves scattered by an electron in the initial and final states of the bremsstrahlung process do not overlap noticeably as in the case of pair production. Integration of the differential cross sections over the angles of the electrons at the end of the process gave the following analytical expression for the Coulomb correction to the pair-production cross section:

$$f(Z) = a^2 \sum_{\nu=1}^{\infty} \frac{1}{\nu(\nu^2 + a^2)}. \qquad (15)$$

The expansion

$$\Sigma = (1 + a^2)^{-1} + 0.20206 - 0.0369\,a^2 + 0.0083\,a^4 - 0.002\,a^6$$

is quite accurate, so that we obtain $f(Z) \sim a^2$ and hence Z^2. For low atomic numbers $\Sigma \simeq 1.2021$ and $f(Z) \simeq 1.2021\,a^2$. The Coulomb correction involves only large momentum transfers, while the correction for screening involves small transfers; thus these corrections are not mutually dependent. Consequently, Davis, Bethe, and Maximon /60/ obtained the following total cross section for the production of electron-positron pairs at very high energies (total screening):

$$d\sigma_{pair} = 4\frac{N}{A}\,\alpha r_0^2 Z^2\,\frac{dE_+}{\nu^3}\left[\left(E_+^2 + E_-^2 + \frac{2}{3}E_+E_-\right)\{\ln(183\,Z^{-1/3}) - f(Z)\} - \frac{1}{9}E_+E_-\right]$$

and, correspondingly, the following integral cross section:

$$\sigma_{pair} = \frac{28}{9}\cdot\frac{Z^2 r_0^2}{137}\left[\ln(183\,Z^{-1/3}) - \frac{1}{42} - f(Z)\right].$$

The fact that the correction to the bremsstrahlung cross section was practically zero led to the following conclusion. Since σ_{pair} for lead decreased by 10% in comparison with the Born approximation, while σ_{rad} remained constant, the ratio of high-energy photons to electrons in a shower developing in lead increases by 10% in comparison with the Born theory, and the radiation length increases by 5%.

Some important corrections in relation to this were introduced by Olsen /61/. As mentioned above, to calculate the probability of a transition between stationary states, the scattered particle at the end of the process

must be represented in terms of wave functions whose asymptotic form is a plane wave plus a converging spherical wave. The necessity for such a representation shows up especially when the cross section for bremsstrahlung at high energies is calculated /59/. On the other hand, it was pointed out that such a choice of the wave functions for the final states is necessary only when the differential cross section for a given direction of scattered particles is calculated (for example, the direction of electrons at the end of bremsstrahlung). Olsen noticed that, if the cross section integrated over the direction of the scattered particles (that is, over their angles of departure) has to be obtained, it is possible to use successfully a wave function of the diverging-wave type to describe the final state of the process. This may be clearer if we note that for bremsstrahlung the direction of motion of a scattered particle actually represents degeneration of the final state of the process. Therefore, a whole set of states can be used to describe the particle. In particular, it may be represented in terms of diverging waves.

Olsen also indicated how to derive the bremsstrahlung cross section, integrated over the angles of the electrons, from the corresponding pair-production cross section, this transformation being completely independent of the presence or absence of screening. Consequently, from the total pair-production cross section, Olsen obtained the following spectrum for bremsstrahlung at high energies:

$$\frac{d\sigma_{rad}}{d\nu} = \left(\frac{d\sigma_{rad}}{d\nu}\right)_{BH} - 4\alpha^2 \frac{e^2}{\hbar c}\left(\frac{\hbar}{mc}\right)^2 \cdot \frac{1}{\nu E_0^2}\left[E_0^2 + E^2 - \frac{2}{3}E_0 E\right] f(Z),$$

where $\left(\frac{d\sigma_{rad}}{d\nu}\right)_{BH}$ is the bremsstrahlung spectrum obtained by Bethe and Heitler using the Born approximation. The Coulomb correction given by the following term is independent of the amount of screening, and its relative value is the same as that of the correction to the pair-production cross section. The discrepancy between the cross-section corrections obtained by Bethe and Maximon /59/ and by Olsen /61/ as a result of the inaccuracy of the Born approximation can be explained as follows: for bremsstrahlung the correction due to the Coulomb field and the correction for screening are not additive* in the differential cross section (they were assumed to be additive by Bethe and Maximon /58/). This is explained by the fact that the Coulomb correction to the Born approximation is also not negligible for low momentum transfers, when the wave functions of the electron are represented in terms of converging waves (that is, under the same conditions as for screening). However, the usual means of allowing for screening, namely multiplication of the cross section by the form factor, is valid only within the Born approximation, that is, only when the matrix element is not changed by the Coulomb correction. This is why Olsen pointed out /61/ that only a calculation of the cross section integrated over the angles of departure of the electrons at the end of the process, with wave functions of the diverging-wave type, is strictly correct.

In a later work, Olsen et al /63/ obtained the differential cross section for bremsstrahlung in a screened field and concluded that the standard shower theory is not modified when Coulomb effects are taken into account. Moreover, a study of the polarization of photons and electrons during

* See Bethe's footnote in /62/.

bremsstrahlung /64–66/ indicated that the screening and Coulomb corrections to the polarization-dependent part of the cross section could be expressed in the same analytical form and just as accurately as the part of the cross section which is not dependent on the polarization (that is, the corrections considered above).

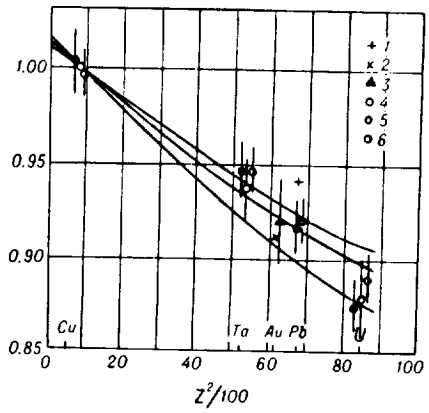

FIGURE 14. Points show ratios between experimental bremsstrahlung cross sections and cross sections calculated from formulas of Bethe and Heitler /3/. Solid curves show ratio of cross sections calculated by Olsen et al /65/ to cross sections calculated from formula of Bethe and Heitler /3/.

1–60MeV /67/; 2–17MeV /68/; 3–247MeV /69/; 4–500MeV /70/; 5–24MeV /71/; 6–34MeV /71/.

The theoretical conclusions concerning the cross sections are confirmed by the available experimental data. In the previously considered article by Malamud /45/, a great number of experimental data on the absorption of high-energy photons in substances with intermediate and high atomic numbers were collected (see Figures 12 and 13). These results agree with the theoretical calculations of Davis, Bethe, and Maximon /60/.

The experimental data on the bremsstrahlung cross section are considerably fewer, and their accuracy somewhat worse, than the data for the pair-production cross section. However, they also agree completely with the theoretical predictions of Olsen /61/.

The results of these studies /67–71/ are shown in Figure 14. An analysis of the data indicates that theory gives a Coulomb correction to the bremsstrahlung cross section which is mainly correct, although to evaluate the absolute accuracy of the theoretical formula more precise experiments must be made.

The Coulomb correction to the cross section was first calculated in a calculation of the t unit by Rossi /72/. However, up to the time when his book was published, theory had not advanced sufficiently. To correct the error introduced by the Born approximation, Rossi suggested multiplying the expression for the radiation length by $[1 + 0.12\,(\frac{Z}{82})^2]$. The numerical coefficient in this expression was selected in order to agree with the

experimental data on the creation of electron-positron pairs in lead at 88 MeV /73/. The values of the cascade unit computed by Rossi according to the formula

$$\frac{1}{t_0} = 4\frac{N}{A}\alpha r_0^2 Z(Z+1)\ln(183Z^{-1/3})\left[1+0.12\left(\frac{Z}{82}\right)^2\right]^{-1}$$

are listed in Table 3.

TABLE 3

Substance	Z	Atomic weight A	t_0, g/cm^2			
			Bethe and Ashkin /41/	Rossi /72/	Ivanenko and Belen'kii /74/	Our results
Hydrogen	1	1.008	58		62	62.8
Helium	2	4.003	85			93.1
Lithium	3	6.940				83.3
Beryllium	4	9.013				66.0
Boron	5	10.820				53.6
Carbon	6	12.010	42.5	44.6	40	43.3
Nitrogen	7	14.008	38	39.4	35.4	38.6
Oxygen	8	16.00	34.2	35.3	32.1	34.6
Fluorine	9	19.00				33.4
Sodium	11	22.977				28.2
Aluminum	13	26.980	23.9	24.5	22.7	24.3
Silicon	14	28.090				22.2
Chlorine	17	36.457				19.5
Argon	18	39.944	19.4	19.8	18	19.7
Potassium	19	39.096				17.4
Calcium	20	40.08				16.3
Iron	26	55.85	13.8	14.1	12.6	13.9
Copper	29	63.54	12.8	13.1	11.6	13.0
Bromine	35	79.916				11.5
Silver	47	107.880				9.0
Iodine	53	126.910				8.5
Tungsten	74	183.92				6.8
Lead	82	207.21	5.8	6.5	5.55	6.4
Air N — 75.52% O — 23.14% A — 1.34%	7.37	14.78	36.5	37.7	34.2	37.1
Water (H_2O)	7.23	14.3	35.9	37.1	33.9	36.4
Clay (kaolin) $Al_2SO_3 \cdot 2SiO_2 \cdot 2H_2O$						28.8
Quartz, SiO_2						27.4
Limestone, $CaCO_3$						24.2
Rock salt, NaCl						22.2
Lithium hydride, LiH						80.0
Nuclear photoemulsion, NIKFI-R*						11.4

* [Nauchno-Issledovatel'skii Kino-Foto Institut (Motion-Picture and Photography Scientific Research Institute).]

However, in the more recent article of Belen'kii and Ivanenko /74/, the coefficient 0.12 in the correction to the Born approximation suggested by

Rossi was replaced by the coefficient 0.06, evidently taking into account the footnote made by Belen'kii during the editing of Rossi's book.*

In accordance with the foregoing, when calculating the radiation length we assumed that the correction for the inaccuracy of the Born approximation is the same for the bremsstrahlung and pair-production cross sections, and we used formula (15).

CONCLUSION

In this study, the effect of total screening, bremsstrahlung and pair production in a field of atomic electrons, as well as corrections for inaccuracy of the Born approximation for the cascade unit, have been accurately taken into account. Accordingly, values of the cascade units for all substances of practical interest were obtained in experiments with high-energy radiation. These values are given in Table 3. For comparison, the cascade units obtained by other investigators are also listed in the table. In some cases the discrepancy between different data may be as much as 20%.

The values of the cascade units obtained by us and listed in the last column of Table 3 agree very closely with recent experimental data and theoretical ideas.

In conclusion, the authors consider it their pleasant duty to thank E. L. Feinberg for his fruitful discussion of our results and to thank B. K. Vainstein and A. I. Nikishov for their helpful consultations.

P. N. Lebedev Institute of Physics of the USSR Academy of Sciences

REFERENCES

1. CARLSON, J. F. and J. R. OPPENHEIMER. –Phys. Rev., **51**, 220. 1937.
2. BETHE, H. A. –Proc. Cambr. Phil. Soc., **30**, 524. 1934.
3. BETHE, H. A. and W. HEITLER. – Proc. Roy. Soc. London, **A146**, 83. 1934.
4. BELEN'KII, S. Z. Lavinnye protsessy v kosmicheskikh luchakh (Cascade Processes in Cosmic Rays). – Gostekhizdat, 1948.
5. KOCH, H. W. and J. W. MOTZ. –Rev. Mod. Phys., **31**, 920. 1959.
6. WHEELER, J. A. and W. E. LAMB. –Phys. Rev., **55**, 858. 1939.
7. THOMAS, L. H. –Proc. Cambr. Phil. Soc., **23**, 542. 1926.
8. FERMI, E. –Zts. Phys., **48**, 73. 1928.
9. BETHE, H. A. –Ann. Phys., 5, 325. 1930.
10. POMERANCHUK, I. –J. of Physics, **8**, 17. 1940.
11. KIRPICHEV, A. and I. POMERANCHUK. –DAN SSSR, **45**, 301. 1944.
12. KOBAYASHI, S., I. MATSUKUMA, S. NAGAI, and K. UMEDA. –J. Phys. Soc. Japan, **10**, 759. 1955.
13. FILON, I. N. G. –Proc. Roy. Soc. Edinburgh, A. **49**, 38. 1929.
14. ROSSI, B. and K. GREISEN. –Rev. Mod. Phys., **13**, 240. 1941.

* See /72/, p. 262 [of Russian edition].

15. LANDOLT-BÖRNSTEIN. - Zweiter Ergänzungsband, 2teil, 584. 1931.

16. BRAGG, W. L. and J. WEST. —Zts. Kristallograph, **69**, 118. 1928.

17. JAMES, R. W., I. WALLER, and D. R. HARTREE. —Proc. Roy. Soc. Lond., Ac **18**, 334. 1928.

18. BRADLEY, A. J. and R. A. H. HOPE. —Proc. Roy. Soc., A **136**, 272. 1932.

19. BRINDLEY, G. W. and P. RIDLEY. —Proc. Phys. Soc. Lond., **50**, 96. 1938.

20. JAMES, R. W. and G. W. BRINDLEY. —Proc. Roy. Soc., A **121**, 155. 1928.

21. BENSCH, H., H. WITTE, and E. WOLFFL. —Zts. Phys. Chem., **4**, 65. 1955.

22. WEISS, R. J. and J. J. DE MARCO. —Rev. Mod. Phys., **30**, 59. 1958.

23. BATTERMAN, B. W. —Phys. Rev. Letters, **2**, 47. 1959.

24. KOMURA, Y., Y. TOMIIE, and R. NATHANS. — Phys. Rev. Letters, **3**, 268. 1959.

25. Mc DONALD, T. R. R. —Acta Crystal, **13**, 113. 1960.

26. BATTERMAN, B. W., D. R. CHIPMAN, J. J. DE MARCO. —Phys. Rev., **122**, 68. 1961.

27. BARTELL, L. S. and L. O. BROCKWAY. —Phys. Rev., **90**, 833. 1953.

28. COMPTON, A. H. —Phys. Rev., **35**, 925. 1930.

29. HARTREE, D. R. —Proc. Camb. Phil. Soc., **24**, 89, 111. 1928.

30. FOK, V. A. —Zts. Phys., **61**, 126. 1930.

31. International Tables for X-Ray Crystallography, **3**, Amsterdam. 1962.

32. THOMAS, L. H. and K. UMEDA. —J. Chem. Phys., **26**, 293. 1957.

33. VIERVOLL, H. and O. ÖGRIM. - Acta Crystal, **2**, 277. 1949.

34. HAUPTMAN, H. and J. KARLE. - Phys. Rev., **77**, 491. 1950.

35. THOMAS, L. H. —J. Chem. Phys., **22**, 1758. 1954.

36. PERRIN, F. —Comptes rendus, **197**, 1100. 1933.

37. LANDAU, L. and G. RUMER. —Proc. Roy. Soc., A **166**, 213. 1938.

38. WHEELER, J. A. and W. E. LAMB. —Phys. Rev., **101**, 1836. 1956.

39. HEISENBERG, W. - Physik. Zts., **32**, 737. 1931.

40. BEWILOGUA, L. —Physik. Zts., **32**, 740. 1931.

41. BETHE, H. A. and J. ASHKIN. Experimental Nuclear Physics, Vol. 1. [Russian translation. 1957.]

42. JOSEPH, J. and F. ROHRLICH. —Rev. Mod. Phys., **30**, 354. 1958.

43. SUCH, K. S. and H. A. BETHE. —Phys. Rev., **115**, 672. 1959.

44. HART, E. L., G. COCCONI, V. T. COCCONI, and T. M. SELLEN. —Phys. Rev., **115**, 678. 1959.

45. MALAMUD, E. —Phys. Rev., **115**, 687. 1959.

46. WYCKOFF, J. M. and H. W. KOCH, —Phys. Rev., **117**, 1261. 1960.

47. LAWSON, J. L. —Phys. Rev., **75**, 433. 1949.

48. MOFFATT, J., J. J. THRESHER, G. C. WEEKS, and R. WILSON. — Proc. Roy. Soc. Lond., A **244**, 245. 1958.

49. MOFFATT, J. and G. C. WEEKS. —Proc. Phys. Soc. Lond., **73**, 114. 1959.

50. DE WIRE, J. W., A. ASHKIN, and L. A. BEACH. —Phys. Rev., **83**, 505. 1951.

51. ANDERSON, J., R. W. KENNEY, and C. A. Mc DONALD. —Phys. Rev., **102**, 1626. 1956.

52. ANDERSON, J., R. W. KENNEY, and C. A. Mc DONALD. —Phys. Rev., **102**, 1632. 1956.

53. COOPER, D. H. –Thesis, California Institute of Technology. 1955.

54. GATES, D. C., R. W. KENNEY, and W. P. SWANSON. – Phys. Rev., **125**, 1310. 1962.

55. BERNSTEIN, D. and W. K. H. PANOFSKY. –Phys. Rev., **102**, 522. 1956.

56. MAXIMON, L. C. and H. A. BETHE. –Phys. Rev., **87**, 156. 1952.

57. DAVIS, H. and H. A. BETHE. –Phys. Rev., **87**, 156. 1952.

58. BETHE, H. A. L. C. MAXIMON, and F. LOW. –Phys. Rev., **91**, 417. 1953.

59. BETHE, H. A. and L. C. MAXIMON. –Phys. Rev., **93**, 768. 1954.

60. DAVIS, H., H. A. BETHE, and L. C. MAXIMON. –Phys. Rev., **93**, 788. 1954.

61. OLSEN, H. –Phys. Rev., **99**, 1335. 1955.

62. BETHE, H. A. and E. E. SALPETER. Quantum Mechanics of One- and Two-Electron Atoms, Berlin, Springer. 1957 [Russian translation. 1960.]

63. OLSEN, H., L. C. MAXIMON, and H. WERGELAND. –Phys. Rev., **106**, 27. 1957.

64. OLSEN, H. and L. C. MAXIMON. –Phys. Rev., **110**, 589. 1958.

65. OLSEN, H., H. WERGELAND, and L. C. MAXIMON. –Bull. Amer. Phys. Soc., **11**, 3, 174. 1958.

66. OLSEN, H. and L. C. MAXIMON. –Phys. Rev., **114**, 887. 1959.

67. BARBER, W. C., A. I. BERMAN, K. L. BROWN, and W. D. GEORGE. –Phys. Rev., **99**, 58. 1955.

68. CURTIS, C. D. –Phys. Rev., **89**, 123. 1953.

69. LANZL, L. H. and A. O. HANSEN. –Phys. Rev., **83**, 959. 1951.

70. FISHER, P. C. –Phys. Rev., **92**, 420. 1953.

71. BROWN, K. L. –Phys. Rev., **103**, 243. 1956.

72. ROSSI, B. High-Energy Particles. New York. 1952. [Russian translation. 1955.]

73. LAWSON, T. L. – Phys. Rev., **75**, 433. 1949.

74. BELEN'KII, S. Z. and I. P. IVANENKO. –UFN, **69**, 591. 1955.

N67-38208

S.I. Nikol'skii

EXTENSIVE AIR SHOWERS OF COSMIC RADIATION

The study of extensive air showers can be divided into three main subjects.

1. Investigation of the structure and composition of the extensive showers. The main purpose of such experiments is to obtain a complete picture of the nuclear-cascade development and the shower absorption.
2. Observations related to the origin of cosmic rays and to their propagation through space (the space physics aspect).
3. Measurements designed to give certain characteristics of elementary acts involving ultrahigh-energy interacting particles.

The second and third subjects are intimately related to the first, since problems of the overall development of a shower will always come up. Research on extensive air showers from the point of view of nuclear interactions and other elementary processes has been discussed thoroughly at conferences, and so it will not be gone into in this report.

The experimental techniques will not be considered here either. All the same, it will be necessary to mention the chief characteristic of experimentation during the last decade, namely the complexity of the apparatus enabling a determination of the total number of particles and the location of the shower axis for each shower recorded.

I. LATERAL DISTRIBUTION AND TOTAL NUMBER OF CHARGED PARTICLES IN EXTENSIVE SHOWERS AT THE OBSERVATION LEVEL

By referring to charged particles, we will avoid having to define the nature of the particles. In the majority of experiments, more than 90% of the particles recorded using gas-discharge counters without any type of filters over them were electrons and positrons. If recordings are made only in the central parts of a shower, the proportion of electrons increases to 98%. The lateral distribution is shown in Figure 1. It is usually most accurate to measure the particle-flux density at distance intervals of 2 to 10 meters. If fluctuations and the weak dependence of the lateral distribution on the number of particles in the shower are neglected, then for showers with from 10^4 to $2 \cdot 10^6$ particles the total number of charged particles can be estimated in terms of the particle-flux density in an interval of 2 to 10 meters as $N = 500\rho(r)r$. Here r is the distance in meters and $\rho(r)$ is the flux density of charged particles per m^2 at the distance r. The factors neglected will limit the accuracy of the estimated total number of

particles, but the inaccuracy of the result obtained will be both statistical and systematic.

Let us consider the dependence of the lateral distribution on the shower intensity. In showers observed at mountain level, less than 10% of the total particle flux falls over distances $r < 10$ meters from the shower axis. Therefore, the distances from 20 to 200 meters are the most interesting, since this is where most of the particles arrive at the observation level (see Figure 1). Averaged experimental data on the lateral distribution of electrons* were obtained for showers with total numbers of particles $N = 7.5 \cdot 10^4$ (curve 1) and $N = 7.5 \cdot 10^5$ (curve 2) /1, 2/. For better comparison between these showers, theoretically obtained functions $2\pi r f^T(r)$ are plotted on the same figure (dashed lines). Calculated lateral distributions /3/ of the electrons in a cascade shower for $s = 1.2$ and $\frac{E_0}{\beta} = \infty$ and for $s = 1$ and $\frac{E_0}{\beta} = 10^5$ were used for the theoretical distribution $f^T(r)$. The calculated curves were normalized to the experimental curves for distances from 1 to 10 meters. The lateral distribution of showers with fewer particles agrees well with the calculation for $s = 1.2$; the distribution of showers with a large number of particles agrees better with the calculation for $s = 1$ and $\frac{E_0}{\beta} = 10^5$. The difference in the lateral distribution leads to different estimates for the total number of particles. For the first group, integration over the distribution observed experimentally leads to $N = 7.5 \cdot 10^4$ instead of $N^T = 500\rho(r)r = 6.5 \cdot 10^4$. For the second group, correspondingly, $N = 7.5 \cdot 10^5$ and $N^T = 8.5 \cdot 10^5$. At present no data are available enabling us to check in detail for such a variation in the lateral distribution. The detected disparity for showers differing in number of particles by only a factor of 10 cannot be interpreted as a substantial change in the lateral distribution of particles within a wide range of primary energies. Actually, the distribution of showers with $N = 1.5 \cdot 10^7$ at practically the same altitude /4/ agrees with the value calculated for $s = 1$. On the other hand, if the scattering angles of π^0 mesons during nuclear interactions do not affect the lateral distribution of electrons in a shower, then (independently of any specific model of the development of a nuclear-cascade shower from the altitude variation of showers with $N < 10^5$) a good fit is to be expected between the average lateral distribution and the calculated function /5, 6/ for a cascade parameter $s = 1.2$ to 1.4. Also, in practice, showers with

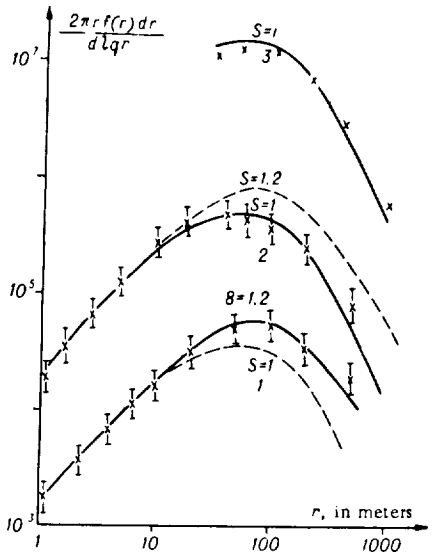

FIGURE 1.

* The contribution of μ mesons and the electrons in equilibrium with them at distances of $r = 100$ meters was taken into account.

$N = 2.1 \cdot 10^4$ particles show a good fit with theory for $s = 1.2$ to 1.4. Consequently, the lateral distribution of electrons in extensive air showers can be described in terms of the distribution function in an electron-photon shower with a specified parameter s for the distance range from 2 to 300 or 500 meters. This is the range within which most of the particles of the shower are observed. The experimental data obtained at a lower altitude by a group from Moscow University /7/ and by Rossi's group /8/ give analogous lateral distributions, taking into account, of course, the change in atmospheric density. For extremely large showers ($N > 10^7$) the following approximation formula /8/, valid for distances from the shower axis of $r = 30$ m, is usually used:

$$\rho(r) = \frac{N}{r_0^2} c(\alpha, \eta) \left(\frac{r}{r_0}\right)\left(1 + \frac{r}{r_0}\right)^{-(\eta-\alpha)};$$

$$c(\alpha, \eta) = \Gamma(\eta - \alpha)\,[2\pi\Gamma(2-\alpha)\,\Gamma(\eta-2)]^{-1}.$$

Here $c(\alpha, \eta)$ is determined from the normalization condition $\alpha = 1$. The parameter η is a gradually increasing function of N ($\eta = 3.5$ for $N = 10^8$ and $\eta = 4.5$ for $N = 10^{10}$).

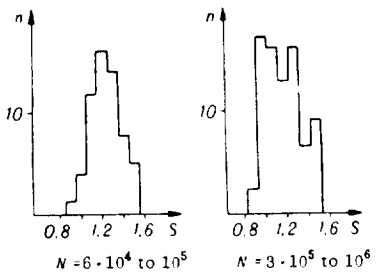

FIGURE 2.

The study of fluctuations in the lateral distribution is very important. Measurements of fluctuations were carried out at mountain altitude (650 g/cm^2) for showers with total numbers of particles $N = 6 \cdot 10^4$ to 10^5 and $N = 3 \cdot 10^5$ to 10^6. The lateral distributions of particles observed experimentally in individual showers agreed with the values calculated from electron-photon cascade theory for different values of the cascade parameter s. A relative representation of the showers corresponding to different values of s for distances from the shower axis of 2 to 60 meters is shown in Figure 2. The distribution for showers with $N = 6 \cdot 10^4$ to 10^5 conforms well to the normal distribution about $s = 1.23$ and a variance of 0.02. For the group with a larger number of particles, the distribution can be described in terms of an average value $\bar{s} = 1.2$ and a variance of 0.03, but only formally, since it does not conform to the normal distribution about a single value (Pearson criterion $\rho(f^2) < 0.006$).

II. THE NUMBER SPECTRUM OF EXTENSIVE AIR SHOWERS.

If the lateral distribution of particles in a shower is known, it is possible to determine with what frequency showers having the number of particles specified above take place. To establish the spectrum of the number of particles [number spectrum] of showers, either direct data on the frequency of occurrence of showers with the above-indicated number of particles, for a determined direction of arrival of the shower axis, or indirect measurements of the "density spectrum" can be used. In the latter case the number spectrum of the showers can be reconstructed for a known shape of the lateral distribution, this shape varying slightly with the shower intensity. For sea level, sufficient data from direct measurements of the frequencies of occurrence for showers with different numbers of particles

are available. The most significant such data are shown in Figure 3. The fewest showers were recorded in /9/, using equipment with a rigid selection criterion. It was assumed that the shape of the lateral distribution is independent of the total number of particles in the interval studied, and also that deviations of the observed particle-flux density from the mean value of the distance (from the shower axis) are described by Poisson's law.

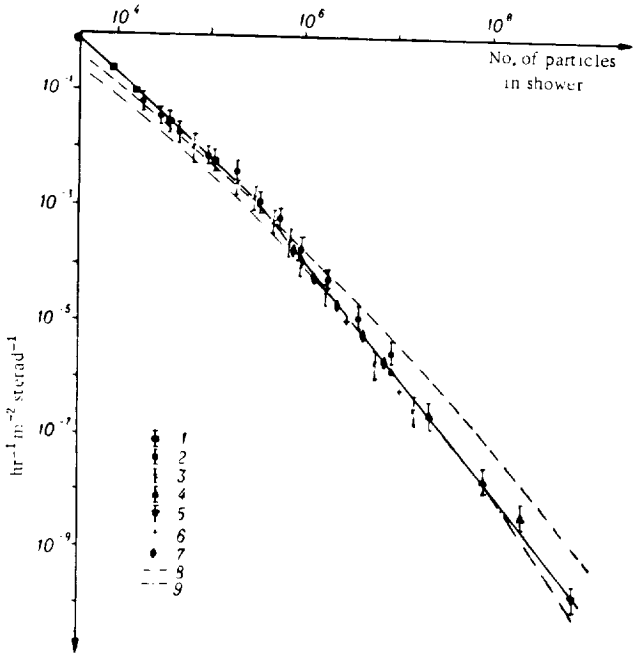

FIGURE 3. Experimental data on the spectrum of extensive air showers at sea level:

1–data of /9/; 2–measurements of /11/; 3–data of /10/; 4–data of /14/; 5–data of /8/; 6–data of /12/; 7–data of /13/; 8–data of survey /15/; 9–data of survey /16/.

For showers with $2 \cdot 10^4 < N < 10^5$, in addition to the results of the measurements indicated above, the data of /10/ (obtained using a complex arrangement of hodoscopic counters) and of /11/ (obtained using scintillation counters) are given. The results of these three studies, which differ in the measurement techniques used, agree well with one another. For showers with $1.5 \cdot 10^5 < N < 8 \cdot 10^5$, only the data of /10/ and /11/ are available, which do not agree very well with one another. The divergences between these data increase for heavier showers, for which, however, we also have the results of other measurements /12, 13, 14/. The most careful measurements /14/ gave a value intermediate between those of /10/ and /11/. The wide range of showers recorded in /14/ was extended up to $N \sim 10^9$ in /8/.

Figure 3 shows that the totality of data on the number spectrum of showers can be approximated by the following power function:

$$F_0(>N) = 1.9 \cdot 10^{-3} \left(\frac{N}{2.5 \cdot 10^5}\right)^{-\varkappa} \text{hr}^{-1}\,\text{m}^{-2}\,\text{sterad}^{-1}.$$

The exponent $\varkappa$ changes in value at $N \simeq 2.5 \cdot 10^5$:

$$\varkappa = 1.44 \pm 0.03 \quad \text{for} \quad N < 2.5 \cdot 10^5,$$

$$\varkappa = 1.9 \pm 0.05 \quad \text{for} \quad N > 2.5 \cdot 10^5.$$

The number spectrum given in the review article /15/, reconstructed on the basis of the "density spectrum," is also plotted in Figure 3. A more recent survey /16/ by the same author gave this spectrum more accurately, and brought it into better agreement with the direct measurements for $N \sim 10^6$. However, as the figure shows, the fit for $N < 10^5$ became worse.

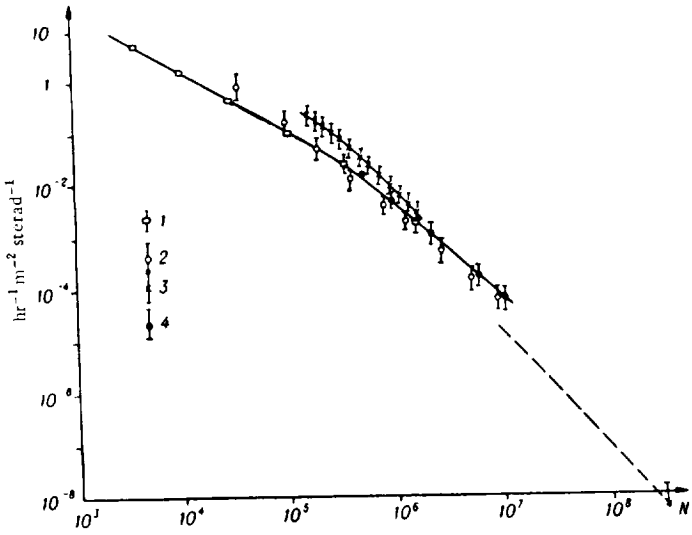

FIGURE 4. Spectrum of extensive air showers at an altitude with a pressure $p = 650\,g/cm^2$:

1–data of /47/; 2–data of /19/; 3–measurements of /18/; 4–data of /17/; dashed line, data of /20/.

So far, comparatively few direct measurements of the intensity of showers with specified numbers of particles have been made at mountain altitudes. In addition, the measurements which have been made pertain to different heights, and to correlate them the number of showers recorded must be known as a function of the observation altitude. Figure 4 shows some data obtained at altitudes of 2770 to 4100 meters above sea level. The absolute intensity was scaled to the level corresponding to a pressure $p = 650\,g/cm^2$, by means of the experimentally observed altitude variation. The data of /17/ and /18/, obtained at the same high-mountain station (2770 meters above sea level), differ considerably from one another, the results of the measurements in /18/ being consistently too high in comparison with the data of other authors. For $N < 10^5$, the results of the measurements in /19/ also deviate from the data of other authors. Just as for the sea-level data, the results can be represented best by means of a power function, with a discontinuity in this case at $N = 3.5 \cdot 10^5$:

$$F_{3860}\,(>N) = 1.9 \cdot 10^{-8} \left(\frac{N}{3.5 \cdot 10^5}\right)^{-\varkappa},$$

$$\varkappa = 1.3 \quad \text{for} \quad N < 3.5 \cdot 10^5;$$
$$\varkappa = 1.9 \quad \text{for} \quad N > 3.5 \cdot 10^5.$$

A comparison of the intensity of extensive showers at an altitude of 3860 meters with the number of showers at sea level gives the following altitude variation of the number of extensive showers in the lower third of the atmosphere: $f(p) \sim e^{-p/140}$ for $N \geqslant 3 \cdot 10^5$.

III. μ MESONS IN EXTENSIVE AIR SHOWERS

The presence of penetrating nuclear-passive particles in extensive showers was established even before the confirmation of the nuclear-cascade scheme of shower development /21/. Now there is no doubt that the penetrating nuclear-passive component of extensive showers is made up of μ mesons. The relatively long lifetimes of $\pi^{\pm}$ mesons means that low-energy pi mesons play the predominant role in μ-meson production, the

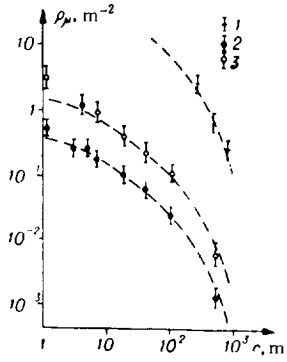

FIGURE 5. Lateral distribution of μ mesons in an extensive air shower at mountain level:

1–data of /23/; 2 and 3–data of measurements in /22/ for showers with $N = 10^5$ and $N = 7.7 \cdot 10^5$, respectively.

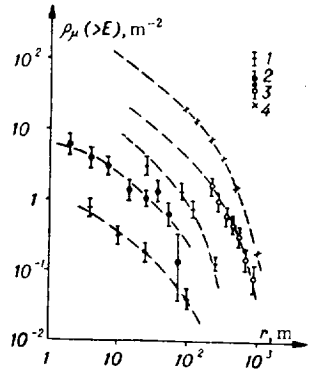

FIGURE 6. Lateral distribution of μ-meson flux in extensive air showers at sea level:

1–results of /24/, for μ mesons with $E_\mu > 10^{10}$ eV; 2–data of /11/, for μ mesons with $E_\mu > 5 \cdot 10^9$ eV; 3–data of /25/; 4–data of /8/.

number of low-energy $\pi^{\pm}$ mesons being especially high near the maximum of a nuclear-cascade shower. Consequently, the spatial and energy properties of the μ-meson component of extensive showers are related to the characteristics of nuclear collisions at low energies ($E < 10^{12}$ eV), and they depend only indirectly on the nature of the collision between the primary particle responsible for the extensive shower and the nucleus of an air atom.

The first information on the lateral distribution was obtained by studying the number of coincidences caused by μ mesons as a function of the distance between recording units. The measurements showed that μ mesons are spread out over greater distances from the shower axis than electrons are. Using complicated setups, it became possible to investigate the lateral

distribution of μ mesons quite thoroughly. Figure 5 shows the lateral distribution of μ mesons in extensive showers with total particle numbers of 10^5 and $7.7 \cdot 10^5$ at an altitude of 3860 meters above sea level. Recordings were made of μ mesons with energies $E_\mu \geqslant 440$ MeV /22/. Data for heavy showers at this same altitude /23/ were obtained for μ mesons with $E_\mu \geqslant 220$ MeV.

Data on the lateral distribution of μ mesons at sea level are quite numerous; Figure 6 shows the results of only the most comprehensive studies /8, 11, 24, 25/. The experimental accuracy attained so far, however, is not sufficient to give the lateral distribution as a function of the total number of particles in a shower or as a function of the observation altitude. To illustrate this, the experimental data were compared with a set of similar curves of the type

$$\rho_\mu(r, E_\mu, N, p) = \frac{0.22\, p \exp\left[-r/r_0(E_\mu)\right]}{\left[2 \cdot 10^8 (p - 500) + E_\mu\right]^{0.25}} \left(\frac{N}{10^5}\right)^{0.81} (2 + r)^{0.75}.$$

Values of $r_0(E_\mu)$ were selected which best fit the detailed data on the energy spectrum and lateral distribution of μ mesons in extensive showers in the lower third of the atmosphere:

$$r_0(E_\mu \geqslant 440 \text{ MeV}) = 300 \text{ m}; \quad r_0(E_\mu \geqslant 10^9 \text{ eV}) = 220 \text{ m};$$

$$r_0(E_\mu \geqslant 5 \cdot 10^9 \text{ eV}) = 100 \text{ m}$$

(p is the pressure in g/cm^2 at the observation altitude). The ratio between the number of electrons and the number of μ mesons will be discussed later. The form of the approximation formula is interesting because in a large number of experimental studies the measurements are made at comparatively small distances from the axis, where the density of the μ-meson flux decreases with distance more slowly than $\sim r^{-2}$. A conversion of these data to the total number of μ mesons in the shower is possible only based on some sort of a priori data in the form of a lateral distribution of the μ mesons.

The approximation given here for the lateral distribution of the μ-meson flux can easily be related to the distribution of transverse momenta of secondary $\pi^\pm$ mesons in nuclear-interaction events. The energies of most particles produced in a nuclear interaction are much less than the energy of the particle causing the interaction. However, the transverse momentum is apparently independent of the energies of the colliding particles. Consequently, we need take into account the deflections from the shower core just in the last nuclear-collision event. The distribution of transverse momenta has been well studied in experiments with photographic emulsions and Wilson cloud chambers. This distribution can be represented analytically in the form

$$W(p_\perp)\, dp_\perp \sim p_\perp e^{-p_\perp/a}\, dp_\perp,$$

$$a = 105 \text{ MeV}/c.$$

Such a distribution fits the experimental data /27/ satisfactorily. Both the most probable value $p_\perp^b = 0.21$ BeV/c and the mean value $p_\perp = 0.315$ BeV/c show good agreement with various photoemulsion measurements /28/. Since $cp_\perp = E \sin\theta$, where θ is the angle between the directions of the primary and secondary particles, the following angular distribution of particles with an energy E can be obtained from the distribution of

different transverse-momentum values:

$$W(E, \theta)\, d\theta = AE^2 \sin^2\theta e^{-\frac{E}{a}\sin\theta} E\cos\theta\, d\theta,$$

where A is a normalization factor.

If we assume that the energy spectrum of the secondary particles is $f(E)\,dE = B\frac{dE}{E^2}$, then the angular distribution of particles with an energy greater than E is

$$W(\theta_1 > E_m) = AB\sin^2\theta\cos\theta\, d\theta \int_{E_m}^{E_0} Ee^{-\frac{E}{a}\sin\theta} dE =$$

$$= ABa^2\cos\theta\left(\frac{E_m}{a}\sin\theta + 1\right) e^{-\frac{E_m}{a}\sin\theta} d\theta.$$

For low-energy particles, the ionization losses over the path from the height at which the particles originate down to the recording level cannot be neglected. Thus, for these particles E_m is a function of the height of particle production h and does not coincide with the energy cutoff E_μ of the recording. For μ mesons this must be taken into account for $E_\mu < 2 \cdot 10^9$ eV. From the angular distribution it is possible to obtain the distribution of distances from the shower axis for particles produced at a height h, assuming that all the particles are produced in the shower core. Such an assumption is valid provided we ignore particle production near the observation level. When $\sin\theta$ and $\tan\theta$ can be replaced by $\theta \sim r/h$, we obtain

$$\rho(r_1 > E_\mu) \sim \frac{dr}{rh}\left(\frac{E_\mu r}{ah} + 1\right)\exp\left(-\frac{E_\mu r}{ah}\right).$$

Consequently, the particles produced at some effective height $h_{\text{eff}} \gg r$ have a lateral distribution which can be used for comparison with the experimental data.

Coulomb-scattering effects and the deflection of μ mesons by the geomagnetic field were compared with the actually observed distribution of μ mesons in extensive air showers /22, 23/. If the lateral distribution of μ mesons with E from 3.5 to 4 BeV is considered, then the observed root-mean-square radius is $r \sim 300$ meters. The Coulomb scattering of mesons produced at a height of 10 km has an RMS radius of ~ 50 meters. The deflection by the geomagnetic field is ~ 50 meters, observed only in the east-west direction. Both of these estimates were made neglecting ionization losses, so that the deflections from the shower axis are exaggerated. In spite of this, the total deflection is considerably less than the value observed experimentally. Hence, the transverse momenta produced by π mesons during nuclear interactions must play a determining role in deflecting μ mesons from the shower axis.

If the lateral distribution of μ mesons is recognized as being independent of the total number of particles, then studies of the dependence of the number of μ mesons on the shower intensity will reduce to measuring the relative proportion of μ mesons at a specified distance from the shower axis. Such measurements were initiated in /29/, by means of varying the areas of the counters included in the coincidence arrangement. This set of measurements established that the relative number of μ mesons decreases with an increase in shower intensity.

Subsequent measurements using more sophisticated techniques were made both at mountain altitudes /8, 22, 23/ and at sea level /24, 25, 30/, and these verified the drop in the proportion of μ mesons as the number of electrons in the shower increased. The authors of these works concluded that either the dependence of the proportion of μ mesons on the number of electrons in the shower is variable or else the decrease is proportional to $N^{-0.25}$. The totality of data given in all the enumerated studies can for the time being be fit to the single dependence $\frac{N_\mu}{N} \sim N^{-0.19 \pm 0.03}$, for showers with $10^4 < N < 10^9$. Moreover, extrapolation of this dependence to extremely light showers ($N \sim 10$) does not lead to absurd results. This relation for the relative number of μ mesons as a function of the total number of particles in a shower agrees well with theoretical calculations /31/.

IV. FLUCTUATIONS IN THE RELATIVE NUMBER OF μ MESONS AT THE LEVEL OF MEASUREMENTS

The accumulation lengths for electrons and μ mesons in an extensive air shower are different, and the mean free paths of μ mesons are relatively large. Thus, the study of fluctuations of the μ-meson flux in a shower should give information on fluctuations during the development of showers in the atmosphere, and on the composition of the ultrahigh-energy primary radiation. The latter two factors undoubtedly affect fluctuations in the μ-meson flux. Therefore, a complete solution of the problem is possible only in conjunction with other data on fluctuations in the shower development over the atmospheric depth or on the composition of the primary radiation in the corresponding energy range. So far, the fluctuations of the μ-meson flux due to the difference in effective cross section for nuclear interactions of primary protons and heavier primary nuclei have been considered the most systematically /25/. The basic assumption of these calculations has been that the μ-meson flux at the level of the measurements is proportional to the total energy lost by the primary particle in the atmosphere, while the number of electrons depends on the height at which the shower originates. To determine experimentally the number of μ mesons in an individual extensive air shower, a large number of meson detectors must be employed to measure the lateral distribution of μ mesons in the shower. The energy of the mesons recorded must be high enough to allow us to neglect their absorption in the atmosphere ($E_\mu \geqslant 2 \cdot 10^9$ eV). In the studies made so far /8, 24, 25, 26/, the area and number of detectors have been insufficient for such measurements.

Let us now consider in more detail a study /32/ in which an analysis of the fluctuations in the relative number of μ mesons leads to the conclusion that the primary radiation with an energy $E_0 \sim 10^{18}$ eV consists of single protons. The relative number of μ mesons over distances from 70 to 300 meters from the shower axis were counted, for extensive showers with $N > 10^8$, both for vertical incidence and for shower arrival at large angles to the vertical. In the former case extensive air showers with $N > 10^8$ at the observation height selected (820 g/cm^2) appear to be at their maximum development, which reduces the fluctuations associated with formation and development of the shower over the depth. However, if the decrease in the

relative number of μ mesons with the rise in the number of electrons in the shower is assumed to depend on the energy of the primary particle, then showers initiated by protons and by heavier nuclei must have different relative numbers of μ mesons, even in the absence of fluctuations in shower development over the depth. Actually, for the same energy of a primary particle in showers caused by primary nuclei, the energy for a single nucleon is $\frac{E_0}{A}$. By taking this into account, and by assuming that the composition of the primary radiation for energies $E_0 \sim 10^{18}$ eV is the same as for $E_0 \sim 10^{12}$ eV, we can compute the probable distribution of extensive air showers with respect to the relative number of μ mesons. The result of such a calculation is shown in Figure 7 in the form of curves. The experimental data (histogram) are also shown in the figure, and they give a considerably narrower distribution of the relative number of μ mesons. From this comparison the authors of /32/ concluded that primary radiation with $E_0 \sim 10^{18}$ eV is uniform in composition (either it consists of protons or of heavy nuclei). For extensive air showers arriving at large angles to the vertical and reaching the stage of maximum development, large fluctuations are observed. This would not be the case if the primary radiation were uniform in composition and consisted of heavy nuclei in the energy range studied.

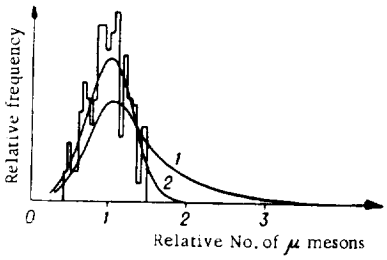

FIGURE 7. Composition of primary radiation: 1–calculation, taking into account the complex composition of the primary radiation; 2–only protons.

However, there is some doubt as to whether the composition of the primary radiation is really uniform. The decision for uniformity was based on the absence of the fluctuations expected in the case of a complex primary composition. Large fluctuations are predicted for the total number of μ mesons in a shower. It was demonstrated experimentally that large fluctuations in the relative μ-meson flux density are absent at distances from 70 to 300 meters from the shower axis; this corresponds to the fluctuations in the total number of μ mesons only in the event of a standard lateral distribution of mesons in the shower. Such a distribution has not been proved as yet either experimentally or theoretically. At the same time, it can be shown that the fluctuations in the μ-meson flux density for $E_\mu > 10^9$ eV over the distances considered in /32/ reflect only the nature of the shower development in the lower part of the atmosphere. Let us assume that: (1) the μ mesons are produced near the shower core, where the nuclear-active component of the shower is concentrated; (2) the main causes of the lateral distribution of the μ mesons in a shower are the transverse momenta which the π meansons acquire upon production. When these factors are taken into account, it follows that μ mesons with an energy E_μ, which originated as a result of the decay of π mesons generated at a height h, will be observed at distances from the shower axis of $r \geqslant h\frac{c\bar{P}_\perp}{E_\mu}$ (where $\bar{p}_\perp \sim 0.3 \cdot 10^9$ eV/c). Thus, the height at which μ mesons with the specified energy, located a distance r from the shower axis, are produced is

$h \leqslant r\frac{E_\mu}{cP_\perp}$. This means essentially that low-energy μ mesons ($E_\mu < 5$ BeV) observed at distances $r < 400$ meters from the shower axis are produced effectively at heights of less than 6 km above the observation level; these are the same heights at which the recorded electron-photon component is produced effectively. This explains the small number of fluctuations in the relative count of μ mesons for a group of showers near the vertical, when, since the showers are at their maximum stage of development, all the fluctuations are smoothed out. The condition that the measured flux of μ mesons with an average energy E_μ include the mesons generated in the upper half of the atmosphere can be expressed as follows:

$$\bar{E}_\mu r > 10^3 cp_\perp.$$

Thus it is evident that measurements of fluctuations of high-energy μ mesons ($E_\mu > 3 \cdot 10^{10}$ eV) are more promising. In /33/ rare events of extremely sharp deviations of the relative number of μ mesons from the average were sought. It is assumed that, once we determine the frequency of occurrence of extensive air showers in which the number of μ mesons is much less than the average (1/50 to 1/100 of the average), it may be possible to estimate the proportion of γ quanta in the ultrahigh-energy primary radiation. The preliminary results indicate that such showers are very infrequent. Only $\sim 0.03\%$ of the showers with $N > 10^6$ have numbers of μ mesons which differ by factors of more than 50 from the average value. The rarity of events imposes high demands on the accuracy of the recording and analysis of events. However, if for energies $E_0 > 10^{15}$ eV interactions are encountered in which there is practically complete energy transfer to π° mesons, the frequency of showers "without μ mesons" ($\sim 0.03\%$) does not characterize the proportion of γ quanta in the primary radiation; rather, it characterizes the probability of the occurrence of elementary acts in which more than 90% of the energy of the primary nucleon is transferred to π° mesons.

V. THE ENERGY FLUXES OF DIFFERENT COMPONENTS OF EXTENSIVE AIR SHOWERS

Measurement of the energy fluxes of the various shower components is of interest because it helps reconstruct the overall formation and development of a shower. Moreover, if we wish to determine the energy of the primary responsible for a shower with a given number of particles at the measurement level, then we must measure: the energy of the electron-photon component and nuclear-active particles at the observation level; the energy expended by shower particles on ionization in the atmosphere down to the observation level; the energy transferred to below the measurement level by μ mesons; and finally, the energy imparted to neutrinos in the atmosphere. The energy transferred to neutrinos cannot as yet be determined experimentally. It has been estimated at half the energy of the μ-meson component. At any rate, the neutrinos do not receive as much energy as the μ mesons /34/, which contain a relatively small part of the energy of the primaries. There are also other means of energy loss which are either completely or partially overlooked during quantitative

observations, but their contribution to the overall energy balance is negligible. The energy fluxes of the μ mesons, the nuclear-active particles, and the electron-photon component of a shower can be determined by integrating over the energy spectrum the corresponding particles in an extensive shower at the observation level. The results for a height of 3860 meters above sea level are shown in the table. The uncertainty in the

	μ mesons	Electron-photon component	Nuclear-active particles	Energy expended on ionization above observation level
Results of integration over energy spectrum	$(2.1\pm^{2}_{0.2})\,10^{14}\times \times\left(\frac{N}{10^6}\right)^{0.81}$ eV	$(2.1\pm0.3)\cdot10^{14}\times \times\left(\frac{N}{10^6}\right)$ eV	$(7\pm1)\cdot10^{13}\times \times\left(\frac{N}{10^6}\right)$ eV	—
Energy flux determined by "calorimetric" method	—	$(2.2\pm0.2)\cdot10^{14}\times \times\left(\frac{N}{10^6}\right)$ eV	$(9\pm2)\cdot10^{13}\times \times\left(\frac{N}{10^6}\right)$ eV	$(8\pm2)\cdot10^{14}\cdot\left(\frac{N}{10^6}\right)^{0.81}$
Energy-flux fluctuations (mean relative deviation)	±30%	±20%	±80%	±30%
Energy flux in showers with $N=3.5\cdot10^6$, taking into account fluctuations	$(0.9\pm^{0.9}_{0.3})\cdot10^{14}$ eV	$(0.75\pm0.16)\cdot10^{14}$ eV	$(0.3\pm0.25)\cdot10^{14}$ eV	$(3.4\pm1.0)\cdot10^{14}$ eV

estimate of the energy transferred by the μ-meson component is a result of the lack of experimental data on the form of the μ-meson energy spectrum for energies $E_\mu > 2\cdot10^{10}$ eV in the extensive air showers with a specified number of particles at the measurement level. The error in the energy flux assigned to the electron-photon component, on the other hand, is a result of a certain arbitrariness in the interpolation of the energy spectrum for 0 to 10^9 eV. The results for the μ-meson and electron-photon components are valid for total numbers of shower particles in the range $10^4 < N < 10^6$. The energy spectrum of nuclear-active particles has not been determined sufficiently well, both at the low-energy end ($E_0 < 10^{10}$ eV) and at the high-energy end, where the number of particles with energies higher than the value of interest may be less than one per shower. Moreover, the energy spectrum depends on the total number of particles in the shower. The energy fluxes given in the table for nuclear-active particles are valid for $10^5 < N < 10^6$.

The energy fluxes of the electron-photon and nuclear-active components were determined differently, by measuring the absorption of these components in lead (calorimetric method). The results of these measurements for showers with $10^5 < N < 10^6$ are shown in the table.

Measurements of the energy lost by shower particles in the atmosphere over the observation level became possible only after a study of the Čerenkov radiation of shower particles in the atmosphere /19, 35/. In these experiments the lateral distribution of the Čerenkov-radiation intensity was measured for extensive showers with different numbers of charged particles at the observation level. The absorption of Čerenkov radiation in the atmosphere is negligible (< 10%). Consequently, by integrating the lateral distribution of the radiation over the entire distance, the total ionization losses in the energy of particles traveling faster than the velocity

of light in the atmosphere can be evaluated. For electrons, which are the major contributors to the ionization of the atmosphere during showers, this corresponds to a cutoff energy of 20 to 100 MeV, depending on the air density. To take into account the energy lost by the ionization of electrons with energies less than the cutoff, it is sufficient to assume that these electrons are absorbed just as described by the electron-photon cascade theory, which specifies the shower development with atmospheric depth, albeit very approximately. For observations of showers with total numbers of particles from 10^5 to 10^6 at heights of ~ 4 km, the latter assumption cannot affect the calculation results, since the showers observed are near the stage of maximum development. The behavior of electrons with energies $E < 100$ MeV in an actual shower also definitely agrees with cascade theory. The energy losses to ionization of the atmosphere over the observation level, determined by this means, are given in the "calorimetric-method" row of the table. The experimental data show that these expressions are valid for showers with total numbers of particles of 10^5 to $2 \cdot 10^6$ at 3860 meters above sea level.

The table also gives tentative estimates of the fluctuations in the energy fluxes of the different shower components. The fluctuations are expressed as mean relative deviations from the average energy fluxes of the respective components.

VI. THE ENERGY SPECTRUM OF THE PRIMARY RADIATION

On the basis of experiments conducted in the Pamirs ($p = 650$ g/cm^2), it is possible to calculate the total energy lost by a primary particle during the initiation of a shower. For this calculation, no arbitrary assumptions concerning the scheme of shower development and the nature of elementary processes at ultrahigh energies are needed. The last row of the table gives the average energy fluxes of the different components of showers with $N = 3.5 \cdot 10^5$. The total energy, taking into account the energy carried off by neutrinos, is $(6 \pm 0.6) \cdot 10^{14}$ eV. The uncertainty in the average value allows for both experimental errors and energy-flux fluctuations from shower to shower. If the data of geomagnetic measurements /36, 37/ are also assumed to be reliable enough, the energy spectrum of the primary radiation for energies of 10^{10} to 10^{15} eV can be represented as $F(> E_0) = c\left(\frac{E_0}{6 \cdot 10^{14}}\right)^{-\gamma}$, where $c = 1.9 \cdot 10^{-2}$ particles/hr m^2 sterad and $\gamma = 1.6 \pm 0.03$. The point corresponding to showers with $N = 3.5 \cdot 10^5$ was not selected by accident: for a further increase in the energy of the primaries, the exponent of the energy spectrum increases. The primary energy spectrum shown in

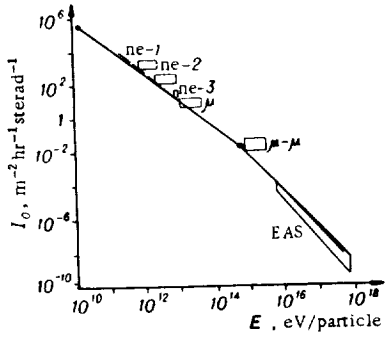

FIGURE 8. Dashed line shows data of /48/. [EAS stands for extensive air showers and ne for nuclear emulsions.]

Figure 8 was plotted from photoemulsion data /38, 39/ and from data on the μ-meson intensity at great depths/40/. Both sets of data give intensities which are too high. The high values resulting from the measurements of high-energy μ mesons can be attributed to the incompleteness of the information on μ-meson production. The error in determining the energy of the particles producing streaks in the photoemulsions is introduced because the effect of fluctuations for a decreasing intensity of the interacting particles at higher energies was not taken into account /41/.

For primary energies exceeding 10^{15} eV, two problems arise. First, what is the shape of the energy spectrum for $E_0 > 10^{15}$ eV, and second, what is the upper limit for the energies encountered in cosmic rays (provided it exists)? The definite power-law shape of the number spectrum for extensive air showers with $10^6 < N < 10^8$ enables us to assume that the energy spectrum of the primaries also follows a power law. To determine the exponent of the spectral function, it must be assumed that the formation and development of a shower at primary energies $E_0 > 10^{15}$ eV is similar to that of a shower in the energy range which has been studied in more detail ($E_0 < 10^{15}$ eV). After the corresponding calculations /14/ for such an assumption, the exponent was found to be $\gamma = 2.17 \pm 0.1$.

The exponent can be evaluated using a less binding assumption concerning the shower development, provided we consider the energy lost by cascade electrons for ionization to be the determining part of the energy of the primaries. A correction allowing for displacement of the maximum of an electron-photon shower due to a variation in the energy of the primary can be obtained from the relative change in the size of the Čerenkov-radiation burst. The exponent obtained in this way /35/ for the integral spectrum of the primary radiation was $\gamma = 2.1 \pm 0.2$ for primary energies $10^{15} < E < 10^{16}$ eV. This correction is not necessary if the spectrum of the extensive showers is observed at maximum shower development. In this case /20/, $\gamma = 2.2 \pm 0.1$ for $10^{16} < E_0 < 2 \cdot 10^{17}$ eV. Therefore, the value $\gamma = 2.15 \pm 0.06$ satisfies all the data considered.

VII. THE SEARCH FOR ANISOTROPY OF THE PRIMARY RADIATION

Anisotropy of the primary radiation at ultrahigh energies is sought in two ways: by measuring the sidereal variations of extensive air showers, recorded over a wide solid angle using simple equipment; or by means of more sophisticated observations of extensive showers in which the point on the celestial sphere is determined from which the primary particle for each recorded shower arrives.

The first method has been applied in a great many studies, and there is no need to cite them here. A correlation with sidereal time of the frequency of recording extensive showers was not observed for showers caused by primaries with energies $E_0 \sim 2 \cdot 10^{13}$ eV (accuracy up to 0.1%) /42/, $E_0 \sim 2 \cdot 10^{15}$ eV (accuracy up to 0.5%) /42/, and $E_0 \sim 3 \cdot 10^{16}$ eV (accuracy up to 3%) /43/. It should be noted that the accuracy of measurements of the sidereal variations of extensive showers caused by primaries with energies of 10^{14} to 10^{16} eV is limited not so much by the counting statistics as by the reliability of introducing corrections.

Recently many experimenters have made systematic determinations of the axis positions in sidereal coordinates for each shower recorded. Analysis of the distribution of points on the celestial sphere, however, has not as yet indicated definitely any preferred regions in which the frequency of arrival of ultrahigh-energy particles is greater. In /8/ some preference was noted for directions lying in a plane perpendicular to the arm of the galaxy, for primaries with $E > 5 \cdot 10^{17}$. However, subsequent data obtained using the same equipment did not verify this preliminary result, and on the basis of this /44/ it can be stated that primary radiation with $E_0 > 3 \cdot 10^{18}$ eV is isotropic with an accuracy up to 40%. In /45/, on the basis of similar measurements, a possible 20 to 40% anisotropy was noted for the particles causing extensive showers with $N > 10^8$, which corresponds to primary energies $E_0 \geqslant 5 \cdot 10^{17}$ eV. The preferential direction was that of the plane of the galaxy. In /44/, where the statistical accuracy was better, no anisotropy in the arrival of these particles was noted (accuracy of 10%). Analyses of the direction of arrival of heavy primary nuclei with $E_0 \sim 10^{16}$eV have also been attempted. The incidence of a heavy nucleus at the limit of atmosphere has been associated with the recording of an extensive air shower rich in μ mesons. Quite high anisotropy was detected /46/. The most preferred directions were those in the plane perpendicular to the galactic arm, but this conclusion has so far not been borne out statistically.

To conclude this brief review of experimental data on extensive air showers, in connection with cosmic-ray research from the point of view of space physics, let us mention the following basic tasks of future experiments.

1. Energy-spectrum studies and the search for anisotropy of the lateral distribution of the primary radiation for $E_0 > 10^{19}$ eV. These subjects are related for two reasons: first, successful measurements in this energy range will require the construction of equipment enabling the effective recording of extensive air showers over areas of tens and hundreds of square kilometers. On the other hand, both a variation of the energy spectrum at extremely high energies and the appearance of anisotropy may be observed in the same energy range.

2. Studies of the chemical composition of the primary radiation. The experiments related to this very difficult subject are still only in the first stages. However, data on the nature of the particles causing extensive air showers are vital for cosmic-ray research, both from the point of view of space physics and from the point of view of nuclear theory.

P.N. Lebedev Institute of Physics of
the USSR Academy of Sciences

REFERENCES

1. NIKOL'SKII, S.I. and V.M. SELEZNEV.— ZhETF, 32, 1250. 1957.

2. DOBROVOL'SKII, S.P., S.I. NIKOL'SKII, E.I. TUKISH, and V.I. YAKOVLEV.— ZhETF, 31, 939. 1956.

3. KAMATA, K. and J. NISHIMURA.— Progr. Theor. Phys. Suppl., No.6, 93. 1958.

4. HERSIL, J., J. ESCOBAR, G. CLARK, S. OLBERT, S. MOORE, and D. SCOTT.— J. Phys. Soc. Japan, 17, Suppl. A-III, 243. 1962.

5. ZATSEPIN, V.I. — ZhETF, **33**, 190. 1957.

6. GRIGOROV, N.L. and V.Ya. SHESTOPEROV.— ZhETF, **34**, 1539. 1958.

7. KHRISTIANSEN, G.B.— ZhETF, **34**, 956. 1958.

8. LINSLEY, J., L. SCARSI, and B. ROSSI.— J. Phys. Soc. Japan, **17**, Suppl. A-III, 243. 1962.

9. MISHNEV, S.I. and S.I. NIKOL'SKII.— ZhETF, **38**, 257. 1960.

10. KULIKOV, G.V. and G.B. KHRISTIANSEN.— ZhETF, **35**, 635. 1958.

11. FUKUI, S., H. HASEGAWA, T. MATANO, I. MIURA, M. ODA, K. SUGA, G. TANAHASHI, and Y. TANAKA.— Progr. Theor. Phys., Suppl. No. 16, 1. 1960.

12. CRANSHAW, T., J. DE BEER, W. GALBRAITH, and N. PORTER.— Phil. Mag., 3, 377. 1958.

13. DELVAILLE, J., F. KENDZIORSKI, and K. GREISEN.— Trudy MKKL, **2**, 107. 1960.

14. ROSSI, B.— Trudy MKKL, 2, 17. 1960.

15. GREISEN, K.— Progr. Elem. Part. Cosm. Ray Phys., **3**, 1. 1956 [Russian translation. 1958.].

16. GREISEN, K.— Ann. Rev. Nucl. Sci., **10**, 63. 1960.

17. HINATANI, K.— J. Phys. Soc. Japan, **17**, 24. 1962.

18. KAMEDA, T., T. MAEDA, and Y. TOYODA.— Trudy MKKL, 2, 56. 1960.

19. CHUDAKOV, A.E., N.M. NESTEROVA, V.I. ZATSEPIN, and E.I. TUKISH.— Trudy MKKL, 2, 47. 1960.

20. CLARK, G.— Proc. of the Fifth Inter-American Symposium on Cosmic Rays. La Paz, Bolivia. 1962.

21. ALEKSEEV, A.D., G.T. ZATSEPIN, and I.R. MOROZOV.— DAN SSSR, 63, 375. 1948.

22. VAVILOV, Yu.N., Yu.F. EVSTIGNEEV, and S.I. NIKOL'SKII.— ZhETF, **32**, 1319. 1957.

23. ANTONOV, Yu.N., Yu.N. VAVILOV, G.T. ZATSEPIN, A.A. KUTUZOV, Yu. V. SKVORTSOV, and G.B. KHRISTIANSEN.— ZhETF, **32**, 227. 1957.

24. KHRENOV, B.A. Candidate's dissertation, Fizicheskii institut Akademii nauk SSSR. 1962.

25. ABROSIMOV, A.T., G.A. BAZILEVSKAYA, V.I. SOLOV'EVA, and G.B. KHRISTIANSEN.— Trudy MKKL, 2, 92. 1960.

26. BENNETT, S. and K. GREISEN.— Phys. Rev., **124**, 1982. 1961.

27. GUSEVA, V.V., N.A. DOBROTIN, N.G. ZELEVINSKAYA, K.A. KOTEL'NIKOV, A.M. LEBEDEV, and S.A. SLAVATINSKII.— Izv. AN SSSR, seriya fizicheskaya, **26**, 549. 1962.

28. SCHEIN, M., D.M. HASKIN, E. LOHRMANN, and M. TEUCHER.— Trudy MKKL, 1, 7. 1960.

29. COCCONI, G., V. TONGIORGI, and K. GREISEN.— Phys. Rev., **75**, 1063. 1949.

30. CLARK, G., J. EARL, W. KRAUSHAAR, J. LINSLEY, B. ROSSI, and F. SCHERB.— Nuovo Cim., **8**, Suppl. 2, 623. 1958.

31. UEDA, A. and N. OGITA.— Prog. Theor. Phys., **18**, 269. 1957.

32. LINSLEY, J. and L. SCARSI.— Phys. Rev. Letters, **9**, 123. 1962.

33. SUGA, K.— Proc. of the Fifth Inter-American Symposium on Cosmic Rays. La Paz, Bolivia. 1962.

34. PUPPI, G. and N. DALLAPORTA.— Progr. Elem. Part. Cosm. Ray Phys., **1**, 263. 1952 [Russian translation. 1954.].

35. NESTEROVA, N.M. Thesis, MGU. 1962.

36. CHARAKHCH'YAN, A.N. and T.N. CHARAKHCH'YAN.— Trudy MKKL, 3, 1960.

37. NEHER, H.V.— Progr. Elem. Part. Cosm. Ray. Phys., **1**, 243. 1952 [Russian translation. 1954].

38. LAL, D.— Proc. Indian Acad. Sci., **38**, 93. 1953.

39. KAPLON, M.F. and D.M. RITSON.— Phys. Rev., **88**, 386. 1952.

40. BARRETT, P.H., L.M.BOLLINGER, G.COCCONI, Y.EISENBERG, and K. GREISEN.— Rev. Mod. Phys. **24**, 133. 1952.

41. NIKISHOV, A.I. and I.L. ROZENTAL'.— ZhETF, **35**, 165. 1958.

42. CACHON, A.— Proc. of the Fifth Inter-American Symposium on Cosmic Rays. La Paz, Bolivia. 1962.

43. GREISEN, K.— Trudy MKKL, **3**, 152. 1960.

44. LINSLEY, J., L. SCARSI, P.J. ECCLES, and B.ROSSI.— Phys. Rev. Lett., **8**, 286. 1962.

45. GREISEN, K.— Proc. of the Fifth Inter-American Symposium on Cosmic Rays. La Paz, Bolivia. 1962.

46. HASEGAWA, H., T. MATANO, I. MIURA, M.ODA, G. TANAHASHI, Y.TANAKA, S. HIGASHI, T. KITAMURA, Y. MISHIMA, S. MIYAMOTO, K. SHIBATA, and Y. WATASE.— Phys. Rev. Letters, **8**, 284. 1962.

47. DANILOVA, T.V., E.V. DENISOV, S.I. NIKOLSKY, and A.A.POMANSKY.— Phys. Soc. Japan, **17**, Suppl. A-III, 205. 1962.

48. BARADZEI, L.T., V.I. RUBTSOV, Yu.A. SMORODIN, M.V. SOLOV'EV, and B.V. TOLKACHEV.— Izv. AN SSSR, seriya fizicheskaya, **26**, 576. 1962.

N67 38209

S.N. Vernov, V.I. Solov'eva, B.A. Khrenov, and G.B. Khristiansen

PRIMARY COSMIC RADIATION IN THE ULTRAHIGH-ENERGY RANGE AND EXTENSIVE AIR SHOWERS

Comprehensive studies of extensive air shows (EAS) were recently made using the detector arrangement of Moscow State University. These studies provided a great deal of experimental material related to primary cosmic radiation at ultrahigh energies. This report presents the total data obtained for 1960 and 1961.

DESCRIPTION OF THE DETECTOR ARRANGEMENT

The arrangement comprised 18 detector points located within a circle 120 meters in radius. The detectors measured the densities of charged particles and μ mesons (Figure 1). The Geiger counters forming the detector system were connected to a hodoscope.

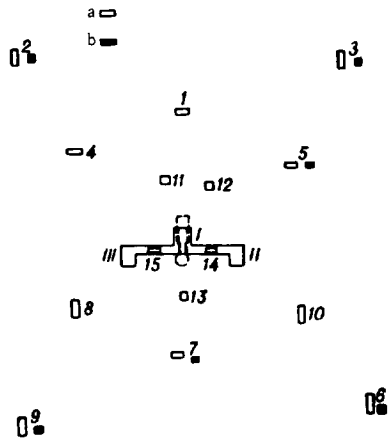

FIGURE 1. Plan of the arrangement.

a – detectors of charged-particle densities;
b – μ-meson detectors ($E \geq 6 \cdot 10^8$).

At the central point (I in Figure 1), 30 charged-particle detectors and 2 μ-meson detectors, located within a circle 7 meters in radius, were

placed at depths of 20 and 40 m. w. e. [meters water equiv.]; these had areas of 3.2 and 6.3 m^2, respectively. The minimum energy required to penetrate a ground layer 20 m. w. e. thick is $5 \cdot 10^9$ eV, and for a layer 40 m. w. e. thick it is 10^{10} eV.

At the other 17 points were placed charged-particle detectors, and at 6 of them were placed detectors of low-energy μ mesons ($E \geqslant 6 \cdot 10^8$ eV), each with an area of 0.8 m^2 (2 muon detectors 60 meters from the center and 4 detectors 120 meters from the center; see Figure 1). This arrangement made it possible to study showers with $N \sim 3 \cdot 10^4$ to $3 \cdot 10^7$ particles. The setup was controlled by means of a system of six counter banks, each with an area $\sigma = 0.132\ m^2$, connected in sixfold coincidence and placed at the central point.

THE MAIN RESULTS

Due to the complexity of the EAS radiation, the Moscow-University arrangement promises to be very effective for studying the ultrahigh-energy primary radiation. The discussion to follow will indicate the special significance of recording fluxes of high-energy μ mesons in an individual shower, using this complicated measuring system.

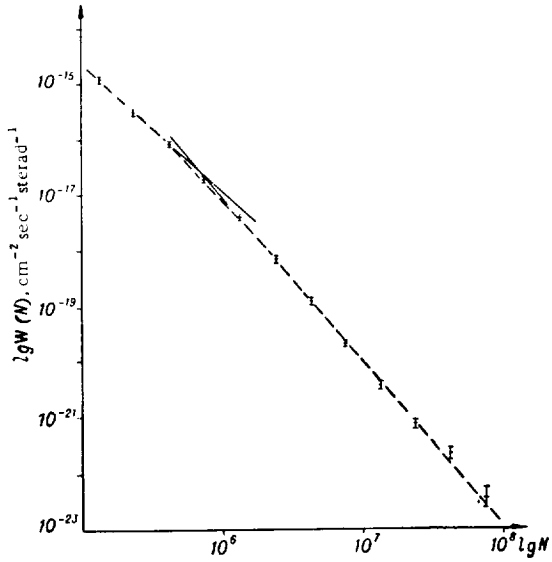

FIGURE 2. Differential number spectrum of showers.

First, let us consider the energy spectrum of the primary radiation. Due to its insufficient reception range, the Moscow-University arrangement cannot be used to determine the intensity of primary radiation with an energy close to the maximum recorded recently by Rossi and Clark /1/. At the same time, in contrast to the equipment of Rossi and Clark, the Moscow-University arrangement enables a detailed study of the energy spectrum in the low-energy range.

As early as 1958, an analysis of the experimental data on EAS obtained by the Moscow group /2/ indicated that there is a quite sharp variation in the index of the integral number spectrum for showers with $N \sim 10^5$ to 10^6 particles. Subsequently this same result was obtained using the Moscow-University arrangement (conference at Borzhomi in 1961; conference in Japan in 1961) /3/, and also by Japanese (1960, 1961) /4/ and English (1962) /5/ investigators.

For interpreting this result, both the integral spectrum, which was obtained in all the above-mentioned studies except /5/, and the differential number spectrum of the showers are of great interest.

Figure 2 shows the differential number spectrum of the showers, obtained from 1960 to 1962 using the Moscow-University arrangement. This spectrum was plotted as follows. To determine the intensity of showers with N particles per unit interval of N, the number of showers I with N between N_1 and N_2 having axes within a circle of radius R (with its center at point I in Figure 1), observed in a time T, was calculated. The location of the shower axis r and the number of particles N were found using the average lateral distribution of charged particles, which has been investigated in a number of works and which agrees with the theoretical distribution of Nishimura and Kamata for a value of the parameter $s = 1.25$. In accordance with experimental data, it was assumed that the lateral distribution does not vary within the interval of N considered. The radius R was so chosen that the probability of recording showers with N from N_1 to N_2 was more than 95% even at the edge of the circle. Therefore, the intensity of showers in the interval $N_1 - N_2$, per unit area and unit solid angle, is $I(0, N) = \frac{I}{\pi R^2 T} \cdot \frac{\nu + 1}{2\pi}$, where ν is the index in the angular distribution of EAS ($I(\theta, N) = I(0, N)\cos^{\nu}\theta$). The experimental data show that, in the interval of N in question, ν is independent of N. The shower intensity per unit interval was related to the value of N^* satisfying the following relation: $N^{*-(\varkappa+1)}(N_2 - N_1) \int_{N_1}^{N_2} N^{-(\varkappa+1)}\, dN$. (As $\varkappa$ varies from 1 to 2, N^* varies by 1.5%.)

The differential number spectrum in Figure 2 can be represented analytically as follows:

$$F(N)\,dN \sim N^{-(2.36 \pm 0.04)}\,dN \quad 10^5 < N \leqslant 1 \cdot 10^6;$$

$$F(N)\,dN \sim N^{-(2.75 \pm 0.10)}\,dN \quad 10^6 < N \leqslant 5.5 \cdot 10^6;$$

$$F(N)\,dN \sim N^{-(2.95 \pm 0.15)}\,dN \quad 5.5 \cdot 10^6 < N \leqslant 1 \cdot 10^8.$$

The sharp variation in the spectral index can be explained by assuming either a sharp variation in the index of the primary energy spectrum, or else a sharp variation in the characteristics of the nuclear-cascade process, leading in turn to a sharp variation in the shape of the cascade curve in the atmosphere as a function of the primary energy E_0. The latter assumption apparently contradicts the available experimental data. At any rate, for showers with N from $\sim 10^5$ to 10^7 studied at sea level, no significant variations with N of the shower structure and composition were observed, in spite of a thorough study of the electron-photon, nuclear-active, and μ-meson components.

Consequently, in the following only the first possibility will be considered. Variations in the index of the primary energy spectrum are to be expected

primarily for the following reason. At quite high energies, the coefficient of diffusion of cosmic rays in the galaxy is no longer constant and rapidly becomes an increasing function of the energy. This is equivalent to assuming that the parameter lH (where l is the dimension of a cloud and H is the strength of the field of the magnetic clouds at which diffusion takes place) has the characteristic distribution: values of lH lower than the most probable value $(lH)_V$ occur with a very low probability. In general, an increase in the diffusion coefficient D leads to a change in the composition of primary radiation with a given energy. This occurs, first, because the variation of D for nuclei begins at higher energies than for protons $\left(E_{\mathrm{cr}\,A} = \frac{A}{Z} E_{\mathrm{cr}\,P}\right)$, and, second, because the probability of fragmentation of nuclei decreases during the journey from the source.

Thus, the variation of the energy spectrum is determined by the distribution of primary radiation with A (that is, by $\varphi(A)dA$) and by the variation of the diffusion coefficient with energy (that is, by $D(E, A)$). The latter function can be related to the distribution of magnetic clouds (with values of lH) by means of the following simple expression /6/:

$$W(lH) \sim \frac{1}{D^2} \frac{dD(E)}{dE}\Big|_{E=300\,lHz}.$$

Let us return to the data in Figure 2. An extensive air shower generated by a primary particle with mass number A and energy E may, at a specified atmospheric depth X, consist of a different number of particles N; this is due to the possibility of fluctuations during development of the nuclear cascade. With an increase in A, of course, the fluctuations become smaller.

In /6/ the experimental data on the number spectrum were analyzed assuming that:

1) the fluctuations during shower development are determined by fluctuations in the height of the initial interaction of the primary particle;

2) the mass-number spectrum produced by supernovae in the energy range considered has the form $\varphi(A)dA = A^{-(n+1)}\,dA$, where n is from 0.5 to 1.0;

3) the energy spectrum produced by supernovae in the energy range considered has the form

$$f(E)\,dE = E^{-(\gamma+1)}\,dE,$$

where γ is from 1.5 to 2.0;

4) a variation in the mass-number spectrum for $E > E_{\mathrm{cr}\,P}$ occurs only due to a variation in the coefficient of diffusion in the galaxy, to a different degree for different A; the decrease in the probability of fragmentation is disregarded. Thus, the energy spectrum for cosmic rays in the galaxy has the form

$$F(E)\,dE = \int f(E)dE \cdot \varphi(A)dA \cdot D^{-1}(E/A).$$

In order to explain the observed variation in spectral index with these assumptions, it must be considered that the diffusion coefficient D varies abruptly from a constant value to $D\left(\frac{E}{A}\right) \sim E^{\alpha}$, where $\alpha > 0.5$ for a tenfold variation of E in the range $E \sim 10^{15}$ to 10^{16} eV, and then for higher energies remains $D\left(\frac{E}{A}\right) \sim E^{\alpha}$. A definite distribution of $W(lH)$ corresponds to such a

dependence of $D\left(\frac{E}{A}\right)$: in the range $lH \sim 10^{-6}$ to 10^{-5} gauss-parsec, the number of magnetic clouds rises sharply, goes through a maximum, and begins to decrease, so that for $lH > 10^{-5}$ gauss-parsec $W(lH) \sim (lH)^{-(\alpha+1)}$. If it is considered that the fluctuations are actually greater than assumed in /6/, the variations in functions $D(E)$ and $W(lH)$ must occur in an even lower range of E and lH. On the other hand, if the variation in the probability of nuclear fragmentation for an increase in the diffusion coefficient is taken into account, the range of E and lH in question may increase somewhat. **Nevertheless, a characteristic property of the distribution of $W(lH)$ obtained in this way must be a sharp rise in $W(lH)$ when lH approaches its most probable value $(lH)_v$ and a relatively low value of $W(lH)$ for $lH < (lH)_v$.** Other factors may also be responsible for the abrupt change in the primary energy spectrum:

1) the acceleration of particles in the clouds of supernovae is limited by the finiteness of the possible values of the corresponding parameter lH. Thus, limiting energies of cosmic rays are to be expected, for which the acceleration in supernovae is possible;

2) a rapid increase in the importance of metagalactic cosmic rays, whose energy spectrum may have a different index, is to be expected, along with a rapid rise, beginning at a certain energy, in the coefficient of cosmic-ray diffusion within the galaxy, and thus an increase in the escape of cosmic rays to beyond the limits of the galaxy.

These factors seem to us to be of low probability, for the following reasons. The energy spectra of the cosmic rays produced in different supernovae must differ considerably. Therefore, a sharp change in the energy spectrum averaged over all the sources is unlikely.

Moreover, with regard to cosmic rays of metagalactic origin, it is highly unlikely that a superposition of energy spectra with completely different natures would result in a comparatively smooth spectrum with one unique property: a rapid transition to a higher spectral index.

In order to ascertain the distribution of $W(lH)$ more accurately, however, more precise experimental data are necessary, as well as additional analysis taking into account the variation in the probability of fragmentation of heavy nuclei.

An experimental determination of the composition of the primary radiation, both for $E \leqslant E_{cr}$ and for $E > E_{cr}$, is very important with respect to this, and it is also of independent interest. The possibility of identifying showers caused by heavy primary nuclei has been discussed in several reports. In /7/ the identification of the primary nuclei on the basis of the core structure of a nuclear cascade in an EAS was considered. However, in /3/ it was pointed out that even statistically such an identification might be ambiguous. The statistical discrimination of nucleus-produced showers by selecting showers with a high flux density of high-energy μ mesons for a given total number of shower particles N was also considered recently /4, 8/. Experiments show /4, 8/ that the flux of high-energy μ mesons for a given N fluctuates considerably; this is related to the fluctuations in shower development, and possibly to a difference in the nature of the primaries producing showers with a given N.

Whatever the fluctuations in the development of the shower itself are, it is clear that they will decrease for higher A. Therefore, to produce a shower with a given N, more energy is required, on the average, in the

case of heavy primary nuclei than in the case of a primary proton. We know that $n_\mu \sim E^\beta$, where $\beta < 1$ (actually $\beta \sim 0.75$ to 0.85). Consequently, the number of μ mesons in such a nucleus-produced shower will also be higher. Moreover, it is reasonable to assume that a shower produced by a nucleus A is equivalent to the superposition of A proton-caused showers each with an energy E/A. Thus, for the primary nucleus, $n_\mu \sim E_0^\beta A^{1-\beta}$ increases with an increase in A.

For example, for showers with a given N, large values of the relative number of μ mesons $n_\mu/\bar{n}_\mu$ may correspond to showers produced by heavy primary nuclei.

In relation to this, it is interesting to compare the experimental distributions $f(n_\mu/\bar{n}_\mu)$ obtained for showers with different N in the range $N \sim 10^5$ to 10^7 (the range in which the variation of the coefficient of cosmic-ray diffusion in the galaxy occurs). At present, unfortunately, experimental data are available only for showers with $N \sim 10^7$. These data are given in Table 1, which shows the percentage of showers recorded over intervals of

TABLE 1

	Moscow data, %	Japanese data, %	Protons, % /10/	Heavy nuclei, % /10/	Protons, % /6/
0—1/3	8±3	6	6	0	0
1/3—2/3	30±5	20	37	15	9.5
2/3—1	22±4	34	24	41	30.5
1—1.5	22±4	26	18	35	60
1.5—3.0	11±3	14	12.5	9	0
>3.0	7±3	0	2.5	0	0

$n_\mu/\bar{n}_\mu$; similar data (Japan) from /9/ are also listed. The table includes theoretical distributions for showers produced by primary protons and heavy primary nuclei ($A=31$); these were obtained using the model considered by Zatsepin and Dedenko /10/, taking into account fluctuations in the development of a nuclear cascade within the atmosphere. The theoretical distribution for protons /6/, taking into account only fluctuations at the level of shower origin, is also given. A comparison of the experimental and theoretical data indicates that the experimental distribution is so wide that it cannot be accounted for by the presence in the primary radiation of heavy nuclei alone. The data in Table 1 are significant for still another reason. It is necessary to take into account the finite probability of low values of n_μ for comparatively high $\bar{n}_\mu$ when evaluating the possibility of studying showers produced by ultrahigh-energy γ quanta.

As pointed out in our report at the conference in Borzhomi, the number of μ mesons in showers produced by primary photons must be 1/100 of the average number in actually observed showers (over a wide range of distances from the axis). Therefore, if the distribution $f(n_\mu/\bar{n}_\mu)$ is not too wide, it should be possible to distinguish showers produced by γ quanta from ordinary showers, even if they occur extremely rarely. In /3, 4/ showers with such values of N were studied and μ-meson detectors with such areas were used that the average number of μ mesons observed over the detector area during showers was ~ 10. Consequently, showers

produced by γ quanta having the same N should not, as a rule, be accompanied by a single μ meson.

Interest in the primary γ radiation has recently grown considerably, since it apparently provides a very effective means of investigating the structure of galactic and, possibly, metagalactic space. However, so far only primary γ radiation of comparatively low energy ($E \geqslant 100$ MeV) has been detected (experiments of Kraushaar and Clark /11/). These experiments gave a flux of γ radiation which was 10^{-3} of the total primary flux. For higher energies the present experimental data enable only an estimate of the upper limit for the flux of primary quanta. According to the data of Duthie et al. /12/, at $E \sim 10^{12}$ eV the upper limit for the ratio between the number of primary γ quanta and the number of primary nuclear particles is 10^{-3}. For ultrahigh energies, the corresponding limit (10^{-2}) was cited in our report at the Borzhomi conference. Due to the processing of recent experimental data, this limit has been reduced considerably.

The experimental data used by us were obtained during 6500 operating hours of the Moscow-University arrangement. Showers with a quite large number of particles ($N > 4 \cdot 10^6$) and quite small distances r of the axis from the detector of μ mesons with $E \geqslant 10^{10}$ eV were selected from all the showers recorded. The maximum allowable distance was decided upon by the condition $f(r, N) = \rho_\mu$, where the function $f(r, N)$ is the familiar average lateral distribution of μ mesons with $E \geqslant 10^{10}$ eV. The density ρ_μ was taken as 1 particle /m^2. Since the area of a μ-meson detector is 6.3 m^2, this means that extensive air showers were chosen for which the expected average number of μ mesons with $E \geqslant 10^{10}$ eV incident on the detector is 6; there were 487 showers which satisfied this criterion. The probability that one of these showers would be one in which not a single meson passes through the μ-meson detector because of Poisson fluctuations is only 0.1. Next, the actual number of μ mesons incident upon the underground and surface μ-meson detectors in each of the selected showers was considered. During each of the showers selected, some μ mesons ($\geqslant 3$) traversed the μ-meson detectors. In all cases but 5, two or more μ mesons with $E \geqslant 10^{10}$ eV traversed a detector. Using our experimental data, therefore, it is possible to determine the probability that pure electron-photon showers will constitute a proportion α of the total number n of showers recorded:

$$P(\alpha n) \sim \sum_{n_i} \sum_{m=0}^{n_i} \frac{[\exp(-\alpha n_i)](\alpha n_i)^m}{m!} \left(1 - e^{\rho_{\mu_i}^{\gamma} \sigma}\right)^m,$$

where n_i is the number of EAS with a μ-meson density $\rho_{\mu_i}^{n}$; here $\rho_{\mu_i}^{\gamma}$ is the μ-meson density in pure electron-photon showers with the same number of particles N as the observed extensive air showers. The probability that α will be less than $2 \cdot 10^{-3}$ is 90%. To determine the ratios of the flux of primary γ quanta to the flux of primary nuclear particles in the same energy range, it must be taken into account that a given value of N for a shower produced by a γ quantum corresponds to a primary energy approximately one half to one fourth that for a shower produced by nuclear particles (here, the uncertainty in the coefficient for converting from N to E_0 for EAS produced by nuclear particles has an effect). Consequently, the upper limit for the proportion of primary γ quanta with $E \sim 10^{16}$ eV turns out to be from 10^{-4} to $4 \cdot 10^{-4}$.

Recent theoretical estimates give a limit of 10^{-3} to 10^{-5} for ultrahigh-energy particles, assuming that the γ radiation is mainly of metagalactic

origin. The validity of this assumption for low energies is confirmed by a comparison of the experimental data of Kraushaar and Clark with a theoretical calculation assuming a definite density of matter in the metagalaxy and assuming an expanding metagalaxy.

In conclusion let us consider the question of isotropy of the primary radiation at extremely high energies. The highest energy which could be recorded with our equipment was $E \sim 10^{17}$ eV. The isotropy of the entire primary radiation at this energy, regardless of its composition, was studied in detail by Rossi, Clark, and their co-workers /1/. These studies showed that for declinations from 0 to 60°, there is right-ascension isotropy to an accuracy up to 4%. (At any rate, no large-scale anisotropy was found.) We had the opportunity of studying the isotropy of the part of the primary radiation responsible for the high values of $n_\mu/\bar{n}_\mu$ in the distribution $f(n_\mu/\bar{n}_\mu)$. Most probably, the high values of $n_\mu/\bar{n}_\mu$ correspond to heavy nuclei in the primary radiation.

TABLE 2

Observation point	Sidereal time 0–6	6–12	12–18	18–20	N	$\frac{n_\mu}{\bar{n}_\mu}$
Moscow	21	26	16	17	$\geqslant 4 \cdot 10^6$	$\geqslant 1.5$
	47		33			
Japan	15	28	8	9	$\geqslant 1 \cdot 10^6$	$\geqslant 2.5$
	43		17			
Moscow	6	9	5	5	$\geqslant 4 \cdot 10^6$	$\geqslant 2.5$
	15		10			
Japan	5	9	3	3	$\geqslant 1 \cdot 10^7$	$\geqslant 2.5$
	14		6			

Table 2 shows data obtained during 4760 hours of operating the Moscow-University arrangement, for showers with $N \geqslant 4 \cdot 10^6$ and for $\frac{n_\mu}{\bar{n}_\mu} \geqslant 1.5$ and $\frac{n_\mu}{\bar{n}_\mu} \geqslant 2.5$. The table gives intervals of sidereal time and the numbers of showers recorded during each interval. Data obtained by the Tokyo and Osaka groups /9/ are given for comparison. Unfortunately, in 1960–1961 the Moscow-University arrangement did not include a system for determining the orientation of the shower axis. Thus, we were unable to specify the declination and right ascension for a shower axis, and we could only record the sidereal time of the vertical direction at the moment of recording an EAS. Consequently, the sidereal time for each shower recorded was established with an uncertainty (± 2 hours, on the average) related to the angular distribution of the shower axes.

If anisotropy exists, this circumstance could contribute only to a reduction of the observed effect. When our data are combined with the Japanese data (regardless of the fact that they pertain to different declination ranges), it is possible to detect a statistical decrease in the intensity of the showers

studied, upon transition from the interval 0h–12h sidereal time to the interval 12h–24h. However, only after further measurements are made will definite conclusions be possible.

Scientific-Research Institute of
Nuclear Physics, Moscow State University

REFERENCES

1. LINSLEY, J., L. SCARSI, and B. ROSSI.— J. Phys. Soc. Japan, 17, Suppl. A-**111**, 91. 1962; CLARK, G., J. EARL, et al.— Phys. Rev., **122**, 637. 1961.

2. KULIKOV, G.V. and G.B. KHRISTIANSEN.— Nuovo Cim., Suppl. 8, 742. 1958; ZhETF, **35**, 635. 1958.

3. VERNOV, S.N., G.B. KHRISTIANSEN, et al.— Izv. AN SSSR, seriya fizicheskaya, **24**, 651. 1962; J. Phys. Soc. Japan, 17, Suppl. **A-III**, 118. 1962.

4. FUKUI, S., H. HASEGAWA, et al.— Progr. Theor. Phys. Suppl., **16**, 1. 1960.

5. ALLAN, H.R., D.M. THOMSON, et al. Preprint. 1962.

6. FOMIN, Yu.A. and G.B. KHRISTIANSEN.— ZhETF, **44**, 666. 1963.

7. PETERS, B.— Trudy MKKL, **3**, p.173. 1960.

8. VERNOV, S.N., V.I. SOLOV'EVA, B.A. KHRENOV, and G.B. KHRISTIANSEN.— ZhETF, **41**, 340. 1961.

9. HASEGAWA, H., M. MATANO, et al.— Phys. Rev. Lett., **8**, 284. 1962.

10. DEDENKO, L.G. and G.T. ZATSEPIN.— Trudy MKKL, **2**, p.222. 1960.

11. KRAUSHAAR, W. and G. CLARK.— J. Phys. Soc. Japan, 17, Suppl. **A-III**, 1. 1962.

12. DUTHIE, J., P.H. FOWLER, et al.— Nuovo Cim., **24**, 122. 1962.

N67-38210

D.D. Krasil'nikov, M.M. Atakova, N.N. Efimov, M.A. Nifontov, and F.K. Shamsutdinova

ATMOSPHERIC-DENSITY EFFECTS IN THE EAS FREQUENCY DURING CYCLONES AND SEASONAL FLUCTUATIONS IN ATMOSPHERIC TEMPERATURE

Studies of atmospheric-density effects in the observed frequency of occurrence of extensive air showers are quite important. First, they indicate what corrections for atmospheric effects must be introduced, and second, they enable a correct estimate of the shower absorption. Such studies are also interesting for the following reason: an estimate of the relative contributions of different atmospheric layers to the observed density effect can in principle help to ascertain the proportion of heavy primary nuclei, the role of decaying particles in EAS development, and the reliability of different models /1-3/ of EAS development.

The effect of the atmospheric density can in general be /4/: (1) a purely geometric effect corresponding to a deformation of the lateral-distribution function of the particles in a shower; (2) a change in the intensity spectrum of the recorded showers, due to a change in the decay probability for unstable particles of the EAS, that is, a decaying-particle effect.

The magnitude and sign of the effect in the first case depend on the geometry of the recording arrangement, whereas the effect of the unstable particles should be roughly the same for arrangements having different geometries. For the model of short-range cascades /2/, the geometric effect would largely reduce to the local effect of an atmospheric layer, adjacent to the observation level, with a thickness $t < 10$ radiation lengths in air. For the other extreme model /3/, the contribution of the atmospheric layers above a thickness $t > 10$ radiation lengths may constitute a considerable portion of the observed geometric effect. A high sensitivity of the observed shower frequency to air-density variations in the highest atmospheric layers ($h < 30$ mb) would indicate that a considerable number of the EAS primaries are heavy nuclei.

Many investigators /5-8, and others/ have studied the effects of the atmospheric density, including ourselves /9, 10, and others/. According to the data of /6, 7/, the geometric effect is a purely local effect of the atmospheric boundary layer, whereas the measurements of /5, 8/ are also consistent with the assumption that the upper half of the atmosphere plays a substantial part in causing this effect. An effect of unstable particles was not observed in these experiments. In /9/ it was concluded that the upper layers of the atmosphere contribute considerably to the temperature effect observed in an EAS. It is evident that the results of different authors are quite contradictory.

All the studies indicated so far had several serious shortcomings. Variations in EAS frequency in the case of long-period (usually seasonal) fluctuations in atmospheric temperature were considered, for which it is especially difficult to discriminate experimentally between the effects of different atmospheric layers. Actually, this sort of temperature fluctuation proceeds similarly in all atmospheric layers, there being a very close positive correlation between the layers /11/.

Moreover, the geometry of the arrangement for observing EAS in the experiments of /6-8/ did not make it possible to separate the geometric effect from other effects. In each case the expected local geometric effect of the lower atmospheric layers was evaluated too roughly, and the accuracy of the experimental data for the EAS was too low.

In view of the above situation, it was advisable to work out a means of discriminating between the effects in the densities of the different atmospheric layers. In /4/ Krasil'nikov suggested a new method for taking into account the local geometric effect of the lower atmospheric layers ($t \lesssim 10$ radiation lengths). Using this method, the density effects of the lower and upper atmospheric layers can be discriminated in the following manner.

Variations in the frequency of EAS recorded using detector arrangements with considerably different geometries are considered. These studies are made over such comparatively short periods that the temperature variations in the upper and lower parts of the atmosphere are opposite in sign. The results are then compared with the results for the seasonal effect on the EAS frequency. A particular instance of a period of opposite tendencies of the temperature fluctuations in the lower and upper parts of the atmosphere is during the passage of a cyclone /11/.

Some preliminary results of our studies of the effect which atmospheric density has on the frequency of EAS during cyclones and seasonal fluctuations in atmospheric temperature will be given in this report. We selected 17 instances of cyclone passage through Yakutsk during 1958 and 1959. The period of each cyclone was divided into 8 equal intervals, 4 before and 4 after the pressure minimum at the observation point. All our data on the state of the atmosphere and the EAS frequency were averaged over each of these intervals.

$C(n, \sigma)$	D	$N_{1/s}$	α_h, %/per mb	β_h, %/per m
C (3; 1.0)	3.8	$1.5 \cdot 10^4$	−0.75	−0.06
C (6; 1.0)	57	10^5	−0.91	0.013

An analysis was made of the frequency variations of EAS observed using four identical arrangements in threefold coincidence C (3; 1.0) having Geiger-counter areas $\sigma = 1.0\,m^2$ and separations $D = 3.8$ m, and by four also identical arrangements in sixfold coincidence C (6; 1.0) having the same counter areas but spaced 57 meters apart /10/. These cases of EAS recordings were chosen because of the convenience of interpreting the results obtained: according to previous calculations /4/, for these EAS recordings the expected geometric effects are of opposite sign.

Corrections for the barometric and geometric effects were introduced, using the corresponding constant coefficients α_h and β_H given in the table. The median intensities $N_{1/s}$ of the recorded EAS and the spacings D of the counter banks are also shown in the table.

Figure 1 shows the results of averaging the state of the atmosphere over all 17 cyclones. The relative time intervals of the cyclones (the 8 intervals referred to above) are laid off on the abscissa. The ordinates correspond to the following mean variations: δh and δt_0, the variations of the atmospheric pressure and temperature at the observation point; δH_{h-100}, the variation of the height of a boundary layer 100 mb thick; δH_{500} and δH_{200}, the variations of the heights of the 500-mb and 200-mb isobaric levels. The uncertainties shown on the curves are RMS values.

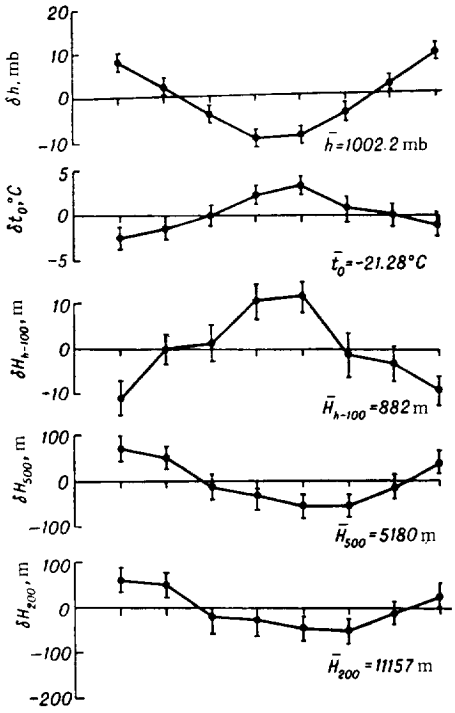

FIGURE 1. Mean variations in pressure and temperature of atmosphere at observation point and in heights of isobaric levels for 17 cyclones.

The curve for the mean variations δH_{h-200} of the height of a boundary layer 200 mb thick is not shown in the figure. It is approximately the same as the δH_{h-100} curve.

Figure 2 shows the mean (over the 17 cyclones) variations in EAS frequency corresponding to the atmospheric states shown in Figure 1. The showers were selected both by the local-recording arrangements (D = = 3.8 m, curves a–c) and by the arrangements of widely separated counters (D = 57 m, curves d–f). Curves a and d show the observed variations without any corrections; curves b and e show the variations with pressure corrections; c and f show the variations with corrections for pressure and for the local geometric effect of the atmospheric boundary layer. The uncertainties shown in this figure represent the corresponding RMS scatter of the mean data for the four identical arrangements.

The residual variations (curves c and f in Figure 2) cannot be explained completely by the errors due to introducing barometric corrections. The barometric coefficients were checked repeatedly in our previous studies (/10, 12, and others/). To eliminate the observed residual variations, it was necessary to increase the barometric coefficient for C (3; 1.0), whereas for C (6; 1.0) it was necessary to reduce the high standard errors in the determination of the variations to 1/7 and 1/4.5 of their former values. It is also impossible to account for the residual variations by the inaccuracy of the corrections for the local geomagnetic effect: the residual variations are opposite in sign to those expected from the observed variation of the height of the boundary layer and they are too large. Moreover, as will be shown below, the seasonal effect on the shower frequency, irrespective of the moments enumerated, also shows that the errors in the barometric and geometric corrections cannot be responsible for the residual variations observed here. At the height of the h – 300 mb level, the fluctuation tendencies of the boundary layers observed in this case become

attenuated, and above this level a transition to opposite fluctuation tendencies takes place. The effect of the levels above h - 300 mb turns out to be 1.5 to 2 times the effect of the underlying levels.

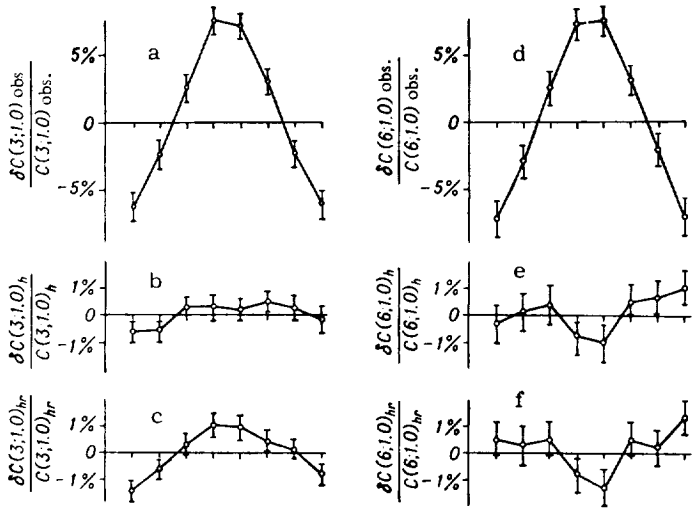

FIGURE 2. Mean variations of frequency of EAS recorded using arrangements with different geometries, during cyclones (compare Figure 1).

The residual variations observed correlate quite closely with the heights of the isobaric levels above 500 mb. Also, they correspond to a geometric effect of the upper layers of the order of $-1.4 \pm 0.3\%$ per 100 meters for $C(3; 1.0; 3.8)$ and $1.0 \pm 0.5\%$ per 100 meters for $C(6; 1.0; 57)$. These estimates pertain to the height of the 500-mb level. This contradicts the model of short-range cascades suggested by Cranshaw and Hillas /2/. It agrees better, however, with the assumption that elementary particle interactions in the middle, and even the upper, atmosphere are a determining factor in creating the lateral distribution of EAS particles observed near sea level. Moreover, since the effect is quite considerable, this means that quite a large number of the primary particles are probably heavy nuclei. Figure 3 shows the results of our study of the seasonal variation in EAS frequency for 1958 to 1960.

The ordinates in the figure, reading from top to bottom, are the mean values of the following quantities for the period in question: the heights of the 100, 500, and h - 100 millibar levels; the pressure h_0 at the observation point; and the frequencies of the EAS selected for Geiger-counter spacings of 3.8 and 57 meters. The last two curves have been corrected for the barometric and local geometric effects according to the table. The uncertainties indicated on these curves represent the RMS scatter of readings in each case of the four identical arrangements for recording EAS. For each curve the horizontal line indicates the average annual value, and the numbers on the left show the range of the seasonal variations.

Obviously, the data on the EAS frequency, corrected in the above-indicated way for pressure and for the height of the atmospheric boundary layer, cannot be correlated either with the pressure or with the heights of

the selected levels. This means that, as pointed out above, the errors in the barometric and local geometric corrections are not responsible for these variations in the shower frequency. In both sets of shower recordings the residual seasonal variations occur in waves of semiannual period, with maxima in April and October and with amplitudes of 2 to 3%. It is impossible to attribute the data for the EAS frequency variation wholly to errors in the barometer readings caused by dynamic effects /13/: taking into account the presence in the case at hand of geometric effects as well, unusually large dynamic effects (of the order of ~5 mb or more) would be necessary.

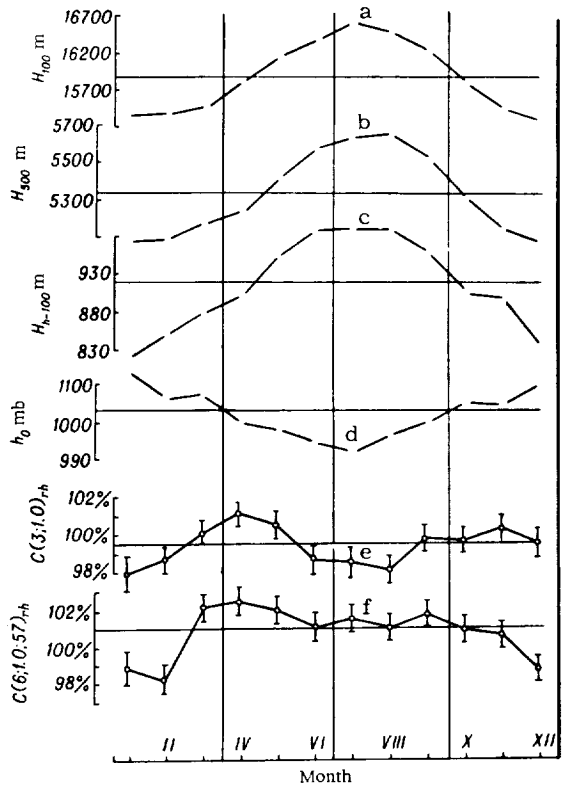

FIGURE 3. Seasonal variations in pressure, heights of isobaric levels, and EAS frequency, at Yakutsk.

a–for $\bar{H}_{100}$ = 15,876 m and $\Delta\bar{H}_{100}$ = 1330 m; b–for $\bar{H}_{500}$ = 5332 m and $\Delta\bar{H}_{500}$ = 577 m; c–for $\bar{H}_{h-100}$ = 917 m and $\Delta\bar{H}_{h-100}$ = 172 m; d–for $\bar{h}_0$ = 1003 mb and $\Delta\bar{h}_0$ = 21 mb; e–for $\overline{C\,(3;\,1.0)\;rh}$ = 9950 showers/day and $\Delta\bar{c}$ = 320 showers; f–for $\overline{C\,(6;\,1.0)\;rh}$ = 1160 showers/day and $\Delta\bar{c}$ = 50 showers.

The positive correlation between $C\,(6;\,1.0)_{hr}$ and $C\,(3;\,1.0)_{hr}$, for which the expected geometric effects are opposite in sign, indicates that in this case decaying particles have an effect. This effect mainly influences the spectrum of EAS intensity, and does not modify the shower geometry. It

was insignificant against the background of quite large geometric effects accompanying relatively small fluctuations in the heights of the isobaric levels. The latter fluctuations take place during ordinary cyclonic pressure drops, but they also show up quite clearly during sharp seasonal fluctuations in the state of the atmosphere, when the range of fluctuations in isobaric-level height in the upper half of the atmosphere is of the order of a kilometer (compare δH_{500} and δH_{100} in Figure 3).

So far it is not known definitely how the observed pattern of the effect (wave with semiannual period) of unstable particles on the seasonal variations is produced. The explanation should be related to the nature of EAS development and to the properties of the unstable particles present in an EAS. It is possible, too, that such a pattern is related to corresponding fluctuations of the extreme outer atmospheric layer ($h \lesssim 50$ mb), unknown at the present time, and to the predominant role which is played by heavy primary nuclei.

A detailed consideration of the questions touched upon here must await a continuation of this analysis of the effects which atmospheric density has on the EAS frequency.

The above results may be summarized as follows:

1) the geometric density effect which atmospheric layers above the $h = 300$ mb level have on the EAS frequency was found to be 1.5 to 2 times the geometric effect expected for the underlying layers (with a thickness $t \lesssim 10$ radiation lengths);

2) preliminary experimental indications of a considerable effect of unstable particles on the sea-level EAS frequency were obtained;

3) the model of short-range cascades /2/ cannot on the whole explain the atmospheric-density effect.

Institute of Space-Physics Research and Aeronomy,
Yakutsk Branch of Siberian Division of USSR
Academy of Sciences

REFERENCES

1. ZATSEPIN, G.T. – Trudy MKKL, 2, p.212. 1959.
2. CRANSHAW, T. and A. HILLAS. – Trudy MKKL, 2, p.231. 1959.
3. GRIGOROV, N.L. and V.Ya. SHESTOPEROV. – ZhETF, 34, 1539. 1958.
4. KRASIL'NIKOV, D.D. – Trudy YaFSO, AN SSSR, seriya fizicheskaya, No.4, 51. 1962.
5. DAUDIN, A. and J. DAUDIN. – Atm. Terr. Phys., 3, 245. 1953.
6. HODSON, A.L. – Proc. Phys. Soc., A64, 1061. 1951.
7. JANOSSY, L., T. SANDOR, and S. SOMOGYI. – Nuovo Cim. Suppl., 8, 801. 1958.
8. CITRON, A. and G. STILLER. – Nuovo Cim. Suppl., 8, 675. 1958.
9. KOVAL'SKAYA, A.I., D.D. KRASIL'NIKOV, and S.I. NIKOL'SKII. – Trudy YaFSO, AN SSSR, seriya fizicheskaya, No.2, 88. 1958.
10. KRASIL'NIKOV, D.D. – Trudy MKKL, 2, p.205. 1959.
11. KHROMOV, S.P. Sinopticheskaya meteorologiya (Synoptic Meteorology). – Moskva–Leningrad, OGIZ. 1948.
12. KRASIL'NIKOV, D.D., N.N. EFIMOV, M.A. NIFONTOV, and F.K. SHAMSUTDINOVA. – Izv. AN SSSR, seriya fizicheskaya, 26, 823. 1962.
13. FEINBERG, E.L. – Sbornik "Mezon," p.91, Moskva–Leningrad. 1947.

NC 38211

D.D. Krasil'nikov

THE μ-MESON SPECTRUM FOR ENERGIES FROM 10^{11} TO 10^{13} eV AT SEA LEVEL

Recently many investigators have become interested in the μ-meson energy spectrum at sea level, for energies from 10^{11} to 10^{13} eV /1–7, and others/.

This subject is important for various reasons. Once the μ-meson spectrum at sea level is measured reliably, a comparison with intensity measurements made deep underground may make it possible to check our assumptions about the energy-loss mechanisms /1–7/. Moreover, it should then be possible to specify more accurately the cross sections for known processes and to investigate additional hypothetical interactions of μ mesons with high and ultrahigh energies.

The μ-meson spectrum has a close relation to the mechanism of μ-meson generation /7, 8/. Therefore, a knowledge of the spectrum will also make it possible to verify certain hypotheses concerning nuclear interactions at ultrahigh energies, in particular with respect to the proportion of K mesons, π mesons, and hyperons among the secondary particles of a nuclear interaction for energies above 10^{11} eV /3, 4, 7–10/.

The study of the μ-meson energy spectrum above 10^{11} eV is quite difficult (due to the complexity of the experiments, the necessity for long-term observations, etc.). So far, statistically workable measurements of the μ-meson spectrum using magnetic spectrometers have been made only up to $E_0 \simeq 5 \cdot 10^{11}$ eV /6/.

For $E_0 \gtrsim 10^{12}$ eV, which is the most interesting energy range from the point of view of the factors indicated above, the spectrum was determined according to the absorption curve. However, due to the uncertainty of some of the energy-loss cross sections, and for other reasons too, the results are contradictory /1, 2, 5/.

Thus, studies of the μ-meson spectrum in terms of the spectrum of muon-caused ionization bursts should be especially interesting /1, 3, 11, 12/. This report will give the results of determining the integral μ-meson energy spectrum at sea level for 10^{11} to 10^{13} eV from the ionization-burst spectrum.

Data from long-term observations of large ionization bursts were obtained using spherical high-pressure chambers /13, 14/. These chambers were mounted at many points in the USSR and abroad to enable continuous recording of the ionization of the hard component of cosmic rays.

A review of the data, together with the burst spectra observed for individual chambers, were given in our previous reports /15, 16/, and the spectra according to all the chambers under consideration, for bursts corresponding to cascade-shower energies from $5 \cdot 10^{11}$ to $2 \cdot 10^{12}$ eV, were given in /11, 12/. The present report will give additional data, compiled

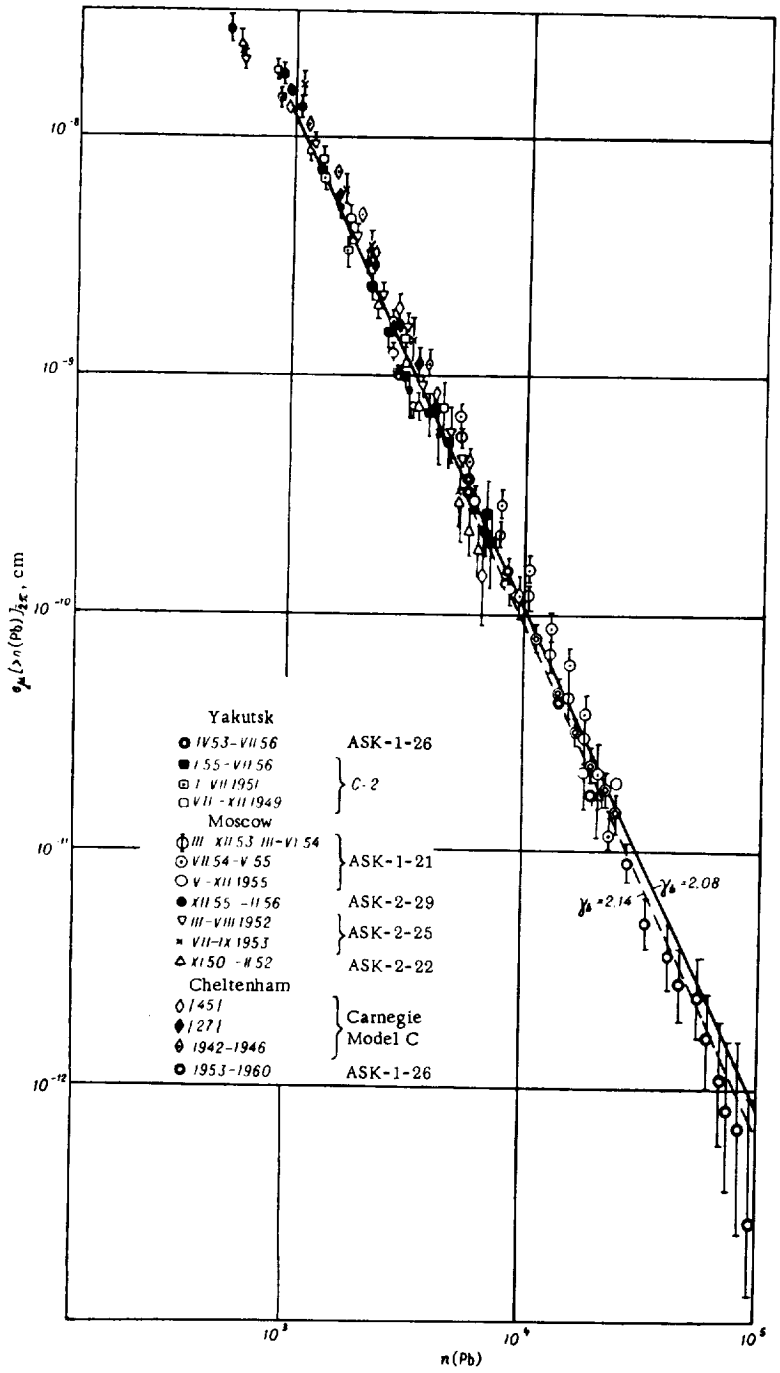

FIGURE 1. Spectrum of muon-caused ionization bursts observed near sea level in spherical chambers (n(Pb) is the number of particles for a shower maximum in lead).

over an 8-year period, on bursts observed with an ASK-1-26 chamber (Yakutsk); the burst energies ranged up to $E_0 \simeq 10^{13}$ eV.

The relation between the size of an observed ionization burst and the intensity of the cascade shower was determined /17/ on the basis of the author's studies of ion recombination /18/ and transition effects /19/ in these chambers.

The proportion of muon-caused bursts in the entire observed burst spectrum was estimated from the variation with height of the burst frequency between levels of 1025 and 690 g/cm^2 (between Cheltenham and Huancayo) /11, 12/. Our determination of the barometric coefficient of the sea-level burst frequency agrees with this estimate. Near sea level, bursts caused by μ mesons in the given chambers constitute from 55 to 75% of all the bursts observed (the percentage varied depending on the observation level and on the amount of additional light matter over the chambers). This estimate also agrees with the recent results in /20/.

The integral spectrum of muon-caused ionization bursts observed at different points near sea level is plotted in Figure 1. The vertical uncertainties (for the ASK-1-26 chamber they correspond to a confidence coefficient $p = 84\%$) represent the statistical Poisson distributions /21/; the horizontal uncertainties represent the probable errors in reading the burst recordings.

The figure shows that, over the entire considered range of muon-caused bursts, the data of different chambers differ by no more than a few dozen percent. It should be noted that under the observation conditions additional differences, not taken into account in the analysis, between the chambers are probable (differences in topography of the locality, in the chamber parameters, etc.). Moreover, some uncertainty in the corrections for bursts of different origin is inevitable, and statistical errors in reading the burst recordings are probable. Consequently, the convergence of the spectra for the different chambers is quite satisfactory.

The upper line in the figure shows the mean burst spectrum /11, 12/. If this spectrum is approximated in the range $10^3 \lesssim n \lesssim 10^4$ by the power law

$$b_\mu(>n) = A \cdot \left(\frac{n}{10^3}\right)^{-\gamma_b},$$

then we find that $A = (1.5 \pm 0.2) \cdot 10^{-8}$ and $\gamma_b = 2.08 \pm 0.08$. Here and in the following n refers to the number of cascade particles in lead n (Pb) /17/.

The lower (dashed) line in the figure shows the mean power-law spectrum for the ASK-1-26 chamber (Yakutsk) for 1953 to 1960. The exponent is $\gamma_b = 2.14 \pm 0.09$ for $5 \cdot 10^3 \lesssim n \lesssim 10^5$. With an accuracy comparable to the measurement error, this spectrum coincides with the previous spectrum for smaller bursts. A direct comparison of this spectrum of the μ-meson bursts with data given in the literature, however, is difficult, since the experiments of other authors usually involve μ mesons from only a part of the hemisphere. Nevertheless, the exponents γ_b given here apparently are close to the exponents quoted in other works /20, 22/.

The next step is to convert this spectrum of muon-caused bursts into an energy spectrum of the μ mesons at sea level. Such ionization bursts can in general be caused by bremsstrahlung, pair production, and δ-electron production, as well as by nuclear interactions of μ mesons. Of these processes, the most important is bremsstrahlung. The combined contribution of the second and third processes to the observed burst frequency was estimated in /23/: for $E_0 \simeq 10^{11}$ eV it is about 7% of the contribution of

bremsstrahlung, and for $E_0 \simeq 10^{12}$ eV it is about 1.5%. The relative contribution of μ-meson interactions is about 10%, provided we use the cross section given in /24/. However, according to /25/, the cross section is really only two thirds of that given in /24/, so that the contribution of μ-meson nuclear interactions is usually completely negligible /7, 22/.

In this report the contributions of the last three processes will be neglected, and the μ-meson spectrum will be calculated assuming that the entire burst spectrum given in Figure 1 is produced by μ-meson bremsstrahlung alone. The consequent exaggeration of the μ-meson intensity will in any case not exceed 17% for $E_0 \simeq 10^{11}$ eV and will be less than $\sim 10\%$ for $E_0 \simeq 10^{12}$ eV.

The spectrum of muon-caused bursts observed using the spherical chambers can be related to the sea-level energy spectrum of the μ mesons by means of the following general formula (also compare /7, 26/):

$$b_\mu [>n]_{2\pi} = 2\pi \int_{W=E_0}^{\infty} \int_{\theta=0}^{\pi/2} \int_{E=E_0}^{W} \int_{t=0}^{\infty} K(W) \cdot \psi(W, \theta) \cdot q(W, E) \cdot W(E, n, t) \sin\theta \, dW \, d\theta \, dE \, dt \cdot \text{cm}^{-2} \text{sec}^{-1}, \quad (1)$$

where

$$E_0 = \frac{3n}{l\left(\frac{E_0}{\beta}\right)}, \quad \beta = 6.4 \cdot 10^6 \text{ eV};$$

$K(W)dW$ is the differential μ-meson spectrum (relative to the vertical intensity);

$\psi(W, \theta)$ is the zenith-angle dependence of the μ-meson intensity, expressed in units of the vertical meson flux;

$q(W, E)$ is the probability, relative to the radiation length, that a μ meson of energy W will produce a photon of energy E;

$W(E, n, t)$ is the probability that a photon which has originated t units deep in a layer of lead will produce a burst of more than n particles in the chamber.

Now let us consider briefly the specific forms of the above functions assumed in the calculation of the spectrum, and also some simplifications. The function $l\left(\frac{E_0}{\beta}\right)$ is a very slightly varying function of the energy, and its values were determined using the calculations in /26, 27/. In the range $10^{11} < E_0 < 10^{13}$ it does not vary by more than 10%, and it is equal to about 0.07.

Next, following the line of reasoning /26, 28/ that the observed burst frequency is mainly produced by showers near maximum development, we take the inner integral as in /26/. However, then n is replaced by E_0, and the logarithmic term containing the slightly varying function $l\left(\frac{E_0}{\beta}\right)$ is neglected. Consequently, in these calculations it was assumed that

$$P(E, E_0) = \int_0^{\infty} W(E, n, t)\, dt \simeq \begin{cases} \frac{2}{\sqrt{\pi}} \cdot \frac{1}{l\left(\frac{E}{\beta}\right)} \cdot \left(\ln \frac{E}{E_0}\right)^{\frac{1}{2}}, & \text{if } E > E_0; \\ 0, & \text{if } E < E_0. \end{cases} \quad (2)$$

The right side of formula (2) is $\sim 3\%$ larger than that given by Belen'kii /26/.

According to /7, 26, 29/, μ mesons have a spin of 1/2 and a normal magnetic moment

$$q(W, E) = \frac{4}{3}\left(\frac{m_e}{m_\mu}\right)^2 \cdot \frac{L^\mu_{\text{rad}}(W,E)}{L^e_{\text{rad}}} \cdot \left(1 - V + \frac{3}{4} \cdot V^2\right) \cdot \frac{1}{E}, \tag{3}$$

where

$$L^\mu_{\text{rad}}(W, E) = \begin{cases} \ln\left[\frac{12}{5} \cdot \frac{1-V}{V} \cdot \frac{W}{m_\mu c^2 \cdot z^{1/3}}\right] - \frac{1}{2} & \text{in the absence of screening } (W \ll 5 \cdot 10^{11} \text{ eV}); \\ b \ln\left(\frac{m_\mu}{m_e} \cdot 183 \cdot z^{-1/3}\right) & \text{for total screening } (W \gg 5 \cdot 10^{11} \text{ eV}); \end{cases} \tag{4}$$

$V = \frac{E}{W}$

b is a coefficient very close to unity; $m_\mu = 206.9 \cdot m_e$ /30/; and $L^e_{\text{rad}} = 4.05$ /31/.

The multiplying factor in parentheses in formula (3) is equal to about 0.7 and it varies only slightly when the fraction of transmitted energy V changes from 0.4 to 0.95, which is a very significant change in this case. Therefore, allowing for an error amounting to some percent, we can simply assume it to be constant:

$$1 - V + \frac{3}{4} \cdot V^2 = 0.7.$$

In order to calculate the intermediate cases approximately, we can simplify the expression for $L^\mu_{\text{rad}}(W, E)$ as follows:

$$L^\mu_{\text{rad}}(W, E) = \begin{cases} \ln \frac{W}{10^9} + \ln \frac{1-V}{V} - 1.15 = a(V), & \text{if } W \leqslant 5 \cdot 10^{10} \text{ eV}; \\ \frac{1}{2}\left[a(V) \cdot \lg \frac{10 \cdot W_1}{W} + 9.07 \lg \frac{10 \cdot W}{W_1}\right], & \text{if } 5 \cdot 10^{10} < W < 5 \cdot 10^{12} \text{ eV}; \\ 9.07 & \text{if } W \geqslant 5 \cdot 10^{12} \text{ eV}. \end{cases} \tag{5}$$

Here

$$W_1 = 5 \cdot 10^{11} \text{ eV}.$$

Then, taking into account the comparatively slight variability of the radiation logarithm $L^\mu_{\text{rad}}(W, E)$ with energy, when calculated separately for each specified value of E_0, we can assume it to be constant, and equal to its median value:

$$L^\mu_{\text{rad}}(W, E) \simeq L^\mu_{\text{rad}}[W(E)_{1/2}, E(E_0)_{1/2}] = L^\mu_{\text{rad}}(E_0)_{\text{eff}}.$$

Values of $L^\mu_{\text{rad}}(E_0)_{\text{eff}}$ calculated for a spectrum of the form $K(W)dW \propto W^{-\gamma-1}dW$, where $\gamma = 2.4$, are listed in Table 1. Similarly calculated values of:

$$l\left(\frac{E_0}{\beta}\right)_{\text{eff}} = l\left[\frac{E(E_0)_{1/2}}{\beta}\right];$$

$$E(E_0)_{1/2} = k_1 \cdot E_0; \quad W(E)_{1/2} = k_2 \cdot E$$

are also given in the table.

To calculate $\eta(W) = \int_{\theta=0}^{\pi/2} \psi(W, \theta)\, d\theta$, values of the function $\psi(W, \theta)$ for two mechanisms of μ-meson generation were taken from /8/. The results of these calculations are given in Table 2.

TABLE 1

E_0	10^{11}	$2\cdot10^{11}$	$5\cdot10^{11}$	10^{12}	$2\cdot10^{12}$	$5\cdot10^{12}$	10^{13}
k_1	1.37	1.36	1.35	1.34	1.33	1.33	1.33
k_2	1.47	1.42	1.38	1.36	1.36	1.35	1.35
$L^{\mu}_{\text{rad}}(E_0)_{\text{eff}}$	6.65	7.50	8.30	8.70	8.95	9.06	9.07
$l\left(\frac{E_0}{\beta}\right)_{\text{eff}}$	0.071	0.069	0.068	0.067	0.066	0.065	0.065

TABLE 2

W, eV	10^{11}	$2\cdot10^{11}$	$5\cdot10^{11}$	10^{12}	$2\cdot10^{12}$	$5\cdot10^{12}$	10^{13}
$\pi\to\mu$	1.01	1.34	1.79	2.13	2.44	2.67	2.79
$K\to\mu$	0.76	0.92	1.20	1.48	1.77	2.17	2.40

After the inner integrals are taken, formula (1) becomes

$$b_{\mu}(>E_0)_{2\pi} = B(E_0)\cdot\int_{W=E_0}^{\infty} 2\pi\cdot K(W)\cdot\eta(W)\cdot\left(\ln\frac{W}{E_0}\right)^{3/2}dW, \qquad (6)$$

where

$$B(E_0) = 4.05\cdot10^{-6}\cdot\frac{L^{\mu}_{\text{rad}}(E_0)_{\text{eff}}}{l\left(\frac{E_0}{\beta}\right)_{\text{eff}}}.$$

The expression $2\pi K(W)\cdot\eta(W)dW$ represents the differential energy spectrum for the global flux of μ mesons. For limited intervals of the variations in W, we can set

$$K(W)\,dW \propto W^{-\gamma-1}dW; \qquad (7)$$

$$\eta(W)\propto W^{\nu}.$$

Then

$$b_{\mu}(>E_0)_{2\pi} = B(E_0)\cdot\frac{\Gamma(1+3/2)}{(\gamma-\nu)^{3/2}}\cdot F_{\mu}(>E_0)_{2\pi},\ \Gamma(1+3/2)=1.33, \qquad (8)$$

or

$$F_{\mu}(>E_0)_{2\pi} = G(E_0,\gamma,\nu)\cdot b_{\mu}(>E_0)_{2\pi},\quad G(E_0,\gamma,\nu)=\frac{(\gamma-\nu)^{3/2}}{\Gamma(1+3/2)}\cdot\frac{1}{B(E_0)}. \qquad (9)$$

The values of ν for two schemes of μ-meson generation are given in Table 3. The last column of the table shows the errors introduced when approximating $\eta(W)$ by a power law.

Some of the inaccuracies in the determination of ν are unimportant. Moreover, formula (9) for the global μ-meson flux $F_{\mu}(>E_0)_{2\pi}$ is in this case practically independent of the choice between the $\pi-\mu$ and $K-\mu$ generation schemes. The uncertainties in the value of the exponent γ, however, may be more important. Judging from the burst spectrum /11, 12, 20, and others/ and from other measurements /2, 4, and others/ at energies from 10^{11} to 10^{13}eV, the probable value of γ is between 2.2 and 3.2. For the calculation of $G(E_0,\gamma,\nu)$, the value of γ was taken as 2.4.

If γ were taken as 2.2, the estimate of the global μ-meson flux from the burst frequency using formula (9) would be reduced by 14%; for $\gamma=3.2$, on the other hand, it would be 63% higher than the flux calculated for $\gamma=2.4$.

The values of $G(E_0, \gamma, \nu)$ calculated for $\gamma = 2.4$ and for an index ν corresponding to the $\pi - \mu$ scheme are given in Table 4, for various E_0.

TABLE 3. Angular-distribution index ν for different ranges of W

W	10^{11}–10^{12}	10^{12}–10^{13}	10^{13}	Error, %
$\pi - \mu$	0.32	0.12	0	3
$K - \mu$	0.26	0.26	0	7

TABLE 4

E_0	10^{11}	$2 \cdot 10^{11}$	$5 \cdot 10^{11}$	10^{12}	$2 \cdot 10^{12}$	$5 \cdot 10^{12}$	10^{13}
$G(E_0, \gamma, \nu) \times 10^{13}$	6.05	5.26	4.66	4.69	4.81	4.68	4.65

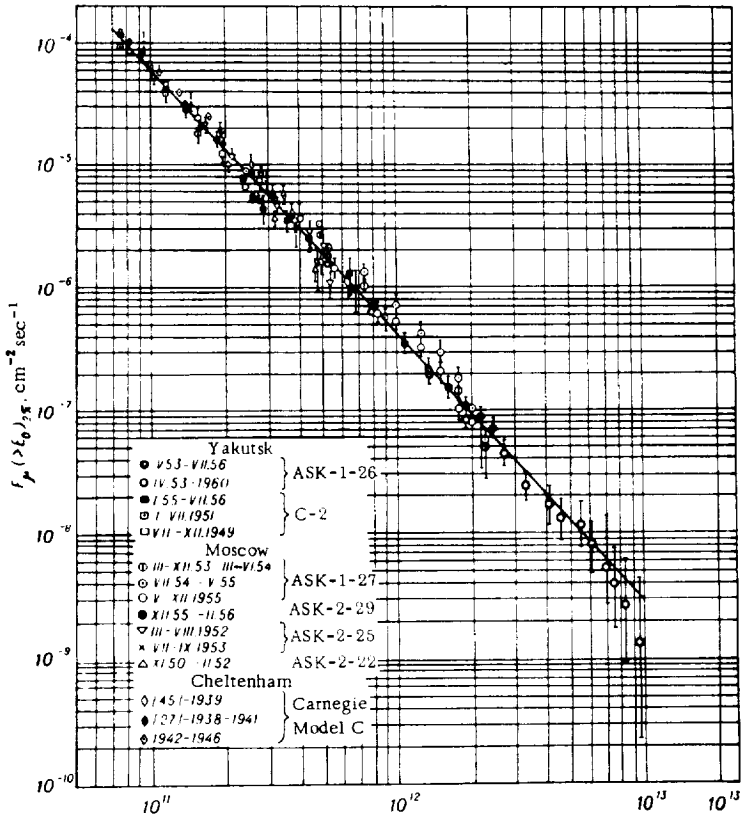

FIGURE 2. Integral energy spectrum of global μ-meson flux at sea level, according to data on muon-caused ionization bursts in spherical chambers at various locations throughout the world (see Figure 1).

$$\left(E_\mu = \frac{\delta n}{l\left(\frac{E_\mu}{\beta}\right)},\ \beta = 6.4 \cdot 10^8\ \text{eV}\right).$$

The results of processing the ionization-burst data in Figure 1 using formula (9) are given in Figure 2. The actual μ-meson spectrum observed at sea level is apparently very close to the average spectrum for all the ionization chambers together. In order to obtain such a weighted spectrum, the data for different chambers were averaged over the energy intervals. Within the averaging intervals, the energies E_0 did not differ by more than 20%. The corresponding mean integral spectrum of the global μ-meson flux observed at sea level with spherical ionization chambers is shown in Figure 3 (open circles).

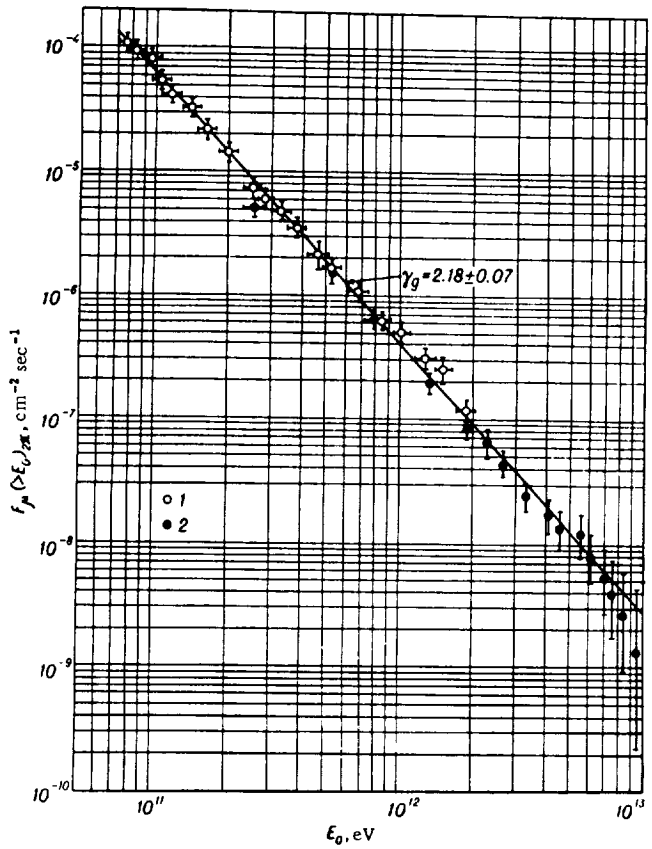

FIGURE 3. Integral energy spectrum of global μ-meson flux at sea level.

1-results of averaging data for many chambers; 2-ASK-1-26 (Yakutsk), 1953-1960.

A conversion from the spectrum of the global μ-meson flux $F_\mu(> E_0)_{2\pi}$ in Figure 3 to the spectrum of the vertical μ-meson flux $F_\mu(> E_0)_\perp$ is possible using the relation

$$F_\mu (> E_0)_\perp = V(E_0, \gamma, \nu) \cdot F_\mu (> E_0)_{2\pi}, \qquad (10)$$

where

$$V(E_0, \gamma, \nu) \simeq \frac{1}{2\pi} \cdot \frac{\gamma - \nu}{\gamma} \cdot \frac{1}{\eta(E_0)} .$$

Values of ν and $\eta(E_0)$ for the $\pi-\mu$ and $K-\mu$ generation schemes were given in Tables 2 and 3. The flux $F_\mu(>E_0)_\perp$ was evaluated assuming that $\gamma = 2.4$. Moreover, the errors related to γ are low in this case, only amounting to a few percent.

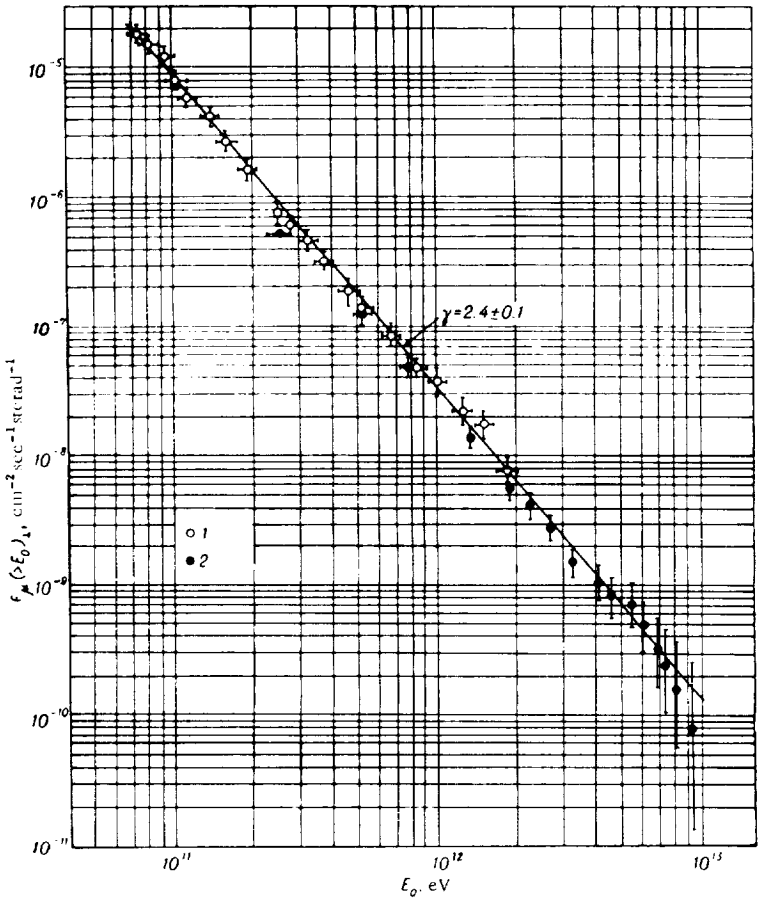

FIGURE 4. Integral energy spectrum of vertical μ-meson flux at sea level, $E_\mu\ (>E_0)_\perp$, obtained from the spectrum of muon-caused ionization bursts, assuming a $\pi-\mu$ generation scheme:

1—results of averaging data for many chambers; 2— ASK-1-26 (Yakutsk), 1953–1960.

Figure 4 shows the results of determining $F_\mu(>E_0)_\perp$ from the frequency of muon-caused bursts in spherical chambers (using relations (9) and (10)), assuming a $\pi-\mu$ generation scheme.

For comparison, Figure 5 gives the results of other authors together with the calculations of $F_\mu(>E_0)_\perp$ made in our study. Our experimental points (denoted as 1 and 2 in the figure) were plotted only for cases of angular dependence according to the $\pi-\mu$ generation scheme, without any normalization to the results of other measurements. The corresponding integral spectrum of the vertical μ-meson flux, assuming a power law, is indicated by curve 8. Curve 9 shows the spectrum determined from the

same data, but assuming an angular distribution conforming to the $K-\mu$ generation scheme.

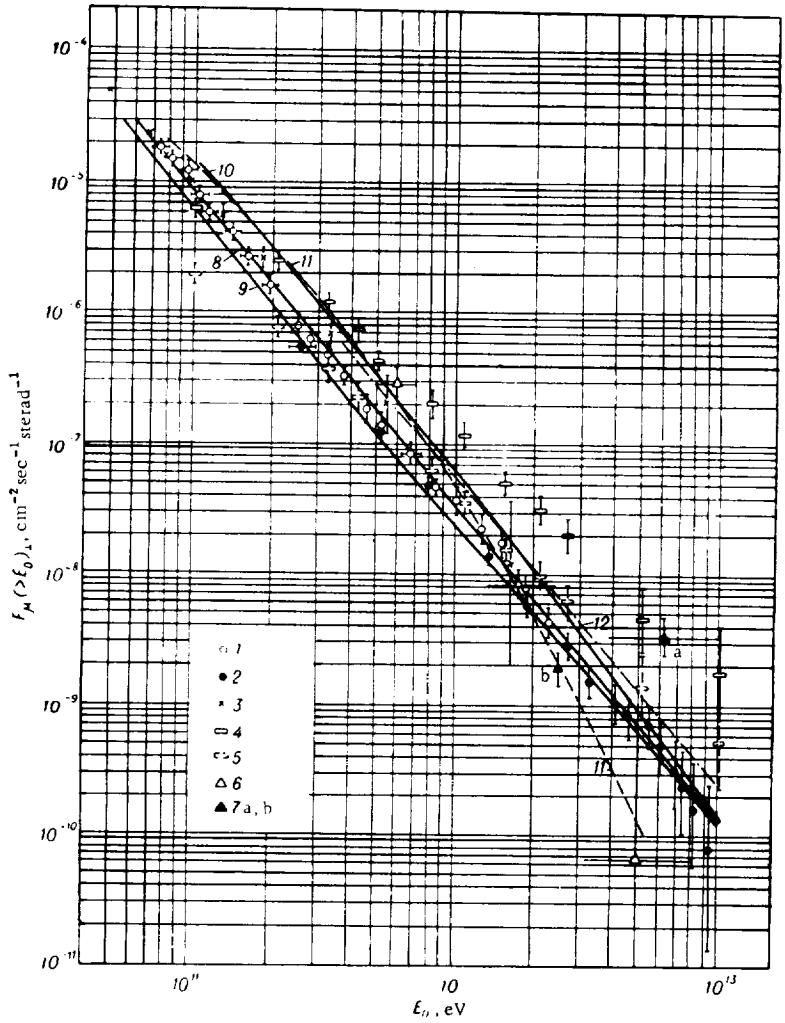

FIGURE 5. Integral energy spectrum of vertical μ-meson flux at sea level, according to various investigators:

1, 2, and 8–from spectrum in Figure 3, assuming a $\pi-\mu$ generation scheme; 3–from /6/; 4 and 5–according to /3/, as originally given by the authors and normalized for $E_0 = 10^{12}$ eV to the spectrum described by curve 8; 6–according to /5/; 7–from the measurements of /31/, if the energy losses are taken into account: a–according to formula (11), and b–according to formula (12); 9–from the spectrum of Figure 3, assuming a $K-\mu$ generation scheme; 10–according to /34/; 11– from /4/, assuming a $\pi-\mu$ generation scheme; 12–according to /2/.

The results of the underground measurements of /3/ are plotted twice: (1) in the form originally given by the authors (denoted in Figure 5 as 4); and (2) normalized for $E_0 = 10^{12}$ eV to the spectrum described by curve 8.

Two different values of the energy flux $F_\mu(>E_0)_\perp$ obtained from measurements of the μ-meson intensity at a single depth underground /31/ are given in Figure 5. These are denoted as points 7a and 7b, where:

point 7a corresponds to the μ-meson energy losses in the ground given in /32/:

$$\frac{dE}{dx} = 2.48 + 4.5 \cdot 10^{-6}E \text{ MeV per g/cm}^2, \tag{11}$$

where E is in eV;

and point 7b is taken from /4/, where

$$\frac{dE}{dx} = 2.05 + 0.076 \ln \frac{E}{10^9} + 2.3 \cdot 10^{-6}E \text{ MeV per g/cm}^2, \tag{12}$$

according to /33/, and a correction for the observation angle is introduced /31/. An analysis /2/ of the same data of /31/, but made assuming μ-meson energy losses of

$$\frac{dE}{dx} = 1.88 + 0.076 \ln \frac{E'_m}{m_\mu c^2} + 3 \cdot 10^{-6} E \text{ MeV per g/cm}^2, \tag{13}$$

results in the spectrum shown by curve 12.

Spectrum 10 was calculated on the basis of /34/, which gives the following differential μ-meson spectrum at sea level:

$$K_\mu(E)\,dE = \frac{A}{1 + \frac{E}{116}} \cdot K_\pi(E)\,dE, \tag{14}$$

where E is in BeV; $A = 0.684$; and $K_\pi(E)dE$ is the differential spectrum of π-meson generation:

$$K_\pi(E)\,dE = I_\pi \cdot E^{-\gamma_\pi - 1}dE, \tag{15}$$

in which $I_\pi = 0.16 \text{ cm}^{-2} \text{ sec}^{-1} \text{ sterad}^{-1} \text{ BeV}^{-1}$ and $\gamma_\pi = 1.62$.

Curve 11 represents the μ-meson spectrum determined from the γ-quantum spectrum measured in the stratosphere using photographic emulsions /4/.

The curve in Figure 3 represents the integral energy spectrum of the global μ-meson flux at sea level, for energies from 10^{11} to 10^{13} eV. From about 10^{11} to $6 \cdot 10^{12}$ eV this spectrum is described by the power law

$$F_\mu(>E_0)_{2\pi} = B \cdot \left(\frac{E_0}{10^{11}}\right)^{-\gamma_g}, \tag{16}$$

where $\gamma_g = 2.18 \pm 0.07$ and $B = (6.5 \pm 0.9) \cdot 10^{-5} \text{ cm}^{-2} \text{ sec}^{-1}$. For energies from $6 \cdot 10^{12}$ to 10^{13} eV, the exponent γ_g tends to increase to 3.5 ± 1.0.

This spectrum is interesting because it was first determined empirically, without regard to assumptions on the angular distribution and energy losses of μ mesons. It may prove to be useful in subsequent studies of the angular distribution of μ-meson intensity and of the meson energy losses.

The integral energy spectrum of the vertical μ-meson flux at sea level, $F_\mu(>E_0)_\perp$, was determined from the observed burst spectrum (see Figure 1), assuming meson generation only according to the $\pi - \mu$ scheme (curve 8 in Figure 4). This flux spectrum has the form

$$F_\mu(>E_0)_\perp = C \cdot \left(\frac{E_0}{10^{11}}\right)^{-\gamma}, \quad 10^{11} \leqslant E_0 \leqslant 6 \cdot 10^{12} \text{ eV}, \tag{17}$$

where $\gamma = 2.4 \pm 0.1$ and $C = (8.8 \pm 1.2) \cdot 10^{-6} \text{ cm}^{-2} \text{ sec}^{-1} \text{ sterad}^{-1}$.

This spectrum agrees with measurements made using a magnetic spectrometer /6/ for energies up to $E_0 \simeq 10^{12}$ eV, and it is close to the spectra given in /2, 34/ for E_0 from 10^{12} to 10^{13}, provided we disregard certain differences between the estimated absolute fluxes. With respect to the absence of a "discontinuity," this spectrum also agrees with the one given in /3/. The fact that the spectrum in /3/ has a curve which is more mildly sloping may possibly be explained, as the authors themselves pointed out, by the influence in the experiment in /3/ of energy losses in the ground; the contribution of μ mesons arriving at inclined directions, which increases with the energy, is then underestimated, since some of the observed bursts may be produced by μ mesons passing outside of the aperture of the instruments, at large zenith angles.

The spectrum given by (17) differs from those /4, 5, 35/ which have a sharp spectral discontinuity in the range $E_0 > 5 \cdot 10^{11}$ eV. Our analysis indicates that, if a discontinuity does exist in the spectrum, it occurs around $6 \cdot 10^{12}$ eV but not before. For the spectrum (17) described in this report, the uncertainty in γ cannot have a significant influence when formulas (9) and (10) are used for conversion from the burst spectrum. The error in the estimate of $F_\mu (> E_0)_\perp$ due to the uncertainty in γ is comparatively small. Moreover, if we take $\gamma = 2.4$, which is considerably less than the value given in /4/, and less than the possibly existing effect of volume ion recombination in an ASK-1-26 chamber, formula (10) would accentuate the discontinuity even more, provided the latter exists. The absence of a "discontinuity" cannot be attributed to an excessively low correction for the contribution of bursts of a different nature for $E_0 \gtrsim 10^{12}$ eV, either, since the given spectrum was obtained from the spectrum of bursts in a spherical chamber, where μ mesons play a very predominant role, and from a comparison of spectrum (17) with the data of underground burst measurements /3/.

The spectral "discontinuity" found from measurements of intensity versus depth /5, 35/ can be explained by the errors in the determination of the μ-meson energy. This follows from a comparison of points 7a and 7b and curve 12 in Figure 5. These errors are related to the considerable uncertainties in the estimated energy losses in the ground (see formulas (11)-(13)). The μ-meson spectrum (17) indicates that the actual μ-meson energy losses in the ground are closer to those specified by formula (13), which was given in /2/. Formula (11) exaggerates these losses, and formula (12) underestimates them. The uncertainties in this case are mainly related to the term which is proportional to the energy.

It is somewhat more complicated to account for the discrepancy with the μ-meson spectrum derived from the spectrum of γ quanta in the stratosphere /4/. No discontinuity shows up in the γ-quantum spectrum obtained from measurements made by means of ionization chambers in the stratosphere /36/. The authors of /36, 37/ explain the difference between the two spectra as follows: emulsions record individual γ quanta, whereas ionization chambers do not distinguish between the members of a group of particles arriving at small angles. Apparently, however, the absence of the discontinuity in the μ-meson spectrum obtained in this analysis cannot be similarly explained: in the μ-meson chambers considered, bursts are produced with a probability of 10^{-4}-10^{-4} [sic], and to smooth out the discontinuity, improbably large numbers of μ mesons would have to be traveling in groups simultaneously each time. Moreover, an analysis of

the burst frequencies in chambers with different areas (conducted by us in /16/ and also more recently) indicated that the bursts are produced by single particles.

Let us assume that in the experiment and analysis of /4/ there are no systematic errors (errors in the method of photometric measurement, in the atmospheric model, etc.), and that in the expected μ-meson spectrum /34/ an error in the constant is possible. In this case, the indicated difference between the spectra of γ quanta /4/ and μ mesons /17/ should mean that, beginning with μ-meson energies $\gtrsim 2 \cdot 10^{12}$ eV, K mesons will play an increasingly larger role in μ-meson production /3/, with a possibility of direct generation /1, 11/. It is interesting that the corresponding spectrum, constructed from our burst spectrum assuming the direct generation of μ mesons, would not contradict the results of the measurements of /3, 6/.

The π mesons resulting from hyperon decay /9/ and K-meson decay cannot be the predominant sources of μ mesons with energies $\lesssim 2 \cdot 10^{12}$ eV. This follows both from the poorer convergence obtained between the burst spectrum and the measurements of /6/ and, what is more significant, from the fact that there would have to be a sharp contradiction with measurements of γ quanta corresponding to the energies in the stratosphere /4, 36/.

A comparison of spectrum (17) with other measurements also indicates that no considerable increase in ion recombination is observed with an increase in shower energy, for argon pressures in the chamber up to 10 atmospheres.

The results obtained in this study can be summarized as follows:

1. The integral spectrum of muon-caused ionization bursts observed at sea level in spherical chambers has the form of a power law:

$$b_\mu (> n)_{2\pi} = A \left(\frac{n}{10^3}\right)^{-\gamma_b}$$

where

$$n = \frac{I\left(\frac{E_0}{\beta}\right)}{\beta} \cdot E_0, \quad \beta = 6.4 \cdot 10^6 \text{ eV};$$

for $10^3 \lesssim n \lesssim 10^4$

$$A = (1.5 \pm 0.2) \cdot 10^{-8} \text{ and } \gamma_b = 2.08 \pm 0.08,$$

whereas for $10^4 \lesssim n \lesssim 10^5$ the exponent is essentially constant at $\gamma_b = 2.14 \pm 0.09$.

2. The integral energy spectra of the global and vertical μ-meson fluxes for energies from 10^{11} to 10^{13} eV were obtained from the frequency of large ionization bursts observed at sea level in spherical chambers. For $10^{11} \lesssim E_0 \lesssim 6 \cdot 10^{12}$ these spectra are described by a power law:

$$F_\mu (> E_0)_{2\pi} = (6.5 \pm 0.9) \cdot 10^{-5} \left(\frac{E_0}{10^{11}}\right)^{-2.18 \pm 0.07} \text{ cm}^{-2} \text{ sec}^{-1}$$

and

$$F_\mu (> E_0)_{\perp, \pi \to \mu} = (8.8 \pm 1.2) \cdot 10^{-6} \left(\frac{E_0}{10^{11}}\right)^{-2.4 \pm 0.1} \text{ cm}^{-2} \text{ sec}^{-1} \text{ sterad}^{-1}.$$

3. In addition to being generated directly /11/, μ mesons with $E_0 \lesssim 2 \cdot 10^{12}$ eV may be products of the decay of π mesons created during the nuclear interactions of primary particles; however, these mesons cannot be caused by hyperon decay, as was maintained by Peters /9/. It may be that, for $E_0 \gtrsim 2 \cdot 10^{12}$ eV, K mesons and direct generation begin to play a part in the μ-meson production, a part which increases with the energy.

4. The μ-meson spectrum at sea level obtained here was compared with the results of measurements of the hard-component intensity deep underground. This comparison indicated that earlier estimates of the energy /38, and others/ were much too high, and that the values in /33/ for $E_0 \gtrsim 10^{12}$ eV were too low.

In the formula describing the total energy losses, the energy-proportional term has a coefficient close to the one used in /2/. Thus, this term is roughly equal to $3 \cdot 10^{-6} E$ MeV per g/cm^2 (where E is in eV). Consequently, all the other hypothetical interactions between μ mesons and matter /7/ hardly play any real part in the overall balance of the μ-meson energy losses.

In conclusion I wish to extend deep thanks to S. I. Nikol'skii for supervising this study, and to F. K. Shamsutdinova and T. F. Panfilova for their assistance in processing the experimental material.

Institute of Space-Physics Research and Aeronomy,
Yakutsk Branch of Siberian Division of USSR
Academy of Sciences

REFERENCES

1. ALEKSEEV, I. S. and G. T. ZATSEPIN.— Trudy MKKL, 1959, **1**, p. 336, Izd. AN SSSR. 1960.
2. PINE, J., R. J. DAVISSON, and K. GREISEN.— Trudy MKKL, 1959, **1**, p. 293, Izd. AN SSSR. 1960.
3. VERNOV, S. N., B. A. DMITRIEV, G. B. KHRISTIANSEN, and GULYAM SADYK MUKHNOI.— Izv. AN SSSR, seriya fizicheskaya, **26**, 661. 1962.
4. DUTHIE, J., P. H. FOWLER, A. KADDOURA, D. H. PERKINS, and K. PINKAU.— Nuovo Cimento, **24**, 122. 1962.
5. BARTON, J. Synopsis of Report at Intern. Cosmic-Ray Conference in Kyoto, Vol. 3. 1961.
6. BROOKE, G., P. J. HAYMAN, F. E. TAYLOR, and A. W. WOLFENDALE. Synopsis of Report at Intern. Cosmic-Ray Conference in Kyoto. 1961.
7. NIKISHOV, A. I. and I. L. ROZENTAL'. Preprint. 1961.
8. ZATSEPIN, G. T. and V. A. KUZ'MIN.— ZhETF, **39**, 1677. 1960.
9. PETERS, B. Preprint of Report at Intern. Cosmic-Ray Conference in Kyoto. 1961.
10. ZATSEPIN, G. T.— Izv. AN SSSR, seriya fizicheskaya, **26**, 674. 1962.
11. KRASIL'NIKOV, D. D.— Izv. AN SSSR, seriya fizicheskaya, **26**, 818. 1962.
12. KRASIL'NIKOV, D. D.— Proceedings of Intern. Cosmic-Ray Conference in Kyoto. 1961 (in press).
13. COMPTON, A. H., E. O. WOLLAN, and R. D. BENNETT.— Rev. Sci. Instr., **5**, 415. 1934.
14. SHAFER, Yu. G.— Trudy YaFSO, AN SSSR, seriya fizicheskaya, No. 2, 7. 1958.
15. KRASIL'NIKOV, D. D.— Uchenye zapiski Yakutskogo universiteta, No. 1, 26. 1956.
16. KRASIL'NIKOV, D. D. and S. I. NIKOL'SKII.— Trudy YaFSO, AN SSSR, seriya fizicheskaya, No. 1, 48. 1955.
17. KRASIL'NIKOV, D. D.— Sbornik: "Kosmicheskie luchi," No. 3, Izd. AN SSSR, Moskva. 1961.
18. KRASIL'NIKOV, D. D.— Nauchnye soobshcheniya YaFSO, AN SSSR, No. 1, 75. 1958.
19. KRASIL'NIKOV, D. D.— Trudy YaFSO, AN SSSR, seriya fizicheskaya, No. 4, 15. 1962.
20. BABAYAN, Kh. P., Ya. S. BABETSKII, et al.— Izv. AN SSSR, seriya fizicheskaya, **26**, 558. 1962.
21. REGENER, V. H.— Phys. Rev., **84**, 161. 1951.

22. HIGASHI, S., T. KITAMURA, M. ODA, Y. TANAKA, and Y. WATASE. Preprint of Report at Intern. Cosmic-Ray Conference in Kyoto. 1961.

23. HIROKAWA, S., H. KOMORI, and S. OGAWA.— Nuovo Cimento, **4**, 736. 1956.

24. BRADDICK, H.J.J., and B. LEONTIC.— Phil.Mag., **45**, 1287. 1954.

25. RESSLER, D. and R. MAZE.— Nuovo Cimento, **5**, 1540. 1957.

26. BELEN'KII, S.Z. Lavinnye protsessy v kosmicheskikh luchakh (Cascade Processes in Cosmic Rays). Moskva-Leningrad. 1948.

27. ZATSEPIN, G.T.— DAN SSSR, **63**, 243. 1948.

28. LANDAU, L.D.— ZhETF, **2**, 32. 1941.

29. CHRISTY, R.F. and S. KUSAKA.— Phys. Rev., **59**, 405. 1941.

30. IVANENKO, D. and A. STARTSEV.— UFN, **72**, 765. 1960.

31. BARRETT, P. and L. BOLLINGER.— Rev. Mod. Phys., **24**, 133. 1952.

32. DUTHIE, J., P.H.FOWLER, A. KADDOURA, D.H. PERKINS, K. PINKAU, and W. WALTER. Preprint of Report at Intern. Cosmic-Ray Conference in Kyoto. 1961.

33. OZAKI, S. Report at Intern. Cosmic-Ray Conference in Kyoto. 1961.

34. ZATSEPIN, G.T. and V.A. KUZ'MIN. Private communication.

35. MENON, M.G.K. Report at Intern. Cosmic-Ray Conference in Kyoto. 1961.

36. BARADZEI, L.T., V.I. RUBTSOV, Yu.A. SMORODIN, M.V. SOLOV'EV, and B.V. TOLKACHEV.— Izv. AN SSSR, seriya fizicheskaya, **26**, 575. 1962.

37. NIKOL'SKII, S.I. and Yu.A. SMORODIN.— ZhETF, **39**, 1156. 1960.

38. WILSON, J.G., editor.— Progress in Elem. Part and Cosmic-Ray Physics, 1, Chap. 7. 1952 [Russian translation. 1954.].

N67-38212

A.I. Kuz'min and G.F. Krymskii

COSMIC-RAY BURSTS

Cosmic-ray bursts are usually defined as intensity increases recorded either by ground-level detectors, by detectors in the stratosphere, or by detectors of the cosmic noise following large solar flares. Such intensity increases are caused by the approach to the earth of particles generated in the vicinity of active regions on the sun. Therefore, studies of cosmic-ray bursts tell us about the mechanism of cosmic-ray production in the solar atmosphere, about the general characteristics of the interplanetary field, and about the geomagnetic field far from the earth. This report gives a brief analysis of the frequency distributions, and of the temporal and energy characteristics, of bursts. In addition, it discusses the main results of experimental studies of bursts, from the point of view of determining the structure of the interplanetary field.

1. THE FREQUENCY DISTRIBUTION OF BURSTS

During the last twenty years detectors of the hard cosmic-ray component, mounted at different points on the earth's surface, have recorded six intensity bursts with amplitudes greater than 3% in the middle latitudes. From this it would appear that about once every three years a burst of particles with energies $\varepsilon \geqslant 4$ BeV occurs. However, in the last decade ground-level stations have been provided with neutron monitors, which are more sensitive to low-energy primaries ($\varepsilon \geqslant 1$ BeV). Over an 8-year period, these detectors registered 8 bursts. Consequently, the introduction of more sensitive detectors raised the observed burst frequency by about a factor of three.

During the IGY, systematic flights of cosmic-ray detectors into the stratosphere were initiated at certain high-latitude points. These detectors were even more sensitive to low-energy particles ($\varepsilon \geqslant 100$ MeV). The readings of these instruments indicated a mean frequency of about one burst per month, which is about 40 times greater than the burst frequency indicated by meson recorders located on the earth's surface. However, if we take into account that the flights have "breaks" in continuity, the mean burst frequency in the stratosphere should be approximately another 2 or 3 times greater than the frequency given by ground-level meson recorders. According to this figure, cosmic-ray bursts occur in the stratosphere every ten to fifteen days. Finally, the use of more sensitive instruments (indicators of cosmic-noise absorption, ionospheric stations, earth currents, etc.) to record particles of even lower energies ($\varepsilon \geqslant 10$ MeV) leads to a severalfold increase in burst frequency.

If these data are used to construct the integral energy spectrum of the burst frequency, a power law with an exponent $\gamma \sim$ is found to describe satisfactorily the experimental material.

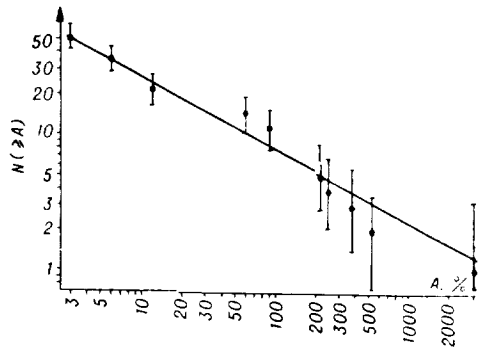

FIGURE 1. Frequency of cosmic-ray increases, as a function of amplitude:

abscissa shows amplitude A of bursts in neutron component; ordinate shows number of bursts in a 20-year period with amplitudes of A or more.

Therefore it can be supposed that the frequency of cosmic-ray intensity bursts drops steeply with an increase in the minimum energy of the primaries responsible for the enhancement of the given recorded component. The observability of a burst using a certain instrument should in principle increase with an increase in the minimum energy of the particles. Thus, the integral distribution of bursts, calculated in terms of the energies of the primaries, is a direct indication of the absence in the vicinity of active solar regions of conditions favorable for protracted action of the acceleration mechanism. In other words, such a distribution of the burst

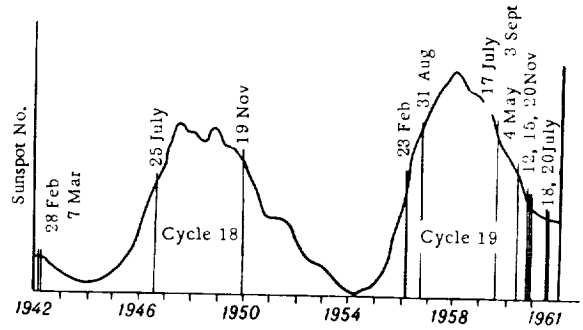

FIGURE 2. Cosmic-ray bursts during the 18th and 19th solar cycles /6/ (solar cosmic rays recorded at sea level).

frequency indicates a short average duration of conditions favorable for particle acceleration in the region of a flare, and it shows that the probability of acceleration decreases with an increase in the duration of these favorable conditions.

Let us now consider the burst frequency as a function of amplitude. Figure 1 shows the integral frequency spectrum for cosmic-ray bursts of different intensities. This spectrum was constructed using the data for all the bursts observed at the earth's surface during the last twenty years. On log-log scale, the ordinate gives the frequency and the abscissa gives the amplitude. To construct this spectrum, the data were reduced to the neutron-monitor readings and to a single time interval.

The figure shows that the integral frequency spectrum for bursts recorded by neutron monitors decreases according to the power law $N(\geqslant A)=\left(\frac{A_0}{A}\right)^{\alpha} N_0$, with an exponent α of about 0.5 to 0.6. Assuming that this spectrum does not undergo any drastic changes in the low-amplitude range, we can evaluate the frequency of intensity bursts, in the neutron component at sea level, which have amplitudes $A \geqslant 0.3\%$. This evaluation shows that during the last twenty years about 100 to 200 bursts could have been recorded in the middle latitudes (about 5 to 10 bursts per year). If this is actually the case, then we can assume that for burst observations the conditions both in the vicinity of the solar flare and in interplanetary space must be especially favorable. Contradictory results have been obtained from a statistical analysis of solar flares with indexes of 2.3 and 3+. Some investigators /1, 2/ appear to have detected effects of small flares, while others /3, 4, 5 /, analyzing the data of the very same stations for the same periods (the IGY and IQSY), have not found any such effects.

Our spectrum of the burst frequency agrees more with the results of the investigators who answer in the negative. The integral energy and amplitude spectra of the bursts show that in many cases chromospheric flares do not have effects which can be recorded with ground-level cosmic-ray detectors.

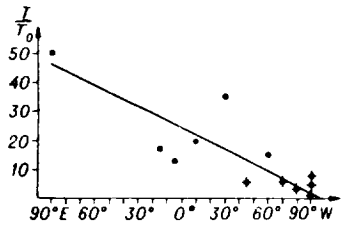

FIGURE 3. Distribution of chromospheric flares responsible for cosmic-ray increases with different time scales:

abscissa shows heliographic longitude of flare; ordinate shows duration of cosmic-ray burst (duration of burst on 4 May 1960 taken as unity). Crosses denote points corresponding to bursts with pronounced impact zones.

The temporal distribution of bursts is also interesting in many respects. Figure 2 shows the distribution of sizable cosmic-ray bursts over the solar-activity cycle /6/. It is clear from the figure that sizable bursts are concentrated in either the rising or descending branches of the solar cycle and are coordinated, on the average, with the mean activity. On the other hand, if chromospheric flares and their immediate surroundings are sources of cosmic rays, then the greatest number of bursts should occur during the period of maximum solar activity. This contradiction can be resolved provided we assume that the average level of solar activity corresponds to conditions especially favorable for the diffusion and propagation of solar cosmic rays throughout interplanetary space and for their arrival at the earth. With respect to this, the asymmetric distribution of effective flares over the solar disk /7/ is also very interesting (Figure 3).

The figure shows that the largest number of cosmic-ray bursts are caused by chromospheric flares on the western side of the solar disk. Hence,

particles emitted from the western hemisphere of the sun have more chance of reaching the earth than particles leaving from the eastern hemisphere.

Another important property of cosmic-ray bursts, whether recorded on the earth or in the stratosphere, is that they are always observed during or after terrestrial magnetic storms. From this it follows that the solar corpuscular streams responsible for geomagnetic storms must bring about the favorable conditions necessary for the propagation of solar cosmic rays.

2. THE TEMPORAL AND ENERGY CHARACTERISTICS OF BURSTS

In some cases the global distribution of the effect of a large flare depends considerably on the longitude. This implies anisotropy of the additional flux of cosmic rays. The most pronounced effects are in the so-called "impact zones" /8/, which are the regions of the earth's surface accessible to cosmic-ray particles coming directly from the sun. It first became possible to study in detail the anisotropy of solar cosmic rays, together with its variation in time, for the flare of 23 February 1956, which was recorded at many points. An analysis /9/ of the effect of this flare, both in the impact zones and outside of them, made it possible to distinguish between the direct flux from the sun and the scattered flux of particles coming from other directions. During the initial period of the phenomenon, the entire flux arrived from the sun within a cone with an opening angle $\leqslant 30°$. This flux reached a maximum after a few minutes, whereas particles began to arrive from other directions about 10 minutes later. After approximately an hour the intensity became isotropic.

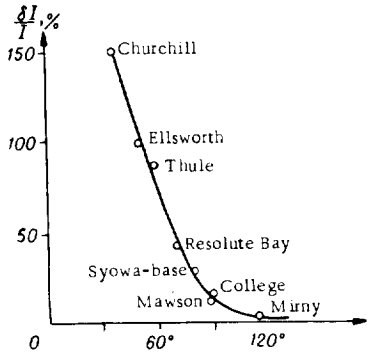

FIGURE 4. Amplitude of cosmic-ray increase on 4 May 1960, as a function of angular distance between asymptotic direction of recording and symmetry axis.

Using the method of asymptotic directions, McCracken /10/ succeeded in plotting the distribution of cosmic-ray intensity, in terms of the directions in space, for the bursts of 4 May, 12 November, and 15 November 1960. The direction of maximum intensity (axis of symmetry of the cosmic-ray flux) is close to the ecliptic plane and is displaced 50–60° to the west of the sun.

Figure 4 shows the intensity of solar cosmic rays as a function of the angular distance from the symmetry axis, for the burst of 4 May 1960. During the period of intensity falloff, the dependence becomes increasingly weaker and the intensity becomes more and more isotropic.

In /11, 12/ it was demonstrated that the temporal profile of a cosmic-ray increase can be described approximately, provided that solar cosmic rays are assumed to propagate from the sun by means of diffusion about inhomogeneities of the magnetic field in the solar system. The solution of

the diffusion equation for a one-dimensional infinite medium has the form

$$n(R_\delta, t) = \frac{Q}{(4\pi Dt)^{3/2}} \exp\left(-\frac{R_\delta^2}{4Dt}\right), \qquad (1)$$

where $n(R_\delta, t)$ is the cosmic-ray density at a distance R_δ for a time t after emission (the finite velocity of the particles is taken into account); D is the diffusion coefficient; and Q is the total number of emitted particles.

The authors of /13/ pointed out that the curves for all cosmic-ray bursts can be matched with one another if the axial scale factors are varied (the abscissa being time and the ordinate being intensity). Different scale factors correspond to different values of D and Q in formula (1). The briefest cosmic-ray increases occur after chromospheric flares at the western limb of the sun.

The duration of a burst as a function of the position of the corresponding chromospheric flare on the solar disk was shown in Figure 3. The degree of anisotropy of the flux of solar cosmic rays also depends on the heliographic longitude of the flare. From Figure 3 it is evident that increases with pronounced impact zones are caused by western chromospheric flares /7/.

The energy spectrum of the flux of solar particles was determined from the dependence of the effect of the increase on the geomagnetic cutoff during the period of isotropy /14/. The differential spectrum for the burst of 23 February 1956 has been determined by many authors:

$$\delta D(p) \sim p^{-6} - p^{-7}.$$

The energy spectrum of the increase of 4 May 1960 is /15/:

$$\delta D(p) \sim p^{-5} - p^{-6}.$$

These two spectra may be assumed as typical for cosmic-ray bursts at the earth's surface. However, the spectrum determined for the period of isotropy characterizes the scattered part of the cosmic-ray flux, and it does not in general coincide with the spectrum of the source on the sun.

Actually, if we assume that the source energy spectrum $Q(p) \sim p^{-\alpha_0}$, and that the diffusion coefficient varies with rigidity as $D(p) \sim p^{\sigma}$, then from formula (1) we obtain

$$\delta D(p) \sim n(p) \sim p^{-\alpha_0 - \frac{3}{2}\sigma} \exp\left[-\frac{R_\delta^2}{4D(p)\,t}\right]. \qquad (2)$$

During the period of isotropy, for $t > t_{max}$, the exponential factor in (2) will differ little from unity and the index of the observed spectrum will be

$$\alpha = \alpha_0 + \frac{3}{2}\sigma. \qquad (3)$$

Pfotzer /16/ attempted to use data from stations located in an impact zone to determine the spectrum of the direct flux from the sun for the burst on 23 February 1956. The spectrum obtained, $\delta D(p) \sim p^{-3.4}$, differs considerably from the spectrum of the scattered radiation. If this is taken as the spectrum of the source, the index σ of the rigidity dependence of the diffusion coefficient can be found: $\sigma = \frac{2}{3}(\alpha - \alpha_0) = 1.8$ to 2.4. This value of σ is not at variance with the assumption concerning the propagation of solar cosmic rays in a magnetic field with inhomogeneities which are much smaller than the gyro radius of the particles (in this case $\sigma = 2$).

3. A MODEL OF THE INTERPLANETARY MAGNETIC FIELD

The discrepancy between the properties of cosmic-ray increases caused by flares at various heliographic longitudes is not due to a difference in the generation conditions. Rather, it reflects a difference in the conditions of particle propagation from the eastern and western parts of the solar disk.

In order to explain the described properties of cosmic-ray bursts, McCracken suggested the following model /7/. In the inner solar system there is a magnetic field with a regular component radial to the sun. This field is twisted by the solar rotation, so that its lines of force connect the earth to the western limb of the solar disk. The dependence of the time scales of cosmic-ray increases upon the heliographic longitudes of flares is explained by the fact that the diffusion of cosmic rays from western flares proceeds along the magnetic field, whereas diffusion from eastern flares is across the field. Since the diffusion coefficient along the field is much greater, increases in the intensity of cosmic rays from western flares will take place more quickly /17, 18/. The propagation of cosmic rays transverse to the field also means that these particles will reach the earth in an isotropic flux, so that the impact zones for eastern flares will not be pronounced. During the motion of cosmic rays from the sun along the magnetic field, the flux must become collimated within a narrow cone with its axis along the line of force, on account of conservation of the adiabatic invariant:

$$\frac{\sin^2\theta}{H} = \text{const.}$$

If the particles moved along the magnetic field without being scattered, they would arrive at the earth within a cone with an angle of opening $<1°$, which, as Figure 4 shows, is not the case. Consequently, it must be assumed that inhomogeneities are present in the radial field, and that the particles are scattered by them.

Therefore, the direction of the force lines of the interplanetary magnetic field in the vicinity of the earth can be considered to be the predominant direction of particle arrival from western flares. As already mentioned, this direction is in the ecliptic plane 50 to 60° to the west of the sun, which is another indication of the tangled nature of the interplanetary field. Similar conceptions of the interplanetary magnetic field also ensue from an analysis of the arrivals of low-energy particles /19, 20/.

Institute of Space-Physics Research and Aeronomy,
Yakutsk Branch of Siberian Division of
USSR Academy of Sciences

REFERENCES

1. KOLOMEETS, E.V. and G.A. SERGEEVA.— Trudy MGG, Part VII, No.4, p.132. 1961.

2. DORMAN, L.I. and E.V. KOLOMEETS.— Geomagnetizm i aeronomiya, **5**, 100. 1961.

3. TOWLE, L.C. and J.A. LOCKWOOD.— Phys. Rev., **113**, 641. 1959.

4. GHIELMETTI, H. et al.— Nuovo Cimento, **15**, 87. 1960.

5. SKRIPIN, G.V., G.F. KRYMSKII, and L.P. BOLTRUSHKO. Report in this collection.

6. CARMICHAEL, H. and J.F. STELJES.— Proc. Kyoto Conference. 1961.

7. Mc CRACKEN, K.G.— J. Geoph. Res., **67**, 447. 1962.

8. FIROR, J.— Phys. Rev., **94**, 1017. 1954.

9. DORMAN, L.I. and G.I. FREIDMAN.— Trudy YaFSO, AN SSSR, seriya fizicheskaya, No.2. 1957.

10. Mc CRACKEN, K.G.— J. Geoph. Res., **67**, 435. 1962.

11. BROWN, R.R.— J. Geoph. Res., **62**, 147. 1957.

12. DORMAN, L.I.— Nuovo Cimento, **8**, Suppl. 2, 180. 1958.

13. Mc CRACKEN, K.G., and R.A.R. PALMEIRA.— J. Geoph. Res., **65**, 2673. 1960.

14. DORMAN, L.I. Variatsii kosmicheskikh luchei (Cosmic-Ray Variations).— Gostekhizdat. 1957.

15. KAMINER, N.S., Ya.L. BLOKH, and L.I. DORMAN.— Trudy MGG, Part VII, No.4, p.146. 1961.

16. PFOTZER, G.— Nuovo Cimento, Suppl. 2, 180. 1958.

17. KRYMSKII, G.F. Report in this collection.

18. SHISHOV, V.I. Report in this collection.

19. REID, G.C. and H. LEINBACH.— J. Geoph. Res., **64**, 1801, 1959.

20. DVORYASHIN, A.S., L.S. LEVITSKII, and A.K. PANKRATOV.— Izv. KAO, **26**, 90. 1961.

N67-38213

A.I. Kuz'min and G.F. Krymskii

THE EFFECT ON COSMIC RAYS OF A VARIATION IN THE GEOMAGNETIC THRESHOLDS

Planetary increases in cosmic-ray intensity during large magnetic storms, which are unrelated to the generation of cosmic rays on the sun, have been noted and investigated in several studies /1-3/. In such cases it was assumed that the increases result from a variation in the geomagnetic thresholds during the storms. Corresponding models were designed /2, 4, 5/, the most correct of which is that of Obayashi and Hakura /5/.

An analysis of the variations related to changes in the geomagnetic threshold is complicated for two reasons. First, the latitude effect of the ground-level cosmic-ray components is quite large, which means that the primary spectrum is quite steep, especially at maximum solar activity. As a result, the variations in question are only slight ($\sim 1-2\%$), even during very large magnetic storms. Second, when analyzing data only for the ground-level components, it is difficult to isolate variations of extra-terrestrial origin having a sufficiently rigid spectrum, for instance, the anisotropy related to Forbush effects.

In order to select the cosmic-ray variations which are of geomagnetic origin, a comparison can in principle be made between the readings of two instruments with approximately the same coupling coefficients (and thus the same response to extraterrestrial variations), but with different responses to changes in the geomagnetic threshold. The coupling coefficients $W(\varepsilon)$ of the instruments must satisfy the relation

$$\int_{\varepsilon_{\lambda_1}}^{\infty} W_1(\varepsilon)\frac{\delta D(\varepsilon)}{D(\varepsilon)}\,d\varepsilon \approx \int_{\varepsilon_{\lambda_2}}^{\infty} W_2(\varepsilon)\frac{\delta D(\varepsilon)}{D(\varepsilon)}\,d\varepsilon, \qquad (1)$$

where $\frac{\delta D(\varepsilon)}{D(\varepsilon)}$ is the spectrum of the variations of extraterrestrial origin.

Relation (1) is satisfied if we use the coupling coefficients of the neutron monitor at Kodaikanal and the underground telescope (7 m.w.e. deep) at Yakutsk. The readings of these instruments for several large magnetic storms do not show any differences which are beyond the limits of statistical error of the neutron monitor. Figure 1 shows the intensity curves recorded with these instruments for the very large magnetic storm on 8 July 1958.

Consequently, for the majority of magnetic storms, the effect which the variation in the geomagnetic thresholds has on the cosmic rays does not exceed $\sim 1\%$.

Appreciable cosmic-ray variations should result from changes in the geomagnetic thresholds during cosmic-ray bursts, whose energy spectra drop sharply ($\sim\varepsilon^{-5}$ to ε^{-7}). Very interesting in this respect is the burst of

12 November 1960, observed at the earth's surface. The two cosmic-ray increases which occurred prior to and during the magnetic storm have different latitude dependences (Figure 2). The dashed curve shows the transformed latitude variation of the burst, assuming that the decrease in

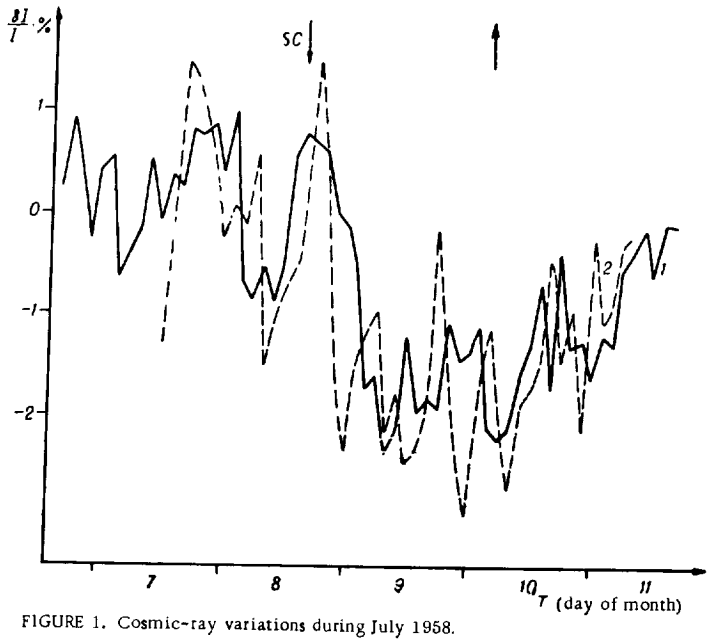

FIGURE 1. Cosmic-ray variations during July 1958.

1-intensity 7 m. w. e. deep at Yakutsk; 2-intensity of neutron component at Kodaikanal. Arrows indicate onset and end of magnetic storm.

geomagnetic thresholds takes place which is predicted by the model of Obayashi and Hakura for a 200-γ reduction of the horizontal component of the geomagnetic field at the equator (the reduction of the horizontal component at Colombo at the moment of the second intensity peak was 160 γ). The dependence of the increase occurring during the magnetic storm upon the geomagnetic threshold agrees with the expected one. Thus, we can conclude that the model of Obayashi and Hakura describes satisfactorily the interaction between the flux plasma and the geomagnetic field which took place on 12 November 1960.

The interesting idea of lunitidal variations of the geomagnetic thresholds was suggested in /6/. According to this theory, lunitidal fluctuations of the plasma in the radiation belts, as a result of the freezing-in there of the geomagnetic field, should lead to a lunar-daily variation in the geomagnetic thresholds and consequently in the cosmic rays.

In /7/ it is shown that the corresponding effect on the cosmic rays may be some tenths of a percent. However, the explanation of the lunar-daily variation observed in /7/ in terms of a tidal action of the moon upon the magnetosphere of the earth is, in our opinion, difficult, for the following reasons.

The tide-producing acceleration along the earth-moon line is

$$g_{\text{tp}} = \left[\frac{L^2}{(L-x)^2} - 1\right] \frac{M_L}{M_e} \left(\frac{R_e}{L}\right)^2 g_e, \tag{2}$$

where L is the distance from the earth to the moon; x is the distance from the earth's center of the point where the acceleration is measured (this is

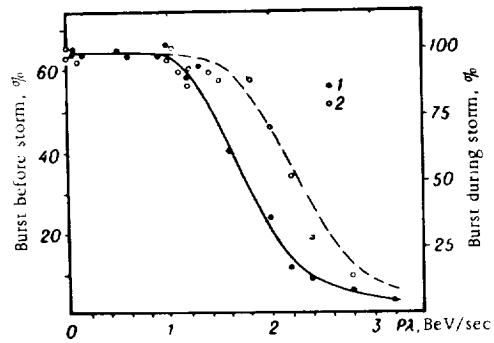

FIGURE 2. Effect of cosmic-ray increase on 12 November 1960, as a function of geomagnetic threshold:

1—first increase (prior to storm); 2—increase during storm.

positive on the side toward the moon); M_L and M_e are the masses of the earth and moon; and R_e and g_e are the radius and gravitational acceleration of the earth. After a series expansion of equation (2) in powers of x (neglecting terms after the x^2 term), we obtain

$$g_{\text{tp}} = \left(\frac{2x}{L} + \frac{6x^2}{L^2}\right)\left(\frac{R_e}{L}\right)^2 \frac{M_L}{M_e} g_e. \tag{3}$$

The first and second terms in this equation correspond to the semi-diurnal and diurnal harmonics (g_2 and g_1) of the tide-producing acceleration. If we assume that the amplitudes of the corresponding harmonics of the lunar-daily cosmic-ray variations are proportional to the accelerations g_2 and g_1, then we obtain

$$\frac{A_1}{A_2} \approx \frac{g_1}{g_2} = \frac{3x}{L}. \tag{4}$$

The characteristic distance in our case may be taken as $x = 3R_e$. Thus, taking into account that $L \sim 60R_e$, we have $\frac{A_1}{A_2} = 0.15$, whereas in /7/ $\frac{A_1}{A_2} > 2$ was obtained.

It is also difficult to imagine that the first harmonic is enhanced by the natural vibrations of the magnetosphere. In order to estimate the order of magnitude of the period of these vibrations, let us assume that they form a standing hydromagnetic wave. Then

$$T \sim \frac{\lambda}{v} = \frac{\lambda \sqrt{4\pi\rho}}{H}, \tag{5}$$

where $\lambda \sim 3R_e$ is the dimension of the region, or the "wavelength"; $\rho \sim 10^{-21}$ to 10^{-20} g/cm^3 is the density of matter there; and $H \sim 10^{-2}$ gauss

is the magnetic-field strength. For the indicated values of the parameters, $T \lesssim 1$ minute.

Therefore, if the lunar-daily variations observed in /7/ are real, they cannot represent lunitidal fluctuations of the magnetosphere. However, these variations may be a consequence of the 27-day modulation of the solar-daily cosmic-ray variation /6, 8/.

Institute of Space-Physics Research and Aeronomy,
Yakutsk Branch of Siberian Division of
USSR Academy of Sciences

REFERENCES

1. YOSHIDA, S. and M. WADA.— Nature, **382**, 1959.

2. KONDO, I., K. NAGASHIMA, S. YOSHIDA, and M. WADA.— Trudy MKKL, **4**, 210. 1960.

3. DORMAN, L.I., Ya.L. BLOKH, and N.S. KAMINER.— Trudy MGG, VII, 4, 5. 1961.

4. ROTHWELL, P.— J. Geoph. Res., **64**, 2026. 1959.

5. OBAYASHI, T. and Y. HAKURA.— Rept. Ionosph. Space Res., **14**, 1. 1960.

6. DORMAN, L.I.— Trudy MGG, VII, **4**, 253. 1961.

7. DORMAN, L.I. and L.Kh. SHATASHVILI.— Geomagnetizm i aeronomiya, **1**, 663. 1961.

8. KRYMSKII, G.F.— Trudy YaFSO, AN SSSR, seriya fizicheskaya, **4**, 108. 1962.

N67-38214

L.I. Dorman, E.V. Kolomeets, L.V. Kozak, V.T. Pivneva, and G.A. Sergeeva

THE VARIATION IN COSMIC-RAY INTENSITY AT THE TIME OF A FORBUSH DECREASE

The enhancement of the cosmic-ray intensity at the minimum of a Forbush effect has been considered in /1-3/. Such an enhancement has been attributed to various causes, including a change in the rigidity threshold for a large reduction of the horizontal component of the geomagnetic field.

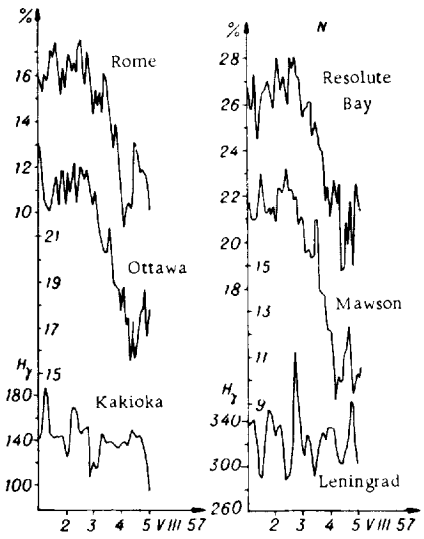

FIGURE 1. Intensity variation of cosmic-ray neutron component and variation of horizontal component of geomagnetic field, for 2-5 August 1957.

In this report, eight instances of intensity increases during a Forbush decrease are considered. What happens is that, during the drop in cosmic-ray intensity at a rate which is usually 1-2% per hour, an intensity increase also sets in at a rate higher than the drop rate. Let us consider separately these cases of an intensity rise at the time of a Forbush decrease.

4 August 1957. Figure 1 shows the neutron-component intensities at Rome, Ottawa, Resolute Bay, and Mawson, and also data on the horizontal component of the geomagnetic field at Kakioka and Leningrad. The figure indicates two cases of an increase in cosmic-ray intensity at the time of the Forbush decrease on 4 August. A comparison of the data for the horizontal field component and the cosmic-ray intensity shows that there is no correlation between them. For this case we calculated the amplitude of the effects, both taking into account the decrease rate and neglecting it. Figure 2a shows the neutron-component increase plotted against the cutoff rigidity for the first effect: the lower data, without taking into account the decrease rate; and the upper data, taking it into account. No definite energy dependence of the effect of the increase is observed from Figure 2a. In addition, no definite dependence on longitude is observed either (Figure 2b). From Figures 2c and 2d we see that there is no definite dependence on the cutoff rigidity for the second effect, and from 2e and 2f that the same is true of the hard component for the first effect.

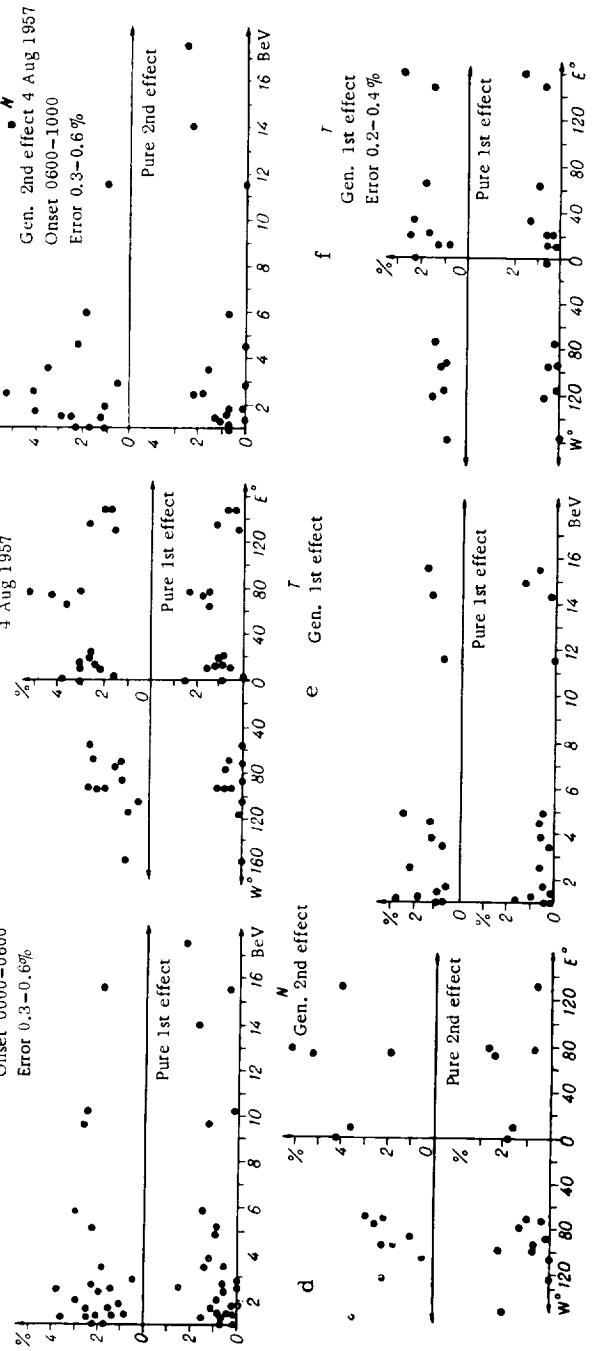

FIGURE 2. Intensity increase of neutron (N) and hard (T) components, plotted against cutoff rigidity and geographic longitude, for 4 August 1957.

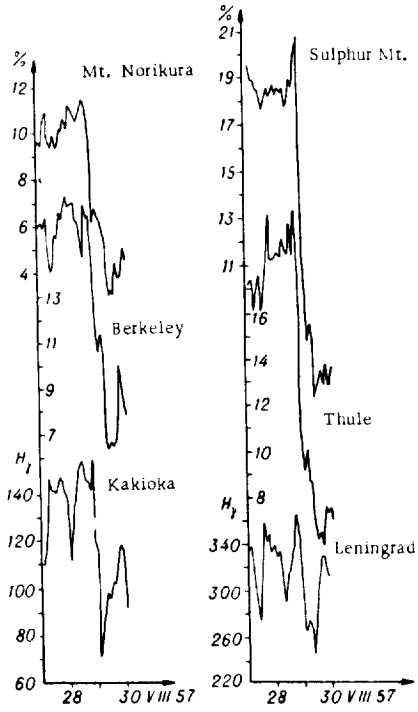

FIGURE 3. Data for 28–30 August 1957.

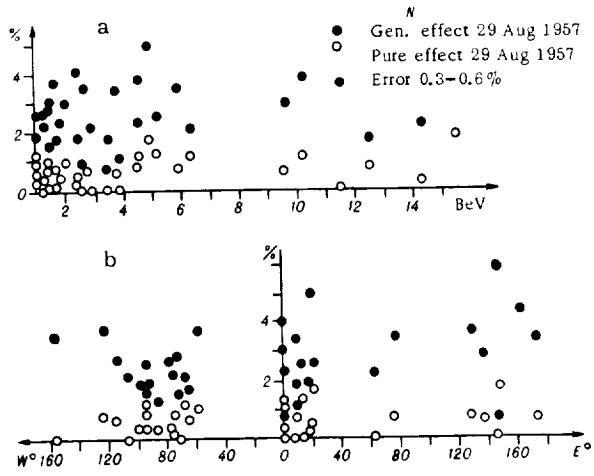

FIGURE 4. Data for 28–30 August 1957.

28–30 August 1957. Figure 3 shows the neutron-component intensity at the Mt. Norikura, Berkeley, Sulphur Mountain, and Thule stations, and also data on the horizontal component of the geomagnetic field for the Kakioka and Leningrad stations. It is clear from the figure that an intensity rise occurs at the time of the decrease in the horizontal field component. This rise is probably due in part to a change in the rigidity threshold. Figures 4a and 4b show the corresponding latitude and longitude dependences of the effect of the intensity rise. As in the previous case, no definite regularity is observed.

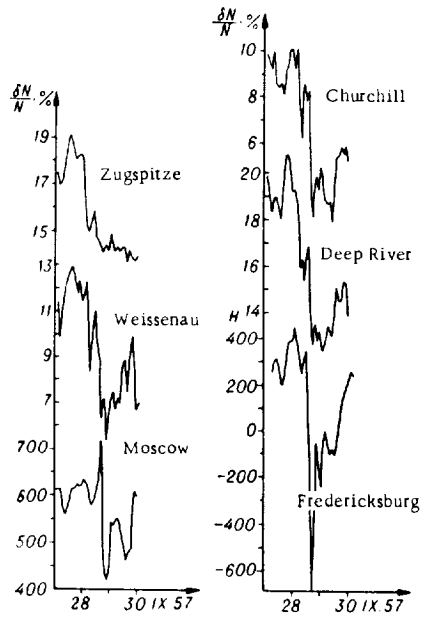

FIGURE 5. Data for 28–30 September 1957.

28–30 September 1957. Figure 5 gives the intensity variation of the neutron component for the stations at Zugspitze, Weissenau, Churchill, and Deep River, and also the variation of the horizontal component of the geomagnetic field at Moscow and Fredericksburg. From the figure it is evident that in this case the intensity decrease began several hours prior to the decrease in the horizontal component of the field. The effect of the intensity rise at the time of the Forbush decrease is also observed before the beginning of the reduction in the horizontal magnetic-field component. In this case, therefore, the intensity increase is definitely not due to a change in the rigidity threshold. Figures 6a–6d show the intensity increase plotted against the cutoff rigidity and the geographic longitude. The data show that the intensity increase depends neither on the rigidity threshold nor on the local time. In Figures 6e–6g, the neutron-component increases are plotted versus the rigidity threshold, for the American, European, and Asian continents separately. Obviously, no regularity can be detected.

20–23 October 1957. Figure 7 shows the neutron-component intensities at Rome, Washington, Yakutsk, and Thule, and the horizontal component of the geomagnetic field at Kakioka and Leningrad. In this case a rise in neutron intensity took place at a time when the horizontal magnetic-field component was a minimum. This was for the second increase. The first rise in neutron intensity, on the other hand, occurred at the beginning of the variation in the geomagnetic field. Figure 8 shows the intensity rise plotted against the cutoff rigidity and the geographic longitude. In this case, too, the intensity increase depends neither on the threshold energy nor on the local time.

25 March 1958. Figure 9 shows the intensity variation of the neutron component and the variation of the horizontal magnetic-field component for 25–26 March 1958. It is clear from the figure that there is no correlation between the variation in the field and the cosmic-ray intensity increase.

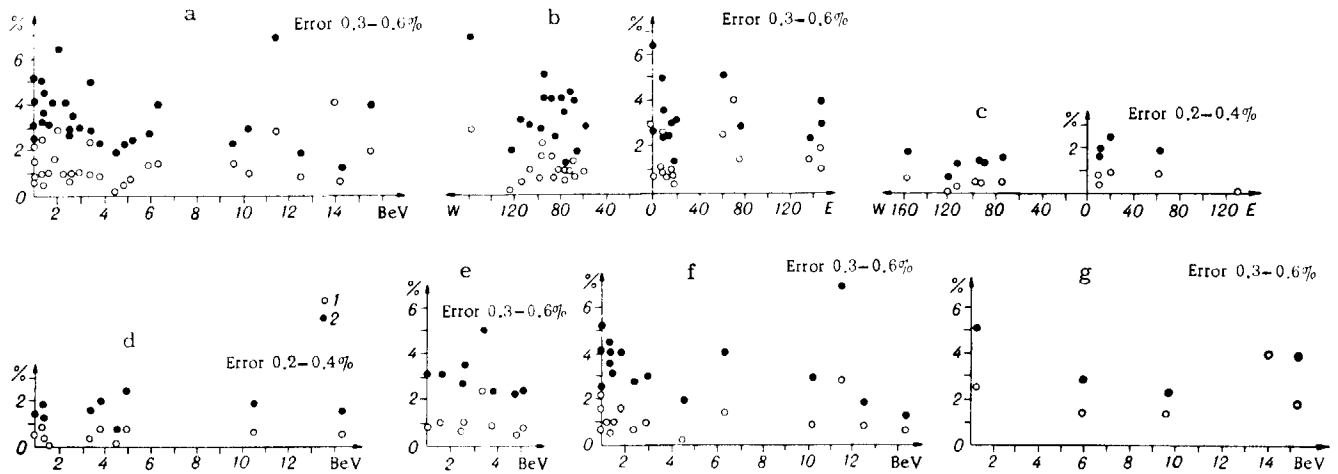

FIGURE 6. Data for 28–30 September 1957.

Intensity increase at time of Forbush decrease: a, b–for N; c, d–for T; e–for N (Europe); f–for N (America); g–for N (Asia). 1 shows increase neglecting decrease rate; 2 takes into account decrease rate.

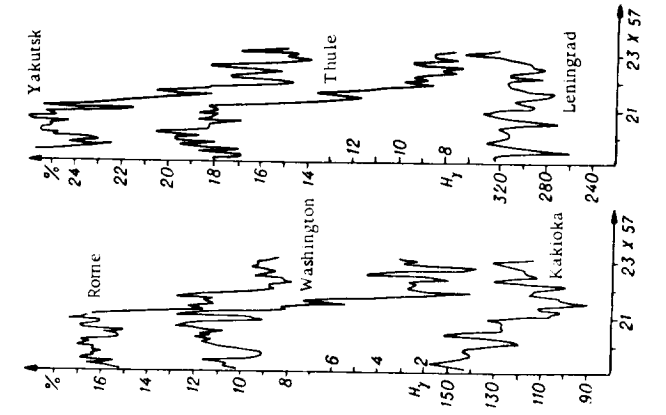

FIGURE 7. Data for 20–23 October 1957.

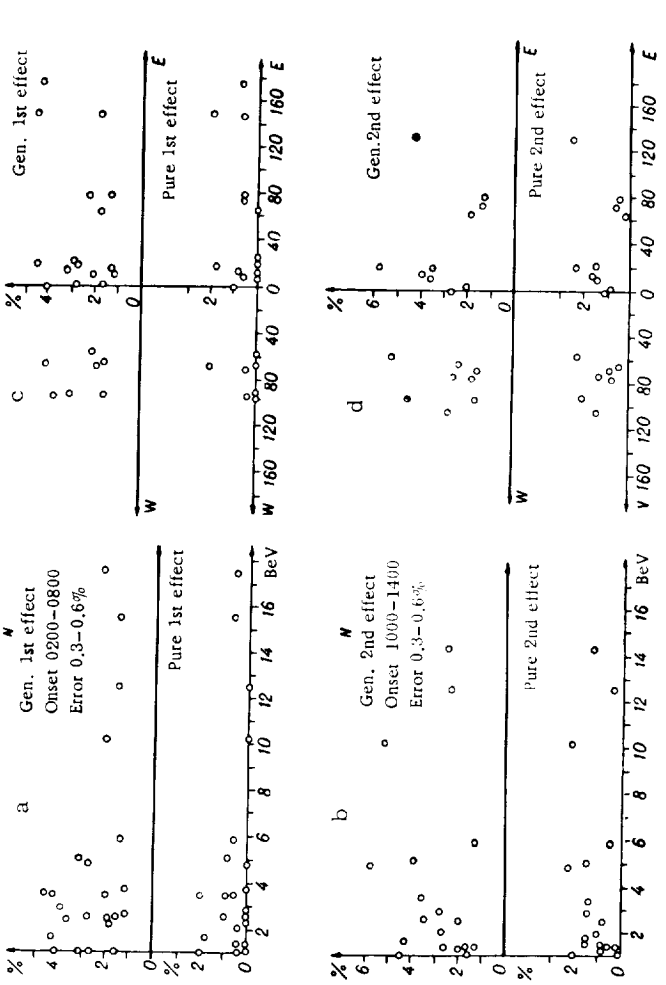

FIGURE 8. Data for 22 October 1957.

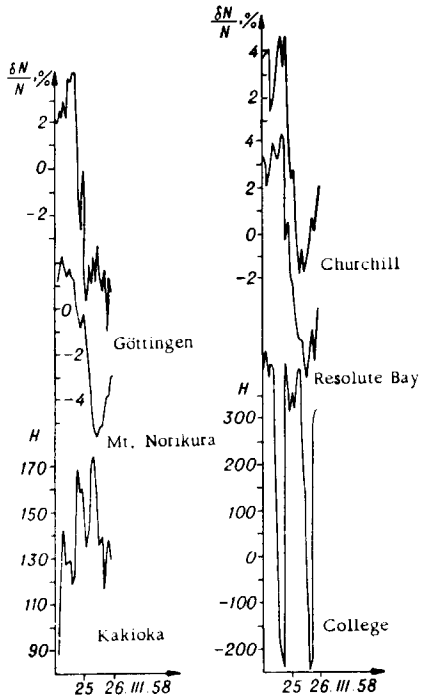

FIGURE 9. Data for 25–26 March 1958.

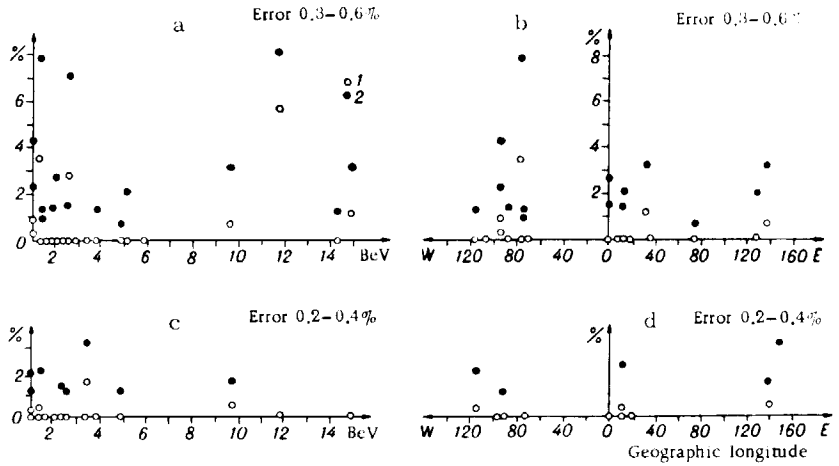

FIGURE 10. Data for 25–26 March 1958.

Intensity increase during Forbush decrease: a, b–for N; c, d–for T; 1–neglecting decrease rate; 2–taking into account decrease rate.

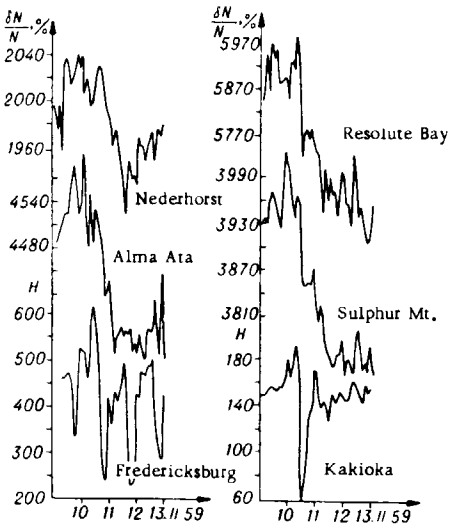

FIGURE 11. Data for 11–12 February 1959.

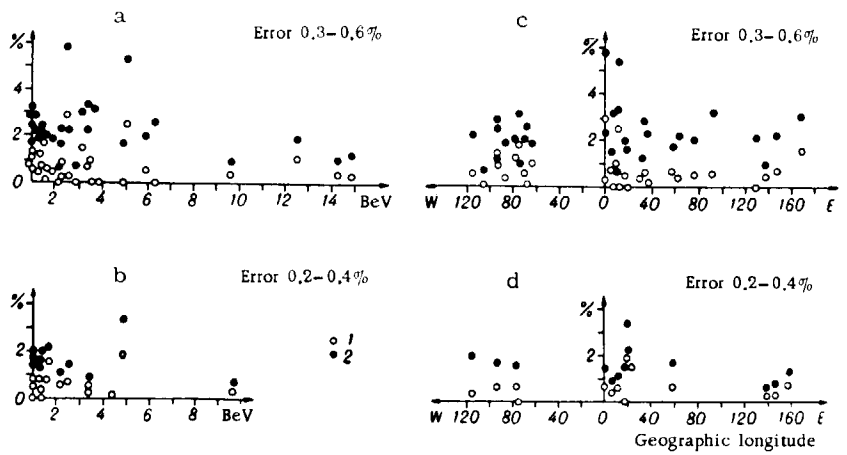

FIGURE 12. Data for 11–12 February 1959.

Intensity increase during Forbush decrease: a–for N; b–for T; c–for N; d–for T; 1–neglecting decrease rate; 2–taking into account decrease rate.

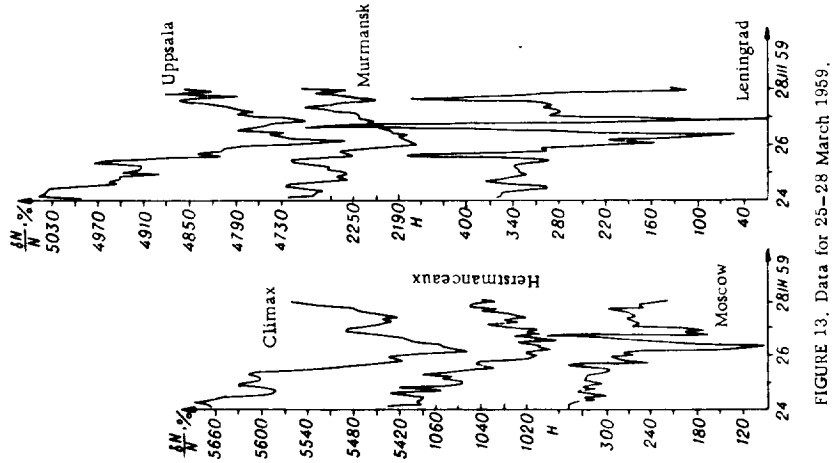

FIGURE 13. Data for 25–28 March 1959.

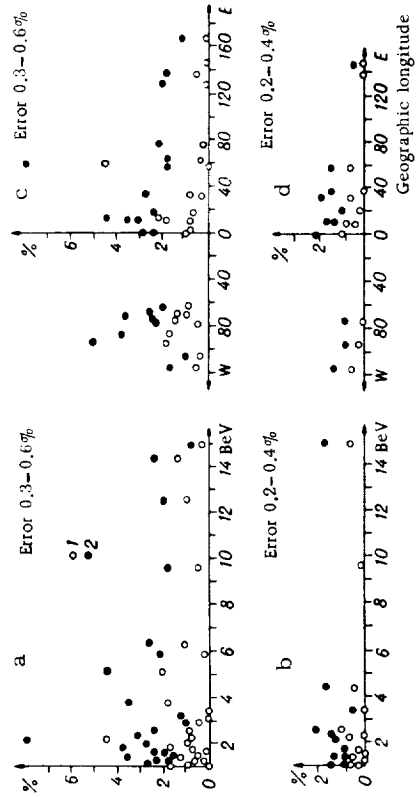

FIGURE 14. Data for 25–28 March 1959.

Intensity increase during Forbush decrease: a–for N; b–for T; c–for N; d–for T; 1–neglecting decrease rate; 2–taking into account decrease rate.

From Figure 10, where the intensity increase is plotted against the cutoff rigidity and the geographic longitude, it is also clear that there is no regularity in the intensity increase of the neutron and hard components as a function of the cutoff energy and geographic longitude.

11–12 February 1959. Figure 11 gives data on the neutron intensity for the stations at Nederhorst den Berg, Alma Ata, Resolute Bay, and Sulphur Mountain, together with data for the horizontal field component at Fredericksburg and Kakioka. The figure shows that the cosmic-ray intensity increases when the horizontal field component is at a minimum.

Figure 12 shows the intensity increase of the neutron and hard components plotted against the threshold energy and the geographic longitude. Here the intensity increase remains constant for changes in energy and geographic longitude.

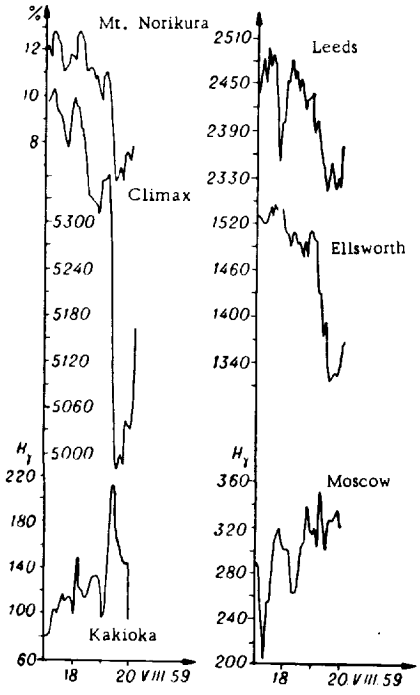

FIGURE 15. Data for 18–20 August 1959.

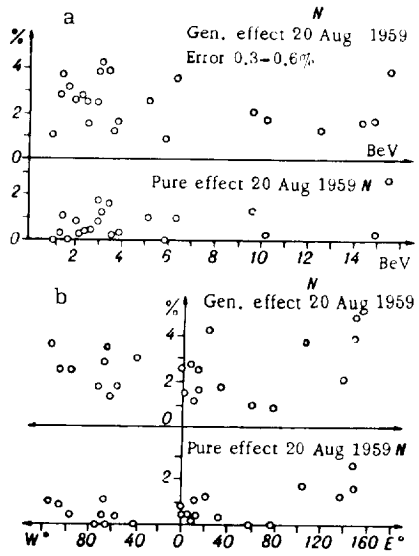

FIGURE 16. Data for 18–20 August 1959.

25–28 March 1959. Figure 13 gives the neutron-intensity variation and the variation of the horizontal field component. Here, the intensity increase occurred when the magnetic-field component began to decrease.

Figure 14 shows the intensity increase in the neutron and hard components plotted against the cutoff energy and the geographic longitude. No definite regularity is observed with variations in energy or longitude.

18–20 August 1959. Figure 15 gives the intensity variation of the neutron component for the stations at Climax, Mt. Norikura, and Ellsworth, together with the variation of the horizontal component of the geomagnetic

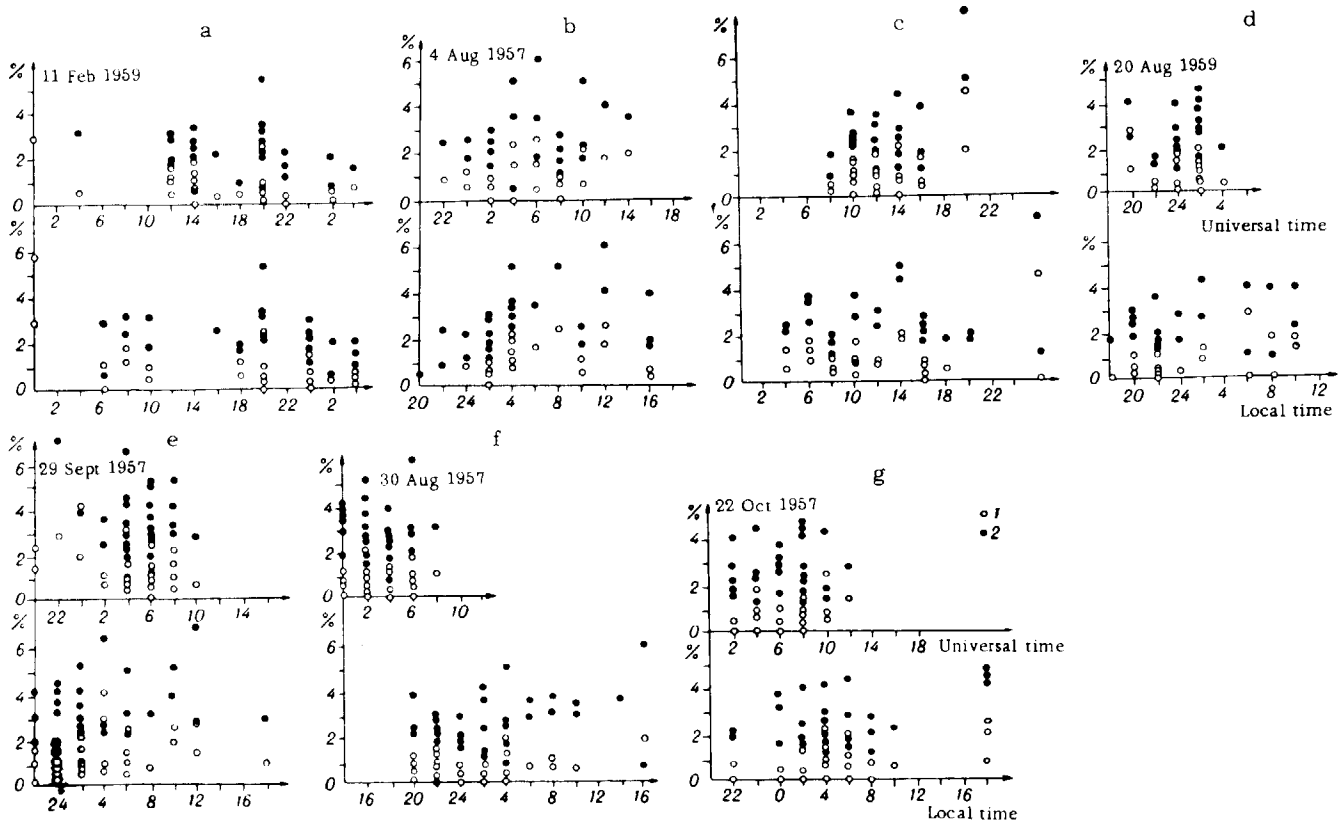

FIGURE 17. The intensity increase during a Forbush decrease, plotted against universal time and local time: 1–pure effect; 2–effect taking into account the rate of decrease.

field at Kakioka and Moscow. No correlation is observed between the variations in cosmic-ray intensity and in the geomagnetic field.

Figure 16 shows the intensity increase plotted against the threshold energy and the geographic longitude. In this case as well, the increase is independent of the rigidity threshold and the geographic longitude.

It is our opinion that the nature of the observed effect is a result of inhomogeneity of the magnetic fields frozen into the corpuscular fluxes. If the velocity of a corpuscular flux is taken as 10^8 cm/sec and the effect in question lasts for 10^4 sec, the transillumination will be 10^{12} cm, which does not contradict the results obtained elsewhere.

Another possible explanation of the observed effect is a sharp change in the cutoff rigidity due to fluctuations in the geomagnetic field at large distances.

Figure 17 shows the increase in cosmic-ray intensity plotted against universal and local time. There is a marked dependence on universal time for the cases shown in Figures 17c, d, f, and g, where the effect is observed within a 6 to 8 hour period. In Figures 17a and b there is a double intensity increase, although the scatter of points in these cases is much greater.

S. M. Kirov Kazan' State University

N67 38215

A.I. Kuz'min, G.F. Krymskii, G.V. Skripin, N.P. Chirkov, Yu.G. Shafer, and G.V. Shafer

COSMIC RAYS IN JULY 1961

1. GENERAL SEQUENCE OF EVENTS AND SOURCES OF DATA USED

From the ninth to the twentieth of July 1961, the large spot group No. 198 /1/, accompanied by a large number of chromospheric flares, traversed the visible disk of the sun. A series of remarkable cosmic-ray events and other geophysical phenomena were associated with the transit of this spot group.

24 hours after a chromospheric flare was observed at 1000 U. T. on 12 July, a magnetic storm commenced suddenly and a drop in cosmic-ray intensity took place.

On 14 and 15 July the cosmic-ray intensity was highly anisotropic. The trend of the anisotropy was opposite to the diurnal rotation of the earth. On 18 July, following a new flare in the same part of the sun, the cosmic-ray intensity (which had not yet recovered from the previous drop) decreased once again.

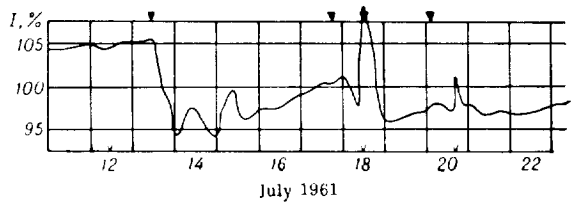

FIGURE 1. The sequence of solar and geophysical phenomena during July 1961.

The flare at 1000 U. T. on 18 July (coordinates 10° S and 60° W) was apparently the source of the solar cosmic rays observed at 1100 U. T. on that day. A second cosmic-ray increase took place on 20 July, after a flare at the western limb of the sun; the anisotropy in this case was pronounced.

All the chromospheric flares responsible for the phenomena in question occurred in a single spot group. The succession of events in July 1961 are shown schematically in Figure 1.

Our study utilizes the results of cosmic-ray recordings at Yakutsk, both at ground level and in the stratosphere, and also data on the hard and neutron components obtained at other stations.

2. THE INTENSITY DROP ON 13 JULY

The drop in cosmic-ray intensity on 13 July (see Figure 1) was related to the arrival of a corpuscular stream which caused a magnetic storm with a sudden commencement at 1112 U. T. The most probable source of this flux was a 3^+ chromospheric flare with coordinates 7° S and 25° E, which began at 1003 U. T. on 12 July and lasted for two hours. The flare was accompanied by very strong radio emission in the meter and decimeter ranges /1/.

The magnetic storm commenced 25 hours and 9 minutes after the flare, which corresponds to a mean flux velocity of $1.6 \cdot 10^8$ cm/sec.

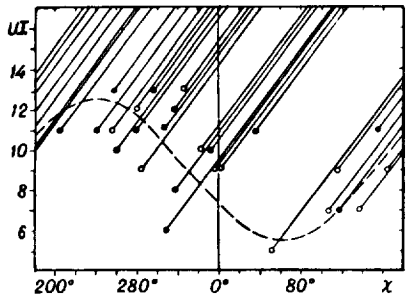

FIGURE 2. Moment of onset of Forbush decrease on 13 July 1961, as a function of direction of recording.

Degrees are reckoned east from E–S line. O denotes meson component; • denotes neutron component. Slanted lines show trajectories of instrument receiving direction as a time-direction diagram.

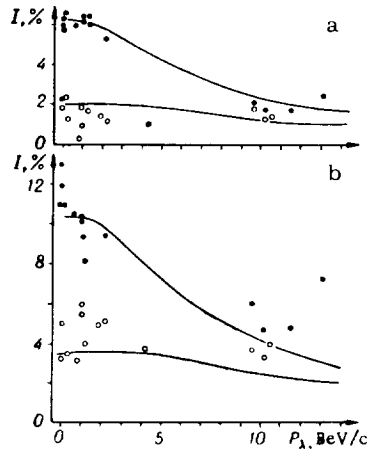

FIGURE 3. Decrease effects as a function of geomagnetic threshold:

a–direction of minimum drop; b–direction of maximum drop; O denotes meson component; • denotes neutron component.

Figure 2 shows the moment of drop onset as a function of the direction of recording of cosmic rays beyond the limits of the geomagnetic field. The intensity begins to drop earlier for the direction 60° east of the earth-sun line (E–S line). This situation is the opposite of that observed for other cosmic-ray decreases /2/. All the intensity decreases studied previously showed an early drop from directions west of the E–S line (see, for example, /3, 4, 5/).

Appreciable anisotropy was observed for two days after the minimum of the cosmic-ray intensity. The intensity in space varied only moderately during the first 12 hours after the minimum (gradual recovery). Consequently, it was possible to measure the effect of the drop separately for the directions of maximum and minimum intensity decrease. The dependence on geomagnetic threshold for these two directions is plotted in

Figure 3. The curves show the dependence of the following intensity-drop spectrum:

$$\frac{\delta D(\varepsilon)}{D(\varepsilon)} = a\varepsilon^{-1}, \qquad (1)$$

where a is a normalizing factor satisfying the requirement that the effect on the neutrons, calculated for a point with geomagnetic threshold $p_\lambda = 1$ BeV/c, agrees with experiment.

The figure shows that the intensity-drop spectrum in the direction of minimum intensity is harder than shown by (1), whereas in the direction of minimum decrease it is softer. The energy spectrum of the effect in other directions will be a combination of these two spectra, as described approximately by formula (1).

3. THE ROTATION OF THE ANISOTROPY VECTOR

The cosmic-ray anisotropy, which appeared in the form of a 24-hour variation following the Forbush minimum, remained until about 1600 U. T. on 15 July (that is, it remained for ~ 40 hours).

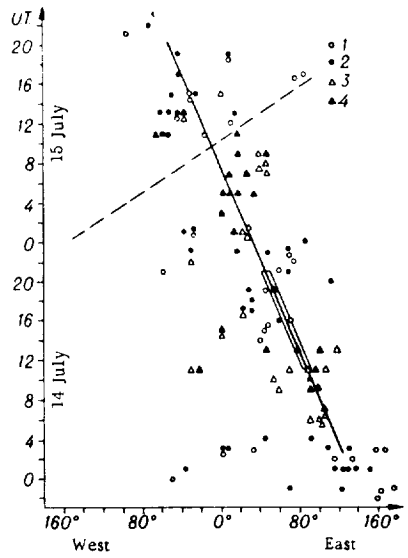

FIGURE 4. Direction of minimum intensity as a function of time, for the meson (1, 3) and neutron (2, 4) components.

1, 2–direction of minimum intensity; 3, 4–direction of maximum intensity, shifted by 180°. Dashed line shows trajectory of receiving direction of instrument.

Figure 4 shows the direction of minimum intensity in the ecliptic plane as a function of universal time, according to the data of 20 stations in the world-wide network. The points corresponding to the moments of maximum have been shifted 180° on the diagram. The geomagnetic drift of the particles was not allowed for, due to the low accuracy of the time estimates (3 to 5 hours). However, it can be roughly taken into account if the scale of the directions is shifted 40° counterclockwise.

It is evident from Figure 4 that the direction of the anisotropy varied in space. During a 40-hour period it changed from ~ 160° E to 0°, that is, the anisotropy vector made a half-turn counter to the diurnal rotation of the earth. It is characteristic that, at the beginning and end of the rotation, the direction of the anisotropy lies close to the E–S line. After dividing the rotation angle by the duration of the rotation, we obtain an angular velocity of the anisotropy of $\omega_A = 4$ degrees/hour.

It is difficult to explain the diurnal variation of 14 to 15 July as a deflection of the particles moving away from the sun by magnetic fields, be they regular /5/ or irregular /6/ fields, since in the given case a gradual 180° variation of the velocity vector would have to be observed. On the

other hand, the sudden Forbush decrease implies that near the earth a considerable gradient of the cosmic-ray density in the presence of the magnetic field may exist at this time, that is, the conditions are suitable for the appearance of anisotropy /7/.

The vector of the anisotropy caused by the cosmic-ray density gradient has the following form /8/:

$$\vec{A}(\varepsilon)=\frac{\rho(\varepsilon)\,[\operatorname{grad} n(\varepsilon)\cdot\vec{H}]}{H\cdot n(\varepsilon)}. \qquad (2)$$

This equation shows that, for a 180° change in A, either the direction of H or grad n must vary. Since particles in a nonuniform magnetic field drift transverse to the field gradient, while the particle intensity in the direction of the drift is constant, the density gradient must be either parallel to or antiparallel to the field gradient. Therefore, rotation of the anisotropy indicates a considerable change either in the direction of the magnetic field in the vicinity of the earth or in the direction of the field gradient.

Such a rapid variation of the magnetic field close to the earth shows that during this period a current system acting as a source of this field apparently passed near the earth. Actually, from 1100 to 2100 U.T. on 14 July, an active period of magnetic storm with a sharp depression of the magnetic field (designated in Figure 4) was observed, indicating passage of the earth through the plasma cloud which carried this current system.

4. THE COSMIC-RAY BURST ON 18 JULY 1961

After the Class-3 solar flare at 0757 U. T. on 17 July, the cosmic-ray intensity dropped again, indicating that the earth entered a new plasma

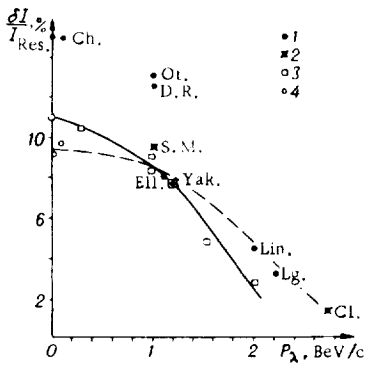

FIGURE 5. Effect of cosmic-ray increase as a function of geomagnetic threshold, for bursts of 18 July 1961 (1, 2, 4) and 12 November 1960 (3).

2–effect at high-mountain stations, reduced to sea level; 1–effect measured after peak of cosmic-ray intensity.

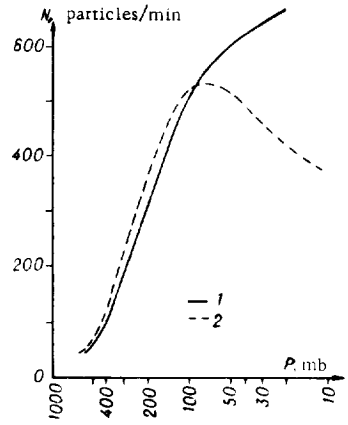

FIGURE 6. Variation of cosmic-ray intensity with altitude over Yakutsk on 19 July 1961 (solid curve).

1–flight on 19 July (0050–0210); 2–average function $I = I(P)$ for 1961.

cloud. The moment of onset of the drop was difficult to specify, due to the masking effects of large intensity fluctuations. During this period, two pulses of sudden-commencement type were observed in the H component (at 1830 on 17 July and at 1020 on 18 July). One of these pulses was probably related to the arrival of the flux causing the cosmic-ray decrease.

By 1000 U. T. on 18 July the intensity at many stations had already reached a minimum, so that the first outburst (at 1830 on 17 July) was apparently associated with the arrival of the corpuscular stream. The velocity of the stream was thus $4 \cdot 10^8$ cm/sec. A solar flare with coordinates 7° S and 60° W, beginning at 0390 on 18 July and reaching a maximum at 1000, was the source of the cosmic rays recorded by the neutron monitors.

In Figure 5 the effect of cosmic-ray increase as a function of the geomagnetic threshold, for the event on 18 July 1961 and the first burst on 12 November 1960, is compared. The effect at high-mountain stations was reduced to sea level, assuming mean free absorption lengths of 140 and 110 g/cm^2 respectively, for galactic and solar radiation /9/.

The data for Ottawa, Deep River, Churchill, and Resolute Bay lie considerably above the data for the other stations in Figure 5. This may be related to the presence of impact zones. Churchill and Resolute Bay had the largest intensity rises. An evaluation was made after the sharp intensity drop, at 1300 U. T. (open circles in Figure 5).

From Figure 5 it is clear that the energy spectrum for the burst on 18 July 1961 is more rigid than the one for the burst on 12 November 1960. The burst on 18 July has a large time scale, indicating a low value of the diffusion coefficient for solar cosmic rays.

Measurements in the stratosphere over Yakutsk at 0100–0200 U. T. on 19 July showed a cosmic-ray increase of $\sim 20\%$ (Figure 6). The presence of this effect in the low-energy part of the spectrum, at a time when the ground-level cosmic-ray intensity had returned to normal, shows that the energy dispersion of the effect was appreciable. Thus, it follows that the diffusion was hindered considerably.

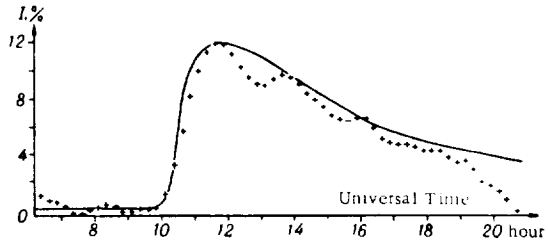

FIGURE 7. Time function of cosmic-ray increase at Deep River on 18 July 1961 (crosses).

The curve shows the variation in cosmic-ray intensity expected for isotropic diffusion.

Figure 7 shows the time variation of the burst at Deep River, smoothed over a 30-minute interval, together with the curve describing the diffusive propagation of particles in a sphere:

$$I(t) = \frac{Q}{(4\pi Dt)^{3/2}} \exp\left(-\frac{R_0^2}{4Dt}\right), \qquad (3)$$

where D is the diffusion coefficient; R_δ is the radius of the earth's orbit; and Q is a factor proportional to the total number of particles emitted by the sun.

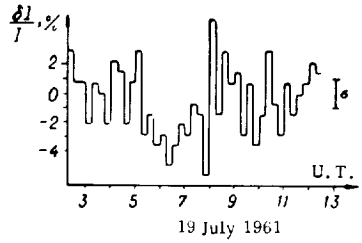

FIGURE 8. Cosmic-ray neutron intensity at Yakutsk on 19 July 1961, during a 15-min interval.

Until 1900 U. T., the time variation of the burst agreed satisfactorily with the curve of equation (3) for $D = 6 \cdot 10^{21}\ \mathrm{cm^2/sec}$. This corresponds to a mean free path of isotropic scattering

$$l = \frac{3D}{c} = \frac{3 \cdot 6 \cdot 10^{21}\ \mathrm{cm^2/sec}}{3 \cdot 10^{10}\ \mathrm{cm/sec}} = 6 \cdot 10^{11}\ \mathrm{cm}. \qquad (4)$$

At 1915 there was a sudden drop in intensity at Deep River (See Figure 7). This was also observed at other stations and proceeded according to local time.

Station	Observed moment	Expected moment
London	1400 U.T.	1400 U.T.
Ellsworth	1730	1750
Deep River	1915	1930
Churchill	2115	2160
Resolute Bay	2200	2330
Yakutsk	0515 (19 July)	0530

The moments of onset of the intensity drop and the drop times to be expected due to the rotation of the earth for 18 July 1961 (adjusted to London Time) are shown in the table. It is clear from these data that the drop was caused by the directional anisotropy which was first observed at 1400 U. T. on 18 July and continued until at least 0500 on 19 July, when an intensity drop was observed in the neutron component at Yakutsk (Figure 8).

An appreciable decrease in cosmic-ray intensity was also observed in the stratosphere over Yakutsk (Figure 9), but it had a somewhat shorter duration. The moments of minimum in the stratosphere and in the neutrons at ground level were identical.

A cosmic-ray burst took place on 20 July, following a flare at the western limb of the sun (90° W). This burst was characterized by a short time scale and low amplitude (Figure 10). The short time scale indicates that the particles reached the earth unhindered. However, since at this time there was still a Forbush decrease, the particles moved along the lines of force. This agrees with Mc Cracken's assumptions, according to

which the force lines of the interplanetary field join the earth to the western limb of the sun. The Churchill station was closer to an impact zone than

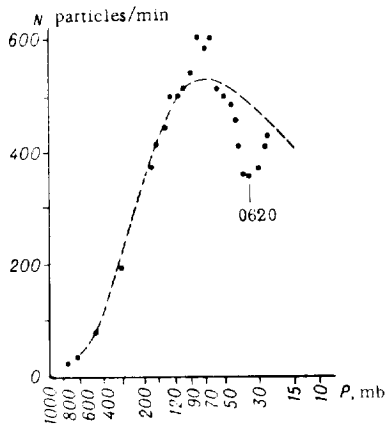

FIGURE 9. Variation of cosmic-ray intensity with altitude over Yakutsk on 19 July 1961 (points). Dashed curve shows average annual variation.

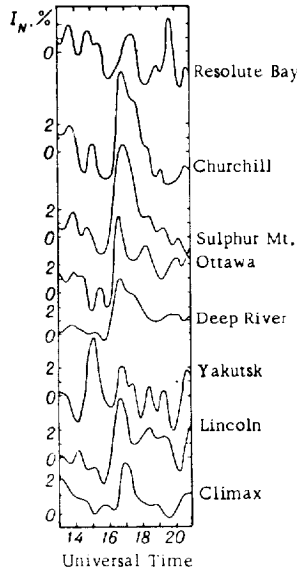

FIGURE 10. Neutron intensity on 20 July 1961, smoothed over a 30-minute interval.

were the other stations, and the largest intensity increase was observed there. At that moment its asymptotic cone was directed toward the sun.

CONCLUSION

Consequently, the active region which traversed the sun's disk between 9 July and 20 July 1961 brought about several interesting phenomena associated with galactic and solar cosmic rays.

1. An analysis of the Forbush effect on 13 July 1961 showed that the amplitude and spectrum of the decrease depend on the direction of arrival of the recorded radiation. The anisotropy of 14 and 15 July varied 180° in its direction during this period, but counter to the diurnal rotation of the earth.

2. The particles of the cosmic-ray burst on 18 July spread via diffusion in an irregular magnetic field. Anisotropy of the arrival of solar particles was observed, the preferred direction being 50–60° west of the earth-sun line. This result agrees with Mc Cracken's findings for several bursts (4 May, 12 November 1960, etc.).

3. The spectrum of the cosmic-ray increase on 18 July was comparatively hard.

4. The cosmic-ray burst on 20 July, following a flare at the western limb of the sun, had a short time scale and pronounced impact zones.

Institute of Space-Physics Research and Aeronomy,
Yakutsk Branch of Siberian Division of
USSR Academy of Sciences

REFERENCES

1. Solnechye dannye, 1961. Byulleten' No. 7.— Moskva-Leningrad. Izd. AN SSSR.
2. FENTON, A.G., K.G. McCRACKEN, D.C. ROSE, and B.G. WILSON. — Can. J. Phys., **37**, 9. 1959.
3. KAMINER, N.S., L.I. DORMAN, and Ya.L. BLOKH.— Sbornik: "Kosmicheskie luchi," No. 4, p.59, Moskva, Izd. AN SSSR. 1961.
4. FEDCHENKO, K.K. Report at Cosmic-Ray Conference in Yerevan. 1961.
5. DORMAN, L.I. Variatsii kosmicheskikh luchei (Cosmic-Ray Variations).— Moskva, Gostekhizdat. 1957.
6. NAGASHIMA, K.— Trudy MKKL, **4**, p. 247, Moskva, Izd. AN SSSR. 1960.
7. ELLIOT, H. Material from Symposium on Geophysical Aspects of Cosmic Rays, Helsinki. 1960.
8. KRYMSKII, G.F.— Trudy YaFSO, AN SSSR, seriya fizicheskaya, No. 5 (in press).
9. KUZ'MIN, A.I., G.V. SHAFER, G.F. KRYMSKII, and Yu.G. SHAFER.— Geomagnetizm i aeronomiya, **1**, 510. 1960.
10. McCRACKEN, K.G.— J. Geoph. Res., **67**, 423. 1962.
11. McCRACKEN, K.G.— J. Geoph. Res., **67**, 447. 1962.

N67-38216

A.I.Kuz'min, G.V. Skripin, S.N. Druzhinin, G.F. Krymskii, and P.A. Krivoshapkin

SOME RESULTS OF AZIMUTHAL MEASUREMENTS OF COSMIC-RAY VARIATIONS AT YAKUTSK

Our basic equipment at Yakutsk for studying azimuthal effects in the cosmic-ray variations is a system of crossed telescopes located both on the earth's surface and at different depths underground /1/. The crossed telescopes are situated in the north-south plane and also in the east-west plane, at 30 and 60° to the zenith.

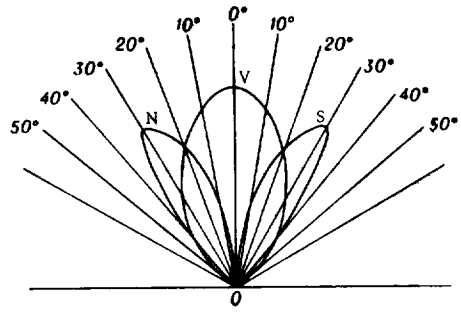

FIGURE 1. Directivity diagrams of crossed telescopes in north-south plane.

Figure 1 is a diagram of the telescopes in the north-south plane. From the diagram it is clear that the meteorological effects must be identical for telescopes located at the same level and having the same angle to the zenith. Therefore, any differences in the variations indicated by the telescopes will have sources which are not atmospheric.

This report will present some results of a statistical analysis of data from azimuthal observations made during the IGY and the IQSY.

The readings of azimuthal instruments during geomagnetic storms are quite interesting. Some storms are accompanied by a characteristic change in the cosmic-ray intensity. For example, during the IGY and IQSY over 40 magnetic storms with marked Forbush effects were observed. The majority of these effects were recorded by our ground-level and underground equipment.

Figure 2 shows the results of a statistical analysis of the moments of onset and minimum for different directions and depths of recording the intensity of the hard cosmic-ray component. The analysis shows that, within the limits of calculational accuracy, the moments of onset and

minimum are independent of the directions and depths of recording the hard-component intensity.

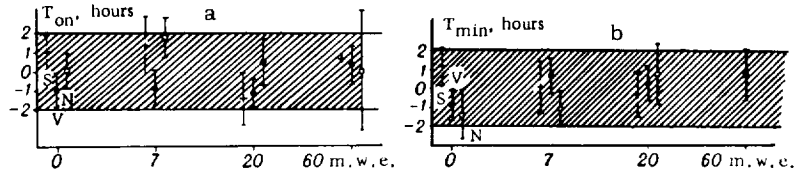

FIGURE 2. Moments of onset (a) and minimum (b) of Forbush effect, for different directions and depths of recording the hard-component intensity.

However, individual instances of a large deviation toward either side are observed. For example, during the magnetic storm of 20 August 1958, detectors facing south at an angle of 30° to the zenith recorded the onset of the intensity decrease about 8 hours earlier than detectors directed north at the same zenith angle. However, during the storm of 14 September 1958, detectors pointing toward the south recorded the onset of the Forbush effect 6 hours later than northward detectors. Such large differences in the moments of onset are observed in 40% of all Forbush decreases. The situation is the same for the moment of minimum intensity and the moment of recovery.

Therefore, in most cases a Forbush decrease will proceed isotropically. However, as the table shows, the amplitude of the main intensity drop recorded by detectors pointing south is greater than for detectors pointing north.

Effect of north-south asymmetry, for intensity at 30° to zenith

Relative no. of cases, %	Type of asymmetry	Recording depth m.w.e. $\frac{2(\delta N_S - \delta N_N)}{\delta N_S + \delta N_N} \cdot 100\%$			
		0	7	20	60
40	$N_S > N_N$	16	20	8	—
7	$N_N > N_S$	12	5	—	—
53	$N_S \approx N_N$	0	0	0	0

Moreover, according to the table, most Forbush decreases take place without any appreciable asymmetry effect. In 40% of the cases, however, there was noticeable asymmetry. In these cases, particles moving in the ecliptic plane were affected more than particles concentrated at large angles to the ecliptic plane. The particles responsible for the asymmetry of the effect had quite high energies ($\varepsilon \leqslant 20$ BeV).

The existence of a direction in which the effect is greater leads to additional diurnal cosmic-ray variations during magnetic storms, with a harder spectrum than on magnetically quiet days. Actually, during some magnetic storms, so-called perturbed diurnal variations are observed.

SOLAR-DAILY VARIATIONS

The first harmonics of the mean diurnal variations for 1958–1959 are shown in Figure 3. These data were obtained for the northern, southern, and vertical directions, using telescopes at ground level and also at 7, 20, and 60 m.w.e. underground. The figure shows that detectors pointing south record larger amplitudes of the mean diurnal variations, and also

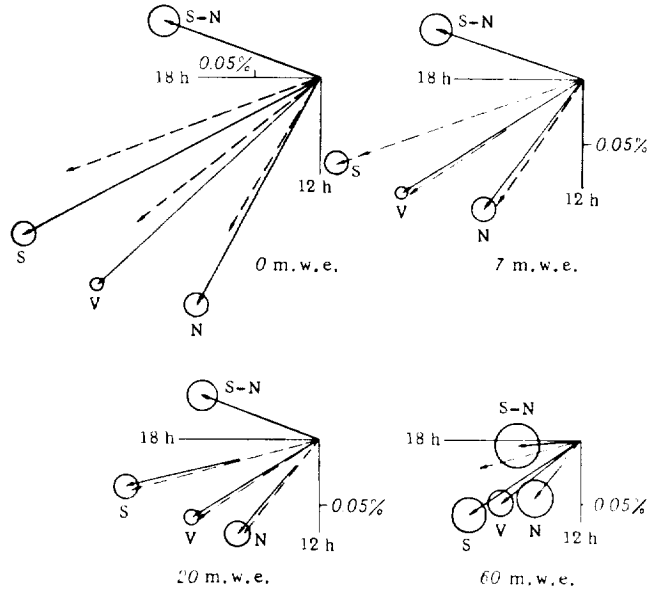

FIGURE 3. First harmonic of diurnal variation for 1958–1959, at ground level and underground.

S, V, and N refer to southern, vertical, and northern orientations respectively. Dashed lines show vectors corrected for pressure; solid lines include corrections for pressure and temperature of entire atmosphere.

later maxima, than detectors pointing north or oriented vertically. The greatest differences are between detectors pointing north and detectors pointing south. At all recording levels a detector oriented vertically indicates intermediate values of both amplitude and moment of maximum. The difference in moments of maximum of the diurnal variations for the directional intensity agrees with that predicted assuming an external source of the variations.

According to the diagrams of Dattner and Brunberg /2/, a recorder pointing south at the latitude of Yakutsk receives radiation, irrespective of the energies of the primaries, at approximately a single direction from the ecliptic plane ($\approx 22°$). Consequently, from the readings of telescopes directed southward and placed at different depths underground, the energy spectrum of the mean variations can be determined. Calculations /3/ show that this spectrum has the following form:

$$\frac{\delta D(\varepsilon)}{D(\varepsilon)} = \begin{cases} 0.16\varepsilon^{-1}, & \text{if } \varepsilon > 13 \text{ BeV}; \\ 0, & \text{if } \varepsilon < 13 \text{ BeV}. \end{cases}$$

This spectrum agrees well with the spectrum found in /4/ from the readings of vertical telescopes, taking into account a change in source intensity. The readings of the entire detector array conform to a source located 83 ± 4° to the left of the earth-sun line /3/.

The data from the entire detector array were used to determine the intensity distribution for the source of the diurnal variations. However, in /3/ the effect of diurnal fluctuations in the temperature of the upper atmosphere was not taken into consideration, and (as was shown in /5/) these fluctuations may be considerable. Moreover, it was demonstrated in /6/ that the predicted diurnal variations due to temperature fluctuations of the atmosphere up to 50 mb were 1.5 to 2 times too high, because the radiation errors were not computed correctly. We used the data of /5, 6/ and calculated the average expected diurnal variations for 2 years due to the temperature variation of the entire atmosphere. The variations obtained were 0.06; 0.01; 0.004; and 0.03%, with maxima at 2.0; 6; 6; and 1 hours local time, for instruments at ground level and at underground depths of 7, 20, and 60 m.w.e., respectively. The diurnal variations, corrected for temperature using the above values, are shown in Figure 3.

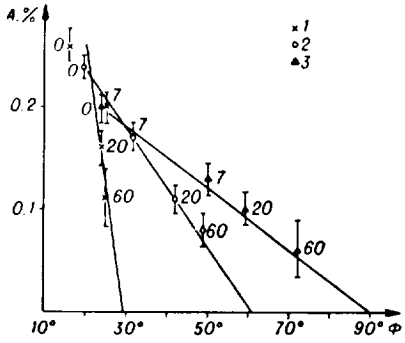

FIGURE 4. Amplitude of solar-daily variation, as a function of drift angle, for different recording directions (numbers at points show recording levels in m.w.e.).

1-south; 2-vertical; 3-north.

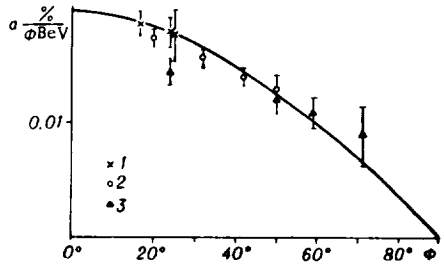

FIGURE 5. Intensity distribution for source of solar-daily variation, in a plane perpendicular to the ecliptic plane.

1-south; 2-vertical; 3-north.

Figure 4 is a diagram of the amplitude of the diurnal variation as a function of the drift angle; here, the variation is corrected for the pressure and temperatures of the whole atmosphere. The readings of southward, vertical, and northward telescopes, respectively, lie along three lines.

The angles of intersection of these lines with the abscissa axis correspond to the angles of inclination of the southward, vertical, and northward telescopes, relative to the terrestrial equator. The vertical telescope indicates the latitude of Yakutsk. Such a dependence of amplitude on latitude is to be expected. Actually, high-energy particles must enter a given telescope from the direction of telescope orientation. Before the diurnal variations were corrected for temperature changes in the upper atmospheric layers (above 50 mb), however, the picture was different: the points were greatly scattered, and it was difficult to draw a straight line or smooth curve through them.

All this attests to the necessity for temperature corrections taking into account temperature fluctuations in the upper atmosphere above 50 mb. Consequently, it is reasonable to recalculate the spectrum of the diurnal variations in the light of these corrections. Using the method of /3/ and the data (shown in Figure 3), corrected for the entire temperature range, we obtained the following energy spectrum of the solar-daily variations: $\frac{\delta D(\varepsilon)}{D(\varepsilon)} = 0.02\,\varepsilon^{-0.5\pm0.3}$ for energies above 8 ± 2 BeV; and $\frac{\delta D(\varepsilon)}{D(\varepsilon)} = 0$ for energies below 8 ± 2 BeV.

This spectrum agrees with the one obtained recently from a study of the latitude-longitude dependence of the diurnal variations of the neutron intensity /7/. On the basis of this spectrum and the data of /3/, we calculated the distribution of the source strength in a plane perpendicular to the ecliptic plane (Figure 5). The figure shows that the source strength is described by the formula $a_\varphi = 0.02 \cos \varphi$. Thus, the mean diurnal variations for 1958–1959 were caused by a single source, located in the plane of the ecliptic and having an intensity which drops with an increase in φ (it decreases as $\cos \varphi$). On the average, particles with energies > 8 BeV are subject to these variations, and the variation amplitude drops with the energy $\left(\frac{\delta D(\varepsilon)}{D(\varepsilon)} \sim \frac{1}{\varepsilon^{0.5}}\right)$.

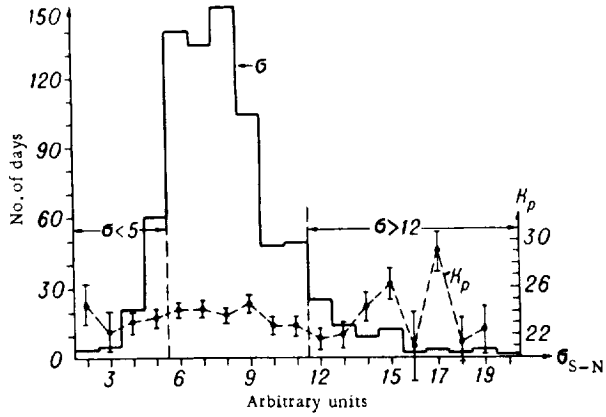

FIGURE 6. Distribution of days with different σ, over a three-year period; also mean values of K_p index corresponding to these days. Vertical dashed lines separate days chosen for study.

However, if the variations on separate days are considered /8/, we see from Figure 6 that there are many days when the north-south difference in the variations is small, and quite a few days when the north-south difference is large. Obviously, days with low σ ($\leqslant 5$)* could have occurred in cases when two sources were responsible for the outer component of the diurnal variations or when the outer component was small.

Days with large σ ($\geqslant 12$), on the other hand, indicate cases when the extraterrestrial variations depend considerably on the direction of recording the radiation and when the angular dimensions of the source are

* [σ is an index indicating the dependence of the diurnal variations on direction.]

limited. Consequently, these distributions can be used to study the properties of the sources of diurnal variations.

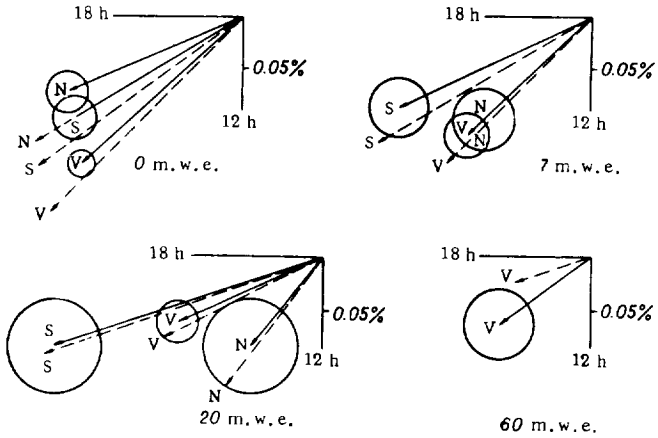

FIGURE 7. First harmonic of mean solar-daily variation of meson component, for the group of days with $\sigma \leqslant 5$, at the earth's surface and underground.

Solid vectors are corrected for pressure and temperature of entire atmosphere; dashed vectors are corrected for pressure and temperature up to the 50-mb level.

In order to evaluate the relation between diurnal variations of the types indicated above and the geomagnetic activity, we compared the geomagnetic-activity indexes in the different groups. It was found that the geomagnetic activity does not change appreciably from days with low $\sigma(\leqslant 5)$ to days with large $\sigma(\geqslant 12)$.

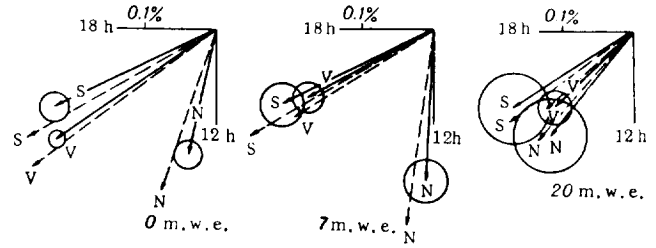

FIGURE 8. First harmonic of mean solar-daily variation of meson component for the group of days with $\sigma \geqslant 12$ (solid and dashed vectors same as in Figure 7).

The mean diurnal variations on days with low σ (80 days) are plotted in Figure 7. It is clear that on these days the variations at ground level in the southern and northern directions are actually identical and coincide with the variations in the direction of the zenith. At the same time, for days with a large index σ of the north-south difference (80 days), Figure 8 shows that the variations in the northern and southern directions, at all recording depths, differ considerably from one another. The amplitude of the variations is appreciably larger for all depths and directions, both in comparison to the mean and in comparison to days with low σ. For $\sigma \leqslant 5$,

the characteristics of the diurnal variations in the zenith and southern directions coincide with the mean, while the vector of the variations in the northward direction has a considerably larger amplitude and is shifted toward a later time until it coincides with the southward vector.

At a depth of 7 m. w. e. such a change in the northern vector is also observed, but to a lesser degree. At a depth of 20 m. w. e. no change is observed.

A study of days with large σ (see Figure 8) indicates that at the earth's surface and at a depth of 7 m. w. e. the northern vector shifts toward earlier times in comparison with the mean, while the southern and vertical vectors do not shift much, just as in the case of days with low σ.

The asymmetry of the transformation of the diurnal variation implies that this transformation is not a result of random causes. The cause of the shift in the northward diurnal variation is limited at low energies ($\leqslant 20$ BeV). The observed difference of the variations during different groups of days is probably not related to a change in the dimensions and spectrum of a single source. Rather, it requires the presence of a high-latitude source with varying properties.

DIURNAL VARIATIONS DURING A PERIOD OF MAGNETIC DISTURBANCE

Figure 9 shows the diurnal-variation parameters for the intensities of the various cosmic-ray components, during days of world-wide quiescence and during magnetic disturbances. The period covered is from March 1958 to February 1960.

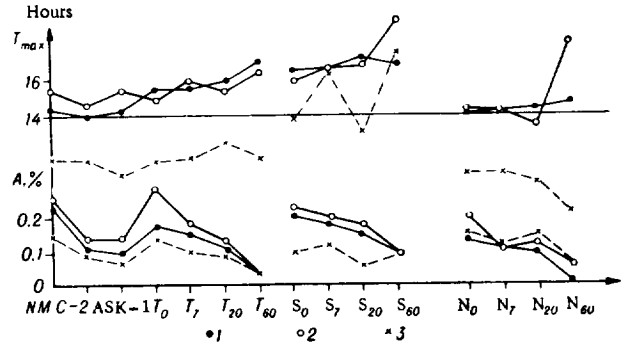

FIGURE 9. Amplitude and phase diagrams for diurnal variations of various cosmic-ray components.

ASK-1, C-2 pertain to ionization-chamber readings; NM pertains to neutron-monitor readings; T_0, T_7, T_{20}, T_{60}, S_0, S_7, S_{20}, S_{60}, N_0, N_7, N_{20} N_{60} denote data of counter telescopes recording meson intensity from the vertical (T), from the south (S), and from the north (N), at the earth's surface and at 7, 20, and 60 m. w. e. underground, respectively; 1–for a two-year period; 2–for quiet days; 3–for disturbed days.

Here, for each group the data for five days in each month were selected according to a list supplied by the International Association of Geomagnetism and Aeronomy.

A study of the results in Figure 9 indicates the following properties. On disturbed days the diurnal variations exhibit earlier maxima for all directions and levels of recording, in comparison with quiet days and with the annual mean. The amplitude of the first harmonic on a disturbed day is 1/1.3 to 1/2 as great for all vertical and southward telescopes. For northward telescopes, however, no amplitude decrease is observed on these days. On disturbed days, as well as on quiet days, telescopes pointing northward have earlier maxima than southward telescopes. This confirms the previously established shift toward an earlier time of the diurnal-variation peak on disturbed days. However, at first glance, the behavior of the diurnal-variation amplitude contradicts the results of this analysis /9/. This can be explained by the fact that on quiet days the diurnal variations were stable compared to days of world-wide disturbance. In other words, the perturbation of the diurnal variations increases with an increase in the disturbance of the geomagnetic field.

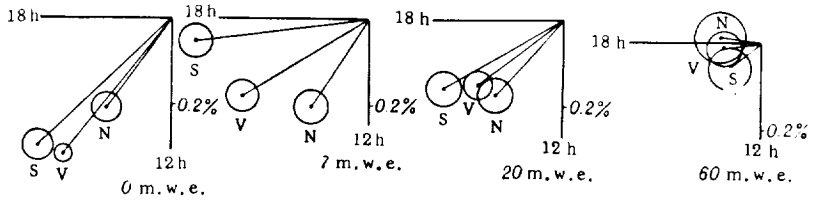

FIGURE 10. First harmonic of solar-daily variation, after main Forbush phase.

S, V, N refer to south, vertical, and north, respectively; solid vectors are corrected for pressure and temperature.

Figure 10 gives the results of a harmonic analysis of the diurnal variations following the main Forbush phase, according to the readings of directional telescopes at ground level and at 20 and 60 m. w. e. underground. The figure shows that detectors pointing south record variations with amplitudes about 1.5 to 2 times greater than those recorded by northward detectors. All the telescopes at the earth's surface recorded variation maxima at the same time. However, the differences in the moments of maximum noted previously for these directions remained for detectors located underground.

A shift to an earlier time of maximum relative to the average is observed for a southward telescope located at the earth's surface, whereas for a northward instrument the opposite is observed. Therefore, detectors located at the earth's surface in north-south directions have the same time of maximum. Consequently, during magnetic storms accompanied by a Forbush effect, effects of a phase shift in the diurnal variations for the southward and northward directions are observed only for instruments at the earth's surface. If this effect is the same as that discovered by Sarabhai /10/, then this implies that the particles responsible for the phase shift do not have very high energies, and that the spectrum of the variations must be considerably softer or else cut off at the top.

It should also be noted that the rotation of the diurnal variations discovered in certain studies /11/ is indicated by azimuthal detectors both on the earth's surface and underground. The properties of the rotation of the diurnal-variation source are difficult to explain by the theory of diurnal variations suggested by Dorman.

COSMIC-RAY BURSTS

In 1956 through 1960, azimuthal instruments recorded several cosmic-ray bursts. For example, a very pronounced effect was observed on 23 February 1956. On this date (see Figure 11), a telescope pointing southward recorded a very high amplitude (200%), while a northward telescope indicated only a rise in intensity of 170%. Such a difference in the effects cannot be attributed to a difference in the screening ($< 10\ g/cm^2$); rather, it is a result of anisotropy of the flux in the north-south plane. Such an anisotropy can be distinguished until the half-way mark of the effect. The two telescopes receive radiation with an energy < 10 BeV from practically the same region near the equator, if the dipole model of the geomagnetic field is used. Therefore, if different effects are observed with detectors pointed in different directions, it must be assumed that a dipole field is not a satisfactory approximation to the actual terrestrial field. The difference of the effects in the northern and southern directions also implies that the angular dimensions of the source are not very large.

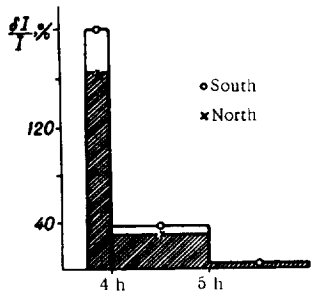

FIGURE 11. The burst on 23 February 1956.

The burst of 22 January 1957 had an amplitude of about 20% according to both northward and southward telescopes, there being no directional difference in amplitude.

The burst of 4 May 1960 had a low amplitude and short duration at Yakutsk. At the moment of the burst, a small intensity rise was observed in the southward direction, whereas toward the north no appreciable effect beyond the limits of measurement error was detected. This effect does not agree with a dipole model of the geomagnetic field, either.

Institute of Space-Physics Research and Aeronomy,
Yakutsk Branch of Siberian Division of
USSR Academy of Sciences

REFERENCES

1. KUZ'MIN, A.I. and A.V. YARYGIN.— Trudy YaFSO, AN SSSR, seriya fizicheskaya, No. 2, 36. 1958.
2. DORMAN, L.I. Variatsii kosmicheskikh luchei (Cosmic-Ray Variations).— Moskva, Gostekhizdat. 1957.
3. SKRIPIN, G.V.— Sbornik: "Kosmicheskie luchi," No.4, p.229, Izd. AN SSSR. 1961.
4. KUZ'MIN, A.I.— Trudy YaFSO, AN SSSR, seriya fizicheskaya, No. 3. 1960.
5. KUZ'MIN, A.I., P.A.KRIVOSHAPKIN, G.F.KRYMSKII, and G.V.SKRIPIN.— Pervoe Vsesoyuznoe soveshchanie po kosmofizike (in press).
6. SKRIPIN, G.V.— Trudy YaFSO, AN SSSR, seriya fizicheskaya, No. 5.
7. DUGGAL, S.P., K. NAGASHIMA, and M.A. POMERANTZ.— J. Geophys. Res., **66**, 1970. 1961.
8. KUZ'MIN, A.I., G.F.KRYMSKII, and G.V.SKRIPIN.— Trudy YaFSO, AN SSSR, seriya fizicheskaya, No. 5.
9. SEKIDO, Y. and S. YOSHIDA.— Rep. Ionosphere Sp. Res. Japan, 4, 37. 1950.
10. RAO, U.R. and V. SARABHAI.— Proc. Roy. Soc., A **263**, 101. 1961.
11. KUZ'MIN, A.I., G.F. KRYMSKII, and G.V. SKRIPIN.— Geomagnetizm i aeronomiya, 1962 (in press).

L.I. Dorman and O.I. Inozemtseva

*A LOCAL SOURCE OF THE DIURNAL COSMIC-RAY VARIATION DURING MAGNETIC STORMS (Synopsis)**

The anomalous diurnal variation during the main phase of an effective magnetic storm was investigated using the directional properties of crossed telescopes. Continuous recordings at Moscow (at sea level) and at Yakutsk (at sea level and at depths of 7, 20, and 60 m. w. e.) provided data on the hard-component intensity in the northward and southward directions.

In the given case a distant source of anisotropy was assumed to exist, which was related to the influence on cosmic rays of the electromagnetic field of the solar corpuscular flux. In addition, a local source, formed as a result of the direct influence of the asymmetrically distorted geomagnetic field on the cosmic rays, apparently acted as well /1/.

This assumption was checked in detail using the data of crossed telescopes at the Capetown station and the data from 40 neutron monitors of the world-wide system of stations. The period chosen for study was the main phase of the magnetic storm on 11 February 1958, when the anomalous effect of the diurnal variation was a maximum compared to the other cases considered and was several times greater than the errors due to statistical fluctuations.

The effect to be expected was evaluated quantitatively using theoretical calculations of the rise in cosmic-ray intensity caused by a distorted geomagnetic field and also using experimental data on the actual variations of the geomagnetic field during this period. The results were then compared with the data of the experiment. It was concluded that there were at least two distinct sources of the anomalous diurnal variation. One, the remote source, acted beyond the sphere of the geomagnetic field. The other, the local source, influenced the cosmic rays within the sphere of the geomagnetic field. The two sources acted in the same direction, giving a maximum effect during the daytime /2, 3/.

REFERENCES

1. DORMAN, L.I. and O.I.INOZEMTSEVA.— Sbornik: "Kosmicheskie luchi," Seriya "Rezul'taty MGG," Part 7, No.4. 1961.

2. DORMAN, L.I. and O.I.INOZEMTSEVA.— Geomagnetizm i aeronomiya, 2, No.3. 1962.

3. DORMAN, L.I. and O.I.INOZEMTSEVA.— Sbornik: "Kosmicheskie luchi," No.5, Izd. AN SSSR, 1962.

* For the complete report, see /1–3/.

N67 30217

G. V. Skripin, G. F. Krymskii, and L. P. Boltrushko

THE CONTRIBUTION OF SOLAR PARTICLES TO THE DIURNAL VARIATION OF THE NEUTRON INTENSITY

Studies of the contribution of cosmic rays from small solar flares to the intensity of the neutron component /1-9/ have given contradictory results. The authors of /1-6/ concluded that solar particles contribute appreciably to this intensity, while in /7-10/ it was decided that the contribution is insignificant.

Since flares occur quite frequently, an intensity rise at the time of a flare should distort the diurnal variation on individual days. Moreover, if solar cosmic rays reach the earth in a sharply anisotropic flux, a distortion of the average diurnal variations, caused by the additional diurnal variation of the solar particles, should also be observed.

The goal of this report is to evaluate the contribution of solar particles both to the diurnal variations on individual days and to the average variation. The data, corrected for the barometric effect, from neutron monitors at three stations were used (Yakutsk, Resolute Bay, and Sulphur Mountain), covering a period from July 1957 to 1960.

In order to obtain the pure flare effect, we subtracted the average monthly value of the bihourly diurnal intensity variation from the data for a flare day. The analysis was made using the method of superposition of epochs. Zero time was the moment of observation of a flare. The values during the six hours preceding a flare and the sixteen hours after a flare were recorded, to the left and to the right of zero time, respectively. Data on chromospheric flares and radio bursts were taken from the collection "Solnechnye dannye," which provided material from observations of the observatory network of the USSR. These data pertained to universal times from 1 to 17 hours. The material was divided into five groups, depending on when the flare occurred: 0-6 h U. T. formed the first group; 6-8 h, the second; 8-10 h, the third; 10-12 h, the fourth; and 12-18 h, the fifth. Data for flares in the eastern and western parts of the solar disk were processed separately.

Figure 1a shows a Chree analysis for the readings of the neutron monitor at Sulphur Mountain. As zero epochs were chosen intervals containing flares with intensities > 2. In selecting the flares to be studied, periods of irregular cosmic-ray variations were excluded. The total number of flares chosen was 238. The intensity was corrected for the diurnal variation on the basis of the average monthly diurnal changes.

As Figure 1 shows, there is no appreciable effect immediately after a flare in any group, for flares in both the western and eastern hemispheres. Thus, flare effects are absent, irrespective of the local time and the

heliographic longitude. The same conclusion follows from Figure 2, which shows the average effect over all groups, including the 238 flares observed at Sulphur Mountain.

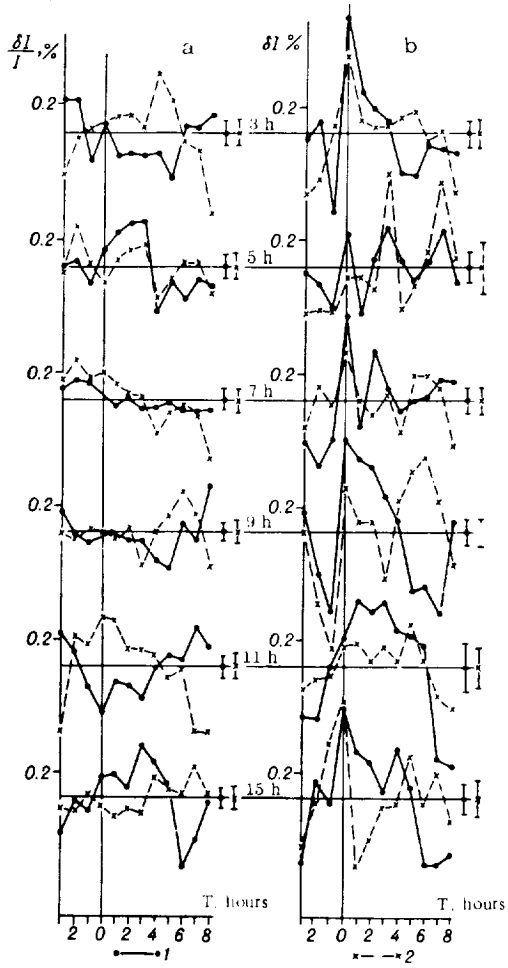

FIGURE 1. Neutron intensity at Sulphur Mountain at the time of solar flares. On the abscissa are shown the bihourly intervals from the zero epoch, the bihourly statistical errors, and the universal time of the zero epoch:

a–for all 238 flares; b–for 69 effective flares; 1–west; 2–east.

Some solar flares are accompanied by intense, prolonged ($\geqslant$20 minutes) radio emission at high frequencies (Type-IV radio burst), associated with the magnetic bremsstrahlung of relativistic electrons in the vicinity of the flare. It is more likely for such flares to emit cosmic rays than for other flares to do so.

From the entire 238 flares, 115 flares with radio emission were selected, and according to their moments an analysis similar to the one described above was carried out. The results of the analysis for Yakutsk and

Resolute Bay, after removing the first harmonic of the average variation, are portrayed in Figure 3 (according to groups) and Figure 2 (average). Here, it is also difficult to note any effect of an intensity rise during the zero and first epochs.

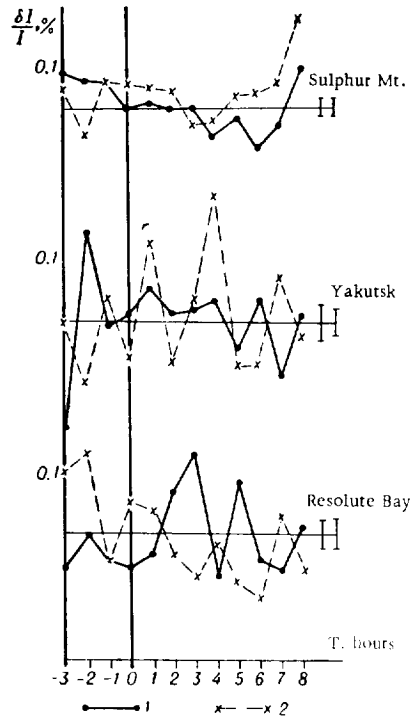

FIGURE 2. Average solar-flare effect on neutron intensity, at Sulphur Mountain, Yakutsk, and Resolute Bay.

1—west; 2—east.

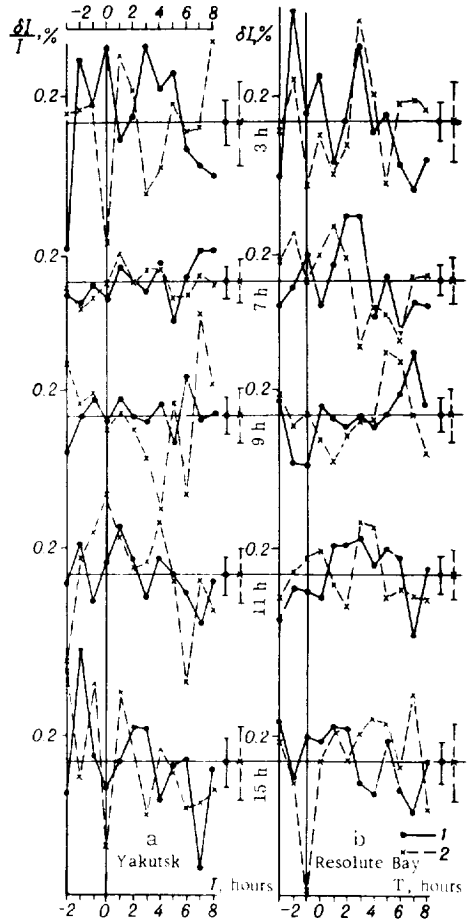

FIGURE 3. Neutron intensity at Yakutsk and Resolute Bay, at the time of solar flares accompanied by radio bursts, for the different groups (Universal Time).

1—west; 2—east.

If the solar particles do contribute, but the contribution does not show up over a short interval, there may still be an effect on the diurnal variation. In such a case, there should be a change in the amplitude and time of maximum of the first harmonic of the diurnal variation, in comparison with the corresponding average characteristics.

The table lists the first-harmonic parameters of the diurnal variations obtained after vector subtraction of the average biennial diurnal-variation vectors from the diurnal wave for flare days.

It is clear from the table that for western and eastern flares the data of each station show considerable residual diurnal variations for the individual groups. The average variations obtained from all the flare data have considerably lower amplitudes. They constitute 20% of the average diurnal variation of the station for Sulphur Mountain and Yakutsk and 70% of the average variation for Resolute Bay.

First-harmonic parameters of residual diurnal variation on days with solar flares, for three stations

Station	Group	Moment of flare		Western region of sun				Eastern region of sun			
		U.T.	L.T.	no.of flares	amplitude	τ_{mU}	τ_{mL}	no.of flares	amplitude	τ_{mU}	τ_{mL}
Yakutsk	1	3	12	11	0.34	8	17	3	0.15	17	2
	2	9	16	20	0.05	20	05	19	0.08	14	23
	3	7	18	16	0.04	14	23	17	0.36	3	12
	4	11	20	15	0.14	13	22	15	0.33	13	22
	5	15	0	11	0.21	14	23	11	0.34	13	22
	Average	9	18	74	0.04	10	19	40	0.02	17	2
Resolute Bay	1	3	21	12	0.27	5	23	3	0.16	14	8
	2	7	1	20	0.25	10	4	18	0.33	11	5
	3	9	3	17	0.17	21	15	8	0.23	21	15
	4	11	5	15	0.20	17	11	8	0.13	15	9
	5	15	9	11	0.17	14	8	3	0.38	4	22
	Average	9	3	75	0.12	13	7	40	0.09	6	0
Sulphur Mt.	1	3	19	14	0.20	20	12	13	0.36	8	0
	2	5	21	13	0.20	9	1	12	0.09	10	2
	3	7	23	28	0.13	10	2	28	0.19	9	1
	4	9	1	34	0.14	2	18	26	0.09	23	15
	5	11	3	22	0.24	2	18	14	0.14	10	2
	6	15	7	21	0.28	19	11	13	0.11	5	21
	Average	9	1	132	0.06	5	21	106	0.04	1	17

Let us now ascertain whether the diurnal variations listed in the table are related to the solar flares or whether they have other causes. If the solar-flare effect on cosmic rays is isotropic, then it must occur according to universal time. However, the table shows that there is no single universal time of maximum (T_{mU}) at the three stations, for either the average residual diurnal variations or the group variations.

On the other hand, if the flare effect in the diurnal cosmic-ray variation is anisotropic, then this effect must be observed at the earth in specific "impact zones" and must proceed according to the local time. In order to analyze this assumption, we used the data of the table and selected flares for which the moment of onset in local time was the same for each station. Then, we compared the corresponding local times of maximum (T_{mL}) of the residual diurnal variation at each of the three stations.

This comparison gave a negative result: actually, T_{mL} for the fourth group at Yakutsk, the first group at Resolute Bay, and the second group at Sulphur Mountain were respectively 22, 23, and 1 for western flares and 22, 8, and 2 for eastern flares.

Thus, relative to these three stations, solar flares took place at 20 hours local time, whereas the flare effect in the diurnal cosmic-ray variation at the earth did not proceed according to local time. The case was just the same for other impact zones. Hence we can conclude that solar particles

at the time of small chromospheric flares do not affect the diurnal variations of the neutron intensity.

The foregoing results agree with the conclusions in /7-10/ and contradict those in /1-6/. Let us now determine the reasons for the disagreement between these studies.

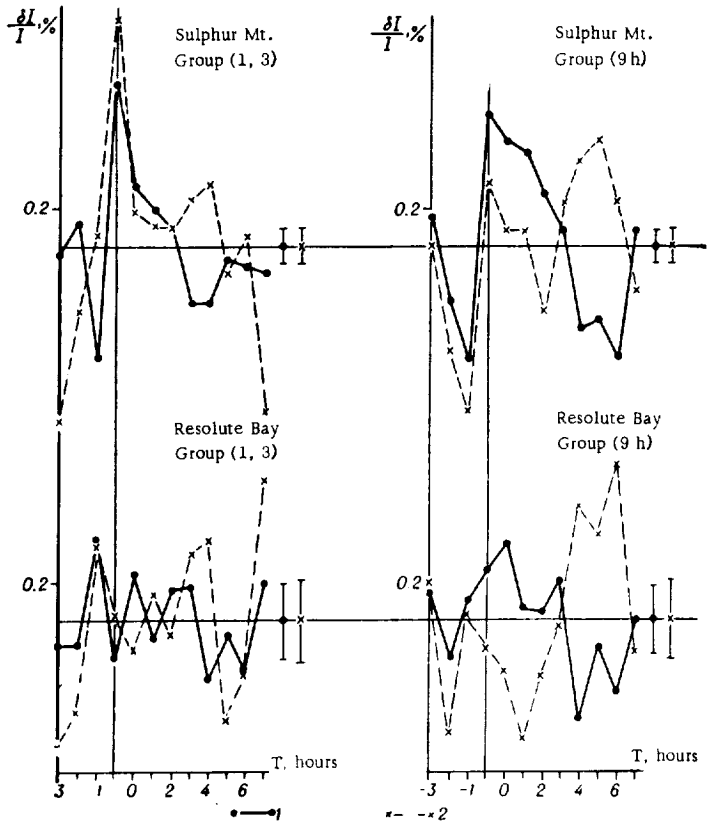

FIGURE 4. Neutron intensity at Sulphur Mountain and Resolute Bay, at the time of flares showing effects at Sulphur Mountain, for two time groups.

1-west; 2-east.

One reason may be the difference in methods of removing the diurnal variations from the solar-flare effect. In /4, 5, 6/ the diurnal variation was eliminated for a given flare day by subtracting the sum of the first and second harmonics of the diurnal variations of the preceding day. This method does not give a completely true representation of the actual variation which must be eliminated, since the electromagnetic conditions determining the nature of the diurnal variation vary considerably from day to day. The monthly average or the yearly average of the diurnal variation, on the other hand, is more likely to represent the main part of the variation present on each individually selected day.

Another reason may be that, as E. V. Kolomeets has pointed out orally, the selection of solar flares in /7–10/ was not so careful, whereas in /3, 4, 5/ only flares which had been recorded at many observatories were used. To check this assumption, for the station at Sulphur Mountain we selected from the entire 238 flares only 69 which were definitely accompanied by an increase in cosmic-ray intensity at the zero epoch. The results for the six flare groups defined previously are shown in Figure 1. The question is whether these selected flares had effects at the other stations. Figure 4 shows the intensities at Resolute Bay and Sulphur Mountain for two of the groups. A comparison of these figures indicates that flares which had a definite effect at Sulphur Mountain did not affect the instruments at the other station. Consequently, the flares selected by us did not have a world-wide effect on the cosmic radiation. At the same time, the existence of the flare effect in each of the six time groups implies that these flares were isotropic. All these results confirm still more the correctness of our previous conclusion that small flares do not affect the cosmic-ray intensity.

Institute of Space-Physics Research and Aeronomy,
Yakutsk Branch of Siberian Division of
USSR Academy of Sciences

REFERENCES

1. FIROR, J.— Phys. Rev., **94**, 1017. 1954.

2. DOLBEAR, D., H. ELLIOT, and D. DANTON.— J. Atm. Terr. Phys., **1**, 187. 1951.

3. KOLOMEETS, E.V.— ZhETF, **36**, 1351. 1959.

4. KOLOMEETS, E.V. and G. SERGEEVA.— Sbornik: "Kosmicheskie luchi," No.4, 132. 1961.

5. DORMAN, L.I. and E.V.KOLOMEETS.— Geomagnetizm i aeronomiya, **5**, 653. 1961.

6. DORMAN, L.I. and E.V.KOLOMEETS.— Geomagnetizm i aeronomiya, **5**, 830. 1961.

7. KUZ'MIN, A.I.— Trudy YaFSO, AN SSSR, seriya fizicheskaya, No.4. 1962.

8. TOWLE, L.C., and J.A. LOCKWOOD.— Phys. Rev. Letters, No.2, 641. 1959.

9. GHIELMETTI, H., J.C. ANDERSON, J.M.CARDOSO, J.R.MANZANO, J.G.ROEDERER, and O.R.SANTOCHI. — Nuovo Cimento, **15**, 87. 1960.

10. ANDERSON, J.C., R.L. CHASSON, and K. MAEDA.— J. Phys. Soc. Japan, **17**, Suppl. A-II, 263. 1962.

N67-38218

N.N. Efimov, M.M. Atakova, T.A. Egorov, D.D. Krasil'nikov, S.V. Maksimov, M.A. Nifontov, and F.K. Shamsutdinova

THE EAS FREQUENCY DURING PERIODS OF VARIOUS EFFECTS IN THE INTENSITY OF INTERMEDIATE-ENERGY COSMIC RAYS

1. The 27-day variations in the intensity of extensive air showers were studied, in relation to the existence of a 27-day recurrence period for atmospheric conditions.

Two methods were used to record the showers. The first entailed threefold coincidences between three counter groups 1 m^2 in area, separated 3.7 meters from one another; this is denoted as C (3; 1.0). The second method involved sixfold coincidences between these counter groups, but separated from one another by 57 meters; this is denoted as C (6; 1.0). Here, the choice of the two different separations is important: in the first case the geometric effect is negative and in the second case it is positive /1/.

The average number of showers recorded by the threefold-coincidence arrangement was $1.5 \cdot 10^4$, and for the sixfold arrangement it was $1.2 \cdot 10^5$. The threefold coincidences of $4 \cdot 10^7$ showers and the sixfold coincidences of $4.8 \cdot 10^6$ showers were processed.

The threefold coincidences were obtained at four points located at the corners of a square. The sixfold coincidences, on the other hand, were obtained on all sides of a square. First, all these recording events were considered separately, and then the average values for all the threefold coincidences and all the sixfold coincidences were computed. The error at each point was determined as the error in the average for the four combinations. Figure 1 shows: the observed 27-day variation of EAS intensity; the variation of the ground-level pressure (h_0); the variation of the height of the isobaric level $h_0 - 100$ mb (H_{h_0-100}); the temperature variation of the layers with 50 and 500 mb pressure; and the variation of EAS intensity corrected for pressure and for the height of the lower atmospheric layers (represented satisfactorily by the height H_{h-100}, so that the correction for this height was used).

The following coefficients were used in the introduction of the corrections /1, 2/:

	α_p	α_h
C(3; 1.0)	— 0.75% per mb	— 0.06% per m
C(6; 1.0)	— 0.91% per mb	— 0.013% per m.

The figure shows that, after the corrections are introduced, the 27-day variation remains, and that it is opposite for the two coincidence arrangements. This opposite variation can be explained as a residual geometric effect.

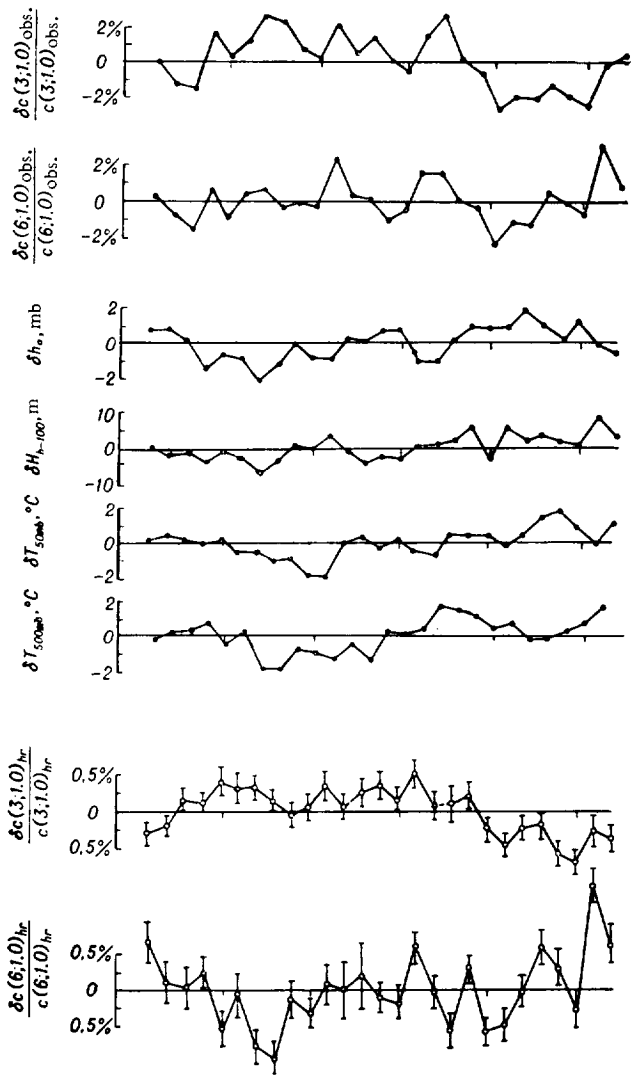

FIGURE 1. 27-day variations of: EAS intensity, recorded for two different counter separations; ground-level pressure (h_0); height of $h_0 - 100$ mb isobaric level (H_{h-100}); and temperatures of 50-mb and 500-mb isobaric levels.

The question also arises as to whether this opposite variation does not indicate a barometric correction for $C(3;\ 1.0)$ which is too low and one for $C(6;\ 1.0)$ which is too high. However, other cases, in which the data were selected according to the times of maximum and minimum temperature in the 50-mb layer, indicate that for the same dependence between the EAS frequency and t_{50mb} the pressure varies differently (Figure 2).

It is evident from Figure 2 that in the cases indicated the variation of the height H_{h-100} has a direct correlation with $C(3;\ 1.0)_{hg}$ and an inverse

correlation with $C\,(6;\ 1.0)_{hg}$. Moreover, for the 27-day variations, in order to remove completely the remaining geometric effect, it would be necessary to use height coefficients which are higher by a factor of 1.3 for the three-fold coincidence and higher by a factor of 5 for the sixfold coincidence, in comparison to the normal height coefficients.

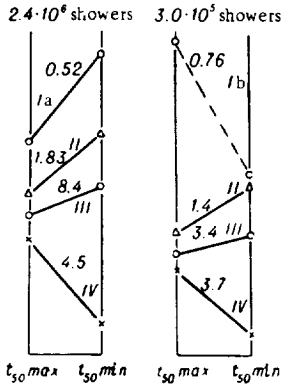

FIGURE 2. Variations in EAS intensity, h_0, and $H_{h\text{-}100}$, for the times of maximum and minimum temperature (t_{50}) in the 50-mb level.

Ia – $\frac{\delta C\,(3;\ 1.0)_{hg}}{C\,(3;\ 1.0)_{hg}}$, %; Ib – $\frac{\delta C\,(6;\ 1.0)_{hg}}{C\,(6;\ 1.0)_{hg}}$, %;

II – δh_0, mb; III – $\delta H_{h\text{-}100}$, m; IV – δt_{50} mb, °C.

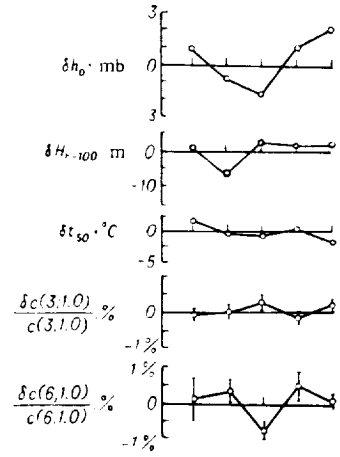

FIGURE 3. EAS intensity, h_0, $H_{h\text{-}100}$, and t_{50}, during a Forbush decrease in the intensity of the neutron cosmic-ray component.

Hence, this residual geometric effect cannot be an effect of the lower atmospheric layers.

It should be noted that, just as in Figure 1, in Figure 2 there is an inverse correlation between T_{50mb} and $C\,(3;\ 1.0)_{hg}$ and a direct correlation between $T_{50\,mb}$ and $C\ \ (6;\ 1.0)_{hg}$.

These results imply that the observed shape of the lateral-distribution function is produced not only over the last t units [cascade units] of the EAS path (as customarily assumed at present) but also over much higher layers of the atmosphere. More detailed studies of this subject will be made later.

2. Similar recordings were made during Forbush decreases of the cosmic-ray intensity. Each Forbush effect on the neutron intensity at Yakutsk was divided into five periods: preonset, decrease, minimum, recovery, and postrecovery.

Forbush effects were selected for which the duration of each of these periods was at least 24 hours. In all, the data for 7 Forbush decreases during 1959–1960 were processed (Figure 3).

An interesting result of this study was the fact that, during the period of Forbush minimum, opposite deviations of $C\,(3;\ 1.0)_{hg}$ and $C\,(6;\ 1.0)_{hg}$ were observed. Moreover, the errors of these points, found as the errors of the average for four combinations, were very small. It can be assumed that

these deviations are also geometric in nature. As yet it is not clear in which layer this effect is produced, but it is definitely not an effect of the lower layers.

The character of the effect itself indicates that during this period there may be a decrease in the height of the layer responsible for the observed effect.

In addition, the amplitude of the effect for sixfold coincidences (that is, for the larger separation) was, just as in the previous cases, considerably greater than for threefold coincidences. The foregoing results indicate that the upper temperature effect of extensive air showers should be studied in more detail. Such a study should provide information on shower development. Moreover, if the temperature effect over the first nuclear units of path is observed, we will learn more about the interaction cross section for ultrahigh-energy primaries, and hence about the chemical composition of these particles.

Institute of Space-Physics Research and Aeronomy,
Yakutsk Branch of Siberian Division of
USSR Academy of Sciences

REFERENCES

1. KRASIL'NIKOV, D.D., N.N. EFIMOV, M.A.NIFONTOV, and F.K. SHAMSUTDINOVA.— Izv. AN SSSR, seriya fizicheskaya, **26**, 823. 1962.

2. KRASIL'NIKOV, D.D.— Trudy YaFSO, AN SSSR, seriya fizicheskaya, No. 4.

G. V. Skripin

DIURNAL VARIATIONS IN COSMIC-RAY INTENSITY

Once investigators /1, 2/ finally became convinced of the nonmeteorological nature of the diurnal variation in cosmic-ray intensity, the importance of cosmic rays for studying interplanetary space and the phenomena in it increased considerably. Scientists began to take more and more interest in these variations, and now we are continually learning more about their properties and regularities. This subject was studied with particular interest during the IGY, when several experimental and theoretical works appeared in which the diurnal variations were considered in relation to geomagnetic and solar-physical phenomena and were used to probe interplanetary space.

The electromagnetic conditions in the space around the earth could be studied very effectively by means of the diurnal cosmic-ray variation, if only certain difficulties, which themselves are of considerable scientific interest, were overcome.

First of all, when primary cosmic rays, especially those with low energies, enter the sphere of action of the geomagnetic field, their directions of motion are varied significantly. The interaction of the magnetosphere of the earth with corpuscular formations ejected by the sun deforms the magnetosphere considerably and possibly causes it to oscillate. Moreover, the conditions for the generation and propagation of the various secondary cosmic-ray components in the atmosphere vary during the course of the day. Thus, there are also diurnal variations of atmospheric origin.

The diurnal intensity variations can therefore be classified into three types, according to origin. The first type of variations are caused by a change in the integral generation time for secondary components in the atmosphere (variations related to temperature and barometric changes). The second type are due to variations of the geomagnetic field (effect of inclination of magnetic-dipole axis, and effect of alteration of the magnetosphere configuration by the solar wind and by magnetic solar formations). Finally, the third type are related to a change in the primary flux beyond the limits of the magnetosphere. This report will give a brief survey of recent studies of the diurnal variations made by Soviet and non-Soviet authors. Detailed information on early investigations of this subject will be found in the thorough reviews of Elliot /3/ and Dorman /4, 5/.

1. DIURNAL COSMIC-RAY VARIATIONS AND METEOROLOGICAL EFFECTS

The effects which diurnal fluctuations of meteorological factors have on the diurnal cosmic-ray variations have still not been definitely determined. It is comparatively easy to introduce barometric corrections by means of a barometric coefficient and the variation of the ground-level pressure. However, it is difficult to remove the influence of diurnal meson-intensity variations resulting from atmospheric temperature changes. The problem is that the aerological-sounding data for a specific day are very meager. Consequently, the expected diurnal variations due to these temperature changes cannot be estimated accurately enough. Actually, even at more progressive weather stations, atmospheric sounding is carried out only three or four times daily and up to heights of no more than 50 mb.

Different means have been employed to compensate for this insufficiency of data. In /6, 7/ temperature variations above 1 km were neglected, and corrections were made using the temperature coefficient and the diurnal variation of the ground-level temperature. In /8-14/ the temperature corrections were calculated, according to the theoretical scheme in /4/, for 2 to 4 moments of sonde launching. Then, the first-harmonic parameters of the predicted wave were found by harmonic analysis and the correction was subtracted from the observed variation.

In /1, 2, 15, 16/ the data of detectors making it possible to eliminate the contribution of atmospheric temperature changes were used. The studies made in /15/ are noteworthy: in this work, the readings of counter telescopes oriented to the north and south of the drift angles in the magnetic field were used to calculate the primary anisotropy and the atmospheric wave.

All these methods make it possible, to some extent, to allow for the average contribution of the atmospheric temperature changes. However,

Expected diurnal variations of cosmic-ray meson intensity, due to atmospheric temperature changes

Author and reference	Method and theoretical scheme	Period, years	Amplitude, %	τ_m	Station
Kuz'min /8/	Day and night, double sounding, Dorman's scheme	1949-1952	0.3	2.0	Yakutsk
Kuz'min/10/	Quadruple sounding, Dorman's scheme	1957-1958	0.21	2.0	Yakutsk
Glokova	Quadruple sounding, Dorman's scheme	1954	0.18	2.0	Moscow
Kaminer /9/	Multiple sounding, Dorman's scheme		0.22	2.0	
Skripin	Triple sounding, Dorman's scheme	1958-1960	0.11	2.5	Yakutsk
Fedchenko /12/	Multiple sounding	1955	0.18	3.0	Cape Schmidt
Sarabhai /6/	Neglecting temperature changes above 2 km	1957-1958	0.15	4.0	Ahmedabad
Quenby and Thambyahpillai /7/	Comparison between chamber and neutron-monitor data	1954-1956	0.11	5.8	Huancayo

they do not enable a study of the diurnal variations on individual days. At present only pronounced large diurnal variations on individual days can be studied reliably.

The table shows all the data known to us concerning the diurnal variation to be expected as a result of the atmospheric temperature changes determined by the different methods. It is clear from the table that the estimates of these expected variations differ considerably from author to author, both in magnitude and in phase.

Non-Soviet scientists, mainly on the basis of the data of Harris /17/, neglected the temperature variations above 2 km and introduced corrections only for the variation in ground-level temperature, using Behr's relation /6/. Soviet investigators, on the other hand, proceeded from experiments /9, 13, 14/ demonstrating the comparatively large temperature changes in the upper atmospheric layers. Quenby and Thambyahpillai /7/ assumed that radiation errors for the sounding during daytime hours crept into the data of Kaminer /9/. They justified this assumption by the fact that differences (toward the high side) in the amplitude of the temperature variations at all sounding levels are observed in the daytime, in comparison with the data of Harris. Recent calculations made by us /11/, on the basis of a more correct allowance for the radiation errors of the wave W_1, give a lower value (0.11%) for Yakutsk, in comparison with previous estimates /8–10, 14/.

However, it is impossible to reconcile a neglect of the temperature variations above 2 km with this. Underground measurements of the meson intensity /18/ indicate that at a level above 50 mb sizable temperature oscillations (3 to 5° in magnitude) exist, which are out of phase with the ground-level variations. When these variations are taken into account, the correction is considerably less.

Experiments on the correlation of the semidiurnal variations (S) of the meson- and neutron-component intensities with the ground-level barometric pressure /19–21/ constitute another, independent, indication of the considerable variability of the atmospheric temperature. In /19/ the barometric coefficient was obtained from a comparison of the monthly average semidiurnal variations of the meson intensity and pressure for 1949 to 1952. The coefficient obtained was three times the value $\beta = 0.11\%/\text{mb}$ calculated from the daily average values. A repetition of these calculations at Yakutsk for 1958 to 1960 resulted in a barometric coefficient for the meson intensity which was twice as large, whereas for the neutron component the coefficients were identical for calculations by the different methods.

Sarabhai and Rao /6/, and Katzman /22/ have pointed out that for comparatively hard mesons at the equator and underground there is a positive correlation between the semidiurnal waves of the pressure and the meson intensity. At Yakutsk semidiurnal variations of the meson intensity at a depth of 20 m. w. e. of the order of 0.05%, with $T_m \approx 6$ hours, were observed; for the pressure these parameters were 0.18 mb and $T_m = 8.5$ hours. All these facts attest to the likelihood of large oscillations of semidiurnal period in the upper atmosphere. The attempts of Nicholson and Sarabhai to explain the positive correlation observed for S_2 by this means were unsuccessful. However, these calculations were made during early experiments, and they should be reconsidered in the light of present-day theoretical ideas concerning meson production in the atmosphere.

Finally, a semidiurnal lunar wave, with an amplitude of about 0.06% and a time of maximum 3 hours before outer culmination of the moon, is present in the meson intensity. This also indicates, as was pointed out in /23/, the considerable influence of tidal temperature oscillations in the atmosphere.

2. DIURNAL COSMIC-RAY VARIATIONS AND THE GEOMAGNETIC FIELD

During the IGY and also after it, continuous recordings of the cosmic-ray neutron intensity were made. These data enabled several investigators to recognize some interesting properties of the diurnal variations, in relation to the penetration of the primaries into the geomagnetic field.

The latitude and longitude dependences of the diurnal variations of the nuclear cosmic-ray component have been discussed in /11, 24–30/. In spite of difficulties related to the experimental errors /31/, some new statistical regularities in the diurnal neutron variations were established.

1. The amplitude of the first harmonic increases slightly with latitude from the equator to the middle latitudes and then decreases to almost zero at the pole /11, 24, 31/.

2. The variation of the monthly average values of the first-harmonic amplitudes for the diurnal neutron variations at different stations is global in character /24, 28/. The corresponding changes in the time of maximum may be statistical /28/.

3. The time of maximum of the first harmonic increases from the equator to the pole, from 9–12 hours to 17–20 hours local time /11, 24, 25, 27–30/.

4. The latitude dependences of the amplitude and time of maximum are different for the Northern and Southern Hemispheres /26/.

5. Slight differences exist between the amplitudes and maximum times of diurnal variations measured at mountain height and at sea level.

6. For high-latitude stations the first harmonic predominates over the second, whereas for equatorial stations the opposite is true /26/.

7. The amplitude and phase of the diurnal neutron variation depend considerably on the geographical longitude of the observation /26, 28/.

8. There is a latitude and longitude effect on the maximum time T_m of the diurnal variation, the minimum being near the geomagnetic equator. T_m for the diurnal variation of the neutron intensity at mountain level is less than the corresponding sea-level value /26/. The minimum value of T_m is in a region stretching from southern Africa through the Pacific Ocean to South America.

9. The moment of minimum $T_{m\,\min}$ on the latitude curve of the monthly phases of the diurnal neutron variation increases with a decrease in solar activity. The spread ΔT_{80-0° of the variation on the latitude curve of the maximum time increases with a rise in solar activity /26/.

10. The global dependence of T_m for the diurnal variation /26, 27/ indicates that the contours of different T_m shift toward the west in the Northern Hemisphere when the solar activity increases, and toward the east when it decreases. In the Southern Hemisphere no such shift is observed. This led to the assumption /26/ that the lines of the geomagnetic field are

deformed toward the west in outer space when the solar activity increases. From this, the authors of /26/ concluded that the position of the cosmic equator varies with time.

A theoretical explanation of the observed latitude-longitude dependence of the diurnal neutron variation was given in /27, 32/. These authors proceeded from the premise that the geomagnetic dipole is inclined to the earth's rotation axis. They calculated the solar-daily variations of the nuclear cosmic-ray component to be expected at various geomagnetic latitudes and longitudes, for different assumptions concerning the spectrum and the source-strength distribution of the diurnal variation.

A comparison of the experimental and theoretical results in /27–29/ shows some interesting things about the diurnal variations:

a) the energy spectrum of the diurnal neutron variation has the form $a\varepsilon^{-0.4}$ for energies of 7 BeV and above and is equal to zero for particles with energies below 7 BeV /29/. This spectrum is considerably harder than that obtained by Dorman and by Nagashima et al. A recent analysis of data on the underground variations at Yakutsk /18/ indicated this same form for the spectrum;

b) the predicted two control maps agree better with the predicted and experimental distributions if the predicted contour map is turned westward about the geographic pole, by 90° near the pole and by 45° near the equator. This fact is explained /27/ by the deformation of the geomagnetic field by some conducting medium which continually surrounds the earth in the exosphere. As pointed out in /26/, on account of this the cosmic equator may shift with time.

The early investigations of Elliot showed that near the earth, within the region of influence of the magnetosphere, a local source of diurnal cosmic-ray variations may sometimes appear. Sarabhai /33/ presented some details about this source, gained from directional cosmic-ray measurements at an equatorial station. The energy spectrum of the diurnal variations from this source has the form $\frac{\delta D(\varepsilon)}{D(\varepsilon)} = a$, where $a = 0$ for $\varepsilon \geqslant \varepsilon_{max} = 40$ to 60 BeV. The source is located in the direction of the sun and appears predominantly on days of high magnetic activity.

In /35/ an attempt was made to explain the appearance of a local source during a large magnetic storm as a result of the direct action on cosmic rays of a geomagnetic field distorted asymmetrically by the corpuscular flux. If such an effect exists, then it will obviously show up better during a magnetic storm accompanied by an intensity increase. In this case the magnetic field of the corpuscular fluxes causing the disturbed diurnal variation has no influence.

The foregoing survey makes it clear that the geomagnetic field and its variations contribute significantly to the production of diurnal cosmic-ray variations. These factors must be taken into account and are of independent interest.

However, with respect to obtaining a more reliable description of this effect, the lack of data from continuous recordings at certain especially important points in the world is keenly felt. There are almost no stations in Africa and in the Pacific. Also, only a few stations exist in the Southern Hemisphere, and they are located at random.

Moreover, data on the diurnal variations at nearby stations with the same latitude sometimes differ greatly /27/. Therefore, when studying the

latitude–longitude dependence of the diurnal variations, particularly for comparatively short averaging periods (a day or a month), the construction of contour maps is difficult.

3. DIURNAL COSMIC-RAY VARIATIONS AND INTERPLANETARY SPACE

It is known that the main source of the diurnal variations is located somewhere in the solar system outside of the geomagnetic field. It may disappear during the period of minimum solar activity and then may reappear, mainly to the left of the earth-sun line, in other periods. Its strength is a maximum in the ecliptic plane and decreases as the cosine of the latitude.

Consequently, the properties of this source are related to the solar activity. This is the reason for the interest in the diurnal variations as an unusual probe of the situation in interplanetary space, which is known to be regulated by solar processes.

The properties of this remote outer source are investigated by studying the variability of the average diurnal variations (secular change, recurrence period, and seasonal changes of the variations). This method makes it possible to distinguish against the background of rapidly varying sources the diurnal-variation source which is stable in space and time.

Another, independent, means of studying "remote" sources is using crossed telescopes.

The studies of Glokova, Sarabhai, and Thambyahpillai and Elliot, dealing with the change in the diurnal variations from year to year, were followed (during the last 4 or 5 years) by several works which utilized the experimental data collected up to 1959. The results of these investigations can be summarized as follows.

1. The variation of the first-harmonic amplitude of the meson-intensity variation correlates positively with the variations in solar and magnetic activity, the correlation with the latter apparently being better /36/. This indicates that the relation to the solar activity is not direct and that, most likely, the electromagnetic state of the interplanetary space has an immediate influence on the diurnal variation.

2. The direction of anisotropy has a tendency to shift toward the morning hours during periods of solar-activity minimum, the amount of shift varying substantially from cycle to cycle.

3. The changes in the second harmonic of the diurnal meson-intensity variation are more complex, and the general properties of these regularities are still not known with any certainty.

4. The data of recent years (1955–1960) on the meson and neutron components confirm Elliot's conclusion that the solar-daily variations undergo 22-year periodic changes /37, 38/. During this period, T_m for the meson and neutron diurnal variations at Ottawa shifted toward later hours.

5. For the high-latitude station at Resolute Bay, a biennial recurrence period of T_m for the first harmonic of the diurnal variations in meson and neutron intensity was found for 1957 to 1960. This result correlates closely with similar variations of the geomagnetic-activity index (K_p) /38/. Since such changes are not observed at stations with geomagnetic latitudes less than 60°, it can be assumed that T_m at Resolute Bay is more sensitive to the interplanetary disturbances measured by the planetary index K_p.

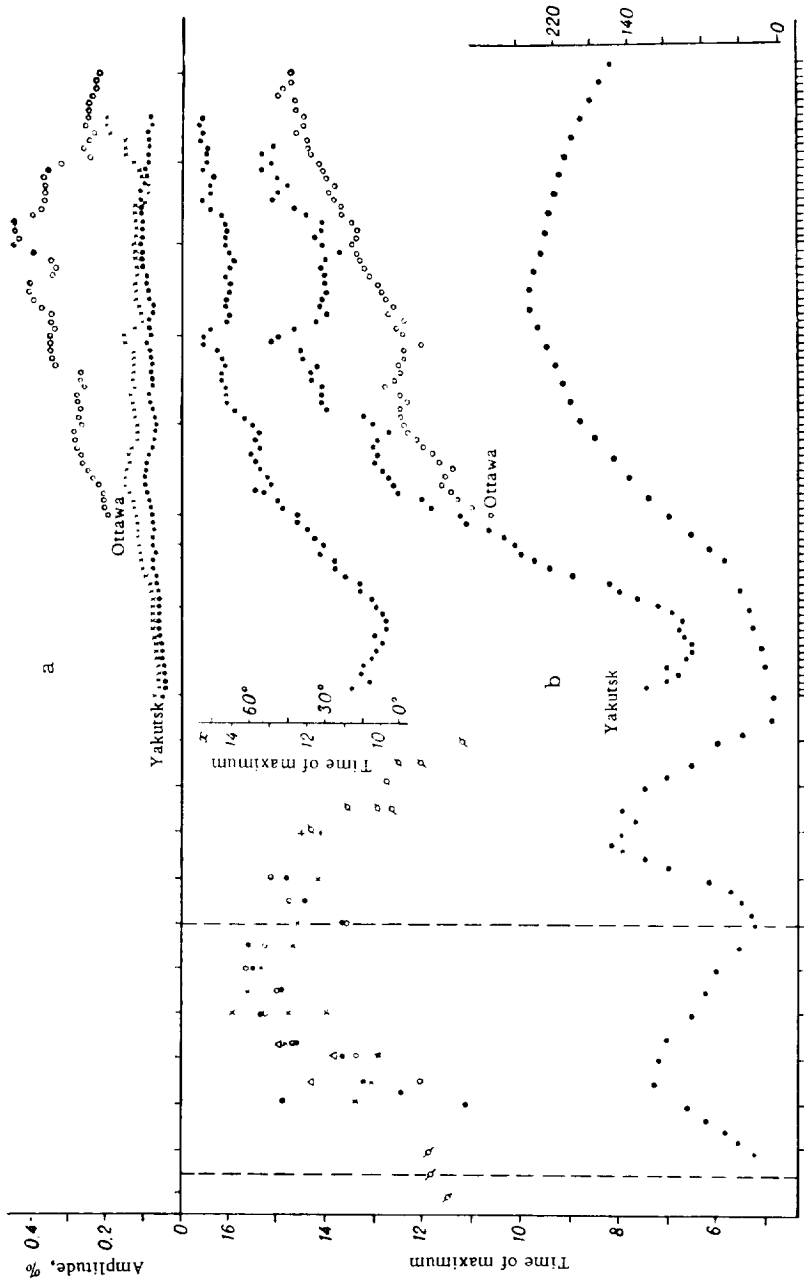

FIGURE 1. Secular variation of the time of maximum meson intensity, for Yakutsk and Ottawa, shown with sunspot-number variation /2/.

a–data corrected for barometric and temperature effects, x denotes angle east of earth-sun line and direction toward source; b–data uncorrected for temperature effect.

In order to check the foregoing experimental facts and conclusions, we made a study of the secular changes in the diurnal variations recorded at the Yakutsk and Tixie-Bay stations. Figure 1 shows the results of this study. It is clear from the figure that up to 1961 T_m for the diurnal meson-intensity variation at Yakutsk shifted toward a later time. The amplitude of this diurnal variation also tended to increase with a rise in solar activity. Therefore, our experiments verify the existence of a 22-year cycle of T_m for the diurnal variation.

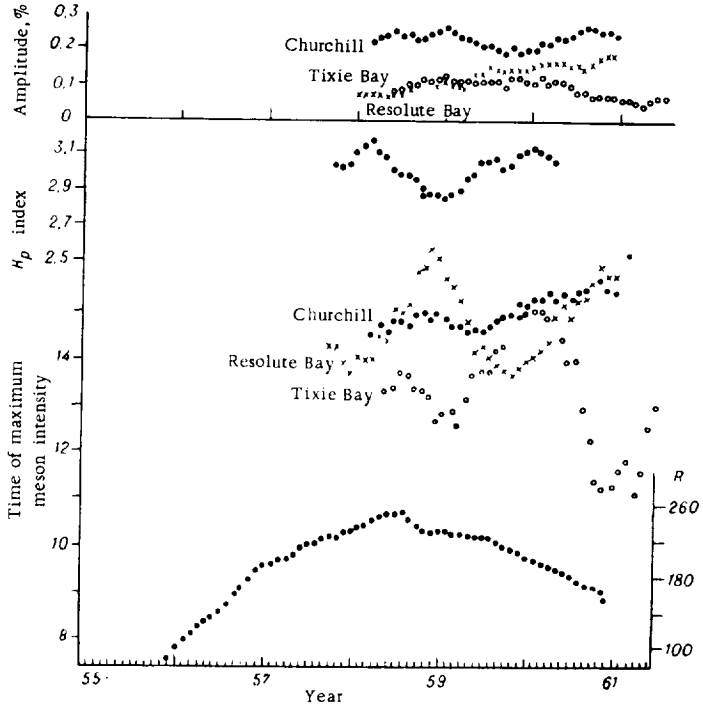

FIGURE 2. Variation of time of maximum meson intensity at Resolute Bay, Tixie Bay, and Churchill, plotted along with variations of magnetic disturbance (K_p index) and solar activity (R).

The biennial wave in the diurnal variations at high-latitude stations, and the absence of this wave at middle-latitude stations, were also verified. Figure 2 shows curves, smoothed over a 12-month interval, for the monthly values of T_m and the amplitude of the diurnal meson-intensity variation, for the stations at Tixie Bay, Resolute Bay, and Churchill. The pronounced biennial wave of the meson-intensity variations at Resolute Bay and Tixie Bay shows up clearly in this figure.

In Figure 3 the correlation coefficients for the variations of T_m and the magnetic-activity index K_p are plotted for the three stations. The coefficients were found using the autocorrelation method. The best correlations (over 90%) were those for the data from Tixie Bay and Resolute Bay. For Yakutsk the correlation was weaker. The largest positive coefficient for the correlation of T_m with K_p for Tixie Bay is obtained if the K_p curve is

shifted 2 months later relative to the T_m curve. For Resolute Bay, on the other hand, this coefficient is negative, and the K_p curve must be moved back 3 months for optimum correlation. From Figure 2 it is clear that the biennial waves of T_m for Tixie Bay and Resolute Bay are almost out of phase. This behavior of the curves led us to assume that the biennial recurrence of T_m for the diurnal variation is due to superposition of the solar-daily variation and a wave with a 24-hour period which proceeds according to universal time and modulates with a period of two years.

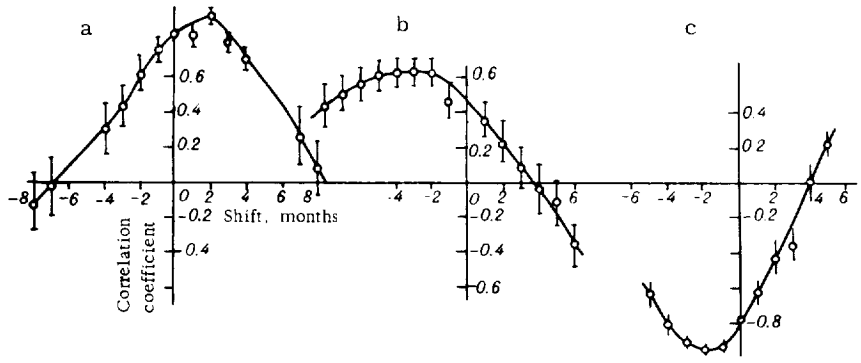

FIGURE 3. Correlation between K_p-index curve and curve of biennial variation in time of maximum, for Tixie Bay (a), Yakutsk (b), and Resolute Bay (c).

Parsons' relation /39/ shows that a global wave is observed, but actually the existence of such a wave is still not definite. It can be assumed that either all of the global wave, or at least a considerable part of it, is caused by a spurious effect due to the influence of Forbush decreases on the monthly average diurnal variation. This influence manifests itself even in cases when data for a steep drop in intensity do not enter into the calculation.

Recurrences of the diurnal variation at periods of about a month and half a month were studied in /11, 40/. It was found that, in addition to the 27-day recurrence of the diurnal variation, there is also a recurrence with a period of 13–14 days, which has an inverse correlation with the solar activity. Diurnal variations with their times of maximum in the morning or night show more tendency to have such a recurrence period.

There are indications /40, 41/ that the lunar-daily variation found in /42, 43/ is a consequence of modulation of the 27-day recurrence of the diurnal variation.

Several studies have been made /11, 34, 44–53/ of changes in the diurnal variations on specific days or groups of days having some special feature. For instance, investigators have paid special attention to the diurnal variations on magnetically disturbed days, including days during the recovery period following a Forbush decrease.

The results of these studies may be summarized as follows.

1. On disturbed days the time of maximum of the diurnal variation is earlier /11, 44, 45, 48, 52/, which agrees with previous results /50/. However, there are also some disturbed days with a later T_m /48/.

2. The amplitude on days of heightened magnetic activity is lower in comparison with quiet days /11, 44, 47/. This effect shows up when large

groups of days are studied. When the diurnal variations on individual days are considered, as was done in /11, 45, 47/, it turns out that the first-harmonic amplitude of the variation is on the average 1.5 to 2 times that on magnetically quiet days. The latter result verifies the earlier findings /50/.

3. Forbush decreases are always related to and flanked by a train of diurnal variations, and, conversely, a train of diurnal variations often includes a more or less definite Forbush decrease. Cattani et al. /46/ have pointed out that such a diurnal-variation train is different in nature from a Forbush decrease. The effects which are found to accompany a Forbush decrease, as well as a predecrease, preincrease, or rise in the diurnal variations during the recovery period, are a result of the superposition of two effects: a Forbush decrease and a train of diurnal variations.

4. In several studies /48, 49, 51, 54/ an interesting phenomenon has been observed, namely a gradual rotation of the diurnal cosmic-ray variations during some effective magnetic storms. Such a rotation was observed at Yakutsk by all the instruments, both at ground level and underground at depths up to 60 m. w. e. /54/. The possible reasons for this rotation of the anisotropy are discussed in /52/. These may be: a gradual change in the position of the anisotropy source; the superposition of an isotropic intensity burst onto the diurnal variation; the appearance of a new, additional modulating source. Here, however, only the general scheme of the phenomena of anisotropy rotation observed at the time of magnetic storms will be given. It is assumed that within a magnetic field closed at the sun there exist isolated magnetic formations which, alternately intersecting the earth, may cause all the various observed kinds of anisotropy rotation.

5. In /34/ it was found that on individual days (not necessarily magnetically disturbed days) ground-level telescopes pointed north and south at Yakutsk registered diurnal variations which were identical in amplitude and phase.

Phase changes relative to the average are detected only by northward-pointing telescopes. This indicated to the authors of /34/ that the observed change may be due to the presence of a high-latitude source of diurnal variations, the properties of which are varying.

The sidereal-time diurnal variation requires separate consideration. This topic has been discussed widely in recent years in relation to the anomalous behavior of the diurnal variations in 1954.

Some new information regarding this effect is presented in /55–57/. The authors of /56/ are of the opinion that two sources of diurnal cosmic-ray variations exist, the basic properties of which vary with the solar activity. A first, low-energy, source lies to the left of the earth-sun line, and a second, high-energy, source has its main strength at large angles to the ecliptic plane. The second source is related to the preference of particles of galactic origin for arrival directions from the center of the galaxy. At minimum solar activity, conditions are the most favorable for the passage of particles from the second source. The existence of the latter must bring about a sidereal-time diurnal variation with varying amplitude and phase.

In /57/ it is pointed out that the second source exists during periods of both maximum and minimum solar activity. This conclusion follows from an analysis of the data of directional meson-intensity measurements at Yakutsk at underground depths of 20 and 60 m. w. e.

CONCLUSION

On the basis of the experimental data considered here and in previous surveys /3, 4, 5/, let us try to give a general description of the formation of diurnal cosmic-ray variations.

Cosmic rays enter the solar system from the galaxy with an intensity which is constant in time and with some degree of spatial anisotropy. This anisotropy manifests itself as a sidereal-time diurnal variation with an amplitude of about 0.1% for particles of less than 200 BeV; it has a maximum in the direction of the galactic center.

In interplanetary space cosmic rays interact with the magnetic fields of celestial bodies and with solar corpuscular streams. Cosmic-ray modulation effects, including the diurnal variations, are apparently connected with these interactions.

The principal anisotropy source possessing very high stability in time is located in the ecliptic plane to the left of the earth-sun line, and it participates in the revolution of the earth about the sun. The properties of this source vary with periods of 22 years and 27 days, and probably also with periods of 2 years and 12 to 15 days. Until recently this source was described satisfactorily by Dorman's proposal /3/ of a mechanism whereby the electric fields of the solar corpuscular streams influence the diurnal variations. However, recent evaluations of the diurnal-variation spectrum /29, 34/ have led to certain difficulties in the explanation of the variations by means of this mechanism.

When corpuscular streams envelop the earth, a whole series of sources of cosmic-ray anisotropy originate, depending on the structure of the flux and on the extent of its interaction with the geomagnetic field. These are primarily the so-called disturbed diurnal variations, having a time of maximum close to midday. At such times situations can also arise which lead to a gradual rotation of the anisotropy (appearance of a rotating source).

As the plasma of a corpuscular stream flows around the geomagnetic field, a nonsymmetrical cavity may also be formed, which can give rise to a local source of diurnal variations.

Finally, atmospheric effects contribute considerably to the diurnal variations of cosmic rays, and this contribution is at present difficult to take into account.

Thus, many sources of diurnal variations exist, the superposition of which produces a complicated picture. As a result, a successful study of the nature of the diurnal variations is at present possible only through a detailed analysis of the data for each day separately, and through a determination of the relation between these data and phenomena on the earth and the sun. However, our present-day experimental techniques for continuous cosmic-ray recording are inadequate for such an analysis. The incomplete coverage of the world with cosmic-ray stations, especially in the Southern Hemisphere and the equatorial latitudes, the insufficient counting rates of the detectors, and the small number of instruments for directional measurements of the cosmic-ray intensity, are the main deficiencies preventing the attainment of the desired goal. If these deficiencies can be eliminated to some extent, a regular probing of the electromagnetic conditions in interplanetary space will become possible.

Institute of Space-Physics Research and Aeronomy,
Yakutsk Branch of Siberian Division of
USSR Academy of Sciences

REFERENCES

1. MALMFORS, K. G. – Tellus, **1**, 55. 1949.
2. ELLIOT, H. and D. DOLBEAR. – J. Atmos. Terr. Phys., **1**, 205. 1951.
3. Progr. Elem. Part. Cosm. Ray Phys., **1**. 1952.
4. DORMAN, L. I. Variatsii kosmicheskikh luchei (Cosmic-Ray Variations). 1957.
5. DORMAN, L. I. – Sbornik: "Kosmicheskie luchi," No. 3. 1961.
6. RAO, U. R. and V. SARABHAI. – Proc. Roy. Soc., **263**, 101. 1961.
7. QUENBY, J. J. and T. THAMBYAHPILLAI. – Phil. Mag., **5**, 54, 585. 1960.
8. KUZ'MIN, A. I. – ZhETF, **28**, 614. 1955.
9. KAMINER, N. S. – Trudy TsAO, No. 16, 48. 1956.
10. KUZ'MIN, A. I. – Trudy YaFSO, AN SSSR, seriya fizicheskaya, No. 3. 1960.
11. SKRIPIN, G. V. – Trudy YaFSO, AN SSSR, seriya fizicheskaya, No. 5 (in press).
12. FEDCHENKO, K. K. Report on Topic No. 5004 for 1956–1957, Arkticheskii nauchno-issledovatel'skii institut Glavsevmorputi.
13. SELEZNEVA, E. S. – Izv. AN SSSR, seriya geograficheskaya i geofizicheskaya, **9**. 1949.
14. GLOKOVA, E. S. N. A. MISHNINA, and N. S. KAMINER. – Trudy YaFSO, AN SSSR, No. 2, seriya fizicheskaya. 1957.
15. BRUNBERG, E. A. Electromagn. Phenom. Cosm. Ray, pp. 386–391. – Cambridge Univ. Press. 1958.
16. KITAMURA, M. and M. KODAMA. – J. Geomag. and Geoelect., **12**, 4. 1961.
17. HARRIS, M. T. – J. Geophys. Res., **64**, 983. 1959.
18. KUZ'MIN, A. I., G. F. KRYMSKII, P. A. KRIVOSHAPKIN, and G. V. SKRIPIN. Report in this collection.
19. KUZ'MIN, A. I. and G. V. SKRIPIN. – Trudy YaFSO, AN SSSR, seriya fizicheskaya, No. 23. 1955.
20. SKRIPIN, G. V. and N. P. CHIRKOV. – Issledovaniya po geomagnetizmu i aeronomii SibIZMIR, 126. 1960.
21. KATZMAN, J. and D. VENKATESAN. – Canad. J. Phys., **38**, 1011. 1960.
22. KATZMAN, J. – Canad. J. Phys., **37**. 1959.
23. KUZ'MIN, A. I. and G. V. SKRIPIN. – ZhETF, **28**, 608. 1955.
24. SCHWACHEIM, G. – J. Geophys. Res., **65**, 3151. 1960.
25. KANE, R. P. and S. R. THAKORA. – Proc. Ind. Acad. Sci., A52, 122. 1960.
26. KANNO, T. and K. MURAKAMI. – Comm. to Intern. Conf. on Cosmic Rays, Kyoto, **47**. 1961.
27. MURAKAMI, K. – Sci. Pap. Inst. Phys. Chem. Res., **55**, 24. 1961.
28. POMERANTZ, M. A., S. P. DUGGAL, and K. NAGASHIMA. – Prepr. 2 Intern. Conf. on C. R. and Earth Storm, Kyoto, MO-11-46-5. 1961.
29. DUGGAL, S. P., K. NAGASHIMA, and M. A. POMERANTZ. – J. Geophys. Res., **66**, 1970. 1961.
30. KATZMAN, J. and D. VENKATESAN. – Canad. J. Phys., **38**, 1011. 1960.
31. KANE, R. P. – Ind. J. Phys. **35**, 5, 213. 1961.
32. NAGASHIMA, K., V. R. POTNIS, and M. A. POMERANTZ. – Nuovo Cimento, **19**, No. 2. 292. 1961.
33. RAO, U. R. and V. SARABHAI. – Proc. Roy. Soc., A263, 101–135 (Parts I, II, III). 1961.
34. KUZ'MIN, A. I., G. V. SKRIPIN, S. N. DRUZHININ, G. F. KRYMSKII, and P. A. KRIVOSHAPKIN. Report in this collection.
35. DORMAN, L. I. and O. I. INOZEMTSEVA. – Geomagnetizm i aeronomiya, No. 3, 453. 1962.

36. THAMBYAHPILLAI, T. and H. ELLIOT.– Nature, **171**, 919. 1953.

37. FORBUSH, S. and D. VENKATESAN.– J. Geophys. Res., **65**, 2213. 1960.

38. KATZMAN, J.– Canad. J. Phys., **39**, 1477. 1961.

39. PARSONS, N.R.– Tellus, **12**, 450. 1960.

40. SKRIPIN, G.V. and L.P. BOLTRUSHKO. Geo– i geliofizicheskie effekty v kosmicheskikh luchakh i polyarnykh siyaniyakh (Geophysical and Solar-Physical Effects on Cosmic Rays and Polar Aurorae). In press.

41. KRYMSKII, G.F. – Trudy YaFSO, AN SSSR, No.4, 108. 1962.

42. BAGGE, E. and O. BINDER.– Trudy MKKL, **4**, 273. 1960.

43. DORMAN, L.I. and L.Kh. SHATASHVILI.– Geomagnetizm i aeronomiya, No.5. 1962.

44. SANDSTRÖM, A.E., E. DYRING, and S. LINDGREN.– Tellus, **12**, 332. 1960.

45. SANDSTRÖM, A.E.—Internat. Conf. on C.R. and Earth Storm, Kyoto, MO–11–4B–8. 1961.

46. CATTANI, D., M. GALLI, and P. RANDI.— Nuovo Cimento, **21**, 923. 1961.

47. CROWDEN, J.B. and P.L. MARSDEN.— Conf. on C.R. and Earth Storm, Kyoto, MO–11–4B–12. 1961.

48. KUZMIN, A.I. and G.V. SKRIPIN.– Trudy YaFSO, AN SSSR, seriya fizicheskaya, No.4. 1962.

49. KUZ'MIN, A.I., G.F. KRYMSKII, G.V. SKRIPIN, V.A. FILIPPOV, N.P. CHIRKOV, and G.V. SHAFER. Report in this collection.

50. SEKIDO, Y. and S. YOSHIDA.– Rep. Ionos. Space Res. Japan, **4**, 37. 1950.

51. KRYMSKII, G.F., N.P. CHIRKOV, G.V. SHAFER, and V.A. FILIPPOV. Report in this collection.

52. KUZ'MIN, A.I., G.F. KRYMSKII, and G.V. SKRIPIN.– Geomagnetizm i aeronomiya (in press).

53. DORMAN, L.I. and O.I. INOZEMTSEVA.– Sbornik: "Kosmicheskie luchi," Seriya "Rezul'taty MGG," No.4. 237. 1961.

54. KUZ'MIN, A.I., G.F. KRYMSKII, and G.V. SHAFER.– Geomagnetizm i aeronomiya.

55. GLOKOVA, E.S.– Sbornik: "Kosmicheskie luchi," Seriya "Rezul'taty MGG," No.4, 225. 1961.

56. DORMAN, L.I. and O.I. INOZEMTSEVA.– Sbornik: "Kosmicheskie luchi," Seriya "Rezul'taty MGG," No.4, 209. 1961.

57. SKRIPIN, G.V. Geo– i geliofizicheskie effekty v kosmicheskikh luchakh i polyarnykh siyaniyakh (Geophysical and Solar-Physical Effects on Cosmic Rays and Polar Aurorae). In press.

N67-38219

N.P. Chirkov, A.I. Kuz'min, G.F. Krymskii, G.V. Shafer, and V.A. Filippov

THE UNUSUAL PHENOMENA RELATED TO THE COSMIC-RAY VARIATIONS IN DECEMBER 1957

During the second half of December 1957, some interesting cosmic-ray phenomena were observed. These phenomena proceeded according to local and universal time and possessed some anomalous features. The neutron-intensity variations at several stations are shown in Figure 1 /1/. These variations were accompanied by three light geomagnetic storms associated with solar flares.

The cause of these geophysical effects was active region No. 603 on the sun (according to the numeration of /2/), whose maximum development occurred at the time of its central-meridian transit. A first Class-2 flare (coordinates 18 N, 77 E) occurred at 1238 U. T. on 14 December, and it was accompanied by Type-IV, Class-3 radio emission with a duration of 17 minutes /3/. A second Class-2 flare was observed at 0735 U. T. on 17 December (at 22 N, 44 E), with Type-IV, Class-3 radio emission which lasted for 31 minutes /3/. A third flare, Class 1^+, appeared at 1712 U. T. on 22 December (at 18 N, 19 W), with Type-IV, Class-3 radio emission for 56 minutes /4/. All these flares occurred in the above-mentioned active region. During the period in question, the geoactivity was quite weak ($K_p \leqslant 5-$), whereas on 22–23 December the magnetic-activity index K_p was $\leqslant 1+$ /5/. The indicated days were in general the quietest days in December 1957.

THE COSMIC-RAY ANISOTROPY ON 18–20 DECEMBER

The general sequence of solar and geophysical phenomena is shown in Figure 2. The cosmic-ray intensity was averaged for the stations at Washington, Göttingen, and Yakutsk, which are separated from one another by about 120° longitude and which have intersecting asymptotic cones.

Figure 2 shows that on 17, 19, and 24 December Forbush decreases were observed, the largest decrease (6 or 7%) being the one on 19 December. In Figure 3 the decrease on 19 December is plotted as a function of the geomagnetic threshold. The effect was estimated as the difference of the intensities on 16 and 22 December. During this period the geomagnetic field was disturbed slightly. For a spectrum of the form $\frac{\delta D(\varepsilon)}{D(\varepsilon)} = a\varepsilon^{-\alpha}$, α is about 0.75, which agrees closely with the value obtained previously in /6, 7/. The onset of the Forbush effect on 19 December is shown as a

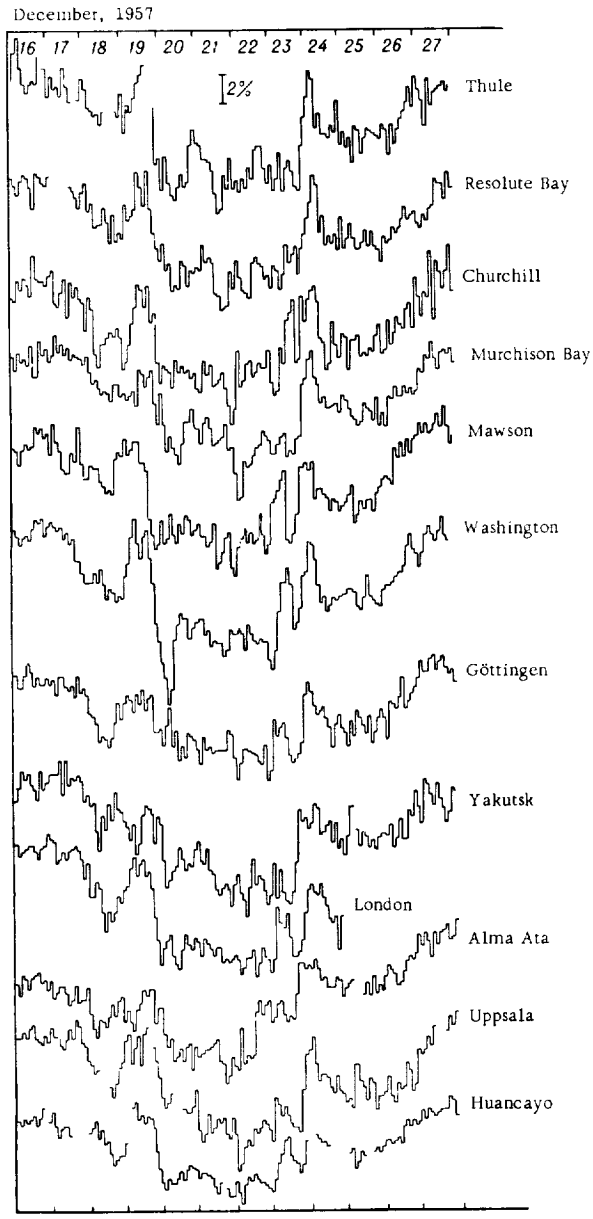

FIGURE 1. Bihourly values of cosmic-ray neutron intensity on 16–27 December 1957, according to data of IGY stations.

function of time in Figure 4. First of all, a decrease began in a direction 60° to the east of the earth-sun line, and after 6–9 hours it could be observed 60° to the west of the line. Usually a Forbush decrease begins to the west of the earth-sun line /8/.

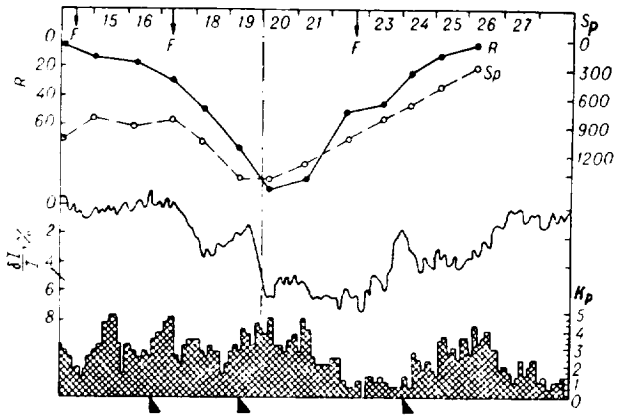

FIGURE 2. Succession of solar and geophysical phenomena in December 1957.

S_p is the total relative spot area in active region No. 603 on the sun; R is the relative spot number in this region; F are Type-IV radio bursts; triangles show onsets of magnetic storms.

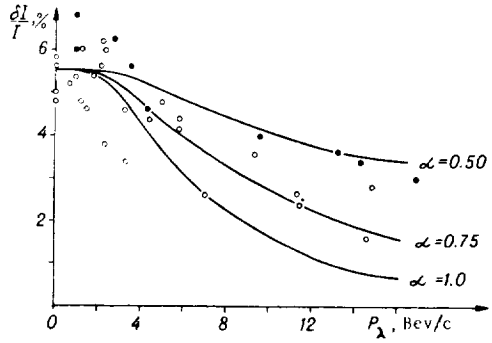

FIGURE 3. Forbush decrease of 19 December 1957 as a function of geomagnetic threshold.

Curves show expected decrease spectrum for different γ; black points show data of high-mountain stations.

Figure 5 shows the average Forbush decreases for two groups of stations located on the average 180° apart and having approximately the same thresholds. It is clear from the figure that the minimum intensity, as well as the onset of the drop, occurs later at the second group of stations than at the first. Consequently, on 19 and 20 December there was a high anisotropy of the cosmic-ray intensity.

In order to determine the properties of this anisotropy, we considered the intensity deviations, from the mean for 18–20 December, for the stations at Yakutsk, Göttingen, and Washington. The results are given in Figure 6, which shows the anisotropy in the plane of the geographical equator as a function of local time. Here, the change in anisotropy during

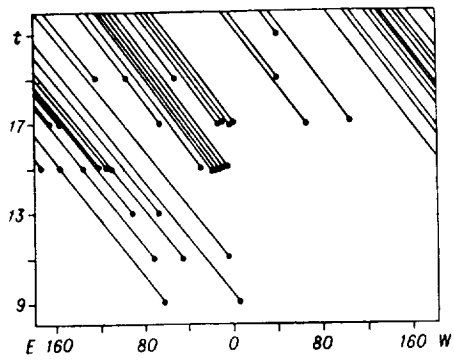

FIGURE 4. Moments of onset of Forbush decrease on 19 December 1957, as a function of recording direction (degrees reckoned from earth-sun line).

Lines show trajectories of receiving direction of instruments, according to time-direction diagram.

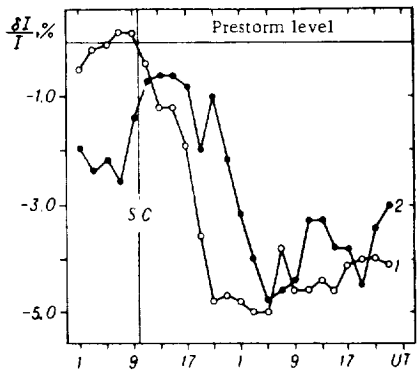

FIGURE 5. Bihourly values of neutron intensity on 19–20 December 1957, averaged for two groups of stations.

1–Mawson, Ushuaia, Rio de Janeiro, Pic-du-Midi; 2–Yakutsk, Wellington, Lae, Alma Ata; S.C. denotes sudden commencement of magnetic storm.

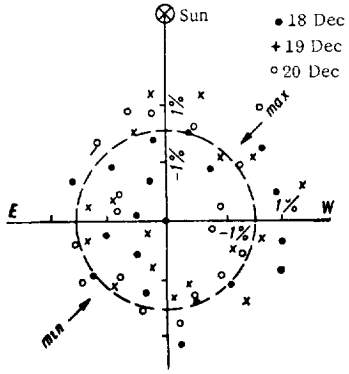

FIGURE 6. Cosmic-ray anisotropy on 18-20 December, in the plane of the geographical equator.

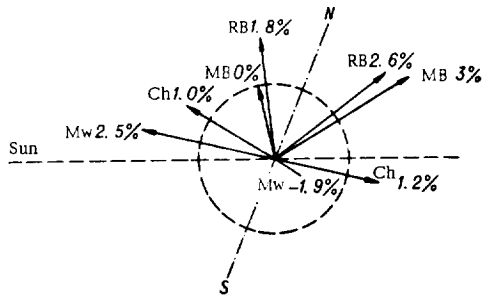

FIGURE 7. Cosmic-ray anisotropy on 19 December 1957, in a plane perpendicular to the ecliptic plane.

the course of a day was assumed to be insignificant. Thus, anisotropy of the cosmic-ray intensity was "felt" by the indicated stations during rotation of the earth.

It is evident from Figure 6 that on 18 and 19 December the cosmic-ray intensity was considerably lower than the average value in a direction to the left of the earth-sun line. Such a trend of the anisotropy is opposite to the direction of the anisotropy giving rise to "quiescent" diurnal variations.

The anisotropy in the plane passing through the sun and the earth's rotation axis (in December this plane is perpendicular to the ecliptic plane) is shown in Figure 7. Data were used from pairs of stations having

asymptotic directions along a single geographic meridian: Mawson and Murchison Bay; and Resolute Bay and Churchill. The geomagnetic

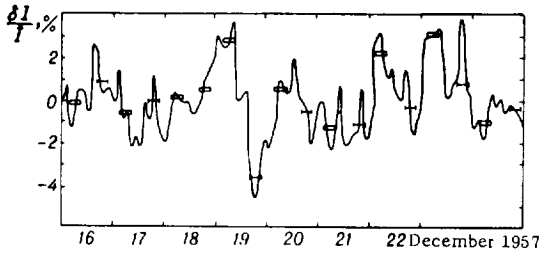

FIGURE 8. Difference curve for neutron intensities at Mawson and Murchison Bay, in December 1957.

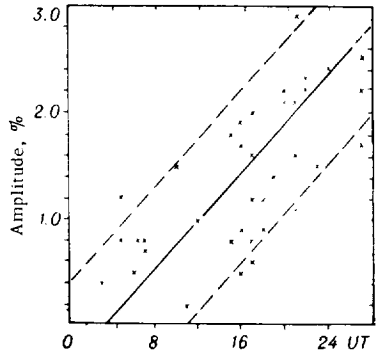

FIGURE 9. Direction of maximum intensity, as a function of time, for 22–23 December 1957. Crosses denote directions of minimum intensity, shifted by 180°.

thresholds of these stations are < 1 BeV/c, so that intensity differences will be due to detector directivity alone. The figure shows that the cosmic-ray

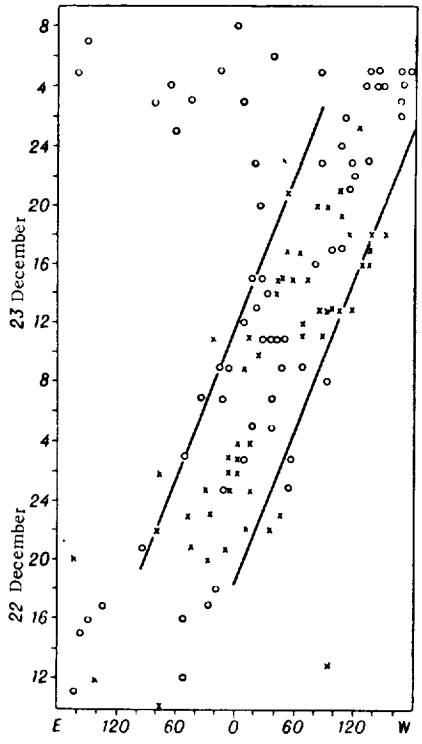

FIGURE 10. Anisotropy amplitude as a function of time, for 23 December 1957.

intensity decreases with the distance from the ecliptic plane, both toward the north and, especially, toward the south. The north-south anisotropy remained for about 24 hours (19 December). This can be seen from Figure 8, where the difference between the intensities recorded at Mawson and at Murchison Bay is plotted. The rectangles and short lines denote moments when the stations receive radiation in the plane of Figure 7 (that is, at local noon and midnight, respectively, taking into account the geomagnetic drift).

ANISOTROPY OF THE COSMIC-RAY INTENSITY ON 22–23 DECEMBER AND ROTATION OF THE ANISOTROPY SOURCE

As mentioned above, during the period in question there were only slight terrestrial effects. On 22–23 December the geomagnetic field was almost completely quiet, except at stations in Antarctica, where minor disturbances were observed /6/. During this time, an anomalous anisotropic increase took place, which reached 6% by the end of 23 December. At first the increase proceeded according to local time, and then according to universal time, when the intensity became isotropic. The anisotropy source shifted in space from 20° E to 120° W, and it rotated in a sense opposite to the diurnal rotation of the earth. These results are shown in Figure 9, which makes use of data from 37 stations. The angle was reckoned from the earth–sun line, taking into account particle drift in the geomagnetic field.

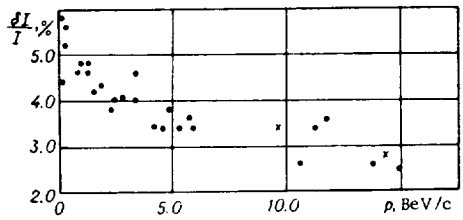

FIGURE 11. Effect of isotropic increase on 23–24 December 1957, as a function of geomagnetic threshold.

Crosses denote high-mountain stations.

According to the data of underground measurements, there was a rotation of the anisotropy source in November 1960 as well /9/. This interesting fact is worthy of special consideration. It should be noted here that such a rotation of the anisotropy source does not agree with the theory of modulation of the cosmic-ray intensity by the electric field of a moving corpuscular flux. The disagreement with theory is shown by the increase in anisotropy amplitude with time in the given case (see Figure 10) and by the rotation of the axis, which is impossible when an electric field is acting. The amplitudes were evaluated from the intensity level on 21–22 December.

Figure 10 shows that early on 24 December an intensity anisotropy set in, which produced a second maximum according to universal time (this was also noted in /10/) and which almost reached the intensity level of 16 December. The isotropy of this maximum is also confirmed by the fact that it was observed at Thule and Resolute Bay, whereas the first maximum according to local time was small at these stations (see Figure 1).

Figure 11 shows the effect of the isotropic increase as a function of geomagnetic threshold, while Figure 12 gives the differential energy spectrum of the flux responsible for this intensity increase. In the energy range $\lesssim 15$ BeV the spectrum was determined from the data of Figure 11, and for high energies the data from underground measurements at Yakutsk were used.

It is evident from Figure 12 that the spectrum over a wide range of energies is described by a power law, with an exponent of 3.5. This energy spectrum is quite different from the spectrum for particles of solar origin, as was pointed out in /11/.

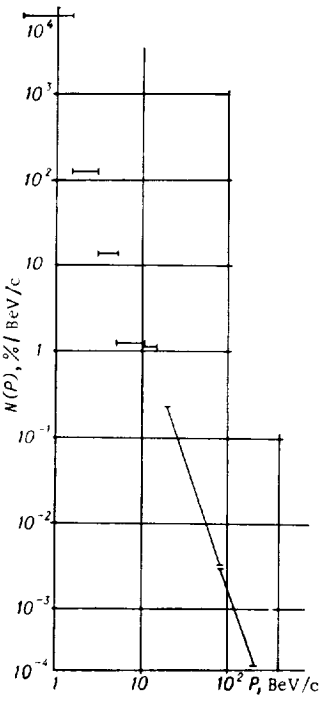

FIGURE 12. Differential energy spectrum of particle flux causing intensity increase on 23–24 December 1957.

DISCUSSION OF THE RESULTS

The considered period of cosmic-ray phenomena represents a rare event from the point of view of solar phenomena. The moment of maximum development and activity (see Figure 2) of spot group 603 coincided with its passage through the central meridian of the sun (00 hours on 20 December). For half a month this group was very active and it determined the entire activity of the sun.

The first large solar flare, observed on 14 December in this active region, occurred at the eastern limb of the disk and gave rise to a light magnetic storm at the end of 16 December and a cosmic-ray intensity decrease on 17 December.

A subsequent large flare on 17 December caused, after 50 hours, a small magnetic storm with sudden commencement and a rather large decrease in the cosmic-ray intensity (about 6%). As indicated above, this decrease was highly anisotropic in character. It began earlier to the east of the earth-sun line, and then, 6–9 hours later, it began to the west. The minimum of the Forbush decrease also occurred later in the west.

Since the magnetic storm commenced suddenly, it is probable that the earth entered the forepart of a corpuscular flux with an average velocity of $0.8 \cdot 10^8$ cm/sec. However, the magnetic storm was brief and of low amplitude, although the decrease in cosmic-ray intensity was considerable and sharply anisotropic. All this implies that we entered a region with a

large gradient of the cosmic-ray density but with a low density of matter. The core of the corpuscular flux bypassed the earth (evidently to the left of the earth-sun line, since the flare was on the eastern side of the solar disk), causing a light magnetic storm. The earth entered a side of the flux with a large gradient of the cosmic-ray density, and we observed an anisotropy of the Forbush decrease in proportion to the entry into the flux.

The anisotropy responsible for the usual diurnal variations is related to the presence of the interplanetary magnetic field and the gradient of the cosmic-ray density (Elliot). The fact that the onset of a Forbush effect is not simultaneous is also related to the action of the interplanetary magnetic field on cosmic rays (Dorman). These two mechanisms require that the interplanetary magnetic field be oriented parallel to the terrestrial field. If in December 1957 the interplanetary field was acting on the cosmic radiation, then the anomalous anisotropy with a minimum intensity to the left of the earth-sun line, and also the onset of the Forbush decrease from the east, indicate that the field in the flux was antiparallel to the terrestrial field.

In this case it must be assumed that during the period in question the magnetic field in the vicinity of the earth was not the general field of the sun. Rather, it was a field carried out of the active region by the flux plasma (otherwise a high rate of magnetic reversal would be required).

The almost constant decrease of the intensity level on 20-22 December indicates that the magnetic screening of the earth from cosmic rays continued.

The complete quiescence of the magnetic field ($K_p \leqslant 1$) leads us to assume that the screening field was not related to the moving plasma of the flux, since inhomogeneities in the plasma density would have to disturb the geomagnetic field. On the other hand, an immobile field must restrict any motions of the plasma and shield the earth from both cosmic rays and geomagnetic disturbances.

The next large flare was observed at 1712 U. T. on 22 December. It gave rise to a light magnetic storm and a decrease in cosmic-ray intensity early on 24 December, indicating that the earth entered a new corpuscular stream. An anisotropic rise in intensity set in approximately 8 hours after the flare and was observed for more than 24 hours, until it became isotropic. The source of the anisotropy rotated in a sense opposite to that of the diurnal rotation of the earth. This was apparently related to a change in the direction of the magnetic field in the flux, during which the field direction must have become almost reversed. This is understandable if we assume that the earth traversed a region in which the force lines of the magnetic field closed upon themselves.

An anisotropic increase began some hours after the flare on 22 December and was observed until the arrival of a new flux early on 24 December. The average velocity of this flux was of the order of $1.1 \cdot 10^8$ cm/sec.

The following is a tentative explanation of the anomalous cosmic-ray phenomena on 23 December: after a corpuscular flux was emitted on 22 December, a previous flux in which the earth happened to be at this time lost contact with the sun and most of its force lines closed upon themselves. The new flux, being more energetic, squeezed and expelled the previous flux (now a cloud), and a gradient of the cosmic-ray density was produced. The rapid penetration of the earth into this cloud gave rise to an anisotropic

increase in the cosmic-ray intensity, bringing it almost up to the level of 15–16 December (the normal galactic intensity level for this time).

Thus, in this case an interaction of corpuscular fluxes apparently took place. In like manner, during the events of July 1959, a superposition of Forbush effects was observed, due to the entry of one flux into another. The present report gives an example of another interaction between magnetized fluxes, acting as two independent systems.

Institute of Space-Physics Research and Aeronomy,
Yakutsk Branch of Siberian Division of
USSR Academy of Sciences

REFERENCES

1. Cosmic Ray Intensity during the International Geophysical Year, No. 1, Japan, 1959.

2. Solnechnye dannye. Byulleten' Glavnoi astronomicheskoi observatorii, No. 7, 1957.

3. WADA, M. and Y. KAMIYA. Rep. Ionos. Res. in Japan, **13**, No. 2, 1959.

4. Solar-Flare Data of the Fraunhofer Institute (Private collection).

5. BARTELS, J., A. ROMANA, and J. VELDKAMP. – Geomagnetic Data 1957, Indexes K and C, Rapid Variations, Amsterdam, 1961.

6. KUZ'MIN, A.I. and G.V. SKRIPIN. – Trudy YaFSO, AN SSSR, seriya fizicheskaya, No. 3, 121, 1960.

7. KUZ'MIN, A.I. and G.F. KRYMSKII. – Trudy YaFSO, AN SSSR, seriya fizicheskaya, No. 5 (in press).

8. FENTON, A.G., K.G. McCRACKEN, D.C. ROSE, and B.G. WILSON. – Can. J. Phys., **37**, 9, 1959.

9. KUZ'MIN, A.I., G.V. SHAFER, G.F. KRYMSKII, and Yu.G. SHAFER. – Geomagnetizm i aeronomiya, **1**, 510, 1961.

10. CHASSON, R. and K. MAEDA. – Trudy MKKL, **4**, 192, Izd. AN SSSR, 1960.

11. KUZ'MIN, A.I., G.F. KRYMSKII, G.V. SKRIPIN, N.P. CHIRKOV, G.V. SHAFER, and Yu.G. SHAFER. – Izv. AN SSSR, seriya fizicheskaya, **26**, 808, 1962.

N67 38220

N. P. Chirkov

IONIZATION-BURST VARIATIONS

Since December 1957 cosmic-ray recordings have been made at Tixie Bay using the ASK-2-34 ionization chamber. Ionization bursts are recorded simultaneously with the meson component, and altogether about 10,300 bursts ($\geqslant$1 scale division) were recorded during a 4-year period.

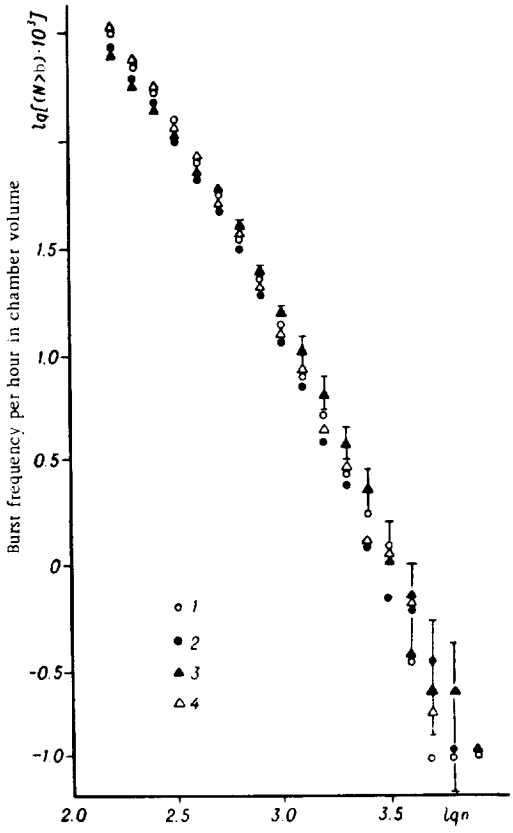

FIGURE 1. Integral spectrum of ionization bursts at Tixie Bay for 1958-1961.

1-1958; 2-1959; 3-1960; 4-1961.

The lapses in burst recording amounted to from 2 to 8% during certain months, and for the entire period considered they were about 1%. The large amount of material available enables us to consider variations in the number of bursts from year to year, during the course of a year, and even over shorter intervals, a type of study which, as far as we know, has hitherto not been made.

Figure 1 shows the integral number spectrum for bursts from 1958 to 1961. This spectrum is described by a power law of the form $N(\geqslant b) = Am^{-\gamma}$, where γ varies from 2.00 to 2.20 for bursts with numbers of particles in the range $440 < m < 3540$, m being the magnitude of the burst in the chamber (the number of relativistic particles). This result agrees with /1, 2/.

It is clear from Figure 1 that some variations in the number of bursts exist which go beyond the limits of statistical error. For example, in 1959 the number of bursts with $440 < m < 3540$ was 20 to 30% lower than in 1960 (and also lower than the number in 1958 and 1961). Moreover, the number of bursts in 1951 and 1955 (see Figure 1 in /1/) was also lower than in other years. Therefore, it seems that the 4-year rhythmic variation in the meson component, noted in /3/, also applies to the burst frequency.

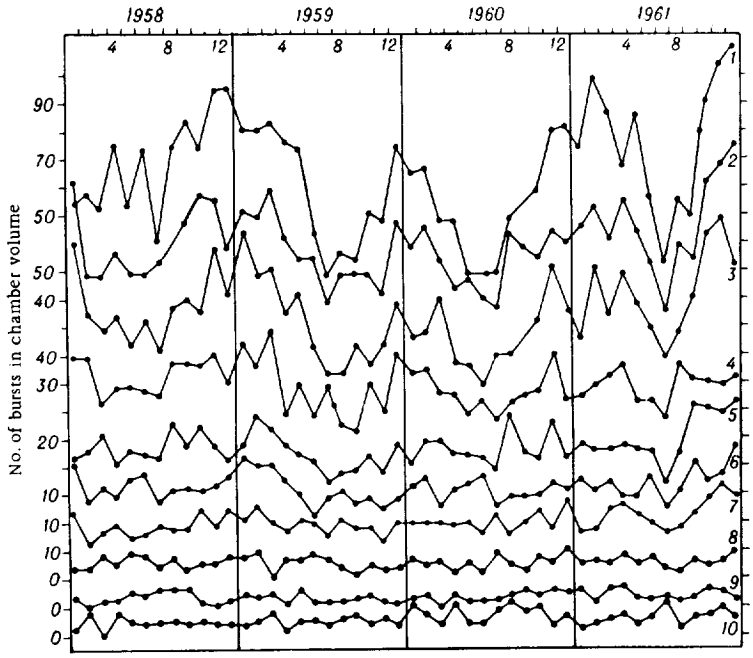

FIGURE 2. Monthly variations in burst number, according to groups in table.

To enable a more detailed consideration of the variations in burst number, we have plotted them in Figure 2 according to months. The data are divided into groups (see table) and normalized to the average month. The figure shows that the number of bursts with $m < 710$ is subject to seasonal variations.

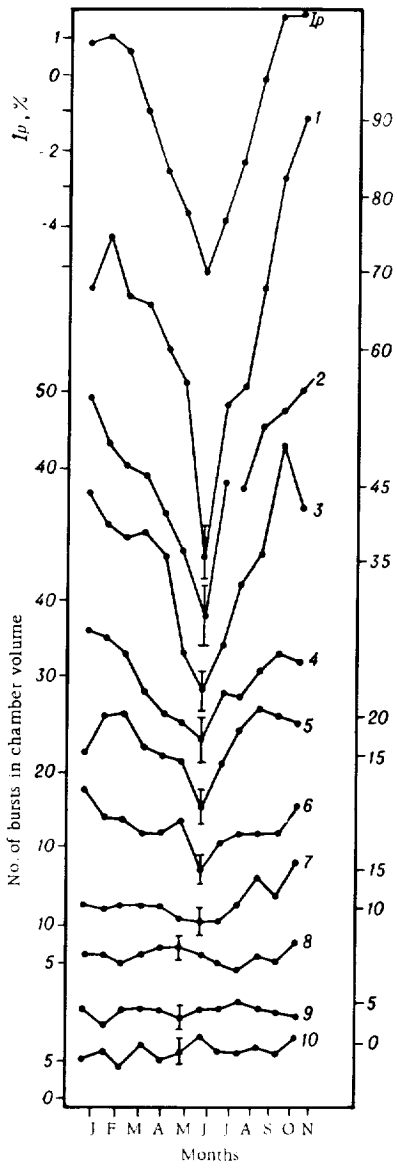

FIGURE 3. Average (over 4 years) variations of hard component (curve *Ip*) and number of bursts, according to groups (curves 1–10).

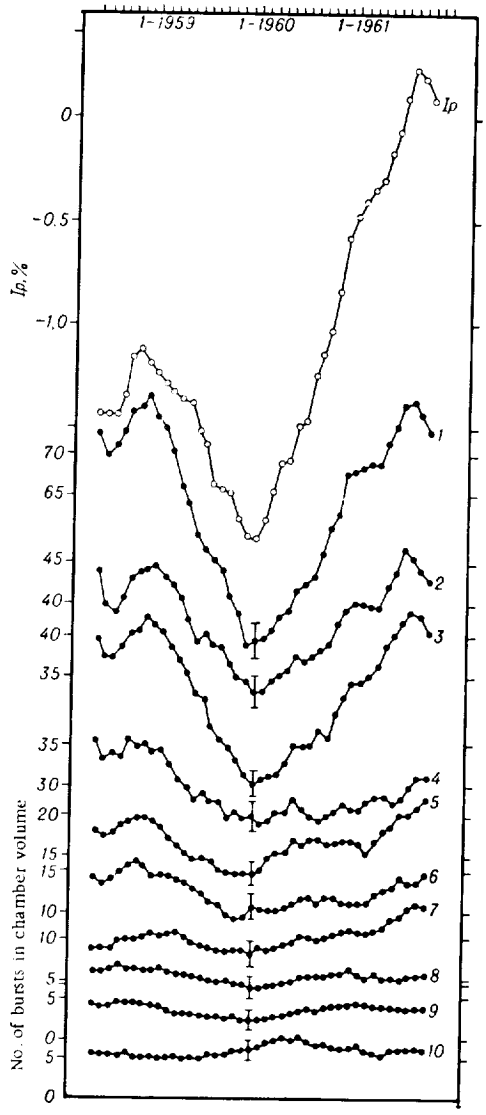

FIGURE 4. Secular variations in muon intensity (curve *Ip*) and number of bursts (curves 1–10).

The average seasonal variations in the burst number are shown in Figure 3. The amplitude of these variations is of the order of 35% for bursts with $m < 710$ particles. As curve *Ip* in the figure shows, during the course of a year, the hard μ-meson component varies only about 3% in amplitude at Tixie Bay. Estimates show that, by changing the slope of the

curve for the recordings of cosmic-ray intensity, it is possible to obtain a seasonal amplitude of the burst number which is not more than 5–10%.

Consequently, variations (during the course of a year) in the number of bursts with $m < 710$, with amplitudes of the order of 25%, apparently exist.

Moreover, as Figures 1, 2, and 4 show, there are also secular variations in the number of bursts. Figure 4 was obtained by moving-average smoothing of the data in Figure 2 for a 12-month interval, in order to eliminate the seasonal burst variations. The number of bursts with $m < 1110$ decreased by 40 to 50% from the end of 1958 till the end of 1959, and it increased by about the same amount up to the middle of 1961. These long-term variations in the burst number almost copy the variations in meson intensity (curve Ip in Figure 4), especially for small bursts.

In an attempt to explain the results obtained, we studied the variations in the number of bursts during the passage of cyclones. Since cyclones are very striking atmospheric phenomena, if any relation exists between bursts and the atmosphere, it should show up at the time of a cyclone.

Figure 5 shows the pressure-corrected variation δIp in the muon intensity at Tixie Bay, during the passage of cyclones at this location. Also shown are the theoretically calculated /4/ intensity variations δW_{200} (the radiosondes did not ascend to over 200 mb). There is a good fit between the two curves.

This figure also shows the variations in the number of bursts at this time. These do not match the variations in muon intensity, but they correlate very well with the temperature variations at the 100-mb level /5/, observed during passage of the cyclones through Yakutsk. The cyclones in question passed through Yakutsk and Tixie Bay at different times. Thus, the meteorological situation in the lower stratosphere when the cyclones hit Yakutsk and Tixie Bay must have been approximately identical. Moreover, the variations in the number of bursts at sea level must have been related to the temperature variations in the lower stratosphere.

If this is the case, then to explain the secular variations in the number of bursts analogous secular changes in the temperature of the upper layers of the atmosphere must be assumed. A preliminary analysis of the aerological material for Yakutsk for 1954–1961 confirms this. A quantitative evaluation will be possible only after further study of these subjects and the introduction of more comprehensive burst-observation data.

Curve numbers in Figures 2, 3, 4	1	2	3	4	5	6	7	8	9	10									
m in scale divisions	$\geqslant 1.0$ < 1.2	$\geqslant 1.2$ < 1.5	$\geqslant 1.5$ < 1.9	$\geqslant 1.9$ < 2.3	$\geqslant 2.3$ < 2.9	$\geqslant 2.9$ < 3.6	$\geqslant 3.6$ < 4.6	$\geqslant 4.6$ < 5.7	$\geqslant 5.7$ < 7.2	$\geqslant 7.2$ < 9.1	$\geqslant 9.1$ < 11.4	$\geqslant 11.4$ < 14.3	$\geqslant 14.3$ < 18.0	$\geqslant 18.0$ < 22.6	$\geqslant 22.6$ < 28.5	$\geqslant 28.5$ < 35.8	$\geqslant 35.8$ < 42.5	$\geqslant 42.5$
m in no. of relativistic particles	> 160 < 190	$\geqslant 190$ < 240	$\geqslant 240$ < 280	$\geqslant 280$ < 350	$\geqslant 350$ < 440	< 440 < 555	< 550 < 710	$\geqslant 710$ < 880	> 880 $\leqslant 1110$	$\geqslant 1110$ < 1410	> 1410 < 1770	> 1770 < 2230	> 2230 < 2810	> 2810 < 3540	> 3540 < 4460	> 4460 < 5620	> 5620 < 7070	$\geqslant 7070$	
$\lg m_{rel}$	2.2	2.3	2.4	2.5	2.6	2.7	2.8	2.9	3.0	3.1	3.2	3.3	3.4	3.5	3.6	3.7	3.8	3.9	
N for 1958–1961	10284	7314	5519	3933	2569	1703	1206	729	453	279	167	100	55	35	20	8	4	2	

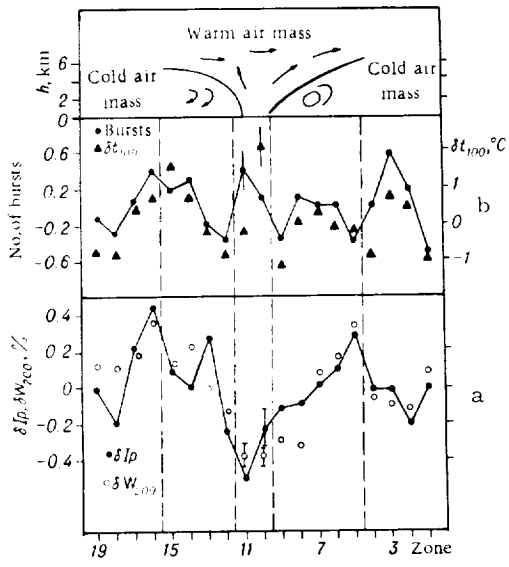

FIGURE 5. Variation of:

a-cosmic-ray intensity (experimental δIp and theoretical δW_{200}); b-number of bursts at Tixie Bay and temperature of 100-mb level (triangles) at Yakutsk during passage of cyclones.

In conclusion, I wish to thank A. I. Kuz'min and D. D. Krasil'nikov for their discussions of this report and M. Samusikova and M. Timofeev for their assistance in preparing it.

Institute of Space-Physics Research and Aeronomy,
Yakutsk Branch of Siberian Division of
USSR Academy of Sciences

REFERENCES

1. MONTGOMERY, C.G. and D.D. MONTGOMERY.— Phys. Rev., **47**, 429, 1935.

2. KRASIL'NIKOV, D.D.— Izv. AN SSSR, seriya fizicheskaya, **26**, 6, 1962.

3. CHIRKOV, N.P. Ritmy v vekovykh variatsiyakh intensivnosti kosmicheskikh luchei (Rhythmic Trends in the Secular Variations of Cosmic-Ray Intensity). See next report in this collection.

4. DORMAN, L.I. Variatsii kosmicheskikh luchei (Cosmic-Ray Variations), Chap. 5.— Gostekhizdat, 1957.

5. KUZ'MIN, A.I., A.A. DANILOV, and N.P. CHIRKOV.— Trudy YaFSO, AN SSSR, seriya fizicheskaya, No.5 (in press).

N67-38221

N. P. Chirkov

RHYTHMIC TRENDS IN THE SECULAR VARIATIONS OF COSMIC-RAY INTENSITY

Data from continuous recordings made from 1938 to 1946 at the stations of the Carnegie Institute were studied in /1/. The author of this work concluded that cosmic-ray intensity variations exist which have periods of 2 or 3 years. Geomagnetic phenomena are also subject to variations with such a period /2/, and the nature of these variations is still obscure. An irregular annual variation with an amplitude of about 0.5% was also found in /1/, and it correlated well with the annual variation of the *C* index.

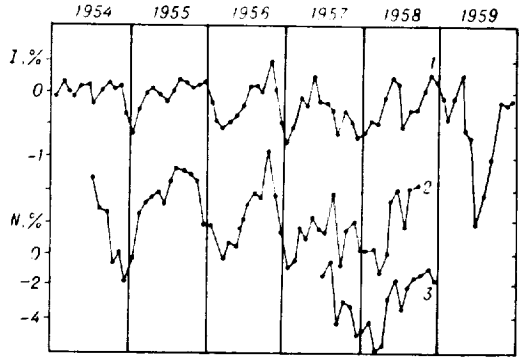

FIGURE 1. Variations of the hard cosmic-ray component at Yakutsk (1), and the neutron components at Washington (2) and Wellington (3). The variations are corrected for the secular change.

For several years, continuous recording of the hard cosmic-ray component has been carried out at Yakutsk. Some results of an analysis of these data were presented in /3/. In particular, the effects of the atmosphere were taken into account systematically in this study, which made it possible to distinguish the variations concurrent with variations in the neutron component (these being variations of world-wide character).

When these data are corrected for the secular variations (by subtracting the data averaged for 24 successive months, using the method of moving averages), the curve in Figure 1 is obtained. This curve shows quite clearly the annual irregular variations in the meson intensity. The actuality of these variations is confirmed by the fact that they also show up in the neutron component, in both the Northern and Southern Hemispheres, with amplitudes up to 2% (Figure 1, curves 2 and 3). In order to verify

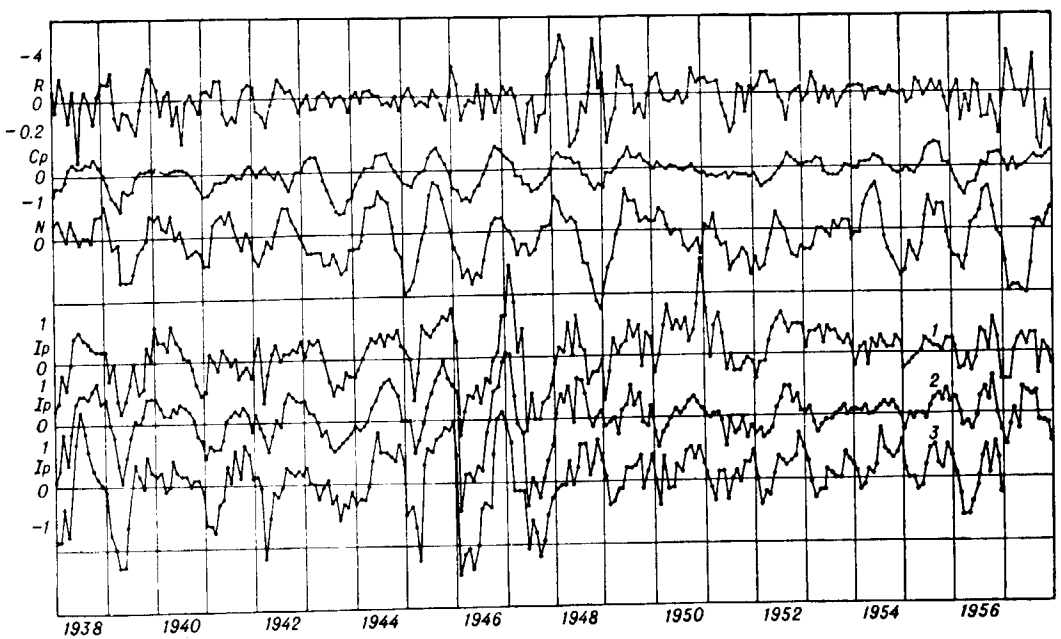

FIGURE 2. Variations of relative sunspot number R; geomagnetic-activity index Cp; number of geomagnetic storms N; and cosmic-ray intensity. Data refer to stations at Cheltenham (1), Huancayo (2), and Christchurch (3) and are corrected for the secular variation.

this result, and to check for a possible change in the character of the annual variations, we made a study of the data from stations of the Carnegie Institute (Cheltenham, Huancayo, Christchurch), compiled over a 20-year period /4/. The results are shown in Figure 2. The data were corrected for the secular variations, using the method described above. The figure also gives the variations in the relative sunspot number R /4/, the geomagnetic-activity index Cp /5/, and the number of heavy and moderate magnetic storms N /2, 6/. The data for the number of storms N and the magnetic activity Cp were first smoothed (by moving averages) over a six-month interval.

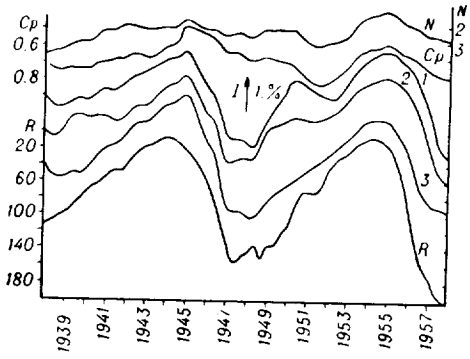

FIGURE 3. Secular variations of total number of magnetic storms N; geomagnetic-activity index Cp; cosmic-ray intensity at Cheltenham (1), Huancayo (2), and Christchurch (3); and relative sunspot number R.

As Figure 3 shows, moving-average smoothing of the data over a 24-month period (R was smoothed over only 12 months) eliminates quite successfully variations with periods less than 11 years. The data on the cosmic-ray intensity used here was corrected for seasonal atmospheric changes. From Figure 2 it is evident that there are annual variations in the cosmic-ray intensity, with a minimum at the beginning of the year and a maximum half way through the year. The variation amplitude is $\leqslant 1\%$. These variations can be followed over the 20 years of operation of the stations. However, during certain years (for example, 1939, 1943, 1947, and 1951), this regularity is disturbed and a deep intensity minimum is observed for some months. It seemed to us that this trend is also regular, and so we averaged all the data for observations within a four-year period. The average curves obtained are shown in Figure 4, along with the average variations of the number of storms N, the geomagnetic activity Cp, and the relative sunspot number R (as in Figures 2 and 3, the curves for Cp, N, and R are reversed to make the analysis more convenient). A close inverse correlation is observed between the changes in the intensity I and the variations in Cp and N. A four-yearly rhythmic trend in the variations of cosmic-ray intensity is observed, which is made up of two annual fluctuations (amplitudes of 0.3 to 0.5%) and one fluctuation with a period of 1.5 to 2 years (amplitude about 0.5%). This same trend is observed in the geomagnetic activity and in the variations of the number of magnetic storms.

The fact that annual variations in the relative sunspot number R are obtained is very interesting. For the first two years of the rhythmic trend the correlation of R with Cp and N is direct and the correlation of R with I is inverse. Then, during the next two years the opposite is true. This explains the conclusion in /1/ that there is no correlation between the annual variations of R and I, while between I and Cp there is a marked inverse correlation. The author of /1/ smoothed the values of R by the method of moving averages over a 12-month period, so that all the annual variations were eliminated.

Consequently, it seems to us that the solar activity varies with a period of about four years, if it is represented in terms of the number of magnetic storms registered at the earth. The orientation of the earth in space and its magnetism /7/ may have some influence on the variations of Cp and in part on the number of magnetic storms. If this is the case, then it is apparently possible to describe the obtained cosmic-ray variations only by assuming for them an extraterrestrial origin of a modulation nature. However, if it is assumed that the observed variations of I are of atmospheric origin, and that (as stated in /8/) the annual temperature fluctuations in the upper layers of the atmosphere are of the order of 30–50° C, while the temperature-coefficient density is about 0.01% per degree centigrade /9/, then annual intensity fluctuations of around 0.3 to 0.5% can be expected, that is, fluctuations with the amplitude and phase found in this study.

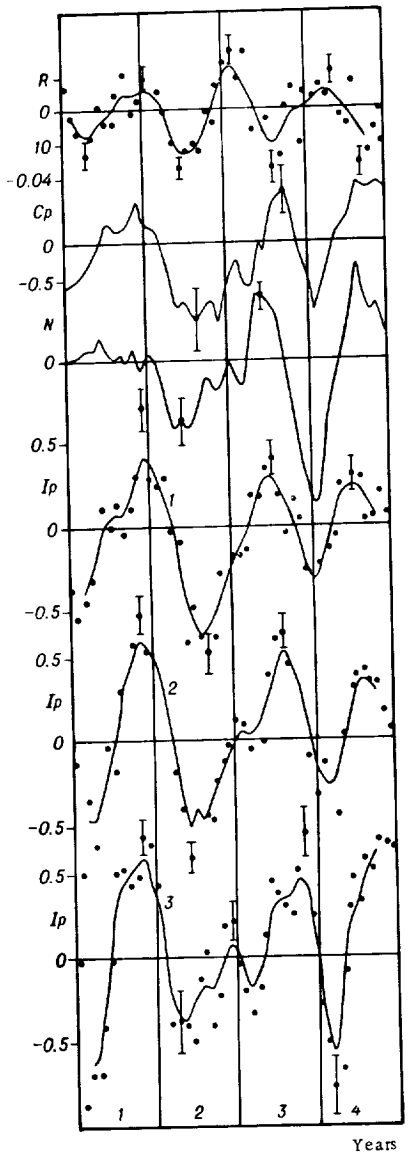

FIGURE 4. Average variations of: relative sunspot number R; geomagnetic-activity index Cp; number of magnetic storms N; and cosmic-ray intensity at Cheltenham (1), Huancayo (2), and Christchurch (3). Solid curves indicate data for R and I smoothed according to formula $(a + 2b + 4c + 2d + e)/10$.

On the other hand, to ensure annual variations in the neutron component, we must assume annual temperature fluctuations in the stratosphere of the order of several hundred degrees, which is quite improbable. It is possible, however, that our allowance for the contribution of the atmosphere to the neutron-component variations was not completely correct, and that the picture of the interaction and the travel of particles to the detector must be revised. The thing is, though, that the intensity decreases at the end of 1954, 1955, 1956, and 1957 are definitely stormlike in character. During this period very pronounced Forbush decreases in I, which were world-wide in character, were observed, and there was an overall drop in the galactic intensity of cosmic rays.

The 4-year rhythmic trend found above for the cosmic-ray intensity variations is confirmed by the data for 1958 to 1961. The large intensity decrease expected for 1959 was actually observed. These sizable drops in the galactic cosmic-ray intensity are

proportional to the level of solar activity. For example, in 1955 the decrease in I was small, whereas in 1947 it was large (> 3%). The next considerable drop in I should occur in 1963, and for the meson intensity it should amount to about 1.0 to 1.5%.*

In conclusion I wish to thank A. I. Kuz'min, G. F. Krymskii, and V. D. Sokolov for their discussions of this report and M. I. Timofeev for his assistance in preparing it.

Institute of Space-Physics Research and Aeronomy,
Yakutsk Branch of Siberian Division of
USSR Academy of Sciences

REFERENCES

1. GLOKOVA, E.S.— Izv. AN SSSR, seriya fizicheskaya, **20**, 47, 1956.

2. AFANAS'EVA, V.I. (editor). Spravochnik po peremennomu magnitnomu polyu SSSR (Handbook on the Variable Magnetic Field of the USSR).— Gidrometeoizdat, 1954.

3. CHIRKOV, N.P., V.A. FILIPPOV, and G.V. SHAFER.— Trudy YaFSO, AN SSSR, seriya fizicheskaya, No.4, pp.122-131, 1961.

4. FORBUSH, S.E.— J. Geophys. Res., 63, 651, 1958.

5. BARTELS, J., A. ROMANA, and J. VELDKAMP.— Geomagnetic Data 1957, Indexes K and C, Rapid Variations, Amsterdam, 1961.

6. Sbornik: Kosmicheskie dannye za 1948-1959 gg. (Collection: Space Data for 1948–1959).— Nauchno-issledovatel'skii institut zemnogo magnetizma, ionosfery i rasprostraneniya radiovoln.

7. AFANAS'EVA, V.I. and Yu.D. KALININ.— Geomagnitnye vozmushcheniya, No.4, pp.5–13, Izd. AN SSSR, 1960.

8. KUZ'MIN, A.I., P.A. KRIVOSHAPKIN, G.F. KRYMSKII, and G.V. SKRIPIN. Izuchenie kolebanii temperatury verkhnei atmosfery po dannym podzemnykh izmerenii kosmicheskikh luchei (A Study of Temperature Fluctuations of the Upper Atmosphere, According to Data of Underground Cosmic-Ray Measurements). Report in this collection.

9. DORMAN, L.I. Variatsii kosmicheskikh luchei (Cosmic-Ray Variations), p.135.— Gostekhizdat, 1957.

* Proofreading note: the decrease in I expected for 1963 was actually observed and was ~ 1% according to the data of the ASK–1 chamber at Yakutsk. These data were corrected for atmospheric pressure and temperature.

N67-30222

D. D. Krasil'nikov

CORRELATION OF THE FREQUENCY OF LARGE IONIZATION BURSTS WITH THE 11-YEAR SOLAR-ACTIVITY CYCLE

Large ionization bursts are observed in the chambers during continuous recordings of the intensity variations of the hard cosmic-ray component. An analysis of the burst frequency reveals unexpectedly large frequency variations (of the order of 20–30% at sea level and up to ~ 100% at mountain heights) which correlate with the 11-year cycle of solar activity. It is difficult to explain these variations in terms of systematic measurement errors, and, whatever their interpretation, they are of great interest. This report will present the observed facts and will discuss them briefly.

1. The ionization bursts were observed in an ASK-1-26 chamber /1/ and a C-type chamber /2/. The former was mounted near sea level (at Yakutsk, 100 m above sea level), and the latter was at mountain height (at Huancayo, 3350 m above sea level).

The data selected for consideration were from burst observations for 1937–1946 using the C chamber /3–5/ and for 1954–1960 using the ASK-1-26 chamber. These data were chosen from several similar sets of observations for the following reason: they were obtained under constant chamber-operation conditions over long periods, representing on the whole two cycles of solar activity. The average yearly values of the Wolf number /6/ were taken as the solar-activity characteristics.

Data on long-period variations of the hard-component intensity (according to the total ionization, with the exception of bursts) were taken from /7–9/.

The bursts considered here were produced either by μ mesons or by nuclear-active particles with energies from 10^{11} to 10^{12} eV /10/. The burst energy released immediately within the chambers in the form of ionization was from 10^9 to $3 \cdot 10^{10}$ eV.

Figure 1 shows a comparison of the average yearly Wolf numbers W for 1936–1960 with the hard-component variations $\delta I_\mu / I_\mu$ for 1937–1960 and with the frequency of bursts with different magnitudes m for 1941–1946 (Huancayo) and 1954–1960 (Yakutsk). The burst magnitude m is given in scale divisions of the chamber electrometer. One scale division corresponds to 650 cascade particles in lead for the C chamber and 2850 such particles for the ASK-1-26 chamber, or to a simultaneous passage through the chamber of 270 and 1200 relativistic particles, respectively /10/.

The observed frequencies of the bursts of all magnitudes considered are evidently subject to very abrupt systematic fluctuations, which have a negative correlation with the 11-year solar cycle. At Huancayo the variation data showed a tendency to lead. The amplitude of the frequency

variations for bursts of different magnitudes fluctuates within limits from 15 to ~50%, at both Huancayo and Yakutsk. It should be noted that this result pertains to data of burst observations at Huancayo which do not include the solar-activity maximum.

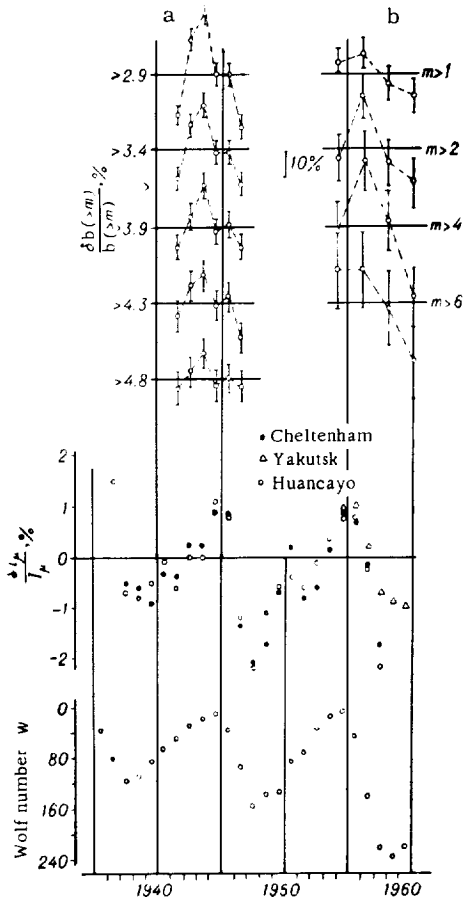

FIGURE 1. 11-year variations of Wolf number W, hard-component intensity $\delta I_\mu / I_\mu$, and frequency of large bursts (m is burst magnitude in electrometer scale divisions).

a–Huancayo (Carnegie model-C chamber); b–Yakutsk (ASK-1-26 chamber).

The average burst spectra for measurements during years of maximum, intermediate, and minimum solar activity at Huancayo have even sharper variations. These spectra are plotted in Figure 2, according to the data of /3-5/. A comparison of the spectra shows that at Huancayo the burst frequency during years of minimum solar activity is twice as great as during years of maximum activity, while for Cheltenham (not shown in the figure) it is ~30% greater. The spectra for periods of intermediate activity lie somewhere between those for years of maximum and minimum.

Let us now consider briefly whether the indicated variations in burst frequency can be explained in terms of statistical errors.

2. The existence of variations in cosmic-ray intensity related to the 11-year solar cycle manifests itself in the form of corresponding variations in the slope ΔI of the photorecording curves (deviations of the total cosmic-ray ionization from the average value).

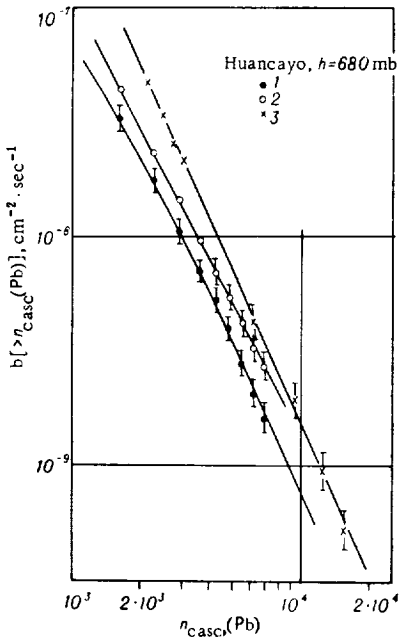

FIGURE 2. Integral burst spectra at Huancayo, for measurements at different periods of solar activity.

1-data of /4/; 2-data of /5/; 3-data of /3/; $n_{casc}(Pb) = l\left(\frac{E_0}{\beta}\right) \cdot \frac{E_0}{\beta}$; $\beta = 6.4 \cdot 10^4$ eV; $l\left(\frac{E_0}{\beta}\right)$ is almost constant, of the order of 0.07; E_0 is energy of cascade shower.

The author examined the technique for reading the photorecordings of bursts in such chambers. This examination showed that the errors in evaluating the burst magnitude are usually about 0.1 electrometer scale divisions. The maximum absolute value of the errors does not exceed 0.4 scale divisions. Moreover, and this is especially important, it was found that the indicated errors correlate with the slope ΔI of the photorecording curve for the total ionization in the chambers. Let us express in electrometer scale divisions both the burst magnitude m and the deviation ΔI of the total cosmic-ray ionization from the mean compensated value. Then, the spurious variations in burst frequency for these chambers can be represented approximately by the formula:

$$\frac{\Delta b(>m)}{b(>m)} \cdot 100 \simeq 0.4 \cdot \Delta I\%.$$

Thus, spurious 11-year variations in burst frequency are possible. Let us now estimate the magnitude of such variations.

The fluctuations ΔI caused by variations in the hard component during the solar-activity cycle have about the same amplitude ($\sim 3\%$) for both sea level and mountain altitudes (see Figure 1). This corresponds to differences ΔI of 14 (Huancayo) and 18 (Yakutsk) electrometer scale divisions. Consequently, an 11-year variation in hard-component intensity of $100\,\delta I_\mu / I_\mu \simeq 3\%$ may be accompanied by spurious burst-frequency variations of only around 6 or 7% at Huancayo and Yakutsk. Taking into account the additional effect of the systematic drift of ΔI at Huancayo /9/ does not change the situation essentially, either: the probable range of spurious variations in burst frequency at Huancayo just increases to 14% instead of 6%.

The obtained discrepancies between the observed and spurious (predicted) 11-year variations in burst frequency cannot be eliminated by assuming any reasonable stronger dependence on ΔI of the errors in the burst evaluation. For instance, to eliminate the differences of the spectra for Huancayo (Figure 2), simultaneously over the whole spectrum errors correlating

with ΔI would have to be made in evaluating the burst magnitudes. Moreover, these errors would have to be many (~ 10) times greater than the maximum absolute errors observed in other analogous cases (see above). The relative errors in the burst magnitude would have to be constant over the entire spectrum and equal to 0.4 times their true value, which is impossible in a range of burst magnitudes measured in tens of electrometer scale divisions.

The suspicion that errors were made in matching the spectra of the different authors (Figure 2) is removed by the fact that analogous spectra of these same authors for Cheltenham (near sea level) agree to within limits of $\sim 30\%$.

Taking into account possible variations in the average yearly values of the atmospheric pressure at the observation point, even assuming that all bursts are produced by nuclear-active particles (absorption length $\lambda \simeq 120$ to $130\,g/cm^3$), does not eliminate to any extent the observed differences between the spectra in Figure 2, either: to do this, variations in burst frequency of the order of $\lesssim 10\%$ would have to take place.

Consequently, a considerable part of the observed burst-frequency variations (especially at Huancayo) which correlate with the 11-year solar cycle are probably real. At present, however, it is not clear how they can be made to agree with the other experimental results and with existing ideas concerning cosmic-ray variations. In particular, the burst-frequency variations are, unexpectedly, sharper than the corresponding variations in the μ-meson energy range (10^9–10^{10} eV) /8, 9, 12/.

3. The result obtained here is somewhat strange and requires further verification. In addition, it would be generally advisable to give special attention to the energy range from 10^{11} to 10^{13} eV, which has remained almost unstudied from the point of view of time variations. These energies are interesting in that particles in this range are affected by the conditions of cosmic-ray diffusion in the part of the galaxy immediately adjacent to the solar system. For this type of research, the continuous observation of the frequency of large ionization bursts is in some respects (better energy discrimination, the absence of a background, relatively low cost) more convenient and more preferable than μ-meson detection deep underground.

The variations in the frequency of large ionization bursts may indicate: (1) the characteristics of the modulation mechanism of the 11-year variations for energies above $\sim 10^{11}$ eV; or (2) the participation in cosmic-ray phenomena, for energies $\gtrsim 10^{10}$ eV, of as yet unknown particles and interaction processes, related to the dissipation of about 10^9 to 10^{10} eV of energy by means of ionization over a path of about a radiation length.

The strong dependence of the burst frequency on the period of observation also implies that, with respect to measurement techniques, the compared burst spectra and their altitude dependences can be obtained with satisfactory accuracy only via measurements using the chambers considered for just the same observation period.

To S. I. Nikol'skii and B. B. Dotsenko I offer deep thanks for their discussions of the results.

Institute of Space-Physics Research and Aeronomy,
Yakutsk Branch of Siberian Division of
USSR Academy of Sciences

REFERENCES

1. SHAFER, Yu.G.— Trudy YaFSO, AN SSSR, seriya fizicheskaya, No. 2, 7. 1958.
2. COMPTON, A.H., E.O. WOLLAN, and R. D. BENNETT.— Rev. Sci. Instr., **5**, 415. 1934.
3. LANGE, I. and S.E. FORBUSH.— Carnegie Institute of Washington, Publication 175. 1948.
4. SCHEIN, M. and P. GILL. – Rev. Mod. Phys., **11**, 207. 1939.
5. LAPP, R.— Phys. Rev., **69**, 321. 1946.
6. Mesyachnye kosmicheskie dannye (Monthly Space Data).— Moskva, Institut zemnogo magnetizma, ionosfery i rasprostraneniya radiovoln Akademii nauk SSSR. 1960.
7. GLOKOVA, E.S.— Trudy Nauchno-issledovatel'kogo instituta zemnogo magnetizma, **8**, 59. 1952.
8. CHIRKOV, N.P., V.A. FILIPPOV, and G.V.SHAFER.— Trudy YaFSO, AN SSSR, seriya fizicheskaya, No.4. 1962.
9. FORBUSH, S.E. Cosmic-Ray Intensity Variations During Two Solar Cycles. —Department of Terrestrial Magnetism, Carnegie Institute of Washington, D.C., 15. 1958.
10. KRASIL'NIKOV, D.D.— Sbornik: "Kosmicheskie luchi," No.3, p.215, Moskva, Izd. AN SSSR. 1961.
11. KRASIL'NIKOV, D.D.— Izv. AN SSSR, seriya fizicheskaya, **26**, 818. 1962.
12. DORMAN, L.I. Variatsii kosmicheskikh luchei (Cosmic-Ray Variations).— Moskva, Gostekhizdat. 1957.

N67-38223

E.F. Vershinin and E.A. Ponomarev

OBSERVATIONS OF THE ULTRALOW-FREQUENCY (ULF) RADIATION OF POLAR AURORAE

Close correlation with disturbances of the geomagnetic field is a characteristic feature of the ULF radiation of polar aurorae. Bursts of ULF radiation of this type at frequencies above 4 kc are closely synchronized with variations in the optical radiation of polar aurorae, observed either visually or with an electrophotometer /1, 2/.

Regular observations of the ULF radiation were made during the IGY, according to a special program employing equipment designed to receive whistler atmospherics. Several possible mechanisms of ULF-radiation generation were suggested by different investigators to explain the observation results.

Ellis /3/ assumed that the auroral radiation at 4–5 kc is caused by the Čerenkov effect. Gallet and Helliwell /4/ suggested a mechanism based on an analogy with a traveling-wave tube. The authors of /5/ considered the radiation at about 800 cps to be radiation with the frequency of proton gyroresonance at the corresponding level of the ionosphere. However, the ULF radiation in this part of the range does not correlate with the polar aurorae.

It is noteworthy that the mechanisms suggested make it possible to explain only some of the frequency regularities in the ULF-radiation spectra.

The ULF radiation was picked up and recorded at Tixie Bay using a setup designed by us. The signal was received by an antenna which formed a horizontal ring 40 meters (104 turns) in diameter, made of lead-coated cable. The signal was sent from the antenna through filters which cut out the interference beyond the operating range of the equipment (820–14,000 cps). The signal was next fed through a wide-band amplifier with a gain of $\approx 10^5$. Then, after an attenuator and another filter, the ULF signal was fed to narrow-band active RC filters. From the filter output through a step selector, the signal was fed to an oscillograph, whose screen was photographed together with a time marker. Then the signal was fed to a balance circuit with a steady line-noise component, at the output of which an N-370 M recorder was connected. The circuit of the automatic equipment made it possible to observe on the oscillograph, to photograph, and to record on the N-370 M recorder, a signal from any of nine channels, and also to obtain the amplitude-frequency characteristics. The setup also made it possible to hear the ULF radiation over a loudspeaker. Observations of the radio emission (mainly at $c = 11$ kc) were made from 1 March to the middle of May 1962, and recordings on the automatic recorder were made from 17 March until May 1962.

To record rapid variations in the visible luminosity of polar aurorae, for wavelengths from 3000 to 6000 Å, we used a setup incorporating an electrophotometer circuit. A photometer with an FEU-19 M photomultiplier, having a viewing angle of about 120° in the vertical plane and 90° in the horizontal plane, was mounted in the plane of the meridian at an angle of 70° to the northern horizon. The response of the FEU unit is about 100^a/lumen. The signal from the FEU unit was fed through a dividing condenser to a 28 IM wide-band amplifier and recorded by an EPP-09 electronic recording potentiometer. Observations were made using this equipment from 23 March to 2 April.

RESULTS OF THF OBSERVATIONS

Some typical recordings of ULF signals, at a frequency of 11 kc, are shown in Figure 1. The calibration was made using an audio oscillator.

The period of observation from 17 March to 2 April was selected for data processing. For this study, the maximum signal level was recorded at 15-minute intervals. Data from visual observations and from electrophotometer observations of the whole sky were used, as well as data from vertical radiosonde observations of the ionosphere and data on the variation of the horizontal geomagnetic-field component. For comparison purposes, the data for each night and day were plotted on a single graph. The results for 2 different observation days are shown in Figure 2. Photos of typical ULF signals observed on an oscillograph for 11 and 14 kc, respectively, are shown in Figures 3a and 3b.

A ULF signal was recorded during 147 out of 231 hours of observations at 11 kc. The relation of the ULF radiation to the polar aurorae, and to the state of the magnetic field and the ionosphere, will be evident from the following comparisons. During the entire observation period, aurorae were recorded visually during 71 hours, and a ULF signal was recorded during 65 of these, giving 91.6% concurrence. In 8.4% of the cases no signal was recorded at the time of the aurorae, and all these cases occurred at moments of total ionospheric absorption. A disturbance of the horizontal component of the geomagnetic field was observed for 79 hours, and ULF radiation for 73 of these (92.4% concurrence). According to the data of an ionospheric station, an E_s layer was noted for 52 hours, and during all 52 hours a ULF signal was recorded.

The figures cited indicate a close correlation between visually observed polar aurorae, disturbances of the geomagnetic field, the appearance of an E_s layer, and ULF radiation. When recordings of the radio emission are compared with electrophotometer recordings for the whole sky, it turns out that in an overwhelming majority of cases the signal maximum coincides with the maximum luminous flux from the polar aurorae. In the event of total ionospheric absorption of the radiosonde observations, a ULF signal was recorded only during large disturbances of the magnetic field, the signal amplitude in this case being low.

Of five 24-hour observations, four had a daytime signal and only one did not. At this time there was total ionospheric absorption. There is reason to believe that a signal recorded in the daytime is related to polar

aurorae on the night side of the earth. This is verified by the fact that in the daytime we picked up, on a loudspeaker connected to the antenna through an amplifier with $k \approx 1000$, a Canadian radio station broadcasting in the telegraphic range.

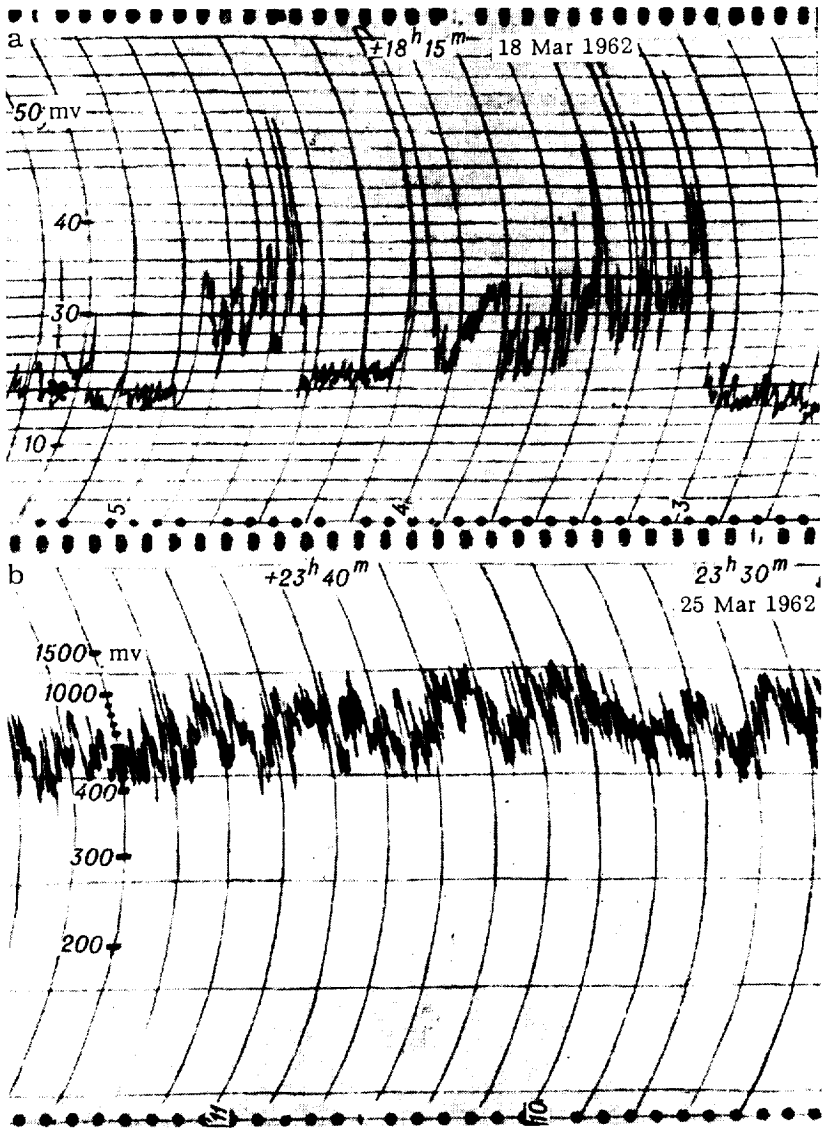

FIGURE 1. Recordings of ULF signals at 11 kc. Signal amplitude at antenna output is indicated in microvolts.

During the observations, short-term signal recordings were made periodically on all the channels. It was noted that during uniform and

pulsating aurorae there was ULF radiation at all frequencies, and that for specific forms of aurorae, as was pointed out in /6/, there is no radiation maximum at any frequency. Some shift in frequency with time was observed.

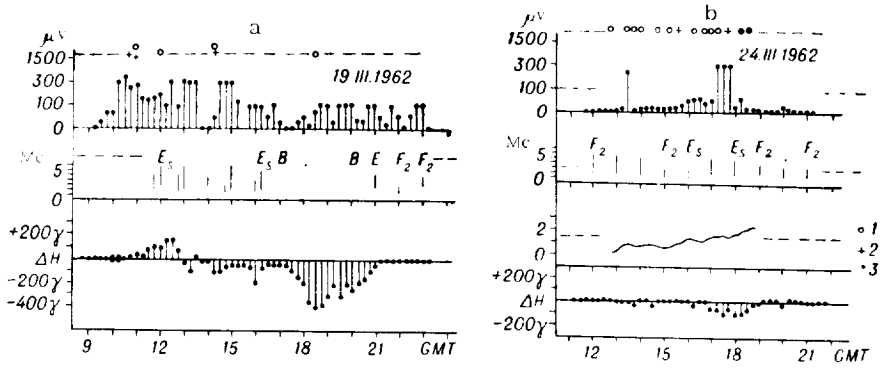

FIGURE 2. Comparison of observation results:

1–homogeneous forms of polar aurorae; 2–radiative forms; 3–pulsating forms. Dashed lines indicate periods during which there were no observations.

In the evening the signal amplitude was higher at low frequencies, whereas after midnight it was higher at high frequencies. The signal bursts at all frequencies were usually short-lived (≤ 2 seconds), but there were cases

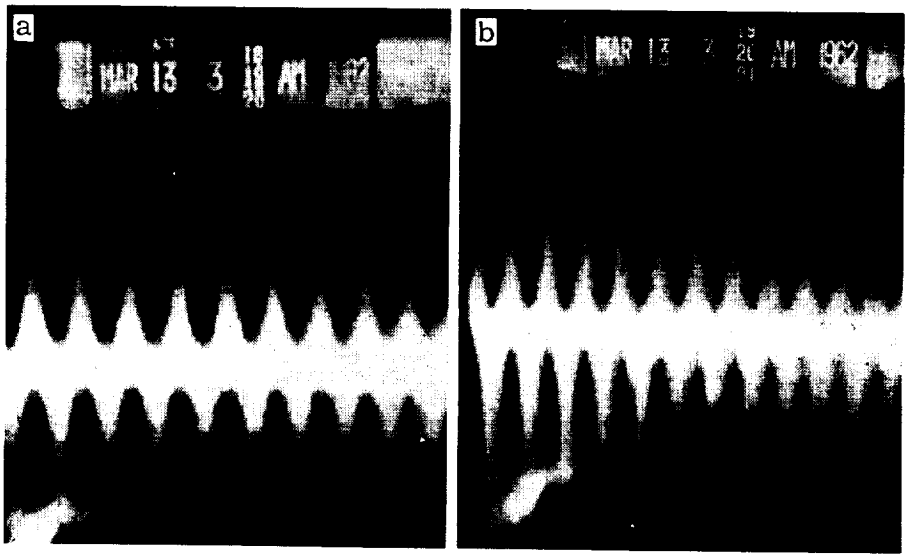

FIGURE 3

in which the signal remained at maximum amplitude for some minutes. The maximum signal amplitude recorded at the antenna output in the 11-kc range

was 1500 μv. This corresponds to a field strength at the earth's surface of $\approx 600\mu$v/m, according to the formula

$$\varepsilon = 2\pi EN \frac{A}{\lambda} \cos\vartheta,$$

which takes into account roughly the influence of the earth on the directivity diagram of the antenna.

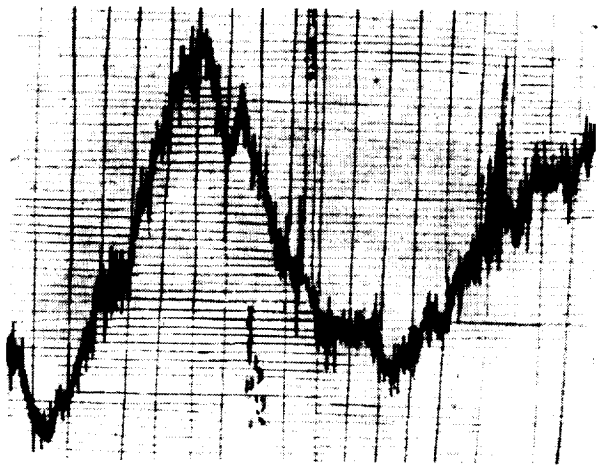

FIGURE 4

Due to the small amount of observational material available from recordings of rapid variations of the optical auroral radiation, no quantitative conclusions can be drawn. It is only possible to remark that the envelope of the modulated optical radiation at 400 cps is the same as the envelope of the ULF radiation (see, for example, Figure 2b). Rapid variations in the optical radiation were observed in a range from 200 to 1700 cps. The maximum was somewhere between 400 and 600 cps. No regularities in the shift of the maximum were observed. A typical recording at 400 cps is shown in Figure 4. The bursts of modulated optical radiation at the indicated frequencies are synchronized with the bursts of ULF radiation, although they often lead the latter by 1 or 2 minutes.

THE INTERACTION OF ULF WAVES WITH THE IONOSPHERE

An important particular case of the propagation of plane monochromatic ULF waves in the ionosphere is the propagation of longitudinal waves ($\vec{k} \parallel \vec{H}^\circ$), where $\vec{H}^\circ$ is the intensity vector of the geomagnetic field. The

longitudinal electrical conductivity in a plasma for the frequencies in question is very high compared to the transverse conductivity. Therefore, let us now consider the case of longitudinal propagation.

The damping of a wave is determined by the imaginary part of the wave vector $\vec{k}$ and by the absorption coefficient $\varkappa$:

$$k^2 = \frac{\omega^2}{c^2}(n - i\varkappa)^2 = \frac{\omega^2}{c^2}(\varepsilon_{xx} + i\varepsilon_{xy}), \tag{1}$$

where ω is the frequency of a monochromatic wave; n is the index of refraction; and ε_{xx} and ε_{xy} are components of the permittivity tensor.

At ultralow frequencies $\omega_n \gg \omega \gg \Omega_n$, where ω_n and Ω_n are the gyrofrequencies of electrons and ions respectively. Thus,

$$\varepsilon_{xx} \pm i\varepsilon_{xy} = 1 - \left(\frac{\omega_0}{\omega}\right)^2 \frac{\omega}{(\pm\omega_n - i\nu_{\text{eff}})}, \tag{2}$$

where $\nu_{\text{eff}} = \nu_{ei} + \nu_{em}$ is the frequency of collision of electrons with molecules and ions. From (1) and (2) it follows that the index of refraction and the absorption coefficient are:

$$n_\pm = \frac{\sqrt{\varepsilon_{xx\pm} + \sqrt{\varepsilon_{xx\pm}^2 + \varepsilon_{xy\pm}^2}}}{\sqrt{2}}; \tag{3}$$

$$\varkappa_\pm = \frac{\varepsilon_{xy\pm}}{\sqrt{2}\sqrt{\varepsilon_{xx\pm} + \sqrt{\varepsilon_{xx\pm}^2 + \varepsilon_{xy\pm}^2}}}, \tag{4}$$

while the group velocity for moderate absorption is

$$V_{\text{gr}} \approx \frac{2c\sqrt{\varepsilon_{xx}}}{1 + \varepsilon_{xx}}.$$

TABLE 1

z, km	N_e	N_m	N_e/N_m	ν_{eff}	V_{gr}, cm/sec
60	8	$8\cdot10^{15}$	10^{-15}	$4.7\cdot10^{7}$	—
70	10^2	$2.5\cdot10^{15}$	$4\cdot10^{-14}$	$1.4\cdot10^{7}$	—
80	$2\cdot10^3$	$5\cdot10^{14}$	$4\cdot10^{-12}$	$1.7\cdot10^{6}$	0.713
90	$3\cdot10^4$	$2\cdot10^{14}$	$1.5\cdot10^{-10}$	$7.6\cdot10^{5}$	0.576
100	10^5	$3.7\cdot10^{14}$	$2.7\cdot10^{-9}$	$1.7\cdot10^{5}$	0.325
110	$1.6\cdot10^5$	$9\cdot10^{13}$	$1.67\cdot10^{-8}$	$5.1\cdot10^{4}$	0.263
120	$1.2\cdot10^5$	$3\cdot10^{13}$	$4\cdot10^{-8}$	$1.8\cdot10^{4}$	0.290
130	$1.3\cdot10^5$	$8\cdot10^{12}$	$1.62\cdot10^{-7}$	$4.8\cdot10^{3}$	0.282
150	$1.5\cdot10^5$	$6\cdot10^{11}$	$2.5\cdot10^{-7}$	$3.4\cdot10^{3}$	0.263
200	$5.0\cdot10^5$	$5.0\cdot10^{11}$	10^{-5}	$1.6\cdot10^{3}$	0.145
300	$1.8\cdot10^6$	$3\cdot10^{10}$	$6\cdot10^{-4}$	$2.7\cdot10^{2}$	0.0755
400	$1.5\cdot10^6$	$5\cdot10^{9}$	$3\cdot10^{-3}$	$1.4\cdot10^{2}$	0.0843
500	$1.1\cdot10^6$	$5\cdot10^{8}$	$2.2\cdot10^{-2}$	$7.5\cdot10^{2}$	0.098
600	$7.5\cdot10^5$	$2\cdot10^{7}$	$3.75\cdot10^{-2}$	$4.2\cdot10^{2}$	0.118
700	$5.0\cdot10^5$	$6\cdot10^{6}$	$8.33\cdot10^{-2}$	$2.2\cdot10^{2}$	0.145
800	$3.7\cdot10^5$	$2\cdot10^{6}$	0.185	140	0.168
900	$2.5\cdot10^5$	10^{6}	0.250	83	0.204
1000	$1.3\cdot10^5$	$4\cdot10^{5}$	0.325	41	0.282

When the field strength at the earth's surface is known from experiment, it is easy to find its value at any level of a specific model of the ionosphere.

We chose a model which represented satisfactorily the properties of the polar ionosphere (Table 1) /7/.

TABLE 2

z, km	E, μv/cm	E/E_p
60	8	—
70	10.8	—
80	19.8	—
90	22.2	—
100	40.5	10^{-2}
110	44.7	$4.44 \cdot 10^{-2}$
120	73.2	0.112
130	111	0.189
150	165	0.249
200	200	0.244
300	444	0.447
400	600	0.602
500	665	0.663
600	732	0.730
700	750	0.753
800	—	0.753

Table 2 lists the field strengths in μv/cm at different heights for $E(0) = 3\,\mu v/cm$. The values of $E(z)$ were determined from the formula

$$\frac{E(z)}{E(0)} = \exp\left(\frac{\omega}{c}\int_0^z \varkappa dz\right). \qquad (5)$$

The damping during the passage through the absorbing thickness of the ionosphere, from the given level down to the surface of the earth, is shown in Figure 5 in decibels.

Due to the large mean free paths in the ionosphere, even relatively weak electric fields can impart to electrons energies comparable to the thermal energy. The criterion for smallness of the field strength of a wave (the relations given above being correct only in this specific case) is the ratio between the field E and the so-called plasma field E_p /8/, which in our case is

$$E_p = \sqrt{3kT\frac{m}{e^2}\delta(\omega_H^2 + \nu_{eff}^2)} \approx 4.2 \times 10^{-10}\sqrt{\delta T(\omega_H^2 + \nu_{eff}^2)}\ v/cm. \qquad (6)$$

If $\frac{E(z)}{E_p(z)} \ll 1$, then the field is weak. The collision frequency here does not depend on the strength of the electric field of the wave. Two wave systems will in this case pass through the same region without interacting.

For $\frac{E(z)}{E_p(z)} \approx 1$, noticeable nonlinear effects begin, primarily crossmodulation. For $\frac{E(z)}{E_p(z)} \approx 20$ or 30, ionization of the ionosphere under the action of the field of the wave may begin /8/. Table 2 lists some values of $\frac{E(z)}{E_p(z)}$ for a frequency of 11 kc, on the above-specified ionospheric model and for longitudinal propagation. The table shows that, although strong nonlinear effects do not occur even in the upper atmosphere, some crossmodulation of radio signals passing through the region of ULF propagation is possible, as well as some heating of the ionosphere by the energy released during damping of the low-frequency oscillations.

Let us consider this in more detail. The power given up by the wave per cm^3 is $\frac{\varepsilon_{ky} - E^2}{4\pi}\omega$. We assume that the energy of the wave is transferred exclusively to an electron gas. This energy will be consumed in heating the "heavy" gas (ions, atoms, and molecules) and in compensating additional losses (via inelastic collisions of electrons with ions and atoms of the "heavy" gas); and, finally, a certain part of the energy will be emitted by electrons during free transitions. The third type of loss can safely be neglected in comparison to the first two, but an evaluation of the relative importance of elastic and inelastic collisions is considerably more difficult. Let us make the following limiting assumptions: 1) the electron gas imparts all the energy to the heavy gas via elastic collisions only; 2) the heavy gas has no energy sinks of its own; 3) the capacity of the energy reservoir of the "heavy" gas is quite large, so that the ionic-atomic or kinetic temperature may be considered constant.

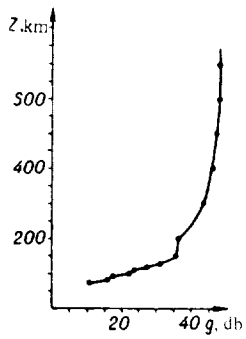

FIGURE 5.

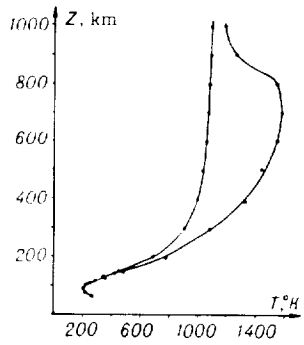

FIGURE 6.

With these assumptions it is not difficult to find the increment in electron temperature due to absorption of the energy of an electromagnetic wave. According to /9/, the amount of energy transferred from the electron gas to the "heavy" gas for a temperature difference $(T_e - T) = \Delta T$ is $\frac{4m}{M} kN_e \nu_{\text{eff}} \Delta T$. The stationarity condition, which we assume to be satisfied (if only as a consequence of assumptions 1–3), gives

$$\Delta T = \frac{M}{4m} k\nu_{\text{eff}} \frac{Q}{N_e},$$

where

$$Q = \frac{\varepsilon_{xy} - E^2}{4\pi} \omega. \qquad (7)$$

The results of computations made according to this formula are given in Table 3, and the temperature distribution with height is plotted in Figure 6. It should be noted that the realization of this situation will be hindered by several factors, the chief one being the limited capacity of the "energy reservoir" of the heavy gas. In the lower ionosphere, where the degree of ionization is low and there are a large number of heavy particles for each electron, this condition is satisfied. However, in the upper atmosphere it

will be violated quite rapidly, since there the characteristic time is

$$\tau_{char} \approx \frac{M}{4m\nu_{eff}} \cdot \frac{N_m + N_i}{N_e} \text{ sec.} \qquad (8)$$

Some values of τ_{char} are given in Table 3. If the time necessary for ULF radiation to travel through the ionosphere is greater than τ_{char}, an appreciable rise in the kinetic temperature of the heavy gas will occur.

TABLE 3

z, km	T, °K	ΔT, °K	τ_{char}, sec
60	260	$7.27 \cdot 10^{-4}$	—
70	219	$5.96 \cdot 10^{-2}$	—
80	205	$4.75 \cdot 10^{-3}$	—
90	210	$6.05 \cdot 10^{-2}$	—
100	230	1.85	$1.51 \cdot 10^{8}$
110	260	2.73	—
120	300	6.66	—
130	350	15.4	—
150	450	31.7	—
200	700	78.2	$4.63 \cdot 10^{5}$
300	900	187	$1.15 \cdot 10^{4}$
400	1000	326	$1.64 \cdot 10^{3}$
500	1000	403	420
600	1000	478	425
700	1000	505	377
800	1000	462	266
900	1000	175	332
1000	1000	96	518

As mentioned above, crossmodulation is a fairly fine nonlinear effect and may even be observed for $\frac{E(z)}{E_p(z)} < 1$. We should expect, therefore, that at high latitudes, where considerable amplitudes of ULF noise are common, this effect will often be observed as a modulation of the modulated and unmodulated emission of radio stations by audio-frequency noise. Actually, such a noise modulation in the range between 12 and about 500 kc was observed repeatedly by us at Tixie Bay during periods of ULF emission. The highest intensity for this type of noise was at about 300 kc, and it was apparently independent of the location of the transmitting station. It is noteworthy that the peaks of the noise envelope almost always corresponded very closely to bursts of ULF radiation.

Let us assume that ULF oscillations cause slight changes in the number of collisions of electrons with ions and with neutral particles, and that they thereby modulate the value of the absorption coefficient of a radio wave, provided that $\frac{\partial \varkappa_2}{\partial \nu} d\nu \ll \varkappa_{02}$, where $\varkappa_2$ is the absorption coefficient of the radio wave and $\varkappa_{02}$ is the first term in the series expansion of $\varkappa_2$. In this case the modulation coefficient p is /8/:

$$p = \frac{\Delta E_2}{E_2} = \frac{e^2 E_1^2 \omega_2 \omega_0}{3mckT} \int_s \frac{\left[\nu_{em} - \frac{3}{2}\left(\frac{T}{T_e}\right)^{5/8} \nu_{ei}\right] \nu_{eff} ds}{(\omega_n^2 + \nu_{eff}^2) \sqrt{(\delta\nu_{eff})^2 + 4\omega_1^2} \left[(\omega_2 \pm \omega_n)^2 + \nu_{eff}^2\right]^{1/4}}. \qquad (9)$$

Here it is assumed that E_1 is the amplitude of the active field of the wave, while $\omega_2 \gg \nu_{im}$. The integration is carried out over the entire path of the

radio wave in the disturbed region. If the dependence on ω_2 of the height of the reflection point is not taken into account, then p will reach a maximum p^m for $\omega_{21}=\frac{\omega_H}{2}\cos\psi$ and $\omega_{22}=\omega_H\cos\psi$, where ψ is the angle of incidence of the wave on the ionosphere. For $\psi\approx 10^\circ$ this is 1 or 2 megacycles. The disagreement with the observation results can be explained by the fact that z_2 as a function of ω_2 was neglected. A rise in ω_2 increases z_2 and reduces ν_{eff}. Since there is a quantity $\sim\nu_{eff}^2$ in the numerator of (9), this reduces p, and so the maximum p^m must be shifted toward lower frequencies (that is, $\omega_{21}<\frac{\omega_H}{2}\cos\psi$ and $\omega_{22}<\omega_H\cos\psi$). The fact that only one maximum is observed in practice cannot serve as a conclusive argument against the explanation presented. The second weaker maximum may not have been observed simply because the experiment was not comprehensive enough, since during the observation period no special importance was attached to the above facts.

In this case, if $\frac{E(z)}{E_p(z)}$ is comparable to unity, and especially if it is greater than unity, the luminous emission of polar aurorae will be modulated by the ULF radiation. However, a discussion of this complex and interesting subject goes beyond the scope of this report.

In addition to the influence of the ULF radio emission of the upper atmosphere on the propagation of medium-frequency radio waves, the influence which electromagnetic oscillations of even lower frequency have on the propagation of ULF waves is also of interest. Actually, the condition for quasilongitudinal propagation of ULF waves is very rigid, and oscillations of the constant magnetic field may violate this condition. In the ionosphere, which is a region where currents flow causing the short-period pulsations of the magnetic field so characteristic of the polar regions, the bending of the magnetic force lines may be considerable. It is important that the vector of the disturbing field is oriented in opposite directions above and below the current. The variations of the absorption coefficient can, to a first approximation, be represented as

$$\varkappa_1=\varkappa_{01}\left(1-\frac{\alpha^2}{2}\frac{\varepsilon_{xx}}{\varepsilon_{zz}}\right), \tag{10}$$

where, roughly speaking, $\frac{\varepsilon_{xx}}{\varepsilon_{zz}}\approx\frac{\omega_H}{\omega}$. Here, α, the angle of deviation of a force line of the geomagnetic field from the average position, is approximately equal to $\frac{\Delta H}{H^\circ}$ (the ratio of the variation of the horizontal component to the total magnetic-field vector). If ΔH is of the order of $10^3\gamma$, then $\frac{\Delta\varkappa}{\varkappa_{01}}$ may be several percent. This mechanism may well explain the repeatedly observed correspondence between the envelope of the ULF noise and the shape of the curve describing the short-period oscillations of the magnetic field.

Institute of Space-Physics Research and Aeronomy,
Yakutsk Branch of Siberian Division of
USSR Academy of Sciences

REFERENCES

1. DUNCAN, R.A. and G.R. ELLIS.— Nature, **183**, 1618, 1959.
2. JØRGENSEN, T.S. and E. UNGSTRUP.— Nature, **194**, 462, 1962.
3. ELLIS, G.R.— J. Atm. Terr. Phys., **10**, Nos.5–6, 302, 1957.
4. GALLET, R.M. and R.A. HELLIWELL.— J. Res. Nat. Bur. Stand., **63D**, 21, 1959.
5. AARONS, J., G. GUSTAFSSON, and A. EGELAND.— Nature, **185**, 149, 1960.
6. MARTIN, L.H., R.A. HELLIWELL, and K.R. MARKS.— Nature, **187**, 751, 1960.
7. AL'PERT, Ya.L. Rasprostranenie radiovoln i ionosfera (Radio-Wave Propagation and the Ionosphere).— Izd. AN SSSR, 1960.
8. GINZBURG, V.L. Rasprostranenie elektromagnitnykh voln v plazme (Propagation of Electromagnetic Waves in a Plasma).— Fizmatgiz, 1960.
9. VLASOV, A.A. Teoriya mnogikh chastits (Many-Particle Theory).— Moskva, Gosudarstvennoe izdatel'stvo tekhnicheskoi i teoreticheskoi literatury, 1950.

N67 38224

N. P. Ben'kova and A.N. Sukhodol'skaya

THE VARIABILITY OF IONOSPHERIC PARAMETERS

In connection with the IGY, a program for the initial processing of data from vertical soundings of the ionosphere was laid out /1/. This program provided for a determination of the monthly median values of the ionospheric parameters and also of the upper and lower quartiles, with a view toward using these to study the variability of the ionosphere. It was demonstrated in /2/ that the parameters of a quiet ionosphere obey the normal law of distribution of random values, and that deviations from a normal distribution indicate a disturbed state of the ionosphere. Therefore, the standard deviation of the hourly parameter values can be determined from the formula for a normal distribution:

$$\sigma = \frac{1}{2}\,\frac{(\lambda_u - m) + (m - \lambda_l)}{0.6745},$$

where λ_u and λ_l are the upper and lower quartiles and m is the median value of the given parameter (see, for example, page 236 of /3/). The degree of deviation of the distribution from the normal can be evaluated using the formula

$$\delta = (\lambda_u - m) - (m - \lambda_l),$$

characterizing the asymmetry of the distribution.

We used data from vertical soundings of the ionosphere, made during the IGY at Yakutsk, Yuzhno-Sakhalinsk, and Tixie Bay. These stations have different latitudes, but they lie in the same longitude sector; thus any possible influence of a longitude effect in the F_2 layer was avoided. With an increase in disturbance of the ionosphere, it can be assumed that σ will increase and that δ will become more negative, increasing in absolute value, since ionospheric disturbances are for the most part accompanied by a reduction of the critical frequencies of the F_2 layer. In other words, the variations of these two quantities (σ and δ) are "out of phase" with one another.

Figure 1 shows the seasonal variation of σ and δ during the IGY at the above three stations. The 24-hour period is divided into three parts: day, from 0900 to 1700 local time; night, from 2100 to 0500; and morning-evening, from 0500 to 0800 and from 1700 to 2000.

At all three stations a rise in σ is observed during the equinoctial months. This rise was especially large in the daytime and was greater at higher latitudes. Near the winter and summer solstices the values of σ were approximately identical, and they amounted to 1/3 to 1/2 of the equinox values for the given part of the day. The fact that the oscillations of δ and σ are out of phase shows up clearly only at night. During the

morning and evening the variation of δ is rather indefinite. During the daytime there is even a tendency for the variations of δ and σ to be in phase, although this tendency is somewhat undefined.

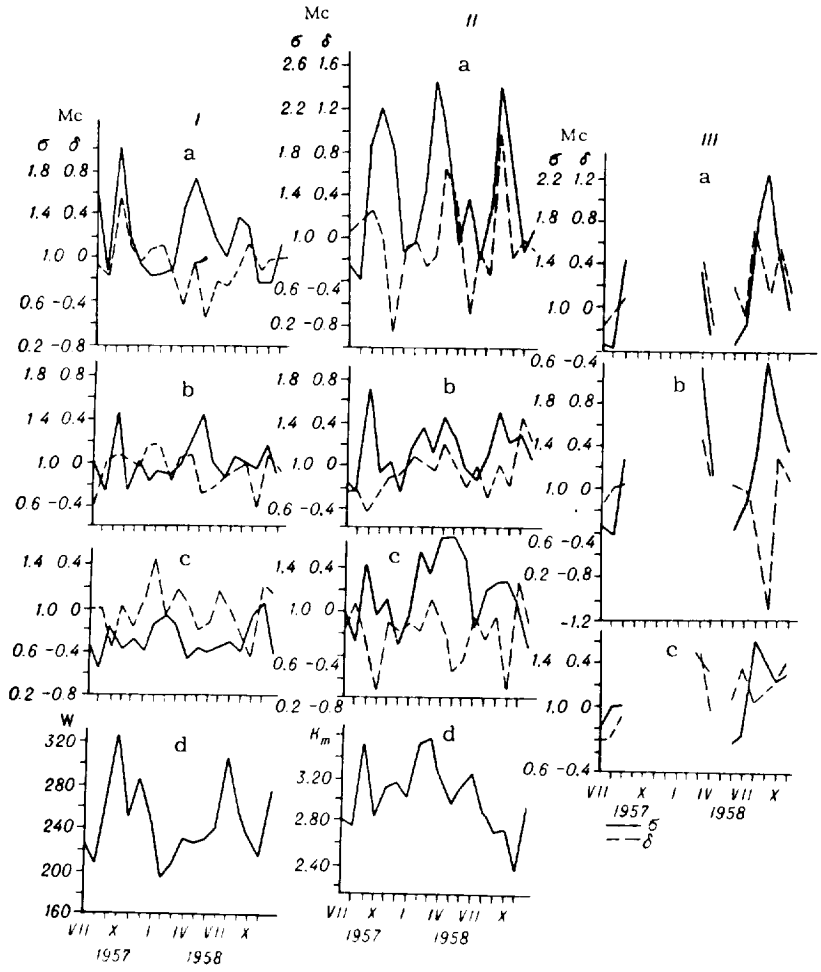

FIGURE 1. Standard deviation (σ) and asymmetry (δ) of critical frequencies of F_2 layer. I–Yuzhno-Sakhalinsk; II–Yakutsk; III–Tixie Bay; a–day; b–morning-evening; c–night.

The diurnal variation of σ (Figure 2) at the time of the solstices is not very definite. Near the equinoxes, on the other hand, the diurnal variation of σ has a definite maximum in the daytime at all the stations, and there is a tendency for σ to begin rising during the night. It is difficult to make any definite comments on the diurnal variation of δ.

An attempt to compare σ and δ with the relative sunspot number (W) did not lead to the desired results, since the correlation was found to be very weak. The variation of the spot number for the period in question is plotted

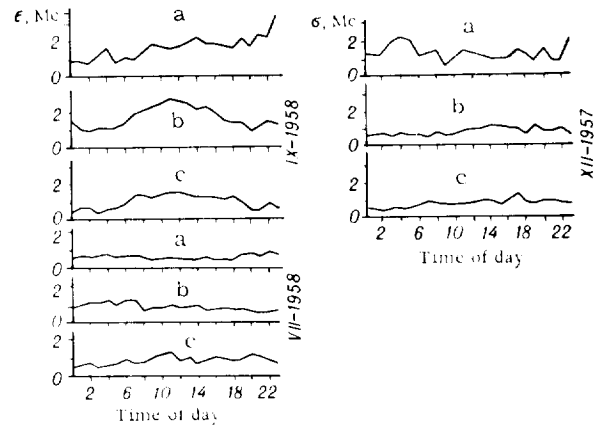

FIGURE 2. Diurnal variation of ε (f_0F_2).

a–Tixie Bay; 2–Yakutsk; 3–Yuzhno-Sakhalinsk.

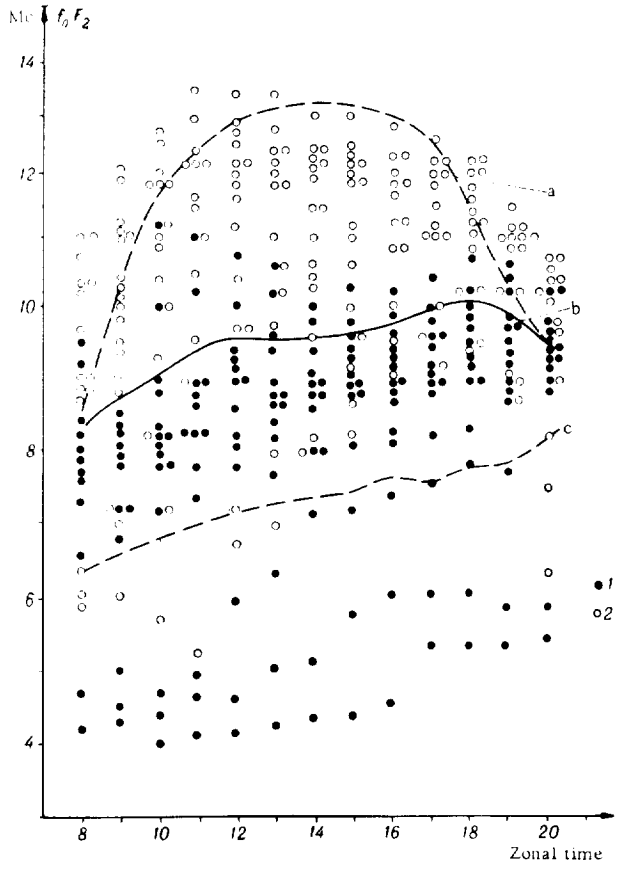

FIGURE 3. Hourly values of f_0F_2 for September 1958 at Yakutsk.

a–median for Oct.; b–median for Sept.; c–median for Aug. 1– f_0F_2 for first half of Sept.; 2– f_0F_2 for second half of Sept.

in Figure 1. There is better agreement between the variations of σ and K_m (the average monthly magnetic-activity index at Soviet stations). The latter index also increases during the equinoctial months.

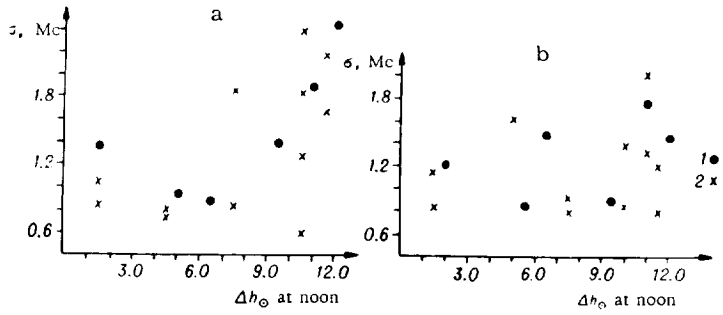

FIGURE 4. $\sigma(f_0F_2)$ as a function of change in sun's height ($\Delta h_\odot$ is the difference in the noon values on the first and last days of the month).

1–increase in $h_\odot$; 2–decrease in $h_\odot$; a–Yakutsk; b–Yuzhno-Sakhalinsk.

However, the rise in σ near the equinoxes, as well as being related to the magnetic-ionospheric disturbance, which has a tendency to increase at this time, is also related to the rapid variation of $f_0 F_2$ occasioned by the regular seasonal change in the ionization density of the layer. The influence of this seasonal change on the distribution of hourly values is illustrated clearly in Figure 3. In this figure all the daytime values of $f_0 F_2$ for September 1958 are plotted against the hour of day. Regardless of variations in the magnetic disturbance, almost all the values of $f_0 F_2$ for the first half of the month are less than the median, while those during the second half of the month are greater than the median. This corresponds to the regular rise in the daytime level of the ionization during the autumn. Since the seasonal variation of the ionization is due to the change in the height of the sun ($h_\odot$), we have plotted σ as a function of this change during the month in Figure 4 ($\Delta h_\odot$ is the difference between the noon values of $h_\odot$ on the first and last days of the month). The figure does not give data for Tixie Bay, since the number of observations made at this station were insufficient.

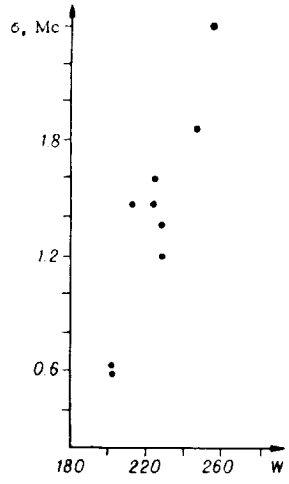

FIGURE 5. Anomalous values of $\sigma(f_0F_2)$ as a function of solar activity.

The two graphs for the stations with different latitudes have the same character. The values of σ on these graphs which appeared to "deviate" from a definite dependence of σ on ($\Delta h_\odot$) were transferred to another graph, where they were plotted as a function of W. These values of σ correlated closely with an increase in the solar activity W (Figure 5), whereas for the aggregate of all the values of $\sigma(W)$ the points are very scattered.

The relation between σ and the change in the height of the sun is also verified by the seasonal variation of σ for the *E* layer during this same period (see table). Since the *E* layer is almost unaffected by disturbances, the rise in σ in the equinoctial periods is probably related only to the change in the sun's height.

1957 month	σ	δ	1958 month	σ	δ	1958 month	σ	δ
VII	0.16	0.12	I	0.11	0.00	VII	0.17	0.00
VIII	0.20	0.08	II	0.13	−0.10	VIII	0.16	0.02
IX	0.18	0.01	III	0.18	−0.06	IX	0.26	−0.11
X	0.12	−0.06	IV	0.14	0.05	X	0.17	−0.05
XI	—	—	V	0.14	0.05	XI	0.19	0.03
XI	0.10	0.07	VI	0.12	−0.05	XII	—	—

The foregoing data show that the standard deviation of the hourly values of the ionospheric parameters, relative to the monthly median, are largely determined by the regular seasonal variation of the parameters. The rise in σ during the equinoctial months is related to the high rate of the seasonal variations as well as to the heightened ionospheric disturbance at this time of year. Consequently, when the characteristics σ and δ are computed according to the quartile values of the parameters, they typify the overall variability of the ionosphere. Thus, they are useful for practical calculations of the range of operating frequencies and for the solution of other radio-communication problems in which the possible deviations of the ionospheric parameters from the monthly medians must be evaluated.

On the other hand, the values of σ calculated according to the quartiles are not a reliable index of the disturbance during the month, since they "react" to a disturbance only in cases when the variation associated with the disturbance exceeds the regular seasonal variations of the parameters (within the given month). Since the seasonal-variation amplitude for the nighttime values of f_0F_2 is less than the amplitude for the daytime values, the nighttime values of σ will naturally characterize the disturbance of the ionosphere better. This is verified by the data in Figure 1, which demonstrates the good fit of the variations of the "nighttime" values with the seasonal change in K_m, and also the fact that the variations of σ and δ are out of phase.

Institute of Terrestrial Magnetism and
Radio-Wave Propagation

REFERENCES

1. Handbook on Vertical Sounding of the Ionosphere (Translation from English edited by N.V.Mednikova and B.S.Shapiro).— Moskva, Izd. AN SSSR. 1957.

2. BEN'KOVA, N.P. and N.I.POTAPOVA.— Trudy VII nauchnoi konferentsii Tomskogo gosudarstvennogo universiteta, Tomsk. 1957.

3. KRAMER, G. Matematicheskie metody statistiki (Mathematical Methods of Statistics).— Moskva, Ob"edinenie nauchno-tekhnicheskikh izdatel'stv. 1948.

N67-38225

E.G. Boss, L.I. Dorman, E.V. Kolomeets, and Zh.S. Takibaev

COUPLING COEFFICIENTS FOR PARTICLE PASSAGE THROUGH THE ATMOSPHERE, TAKING INTO ACCOUNT NUCLEAR INTERACTIONS

When calculating the coupling coefficients in the high-energy range, it is necessary to take into account the cascade multiplication of the nuclear-active component produced when a primary particle of energy E_0 is incident upon the limit of atmosphere. Let us assume that the primary is a nucleon and that it loses the same fraction of its energy in each elementary collision with the nucleus of an air atom. The coefficient of inelasticity K_N for cosmic rays has been found by different methods /1–3/ to be $\simeq 0.3$. In the energy range to be considered here ($E > 10^{10}$ eV), the scattering of the energetically isolated nucleon can, to a first approximation, be neglected, since the transverse impulse of a nucleon is low ($P_\perp \lesssim 5 \cdot 10^8$ eV/c).

Let us consider the i th elementary interaction of a primary nucleon with the nucleus of an air atom. As a first approximation, we assume that only π mesons are produced. The maximum energy of the π mesons generated is

$$\varepsilon^i_{\pi_{max}} = K_N (E_{N_{i-1}} - M). \tag{1}$$

The distribution of these π mesons according to angles θ and energies ε_π can be written as

$$d^2 f_N = a^i_N \omega_N (\varepsilon_\pi, \theta)\, d\cos\theta \cdot d\varepsilon_\pi, \tag{2}$$

where a^i, the normalizing coefficient, is

$$a^i_N = 1 \Big/ \int_{\cos\theta_{min}}^{\cos\theta_{max}} d\cos\theta \int_{\varepsilon_{min}}^{\varepsilon_{max}} \omega_N (\varepsilon_\pi, \theta)\, d\varepsilon_\pi.$$

The average energy of the π mesons at the i th event is

$$\overline{\varepsilon^i_\pi} = a^i_N \int_{\varepsilon_{min}}^{\varepsilon_{max}} \varepsilon_\pi d\varepsilon_\pi \int_{\cos\theta_{min}}^{\cos\theta_{max}} \omega_N (\varepsilon_\pi, \cos\theta)\, d\cos\theta. \tag{3}$$

The average multiplicity is $\overline{n^i_\pi} = K_N (E_{N_{i-1}} - M)/\overline{\varepsilon^i_\pi}$. The distribution of charged π mesons with respect to angles and energies may be written in the form

$$dN^i_N = A^i_N \cdot \omega_N (\varepsilon_\pi, \cos\theta)\, d\varepsilon_\pi d\cos\theta; \tag{4}$$

where

$$A_N^l = \frac{2}{3}\frac{K_N(E_{N_{l-1}} - M)}{\int\limits_{\varepsilon_{min}}^{\varepsilon_{max}} \varepsilon_\pi d\varepsilon_\pi \int\limits_{\cos\theta_{min}}^{\cos\theta_{max}} \omega_N(\varepsilon_\pi, \cos\theta)\, d\cos\theta}. \quad (5)$$

Next let us assume that the average effective mass with which the primary nucleon collides is $m_2 \sim M$, and that the total momentum of the generated mesons in the center-of-mass $(M - m_2)$ system is zero. The energy of the nucleon can then be represented as a function of K_N and $E_{N_{l-1}}$, so that

$$E_{N_l} = E_{N_{l-1}} - K_N(E_{N_{l-1}} - M) - (E_{\delta_l} - M). \quad (6)$$

The energy E_{δ_l} of the δ nucleons turns out to be $\sim M$, and so the contribution of these nucleons to the creation of secondary π mesons can be neglected.

Let us make an additional assumption concerning the form of the function ω_N, namely that the transverse impulses of all the mesons generated must be constant. Then

$$\omega_N(\varepsilon_\pi, \cos\theta)\, d\cos\theta\, d\varepsilon_\pi = \omega_N(\varepsilon_\pi)\,\delta\left(\cos\theta - \sqrt{\frac{\varepsilon_\pi^2 - m_\pi^2 - p_\perp^2}{\varepsilon_\pi^2 - m_\pi^2}}\right) d\varepsilon_\pi d\cos\theta. \quad (7)$$

In the high-energy range this requirement is satisfied over a very wide interval of primary energies.

On this assumption, we obtain

$$\sqrt{p_\perp^2 + m_\pi^2} \sim \varepsilon_{\pi_{min}}^l \leqslant \varepsilon_\pi \leqslant \varepsilon_{\pi_{max}}^l = K_N(E_{l-1} - M)$$

$$0 \leqslant \cos\theta \leqslant \left\{\frac{[K_N(E_{N_{l-1}} - M)]^2 - m_\pi^2 - p_\perp^2}{K_N^2(E_{N_{l-1}} - M)^2 - m_\pi^2}\right\}^{1/2},$$

and so

$$A_{N_l} = A_{N_l}(E_{N_{l-1}},\ K_N,\ p_\perp).$$

Data on $\pi - N$ collisions at 7.5 BeV /4/ and 17 BeV /5/ indicate similar patterns for the elementary interactions between π mesons and nucleons for these energies, the only difference being that the energetically isolated meson retains for itself 1/3 of the initial energy ($K_\pi \approx 0.7$). The energy of the π meson becomes dissipated considerably more rapidly. The distribution function for the generated $\pi^\pm$ mesons can be written as*

$$dn_\pi = A_{l_\pi}^j \cdot \omega_\pi(\varepsilon_\pi') \cdot \delta\left(\cos\alpha - \sqrt{\frac{\varepsilon_\pi'^2 - p_\perp^2 - m_\pi^2}{\varepsilon_\pi'^2 - m_\pi^2}}\right) d\cos\alpha\, d\varepsilon_\pi', \quad (8)$$

where

$$A_{l_\pi}^j = \frac{2}{3} K_\pi(\varepsilon_{\pi_{j-1}} - m_\pi) \Big/ \int\limits_{\varepsilon_{\pi_{min}}^j}^{\varepsilon_{\pi_{max}}^j} \varepsilon_\pi' d\varepsilon_\pi' \int\limits_{\cos\theta_{min}}^{\cos\theta_{max}} \omega_\pi(\varepsilon_\pi',\ \cos\alpha) \cdot d\cos\alpha.$$

Here

$$\sqrt{p_\perp^2 + m_\pi^2} \sim \varepsilon_{\pi_{min}}^j \leqslant \varepsilon_\pi' \leqslant \varepsilon_{\pi_{max}}^j = K_\pi(\varepsilon_\pi'^{-1} - m_\pi), \quad (8')$$

$$0 \leqslant \cos\alpha \leqslant \left[\frac{K_\pi^2(\varepsilon_{\pi_{j-1}} - m_\pi)^2 - m_\pi^2 - p_\perp^2}{K_\pi^2(\varepsilon_{\pi_{j-1}} - m_\pi)^2 - m_\pi^2}\right]^{1/2}.$$

* The index j indicates the j th collision of the "primary" π meson created in the i th collision of the primary nucleon.

The energy of the isolated ("primary") meson in the j th event is determined by analogy with (6):

$$\varepsilon_{\pi_j} = \varepsilon_{\pi_{j-1}} - K_\pi(\varepsilon_{\pi_{j-1}} - m_\pi) - (E_\delta^j - M), \qquad (8'')$$
$$E_\delta^j = f(M,\ \varepsilon_{\pi_{j-1}},\ K_\pi).$$

Let us now go back to the meson cascade caused by the primary nucleon. According to /6/, the probability that a nucleon incident vertically upon the limit of atmosphere will reach a depth h' after $(j-1)$ collisions and will interact at a depth dh' is

$$d\psi_N^j(h') = \frac{(h')^{j-1}}{(j-1)!\lambda^{j-1}} e^{-h'/\lambda} \cdot dh'/\lambda, \qquad (9)$$

where λ is the interaction mean free path.

The number of π mesons produced at a depth h' in the i th event, for the energy interval from ε_π to $\varepsilon_\pi + d\varepsilon_\pi$ and for angles from $\cos\theta$ to $\cos\theta + d\cos\theta$, is obviously

$$dn_N^i = A_N^i \omega_N(\cos\theta,\ \varepsilon_\pi) \cdot d\cos\theta d\varepsilon_\pi d\psi_N^i(h'). \qquad (10)$$

Collisions right down to $i_1(\varepsilon_\pi)$, which is determined by the condition $K_N(E_{N_{i_1}} - M) = \varepsilon_\pi$, can contribute to the energy ε_π.

The probability that a meson of energy ε_π, traveling at an angle θ, will reach a depth h is given by the formula

$$\varphi_\pi(\varepsilon_\pi,\ \cos\theta,\ h',\ h) = \exp\left[-\frac{h-h'}{\lambda\cos\theta} - \frac{m_\pi}{\tau_\pi\sqrt{\varepsilon_\pi^2 - m_\pi^2\cos\theta}}\int_{h'}^{h}\frac{dh}{\rho(h)}\right], \qquad (11)$$

provided we assume identical interaction mean free paths for π mesons and nucleons in the atmosphere. Here, τ_π is the lifetime of a $\pi^\pm$ meson, and $\rho(h)$ is the density of the atmosphere. Assuming an isothermal atmosphere $\left(\rho = \frac{hg}{RT}\right.$, where g is the acceleration of gravity, T is temperature, and R is the universal gas constant), we have

$$\varphi(\varepsilon_\pi,\ \cos\theta,\ h,\ h') = \left(\frac{h'}{h}\right)^{\frac{RT}{g}} \cdot \frac{m_\pi}{\sqrt{\varepsilon_\pi^2 - m_\pi^2\cos\theta}\cdot\tau_\pi} \cdot \exp -\frac{h-h'}{\lambda\cos\theta}. \qquad (12)$$

The number of mesons arriving from the i th collision, which occurs at any depth $h' \leqslant h$, will obviously be

$$dN_N^i = \int dn_N^i \varphi(\varepsilon_\pi,\ \cos\theta, h, h') =$$
$$= A_N^i \omega_N(\varepsilon_\pi,\ \cos\theta) \cdot d\varepsilon_\pi d\cos\theta \int_0^h \exp\left(-\frac{h-h'}{\lambda\cos\theta}\right) \cdot \left(\frac{h'}{h}\right)^q \cdot \frac{(h')^{i-1}}{(i-1)!\lambda^{i-1}} \times$$
$$\times \exp\left(-\frac{h'}{\lambda}\right)\frac{dh'}{\lambda} = \frac{1}{(i-1)!\lambda^i \cdot h^q}\left(\frac{\lambda\cos\theta}{1-\cos\theta}\right)^{q+i} \exp -\frac{h}{\lambda\cos\theta} \times$$
$$\times \int_0^{\frac{h(1-\cos\theta)}{\lambda\cos\theta}} \exp x \cdot x^{q+i-1} dx \cdot A_N^i \omega_N(\varepsilon_\pi,\ \cos\theta) \cdot d\varepsilon_\pi d\cos\theta; \qquad (13)$$

here, since $q + i - 1 > 0$, the integral $\int_0^{\frac{h(1-\cos\theta)}{\lambda\cos\theta}} \exp x \cdot x^{q+i-1} dx$ converges. The total number of π mesons at a depth h, with energies from ε_π to $\varepsilon_\pi + d\varepsilon_\pi$ and angles from $\cos\theta$ to $\cos\theta + d\cos\theta$, as a result of all possible collisions of the

nucleon at smaller depths into the atmosphere, is

$$dN_N = \Phi_1(h,\ \varepsilon_\pi,\ \cos\theta,\ E_0)\, d\varepsilon_\pi d\cos\theta, \tag{14}$$

where

$$\Phi_1 = \sum_{i=1}^{i_1} \frac{A_N^i \omega_N(\varepsilon_\pi \cos\theta)}{(i-1)!\lambda^i h^q} \left(\frac{\lambda\cos\theta}{1-\cos\theta}\right)^{q+i} \exp -\frac{h}{\lambda\cos\theta} \int_0^{\frac{h(1-\cos\theta)}{\lambda\cos\theta}} \exp x \cdot x^{q+i-1} dx,$$

$$q = \frac{RT\cdot m_\pi}{g\sqrt{\varepsilon_\pi^2 - m_\pi^2}\cdot\cos\theta\cdot\tau_\pi}.$$

Formula (14) indicates the main contribution to the total π-meson flux at a depth h. Since all these mesons originate from primary nucleons, let us call them first-generation mesons.

At a depth h this flux will be accompanied by a flux of mesons produced in secondary events ($\pi - N$ collisions). Let us now determine the contribution of the first-generation mesons. We consider a π meson emitted at a depth h', with an energy between ε_π and $\varepsilon_\pi + d\varepsilon_\pi$ and with an angle between $\cos\theta$ and $\cos\theta + d\cos\theta$.

The probability that this meson will reach a depth h and will interact within a layer dh is

$$\frac{dh}{\lambda\cos\theta}\cdot W_0 = \frac{dh}{\lambda\cos\theta}\left(\frac{h'}{h}\right)^q \exp -\frac{h-h'}{\lambda\cos\theta}. \tag{15}$$

The probability that the π meson will reach a depth h after the first interaction and will interact within a layer dh is

$$\frac{dh}{\lambda\cos\theta} W_1 = \int_{h'}^{h} \varphi(h'',\ h)\cdot W_0(h'',\ h')\frac{dh''}{\lambda\cos\theta} = \exp -\frac{h-h'}{\lambda\cos\theta} \times$$

$$\times \frac{1}{\lambda\cos\theta\,(q_1 - q + 1)}\left\{\frac{h'^q}{h^{q-1}} - \frac{(h')^{q_1+1}}{(h)^{q_1}}\right\}\frac{dh}{\lambda\cos\theta}. \tag{16}$$

In the same way, it is possible to calculate the probability that the π meson will be at a depth h after the second interaction:

$$\frac{dh}{\lambda\cos\theta} W_2 = \int_{h'}^{h} W_1(h'',\ h')\frac{dh''}{\lambda\cos\theta}\varphi(h,h'') =$$

$$= \frac{\exp -\frac{h-h'}{\lambda\cos\theta}}{\lambda^2\cos^2\theta}\cdot\frac{1}{q_2 - q_1 + 1}\left\{\frac{1}{q_2 - q + 2}\cdot\left(\frac{(h')^q}{(h)^{q-2}} - \frac{(h')^{q_2+2}}{(h)^q}\right) -\right.$$

$$\left. - \frac{1}{q_2 - q_1 + 1}\left(\frac{(h')^{q_1+1}}{(h)^{q_1+2}} - \frac{(h')^{q_2+2}}{h^{q_2}}\right)\right\}\frac{dh}{\lambda\cos\theta}. \tag{17}$$

Finally, for the $(j-1)$ th interaction, the probability is

$$\frac{dh}{\lambda\cos\theta} W_{j-1} = \frac{dh}{\lambda\cos\theta}\int_{h'}^{h} W_{j-2}(h'',\ h')\varphi(h'',\ h)\cdot\frac{dh''}{\lambda\cos\theta}. \tag{18}$$

Everywhere in the above, the energetically isolated π meson is assumed to retain its initial direction. For each event the distribution with respect to angles and energies of the mesons produced is given by formula (8). The number of secondary mesons in the intervals $\cos\alpha$, $\cos\alpha + d\cos\alpha$, $\varphi, \varphi + d\varphi$; ε'_π, $\varepsilon'_\pi + d\varepsilon'_\pi$, due to possible collisions of the primary meson at a depth $h + dh$ is

$$dN_\pi^\pm = \sum_{j=1}^{j_1} A_{j_\pi}^j \omega_\pi(\varepsilon'_\pi)\,\delta\left(\cos\alpha - \sqrt{\frac{\varepsilon_\pi'^2 - m_\pi^2 - p_\perp^2}{\varepsilon_\pi'^2 - m_\pi^2}}\right)\cdot W_{j-1}\frac{1}{2\pi\lambda\cos\theta} d\varepsilon_\pi d\cos\alpha d\varphi\cdot dh. \tag{19}$$

A contribution to the energy ε'_π may be made by collisions down to the j_1 th, which is determined by the condition

$$K_\pi(\varepsilon_{\pi_{j_1-1}} - m_\pi) = \varepsilon'_\pi.$$

The azimuthal angle φ and the plane angle α are measured from the direction of motion of the "primary" meson.* However, the angle θ' relative to the vertical is usually the angle of interest. Spherical geometry gives us the following formula relating these angles:

$$\cos\theta' = \cos\alpha\cos\theta + \sin\alpha\sin\theta\cos\varphi. \tag{20}$$

For specified values of α and θ,

$$d\varphi = \frac{-d\cos\theta'}{\sqrt{1-\cos^2\alpha-\cos^2\theta-\cos^2\theta'+2\cos\theta\cos\theta'\cos\alpha}}. \tag{21}$$

Thus, formula (19) can be rewritten as

$$dn_\pi = \sum_{j=1}^{j_1} A^j_{i_\pi}\omega_\pi(\varepsilon'_\pi)\cdot\delta\left(\cos\alpha - \sqrt{\frac{\varepsilon'^2_\pi - m^2_\pi - p^2_\perp}{\varepsilon'^2_\pi - m^2_\pi}}\right) W_{j-1}\times$$

$$\times\frac{dh}{\lambda\cos\theta}\frac{d\varepsilon'_\pi d\cos\alpha}{2\pi}\frac{d\cos\theta'}{\sqrt{1-\cos^2\alpha-\cos^2\theta-\cos^2\theta'+2\cos\theta\cos\theta'\cos\alpha}}. \tag{22}$$

For a selected function describing the angular distribution of π mesons in an elementary event, it is easy to carry out the integration with respect to α. The number of $\pi^\pm$ mesons produced at a depth dh and traveling at an angle θ' with an energy ε'_π will be

$$dn'_\pi = \sum_{j=1}^{j_1} A^j_{i_\pi}\omega_\pi(\varepsilon'_\pi)\,W_{j-1}\cdot\frac{dh}{\lambda\cos\theta}\frac{d\varepsilon'_\pi}{2\pi}\times$$

$$\times\frac{d\cos\theta'}{\sqrt{1-\cos^2\theta-\cos^2\theta'-\left(\frac{\varepsilon'^2_\pi-m^2_\pi-p^2_\perp}{\varepsilon'^2_\pi-m^2_\pi}\right)+2\cos\theta\cos\theta'\left(\frac{\varepsilon'^2_\pi-m^2_\pi-p^2_\perp}{\varepsilon'^2_\pi-m^2_\pi}\right)^{1/2}}}. \tag{23}$$

Correspondingly, the flux of $\pi^\pm$ mesons at a depth h, with an energy ε'_π in the angular interval $\cos\theta' + d\cos\theta'$, will be

$$dn_\pi = \int_{h'}^{h} dn'_\pi\varphi_\pi(h'',\ h,\ \varepsilon'_\pi,\ \cos\theta') = \sum_{j=1}^{j_1}\times$$

$$\times\frac{A^j_{i_\pi}\cdot\omega_\pi(\varepsilon'_\pi)\,G_{j-1}(h,\ h')\,d\cos\theta'\,d\varepsilon'_\pi}{2\pi\sqrt{1-\cos^2\theta-\cos^2\theta'-\left(\frac{\varepsilon'^2_\pi-m^2_\pi-p^2_\perp}{\varepsilon'^2_\pi-m^2_\pi}\right)+2\cos\theta\cos\theta'\left(\frac{\varepsilon'^2_\pi-m^2_\pi-p^2_\perp}{\varepsilon'^2_\pi-m^2_\pi}\right)^{1/2}}}, \tag{24}$$

where

$$G_{j-1}(h,\ h') = \int_{h'}^{h} W_{j-1}(h'',\ h')\left(\frac{h''}{h}\right)^{q'}\cdot\exp-\frac{h-h''}{\lambda\cos\theta}\cdot\frac{dh''}{\lambda\cos\theta}, \tag{25}$$

$$q' = \frac{RTm_\pi}{g\sqrt{\varepsilon'^2_\pi - m^2_\pi}\cdot\cos\theta'\cdot\tau_\pi}.$$

Using formulas (16), (17), and (18), it is possible to calculate the coefficients $G_{j-1}(h, h')$, which are the functions

$$q,\ q_1,\ q_2,\ \ldots,\ q_{j-\perp},\ q',\ h,\ h'.$$

* The angle φ is reckoned in a plane perpendicular to θ, from the bottom of its intersection with the vertical plane passing through the direction of motion of the primary nucleon.

The total number of $\pi^{\pm}$ mesons at a depth h generated by "primary" mesons with energies from ε_π to $\varepsilon_\pi + d\varepsilon_\pi$ and angles from $\cos\theta$ to $\cos\theta + d\cos\theta$ is

$$dN_\pi^{\pm} = \int_0^h dh_\pi(h,\ h')\, dN_N(h')\, \frac{dh'}{\lambda \cos\theta} =$$

$$= \sum_{i=1}^{i_1} \sum_{j=1}^{j_1(i)} D_{j-1}^{i}\ \frac{A_N^i A_{\pi_l}^l}{2\pi\cdot(i-1)!\lambda^i} \cdot \left(\frac{\lambda\cos\theta}{1-\cos\theta}\right)^{q+l} \times$$

$$\times \frac{\omega_\pi(\varepsilon_\pi')\, d\cos'\theta\ \ d\varepsilon_\pi' \omega_N(\varepsilon_\pi,\ \cos\theta)\, d\varepsilon_\pi d\cos\theta}{\sqrt{1-\cos^2\theta-\cos^2\theta'-\left(\frac{\varepsilon_\pi'^2-m_\pi^2-p_\perp^2}{\varepsilon_\pi'^2-m_\pi^2}\right)+2\cos\theta\cdot\cos\theta'\cdot\left(\frac{\varepsilon_\pi'^2-p_\perp^2-m_\pi^2}{\varepsilon_\pi'^2-m_\pi^2}\right)^{1/2}}}, \qquad (26)$$

where

$$D_{j-1}^{i}(h,\ q,\ q_1,\ q_2 \ldots q_{j-1},\ q',\ \cos\theta,\ \cos\theta') =$$

$$= \int_0^h \frac{dh'}{\lambda\cos\theta}\, G_{j-1}\cdot\frac{1}{(h')^q}\exp-\frac{h'}{\lambda\cos\theta}\cdot\int_0^{\frac{h'(1-\cos\theta)}{\lambda\cos\theta}} \exp x\cdot x^{q+l-1}\, dx. \qquad (27)$$

By specifying a function

$$\omega_N(\varepsilon_\pi,\ \cos\theta) = \omega_N(\varepsilon_\pi)\cdot\delta\left(\cos\theta-\sqrt{\frac{\varepsilon_\pi^2-m_\pi^2-p_\perp^2}{\varepsilon_\pi^2-m_\pi^2}}\right),$$

it is easy to integrate (26) with respect to the angles of emergence of the first-generation mesons:

$$dN_\pi^{\pm} = \sum_{i=1}^{i_1}\sum_{j=1}^{j_1(i)} D_{j-1\perp}^{i}\left(h,\ Q,\ Q_1,\ Q_2,\ \ldots,Q_{j-1},\ q',\right.$$

$$\left.\sqrt{\frac{\varepsilon_\pi^2-p_\perp^2-m_\pi^2}{\varepsilon_\pi^2-m_\pi^2}},\ \cos\theta'\right)\frac{A_{i_\pi}^l A_N^i}{2\pi(i-1)!\lambda^i}\left(\frac{\lambda\sqrt{\varepsilon_\pi^2-p_\perp^2-m_\pi^2}}{\sqrt{\varepsilon_\pi^2-m_\pi^2}-\sqrt{\varepsilon_\pi^2-p_\perp^2-m_\pi^2}}\right)^{Q+l}\times$$

$$\times\frac{\omega_\pi(\varepsilon_\pi')\, d\varepsilon_\pi' d\cos\theta'\cdot\omega_N(\varepsilon_\pi)\cdot d\varepsilon_\pi}{\sqrt{1-\left(\frac{\varepsilon_\pi^2-m_\pi^2-p_\perp^2}{\varepsilon_\pi^2-m_\pi^2}\right)-\left(\frac{\varepsilon_\pi'^2-m_\pi^2-p_\perp^2}{\varepsilon_\pi'^2-m_\pi^2}\right)-\cos^2\theta'+}}\rightarrow$$

$$\leftarrow\frac{}{+2\cos\theta'\left(\frac{\varepsilon_\pi'^2-m_\pi^2-p_\perp^2}{\varepsilon_\pi'^2-m_\pi^2}\right)^{1/2}\left(\frac{\varepsilon_\pi^2-m_\pi^2-p_\perp^2}{\varepsilon_\pi^2-m_\pi^2}\right)^{1/2}}}, \qquad (28)$$

where

$$Q = \frac{RT}{g\tau_\pi\sqrt{\varepsilon_\pi^2-p_\perp^2-m_\pi^2}};\quad Q_l = \frac{RT}{g\tau_\pi}\frac{\sqrt{\varepsilon_\pi^2-m_\pi^2}}{\sqrt{(\varepsilon_{\pi_{j-1}}^2-m_\pi^2)(\varepsilon_\pi^2-p_\perp^2-m_\pi^2)}},$$

$\varepsilon_{\pi_{j-1}}$ being the energy of a π meson which is primary for the j th event. The expression obtained determines the flux of secondary mesons produced by the first-generation mesons. These will be called second-generation mesons.

In order to obtain a function describing the distribution of second-generation π mesons with respect to angles θ' and energies ε_π', equation (28) must be integrated over ε_π. Here we must keep in mind that the contributions of the integrals of the different terms in the sum in (28) will be different.

On the basis of energy-balance equations (6) and (8''), together with expressions (1) and (8') determining the maximum energy of the π mesons in

generation events, it is possible to find the limit values $j_1(i, K_\pi, K_N, \varepsilon'_\pi, E_0)$ and $i_1(K_N, K_\pi, \varepsilon'_\pi, E_0)$ of the summation indexes.

Let us consider the first collision of the nucleon $i = 1$ and all the subsequent collisions of the π meson ($j = 1, 2, \ldots, j_1(i = 1)$). The limits of the integration with respect to ε_π are:

$$i = 1;\ \varepsilon_{\pi_{\max}} = K_N (E_0 - M);$$

$$j = 2;\ \varepsilon_{\pi_{\min}} = \varepsilon'_\pi / K_\pi + m_\pi.$$

For the second collision ($i=1, j=2$), only the values of ε_π which satisfy the following condition can contribute to the energy ε'_π:

$$i = 1;\ \varepsilon_{\pi_{\max}} = K_N (E_0 - M);$$

$$j = 2;\ \varepsilon_{\pi_{\min}} = m_\pi + \frac{1}{K_\pi} m_\pi + \frac{\varepsilon'_\pi}{K_\pi^2}.$$

For $i = 1$ and arbitrary values of j, similar reasoning leads to

$$i = 1;\ \varepsilon_{\pi_{\max}} = K_N (E_0 - M);$$

$$j;\ \varepsilon_{\pi_{\min}} = m_\pi \left(\sum_{\beta=0}^{j-1} K_\pi^{-\beta} + \frac{\varepsilon'_\pi}{m_\pi \cdot K_\pi^j} \right).$$

For the ith collision, the determination of the lower limit $\varepsilon_{\pi_{\min}}$ does not change. Therefore, equation (28) can be integrated with respect to ε_π in the form

$$dN_{\pi^\pm} = \Phi_2 (\varepsilon'_\pi, \cos\theta', h)\, d\varepsilon'_\pi d\cos\theta', \tag{29}$$

where

$$\Phi_2 = \sum_{i=1}^{i_1} \frac{A_N^i}{2\pi (i-1)! \lambda^i} \sum_{j=1}^{j_1(i)} \int_{m_\pi \left(\sum_{\beta=0}^{j-1} K_\pi^{-\beta} + \frac{\varepsilon'_\pi}{K_\pi^j m_\pi} \right)}^{K_N (E_N^{i-1} - M)} D_{j-1}^i \cdot A_{i_\pi}^j \cdot \omega_N (\varepsilon_\pi) \times$$

$$\times \left[\frac{\lambda (\varepsilon_\pi^2 - p_\perp^2 - m_\pi^2)^{1/2}}{(\varepsilon_\pi^2 - m_\pi^2)^{1/2} - (\varepsilon_\pi^2 - m_\pi^2 - p_\perp^2)^{1/2}} \right]^{Q+i} \times$$

$$\times \frac{d\varepsilon_\pi}{\sqrt{1 - \left(\frac{\varepsilon_\pi^2 - m_\pi^2 - p_\perp^2}{\varepsilon_\pi^2 - m_\pi^2} \right) - \left(\frac{\varepsilon'^2_\pi - m_\pi^2 - p_\perp^2}{\varepsilon'^2_\pi - m_\pi^2} \right) - \cos^2\theta' + 2\cos\theta' \left(\frac{\varepsilon'^2_\pi - p_\perp^2 - m_\pi^2}{\varepsilon'^2_\pi - m_\pi^2} \right)^{1/2} \left(\frac{\varepsilon_\pi^2 - p_\perp^2 - m_\pi^2}{\varepsilon_\pi^2 - m_\pi^2} \right)^{1/2}}}.$$

Consequently, the total number of π mesons of the first and second generations at a depth h, averaged over the different generation levels, is

$$dN_{\pi^\pm} = (\Phi_1 + \Phi_2)\, d\varepsilon'_\pi d\cos\theta'. \tag{30}$$

In a similar way, it is possible in principle to compute the contribution Φ_3 of the third and following generations. This would solve the entire problem, since equation (30) could be integrated with respect to the energies and angles and the total multiplicity of $\pi^\pm$ mesons at a specified observation level h could be obtained. To do this, of course, the pattern of elementary events would have to be worked out in further detail, by selecting a specific energy spectrum for π-meson generation and by determining more precisely the energy dependence of $\varepsilon'_{\min}$.

The scheme presented (K_N constant and K_π constant) implies that the meson energy spectrum has the same general form as the spectrum of the primary nucleons, so that for $\varepsilon_\pi \gg m_\pi$ it obeys a power law ($\sim 1/\varepsilon_\pi^\gamma$), where γ is the spectral index for the primary nucleons.

Let us estimate the probable contribution W of the function Φ_3 to (30). We take $\gamma \approx 2.5$ and assume a minimum multiplicity for $\pi^{\pm}$-meson production of $n_{\pi}^{\pm} = 3$. Then

$$W < \left(\frac{K_{\pi}}{n_{\pi^{\pm}}}\right)^{3\gamma} \approx 10^{-3}.$$

This approximate estimate indicates that Φ_3 can in practice be neglected. Thus, Φ_2 need be calculated only as far as terms which have orders of magnitude of 1/1000 of Φ_1.

The integral

$$N_{\pi^{\pm}} = \int_{\Delta\varepsilon_{\pi}}^{\varepsilon_{\pi\max}} d\varepsilon_{\pi}' \int_{0}^{\pi/2} d\cos\theta' \cdot (\Phi_1 + \Phi_2) \tag{31}$$

gives the total multiplicity of $\pi^{\pm}$ mesons at a depth h which have energies greater than the specified threshold energy $\Delta\varepsilon_{\pi}$ that can be recorded by the detectors.

Let us now calculate the energy spectrum and multiplicity of the μ mesons. We assume that the sole source of μ mesons is $\pi \to \mu + \nu$ decay. For energies $\varepsilon_{\pi}' > m_{\pi}$, the maximum μ-meson deviation $\alpha_{\max} \sim m_{\pi}^2/2 \cdot m_{\mu} \cdot \varepsilon_{\pi}'$ is found to be small. Therefore, only a slight error is introduced if we assume that the μ meson retains the original angle of emergence θ' of the π meson.

For a specified π-meson energy ε_{π}', the μ-meson energy ε_{μ} varies over a quite wide interval, $\frac{\varepsilon_{\pi}' \cdot m_{\mu}^2}{m_{\pi}^2} \leqslant \varepsilon_{\mu} \leqslant \varepsilon_{\pi}'$, within which the distribution is uniform:

$$dN_{\mu} = \frac{m_{\pi}^2}{(m_{\pi}^2 - m_{\mu}^2)} \frac{d\varepsilon_{\mu}}{\sqrt{\varepsilon_{\pi}'^2 - m_{\pi}^2}}. \tag{32}$$

The probability that a μ meson generated at a depth h' with an energy ε_{μ} will reach a depth h, allowing for specific ionization losses $K = 2.2 \times 10^6 \frac{\text{MeV} \cdot \text{cm}^2}{2}$, is*

$$P_{\mu}(\varepsilon_{\mu}, \cos\theta', h, h') = \left\{\frac{h' [\varepsilon_{\mu} \cos\theta' - K(h - h')]}{h \cdot \varepsilon_{\mu} \cos\theta'}\right\}^{\frac{m_{\mu} RT}{\tau_{\mu} g (\varepsilon_{\mu} \cos\theta + h' K)}}, \tag{33}$$

where τ_{μ} is the lifetime of a μ meson. If we convert to the energy $\varepsilon_{\mu}' = \varepsilon_{\mu} - \frac{(h - h')K}{\cos\theta}$ of the μ mesons at the level of observation h, then (33) becomes

$$P_{\mu}(\varepsilon_{\mu}', \cos\theta', h, h') = \left\{\frac{h' \cdot \varepsilon_{\mu}' \cos\theta'}{\cos\theta' \varepsilon_{\mu}' + (h - h') K}\right\}^{\frac{m_{\mu} RT}{\tau_{\mu} g (\varepsilon_{\mu}' \cos\theta' + hK)}}. \tag{34}$$

The probability that a π meson with an energy ε_{π}' will decay at a height between h' and $h' + dh'$ is

$$dW_{\pi} = \frac{m_{\pi} RT}{g \cdot \tau_{\pi} \cdot \sqrt{\varepsilon_{\pi}'^2 - m_{\pi}^2} \cos\theta'} \frac{dh'}{h'}. \tag{35}$$

* The velocity of light c is everywhere taken as unity.

The differential density of the μ-meson distribution with respect to angles θ' and energies ε'_μ at the level of observation h is given by the following expression:

$$dN_\mu = F \cdot d\varepsilon'_\mu d\cos\theta',$$

where

$$F = \frac{m_\pi^3 RT}{(m_\pi^2 - m_\mu^2)\, g\tau_\pi \cos\theta'} \int_0^h dh' \int_{\frac{m_\pi^2}{m_\mu^2}\left(\varepsilon'_\mu + \frac{K(h-h')}{\cos\theta'}\right)}^{\varepsilon_{\pi\max}} \frac{d\varepsilon_\pi}{\sqrt{\varepsilon_\pi^2 - m_\pi^2}} \times$$

$$\times \left\{\frac{h'\varepsilon'_\mu \cos\theta'}{\cos\theta' \cdot \varepsilon'_\mu + (h-h')K}\right\}^{\frac{m_\mu RT}{\tau_\mu g(\varepsilon'_\mu \cos\theta' + hK)}} \cdot (\Phi_1 + \Phi_2). \qquad (36)$$

The total multiplicity of μ mesons at the observation level h is

$$N_\mu = \int_0^{\pi/2} d\cos\theta' \int_{\Delta\varepsilon_\mu}^{\varepsilon_{\mu\max}} F \cdot d\varepsilon'_\mu, \qquad (37)$$

where $\Delta\varepsilon_\mu$ is the threshold energy for μ mesons recorded by the detector.

Using formulas (31) and (37), we can find the coupling coefficients /6/ for $\pi^\pm$ mesons and μ mesons:

$$W_{\pi^\pm}(E_0,\ \Delta\varepsilon_{\pi,h}) = \frac{D(E_0)\, N_{\pi^\pm}(E_0,\ h)}{\int_{\Delta\varepsilon_\pi}^{\varepsilon_{\pi\max}} N_{\pi^\pm}(E_0,\ h)\, D(E_0)\, dE_0}, \qquad (38)$$

$$W_\mu(E_0,\ \Delta\varepsilon_\mu,\ h) = \frac{D(E_0)\, N_\mu(E_0,\ h)}{\int_{\Delta\varepsilon_\mu}^{\varepsilon_{\mu\max}} N_\mu(E_0,\ h) \cdot D(E_0)\, dE_0}, \qquad (39)$$

where $D(E_0) \sim 1/E_0^\gamma$ is the spectrum of the primary nucleons.

Final results in the form of working curves can be obtained only after a large amount of calculational work; the foregoing calculations can be used in the computer programming.

Nuclear-Physics Institute of the
Academy of Sciences of
the Kazakh SSR

S. M. Kirov Kazakh
State University

REFERENCES

1. BOSS, E.G. and Zh.S.TAKIBAEV.— Trudy MKKL, **1**, p.76, Moskva. 1959.

2. DOBROTIN, N.A. and S.A. SLAVATINSKII. Report at Xth conference, Rochester. 1960.

3. DOBROTIN, N.A., G.T. ZATSEPIN, I.L.ROZENTAL', L.I.SARYCHEVA, G.B.KHRISTIANSEN, and L.Kh. EIDUS.— UFN, **49**, 185. 1953.

4. GROTE, C., I. KABUHN, U. KRECKER, U.KUNDT, K. LANIUS, and H.W. MEIER. Inelastic π^--Nucleon Interactions at 7.5Gev. in the Emulsion.—Nuovo Cim. (in press).

5. COCCONI, G. Experimental Results Obtained with the 25 Gev CERN Accelerator.— CERN Symposium. 1961.

6. DORMAN, L.I. Variatsii kosmicheskikh luchei (Cosmic-Ray Variations).— Moskva, Gostekhizdat. 1957.

N67 38226

A.I. Kuz'min, P.A. Krivoshapkin, G.F. Krymskii, and G.V. Skripin

A STUDY OF TEMPERATURE FLUCTUATIONS OF THE UPPER ATMOSPHERE, ACCORDING TO DATA OF UNDERGROUND COSMIC-RAY MEASUREMENTS

At present the characteristics of the upper atmosphere are studied in three ways: by means of radiosondes; from the luminous emissions of the night sky; and by sporadic flights of meteorological rockets. The information gained using radiosondes is limited to an altitude of 16 to 20 km, while spectral studies of the luminosity of the night sky pertain to the layer between the 80-km and 120-km levels. Meteorological rockets are launched very infrequently and at only a few points in the world. Consequently, practically no systematic data are available on the dynamics of the atmospheric layer between 20 and 80 km.

On the other hand, to understand the relation between solar-terrestrial phenomena and the general circulation of the atmosphere, it is important to have information on the dynamics of the middle atmosphere (mesosphere) which is as complete as possible.

This report will present some results concerning tne periodic temperature fluctuations in the mesosphere. The data were obtained from underground measurements of the cosmic-ray intensity at Yakutsk. The results of continuous recordings in 1959–1960 of the cosmic-ray intensity, for zenith angles of 30° and 60°, at ground level and at 20 and 60 m. w. e. underground, are used.

The experimental equipment is described in /1/. It was assumed that the intensity variations of cosmic rays with 60° zenith angles, measured at 20 and 60 m. w. e. underground, were due solely to temperature fluctuations of the atmosphere. The contribution of temperature variations in the atmospheric layer from the earth's surface to the 50-mb level was taken into account using radiosonde data provided by the Yakutsk Aerological Station. The rest of the variation was assumed to be due to the layer above 50 mb. On the basis of these assumptions, the anticipated variations of the mesosphere temperature were evaluated for various density coefficients of the temperature effect. The above assumptions appear to be plausible in the light of findings /2/ concerning the energy dependence of the different cosmic-ray variations. The primary diurnal variations, for example, are described by a decreasing spectrum with an exponent of ~ 1.0. If the ground-level diurnal variation at the latitude of Yakutsk has an amplitude of 0.3%, then at 60 m. w. e. underground the variation amplitude will be $\sim 0.06\%$, and at a zenith angle of 60° it will be not more than 0.005%. Such primary variations lie at the limits of error of our measurements and thus we have not taken them into account. This is in fact also true for the 27-day, seasonal, and other regular cosmic-ray fluctuations.

The integral method of Feinberg and Dorman /3/ was applied to compute the temperature contribution to the cosmic-ray intensity:

$$\left(\frac{\delta I}{I}\right)_{\text{temp}} = \int_{h}^{h_0} W(h)\,\delta T(h)\,dh,$$

where $W(h)$ is the temperature-coefficient density; $\delta T(h)$ is the temperature variation in the layer for a pressure h; and h_0 is the recording level.

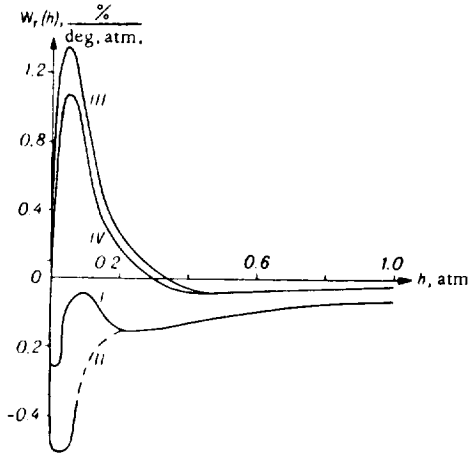

FIGURE 1. Temperature-coefficient density at depths of 20 and 60 m.w.e., for a 60° zenith angle.

I — $\gamma = 2$; II — $\gamma = 3$ for 20 m.w.e.; III — $\gamma = 2$; IV — $\gamma = 3$ for 60 m.w.e.

Figure 1 shows the temperature-coefficient density for the cosmic-ray intensity (zenith angle of 60°) at depths of 20 and 60 m. w. e. The curves for two different exponents of the differential energy spectrum for π-meson generation are given. The temperature-coefficient density was calculated according to a two-meson scheme for the generation of the hard component. The values of the parameters used were:

$$m_\mu = 215 m_e;\ \tau_\mu = 2.15 \cdot 10^{-6}\ \text{sec};$$

$$m_\pi = 276 m_e;\ \tau_\pi = 2.5 \cdot 10^{-8}\ \text{sec};$$

where m_μ, m_π, τ_μ, and τ_π are the masses and lifetimes of μ mesons and π mesons. The mean free path of a π meson until nuclear capture is $l_\pi = 120\ \text{g/cm}^2$. The average coefficient of energy transfer for $\pi \rightarrow \mu$ decay is $\alpha = 0.65$.

The thickness of the solid shielding above the equipment (along the vertical) was:

$\Delta\varepsilon = 4.52$ BeV for the 20 m. w. e. level;

$\Delta\varepsilon = 16.2$ BeV for the 60 m. w. e. level.

The ionization losses in the atmosphere were allowed for roughly by adding an extra 2 BeV for the shielding above the equipment. Values of the

effective indexes of the differential π-meson spectrum for underground equipment were taken from /4/. These indexes were 2.3, 2.8, and 3.0, for 20 and 60 m. w. e. respectively.

TABLE 1. Temperature coefficients for directional underground intensity.

Depth and direction	0–25 mb	0–50 mb
20 m. w. e., 60°	– 0.009%/deg.	– 0.020%/deg.
60 m. w. e., 60°	0.003%/deg.	0.04 %/deg.

Table 1 lists the specific temperature coefficients of the 0 to 50 mb layer, for the intensity recorded at 20 and 60 m. w. e. (60° zenith angle). Identical temperature variations are assumed throughout the entire layer.

THE SEASONAL VARIATION

The seasonal variations were computed from the average monthly values of the cosmic-ray intensity at 30 and 60° zenith angles, for ground level and for 20 and 60 m. w. e. underground. A correction for the barometric effect was introduced for the following values of the coefficients: $\beta\alpha_p = -0.13\%$/mb at the ground level and a 30° zenith angle; $\beta\alpha_p = -0.05\%$/mb at 20 m. w. e. and a 60° zenith angle; $\beta\alpha_p = 0.03\%$/mb at 60 m. w. e. and a 60° zenith angle. At the surface of the earth the actual seasonal variation is distorted considerably by different variations of extra-atmospheric origin. In order to reduce the effect of the distorting factors, we introduced corrections for the secular variation and the Forbush effect. The secular variation was corrected for roughly by means of a line joining the two end points of the seasonal variation (January and December). The Forbush effect was eliminated using neutron-component data, assuming a ratio of 2.5 between the effects upon the neutron and μ-meson components.

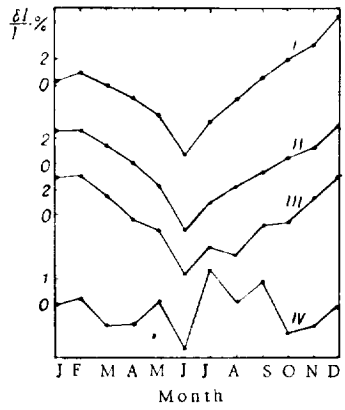

FIGURE 2. Seasonal variation of μ-meson intensity at earth's surface:

I–corrected for pressure; II–pressure effects and secular variation eliminated; III–pressure effects, secular variation, and Forbush effect eliminated; IV–intensity after successive elimination of pressure effects, secular variation, Forbush effects, and temperature effects up to 50-mb level ($\gamma_{eff} = 2.3$).

The seasonal intensity variations at the earth's surface, for a 30° zenith angle, are plotted in Figure 2. The curves were corrected successively for pressure, secular variation, Forbush effect, and temperature up to the 50-mb level. Figure 3 gives the seasonal variations of the directional intensity at depths of 20 and 60 m. w. e. The curves show the observed intensity variations and the variations corrected for the influence of various factors.

Curve III in Figure 2 and curves II in Figure 3 show that a seasonal variation can be distinguished at all depths of cosmic-ray recording. The correction for the change in atmospheric temperature up to the 50-mb level reduces the seasonal wave at the earth's surface by 3%; at depths of 20 and 60 m. w. e., it reduces the variation by 1.2 and 0.3%, respectively.

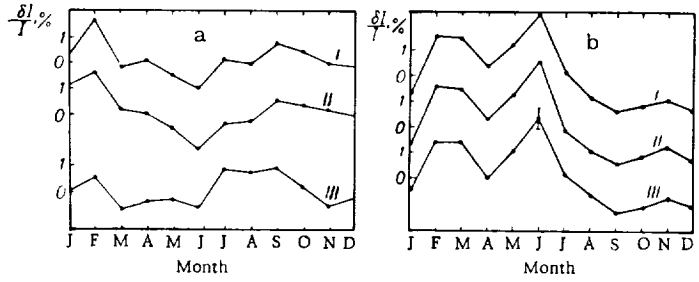

FIGURE 3. Seasonal variation of μ-meson intensity for 60° zenith angle: a) at 20 m.w.e., b) at 60 m.w.e.

I–observed intensity; II–corrected for pressure; III–variation remaining after removing pressure effects and temperature effects up to 50-mb level ($\gamma_{eff} = 2.8$).

The residual seasonal wave at ground level and at 20 m. w. e. (IV in Figure 2 and III in Figure 3a) is dephased for three months, relative to the seasonal wave before introduction of the temperature corrections. For

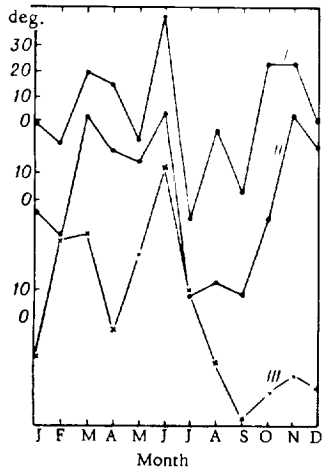

FIGURE 4. Expected seasonal temperature fluctuation in layer above 50 mb.

I–recorded at earth's surface; II–recorded at 20 m.w.e.; III–recorded at 60 m.w.e. (zenith angle of 60°).

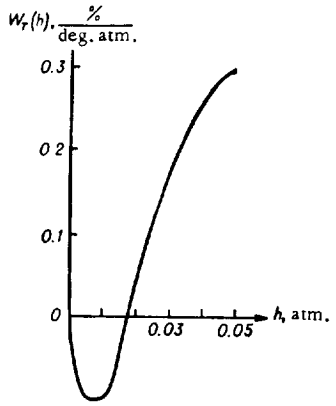

FIGURE 5. Density of temperature coefficient, for sum of instrument readings at depths of 20 and 60 m.w.e. (60° zenith angle).

the 60-m. w. e. level, on the other hand, the phase of the seasonal wave remains unchanged (III in Figure 3b).

The seasonal variations at the earth's surface and at 20 m. w. e. are out of phase with the variation at 60 m. w. e. This means that the residual seasonal wave is a result of atmospheric causes only, apparently of the temperature fluctuation above the 50-mb level. Moreover, this shows that the two-meson scheme adopted as a basis for the calculations is correct. Consequently, using the temperature coefficients, we can find the average temperature fluctuation to be expected above the 50-mb level. The average expected temperature variation in the layer from 0 to 50 mb is plotted in Figure 4, according to the data of three recordings at three depths. This figure shows that the spread of the seasonal temperature variations over Yakutsk in the layer above 50 mb is 70 to 100°C, with the maximum temperature during the spring months.

This seasonal variation of the temperature above 50 mb matches the annual variation in the ozone content of the ozone layer at high latitudes /5/.

It is possible to localize the layer between 0 and 50 mb which is responsible for the largest temperature variations. Let us take the sum of the readings of inclined instruments placed at depths of 20 and 60 m. w. e. The density of the temperature coefficient of this "component" is plotted in Figure 5. This density has different signs above and below the 20-mb level. Therefore, since the phase of the seasonal wave of the intensity is known, the layer making the largest contribution can be established. Analysis shows that the part of the atmosphere between 20 and 50 mb makes the largest contribution.

THE 27-DAY VARIATION

We used data from continuous cosmic-ray recordings (1959–1960) to investigate the 27-day variations. The recordings were made underground at depths of 20 and 60 m. w. e., for zenith angles of 30 and 60°. A 27-day wave with an amplitude of $\sim 0.3\%$ was detected at a depth of 60 m. w. e., by the method of mean values. The pressure correction increases the magnitude of the effect by 0.04%. The correction for the temperature effect from the earth's surface up to 50 mb, on the other hand, reduces the effect by 0.06%. This indicates that the 27-day wave at a depth of 60 m. w. e., for a zenith angle of 60°, is not very sensitive to pressure changes and temperature fluctuations below the 50-mb level.

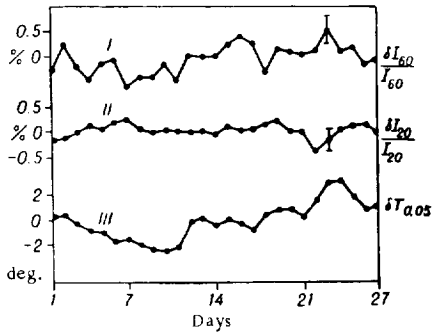

FIGURE 6. The 27-day variation in cosmic-ray intensity:

I, II–27-day intensity variation at depths of 20 and 60 m. w. e., for zenith angles of 30 and 60°, respectively; III–27-day fluctuation of temperature of 50-mb layer, averaged for 1959–1960.

Using the same method, we studied the 27-day wave at a depth of 20 m. w. e., for a zenith angle of 30°.

Figure 6 shows the 27-day intensity wave at 20 and 60 m. w. e., after correcting for the pressure and temperature up to the 50-mb level. The 27-day temperature fluctuations at the

50-mb level are also plotted in the figure. It is evident from Figure 6 that there is no considerable 27-day intensity wave at a depth of 20 m. w. e., for a zenith angle of 30°. However, a tendency toward fluctuations opposite to the 27-day intensity variations at a depth of 60 m. w. e., for a zenith angle of 60°, is noted.

The absence of a noticeable 27-day intensity wave at 20 m. w. e., for a 30° zenith angle, together with the presence of a considerable 27-day wave at 60 m. w. e., for a 60° zenith angle, confirm the atmospheric origin of these variations. Moreover, there is a direct correlation between the temperature fluctuations at the 50-mb level and the 27-day intensity wave at 60 m. w. e., for a zenith angle of 60°.

Consequently, the 27-day variation at 60 m. w. e. (curve I in Figure 6) is due to temperature fluctuations above 50 mb. The linear correlation between the cosmic-ray intensity at 60 m. w. e. and the temperature at the 50-mb level gives a regression coefficient of 0.12%/degree for a correlation coefficient of 60%. By comparing the regression coefficient with the temperature coefficient for the 0 to 50 mb layer, we find that the 27-day variations in the layer above 50 mb are on the average three times greater than at the 50-mb level, where the variations have a spread of about 6°. Hence the lower limit of the 27-day temperature fluctuations in the layer from 0 to 50 mb lies between 15 and 20°C.

THE DIURNAL VARIATION

Figure 7a shows the diurnal variations of the bihourly values of the meson intensity, measured underground at depths of 20 and 60 m. w. e., for a 60° zenith angle. The parameters of the 1st and 2nd harmonics of the diurnal

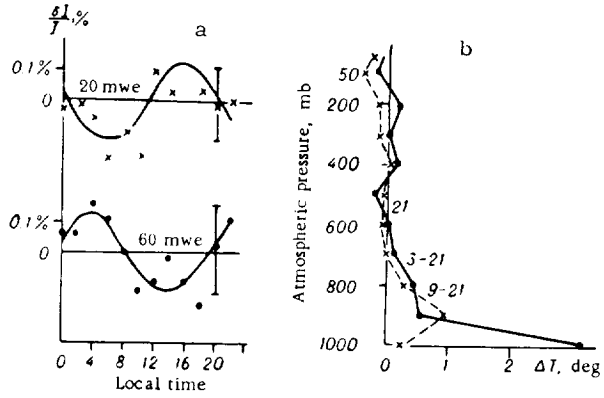

FIGURE 7. a-diurnal variation of cosmic-ray intensity; b-variation of temperature with height, in atmospheric section up to 50 mb.

intensity variation, after correcting for the barometric and temperature effects, are listed in Table 2. The diurnal temperature wave was determined from the data of three soundings of the atmosphere up to the 50-mb level; the technique described in /3/ and the temperature-coefficient density plotted in Figure 1 were used. Figure 7b shows a section through

the atmosphere, for the temperature variation with height up to the 50-mb level. The data were obtained from atmospheric soundings over Yakutsk at local times of 0300, 0900, and 2100 during 1958 and 1959. The data were normalized to the temperature variation with height for a radiosonde sent up at 2100.

TABLE 2. Amplitudes and phases of 1st and 2nd harmonics of diurnal meson-intensity variations, measured at Yakutsk in 1958–1959 using telescopes oriented 60° to the zenith (south-north)

Observation level	Correction	No. of recording days	A_1	t'_m	A_2	t''_m
20 m.w.e.	Pressure	530	0.12 ± 0.05	17.0 ± 1.6	0.07 ± 0.05	3.0 ± 2.7
	Temperature and pressure		0.14	16.2		
60 m.w.e.	Pressure	620	0.11 ± 0.06	2.6 ± 2.0	0.03 ± 0.06	3 + 7.0
	Temperature and pressure		0.14 ± 0.06	2.4 ± 2.0		

From Figure 7 and Table 2 it is evident that: (a) the diurnal variation at 20 m.w.e. is out of phase with the wave at 60 m.w.e.; (b) the correction for changes in atmospheric temperature up to the 50-mb level increases the amplitude of the first harmonic at both recording levels by 15–30%. This indicates that the average diurnal fluctuations in atmospheric temperature up to the 50-mb level are not in phase with the corresponding intensity fluctuations underground at 60 and 20 m.w.e., for a zenith angle of 60°. On the other hand, the temperature coefficient for the atmospheric layer above 50 mb has opposite signs for instruments located at depths of 20 and 60 m.w.e. Consequently, the observed intensity variations are due to the diurnal temperature fluctuations of the upper atmosphere. The data in Tables 1 and 2 can therefore be used to evaluate the diurnal variation in atmospheric temperature above the 50-mb level. The amplitude of the diurnal temperature fluctuations, according to Tables 1 and 2, are: $(0.14 \pm 0.06)/0.02 = 7 \pm 3°$ and $(0.14 \pm 0.08)/0.04 = 3.5 \pm 2°$, on the basis of instrument readings at depths of 20 and 60 m.w.e., respectively. The moment of maximum of the diurnal temperature fluctuations of the upper atmosphere (0–50 mb) must coincide with the moment of maximum of the diurnal intensity wave recorded 60 m.w.e. underground (0000 to 0400 local time).

CONCLUSION

An analysis of cosmic-ray measurements made at large equivalent depths underground (120 and 40 m.w.e.) indicates that the scheme accepted at present, explaining the generation of the hard component as being due to intermediate nuclear-active mesons, is correct. On the other hand, considerable periodic temperature variations are observed in the upper atmosphere, which originate at the height of the ozone layer. The amplitude of the seasonal variations in ozonosphere temperature is 35 to 50°, that of the 27-day variations is 5 to 10°, and that of the diurnal variations is 3 to 7°.

The annual temperature variation reaches a maximum during the spring months, and the maximum of the diurnal variation is during the night.

When the seasonal temperature variations of the level above 50 mb are taken into account, the residual seasonal wave indicated by the recordings of ground-level detectors of the hard component becomes smoothed out.

It is important to take into consideration the temperature oscillations in the upper atmospheric layers, when studying the 27-day and diurnal variations of the hard component.

We should also note that the course of the temperature oscillations shows a good fit with data obtained from spectral observations of the luminous emission of the night sky. Temperature fluctuations of the upper atmosphere measured by spectral methods pertain to heights from 80 to 120 km. The amplitudes of these fluctuations exceed severalfold the corresponding amplitudes reported by our measurements in the layer from 20 to 50 mb.

Institute of Space-Physics Research and Aeronomy,
Yakutsk Branch of Siberian Division of
USSR Academy of Sciences

REFERENCES

1. KUZ'MIN, A.I. Thesis, Nauchno-issledovatel'skii institut yadernoi fiziki, Moskovskii gosudarstvennyi universitet. 1960.

2. KUZ'MIN, A.I.— Trudy MKKL, 4. 1960.

3. DORMAN, L.I. Variatsii kosmicheskikh luchei (Cosmic-Ray Variations).— Moskva, Gostekhizdat. 1957.

4. KUZ'MIN, A.I. and A.A.DANILOV.— Trudy YaFSO, ANSSSR, seriya fizicheskaya, No. 3.

5. PROKOF'EVA, I.A. Atmosfernyi ozon (Atmospheric Ozone).— Izd. AN SSSR. 1951.

V. V. Smirnov and K. K. Fedchenko

THE BAROMETRIC EFFECT FOR THE ASK-3 IONIZATION CHAMBER AT MURMANSK (Synopsis)

The method of multiple correlation was applied to find the monthly values of the barometric coefficients for the ASK-3 ionization chamber at Murmansk. The data used, covering the period from December 1958 to January 1961, were corrected for the variation of atmospheric temperature (according to the method of Dorman and Feinberg).

In order to eliminate the influence of the primary cosmic-ray component, data on the neutron intensity for the period in question, obtained at Murmansk and Heiss Island, were used. The calculated values of the barometric coefficient show an appreciable annual variation, with fluctuations of about 20% from the mean for the period considered (the mean was 0.220 ± 0.003%/mb), and with a maximum at the beginning of January. This mean value of the coefficient is almost half again as large as the theoretical and experimental values for most ionization chambers (0.14 to 0.17%/mb).

It was assumed that the excessive value of the barometric coefficient for the ASK-3 chamber at Murmansk is not related to any properties of the meteorological conditions, but rather is instrumental in origin. In order to verify this assumption, the meson-component variations for the Murmansk chamber were compared with data from similar equipment at Cape Schmidt and Tixie Bay. The variations related to the change in the primary component for the Murmansk chamber were found to be 1.5 times greater than the corresponding variations recorded at the other stations. This confirms the above assumption of an instrumental reason for the excessive variations of the meteorological effect (the high barometric coefficient) and for the excessive variations related to the primary component.

The entire text of this report will be published in the collected proceedings of the Polar Geophysical Institute, entitled "A Study of Geophysical Phenomena of the Electromagnetic Complex at High Latitudes."

Polar Geophysical Institute,
Kola Branch of USSR Academy
of Sciences

N67-38227

A.A. Danilov

A COMPARISON BETWEEN THE DIURNAL VARIATIONS OF THE GEOMAGNETIC FIELD AND THE CORRESPONDING VARIATIONS OF COSMIC-RAY INTENSITY

I. INTRODUCTION

In /1, 2, 3/ the relation between the diurnal cosmic-ray variations and the variations of the geomagnetic field were studied. In some cases epochs were selected for consideration according to the level of geomagnetic activity, the average daily characteristics (such as the K_p index, the C_p index, and the H component during magnetic storms) being taken as a measure of the activity. In other cases epochs were selected according to some cosmic-ray criterion, and the correlation with geomagnetic activity was determined. This means of studying the cosmic-ray variations at the time of magnetic storms treated geomagnetic processes merely as indicators of large-scale phenomena in the vicinity of the earth.

In these studies it was assumed that all observable cosmic-ray variations are produced by sources located far away from the earth, and that variations of the geomagnetic field do not influence the cosmic-ray intensity, at least not within the limits of measurement accuracy.

However, the picture became changed when it was demonstrated /4, 5, 6, 7/ that local sources of cosmic-ray anisotropy exist, acting in the immediate vicinity of the earth, where the geomagnetic field can still affect the trajectories of charged particles considerably. It was shown in /4/ that a local source can form as a result of the direct action upon cosmic rays of a geomagnetic field which is asymmetrically distorted by a corpuscular flux.

If this is so, then it should be possible to find variations in cosmic-ray intensity when current systems, which can to some degree vary the geomagnetic field, are present in the ionosphere. In order to study this subject, it is important to select typical variations of the geomagnetic field which will have pronounced differences and which will make it possible to gather sufficient statistical data. Such variations are the solar-daily variations of the magnetic field, according to quiet days (S_q) and disturbed days (S_D), and also the seasonal variations for these days.

The S_q variations of the geomagnetism have been studied quite thoroughly /8–10/. At Yakutsk they take place with great regularity, recurring annually. The S_D variations have also been investigated thoroughly /8, 9, 11/, but they are less regular and their seasonal variations are less pronounced. Consequently, it is reasonable to consider the S_D variations

with respect to the locality of the station whose data are used and with respect to the period involved. This study makes use of data for the International Geophysical Year and the International Quiet-Sun Year, covering the time from 1 July 1957 to 31 December 1959. First, the regularities in the S_D variations at Yakutsk and the corresponding seasonal variations will be considered. Then a comparison with the intensity variations of the cosmic-ray neutron component will be made.

II. SOME REGULARITIES IN THE SEASONAL SHIFTS OF THE S_D VARIATIONS AT YAKUTSK

The initial data for our study of the S_D variations were the average hourly values of the geomagnetic-field elements. The variations were computed according to the scheme: $S_D = S_d - S_q$, where S_d are the average hourly values of the magnetic-field elements for disturbed days, and S_q are the average hourly values for 5 days of worldwide quiescence.

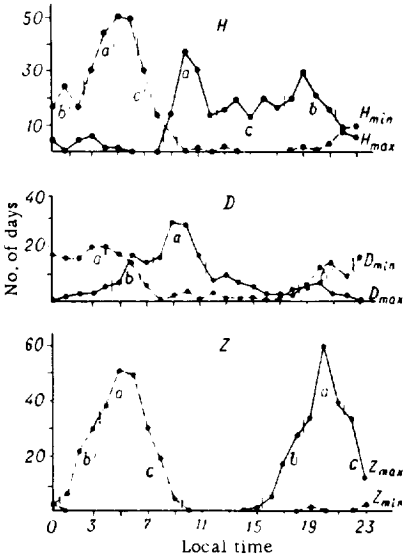

FIGURE 1. Diurnal variation of frequency of occurrence for extrema of: horizontal component H, declination D, and vertical component Z.

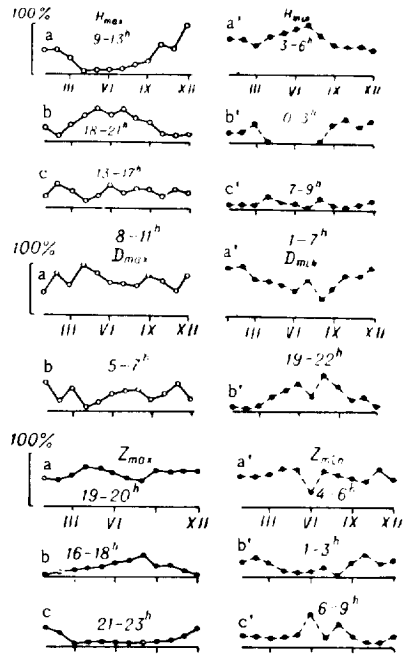

FIGURE 2. Seasonal variation of extrema of H, D, and Z for specific hours of the day.

For the period investigated, about 370 disturbed days were selected. Days on which $A<20\gamma$ were not considered, nor were days which coincided with the main phase of a storm, when the values of D_i and D_{st} were high (here, A is the amplitude of the S_D variations, D_i are the irregular

fluctuations, and D_{st} is the aperiodic variation). By considering each element separately according to the times of maximum and minimum, we determined the frequency of occurrence of extrema during the course of 24 hours. Figure 1 shows the diurnal variations of the frequency of occurrence for extrema of elements H, D, and Z. The frequency curves for the maxima and minima of these elements are separated [by vertical dashes] for the periods a, b, c and a', b', c', respectively. In Figure 2 the extrema corresponding to each of these periods are considered according to months. The curves in Figure 2 are normalized with respect to the total number of S_D days considered during the month. The number of days with extrema during periods a, b, c, etc. was determined as a percentage ratio to the entire number of S_D days considered. For example, for January, a total of 21 S_D days were considered with respect to a minimum of H; of these, 14, 4, and 1, respectively, had minima during periods a', b', and c'. This corresponds to values of 70, 20, and 0.5% in Figure 2. The other two days had minima at times which were not included in periods a', b', and c'.

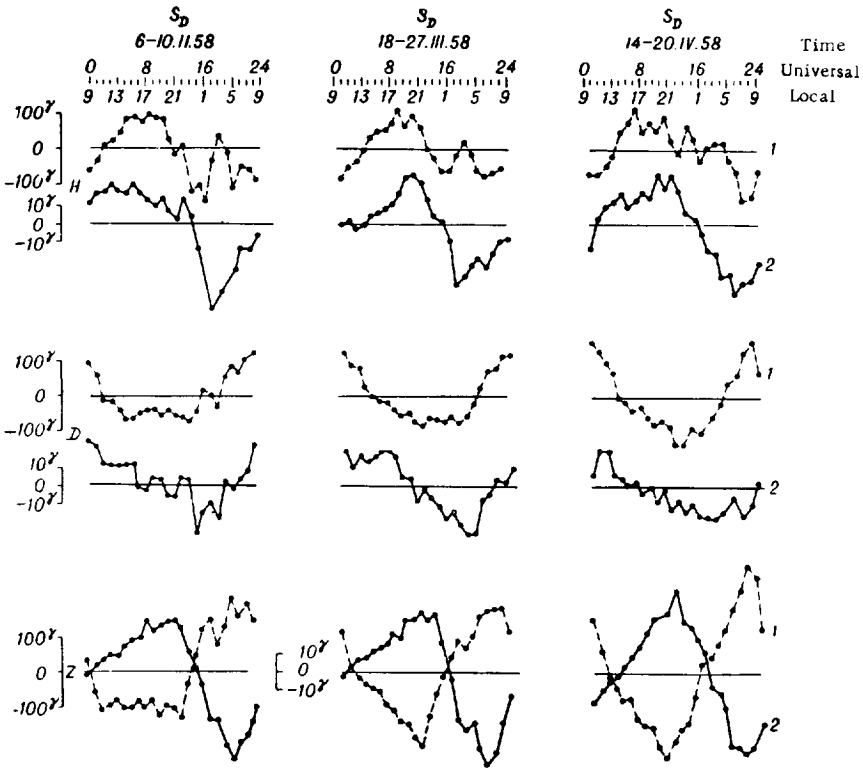

FIGURE 3. S_D variations of magnetic elements at Cape Chelyuskin (1) and Yakutsk (2). For Z the left scale pertains to Cape Chelyuskin and the right scale to Yakutsk.

The curves in Figures 1 and 2 reveal the following features of the S_D variations at Yakutsk.

I. The frequency of occurrence of H_{max} is distributed over times from 0900 to 2300 local time, while H_{min} occurs between 2200 and 0900.* It is noteworthy that the frequency curve for H_{max} covers a wider interval of time and has two maxima, whereas H_{min} is concentrated in a narrower interval and has a single maximum.

The extremum curves for periods a, b, and c, plotted over the months, indicate that a maximum occurs between 0900 and 1300 local time (period a) mainly during the winter months, while a maximum occurs between 1800 and 2100 (period b) mainly during the summer.

A minimum of H occurs between 0400 and 0600 hours, but there are instances of a shift toward earlier and later times of day. A shift toward earlier minima is observed in winter and at the equinox, but not during summer, when the minimum is shifted toward later times.

II. Extrema of D may occur at any time of day. D_{max} is observed more frequently between 0700 and 1100 hours (the largest absolute value of D, that is, the maximum deviation of the magnetic vector toward the west, is taken arbitrarily as the maximum). D_{min}, on the other hand, occurs more often between 2100 and 0600 local time.

III. The times of extrema of Z during the diurnal variation of this element follow a more definite pattern. The maximum occurs between 1900 and 2100, and the minimum between 0400 and 0600. There is a shift toward maxima at earlier hours in the summer and toward maxima at later hours in the winter. The shifts of the minima in the summer and winter are just the opposite of those of the maxima.

The foregoing analysis makes it possible to establish certain regularities in the S_D variations at Yakutsk. The results agree in the main with previous results presented in works on geomagnetism /8, 9, 11, 12/. However, the following distinctive features should be noted:

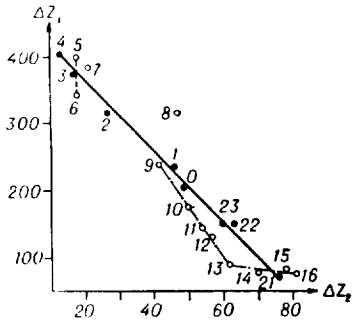

FIGURE 4. Relation between variations ΔZ_1 and ΔZ_2 of vertical vectors at Cape Chelyuskin and Yakutsk, respectively. Numbers at points denote hour of day.

1. The time of maximum H varies with the season of the year. The maximum in the summer is at about 1800 local time and in the winter it is at about 1000.

2. The time of minimum H is shifted toward later hours upon transition from winter to summer.

3. The maximum of D is shifted toward earlier hours in summer and toward later hours in winter.

4. The minimum of D is shifted toward earlier hours in winter and toward later hours in summer.

In order to explain the seasonal shifts of the S_D variations at Yakutsk, we made an approximate determination of the effective position of the source of these variations in the horizontal plane. To do this, we compared the variations at Yakutsk with those at Cape Chelyuskin.

Figure 3 shows the S_D variations of H, D, and Z at Cape Chelyuskin and Yakutsk, for three magnetic storms. The correlation between each pair of curves is good, especially for the Z component. It is significant that

* Local time only will be used throughout this report.

the variations of H and D have the same trend for the two locations, while the variations of Z have opposite trends.

It follows from this that if the S_D variations are caused by the magnetic field of a horizontal current, then the latter must be located between Cape Chelyuskin and Yakutsk. Figure 4 is a graph of the relation between ΔZ_1 and ΔZ_2, the hourly variations of the vertical components relative to the average diurnal values, for Cape Chelyuskin and Yakutsk respectively.

The table lists the ratios between ΔZ_1 and ΔZ_2 for several storms. Numbers indicate the ratios when the relation between ΔZ_1 and ΔZ_2 is linear, and lines indicate the absence of a linear relation. From Figure 4 and the table it is clear that three significant periods exist for the ratio $\frac{\Delta Z_1}{\Delta Z_2}$. The first period is from 2200 to 0600 and from 1000 to 1400, local time; the second period is from 0700 to 1000; and the third period is from 1500 to 2100. It should be noted that between 1000 and 1400 the variability of $\frac{\Delta Z_1}{\Delta Z_2}$ is slight.

Ratio between variations of vertical vectors at Cape Chelyuskin and Yakutsk (local time)

Month	Year	Time of day: 0	1	2	3	4	5	6	7	8	9	10	11	12	13	14	15	16	17	18	19	20	21	22	23
		1st period							2nd period				1st period				3rd period							1st period	
VIII	1957	7.5	7.5	7.5	7.5	7.5	7.5	7.5	—	—	—	—	—	9.0	9.0	9.0	9.0	0	0	0	—	—	—	—	7.5
X	1957	5.2	5.2	5.2	5.2	5.2	—	—	—	—	—	—	7.3	7.3	7.3	0	0	0	—	—	—	—	5.2	5.2	5.2
XI	1957	4.5	4.5	3.8	3.8	3.8	3.4	3.4	3.4	3.4	3.4	7.3	8.6	8.6	8.6	8.6	8.6	0	0	0	0	0	0	4.5	4.5
XI	1957	2.4	2.4	2.4	8.8	8.8	8.8	8.8	—	—	—	11.1	11.1	11.1	0	0	0	0	0	—	—	—	—	2.4	2.4
II	1958	2.7	2.7	2.7	2.7	2.7	2.7	2.7	2.7	—	—	9.1	9.1	9.1	9.1	9.1	0	0	0	0	0	0	0	2.7	2.7
IV	1958	12.1	—	—	—	—	—	—	—	—	—	10.2	10.2	10.2	10.2	—	0	0	0	0	0	12.1	12.1	12.1	12.1

Figure 5 is a schematic representation of the distribution of the magnetic-field vectors of a horizontal current. In the figure, A refers to Cape Chelyuskin, B to Yakutsk, and h to the height of the current above the earth's surface. At point C the proposed current flows perpendicular to the plane of the drawing. Let us assume that the magnetic variations at Cape Chelyuskin and Yakutsk have a single source with a magnetic moment $M = Hr^3$, where H is the field strength at the given point and r is the distance from the source to the observation point. In this case, for Cape Chelyuskin and Yakutsk, we find that $H_1 r_1^3 = H_2 r_2^3$, from which it follows that

$$\frac{r_1}{r_2} = \sqrt[3]{\frac{H_2}{H_1}}. \qquad (1)$$

From triangle ABC in Figure 5, we have

$$r_1^2 = (x - d)^2 + h^2, \qquad (2)$$

and also

$$r_2^2 = x^2 + h^2, \qquad (3)$$

where $d = AB \approx 1800$ km.

During the period from 0900 to 1400 local time the currents are oriented perpendicular to the meridian. Thus, the ratio $\frac{\Delta Z_1}{\Delta Z_2}$ for this period can be used to calculate the distance x. Let us take $\frac{\Delta Z_1}{\Delta Z_2} = 9.0$, and a current height $h = 300$ to

500 km /11/. Then, from (1), (2), and (3), we obtain $x = 1240$ km for $h = 300$ km and $x = 1360$ km for $h = 500$ km. The latitude variation corresponding to 1 degree of arc is about 110 km. Consequently, the currents causing the variations at Yakutsk are situated at a latitude of 63 to 65°, that is, in the zone of maximum polar aurora.*

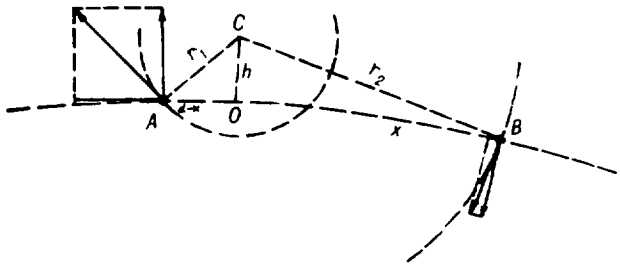

FIGURE 5. Diagram of magnetic field of horizontal linear current.

If we assume that the S_D variations are caused by a system of electrical currents in the upper layers of the atmosphere /8, 9, 11/, then spherical analysis indicates that this current system for the northern hemisphere consists of four current vortexes. Two vortexes are located on the morning and evening sides of the polar cap, and two are in the middle latitudes. According to /11/, over the Soviet Union the centers of the middle-latitude vortexes pass between 40 and 50° geomagnetic latitude and are subject to seasonal variations. The positions of the centers of these vortexes move south during the summer and north during the winter.

In view of the foregoing, the seasonal shifts of the S_D variations at Yakutsk can be reconciled with the constructed current systems if we make the following assumptions.

1. During the summer: (a) the middle-latitude vortexes move south; (b) the morning-side polar vortex moves down toward the south and migrates clockwise (that is, toward later hours); the evening-side polar vortex moves toward the south with its night edge and toward the north with its day edge.

2. During the winter: (a) the middle-latitude vortexes move upward; (b) the polar vortexes move in directions opposite to those in which they move during the summer.

Consequently, the following conclusions can be made.

1. The S_D variations at Yakutsk are caused, to a larger extent, by condensations of the current lines along the zone of polar aurorae, and, to a lesser extent, by the current lines of the middle-latitude vortexes.

2. The seasonal shifts of the S_D variations at Yakutsk are caused by changes in the locations of the vortex centers.

3. The condensations of current lines in the polar vortexes, which are responsible for the S_D variations at Yakutsk, pass closer to Yakutsk during the summer, at 0800 and 1900 local time.

* Some rough approximations were made in the calculation of x, but this is justified by the fact that the value was only estimated.

III. COMPARISON OF THE DIURNAL GEOMAGNETIC-FIELD VARIATIONS WITH THE COSMIC-RAY VARIATIONS

Data from the neutron monitor at Yakutsk were used for this comparison. In order to eliminate the influence of certain factors which are difficult to allow for, we tried to make the material uniform. Thus, the neutron data do not contain definite Forbush effects or sharp deviations due to other causes. The days were selected according to the same calendar as the magnetic data. The mean statistical error for the neutrons was calculated from the formula

$$M = \pm \frac{m}{\sqrt{n}} = \pm \frac{0.56}{\sqrt{n}},$$

where 0.56 is the bihourly statistical error of the neutron recording at Yakutsk. The neutron intensity is calculated to the 1000-mb level.

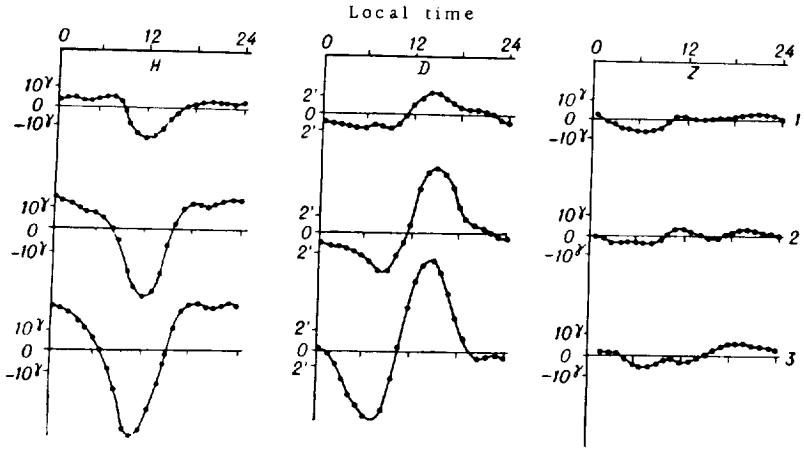

FIGURE 6. Diurnal variations of H, D, and Z for quiet days.
1–winter; 2–equinoxes; 3–summer.

Figure 6 shows the S_q variations of H, D, and Z at Yakutsk, according to seasons. The S_q variations of H and D are found to increase from winter to summer, the nature of the variations remaining the same. There are almost no S_q variations of Z at any time. It can be assumed that seasonal shifts of the S_q variations at Yakutsk take place only owing to a change in the intensity of the currents.

Figure 7 gives the diurnal variations of the neutron intensity for winter (W), the equinoxes (E), and summer (S). The solid curves pertain to quiet days, and the dashed curves to disturbed days (planetary index $K_p \leqslant 4$). A comparison of the solid and dashed curves confirms the existence of the obtained diurnal variations. It is evident from Figure 7 that the diurnal variation of neutrons during the winter has the form of a simple wave with a single maximum, whereas in the summer and at the equinoxes the wave is complex, having two maxima. During the IGY and IQSY, the diurnal neutron variations were subject to pronounced seasonal shifts. A

comparison of the diurnal variations in winter with those in the other seasons shows that the latter can be obtained by superimposing a simple wave with a daytime minimum onto the wave of the winter variations. This simple wave, moreover, is very similar to the diurnal variation of the H component for quiet days.

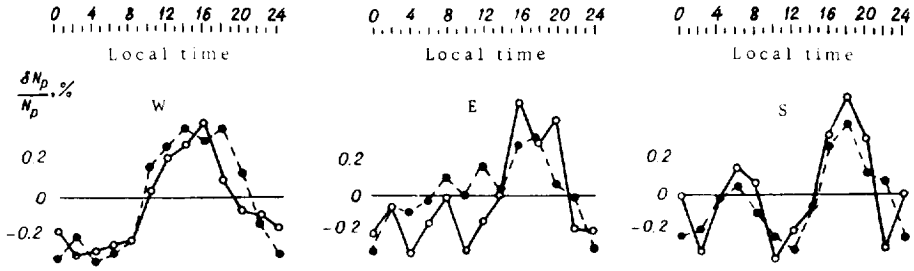

FIGURE 7. Diurnal variation of neutron intensity at Yakutsk, according to seasons.

W–winter; E–equinoxes; S–summer. Solid curves pertain to quiet days, dashed curves to disturbed days ($\bar{K}_p \leq 4$).

Diurnal-variation difference curves for the neutron intensity and the horizontal magnetic-field component are plotted in Figure 8, for the difference between summer and winter (a) and between the equinoxes and winter (b). The correlation between the curves is good.

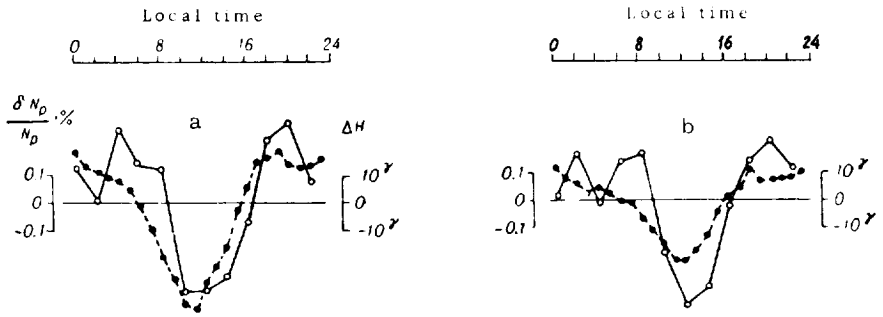

FIGURE 8. Difference between diurnal variations in summer and winter (a) and at the equinoxes and in winter (b), for quiet days. Dashed curves show variations of horizontal magnetic-field component, and solid curves show variations of neutron intensity. Left scale pertains to neutron intensity in percent. Right scale pertains to horizontal field component (in gammas).

Next let us consider the diurnal neutron-intensity variations on disturbed days. Figure 9 shows typical S_D variations of H, D, and Z at Yakutsk for summer and winter. The left graph in Figure 10 shows the disturbed diurnal neutron-intensity variations obtained according to the calendar of typical S_D variations in Figure 9. If it is assumed that the diurnal neutron-intensity variation for quiet days is present on all days, then the subtraction of this basic variation from the data for disturbed days will give a residual wave characteristic of the disturbed periods. Such a wave is plotted on the right graph in Figure 10. In the summer the residual wave for disturbed

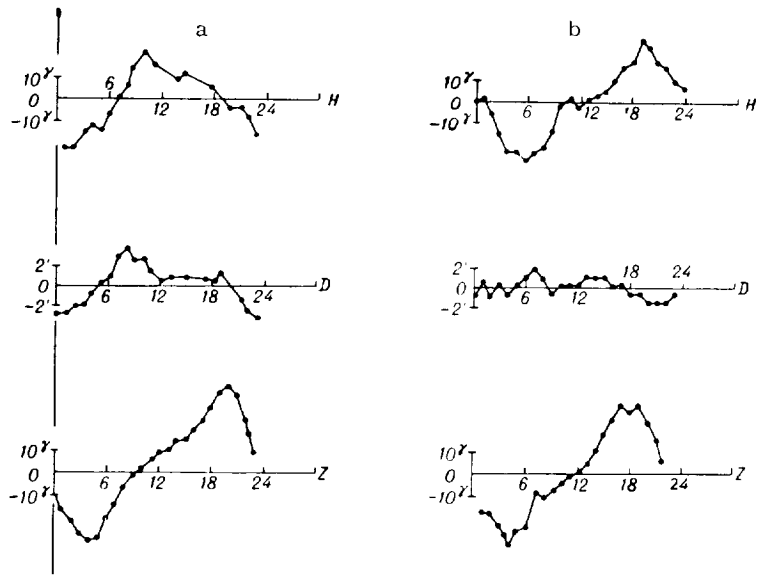

FIGURE 9. Typical S_D variations of magnetic elements at Yakutsk, for winter (a) and for summer (b).

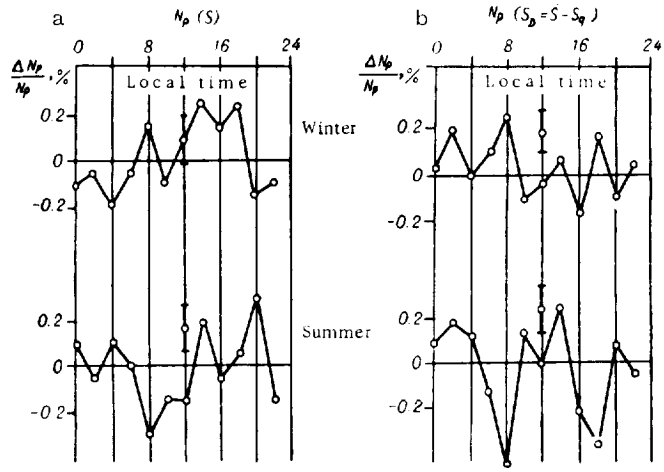

FIGURE 10. a–diurnal neutron-intensity variations at Yakutsk, for disturbed days; b–the same, but taking into account the variations on quiet days.

days has two sharp minima, one at 0600 to 0800 and one at 1600 to 1800, local time. It was pointed out above that, at just these times, the polar currents responsible for the S_D variations pass the closest to Yakutsk (the absence of a residual wave in winter is probably due to the fact that the selected S_D days differed little from the quiet days).

Figure 11 shows the differences between the summer and winter diurnal variations of the neutron intensity and horizontal field component for

disturbed days. The correlation between the curves for (ΔH) and (ΔN_D) is also good. At the same time, a comparison of Figures 8 and 11 indicates a poor correlation between the summer-winter difference curves for quiet and disturbed days. A "well" appears from 1000 to 1800 local time in the summer-winter difference curve for quiet days, while for disturbed days the "well" is from 0600 to 1800. Consequently, the seasonal shifts in the diurnal neutron-intensity variation are different for the different types of variations (S_q and S_D). However, for each type, the seasonal shifts of the diurnal neutron-intensity variation correlate well with the corresponding H-component shifts. This fact indicates that the shifts in the diurnal neutron variation from season to season are closely connected with shifts in the horizontal geomagnetic-field component.

It will be possible to describe the causes of the above regularities only after the latter have been verified using the data of the worldwide network of stations.

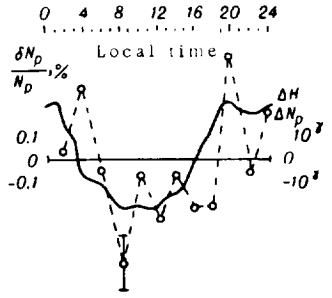

FIGURE 11. Difference between summer and winter diurnal variations of H component and neutron intensity, for disturbed days.

Solid curve is H component (ΔH), and dashed curve is neutron intensity (ΔN_D). Left scale pertains to neutrons and right scale to H component.

CONCLUSIONS

1. The S_D variations of the magnetic field at Yakutsk are caused mainly by systems of electric currents situated in the polar regions. The locations of these current systems vary from season to season. Condensations of the current lines pass closer to Yakutsk in the summer, at 0800 and 1900 local time.

2. During the IGY and IQSY, seasonal shifts in the diurnal variation of the cosmic-ray neutron-component intensity took place. If we take the winter diurnal variation of the neutron intensity on quiet days as the "normal" variation, then the corresponding diurnal variations on quiet days at the equinoxes and in summer can be represented as the sum of two waves: the "normal" wave plus a simple wave with a minimum in the daytime (Figure 8). The diurnal variation of the neutron intensity for disturbed days in the summer can be represented as the sum of three waves: the "normal" wave, a simple wave with a minimum in the daytime (Figure 8), and a wave with minima at 0800 and 1800 local time (Figure 10).

3. The seasonal shifts in the diurnal variation of the neutron intensity at Yakutsk correlate well with the corresponding seasonal shifts of the horizontal component of the geomagnetic field.

The author expresses thanks to A. I. Kuz'min, G. F. Krymskii, and G. V. Skripin for their valuable remarks and advice, and to G. G. Samsonov and T. G. Komarenko for their aid in preparing the report.

REFERENCES

1. SEKIDO, Y. and S. YOSHIDA.— Rep. Ion. Res. Japan, **4**, 37. 1950.
2. KUZ'MIN, A.I. and G.V. SKRIPIN.— Trudy YaFSO, AN SSSR, No.4. 1962.
3. KANE, R.P.— Indian Journ. of Physics, **36**, No.3, 237–281. 1962.
4. DORMAN, L.I. and O.I. INOZEMTSEVA.— Geomagnetizm i aeronomiya, II, 3, 454. 1962.
5. ELLIOT, H. and P. ROTHWELL.— Phil. Mag., **1**, 669. 1956.
6. SARABHAI, V., S.P. DUGGAL, U.R.RAO, H. RAZDAN, T.S.G. SARTRY, and R. PALMEIRA.— Trudy MKKL, No.4, p.237. 1960.
7. KUZ'MIN, A.I., S.N. DRUZHININ, G.V. SKRIPIN, and G.F.KRYMSKII. Report in this collection.
8. YANOVSKII, B.M. Zemnoi magnetizm (Terrestrial Magnetism).— Gostekhizdat. 1953.
9. CHAPMAN, S and J. BARTELS. Geomagnetism.— Clarendon Press, Oxford. 1940.
10. BEN'KOVA, N.P. Spokoinye solnechnosutochnye variatsii zemnogo magnetizma (Quiescent Solar-Daily Variations of Terrestrial Magnetism).— Trudy Nauchno-issledovatel'skikh uchrezhdenii gidrometeosluzhby, Ser. VI, No.1. 1941.
11. BEN'KOVA, N.P. Magnitnye buri i sistemy elektricheskikh tokov (Magnetic Storms and Systems of Electric Currents).— Trudy nauchno-issledovatel'skogo instituta zemnogo magnetizma. 1953.
12. AFANAS'EVA, V.I. (editor). Spravochnik po peremennomu magnitnomu polyu SSSR (Handbook on the Variable Magnetic Field of the USSR).— Gidrometeoizdat. 1954.

N67-30228

A. T. Abrosimov and Ya. L. Blokh

THE STUDY OF SHORT-PERIOD VARIATIONS AND MICROVARIATIONS IN COSMIC-RAY INTENSITY BY MEANS OF SINGLE SCINTILLATION COUNTERS

I. INTRODUCTION

Until recently the only time variations of cosmic-ray intensity which were separately distinguished were long-period variations /1/, (such as the 22-year and 11-year variations), variations with periods of 2 to 3 years, and annual variations. The other variations which were known previous to the IGY had durations of the order of days (27-day, diurnal, and semidiurnal variations; effects of magnetic storms on cosmic rays; large cosmic-ray bursts), and they constituted the remaining part of the variation types.

On the basis of the large amount of material collected during the IGY and after it, however, many studies of variations with shorter periods (of the order of several hours or even less) were made. The fine structures of the Forbush effect and the flare effect can be related to these new short-period variations. For example, the following effects were discovered:

1) an intensity rise prior to a magnetic storm /2, 3, 4, 5/, lasting some hours;

2) a predecrease prior to a magnetic storm /6, 7/, lasting some hours;

3) an intensity rise at the Forbush minimum /8, 9, 10/, lasting some hours;

4) effect of nonsimultaneous onset of the main phase of a Forbush decrease /2/, lasting some hours;

5) effect of disturbed solar-daily variations /11/ having phases some hours different from phases of quiet-sun variations;

6) effect of short-duration flares /12/, such as the one on 4 May 1960, which lasted 40 minutes;

7) effect of small flares /13, 14/ lasting some hours;

8) effect of modulation of solar particles by a corpuscular flux at the time of a large flare /15, 16/, lasting 10-15 minutes.

Nearly all the above variations were studied using the bihourly data of the world-wide system of stations. In only a few cases were 5, 10, and 15-minute data employed. The data used were, as a rule, averaged over many stations, so as to enable a more reliable discrimination of the effects. This was necessary because in certain cases the statistical accuracy of each instrument was insufficient compared to the amplitude of the effect.

II. THE NECESSITY FOR NEW INSTRUMENTS TO STUDY THE VARIATIONS

An analysis of these short-period variations having durations of a few hours or less indicates that they can be studied reliably only via a continuous recording of the various secondary cosmic-ray components by means of "superdetectors" (neutron monitors, cubical and azimuthal telescopes, underground telescopes, and other detectors) having statistical accuracies of some tenths of a percent for an averaging period of some minutes.

Such superinstruments are necessary because they will enable a detailed study of the short-period variations, together with their inherent properties, for different equipment and for observation points located in different parts of the world, without averaging the data over many stations. For instance, in general an intensity rise /2/ depends strongly on the longitude but depends less on the latitude. The rise at the time of a Forbush minimum /8/ depends on both latitude and longitude. The effect of the onset of a sharp drop at the time of a magnetic storm has a sharp longitude dependence. Finally, the effects of certain small flares /13/ depend on both latitude and longitude (impact zones).

Most studies of the short-period variations were made using the conventional instruments (standard neutron monitors, cubical telescopes, underground telescopes, etc.) of the world-wide system of IGY stations. This made it possible just to gain information concerning the existence of short-period variations and to find their overall regularities for a whole series of stations, the data of the latter being averaged over different station groups for each separate phenomenon. A considerably smaller system of superdetectors will make it possible to continue studying individual geophysical phenomena of interest and also to investigate the properties of these phenomena for each station separately. This will lead to a better understanding of the mechanism of short-period variations, and of all the fine-structure details related to them. In addition, a more detailed study of electromagnetic conditions in the interplanetary medium, in the galaxy, in the space around the sun, and in the vicinity of the earth will be possible, by means of the variations in cosmic-ray intensity. The establishment of a relatively small system of stations (10 or 15) with superdetectors, in addition to the existing stations, will make it possible to investigate cosmic-ray variations from a new point of view. Thereby an entirely new stage in the study of the universe by means of cosmic rays will be initiated.

Microvariations

In addition to enabling a closer study of the above-described short-period variations, instruments possessing superhigh statistical accuracies will make it possible to probe a completely new, uninvestigated range of variations in cosmic-ray intensity, namely the range of variations with periods of only a few minutes or even less. Let us call such variations microvariations. Microvariations were first studied at the Cosmic-Ray Laboratory of the Nuclear-Research Institute at Tokyo /17/. Instruments

with a high statistical accuracy (0.3% per minute) were employed, which will be described below. In the Tokyo studies the overall ionizing component was recorded continuously for a comparatively short period (April-May 1959). This made it possible to investigate variations of the short-period fluctuations, with periods from several minutes to several tens of minutes, which were unrelated to the statistical fluctuations.

Diurnal variations of the amplitude of the short-period fluctuations were detected. The variation amplitude was 2% and the maximum occurred between 1300 and 1500 local time. Variations of the average daily values of the short-period fluctuations were also found, which reached about ± 10% and which correlated with the average daily values of the meson intensity (correlation coefficient of 48%). Here, the amplitude of the short-period fluctuations refers to the difference between the largest and smallest intensity values during a 10-minute recording interval. The detector is assumed to have a counting rate with an averaging-time constant of 1 minute.

In /17/ the method of periodogram analysis was used to look for periodic variations of the fluctuations. Data for 26 to 29 May 1959 were used, and variations with periods between 5 and 50 minutes were sought. No such variations were found.

Thus, the initial step in the study of microvariations was taken, in that variations of the fluctuations of the data over some minutes were sought. In /17/ the possible causes of such variations were also analyzed, such as changes in atmospheric pressure and temperature and variations of the geomagnetic field.

III. METHODS FOR STUDYING SHORT-PERIOD VARIATIONS AND MICROVARIATIONS

Instruments designed to record continuously the short-period variations must have a high statistical accuracy and must provide data pertaining to short time intervals (several minutes or less). It is advisable to set up several identical recording channels (say, from 3 to 5) in order to increase the reliability of the results. Such equipment will have less rigid requirements imposed upon it with respect to stability over long periods (days or years).

One of the first detectors to provide continuous recording of the short-period variations of the hard component at sea level was the scintillation telescope of the MIT group /18/. This supertelescope consisted of three assemblies, each of which contained 8 circular plastic scintillators 1 meter in diameter and 10 cm thick. Four of the 8 plastic scintillators were arranged on one level in a lower row, and the other 4 were arranged in an upper row. Two parallel photomultipliers, with photocathode diameters of 12 cm, were provided for each set of 4 plastic disks. This supertelescope gave 1000 pulses/sec, with an accuracy of 0.4% per minute.

The first supermonitor was constructed in Canada in 1959 /19/. It consisted of 4 large neutron pulse ionization chambers filled with BF_3 gas. In 1960 the chambers were replaced by large proportional neutron counters (2 meters long and 15 cm in diameter) mounted in a cubical graphite container with a total weight of 22 tons. The statistical accuracy of this monitor was 0.3% per hour. On the basis of these counters, the

supermonitor described in /20/ was constructed. This is an assembly of 18 neutron counters; the overall area of the lead detector is 18 m^2, and the counting rate is 40,000 pulses/hour per square meter of detector surface (one counter). This supermonitor consists of three sections, each containing six counters. Polyethylene is used as a moderator and reflector, instead of the more usual paraffin. The steel counters have walls 0.8 mm thick. They are filled with BF_3 gas (boron enriched by 10 to 96%) to a pressure of 30 cm Hg. The differential amplitude spectrum for this counter is plotted in Figure 1 (potential of 2600 volts for 20 cm Hg pressure). Usually the counter had a potential of 3500 volts. The total number of neutrons counted by the monitor is equivalent to about $7 \cdot 10^5$ pulses/hour.

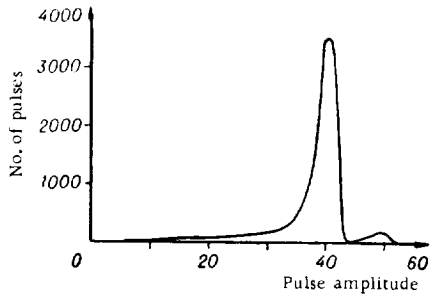

FIGURE 1. Pulse-amplitude distribution for neutron counter (2600 volts).

Single plastic scintillators were first used to investigate microvariations of the general ionizing component in /17/. In this same arrangement the scintillators enabled a simultaneous study of extensive air showers. The Tokyo arrangement made use of 10 m^2 (10 pieces) of plastic scintillator material in the single-count regime. A discriminator was used to select cosmic-ray particles which released around 20 MeV in the plastic scintillator (for vertically incident μ mesons). This made it possible to eliminate with reliability pulses due to radioactivity of the air and of surrounding objects, and also pulses related to the photomultiplier noise. The photomultipliers used in the counters were high-stability Dumont 6364 types, 240 mm in diameter. The statistical accuracy of the arrangement was 0.3% per minute.

IV. REQUIREMENTS FOR PHOTOMULTIPLIERS USED IN SCINTILLATION COUNTERS

When designing instruments for the study of variations in cosmic-ray intensity, it is difficult to ensure the constancy in time of the equipment parameters. If scintillation counters are used as pulse transmitters, moreover, stability of operation of the counter is especially important, since the photomultiplier operation has a decisive effect upon the performance of the equipment as a whole.

Even when the external conditions influencing photomultiplier operation are stabilized, by providing a high-stability voltage supply for the photomultiplier, and by shielding the photomultiplier from large temperature changes and from electric and magnetic fields, operational instability may arise due to causes inherent in the technology of preparing and constructing the photomultiplier. Consequently, the instability can depend considerably on the type of photomultiplier used in the scintillation counter.

The instability resulting from a gradual change in photomultiplier gain as time goes by (after thousands of hours) will not be considered here.

Such changes will naturally take place due to aging of the photomultiplier and due to changes in its "memory." In other words, instability which depends on the conditions existing prior to the period of the experiment (for instance, whether the photocathode was exposed to light or aged in darkness before the experiment) will be neglected.

The latter two types of instability are easily controlled during the operation of an assembly of scintillation counters, which is usually operated for tens, or even hundreds, of hours. Obviously, for such an operating regime, instability of the photomultiplier associated with its "memory," as well as instability due to the finite time required to establish steady performance of the multiplier, will be unimportant. The photomultipliers are continually within the lightproof cases of the scintillation counters, while the time for establishment of stability (about two hours) practically coincides with the time required to put the entire group of instruments into operation and to establish the temperature regime for all the electronic equipment.

However, it is necessary in practice to allow for, and to compensate for by means of auxiliary circuits, the integral sensitivity of the photomultiplier following the period of regime establishment (over several tens of hours). This is the kind of photomultiplier instability which we have studied.

The types of photomultipliers with louvered dynodes selected for test were FEU-11, FEU-13, FEU-14, and FEU-52; the FEU-24 multiplier was also studied. Photomultiplier types FEU-12, FEU-S, and FEU-33, respectively, were studied in /21, 22, 23/. A comparison of the performance of these photomultipliers under identical operating conditions will indicate which multiplier is the most stable.

The above types of photomultipliers were selected for study because they are the most appropriate for use in the scintillation counters designed to record cosmic radiation. Here, such multiplier parameters as integral sensitivity, photocathode area, amplitude resolution, and resolving time were taken into account. After additional investigation it will also be possible to allow for the temperature dependences and the operational stability. The latter, as will be shown in the following, can be allowed for by selecting a certain type of photomultiplier for operation. The large number of photomultiplier types studied is due to the fact that, for large cosmic-ray scintillation counters, it is not possible to select a single type of multiplier having large cathode area and the required gain, which in addition has good amplitude resolution and resolving time. It should be noted, however, that the new FEU-52 photomultiplier does satisfy both of these requirements /24, 25/.

V. EQUIPMENT FOR STUDYING THE OPERATIONAL STABILITY OF PHOTOMULTIPLIERS

All the photomultiplier types listed above were tested for operational stability by means of a setup consisting of different types of scintillators, a high-voltage rectifier, an amplitude analyzer, a ratemeter, two recorders, and a calibration generator. The photomultipliers being tested operated in three kinds of scintillators. Figure 2 shows a block diagram of the testing equipment.

In scintillators D-1 and D-2, which differed by the unsoldering of the constant resistances of the voltage divider, it was possible to select the potential distribution over the first three and last three photomultiplier electrodes for individual photomultiplier specimens. The voltages for the other dynodes were adjusted to the factory-specified values, which as a rule gave a uniform distribution of potential. The best results were obtained using the divider recommended in /25/. For the FEU-24 photomultiplier the voltage was so regulated that, at the time of selection, for the entire dynode system a constant potential (found experimentally) was maintained at the cathode gap (between the photocathode and the ring) /26/. The other type of scintillator (DS-1) was described in /27/.

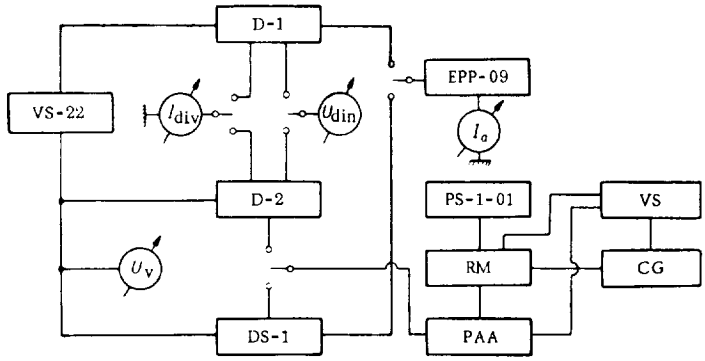

FIGURE 2. Block diagram of equipment for studying operational stability of photomultipliers.

D-1, D-2, and DS-1 are scintillators; PS-1-01 and EPP-09 are electronic recording potentiometers; RM is a counting-rate meter; PAA is a single-channel pulse-amplitude analyzer; VS-22 is a high-voltage rectifier with electronic stabilization; I_a is an LM-type microammeter; U_{din} is a device for measuring the interstage voltages of the photomultiplier; I_{div} is a milliammeter for measuring the divider current of the photomultiplier; VS is a stabilized rectifier; CG is a calibration generator; and U_v is a device for measuring the voltage supplied to the scintillators.

Switching circuits made it possible to use scintillators D-1 and DS-1 to study photomultiplier stability under conditions of constant lighting (uniform illumination of the entire photocathode surface by a constant light source). The photomultiplier output current was measured and recorded on the tape of an FPP-09 electronic recording potentiometer.

Scintillators D-2 and DS-1 were used to investigate the operational stability of photomultipliers under single-pulse conditions. In this study, the position of the maximum of the pulse-amplitude distribution was measured according to the readings of a single-channel amplitude analyzer and a counting-rate meter RM, operating according to the scheme described in /28/. The results were printed on the tape of a PS-1-01 recorder. The variation in the position of the maximum of the pulse-amplitude distribution was determined from the known shape of the differential amplitude spectrum of the recorded pulses.

During the measurements the current through the voltage divider for the photomultiplier was continually checked to see if it was constant. The operation and calibration of the electronic potentiometers were monitored by an LM microammeter.

The amplification of a photomultiplier is a function of the voltage of the power supply. Consequently, to ensure stable operation of the photomultiplier, the supply voltage must be highly stabilized. In practice, the required stability of the power-supply voltage must be an order of magnitude higher than the operational stability expected for the photomultiplier /29/. The shift in gain as a function of a change in supply voltage can be written as

$$\frac{dM}{M} = c \cdot n \cdot \frac{du}{u},$$

where n is the number of photomultiplier dynodes, and c is 0.7 /26/.

In our experiments the voltage for the electrical circuit of the photomultiplier was supplied by a VS-22 high-voltage rectifier with electronic stabilization. The stability of the output voltage of this power supply is better than ± 0.01% and for continuous operation it is better than ± 0.05%. The positive terminal of the power supply was grounded.

In spite of the fact that grounded-photocathode operation ensures high stability, the connection used in this case facilitates measurement of the average output current of the photomultiplier /30/. It is true that switching operations in the electronic potentiometer which change the polarity of its circuit are also necessary /31/; however, operation with a grounded positive terminal does not require the use of condensers with high working voltages.

VI. RESULTS OF THE PHOTOMULTIPLIER TESTS

Tests were run on 20 specimens of the FEU-24 photomultiplier and on 20 specimens of photomultipliers with focused multiplying systems.

The FEU-11, FEU-13, and FEU-14 photomultipliers were operated under conditions of average anode currents of about 35 to 40 μa. Photomultipliers with fused dynodes have higher stability when large currents are used, in comparison with those having antimony-cesium dynodes /32/. Therefore, these photomultipliers were tested at increased output currents, in order to provide a better check of their unstable operation. Above this value of the anode current, most photomultipliers cannot in general maintain steady-state operation, even if the additional current increase is only 10 or 15μa. The results of the tests of louvered-dynode photomultipliers indicated that only specimens with instabilities not exceeding 1% (from 7 to 10% of those tested) can be selected for use. The FEU-24 photomultipliers were tested for currents of about 2 or 3μa. This value of average anode current corresponds to the operating conditions for the photomultiplier in a non-shielded scintillation counter 0.5 m^2 in area, when it is exposed to particles from the cosmic-radiation background at sea level. For currents of tens of μa, moreover, the operational instability of these photomultipliers increases sharply.

The instability of the FEU-24 photomultipliers was several times greater than that of the FEU-11, FEU-13, and FEU-14 photomultipliers,

specimens known to have high instability having been selected beforehand. Let us note that, apart from the selection, it is important here that the photomultipliers operated with low output currents, so that changes in the gain of the photomultiplier were determined only by the last electrode and, consequently, were less than the changes at high anode currents.

All the photomultipliers were tested over a period of about 30 hours. In order to evaluate the expected operational instability, it must be taken into account that the scintillators employed in cosmic-ray detectors usually operate under field conditions. Thus, an additional change in the photomultiplier gain can take place depending on the temperature of the surrounding medium. If the temperature fluctuations are of the order of tens of degrees, then for certain types of photomultiplier this change may be comparable to the level of operational instability considered above.

The temperature stability of photomultipliers depends greatly on the photocathode material and on the method used to attach the cathode. FEU-11 photomultipliers, which have a photocathode with a metal backing, possess a high stability.

VII. STABILIZING THE OPERATION OF SCINTILLATION COUNTERS

Thus, for various reasons, the unstable operation of a photomultiplier leads to instability of the scintillation counter as a whole. Even for selected photomultipliers, moreover, this instability is quite considerable. The data obtained show that counters used for variation studies require additional automatic devices which will stabilize their operation.

Stabilization by the use of special dynode characteristics is possible /33, 34, 35/. However, such stabilization, which is quite simple to carry out technically, has several shortcomings. The reduction of the gain of the stabilizing dynode lowers the gain of the entire photomultiplier. Moreover, the focusing conditions are disturbed because of the nonproportional change in the dynode potentials, so that the range of gain variation is limited

Stabilization by means of external feedback loops is a popular method /36, 37/. Using feedback, it is possible to affect the electronic circuits following the photomultiplier as well (preamplifier, amplifier, etc.), so that compensation for a change in the amplitude of the photomultiplier output pulses will take place irregardless of the point of origin of the instability.

This method, which is more involved than the first one and which complicates the construction of the equipment, has several significant advantages. It does not decrease the photomultiplier gain, and also stabilization turns out to be possible over a wider range. Working signals passing through the amplifier stage of the scintillation counter can be used as control pulses.

This method was suggested, for example, in /38, 39/. These studies made use of the fact that there is a quite pronounced peak in the spectrum of the cosmic radiation recorded by a scintillation counter. Since this is the case, two differential channels with thresholds situated on the two sides of the maximum can be connected, the counting rates in the two channels being equalized, in such a way that a change in the gain of the counter will

result in a change in the counting rates in the channels. By means of differential counting-rate meters, a difference in the counting rates of the channels can be converted into a potential difference which will actuate the regulating mechanism.

To provide control pulses from auxiliary sources, either pulsing light sources or the monoenergetic radiation from a radioactive preparation /37/ are usually employed (the latter produces a standard pulse of light when it is totally absorbed in a scintillator). In the absence of Compton blurring, no pulses are produced in the low-energy part of the spectrum obtained. This method has been called the method using pilot radiation (or a pilot light source). It is convenient to use α-emitting elements (such as radium *D* or plutonium 239) as the radioactive preparation.

Control via a feedback loop is possible either using a discrimination circuit and amplifier or else using the photomultiplier itself plus a programed high-voltage power supply.

An auxiliary crystal can be inserted together with the radioactive preparation, in order to simplify the control circuit. Also, the light emitted by the basic scintillator can be attenuated additionally. If this is done, the pulses from the pilot source will have a greater amplitude than any pulses from the main scintillator. If the counting rate is then converted into a potential difference across some condenser, it is possible to compare this voltage with some standard reference source. The voltage difference obtained from this comparison is fed into the amplifier grid loop of the regulating circuit. In this way, for the energy range of the spectrum around 2 MeV, the calibration drift was less than 50 keV.

By using pulsing light sources as a pilot source, it is possible to increase the output-amplitude stability of the photomultipliers of counters to some tenths of a percent. However, as pointed out above, the scintillation counters in question are intended to operate under field conditions, in the presence of considerable fluctuations in the surrounding temperature. Under such conditions, the indicated stabilizing device will be ineffective, due to differences in the spectral compositions of the light from the source and the actual light from scintillations. An additional variation in the amplitude of the photomultiplier output pulses, associated with temperature variations of the spectral response of the photocathodes, will be observed.

It is easy to provide a regulating device by using a high-voltage photomultiplier supply whose output voltage can be varied according to a specified program /40/. If its general specifications are good (stabilization coefficient of output voltage correct to $\pm$ 0.01% and pulsations not exceeding 5 mv), such a source can guarantee a voltage change in accordance with the commands of a programing device with a quite high rate. The variation of the response rate of the rectifier to the commands given is specified.

In conclusion, let us note that another means of increasing the operational stability of scintillation counters is possible. Special photomultipliers have recently been developed which are characterized by extremely high stability /41/. One such unit is the new FEU-9367-V photomultiplier, which has antimony-cesium dynodes and a louvered multiplier system. The quantum yield of the photocathode is 12%, for radiation with a wavelength of 4200 Å; the photocathode response is 70 to 100 μa/lumen. This photomultiplier is recommended for use in cases when high stability of the

gain is required, and when good linearity of the photomultiplier characteristics is important. Finally, the ratio of dark current to gain for this photomultiplier is also good.

Institute of Terrestrial Magnetism, the Ionosphere, and Radio-Wave Propagation, USSR Academy of Sciences

Scientific-Research Institute for Nuclear Physics, Moscow State University

REFERENCES

1. DORMAN, L. I. Variatsii kosmicheskikh luchei (Cosmic-Ray Variations). — Gostekhizdat. 1957.

2. BLOKH, Ya. L., L. I. DORMAN, and N. S. KAMINER. — Trudy MKKL, **4**, p. 178. 1960.

3. BLOKH, Ya. L., L. I. DORMAN, and N. S. KAMINER. — Rezul'taty MGG, seriya kosmicheskie luchi, No. 2, p. 5. 1960.

4. TRUMPY, B. and T. SVANES. — Arb. Univ. Bergen, Mat.-Naturv. serie, No. 8. 1961.

5. BLOKH, Ya. L., L. I. DORMAN, and N. S. KAMINER. — Monographie, No. 12. p. 83, Paris. October 1961.

6. DORMAN, L. I., N. S. KAMINER, and Ya. L. BLOKH. — Rezul'taty MGG, seriya kosmicheskie luchi, No. 4, p. 49. 1961.

7. FENTON, A. G., K. G. McCRACKEN, D. C. ROSE, and B. G. WILSON. — Canad. J. Phys., **37**, 967. 1959.

8. DORMAN, L. I., Ya. L. BLOKH, and N. S. KAMINER. — Rezul'taty MGG, seriya kosmicheskie luchi, No. 4, p. 5. 1961.

9. YOSHIDA, S. and M. WADA. — Nature, **183**, 381. 1959.

10. KONDO, I., K. NAGASHIMA, S. YOSHIDA, and M. WADA. — Proc. Moscow Cosmic-Ray Conference, **4**, p. 208. 1960.

11. DORMAN, L. I. and O. I. INOZEMTSEVA. — Rezul'taty MGG, seriya kosmicheskie luchi, No. 4, p. 237. 1961.

12. KAMINER, N. S., Ya. L. BLOKH, and L. I. DORMAN. — Rezul'taty MGG, seriya kosmicheskie luchi, No. 4, p. 146. 1961.

13. KOLOMEETS, E. V. and G. A. SERGEEVA. — Rezul'taty MGG, seriya kosmicheskie luchi, No. 4, p. 132. 1961.

14. WILSON, B. G., D. C. ROSE, and M. D. WILSON. — Canad. J. Phys., **40**, 540. 1962.

15. BLOKH, Ya. L., O. I. INOZEMTSEVA, N. S. KAMINER, Yu. M. KOPYLOV, V. K. KOIAVA, and A. V. SERGEEV. — Geomagnetizm i aeronomiya, **1**, 441. 1961.

16. TRUMPY, B. and T. SVANES. — Arb. Univ. Bergen, Mat.-Naturv. serie, No. 14. 1961.

17. TORIZUKA, K. and M. WADA. — Sci. Papers IPCR, **54**, 162. 1960.

18. PALMEIRA, R. and R. W. WILLIAMS. — Nuovo Cimento, **8**, 358. 1958.

19. STEIJES, J. F. and H. CARMICHAEL. — J. Geoph. Research, **60**, 1363. 1961.

20. CARMICHAEL, H., NM-64 Neutron Monitor Specification. — Cospar Information Bulletin, No. 8, p. 15. 1962.

21. NEMILOV, Yu. A., V. M. OVCHINNIKOV, A. N. PISAREVSKII, and E. D. TETERIN. — Atomnaya energiya, **1**, 4. 51. 1956.

22. MELIORANSKII, A. S., I. V. ESTULIN, and L. F. KALINKIN. Report at Conference on Nuclear Radio Electronics, Moskva. 1959.

23. AKIMOV, Yu. K. Preprint, OIYal, **26**, p. 404. 1959.

24. VIL'DGRUBE, G. S., N. V. DUNAEVSKAYA, and I. A. KHARITONOVA. — Pribory i tekhnika eksperimenta, No. 6, 9. 1961.

25. VIL'DGRUBE, G.S., N.K.DALINENKO, N.V.DUNAEVSKAYA, and Zh.M. RONKIN.—Izv. AN SSSR, seriya fizicheskaya, **25**, 1183. 1961.

26. HARTMANN, V. and F.BERNHARD. Fotoelektronnye umnozhiteli (Photomultipliers), p. 194.—Moskva-Leningrad, Gosenergoizdat. 1961.

27. ABROSIMOV, A.T.—Pribory i tekhnika eksperimenta, No. 6, 48. 1960.

28. ELMORE, W.C. and M. SANDS. Electronics, Experimental Techniques.— Mc Graw-Hill, N.Y. 1949 [Russian translation. 1953.].

29. MATVEEV, V.V. and A.D.SOKOLOV. Fotoumnozhiteli v stsintillyatsionnykh schetchikakh (Photomultipliers in Scintillation Counters), p. 114.—Moskva, Gosatomizdat. 1962.

30. MATVEEV, V.V., A.D.SOKOLOV, and I.E.SULIMOVA.—Sbornik No. 2: "Uzly novoi apparatury dlya issledovaniya yadernykh izluchenii," p. 138, Moskva, Gosatomizdat. 1961.

31. KOMIONKO, L.A. and L.M. KOTLYAR.—Pribory i tekhnika eksperimenta, No. 6, 118. 1959.

32. VIL'DGRUBE, G.S.— Izv. AN SSSR, seriya fizicheskaya, **22**, 6, 517. 1958.

33. MORTON, G.A.—RCA Rev., **10**, 525. 1949.

34. KHACHATUROV, Yu.G.—Pribory i tekhnika eksperimenta, No. 4, 63. 1957.

35. ZLOBIN, L.I. and G.A.RADYUK.—Pribory i tekhnika eksperimenta, No. 2. 134. 1961.

36. ZLATAROV, V.K. Thesis, MGU. 1961.

37. SCHERBATSKOY, S.A.—RSJ, **32**, 599. 1961.

38. ABROSIMOV, A.T. and Ya.L.BLOKH.—Sbornik: "Kosmicheskie luchi," No. 5, 190. 1962.

39. BLOKH, Ya.L. and V.Kh.LEONOV.— Sbornik: "Kosmicheskie luchi," No. 5, 208. 1962.

40. Report of Carad Corp.—RSJ, 33, No. 1, 151. 1962.

41. Report of Electr. Tube Div., EMI.—RSJ, **33**, 154. 1962.

M. M. Daion and G. A. Leksin

SPARK DETECTORS FOR CHARGED PARTICLES (Synopsis)

During the last two or three years a very promising new method for recording charged particles and studying elementary processes has been worked out. This method, which saw a rapid development both in the Soviet Union and abroad, makes use of spark detectors (counters and chambers). Spark detectors make it possible to observe the trajectories of charged particles and to determine their coordinates with a high accuracy.

Such detectors are controlled instruments. Since their memory times can be made very short (some fractions of a microsecond), they can be used successfully in intensive particle fluxes. On the other hand, detectors of this type can also be made with long "memories" (hundreds of microseconds), which is necessary in certain special experiments.

A very important feature of spark detectors, even those with large dimensions (areas of thousands of cm^2), is that they are simple to construct, stable in operation, and do not necessitate high material costs during manufacture. They can be made entirely in laboratories possessing large material and technical resources.

Spark-chamber applications are particularly promising for cosmic-ray research in that such relatively simple, controlled detectors of particle tracks can be constructed with large dimensions and still have good spatial resolution.

For studies made from aircraft, artificial satellites, etc., an additional advantage of these detectors is light weight.

In this report, a brief introduction dealing with the history of the subject is followed by a discussion of the different types of spark counters and chambers, and of their characteristics and structural features. As an example, some more important studies with accelerators and cosmic-ray studies are cited, in which the new method was applied. In particular, we noted the wide use of spark chambers in the research works reported at the Conference on the Physics of High-Energy Particles at Geneva in 1962. It is enough to point out that the most interesting experimental studies related to the detection of V_e and V_μ could not have been made without using spark chambers.

The entire contents of the report can be found in the survey "Spark Detectors for Charged Particles" (Preprint, Institute of Theoretical and Experimental Physics, USSR Academy of Sciences, No. 77, 1962).

Institute of Theoretical and Experimental Physics, USSR Academy of Sciences

N67-38229

N.N. Nurgozhin and R.A. Nam

AN AIR-FILLED SPARK CHAMBER

We constructed a small experimental spark chamber in order to become familiar with the operation and construction of spark chambers, with a view toward building a large, multilayer chamber to record showers caused by high-energy cosmic-ray particles.

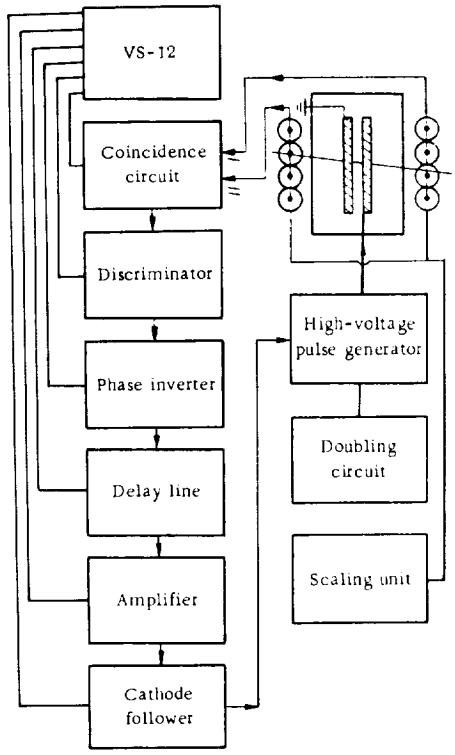

FIGURE 1. Block diagram of experimental equipment.

The experimental equipment (Figure 1) consisted of the spark chamber, a high-voltage generator, and auxiliary electronic circuits (high-voltage 20 kv rectifier, control circuit, etc.). The spark chamber was a stack of plane-parallel plate electrodes, assembled of four, three, and two plates

$180 \times 100\ mm^2$ in area and 3 mm thick; the plates were separated by cylindrical Teflon disks. The interelectrode gaps constituted the working volume of the chamber, in which the trajectories of charged particles were recorded. The distance between electrodes was determined by the height of the cylindrical spacers, which could be varied from 2 to 6 mm. The electrodes were polished rectangular steel plates with rounded-off edges. The chamber was placed in a transparent Plexiglas case with a cover. The working mixture used was air at atmospheric pressure. The sparks were observed visually through a side wall of the case, and also by means of millimeter graph paper, which was introduced into the spark gap, and which, when the spark current was high enough at the point of breakdown, had a hole burned in it with a diameter of about 0.1 mm. The introduction of the millimeter graph paper, by the way, did not make the chamber work less effectively.

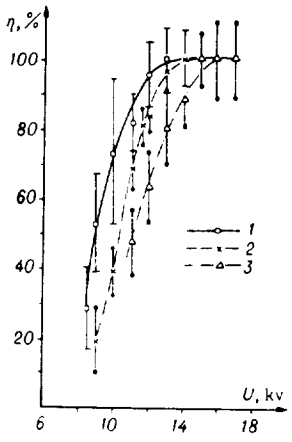

FIGURE 2. Chamber efficiency η as a function of amplitude of high-voltage pulses.

1 – $d = 2$ mm; 2 – $d = 4$ mm; 3 – $d = 6$ mm; $v_{cl} = 0$ volts, $\tau_{del} = 0.6\ \mu$sec.

The spark chamber, which was devised as a spark counter with a pulse voltage supply /1/, was controlled by a telescope consisting of two rows of MS-6 Geiger counters, one located above the chamber and one below it. The dimensions of the rows of counters were such that cosmic-ray particles recorded by the telescope passed through the sensitive volume of the chamber.

Pulses from the counters were fed through shaping multivibrators to a two-channel coincidence circuit with a resolving time of about 10^{-7} sec. The discriminated and amplified pulse from the coincidence circuit then actuated a high-voltage pulse generator, employing a type TGI-1 325/16 hydrogen thyratron. When the thyratron was triggered, a pulse was fed to the chamber electrodes; this pulse had a rise time of about 0.06 microseconds and an amplitude approximately equal to the peak anode voltage (5 to 16 kv) of the thyratron, and it decayed exponentially $\tau_d = 0.2\ \mu$sec).

The delay between the passage of a cosmic-ray particle through the chamber and the delivery of a high-voltage pulse to the chamber electrode was $0.6\ \mu$sec.

To check the background of random breakdowns of the high-voltage generator, a relaxation oscillator which was not associated with the passage of charged particles was used; this oscillator employed an MTKh-90 thyratron with a frequency of 40 pulses/minute. The number of random sparks amounted to 1 or 2%.

The operation of a spark chamber has, to a considerable degree, the properties of an individual spark gap with the same construction and supply as an air-filled counter.

In /2/ it was shown that, for a spark chamber ($10 \times 4\ cm^2$) consisting of four spark gaps with an interelectrode distance of 2 mm and filled with air at atmospheric pressure, a spark breakdown occurs, as a rule, only at

one gap (and at only one point in this gap). When we used four electrodes separated by 2 mm, a spark breakdown occurred in only one of the chamber gaps, although there were cases of two or more simultaneous breakdowns. Discharge in the chamber began at a voltage of 8 to 10 kv. The efficiency of a single chamber gap reached about 98% for a fixed value of the clearing field ($V_{cl} = 0$) and a delay time of 0.6 μsec.

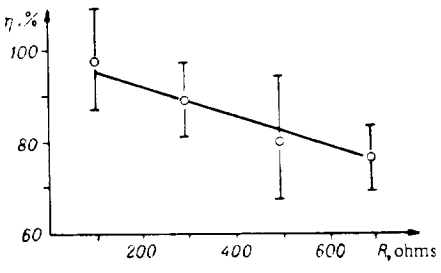

FIGURE 3. Efficiency as a function of limiting resistance R.

$V = 13$ kv; $v_{cl} = 0$; $\tau_{del} = 0.6$ μsec.

Improvement of the chamber operation using three electrodes was attained by selecting a limiting resistance ($R \sim 400$ ohms), connected in series with the chamber, when a discharge took place simultaneously in the two gaps, for a voltage of 14 to 16 kv and a 2-mm interelectrode distance (efficiency of about 80%).

For the chamber with two electrodes, the efficiency was plotted as a function of the amplitude of the high-voltage pulse (Figure 2), the interelectrode distance, and the value of the limiting resistance (Figure 3).

For an increase of the interelectrode distance from 2 to 6 mm, the beginning of the plateau shifts toward higher voltages. In this case the efficiency reaches about 100%. It should be noted that the efficiency drops with an increase in the limiting resistance. A similar result is observed for an increase in the chamber capacitance with a fixed value of the limiting resistance ($R \sim 200$ ohms). This can be explained by the action of the pulse front: before the pulse reaches the maximum value, required to detach an electron from an oxygen molecule, it accelerates the ions and brings about an action similar to that of the clearing field. An increase in RC makes the field act on the ions for a longer time, and consequently it reduces the efficiency.

The preliminary results indicate that, for a specified selection of the chamber parameters and circuit, it is feasible to record cosmic-ray particles using air-filled spark chambers.

Students V. A. Likhoded and V. K. Shirokii participated in this study.

S. M. Kirov Kazakh
State University

REFERENCES

1. CRANSHAW, T. E. and J. F. DE BEER. – Nuovo Cimento, 5, 1107, 1957.

2. BAYUKOV, Yu. D., G. A. LEKSIN, and D. A. SUCHKOV. – Pribory i tekhnika eksperimenta, No. 3, 66, 1961.

N67-38230

M.I. Pak and Yu.T. Lukin

A SPARK COUNTER FOR RECORDING COSMIC-RADIATION PARTICLES

Recently many articles have been published, in the Soviet Union and elsewhere, on spark counters and chambers intended for research in the physics of high-energy particles. Cranshaw and de Beer /1/ were the first to demonstrate that the efficiency of a charged-particle detector increases sharply if, in place of a constant voltage, a high-voltage pulse is applied to the counter electrodes after the passage of each particle.

This report deals with the design of a spark counter of large area, operating in conjunction with an ionization calorimeter and photographic emulsions. The efficiency of such a counter will also be studied.

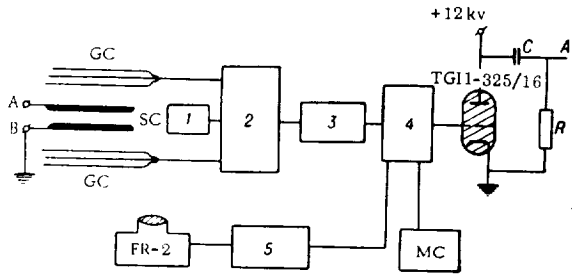

FIGURE 1. Block diagram of the equipment.

1-generator; 2-coincidence circuit; 3-delay line; 4-stage for shaping the delayed pulses; 5-camera circuit.

A diagram of the experimental equipment is shown in Figure 1. A Geiger-counter telescope (GC) connected in coincidence emits a pulse when an ionizing particle passes through the spark counter (SC). This coincidence pulse triggers a circuit which feeds a high-voltage pulse to the electrodes of the spark counter.

The triggering pulse actuates a mechanical counter which registers the number of coincidences, and also a type FR-2 photographic recorder which registers the number of breakdowns. The number of breakdowns is determined both visually and audially. In order to determine the number of spurious breakdowns of the spark counter, pulses were fed to the coincidence circuit from a relaxation oscillator. The triggering frequency of the oscillator was 0.23 cps.

The resolving time of the coincidence circuit was about 4μsec. A type-SN delay unit served as a delay line for counting coincidences and anti-coincidences.

The delay time of the high-voltage pulse was 3 μsec. In order to clear the spark-counter gap of "old" ions, a clearing field of from 0 to 300 volts was applied to the gap at points A and B.

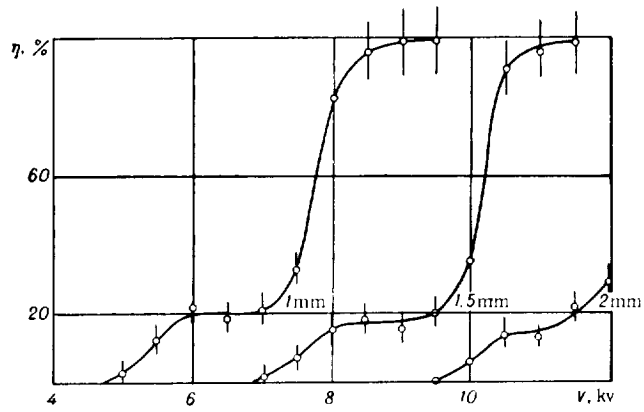

FIGURE 2. Spark-counter efficiency as a function of potential difference between electrodes ($t = 3\mu s$, $v_{cl} = 0$ volts). Numbers next to curves denote interelectrode distance.

The spark counter consisted of two parallel aluminum plates $23 \times 30\,cm^2$ in area and 3 mm thick. Plexiglas knobs were placed between the plates, and by varying the height of the knobs it was possible to vary the gap between the plates. Gaps of 1, 1.5, and 2 mm were used. The aluminum plates were polished to a mirror finish and their edges carefully rounded to eliminate edge effects.

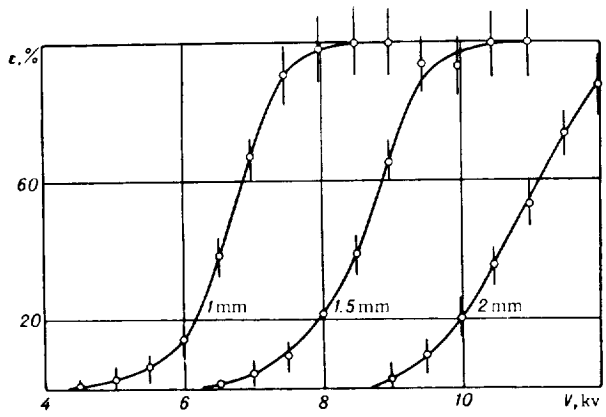

FIGURE 3. Efficiency for random and spurious breakdowns, as a function of potential difference between electrodes ($t = 3\mu s$, $v_{cl} = 0$ volts).

The experimental efficiency was determined as the ratio of the number of breakdowns to the number of coincidences. Cranshaw and de Beer give

a theoretical determination of the efficiency, assuming that the presence of a negative ion in the gap, at the moment when the applied high-voltage pulse reaches a critical value, is a necessary and sufficient condition for triggering a spark discharge. In this case the efficiency ε of the counter equals the probability that an ion which can bring about a breakdown be in the counter gap at the time when the pulse is fed in. Thus

$$\varepsilon = 1 - \exp[-n(d - vt)], \qquad (1)$$

where n is the specific ionization of the ionizing particle in air; d is the distance between the plates; t is the delay time of the arrival of the high-voltage pulse; and v is the velocity of the ions (equal to Kb, where K is the ion mobility and b is the clearing-field voltage).

Formula (1), however, does not give the counter efficiency as a function of the amplitude of the high-voltage pulse. Some investigators /1, 4, 5 / have indicated that there is a definite critical value of the high-voltage pulse, beginning at which the counter efficiency remains unchanged with an increase in pulse amplitude (in other words, that a "plateau" exists). We studied the efficiency of a spark counter as a function of the applied high voltage for gap distances of 1, 1.5, and 2 mm. The results are plotted in Figure 2, where the abscissa is the high voltage at the thyratron anode (measured to within ± 0.1 kv) and the ordinate is the efficiency. The measurement errors cited are statistical.

The curves for the efficiency as a function of the high voltage show that a definite critical value of the pulse amplitude does exist. We also measured the number of random and spurious breakdowns for the same voltages (Figure 3). The figure shows that for a gap of 1 mm there is a "plateau" between pulse amplitudes from 6.5 to 7.5 kv, where the efficiency for random and spurious breakdowns depends only slightly on the pulse amplitude. In our opinion, this "plateau" is a result of random coincidences

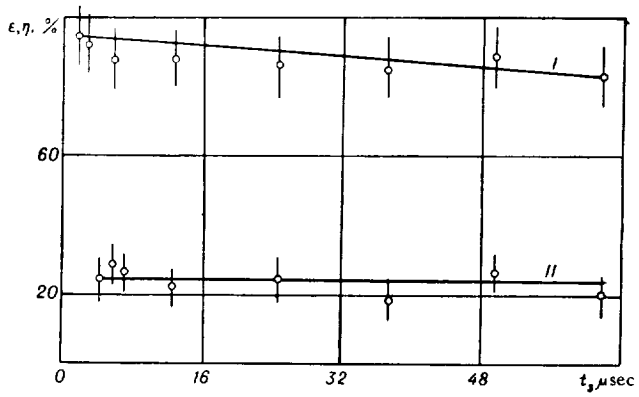

FIGURE 4. Effect of pulse-delay time on counter efficiency (I) and on efficiency for random and spurious breakdowns (II). Here, $V = 10$ kv, $v_{cl} = 0$ volts, and $d = 1.5$ mm.

produced because of the finite resolving time of the circuit. A further increase in the amplitude of the supply pulse leads to a sharp rise in the number of spurious breakdowns. A similar situation exists for other gap distances. Thus it is clear that the operating point for the counter should

be chosen somewhere in the region of the "plateau" of the efficiency for random and spurious breakdowns, in spite of the fact that at these voltages the efficiency for counting genuine pulses has not yet reached the saturation level.

For a gap of 1.5 mm, the efficiency of the spark counter was determined as a function of the delay time of the high-voltage pulse and also as a function of the voltage of the positive clearing field. The results are plotted in Figures 4 and 5. A change in delay time from 3 to 60 μsec was found to reduce the efficiency from 95 to 83%.

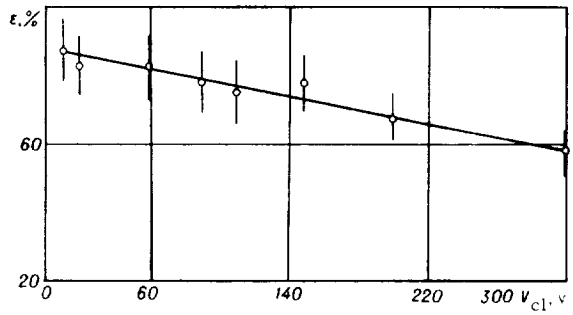

FIGURE 5. Effect of positive clearing field on counter efficiency.

Figure 4 also shows the efficiency for random and spurious breakdowns, which remained constant (about 20%) within the limits of measurement error. If the number of random breakdowns is subtracted, by the way, the number of spurious pulses is negligible (about 1 to 5%).

This indicates that a spark counter of this size and with this gap between its plates can be used successfully, along with an ionization calorimeter, to study the interaction of cosmic-radiation particles with matter.

CONCLUSIONS

1. Values of the supply voltage for a spark counter were recommended.
2. It was shown that the efficiency of a spark counter depends not only on the strength of the electric field but also on other structural features of the counter, the remaining parameters being the same.
3. A spark counter $23 \times 30\ cm^2$ in area with a 1.5 mm gap can be used in conjunction with an ionization calorimeter to study high-energy cosmic-ray particles.

The authors express thanks to A. A. Enin and to S. K. Vasilevskaya for their daily help in setting up and adjusting the experimental equipment and in carrying out the measurements.

Nuclear-Physics Institute of the Academy of Sciences of the Kazakh SSR

REFERENCES

1. CRANSHAW, T.E. and J.F. DE BEER. — Nuovo Cimento. **5**. 1107. 1957.
2. FUKUI, S. and S. MIYAMOTO. — Nuovo Cimento, **1**, 113. 1959.
3. MIKHAILOV, V.A., V.N. ROINISHVILI, and G.E. CHIKOVANI. — Pribory i tekhnika eksperimenta, No. 1, 39. 1961.
4. DAION, M.M., V.Kh. VOLYNSKII, and A.N. KOZHANOV. — Pribory i tekhnika eksperimenta, No. 2, 47. 1961.
5. BEALL, E.F., B. CORK, P.G. MURPHY, and W.A. WENZEL. — Nuovo Cimento, **20**, 502. 1961.
6. BAYUKOV, Yu.D., G.A. LEKSIN, and D.A. SUCHKOV. — Pribory i tekhnika eksperimenta, No. 3, 66, 1961.

N67-38231

I. Ya. Chasnikov

THE USE OF δ ELECTRONS TO DETERMINE THE NATURE AND ENERGY OF CHARGED PARTICLES

In nuclear-emulsion studies of the cosmic radiation, δ electrons are often used to determine the nature of the primary particles. Since the charge distribution of the primaries is intimately associated with the origin of the primary radiation, this subject is being given a great deal of attention by cosmic-ray physicists.

The charge of the particles is determined from a simple relation obtained by transforming the Rutherford formula for the interaction of the atomic electrons of the emulsion material with nuclei. The number of δ electrons with energies between T_1 and T_2 produced by a rapid charged particle with a charge z will be

$$N_\delta = 2\pi N \frac{e^4 z^2}{mc^2\beta^2}\left\{\frac{1}{T_1} - \frac{1}{T_2}\right\}, \qquad (1)$$

where N is the number of electrons per cm^3 of emulsion, βc is the velocity of the incident particle, and m is the electronic mass. In determining N_δ, δ electrons with energies $T_1 \sim 1.5$ keV and above are counted, since they usually leave tracks of four or more grains in the emulsion (including the grain at the track of the primary). The value of T_2 is about 7.5 keV, or for slow particles $T_{max} = [2\beta^2/(1-\beta^2)]\cdot mc^2$. In practice it can be assumed that T_2 always corresponds to T_{max}.

It should be noted that the use of expression (1) to determine the charge involves several assumptions. First, in the derivation of (1) it is considered that the atomic electrons are free. In reality, many of the electrons in the silver and bromine atoms of the emulsion have orbital velocities of about 0.1, which is not much less than the velocities of δ electrons with energies of T_1 ($\beta \sim 0.25$) /1/. Formula (1) does not take into account the spin of the interacting particles either. It is assumed that N_δ is practically independent of the velocity of the incident particle for $\beta > 0.75$ /2/. There are also some experimental difficulties related to counting the δ electrons, such as distinguishing genuine δ electrons from false (background) ones. The number of background electrons depends on the amount of time the emulsion is exposed, on the way it is prepared, and also on the subjective errors of the experimenter. Evaluations of the number of background electrons vary considerably from author to author and also for different experimental conditions (from several tens of electrons to several electrons per cm) /3-8/. Thus the value of N_δ given by (1) is only approximate. Consequently, it is reasonable to make calibration measurements for the tracks of the particles of known charge and velocity.

Table 1 lists experimental data on the number of δ electrons produced by protons with energies of 2, 4, and 9 BeV in NIKFI-R emulsions and by 20-BeV protons and 17.5-BeV π mesons in Ilford G5 emulsions.

TABLE 1

Emulsion type	Year of accelerator experiments	Nature of primary particle	Energy of primary particle, BeV	N_δ per cm	N_d per cm
NIKFI-R	Dubna 1960	Proton	9	8.9 ± 0.3	2.50 ± 0.16
	" 1961	"	9	7.5 ± 0.3	1.49 ± 0.13
	" 1961	"	4	9.4 ± 0.7	3.00 ± 0.39
	" 1961	"	2	10.9 ± 0.3	2.2 ± 0.16
Ilford G5	Geneva 1961	"	20	12 ± 0.8	1.93 ± 0.25
	" 1961	π meson	17.5	9.2 ± 0.8	1.70 ± 0.29

In the NIKFI-R emulsions, δ electrons were counted over a total track length of more than 5 meters, and in the Ilford G5 emulsions over about 0.5 meter. Table 1 gives the average values of N_δ for clear cases of δ electrons and also for doubtful cases (N_d). The errors in the determinations of N_δ and N_d are statistical.

TABLE 2

No. of plate	N_δ per cm
18	7.8 ± 1.0
28	9 ± 0.8
99	9.1 ± 0.5
133	9.5 ± 1.2
176	8.9 ± 0.8
199	8.8 ± 0.7

The number N_d includes δ electrons which could not be definitely established (when a track may have been made by a δ electron, by a background electron, or by a random accumulation of grains). Unskilled observers obtain values of N_d which differ considerably, and which may be quite high. However, dependable counts of N_d for the emulsions indicated will generally fluctuate about average values of 2 or 3. In the δ-electron count the four-grain criterion was applied. As Table 1 shows, the average number of δ electrons differs somewhat for different emulsion batches. In the Ilford G5 emulsions N_δ was higher than in the NIKFI-R emulsions. The blob density for the primary tracks, on the other hand, was less (15–19 and 22–24 per 100μ).

Table 2 lists the values of N_δ for different photographic plates from a single stack of NIKFI-R emulsions exposed in 1960. No dependence of N_δ on the number of the plate is observed. Measurements show that no dependence of N_δ on the immersion depth of the track into the emulsion exists either, which is very important from the methodological point of view.

In 1961 stacks of NIKFI-R emulsions were exposed twice, almost simultaneously. One stack was exposed to 9-BeV protons and, in a perpendicular direction, to 2-BeV protons. Another stack was similarly exposed to 9-BeV and 4-BeV protons. This made it possible to ascertain the dependence of N_δ

on β. As Table 1 shows, such a dependence does exist. For the first two proton energies, formula (1) gives a ratio $N_{\delta 2}/N_{\delta 9}$ of 1.12, whereas experiment gives 1.45 ± 0.07. Correspondingly, for the 4-BeV and 9-BeV protons these ratios are 1.04 and 1.26 ± 0.11. The discrepancies are apparently due to the assumptions mentioned above. The assumption that N_δ is constant for $\beta > 0.75$, for example, is not satisfied.

If sufficient statistical data are available (the track length must be several cm), N_δ as a function of β can be used to determine the nature of a singly charged particle according to the number of δ electrons. For this, the approximate value of $p\beta c$, which can be determined from multiple-scattering measurements, must be known. This method is applicable in the range $1.5\ \text{BeV} \leqslant p\beta c \leqslant 2.5\ \text{BeV}$, when it is impossible to ascertain the nature of the particles from measurements of the ionization and of $p\beta c$ /9/.

The energy (more precisely, $\gamma = 1/\sqrt{1-\beta^2}$) of a primary particle can be determined by measuring the angle of emergence and the kinetic energy T of an energetic δ electron. The kinematics of the elastic interaction between the particle and an atomic electron of the emulsion material gives the following formula /10, 11/:

$$\gamma = \left[\frac{T + 2mc^2}{2mc^2 - T\,\mathrm{tg}^2\,\theta}\right]^{1/2}.$$

If the approximate value of $p\beta c$ is known, then it is also possible to ascertain the nature of a singly charged particle /9/. However, very few δ electrons are useful in this respect. Table 3 shows the calculated and experimental values of n_e, the number of δ electrons with $T > 1$ MeV, as functions of γ, for 10 cm of the track of a singly charged particle.

TABLE 3

γ	3.1	10.5	27
n_e calculated	1.8	2.38	2.45
n_e experimental	1 ± 0.3	1.9 ± 0.5	1.5 ± 0.5

For multiply charged particles, n_e is higher by a factor of z^2. The experimental value of n_e includes only those electrons which are suitable for the measurement of multiple scattering. A somewhat more detailed discussion of the determination of γ particles by means of energetic δ electrons is given in /9/.

In conclusion, I wish to thank Zh. S. Takibaev for his interest in this study and also Z. V. Anzon for his aid in processing the experimental material.

Nuclear-Physics Institute of the
Academy of Sciences of the
Kazakh SSR

REFERENCES

1. POWELL, S.F., P.H.FOWLER, and D.H.PERKINS. The Study of Elementary Particles by the Photographic Method.— London, Pergamon. 1959 [Russian translation. 1962.]

2. BRADT, H.L. and B. PETERS.— Phys. Rev., 80, 943. 1950.

3. WADDINGTON, C.S.— Phil. Mag., **2**, 1059. 1957.

4. BRADT, H.L. and B. PETERS.— Phys. Rev., **77**, 54. 1950.

5. SAII, P.L.— Nuovo Cimento, **13**, 2411. 1959.

6. MATHIESEN, O.— Ark. Fys., **17**, 441. 1960.

7. DAINTON, A.D., P.H.FOWLER, and D.W. KENT.— Phil. Mag., **43**, 729. 1952.

8. DAINTON, A.D., P.H. FOWLER, and D.W. KENT.— Phil. Mag., **42**, 317. 1951.

9. CHASNIKOV, I. Ya.— Vestnik Akademii Nauk Kazakhskoi SSR, No.8, 96. 1962.

10. BISWAS, S., P.J.LAVAKARE, K.A. NEELAKANTAN, and P.G.SHUKLA.— Trudy MKKL, **3**, 116. Izd. AN SSSR. 1960.

11. JAIN, P.L.— Phys. Rev., **120**, 293. 1960.

E. T. Frantsuz

THE ORGANIZATION OF STRATOSPHERIC COSMIC-RAY OBSERVATIONS AT APATITY

Cosmic-ray observations in the stratosphere are being organized at the Cosmic-Ray Laboratory of the Polar Geophysical Institute. Measurements of the cosmic-ray intensity are to be made with a counter telescope and an individual counter borne aloft by sounding balloons. The telescope consists of two STS-6 gas-discharge counters separated by a 7-mm thick aluminum shield. The individual STS-6 counter is directed toward the zenith.

The new radiosonde design worked out in the laboratory differs from the designs hitherto used for such purposes /1, 2/. The coincidence circuit and transmitter modulator were constructed using P13 transistors. The resolving time of the coincidence circuit is 20 μsec and the input capacitance is 10 $\mu\mu$f. The duration of a transmitter pulse is 500 μsec. The radiosonde transmitter is built according to the A-36 radio-unit circuit used in the A-22-III meteorological radiosonde, and it operates in the 200-Mc range. The radio-circuit supply comprises two copper magnesium chloride batteries especially designed for radiosondes. The battery, which weighs about 200 grams, can provide a current of about 25 ma over a 2-hour period, at a potential of 50 volts. The use of such batteries makes it possible to reduce considerably the weight of the radiosonde.

The high-voltage circuits of the gas-discharge counters and of the transmitter anode are supplied by a voltage converter employing a P26 transistor. The 390 volts across the STS-6 counters is stabilized by means of an SG-301S corona-discharge stabilitron tube. The total weight of the radiosonde is less than 1 kg.

Test flights of the radiosondes are now being made at the experimental base of the laboratory, which is equipped with an aerological pavilion and a receiving point.

Polar Geophysical Institute,
Kola Branch of USSR
Academy of Sciences

REFERENCES

1. CHARAKHCH'YAN, A.N.— Sbornik: "Kosmicheskie luchi," No.3, p.134, Seriya "Rezul'taty MGG," Moskva, Izd. AN SSSR. 1961.

2. BELOMESTNYKH, V.A., B.S. NEDZVEDSKII, and Yu.G. SHAFER.— Trudy YaFSO, AN SSSR, seriya fizicheskaya, No.3, 15. 1960.

N67-38232

R.Z. Denikaev, E.V. Kolomeets, L.V. Kozak, L.A. Mirkin, B.A. Prilepskii, and V.G. Roshchupkin

OPERATION OF A NEUTRON MONITOR AND μ-MESON TELESCOPE

I. The neutron monitor at the Cosmic-Ray Station of the Kazakh State University was designed especially for studies of cosmic-ray variations, in accordance with the IGY program /1/. The monitor has been in operation since 1957. Due to unreliable functioning of the monitor subassemblies, certain changes and additions, in both the circuits and the construction of the monitor, were necessary. The main changes and additions made were the following.

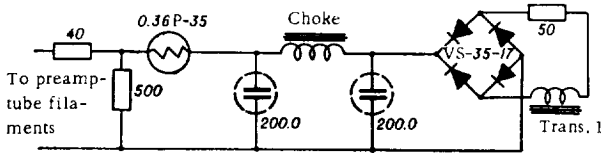

FIGURE 1. Power-supply circuit for first tube of monitor preamplifier.

1. In order to reduce charge leakage at the insulator surfaces, calcium chloride driers were inserted in the connecting high-voltage chassis, and all the high-voltage conductors were shielded to eliminate inductive pickup.

2. All the switching condensers, both in the amplifier and in the scaling unit, had to be replaced by condensers with higher working voltages (500-600 volts).

3. The one-watt plate-load resistors in all the amplifier stages, as well as the cathode resistor of the output stage (6NIP tube), were replaced by two-watt and four-watt resistors.

4. The operating regime selected for the ballast tube (03B17-35) stabilizing the heater current of the preamplifier tube in the SCh-3 assembly (at any rate for the equipment manufactured in 1956-1958) was obviously incorrect. This circuit had to be changed to the one shown in Figure 1.

5. From the very first, it was found that for a scaling factor of 16 the SB-1M counter (numerator) often operated at the 8th and 12th pulse and, in addition, gave "double" pulses. This malfunction was also characteristic of the five reserve units available at our station. It was eliminated by changing the operating regime of the 6NI5P tube (power amplifier) to conform with the circuit in Figure 2.

6. To check for constancy of the gain of the monitor, a 3G-10 oscillator is used in conjunction with a diode voltmeter employing a 6×6 tube. The rectified current is measured by means of a laboratory milliammeter with

a high accuracy (0.1%). Both the input and output voltages of the amplifier are measured by such a voltmeter.

The diode heater is stabilized by means of a ballast tube. The same oscillator (3G-10) is used to calibrate the Schmitt discriminator, since the "threshold of discriminator triggering" of the scale division in the SCh-3 Unit does not correspond to reality.

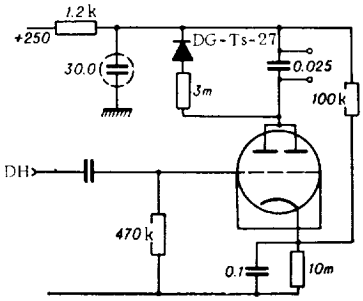

FIGURE 2. Power-amplifier circuit of output stage of scaler.

7. In the first version of the photo-recording equipment (FR), PK-10 scalers were used. However, their performance was completely unsatisfactory. Therefore, this memory unit was replaced by SB-1M numerators, controlled by ordinary blocked multivibrators.

8. For greater reliability, a second FR unit was assembled and put into operation. This completely excluded the possibility of data losses due to one of the FR units getting out of order, due to incorrect exposure, and due to unsuccessful processing of the film.

9. The relay indicating termination of the film was moved to the intake of the film winder. Thus, data losses while the end of the film passes through the film winder are completely eliminated.

10. To enable automatic recording of the atmospheric pressure with an accuracy up to 0.1 mb, a differential pressure transducer was designed, and its readings photographed onto the main film /2/.

As a result of the foregoing revisions and additions, the operation of the neutron monitor at the Cosmic-Ray Station of the Kazakh State University has been very stable for four years.

II. Since 1962, an azimuthal μ-meson telescope has been in operation at the Cosmic-Ray Station. This telescope is designed to record continuously the directional intensity of the hard cosmic-ray component.

The telescope consists of four identical sections. Each pair of sections records particles having equal zenith angles but opposite azimuths. Thus, a double recording of the intensity from each direction is made. The two pairs of sections are mounted on a frame and, by means of a special fly-wheel rotating the sections about a horizontal axis, are swung up to the required zenith angle (from 0 to 60°). The telescope frame is mounted on a platform which rotates about a vertical axis, giving the required azimuth. A block diagram of the telescope is shown in Figure 3a.

Each section of the telescope consists of three trays of counters, each tray containing 4 SI-5G counters connected in parallel. In order to isolate the hard component, a lead shield 10 cm thick is introduced between the lower and middle trays.

Each counter tray has its own quenching circuit (Figure 3b), which cuts off the trailing edge of the pulse and thereby increases the service period of the counter by a factor of 2 or 3. Except for some minor changes, the quenching circuit follows the plan described in /3/.

The quenching-circuit parameters are as follows: duration of quenching pulse 20 μsec, rise time 0.5 μsec, amplitude $\geqslant$ 100 volts, amplitude of output pulse fed to coincidence circuit 35 volts.

The counter trays are connected in threefold coincidence, the coincidence circuit being constructed with DG-Ts27 crystal diodes.

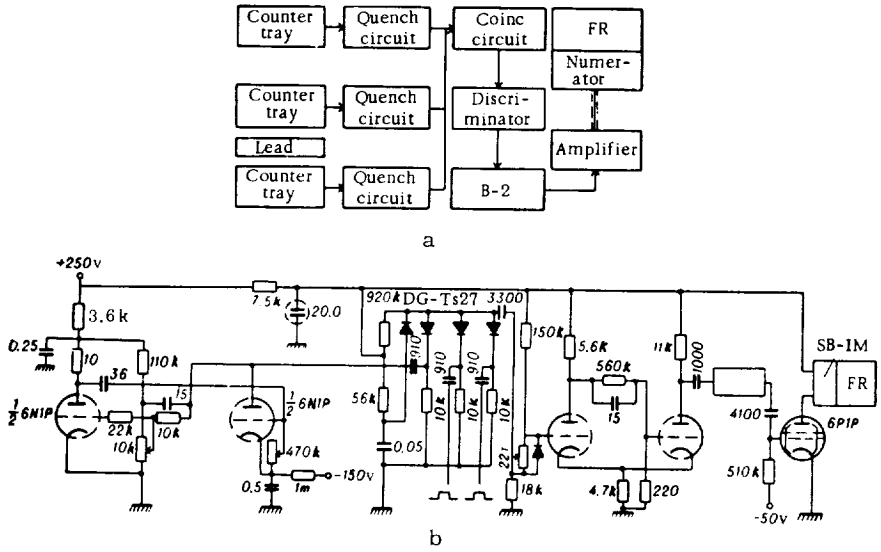

FIGURE 3. Block diagram of μ-meson telescope.

The coincidence circuit provides an output pulse with an amplitude of 11 volts; it has a resolving time $\tau = 1\,\mu$sec, and a selection coefficient $K = 16$. The signal amplitude A for which the circuit begins to operate normally is 8 volts.

The pulses from the coincidence circuit are fed to an amplitude discriminator employing a 6NI5P tube. The discrimination threshold can be regulated by means of a potentiometer. When the discriminator is triggered, it sends out a standard rectangular pulse.

The pulse is then fed from the discriminator to a calculating machine, the B-2 radiometer. The high-voltage stage of this radiometer is used to supply the SI-5G counters.

SB-IM doubling counter-numerators are mounted at the signal panel of the neutron-monitor photorecorder. Therefore, their readings can be recorded on photographic film every 5 to 15 minutes.

In conclusion, the authors wish to thank Senior Engineer Yu. Kapitonov for his advice and assistance during the study.

REFERENCES

1. KOPYLOV, Yu. M. Sovietskie stantsii kosmicheskikh luchei (Soviet Cosmic-Ray Stations).—Moskva, Izd. AN SSSR. 1960.

2. KOLOMEETS, E. V. and B. A. PRILEPSKII.—Sbornik: "Kosmicheskie luchi," No. 5, Moskva, Izd. AN SSSR. 1962.

3. INOZEMTSEVA, O. I. and Yu. M. KAPITONOV.—Sbornik: "Kosmicheskie luchi," No. 3, p. 105, Moskva, Izd. AN SSSR. 1961.

N67 38233

I.N. Kapustin and A.V. Kapustina

A POSSIBLE CAUSE OF INSTRUMENTAL ERRORS FOR A NEUTRON MONITOR

The cosmic-ray variations recorded by a neutron monitor consist of the true variations plus the statistical scatter of the readings. The scatter should conform to a Poisson distribution:

$$P_n = \frac{e^{-\bar{n}} \cdot \bar{n}^n}{n!}. \qquad (1)$$

A study of the statistical scatter of the readings of a standard neutron monitor, however, made on the basis of five-minute data, indicates that it lies far outside the limits of the Poisson distribution.

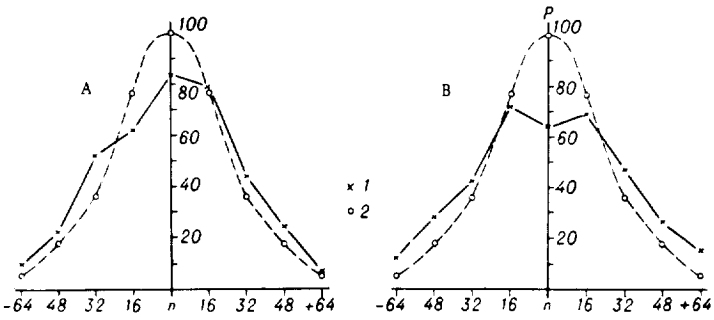

FIGURE 1. Distribution curves for readings of sections A and B of neutron monitor, before soldering the counters.

1-actual distribution; 2-Poisson distribution.

Figure 1 shows the distribution curves for the instrument readings, relative to the arithmetic mean values for sections A and B of the monitor. Each of the curves was plotted according to 380 measurements of the five-minute data. During the processing, the arithmetic mean was computed separately for each two-hour interval, as well as the number of deviations from this mean toward each side. The dashed lines show the curves constructed according to formula (1). In order to explain the deviations from the Poisson distribution, it was assumed that the increased scatter is caused by the presence of an oxide film which forms at the contacts of the high voltage and the central counter electrodes.

The connection between an SNM-8 counter and the electronic circuit is shown schematically in Figure 2.

Due to the presence of an oxide film on the contacts, the latter are insulated from the counters; breakdown of the film will occur only when a certain potential difference between contacts and counters is attained. Consequently, the potential on the counter case (U_{coun}) will not be equal to U_{cont}, and it will vary as shown in the graph of Figure 2.

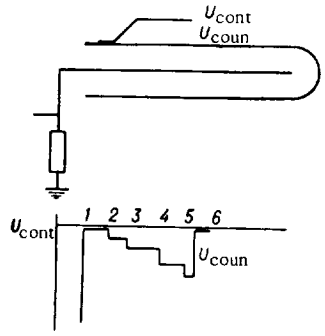

FIGURE 2

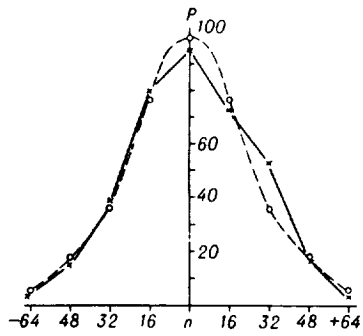

FIGURE 3. Distribution curve for readings of section B of neutron monitor after soldering the counters.

The step curve in the figure shows the variation of the potential on the counter case. When the voltage is connected, the oxide film breaks down (point 1), due to the large potential drop between the power-supply contact and the counter case, and so the potential on the case becomes close to the power-supply voltage. As a result of energy consumption during the formation of pulses in the counter, the potential on the counter case drops by stages (points 2, 3, 4, and 5). Since pulses occur very rarely (8 to 10 pulses/min), an oxide film is able to form once again between the contacts. Finally, the potential difference between the counter case and the contact becomes so great that the film breaks down again (point 6). This produces a negative potential drop at the case, which may reach some tens of millivolts. This drop reaches the amplifier input through the internal capacitance of the counter and is recorded as a spurious pulse.

It can be demonstrated that, at the contact of the central electrode, the situation will be the opposite, so that some of the pulses will be lost. The number of extraneous pulses counted, as well as the number lost, can vary considerably as a function of the surrounding conditions and time, and they may produce spurious intensity variations. In order to provide an experimental check of the foregoing assumption, all the contacts which could contribute to the spurious scatter of the counts were soldered. The curve of the pulse distribution relative to the arithmetic mean values, plotted from 380 measurements of the five-minute data after soldering of the counters, is shown in Figure 3. This curve fits the Poisson curve very well.

It should be noted that, before this study was made, the "Schmitt" univibrator of the standard neutron monitor was replaced by a semiconductor univibrator (Figure 4). This was advisable since, from the beginning, the circuit did not possess a stabilized dead time, which could be varied (depending on the discrimination level, the pulse amplitude, and the

amplification) from 20 to 100 μsec. Since the intervals between pulses produced by stars in the lead shield lie in this range, the magnitude of the additional variations may have been considerable.

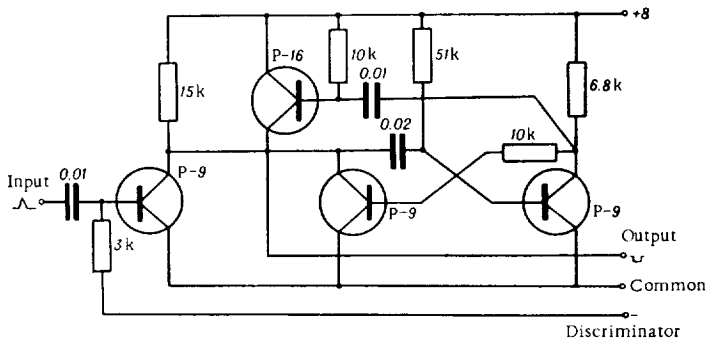

FIGURE 4. Circuit of discriminator-univibrator.

The dead time selected for the discriminator was 1 μsec $\pm$ 10%, a value which exceeded considerably the possible intervals for pulses from a single star.

Polar Geophysical Institute,
Kola Branch of USSR
Academy of Sciences

I.N. Kapustin

VISIBLE RECORDING OF THE COSMIC-RAY INTENSITY BY MEANS OF A MULTIPLE-POINT AUTOMATIC POTENTIOMETER

At the Cosmic-Ray Station of the Polar Geophysical Institute, a six-point 2.5-second EPP-09M automatic electronic potentiometer with a 100-mv scale is used to duplicate the recordings of the main recorder of the neutron monitor data.

At present recordings are being made using only two channels of the neutron monitor, with hourly time markings. In principle, however, this setup can be used for simultaneous recordings on six channels. If a 12-point potentiometer is used, moreover, recordings can be made on 12 channels. The number of pulses received during five-minute time intervals are recorded on chart tape. The potentiometer is switched in by means of a contact clock and is switched out automatically at the end of one cycle of operation.

From the output of each section of the neutron monitor, the negative pulses being recorded are fed through the filter R_1C_2 to a shaping univibrator. Then they are fed to a scaling unit, consisting of six stable triggers (semiconductor circuits), with an overall scaling factor of 64,

The outputs of the triggers are connected through resistors R_{15} through R_{20} to the summing resistor R_Σ. The conductances $\frac{1}{R_{15}}$ through $\frac{1}{R_{20}}$ are proportional to the discharges of the corresponding triggers. Consequently, the current through R_Σ will be approximately proportional to the number of pulses stored in the scaling unit /1, 2/. In this case the nonlinearity of the circuit is less than 0.1%.

The EPP-09M1 automatic potentiometer /3/ used in the setup has been altered somewhat (see diagram). The measuring bridge has been completely disconnected, and the remaining circuit elements (amplifier with reversing motor, slide wire, and channel selector) are connected as shown in the circuit diagram. Resistors R_{21} and R_{22} were added to the potentiometer circuit. The "alternating-cycle" mechanism and the "mechanism for checking and establishing the working current" have been disconnected.

In the normal state the contacts of the two selectors are at the six commutator segments. Upon closure of the five-minute contacts of the clock, a negative pulse is fed through diode D-2, R_{29}, and C_{10} to the winding of the relay RP-4. The relay is switched and actuates a second relay, which: (I) turns on the motor drawing the tape; (II) applies voltage to the vibrating-reed converter [chopper]; and (III) applies plate voltage to the amplifier output tubes (the first two amplifier stages and the filaments of all the tubes are constantly connected).

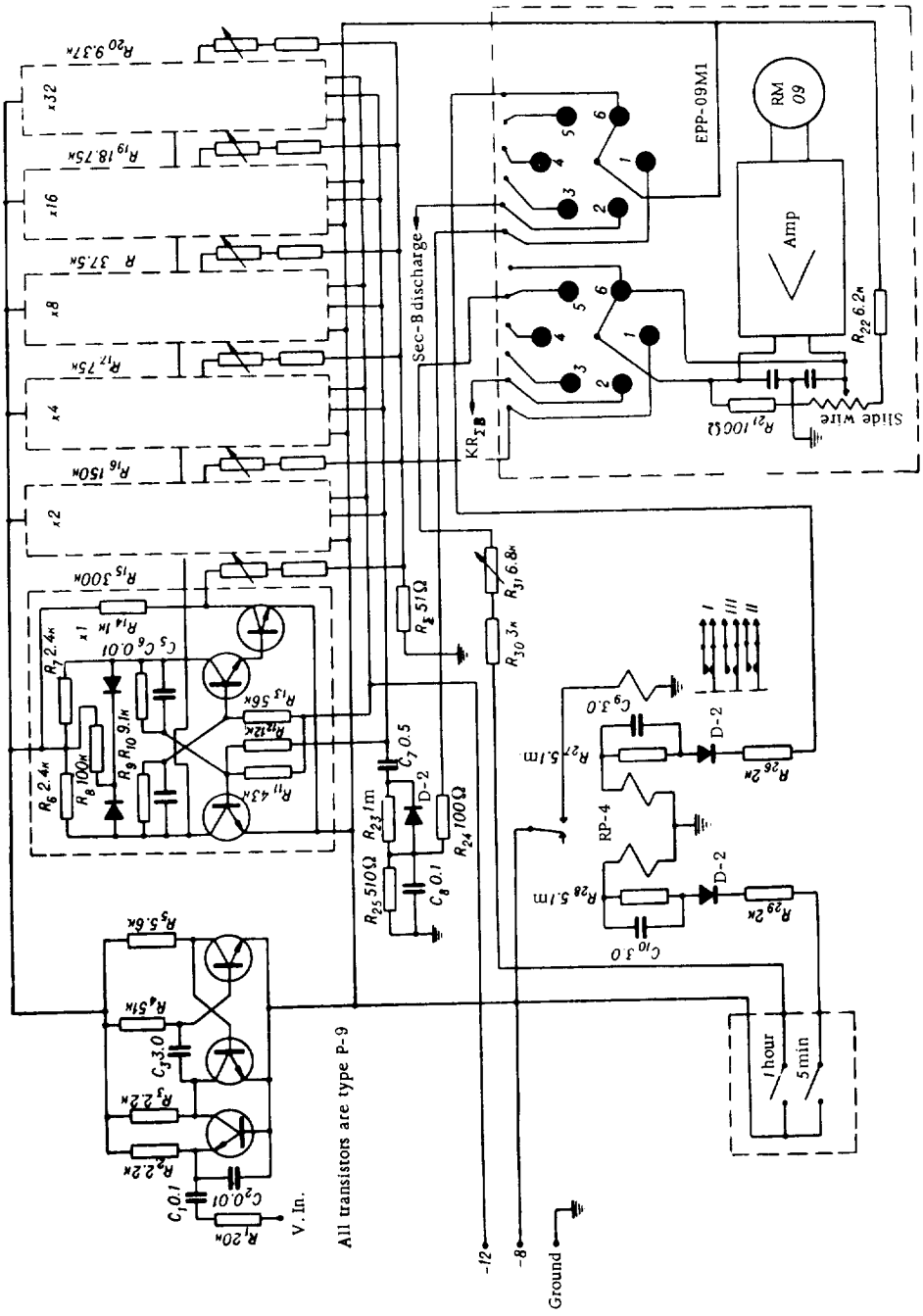
EPP-09M1
RM 09
Amp
Slide wire
Sec-B discharge
All transistors are type P-9
V. In.
-12
-8
Ground
1 hour
5 min
RP-4
D-2

Simultaneously with the drawing of the tape, the sliding contacts of the channel selector begin to move over the commutator segments. When the first positions are contacted, one amplifier input is connected to $R_{\Sigma A}$ (section-A summing resistor); the second is always connected to the slide wire.

The voltage across $R_{\Sigma A}$ is proportional to the accumulated information from section A. Therefore, at the amplifier output a signal controlling the reversing motor is produced. The motor shifts the moving contact along the slide wire until the voltages at the two amplifier inputs are equal.

A record is then printed out on the chart tape, while the sliding contacts of the channel selector proceed to the second commutator segments. At this moment the voltage supply (8 volts) is disconnected from resistor R_{25}, and condenser C_7 discharges through the internal resistance of the discharge loop of the triggers, through the forward resistance of the D-2 diode, and through resistor R_{25}.

A positive triggering pulse is fed to the bases of the left transistors in the trigger circuits and they drop to zero. R_{24} and C_8 are noise filters.

At the second position of the channel selector, a voltage proportional to the number of pulses in section B is applied to the slide wire, etc. The fifth commutator segment serves as a time-marking recording, the time markings being fed through resistors R_{30} and R_{31} from the hour contact of the clock. To mark the time, the potentiometer makes a dot at the 100th scale division. This dot also serves as a control in case the chart tape goes off to the side. At the sixth channel-selector position, a pulse is applied to the second winding of the RP-4 relay (through the D-2 diode, R_{26}, and C_9). The relay then operates and switches out the potentiometer.

Information begins to accumulate in the triggers immediately after discharge. This continues until the moment when the result is printed out, after which the process is repeated. The time interval between the printing of the data for the preceding five minutes and the beginning of the accumulation of new information (the dead time of the system) is less than one second for each five minutes (about 0.3%), and it is maintained by the stability of the power-supply system. For a maximum power-supply instability of ± 10%, the instability of the information loss will be about 0.03%.

The contact-starting clock of the standard neutron monitor is used to indicate the five-minute and hourly time intervals. Three of the four teeth on the contact disk for 15-minute closures were filed off.

The photographic recorder was converted to hourly photographing of the counter panel. This facilitated the data processing and reduced the expenses for movie film to one fourth of the original amount.

Polar Geophysical Institute,
Kola Branch of
USSR Academy of Sciences

Institute of Space-Physics Research and
Aeronomy, Yakutsk Branch of Siberian
Division of USSR Academy of Sciences

REFERENCES

1. NETREBKO. Printsipy konstruirovaniya tsifrovykh kodiruyushchikh avtomaticheskikh kompensatorov (Principles of Constructing Automatic Digital Coding Compensators).— Proc. 1st Int. IFAC Conf. 1961.

2. RICHARDS, Richard Kohler. Digital Computer Components and Circuits.— Van Nostrand, Princeton. 1957.

3. Elektronnye avtomaticheskie samopishushchie potentsiometry s zapis'yu na lentochnoi diagramme EPP-09MI (The Model EPP-09MI Automatic Electronic Recording Potentiometer, with Recording onto a Tape Chart).— Tsentral'noe byuro tekhnicheskoi informatsii, Ioshkar-Ola. 1960.

N67-38234

L.V. Granitskii, A.F. Neermolov, Yu.K. Vorob'ev, and G.V. Kononova

AN AUTOMATIC PROGRAMED SCALER

The automatic programed scaler is intended for research work with radioactive materials. It can be used in cases where statistically distributed pulses are to be recorded.

The scaler consists of the following basic units (see diagram): first counting channel; second counting channel; time channel; code converter; output unit; programing unit; recording device; and power supply.

The first counting channel contains the following elements.

1. The recorded-pulse switch S_1, which enables the separation of positive, negative, or both [positive and negative] pulses. This switch also feeds time-channel pulses to the input of input unit IU-1.

2. Input unit IU-1 shapes the recorded pulses and switches them to the input of the counting channel. The negative-pulse amplifier employs a P-403 transistor with emitter load; for positive pulses the collector is loaded. The control by the input unit is effected by means of connecting [go] and disconnecting [no-go] pulses. Upon reception of a go pulse, the signals entering the input unit are fed to the counting channel. When a no-go pulse is received, the counting of pulses ceases.

3. Counting decade D_1 is made up of transistor elements. The decade consists of four triggers, a diode switch, and an information-readout system. The basic element of the decade is a symmetric automatic-bias trigger made up of P-403 transistors.

4. The six counting decades D_2 through D_7, which operate at lower frequencies, are made up of binary units. A P16B transistor is used in the second decade of each channel, and P13A transistors are used in the other decades. The basic element of each decade is a binary unit, which possesses a high working reliability and at the same time is sufficiently rapid-acting (more than 50,000 pulses/sec).

5. The noise-eliminating circuit NEC-1.

6. The nine-step register of information-readout drift. The basic element of the drift register is a ferrite-diode unit. Blocking oscillators BO-29 and BO-8 are used to control the drift register.

The second counting channel is constructed analogously to the first and contains the same elements. In addition, an alternate-operation switch S_{11} is provided, which uses the pulse disconnecting the first channel to connect the second channel, and vice versa. An OR-gate circuit designed to switch the information signals to the code-converter input during readout is provided for both the first and second channels.

The time channel contains the following elements:

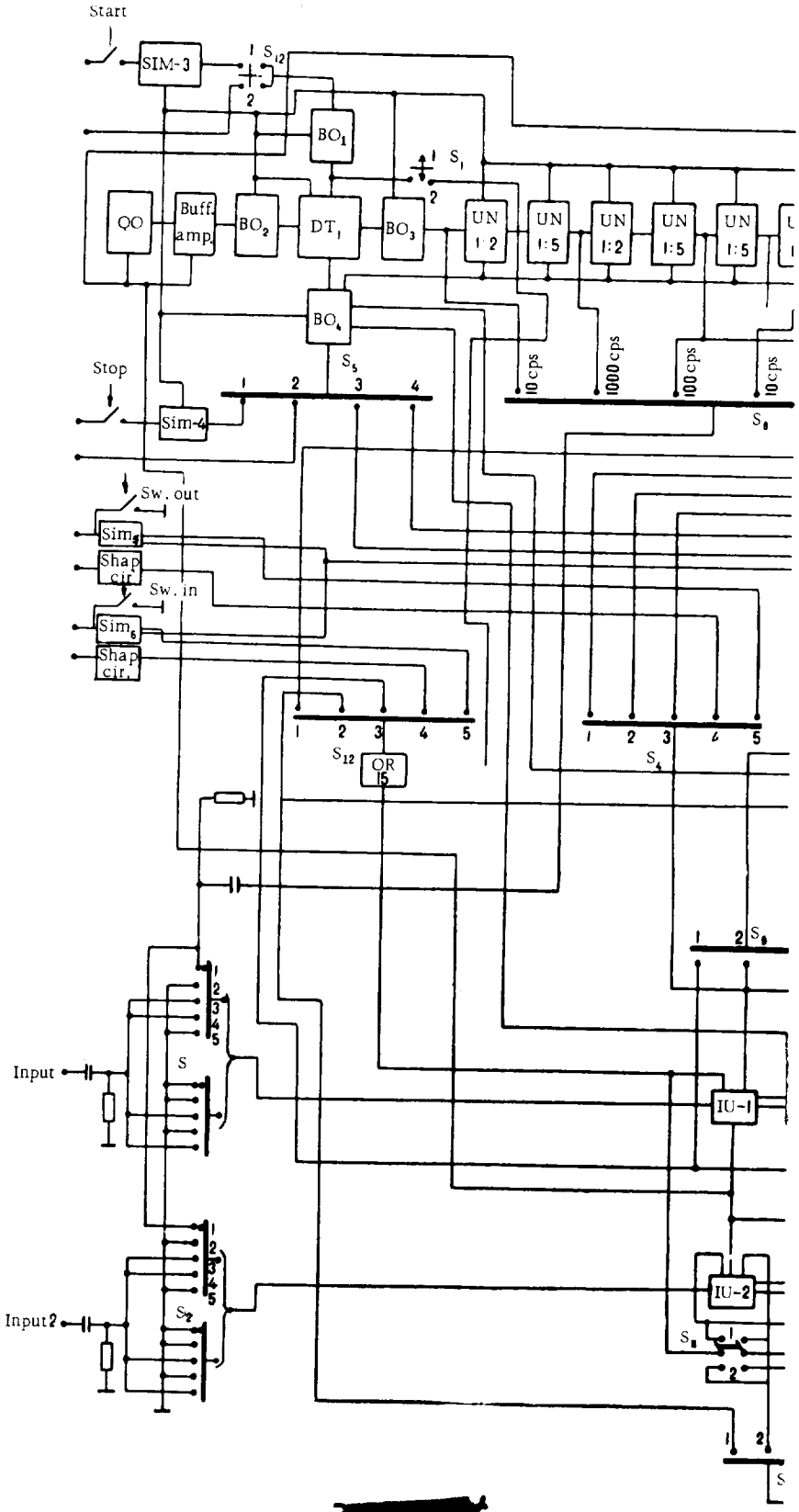

1814/300-301/

Fig 1

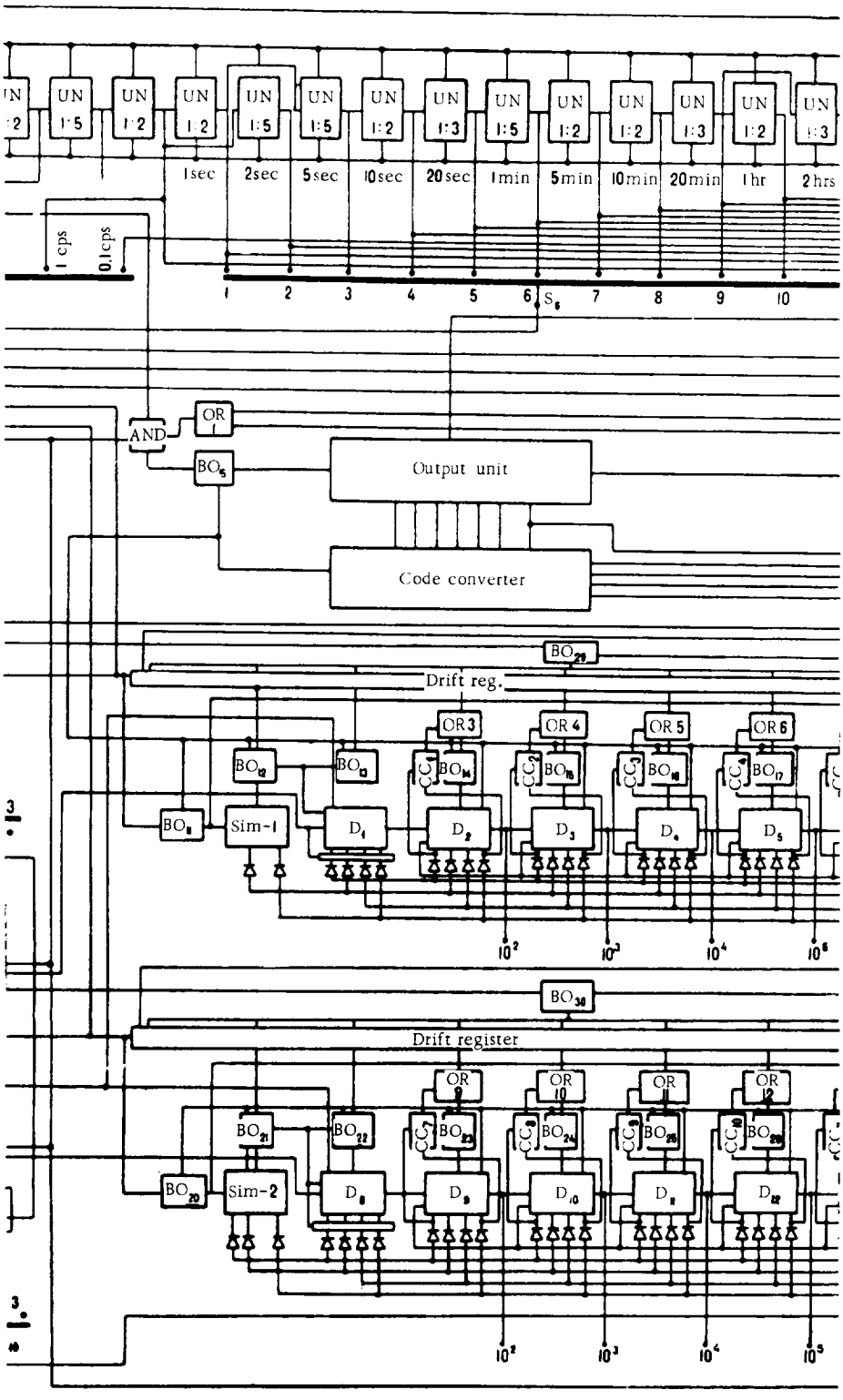
UN 1:2
UN 1:5
UN 1:2
UN 1:2
UN 1:5
UN 1:5
UN 1:2
UN 1:3
UN 1:5
UN 1:2
UN 1:2
UN 1:3
UN 1:2
UN 1:3
1sec
2sec
5sec
10sec
20sec
1min
5min
10min
20min
1hr
2hrs
1 cps
0.1cps
1 2 3 4 5 6 S6 7 8 9 10
AND
OR
BO5
Output unit
Code converter
BO29
Drift reg.
OR 3
OR 4
OR 5
OR 6
BO12
BO13
BO14
BO15
BO16
BO17
BO11
Sim-1
D1
D2
D3
D4
D5
10²
10³
10⁴
10⁵
BO30
Drift register
OR 9
OR 10
OR 11
OR 12
BO21
BO22
BO23
BO24
BO25
BO26
BO20
Sim-2
D8
D9
D10
D11
D12
10²
10³
10⁴
10⁵

Fig 2

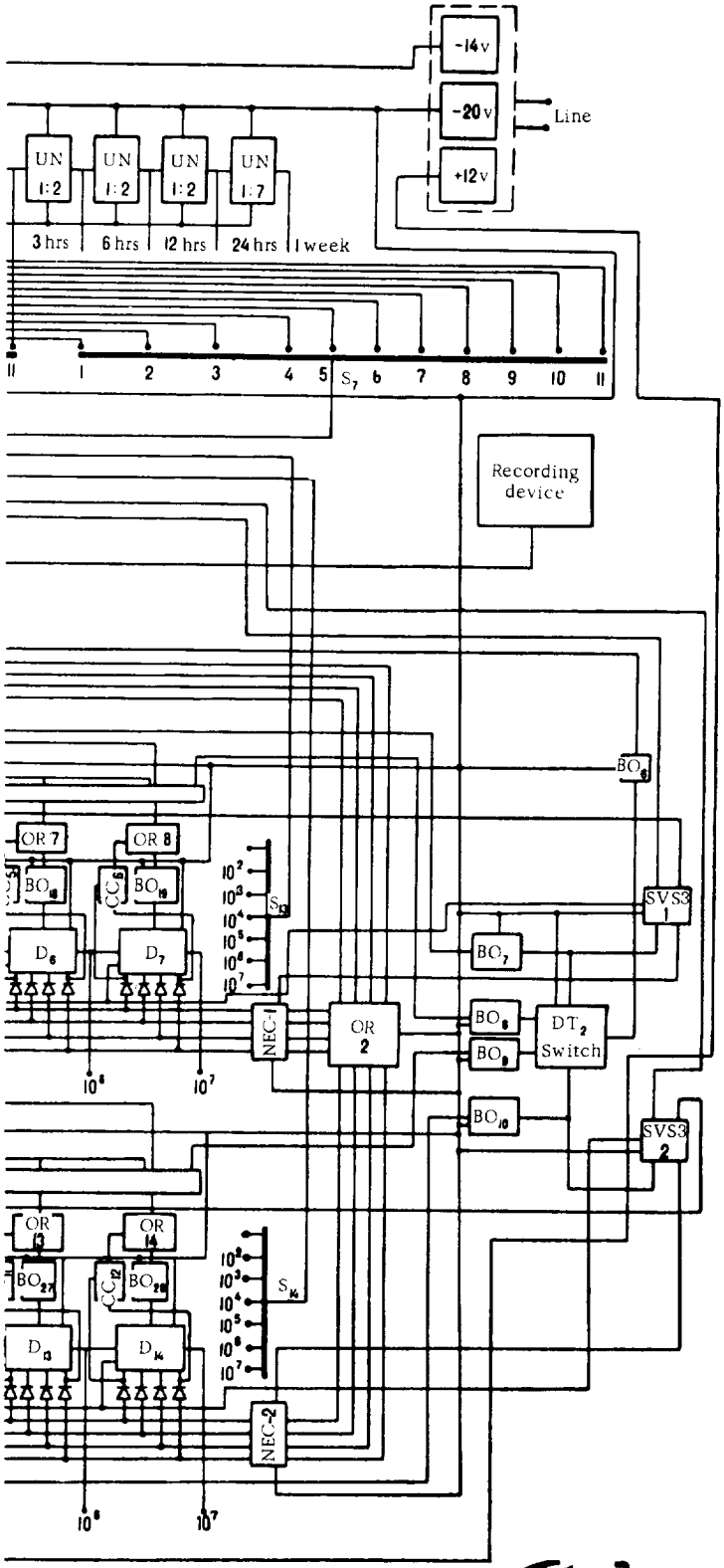
-14v
-20v
+12v
Line
UN 1:2
UN 1:2
UN 1:2
UN 1:7
3 hrs
6 hrs
12 hrs
24 hrs
1 week
1
2
3
4
5
S7
6
7
8
9
10
11
Recording device
OR 7
OR 8
BO16
BO18
CC8
D6
D7
S13
NEC-1
OR 2
BO6
BO7
BO8
BO9
DT2 Switch
BO10
SVS3 1
SVS3 2
OR 13
OR 14
BO27
BO28
CC12
D13
D14
S14
NEC-2

Fig 3

1. A 10-kc quartz-crystal master oscillator QO, employing a P13A transistor with a grounded collector and a capacitive divider.

2. A three-stage buffer amplifier.

3. A dynamic trigger DT_1, designed to switch the pulses fed to the input of the first divider of the time channel.

4. 23-stage ferrite-triode units UN-1 through UN-23.

5. A dynamic trigger-switch DT_2 for switching the readout of the information from the counting channels.

The time channel makes it possible to obtain control pulses at the following time intervals: 10^{-4}, 10^{-3}, 10^{-2}, 10^{-1}, 1, 2, 5, 10, 20 seconds; 1, 5, 10, 20 minutes; 1, 2, 3, 6, 12 hours; 1 week.

The code converter is intended to convert the four-digit binary-decimal parallel code to the standard five-digit parallel code II of the standard telegraph apparatus (STA).

The code converter contains 14 ferrite cores with rectangular hysteresis loops, conforming to the number of converted combinations. The core corresponding to a given code combination is selected by means of switching units. Current coincidence is used in this code converter, in contrast to a diode code converter, in which voltage coincidence is used. Diode code converters have several shortcomings. First of all, high-quality diodes with specially selected forward and backward resistances are required. Also, to operate a diode code converter, timing pulses of short duration and large amplitude ($\tau = 2\mu$sec; $U = 50$ volts) are necessary, and these are difficult to obtain by means of semiconductor circuits. Moreover, high demands, with respect to the working voltages on the condenser of the coupling quadripole, are imposed upon the input register controlling the operation of the code converter. The code converter using ferrite cores with rectangular hysteresis loops, however, does not have these shortcomings.

The output unit converts the parallel five-digit code coming from the code converter into the type-II telegraph code.

The programing unit is made up of: switches S_6, S_7, and S_8 for selecting the appropriate signals from the time channel; switches S_3 and S_4 for the pulses connecting and disconnecting the input unit; switches S_9 and S_{10} for the information-readout pulses; switches S_1 and S_2 for the input units of the first and second channels; switches S_{13} and S_{14} for the pulses from the first and second channels when the input unit is disconnected; switches S_1 and S_2 for connecting and disconnecting the time channel; knobs K_1 and K_2 for connecting and disconnecting the time channel and counting channels; and switch S_{11} for alternate operation of the channels. The basic element of the programing unit is the time channel, since it generates almost all the control signals.

The recording device is a printing standard telegraph apparatus (STA), which prints out seven-digit figures corresponding to the number of pulses collected in the counting channels. Simulators SIM-1 and SIM-2, which provide identification combinations, are used to identify the channels. The letter "Sh" is used to identify the first channel; in the five-digit code the combination of this letter is 01011, while in the four-digit code it is 0101. The simulator for the combination 0101 is made up of two PP-24 rings. The letter "Yu" is used to identify the second channel; in the five-digit code the combination of this letter is 11001, and in the four-digit code it is 1101. The simulator for the combination 1101 is made up of three rings.

The scaler can operate according to the following prespecified programs.

1. For a given time lag, the number of pulses for one or two counting channels are counted. For example, the number of pulses from two pulsing units during 5 seconds are counted, the pulses from the first unit being negative and those from the second being positive and negative. The pulse range is ± 10 to 12 volts. In order to carry out the assigned program, the following switchings are necessary: S_1 is set to position 4; S_2 to position 3; S_3 to 1; S_6 to 3; S_7 to 4; S_{11} to 1; S_9 to 2; S_{10} to 1; S_{12} to 1; and S_5 to 3. After the indicated switchings, the "start" button is pressed.

2. Measurements are made at definite time intervals, the interval between successive measurements and the time lag being specified. For example, measurements are made at 10-second intervals, the time lag is 5 seconds, and the measurements must last for at least 24 hours. The measurements are terminated by command of the operator. The data of the recorded pulses will be the same as in the first case. To carry out this program, the following switchings are necessary: S_5 is set to position 1, and the other switches are set to the same positions as in the first program. The beginning of operation, and the readout of information from the first and second channels, are also as in the first program. After completion of the first cycle, the dynamic trigger DT_1 will not be disconnected; the next pulse for switching in the input units, which follows 5 seconds after these units are disconnected, will put them into operation again. Five seconds later, the keys, the information readout, etc., will be disconnected. The measurements will continue as long as the dynamic trigger DT_1 is not switched out.

3. Since the scaler has two counting channels, continuous measurements are possible. In this case the channels operate alternately: when the first channel is connected for measurement, readout of information from the second takes place. For example, continuous monitoring by a single pulsing unit is to be carried out without any information loss, over a period of at least three days. The delay time is 5 seconds. The pulsing unit provides positive pulses. In this case the pulsing unit must be connected to the first and second channels. Switches S_1 and S_2 are set to position 5; S_{11} is set to 2; and S_{10} is set to 2. The other switches are set to the same positions as in the second program. Five seconds after switching on the dynamic trigger DT_1, the first-channel input unit is connected; the second-channel input unit was switched out, but the pulse disconnecting it is the signal for information readout. Zeros are printed out on the tape, along with the second-channel mark. After a delay of 5 seconds, the pulse switching out the first channel connects the second channel for operation. The readout of information from the first channel begins simultaneously. The cycles will be repeated until dynamic trigger DT_1 is switched out.

4. For a specified number of pulses, it is possible to measure the interval of time during which the pulses were collected. In this case only one counting channel is used. The time intervals are recorded in the channel which is not used for counting pulses. The accuracy of the report depends on the frequency stability of the quartz-crystal oscillator. Since the instability of the oscillator frequency is $5 \cdot 10^{-5}$, the time error for a 24-hour period will not exceed 1 second.

5. The scaler can be used to record the time between any two short-duration processes. In this case one channel is used, and it is connected to the time channel. The input unit is operated by the pulses between which it is necessary to measure the time.

As required, various other programs can be set up for the scaler, including remote-control switching in and switching out. The device can be used for frequency comparison and frequency measurement, and (by means of certain simple attachments) it can be used to measure the phase difference between two periodic oscillations. The scaler can also be used as a recording-printing apparatus for the multichannel processing of information. Using converters which change continually varying quantities into discrete quantities, it is also possible to use the scaler to record current voltages and other electrical and nonelectrical quantities.

Using the standard telegraph code II and simultaneous perforation of the tape during recording, the problem of information exchange between individual points and the computing center can be solved successfully.

Institute of Inorganic Chemistry,
Siberian Division of USSR
Academy of Sciences

APPENDIX

TECHNICAL SPECIFICATIONS OF SCALER

1. Maximum counting rate	500 pulses/sec.
2. Input-pulse amplitude (both polarities)	5 to 20 volts.
3. Output resistance of pulse source	less than 10 k.
4. Rise time of pulse	less than 0.5 μsec.
5. No. of channels for simultaneous counting	2.
6. Maximum channel capacity	10^7.
7. Instability of time-channel quartz-crystal oscillator	less than $\pm 5 \cdot 10^{-5}$.
8. Time channel provides signals for programed switching on of the scaler after	2, 5, 10, 20 sec 1, 5, 10, 20 min, 1, 2 hours;
and signals for display after	1, 2, 5, 10, 20 sec, 1, 5, 10, 20 min, 1, 2 hours.
9. Power consumed by scaler:	
without digital printer	24 watts;
with digital printer	100 watts.
10. Overall dimensions of equipment (without STA)	540×360×300.
11. Weight of equipment (without STA)	about 20 kg.

EXPLANATORY LIST OF ABBREVIATED NAMES OF USSR INSTITUTIONS, JOURNALS, ETC., APPEARING IN THIS BOOK

Abbreviation	Full name (transliterated)	Translation
AZh	Astronomicheskii Zhurnal	Astronomical Journal
DAN SSSR	Doklady Akademii Nauk SSSR	Proceedings of the Academy of Sciences of the USSR
KAO	Krymskaya Astrofizicheskaya Observatoriya	Crimean Astrophysical Observatory
MGG	Mezhdunarodnyi Geofizicheskii God	International Geophysical Year
MGU	Moskovskii Gosudarstvennyi Universitet	Moscow State University
MKKL	Mezhdunarodnaya Konferentsiya po Kosmicheskim Lucham	International Conference on Cosmic Rays
OIYal	Ob"edinennyi Institut Yadernykh Issledovanii	Joint Institute for Nuclear Research
TsAO	Tsentral'naya Aerologicheskaya Observatoriya	Central Aerological Observatory
Uch. Zap. Yak. Un.	Uchenye Zapiski Yakutskogo Universiteta	Scientific Annals of Yakutsk University
UFN	Uspekhi Fizicheskikh Nauk	Advances in Physical Science
YaFSO AN SSSR	Yakutskii Filial Sibirskogo Otdeleniya Akademii Nauk SSSR	Yakutsk Branch of the Siberian Division of the Academy of Sciences of the USSR
ZhETF	Zhurnal Eksperimental'noi i Teoreticheskoi Fiziki	Journal of Experimental and Theoretical Physics

ABROSIMOV, A.T. 101, 266, 276
Accelerators 1-2, 26-28, 76, 277
AFANAS'EVA, V.I. 215, 265
AIZU, H. 18
AKIMOV, Yu.K. 275
ALEKSEEV, A.D. 101
ALEKSEEV, I.S. 131
ALLAN, H.R. 111
AL'PERT, Ya.L. 231
ANDERSON, J.C. 50, 179
Antimatter 33-35
Antineutrino 22-40
Antistar 30, 35
ANTONOV, Yu.N. 101
ANZON, Z.V. 288
APPA RAO, M.V.K. 18
ASHKIN, A. 84
ASHKIN, J. 75, 82, 84
ATAKOVA, M.M. 112, 180
Aurorae 221-31, 269
Azimuthal measurements 164-172, 267, 292

BABAYAN, Kh.P. 131
BABETSKII, Ya.S. 131
BAGGE, E. 196
Balloon measurements 1, 16, 50, 290
BARADZEI, L.T. 102, 132
BARBER, W.C. 85
Barometric effect 113—116, 166, 174-176, 180-187, 248, 254
BARRETT, P.H. 102, 132
BARTELL, L.S. 84
BARTELS, J. 205, 215, 265
BARTON, J. 131
BATTERMAN, B.W. 84
BAYUKOV, Yu.D. 280, 285
BAZILEVSKAYA, G.A. 101
BEACH, L.A. 84
BEALL, E.F. 285
BEHR, 186
BELEN'KII, S.Z. 67, 82-85, 121, 132
BELOMESTNYKH, V.A. 290
BEN'KOVA, N.P. 232, 236, 265
BENNETT, R.D. 131-220
BENNETT, S. 101
BENSCH, H. 84
BERMAN, A.I. 85
BERNHARD, F. 276
BERNSTEIN, D. 78, 85
BETHE, H.A. 63, 66, 67, 74, 75, 78-85
BEWILOGUA, L. 84
BINDER, O. 196
BISWAS, S. 18, 289
BLOKH, Ya.L. 44, 139, 143, 163, 266, 275-6
BLUDMAN, S.S. 39
BOLLINGER, L.M. 102, 132
BOLTRUSHKO, L.P. 139, 174, 196
Born approximation 63-64, 71-83
BOSS, E.G. 237, 245
BRADDICK, H.J.J. 132
BRADLEY, A.J. 84
BRADT, H.L. 288-9
BRAGG, W.L. 67, 69, 70, 84
Bremsstrahlung 31-32, 37, 63-64, 73-83, 120-121, 175
BRINDLEY, G.W. 84
BROCKWAY, L.O. 84
BROOKE, G. 131
BROWN, K.L. 85
BROWN, R.R. 139
BRUNBERG, E.A. 166, 195
Bursts, solar. See Cosmic rays, bursts

CACHON, A. 102
CAMERON, A.G. 6, 18
CARDOSO, J.M. 179
CARLSON, J.F. 63, 83
CARMICHAEL, H. 139, 275
Cascade parameter 88, 105
Cascade unit. See Radiation length
CATANNI, D. 193, 196
Čerenkov counters 8-10, 13, 16-17
Čerenkov radiation 45, 97, 99, 221
CHAPMAN, S. 265
CHARAKHCH'YAN, A.N. 44, 50, 62, 101, 290
CHARAKHCH'YAN, T.N. 44, 62, 101
CHASNIKOV, I.Ya. 286, 289
CHASSON, R.L. 179, 205
CHEN, N.Y. 38
CHIANG, T.L. 38
CHIKOVANI, G.E. 285
CHIPMAN, D.R. 84
CHIRKOV, N.P. 44, 156, 195-197, 205, 210-211, 215, 220
CHRISTY, R.F. 132
CHIU, H.Y. 39
CHUDAKOV, A.E. 39, 45, 47, 101
CITRON, A. 117
CLARK, G.W. 19, 101, 104, 109-111
Cloud chambers 12, 92
COCCONI, G. 45, 47, 84, 101, 102, 245
COCCONI, V.T. 84
Coherent process 73-75
Coincidence counters 52, 93, 104, 113-116, 180-183, 279-283, 290-293
COMPTON, A.H. 71, 84, 131, 220
COOPER, D.H. 85
CORK, B. 285
Corpuscular stream 14, 49, 157, 160, 173, 194, 202-4, 266
Cosmic rays
  Anisotropy 42-44, 99-100, 110, 136-138, 156-163, 172 173, 178, 189, 194, 197-205
  Atmospheric effects 112-117, 166-70, 184-87, 209-10, 213, 215, 246-253
  Bursts vi, 17, 55, 60, 118-142, 159-162, 172, 206-220, 266
  Electron component 11-12, 96, 98, 109
  Galactic 3, 11-14, 48-9, 53-6, 59, 100, 106-7, 160, 193, 214
  Meson component 20-1, 25-6, 28, 36, 87, 91-7, 118-31, 157-8, 169-70, 186, 206-11, 216, 237-45, 287, 291-293

Cosmic rays
Neutron component 42, 133-5, 144-162, 174-9, 182, 187-90, 197-201, 211-14, 254, 260-4
Nuclear component 4-19, 55, 95-7, 100, 107-10
Origin vi, 1, 3, 7, 55, 286
Photon component 45-7, 96, 108-9, 121
Primary 1-19, 45-56, 95-100, 103-11, 117, 130, 134, 140, 166, 184, 237-8, 254
Proton component 12-13, 36, 108, 287
Showers vi, 12, 45-7, 63, 74, 86-117, 180-3, 216-220, 269, 278-80.
Solar 2, 12-17, 30, 35-6, 41-50, 135-40, 160-79
Variations vi, 53-6, 144-55, 164-79, 184-94, 197-215, 248-75
Cosmogony 32-34, 37
COWAN, C.L. 22, 33, 37, 38
CRANSHAW, T. 101, 115, 117, 280-5
CRITCHFIELD, C.L. 18
Crossed telescopes 164-5, 173
Cross section 21-31, 63-4, 73-81, 118, 121
CROWDEN, J.B. 196
CURTIS, C.D. 85
Cyclones 112-117, 209-10

DADYKIN, V.L. 45
DAINTON, A.D. 289
DAION, M.M. 277, 285
DALINENKO, N.K. 275
DALLAPORTA, N. 101
DANDY, G. 38
DANIEL, R.R. 11, 18
DANILOV, A.A. 210, 253, 255
DANILOVA, T.V. 102
DANTON, D. 179
DATTNER, A. 166
DAUDIN, A. 117
DAUDIN, J. 117
DAVIS, H. 79, 81, 85
DAVIS, R. 33, 38
DAVISSON, R.J. 131
DE BEER, J. 101, 280-6
DEDENKO, L.G. 108, 111
Delta electrons 120, 286-8
DELVAILLE, J. 101
DE MARCO, J.J. 84
DENIKAEV, R.Z. 291
DENISOV, E.V. 102
DE WIRE, J.W. 84
Diffusion, cosmic ray 41-4, 53, 60-2, 106-7, 135-8, 160-2
DIRAC 72-3
Diurnal variations 166-179, 184, 188-194, 200, 204, 233-6, 246, 251-268
DMITRIEV, B.A. 131
DOBROTIN, N.A. 101, 245
DOBROVOL'SKII, S.P. 100
DOLBEAR, D. 179, 195
DORMAN, L.I. 44, 138, 139, 143, 144, 163, 171-3, 179, 184, 188, 194-6, 204, 210, 215, 220, 237, 245, 247, 253, 254, 265, 275
DOTSENKO, B.B. 219
DOVZHENKO, O.I. 63
DRUZHININ, S.N. 164, 195, 265
DUGGAL, S.P. 172, 195, 265
DUNAEVSKAYA, N.V. 275-276
DUNCAN, R.A. 231
DURGAPRASAD, N. 11, 18
DUTHIE, J. 109, 111, 131, 132
DVORYASHIN, A.S. 44, 62, 139
DYRING, E. 196

EARL, J.A. 12, 18, 101, 111
Earth currents 259-61
ECCLES, P.J. 102
EGELAND, A. 231
EGOROV, T.A. 180
EFIMOV, N.N. 112, 117, 180, 183
EISENBERG, Y. 102
Electron gas 228
ELLIOT, H. 163, 179, 184, 188-9, 195-6, 204, 265
ELLIS, G.R. 221, 231
ELLISON, M.A. 62
ELMORE, W.C. 276
Emulsions. See Photoemulsions
ENIN, A.A. 284
ERICKSON, W.C. 62
ESCOBAR, J. 101
ESTULIN, I.V. 275
EVSTIGNEEV, Yu.F. 101
Extensive air showers. See Cosmic rays, Showers

FEDCHENKO, K.K. 163, 185, 195, 254
FEINBERG, E.L. 83, 117, 247, 254
FENTON, A.G. 163, 205, 275
Fermi constant 25
FERMI, E. 37, 66, 83
FEYNMAN, R.P. 28, 38
FICHTEL, C.E. 14, 18
FILIPPOV, V.A. 196-7, 215, 220
FILON, I.N.G. 67, 83
FILZ, R. 18
FIROR, J. 139, 179
FISHER, P.C. 85
FOK, V.A. 69, 71, 84
FOMIN, Yu.A. 111
Forbush decreases 53-54, 140, 144-65, 171, 182, 192-205, 214, 248.
FORBUSH, S.E. 196, 215, 220
Fourier integral 66-7
FOWLER, P.H. 111, 131, 132, 288-9
FRADKIN, M.I. 4, 18, 19
FRANK-KAMENETSKII, D.A. 39
FRANTSUZ, E.T. 290
FREIDMAN, G.I. 44, 139
FRIEDMAN, H. 33
FUJIMOTO, Y. 18

GALBRAITH, W. 101
GALLARD, I. 38
GALLET, R.M. 221, 231

GALLI, M. 196
GAMOW, G. 39
GANDEL'MAN, G.M. 39
GARWIN, R.L. 38
GATES, D.C. 85
GELL-MANN, M. 28, 37, 38
Geomagnetic threshold 12, 53, 137, 140-4, 156-62, 197-203
GEORGE, W.D. 85
GHIELMETTI, H. 138, 179
GILL, P. 220
GINZBURG, V.L. 1-4, 18, 19, 55, 231
GLOKOVA, E.S. 185, 189, 195-6, 215, 220
GOLDHABER, M. 38
GOULIANOS, K. 38
GRANITSKII, L.V. 300
GREISEN, K. 39, 67, 83, 101, 102, 131
GRIGOROV, N.L. 101, 117
GUSEVA, V.V. 101
GUSS, D.E. 18
GUSTAFSSON, G. 231

HAKURA, Y. 140-143
HANSON, A.O. 85
HARRIS, M.T. 186, 195
HART, E.L. 84
HARTMANN, V. 276
HARTREE, D.R. 69, 71, 84
Hartree-Fok model 70-73
HASEGAWA, H. 101, 102
HASEGAWA, S. 18
HASKIN, D.M. 101
HAUPTMAN, H. 84
HAYAKAWA, S. 11, 16
HAYMAN, P.J. 131
HEISENBERG, W. 75, 84
HEITLER, W. 63, 74, 78-83
HELLIWELL, R.A. 221, 231
HERSIL, J. 101
HEWISH, 57
HIGASHI, S. 102, 131
HILLAS, A.M. 115, 117
HINATANI, K. 101
HIROKAWA, S. 132
HODSON, A.L. 117
HOFFMAN, R. 51
HOPE, R.A.H. 84

IGY 48, 51, 133, 135, 164, 184, 187, 198, 205, 221, 232, 256, 261-7, 291, 304
Impact zones 136-8, 160-2, 177-8, 267
INOZEMTSEVA, O.I. 173, 195-6, 265, 275, 293
Ionization chambers 1, 50, 52, 118-30, 170, 206-10, 215-20, 254, 268, 280-4
Ionosphere 224-36
IVANENKO, D. 132
IVANENKO, I.P. 82, 85
ITO, K. 18

JAIN, P.L. 289
JAMES, R.W. 84
JANOSSY, L. 117
JØRGENSEN, T.S. 231
JOSEPH, J. 75-7, 84

KABUHN, I. 245
KADDOURA, A. 131, 132
KALININ, Yu.D. 215
KALINKIN, L.F. 275
KAMATA, K. 100, 105
KAMEDA, T. 101
KAMINER, N.S. 44, 139, 143, 163, 185-6, 195, 275
KAMIYA, Y. 205
KANE, R.P. 195, 265
KANNO, T. 195
KAPITONOV, Yu.M. 293
KAPLON, M.F. 102
KAPUSTIN, I.N. 294, 297
KAPUSTINA, A.V. 294
KARLE, J. 84
KATZMAN, J. 186, 195-6
KENDZIORSKI, F. 101
KENNEY, R.W. 84, 85
KENT, D.W. 289
KHACHATUROV, Yu.G. 276
KHARITONOV, V.M. 40
KHARITONOVA, I.A. 275
KHRENOV, B.A. 101, 103, 111
KHRISTIANSEN, G.B. 101, 103, 111, 131, 245
KHROMOV, S.P. 117
KIRPICHEV, A. 67, 69, 70, 73, 83
KITAMURA, M. 195
KITAMURA, T. 102, 132
KOBAYASHI, S. 83
KOBZAREV, P.Yu. 27, 38
KOCH, H.W. 83, 84
KODAMA, M. 195
KOLAVA, V.K. 275
KOLOBYANINA, T.N. 18
KOLOMEETS, E.V. 138, 144, 179, 237, 275, 291, 293
KOMARENKO, T.G. 264
KOMIONKO, L.A. 276
KOMORI, H. 132
KOMURA, Y. 84
KONDO, I. 143, 275
KONONOVA, G.V. 300
KOPYLOV, Yu.M. 275, 293
KORCHAK, A.A. 7, 18
KOSHIBA, M. 18
KOTEL'NIKOV, K.A. 101
KOTLYAR, L.M. 276
KOVAL'SKAYA, A.I. 117
KOZAK, L.V. 144, 291
KOZHANOV, A.N. 285
KRAMER, G. 236
KRASIL'NIKOV, D.D. 112, 113, 117, 118, 131, 180, 183, 210, 215, 220

KRAUSHAAR, W.L. 19, 101, 109-11
KRECKER, U. 245
KRIVOSHAPKIN, P.A. 164, 172, 195, 215, 246
KRYMSKII, G.F. 41, 133, 139, 140, 143, 156, 163-4, 172, 174, 196-7, 205, 215, 246, 264-5
KUKLIN, G.V. 44
KULIKOV, G.V. 101, 111
KUNDT, U. 245
KURNOSOVA, L.V. 4, 18, 19
KUSAKA, S. 132
KUTUZOV, A.A. 101
KUZ'MIN, A.I. 133, 140-56, 163, 164, 172, 179, 185, 195-7, 205, 210, 215, 246, 253, 264-5
KUZ'MIN, V.A. 39, 44, 131, 132

LAL, D. 101
LAMB, W.E. 74-8, 83, 84
LANDAU, L.D. 24, 38, 74, 84, 132
LANDOLT-BÖRNSTEIN, 84
LANGE, I. 220
LANIUS, K. 245
LANZL, L.H. 85
LAPP, R. 220
Lateral distribution 86-92, 95, 97, 100, 105
Latitude cutoff 12, 50, 55
LAVAKARE, P.J. 289
LAWSON, J.L. 84
LEBEDEV, A.M. 101
LEDERMAN, L.M. 38
LEE, T.D. 38
LEINBACH, H. 44, 139
LEKSIN, G.A. 276, 280, 285
LEONOV, V.Kh. 276
LEONTIC, B. 132
LEVITSKII, L.S. 44, 62, 139
LIKHODED, V.A. 280
LINDGREN, S. 196
LINSLEY, J. 101, 102, 111
LOCKWOOD, J.A. 138, 179
LOGACHEV, V.I. 4, 18, 19
LOHRMANN, E. 101
LOTOVA, N.A. 59
LOW, F. 85
LUKIN, Yu.T. 281

MAEDA, K. 179, 205
MAEDA, T. 101
Magnetic field
  Interplanetary, 138, 155, 161-2, 204, 222
  Radial 57-62, 138
Magnetic storms 53, 136, 140-1, 157-60, 164-5, 170-3, 188, 197-204, 211-5, 255-7, 266-7
MAKSIMOV, S.V. 180
MALAMUD, E. 81, 84
MALMFORS, K.G. 195
MANZANO, J.R. 179
MARKOV, M.A. 36, 38-9
MARKS, K.R. 231
MARSDEN, P.L. 196
MARTIN, L.H. 231
MARX, G. 39
MATANO, M. 111
MATANO, T. 101, 102
MATHIESEN, O. 289
MATINYAN, S.G. 39
MATSUKUMA, I. 83
MATVEEV, V.V. 276
MAXIMON, L.C. 79-81, 85
MAZE, R. 132
McCRACKEN, K.G. 44, 62, 136, 138, 139, 161-3, 205, 275
McDONALD, C.A. 84
McDONALD, F.B. 18
McDONALD, T.R.R. 84
McILWAIN, C.E. 51
McKENNA, S.M.P. 62
MEIER, H.W. 245
MELIORANSKII, A.S. 275
MENON, M.G.K. 132
MENYHARD, N. 39
Mesons. See Cosmic rays, Meson component
MEYER, P. 12, 18
MIKHAILOV, V.A. 285
MIRKIN, L.A. 291
MISHIMA, Y. 102
MISHNEV, S.I. 101
MISHNINA, N.A. 195
MISTRY, N. 38
MITO, I. 18
MIURA, I. 101, 102
MIYAKE, S. 39
MIYAMOTO, S. 102, 285
MOFFATT, J. 84
MONTGOMERY, C.G. 210
MONTGOMERY, D.D. 210
MOORE, S. 101
MOROZOV, I.R. 101
MORRISON, P. 39
MORTON, G.A. 276
MOTZ, J.W. 83
MUKHNOI, G.S. 131
MURAKAMI, K. 195
MURPHY, P.G. 295

NAGAI, S. 83
NAGASHIMA, K. 143, 163, 172, 188, 195, 275
NAM, R.A. 278
NARASIMHAN, V.S. 39
NATHANS, R. 84
NEDZVEDSKII, B.S. 290
NEELAKANTAN, K.A. 289
NEERMOLOV, A.F. 300
NEHER, H.V. 50, 101
NEMILOV, Yu.A. 275
NESTEROVA, N.M. 45, 101
NETREBKO, 299
Neutral currents 28-9, 32
Neutrino, vi, 20-40, 96-8

Neutrino
Free 22, 24
Polarization 22-4
Neutron monitors 50, 133-5, 140, 160, 170, 173-5, 267-9, 291-9
NEY, E.P. 12, 18
NICHOLSON 186
NIFONTOV, M.A. 112, 117, 180, 183
NIKISHOV, A.I. 83, 102, 131
NIKOL'SKII, S.I. 86, 100, 101, 117, 131, 132, 219
NIKOLSKY [NIKOL'SKII], S.I. 102
NISHIMURA, J. 18, 100, 105
Number spectrum 88, 105-9, 207
NURGOZHIN, N.N. 278

OBAYASHI, T. 140-143
ODA, M. 101, 102, 132
O'DELL, F.W. 8-10, 18
OGAWA, S. 132
OGITA, N. 101
ÖGRIM, O. 84
OKUN', L.B. 27, 38
OLBERT, S. 101
OLEKSA, S. 12, 18
OLSEN, H. 79-81, 85
OPPENHEIMER, J.R. 63, 83
OVCHINNIKOV, V.M. 275
OZAKI, S. 132

Pair production 63-4, 73-83, 120
PAK, M.I. 281
PALMEIRA, R. 265, 275
PANFILOVA, T.F. 131
PANKRATOV, A.K. 44, 62, 139
PANOFSKY, W.K.H. 78, 85
PANOVKIN, B.N. 57, 59, 62
Parity 22-4
PARSONS, N.R. 192, 196
PAULI, W. 20
PERKINS, D.H. 131, 132, 288
PERRIN, F. 73, 84
PETERS, B. 111, 130, 131, 288-9
PFOTZER, G. 137, 139
Photoemulsions 11, 14-16, 92, 99, 127-9, 281, 286-8
Photomultipliers 9, 45-7, 222, 268-75
PIDDINGTON, G.H. 58
Pi-mu decay 122-8, 244-5, 247-8
PINAEV, V.S. 39
PINE, J. 131
PINKAU, K. 131, 132
PISAREVSKII, A.N. 275
PIVNEVA, V.T. 144
Poisson's law 89, 120, 294-5
POMANSKII, A.A. 63
POMANSKY [POMANSKII], A.A. 102
POMERANCHUK, I. 67, 69, 70, 73, 83
POMERANTZ, M.A. 50, 172, 195
PONOMAREV, E.A. 221
PONTECORVO, B. 20, 38, 39
PORTER, N. 101
POTAPOVA, N.I. 236
POTNIS, V.R. 195
POWELL, S.F. 288
PRILEPSKII, B.A. 291, 293
PROKOF'EVA, I.A. 253
PUPPI, G. 101

QUENBY, J.J. 185-6, 195

Radiation belts 2, 49, 51-2
Radiation length, 63-83, 113, 121, 219
Radiation logarithm 65-73, 122-4
Radio emission 3, 12-13, 45-7, 57, 157, 174-6, 197, 221-31
Radiosondes 246-7, 290
RADYUK, G.A. 276
RAMANA MURTYH, P.V. 39
RANDI, P.. 196
RAO, U.R. 172, 186, 195, 265
RAZDAN, H. 265
RAZORENOV, L.A. 4, 18, 19
Red shift 33
REEVES, H. 39
REGENER, V.H. 131
REID, G.C. 44, 139
REID, J.H. 62
REINES, F. 22, 28, 33, 37, 38
Relativity 33-4
RESSLER, D. 132
RICHARDS, R.K. 299
RIDLEY, P. 84
Rigidity 4-5, 15, 53, 144, 155
RITSON, D.M. 102
RITUS, V.I. 39
ROEDERER, J.G. 179
ROHRLICH, F. 75-7, 84
ROINISHVILI, V.N. 285
ROMANA, A. 205, 215
RONKIN, Zh.M. 276
ROSE, D.C. 163, 205, 275
ROSHCHUPKIN, V.G. 291
ROSSI, B. 67, 81-5, 88, 101, 102, 104, 110, 111
ROTHWELL, P. 51, 143, 265
ROZENBAUM, E. 37
ROZENTAL', I.L. 102, 131, 245
RUBTSOV, V.I. 102, 132
RUMER, G. 74, 84
Rutherford formula 286
RYNDIN, R.M. 38

SALAM, A. 37, 38
SALPETER, E.E. 85
SAMSONOV, G.G. 264
SAMUSIKOVA, M. 210
SANDOR, T. 117
SANDS, M. 276
SANDSTRÖM, A.E. 196
SANTOCHI, O.R. 179
SARABHAI, V. 171-2, 185-9, 195, 265

SARTRY, T.S.G. 265
SARYCHEVA, L.I. 245
Satellites, artificial vi, 2, 4-8, 16-17, 48, 51-6, 277
Scaler, 297-303
SCARSI, L. 101, 102, 111
Scattering, atomic 65-70
  Coulomb 93
  In crystals 67-8
  X-ray 70-1
SCHEIN, M. 18, 102
SCHERB, F. 101
SCHERBATSKOY, S.A. 276
SCHOENBERG, M. 39
SCHWACHEIM, G. 195
SCHWARTZ, M. 38
Scintillation counters 12, 22, 28, 35, 52, 266-75
SCOTT, D. 101
SEKIDO, Y. 172, 196, 165
SELEZNEV, V.M. 100
SELEZNEVA, E.S. 195
Self-consistent field 71-3
SELLEN, T.M. 84
SERGEEV, A.A. 62
SERGEEV, A.V. 44, 275
SERGEEVA, G.A. 138, 144, 179, 275
SHAFER, G.V. 44, 156, 163, 196-7, 205, 215, 220
SCHAFER, Yu.G. 48, 131, 156, 163, 205, 220, 290
SHAMSUTDINOVA, F.K. 112, 117, 131, 180, 183
SHAPIRO, M.M. 8-10, 18
SHATASHVILI, L.Kh. 143, 196
SHESTOPEROV, V.Ya. 101, 117
SHIBATA, K. 102
SHIROKII, V.K. 280
SHISHOV, V.I. 59, 60, 139
SHUKLA, P.G. 289
SIMPSON, 51
SINGER, S.F. 11, 18
SIROTKIN, I.A. 18, 19
SKRIPIN, G.V. 44, 139, 156, 164, 172, 174, 184, 185, 195-6, 205, 215, 264-5
SKVORTSOV, Yu.V. 101
SLAVATINSKII, S.A. 101, 245
SLEE, 57, 58
SMIRNOV, V.V. 254
SMORODIN, Yu.A. 102, 132
SMORODINSKII, Ya.A. 39, 40
SOKOLOV, A.D. 276
SOKOLOV, V.D. 215
Solar activity, 54-6, 133-8, 156-63, 187-98, 203-4, 212-20, 233-6
Solar flares 12-16, 43-4, 49-50, 55, 58-62, 133-8, 156-63, 174-9, 197-204, 266-7
Solar wind 51-4, 184
SOLOV'EV, M.V. 102, 132
SOLOV'EVA, V.I. 101, 103, 111
SOMOGYI, S. 117
Space physics vi, 1-2, 48, 86, 100
Spark chambers 27, 277-85
STARTSEV, A. 132
STEINBERGER, I. 38
STELJES, J.F. 139, 275
Stellar evolution 31, 34, 37
STEPANYAN, A.N. 44
STILLER, B. 8-10, 18
STILLER, G. 117
SUCH, K.S. 78, 84
SUCHKOV, D.A. 280, 285
SUESS, H. 6, 18
SUGA, K. 101
SUKHODOL'SKAYA, A.D. 276
SUKHODOL'SKAYA, A.N. 232
SULIMOVA, I.E. 276
Superdetectors 267-9
Supernovae, 32, 47, 106-7
SVANES, T. 275
SWANSON, W.P. 85
SYROVATSKII, S.I. 3, 7, 14, 18

TAKIBAEV, Zh.S. 237, 245, 288
TANAHASHI, G. 101, 102
TANAKA, Y. 101, 102, 132
TAYLOR, F.E. 131
Temperature effects 185-7, 209-10, 215, 246-53
TERASHIMA, Y. 18
TETERIN, E.D. 275
TEUCHER, M.W. 101
THAKORA, S.R. 195
THAMBYAHPILLAI, T. 185-6, 189, 195-6
Thomas — Fermi model 67, 69-76
THOMAS, L.H. 66, 83, 84
THOMSON, D.M. 111
THRESHER, J.J. 84
Tidal effects 141-3
TIMOFEEV, M. 210, 215
TOLKACHEV, B.V. 102, 132
TOMIIE, Y. 84
TONGIORGI, V. 101
TORIZUKA, K. 275
TOWLE, L.C. 138, 179
TOYODA, Y. 101
Transverse momentum 92-3, 238
TRUMPY, B. 275
TSPLOSANI, N.N. 39
TUKISH, E.I. 100, 101
TULINOV, V.G. 44, 62
TYAPKIN, A.A. 39

UEDA, A. 101
UMEDA, K. 83, 84
Underground measurments 27, 35-6, 103-4, 118, 126-8, 131 140-2, 164-73, 186, 188, 193, 202, 246-53, 267
UNGSTRUP, E. 231
Urca process 32
UREY, H.C. 6, 18

VAINSTEIN, B.K. 83
VAN ALLEN, J.A. 51
VASILEVSKAYA, S.K. 284
VASILEVSKY, N.M. 39
VAVILOV, Yu.N. 101

VEKSLER, V.I. 39
VELDKAMP, J. 205, 215
VENKATESAN, D. 195-6
VERNOV, S.N. 48, 51, 103, 111, 131
VERSHININ, E.F. 221
VIERVOLL, H. 84
VIK, G. 38
VIL'DGRUBE, G.S. 275-6
VISHNYKOV, V.V. 39
VITKEVICH, V.V. 57, 59, 62
VLASOV, A.A. 231
VOGT, R. 12, 18
VOLYNSKII, V.Kh. 285
VOROB'EV, Yu.K. 300

WADA, M. 143, 205, 275
WADDINGTON, C.J. 7-10, 18, 289
WALLER, I. 84
WALTER, W. 132
WATASE, Y. 102, 131
Weak interactions 22-8, 31
WEBBER, W.R. 10, 18
WEEKS, G.C. 84
WEINBERG, S. 40
WEINRICH, M. 38
WEISS, R.J. 84
WENZEL, W.A. 285
WERGELAND, H. 85
WEST, J. 67, 69, 70, 84
WHEELER, J.A. 74-8, 83, 84
WILLIAMS, R.W. 275
WILSON, B.G. 163, 205, 275
WILSON, J.G. 132
WILSON, R. 84
WINCKLER, J.R. 50, 51, 55
WITTE, H. 84
WOLFENDALE, A.W. 131
WOLFFL, E. 84
WOLLAN, E.O. 131, 220
WU, C.S 38
WYCKOFF, J.M. 84

YAGODA, H. 16, 18
YAKOVLEV, V.I. 100
YANG, C.N. 38
YANOVSKII, B.M. 265
YARYGIN, A.V. 172
YOKOI, K. 18
YOSHIDA, S. 143, 172, 196, 265, 275
YUKAWA, 24

ZATSEPIN, G T. 39, 45, 47, 101, 108, 111, 117, 131, 132, 245
ZEL'DOVICH, Ya.B. 40
ZELEVINSKAYA, N.G. 101
ZLATAROV, V.K. 276
ZLOBIN, L.I. 276